International Atomic Energy Agency

INDC(NDS)–220
Distr.: L

INDC INTERNATIONAL NUCLEAR DATA COMMITTEE

PHYSICS OF NEUTRON EMISSION IN FISSION

PROCEEDING OF A CONSULTANTS MEETING
ON PHYSICS OF NEUTRON EMISSION IN FISSION
ORGANIZED BY THE
INTERNATIONAL ATOMIC ENERGY AGENCY
AND HELD IN
MITO CITY, JAPAN, 24–27 MAY 1988

H. D. LEMMEL (ed.)

JUNE 1989

IAEA NUCLEAR DATA SECTION, WAGRAMERSTRASSE 5, A-1400 VIENNA

INDC(NDS)-220
Distr.: L

PHYSICS OF NEUTRON EMISSION IN FISSION

Proceedings of an
IAEA Consultants' Meeting

Mito City, Japan, 24-27 May 1988

H.D. Lemmel (ed.)
June 1989

Abstract

This document contains the proceedings of the IAEA Consultants' Meeting on the Physics of Neutron Emission in Fission, Mito City, 24-27 May 1988. Included are the conclusions and recommendations reached at the meeting and the papers presented by the meeting participants. These papers cover the following topics: Energy dependence of the number of fission neutrons $\bar{\nu}$, multiplicity distribution of fission neutrons, competition between neutron and γ-ray emission, the fission neutron yield in resonances, and the energy spectrum of fission neutrons in experiment, theory and evaluation.

Reproduced by the IAEA in Austria
July 1989

89-02946

Foreword

Upon recommendation of the International Nuclear Data Committee (INDC) the International Atomic Energy Agency convened a consultants' meeting on the Physics of Neutron Emission in Fission, which was hosted by the Japan Atomic Energy Research Institute (JAERI) and took place in Mito City, 24-27 May 1988.

There were 21 participants from 9 countries and two international organizations. The meeting was divided in two sessions, one on the fission neutron yield and related topics, the other on the energy spectrum of fission neutrons.

The primary objective of the meeting was to review recent experiments, developments of theory, and the conclusions from evaluations on all aspects of this process. For each of the two sessions the present status of knowledge was reviewed and summarized, and the resulting conclusions and recommendations were presented.

The IAEA wishes to express its sincere thanks to J.W. Boldeman and D. Seeliger not only for their excellent chairmanship during the meeting but also for the final wording of the conclusions. The Agency also wishes to thank S. Igarasi, I. Kanno and their assistants for their thorough organization of the meeting, the Japan Atomic Energy Research Institute for the splendid hospitality and, last but not least, K. Iwamoto, Deputy Director General of JAERI, for the opening address.

Note:

In addition to the papers contained in this document, the following papers were also presented and discussed during the meeting.

Multiplicity distribution and variances by F.G. Perey (Oak Ridge).

Nu-bar and total fragment kinetic energy for neutron-induced fission of Th-230 and Th-232 near threshold, by J. Trochon (Bruyeres-le-Châtel, France), presented by J.E. Fréhaut.

Watt spectrum fit to Cf-252 prompt fission neutron spectra, by F.H. Fröhner (Karlsruhe, FRG), presented by W. Mannhart. See also IAEA-TECDOC-483 p. 160.

CONTENTS

SUMMARY, CONCLUSIONS and RECOMMENDATIONS

The meeting was organized in two seesions, the first dealing with fission neutron yield and related topics and the second with aspects of the energy spectrum of fission neutrons. For each session a working party was set up to summarise the status of knowledge. This was then presented to a plenary session of the meeting for consideration and endorsement. This paper presents the summary and recommendations from the meeting for both working groups.

Session 1. Fission Neutron Yield and Related Topics

Participants:
J W Boldeman (Chairman)
J Frehaut
Huang Shengnian
I Kanno
H Knitter
B Kuzminov
H Lemmel
Y Nakagome
F Perey

Working Group 1 discussed in detail the status of data on the general topic of "Fission Neutron Yield and Related Topics". The session on this subject was divided into 5 separate topics and conclusions and recommendations for each topic is presented below.

Topic 1. Energy Dependence of $\bar{\nu}_p$

1. The $\bar{\nu}_p$ value for the reference standard, ^{252}Cf, is known to high accuracy. The recommended value is 3.7661 ± 0.0054 from the review by Axton. The accuracy of the value for this standard is adequate for all current applications of $\bar{\nu}_p$ data. However, the internal consistency of the data suggests that there may be a systematic difference between the average value derived by $MnSO_4$ bath experiments and the average of the values derived from large liquid scintillator tank determinations. Since the liquid scintillator average is dominated by the value from the recent measurement by Spencer (ORNL), the systematic difference is essentially one between this measurement and the $MnSO_4$ bath determinations. The other scintillator measurements are consistent with the average of the $MnSO_4$ bath measurements.

2. The values of $\bar{\nu}_p$ for thermal neutron fission determined from a comprehensive analysis of all 2200 ms^{-1} and Maxwellian averaged thermal data and the $\bar{\nu}_p$ value for ^{252}Cf are adequate for all current applications. The recommended values are also those of Axton. There are however, minor inconsistencies in the data which compensate in the overall averaging process. A comprehensive experimental program to resolve all such matters would be very extensive and is difficult to justify at the present time.

   Axton in his evaluation drew attention to the need to improve fission neutron spectra because corrections are required in $\bar{\nu}_p$ measurements for differences in the efficiencies of the neutron detector for the fission

neutron spectrum of the measured fission process and that of the standard ^{252}Cf. Although the data for ^{252}Cf have improved, those for other important fission processes have not. Some further measurements (for neutron fission of ^{235}U for example), especially comparative measurements with ^{252}Cf, would be valuable.

The recent evaluation of the neutron resonance fission cross section data for ^{239}Pu carried out by Fort et al. leads to some modifications to the values of $\bar{\nu}_p$ for ^{239}Pu in the thermal region. It should be investigated if this affects the evaluation of Axton. It should also be investigated if smaller statistical fluctuations known to occur for the resonances of ^{235}U affect the evaluated data.

3. Although the data for the energy dependence of $\bar{\nu}_p$ for neutron fission of ^{233}U, ^{235}U and ^{239}Pu are satisfactory for nuclear reactor applications, a discrepancy of 0.5% exists between the data obtained by ORNL and the combined data obtained by the French and Australian groups for all three cases. It is conceivable that this discrepancy is also that in the absolute values of $\bar{\nu}_p$ for ^{252}Cf. Possible sources of error were discussed in detail, but no solutions were obtained. Resolution of this discrepancy should be given priority.

4. Minor structures have been observed in the energy dependence of $\bar{\nu}_p$ for neutron fission of the three most important fissile nuclei ^{233}U, ^{235}U and ^{239}Pu. The magnitudes of such structures have always been small, and the consistency between different determination has not been exact. The following comments summarise discussion on this topic:

   (a) The structure in $\bar{\nu}_p(E_n)$ for ^{233}U (at 200 keV) recommended in evaluations of the data was not observed in the recent measurement by Gwin et al. and probably does not exist.

   (b) The recent measurement of $\bar{\nu}_p(E_n)$ for ^{235}U by Gwin found a minimum at 40 keV. There are no comparable $\bar{\nu}_p(E_n)$ or $\bar{E}_K(E_n)$ data at this energy. It was noted that the fission fragment anisotropy has a minimum at approximately this energy.

   (c) There appears to be no complementarity of fine structures observed in $\bar{\nu}_p(E_n)$ and $\bar{E}_K(E_n)$. This is not surprising in view of the complexity of the fission process.

   (d) The energy dependence of $\bar{\nu}_p$ for neutron fission of ^{237}Np has been measured by three groups. The two measurements from Kuzminov and Vesser differ from the third measurement (Fréhaut) by 3 percent. An independent measurement is required.

   (e) There exists some variation in the linear dependence of $\bar{\nu}_p$ due to multiple chance fission. This has been observed in some nuclei e.g. ^{232}Th, but not all nuclei. This behaviour was explained in the framework of a two spheroid model combined with the generalised Madland-Nix Model.

   (f) Most recent data for $\bar{\nu}_p(E_n)$ have not been included in the readily available data files and this matter should be addressed urgently.

Topic 2. Multiplicity Distribution and Variances

1. Neutron multiplicity data are extremely accurately known for thermal neutron fission and for the spontaneous fission of ^{252}Cf, ^{240}Pu and ^{242}Pu. There have been several recent measurements of high precision plus several evaluations of the experimental data. (See for example measurements by Boldeman and Hines, Gwin et al and evaluations by Zucker and Holden).

2. The trends in the variation of the multiplicity with energy in neutron emission were reported by Fréhaut and are seen to show consistent behaviour. However, in the specific case of neutron fission of ^{239}Pu where high precision is required for safeguards applications, much higher precision is requested. The appropriate method of treating experimental multiplicity data to derive accurate assessments of the precision was presented by Perey.

3. An improved method of treating high multiplicity data, particularly eliminating the effect of oscillations which appear in current analyses, is requested.

4. A larger data set on the variation of multiplicity with incident neutron energy is also required. Presently data are available from only one experiment. Experimental data from Gwin et al. and Boldeman and Walsh should be analysed.

Topic 3. Competition Between Neutron and γ Ray Emission

1. Data exist on the variation of total gamma ray energy and multiplicity with fragment mass for thermal neutron fission of ^{235}U (Pleasonton) and spontaneous fission of ^{252}Cf (Signarbieux). Furthermore the variation in total gamma ray emission with energy in the neutron fission of ^{235}U, ^{237}Np and ^{232}Th has been measured by Fréhaut and co-workers. For all processes a direct correlation has been observed between $\bar{\nu}_p$ and $\bar{E}\gamma$ (and multiplicities for the first two experiments). A theoretical description is required. Furthermore, more comprehensive data are required. In particular, data on the variation of total γ ray energy and spectra as a function of fragment mass for a specific fissioning system (spontaneous fission of ^{252}Cf for example) would be valuable.

2. The systematics of the $(n,\gamma f)$ process are well understood especially for the case of neutron fission of ^{239}Pu.

   Statistical fluctuations of $\bar{\nu}_p$ correlated with the mass distribution and kinetic energy have been observed for resonances in the neutron fission of ^{235}U. These fluctuations are not correlated with spin and are not related to the $(n,\gamma f)$ process which is extremely small in this system.

   These statistical fluctuation will probably occur for other fission systems and may therefore influence slightly the analysis of the $(n,\gamma f)$ process for neutron resonances in ^{239}Pu.

Topic 4. Fission Neutron Emission Near Threshold

1. Although measurements of the variation of $\bar{\nu}_p(E_n)$ and $\bar{E}_K(E_n)$ for subthreshold and near threshold fission are extremely difficult the experimental data are generally consistent. Recent data were presented

by Kuzminov. Analyses by Fréhaut and Trochon, Kuzminov and Boldeman were discussed.

2. For vibrational resonances in the neutron fission of ^{230}Th, ^{232}Th, ^{234}U, ^{236}U and ^{238}U the value of the average fission fragment kinetic energy decreases significantly. Since the fission fragment angular distributions for such resonances show strong non-isotropic behaviour because of the specific value of K associated with each resonance, the dip in the average fission fragment kinetic energy is also reflected in different values of the average kinetic energy at 0° and 90° to the incident neutron direction.

3. Similarly the $\bar{\nu}_p(E_n)$ dependences also in general show a great deal of structure in the vicinity of the vibrational resonances.

4. However, the $\bar{\nu}_p(E_n)$ and $\bar{E}_K(E_n)$ dependences are not complementary in character.

5. Surprisingly, the $\bar{\nu}_p(E_n)$ data for neutron fission of ^{230}Th show no structure for the vibrational resonance at 715 keV.

6. One analysis of the $\bar{\nu}_p(E_n)$ data for ^{232}Th shows that $\bar{\nu}_p$ is strongly correlated with the quantum number K of the fission channel.

7. An exact explanation of the structure in $\bar{\nu}_p(E_n)$ and $\bar{E}_K(E_n)$ in the threshold region is required if the fission process is to be fully understood. However, such an explanation cannot be attempted until consistent channel analyses are obtained of the fission cross sections.

Topic 5. $\bar{\nu}$ in Resonances

1. The work of Fort et al. shows that resonance variations of $\bar{\nu}_p$ should be included in data files. The additional data that should be listed include the resonance spin variation of $\bar{\nu}_p$ and data for the (n,γf) process.

2. From a general discussion of the (n,γf) process, it was noted that the size of the process for neutron resonances of ^{241}Pu should be similar to that for resonances in ^{239}Pu. For ^{235}U on the contrary, the size of the process should be smaller. However, the (n,γf) process only significantly affects resonances in which the fission width is small. Therefore, the effect of the (n,γf) process on resonances in ^{241}Pu and ^{235}U is minimal.

Session 2. 'Energy Spectrum of Fission Neutrons'

Participants: Baba
Blinov
Hirakawa
Huang
Kapoor
Knitter
Madland
Märten
Mannhart
Seeliger (Chairman)

The Working Group 2 discussed in detail the status of investigations considered in topics 6 to 9 of the Consultants' Meeting and came to the following conclusions and recommendations:

Topic 6. Measurements of Neutron Induced Fission Neutron Spectra

Most of the experiments in this field were carried out prior to the beginning of the 70's, using experimental techniques that were available at that time. At the present CM new measurements at the Tohoku University and TU Dresden have been presented by Baba and Seeliger for neutron-induced prompt-fission-neutron-spectra for ^{232}Th at 2 MeV and 7.3 MeV, respectively. Blinov reported that similar experiments are underway at RI Leningrad at 3 MeV and 14 MeV. In addition, new measurements of the total neutron emission spectra from ^{238}U at 14 MeV incidence energy are in progress in a few laboratories. Relevant reports and brief information papers have been presented at the CM from Tohoku University, TU Dresden, IAE Beijing and RI Leningrad.

During the discussions in the working group the importance of new, high quality measurements at several incident energies was stressed, especially for checking the predictability of new theories for prompt fission neutron spectra. Resulting from the present status of the experiments, the following cases are recommended in particular for careful theoretical analysis and intercomparisons of the experimental data.

(i) ^{235}U at thermal neutron energy (a prompt neutron fission spectrum which was well-investigated in the past);

(ii) ^{232}Th at 2 MeV incident energy (a pure fast neutron induced first chance fission neutron spectrum);

(iii) ^{232}Th at 7.3 MeV incidence energy measured in coincidence with a fission chamber (a case, where first and second chance fission neutrons are mixed);

(iv) ^{238}U at 14 MeV incidence energy measured with and without coincidence to a fission chamber (in this case the experimental spectra represent a complicated mixture of direct, pre-equilibrium and equilibrium pre-fission neutrons with prompt fission neutrons up to the third order of fission).

Fission neutron models which proved to be successful in these cases could be used for the prediction of unmeasured neutron spectra for primary and secondary actinides, resulting in corresponding improvement of evaluated nuclear data files.

Besides these, other high quality measurements of neutron induced fission spectra are encouraged by the working group, especially near the energy regions, where new reaction channels open (e.g. the (n,n'f) and (n,2nf) channels).

Finally, it was pointed out that during the last few years no measurements were reported concerning neutron-fragment-correlation for neutron induced fission. It might be reasonable to carry out such measurements, e.g. at thermal energies, using for this purpose the new techniques developed in connection with the differential experiments for ^{252}Cf s.f., mentioned in Topic 7 of this report.

Topic 7. Studies of Neutron-Fragment-Correlation for ^{252}Cf Spontaneous Fission

At the present CM new measurements of $N(E,\theta)$ for ^{252}Cf s.f. have been presented by Knitter, Seeliger and Blinov from CBNM Geel, TU Dresden and RI Leningrad, respectively.

By these experiments, which in particular were carried out with new techniques, very detailed experimental information concerning the neutron emission from specific fission fragments in a wide emission energy range and with high angular resolution was obtained. This tremendous bulk of new data provides the challenge of detailed studies of the mechanism of neutron emission. At present, the initial steps in a physical interpretation of the data have been undertaken, showing that these experiments do not indicate a significant scission neutron component. The upper limit from the preliminary studies is estimated to be not higher than 5%.

The working group encouraged the laboratories mentioned above to finalise the data analyses for these measurements and to provide other laboratories with the measured data upon request for detailed physical discussions and comparisons with theoretical calculations.

These laboratories are asked also to derive angular integrated data from their measurements for comparisons with the ^{252}Cf s.f. standard nuclear data file. An intercomparison of neutron c.m. spectra from individual fragments as deduced by different experimental groups also seems to be useful.

Further exchange of information between all laboratories using these unique sets of data for comparison with theoretical models and physical conclusions is highly recommended by the working group. Beyond the search for neutrons which are not emitted from fully accelerated fragments, of special interest are investigations of neutron and gamma ray multiplicities for different fragmentations. In addition there is a great deal of interest in the level densities of fission fragments.

The working group stressed, that it should be investigated, whether new experiments of the type being carried out at CBNM Geel, could be started also for other spontaneous fissioning nuclei like the Fm-isotopes (in this case the fission would be largely symmetric in contrast to that of Californium fission).

The importance of obtaining information about the gamma emission from the ^{252}Cf s.f. thereby leading to improved knowledge about the average gamma energy $\bar{E}_\gamma$, the energy balance of fission and the angular momenta of fission fragments was also mentioned. In particular, it was recommended

that the bulk of data measured during the last year using crystal ball detectors be analysed carefully in this sense. In future, measurements with high resolution detectors could also give useful spectroscopic information about the structure and level schemes of the neutron rich fragment nuclei.

The working group was informed, that new gamma ray measurements are underway at Dresden by a TUD/CINR collaboration.

Topic 8. Theory of Fission Neutron Spectra

At the beginning of this topic, the working group discussed the question of terminology used at present in different publications concerning the mechanism of fission neutron emission. At present, a growing diversity of terms is used, which can be is misleading (e.g. central component neutrons, pre-acceleration neutrons, scission neutrons, catapult neutrons, rupture neutrons, etc.). The working group recommends the use in future of the following terms:

(i) pre-fission neutrons

These include the direct, pre-equilibrium and equilibrium components of neutron emission before fission from reactions like (n,n'f), (n,2nf), (n,pnf) etc.;

(ii) scission neutrons

These are all neutrons emitted by different possible mechanisms during the descent from saddle to scission point, including the neutron emission at the rupture of the fissioning nucleus;

(iii) neutrons from accelerating fragments;

(iv) and neutrons from fully accelerated fragments.

For completeness it should be mentioned that besides the prompt neutron emission considered here, there are additionally delayed neutrons, emitted as a result of specific beta decay from the fragments.

Concerning the development of fission neutron theories, the great progress in this field during the last years was highlighted by the working group. In particular, the theories of the description of neutron emission from fully accelerated fragments, which have been developed at LASL, TUD and RIL in the frame of the statistical approach, have strongly increased the predictive capability of theory especially as it is now known that these neutrons are by far the dominating component of all prompt fission neutron. Besides these a few other theoretical approaches to different possible mechanisms of fission neutron emission have been reported in the literature during the recent years. However, the missing, so far, capability of quantitative predictions of this approaches at the one side and the stated above dominance of the neutron emission from fully accelerated fragments of the other side do not allow, at present, a definitive conclusion about the real observations of one of these mechanisms in neutron experiments (this is in contrast to the situation for the emission of light charged particles). Nevertheless, further theoretical studies in this direction are needed. In particular, on the long time scale a full-range time-depending Hartree-Fock theory for the fission process, including neutron emission, should be developed. In any

case, the theoretical description of the main component of neutron emission in the frame of the statistical model has to be further improved as much as possible.

The presently existing approaches in the frame of the statistical model could be divided into three categories, as follows:

(i) Approaches within an approximative statistical model, partially using input parameters averaged over fission fragment distributions. The development of this type of models was started by Madland and Nix at LASL. Later Märten and Seeliger from TUD proposed a more detailed approach of this type, including detailed distributions over fission fragment mass number A, as well as a rough consideration of n-γ-competition and c.m. anisotropy of neutron emission (so-called GMNM). At the present CM, Madland reported about the introduction of further improvements into this approach, e.g. the fragment charge distribution.

After all this development, these models are now capable for the description of angle integrated spectra as well as differential spectra $N(E,\theta)$ for the ^{252}Cf spontaneous fission neutron emission (examples for this were presented by Madland and Märten). But the most promising capability of this approach seems to be the prediction of neutron induced fission neutron spectra, including multiple chance fission, over a broad range of incidence energies. Examples of this, again have been presented at the CM by the laboratories mentioned above. For the determination of input parameters a simple two-spheroid model (TSM) was developed at TUD.

(ii) Approaches within the Weisskopf-Ewing statistical theory, being valid for continuous state densities in the final nuclei, including all steps of cascade particle emission.

The cascade evaporation model (CEM) developed at TUD, is an approach of this type of approximation, taking into account the diversity of distributions in the fission fragments, including individual level density parameters. Due to the need for the knowledge of many input parameters of the fissioning system, so far, the application of this model is limited to well-investigated cases like the ^{252}Cf spontaneous fission. The further application of this theory to the description of the new experimental differential data $N(E,\theta)$ for ^{252}Cf s.f. seems to be very useful for the physical understanding of this process. First examples of such analyses have been presented at the CM by Märten.

(iii) The most general approach within the statistical model, including angular momentum coupling, can be provided by the Hauser-Feshbach theory using the whole diversity of input distributions over all fission fragments. At present, attempts in this direction are undertaken at the RI Leningrad, but still within a limited scale (concerning the diversity of fission fragment distribution and angular distributions). Examples for this approach were presented at the CM by Blinov.

In the long term a fully established HF-code for the calculation of fission neutron spectra seems desirable. However, the broad-range application of this theory needs an improved situation concerning our knowledge of necessary input distributions (over E*, I, A, Z, TKE, etc.), level density parameters and the isospin-dependence of the optical model parameters.

It should be pointed out also, that a fully-established description of neutron emission from fissioning nuclei need also a proper theoretical description of pre-fission neutrons and accompanying neutron induced reactions including collective direct and particle-hole excitations. Besides well established codes like STAPRE, newly developed multisteps statistical theories could be used as a proper base for this.

Finally, it was mentioned, that the knowledge about level density parameter obtained from fission neutron studies could also serve as a useful information for the understanding of astrophysical processes.

Topic 9. Evaluation

The status of the present ^{252}Cf spontaneous fission neutron spectrum evaluation was presented in detail by Mannhart from PTB and discussed in the working group.

The conclusion of this discussion was, that the present evaluation is in a good shape, presenting the spectrum with evaluated uncertainties of $\leq$ 3% between 150 keV and 11 MeV and at last $\leq$ 1.5% between 1 MeV and 5 MeV. Outside at the quoted ranges the uncertainties increase up to 10% at the lowest and 30% at the highest energies. For the practical use the smooth curve of the data evaluation available in numerical form from the Nuclear Data Centres is recommended (in special cases, like comparison with refined theories, it may be justified to go back to the original evaluated point data).

Between 10 keV and 20 MeV the existing evaluation agree within less than 3% with the CEM calculation

It is recommended to update the evaluation from time to time and especially to include as soon as possbile the existing fully documented experimental data (experiment TUD/PTB and recent modifications of Lajtaj data).

The working group noted the attempt by Froehner to approximate the spectrum by a fitted Watt distribution. This parameterisation seems to be useful for a fast and simple representation of the spectrum by two parameters without high requirements concerning the uncertainty.

General Recommendation

The rapid development of modern techniques for multi-parameter measurements of the properties of the fission process promises an opportunity to improve substantially the current understanding of this extremely complicated nuclear process. Furthermore, these measurement techniques provide a real method to aid the transfer of technology not only to the developing countries but also between developed ones. It is proposed therefore that a Coordinated Research Program be established to study "Nuclear Data on Neutron Emission in the Fission Process and its Understanding". A number of laboratories have expressed a great deal of interest in this idea.

Having in mind the fast development in this field during the recent years, but also the common interest of laboratories oriented both forwards basic as well as nuclear data research, it was recommended by the working group to establish by the INDC of the IAEA a new Coordinated Research

Program on "Physics of Fission Neutron Emission and its Nuclear Data Applications". This CRP could be also a way for the transfer of the newly developed techniques and technologies in the field of fission research to appropriate laboratories in developing countries and therefore, it could contribute to the IAEA "Interregional Project for the Transfer of Nuclear Technology to Developing Countries".

SESSION 1

FISSION NEUTRON YIELD AND RELATED TOPICS

Chairman:

J.W. Boldeman

(Lucas Heights, Australia)

THE ENERGY DEPENDENCE OF $\bar{\nu}_p$

J W BOLDEMAN
AUSTRALIAN NUCLEAR SCIENCE
AND TECHNOLOGY ORGANISATION
LUCAS HEIGHTS RESEARCH LABORATORIES
AUSTRALIA

1. INTRODUCTION

Studies of the energy dependence of $\bar{\nu}_p$ (the average number of prompt neutrons emitted per fission) were needed for two reasons - the design of nuclear power systems and the understanding of the physics of the nuclear fission mechanism. The first published measurements go back to the 1940's and were followed by intense activity when the broad outlines of the dependence were established. In the 1960's the quality of the experimental apparatus improved significantly as did the quality of the data. During this period a number of controversial issues appeared, namely fine structure in the $\bar{\nu}_p$ ($\bar{E}_n$) dependence, resonance fluctuations in the value of $\bar{\nu}_p$, the so called $\bar{\nu}$-η discrepancy and the most serious discrepancy of all - the systematic difference of 2 percent between liquid scintillator and manganese sulphates bath measurements of $\bar{\nu}_p$ for the spontaneous fission of ^{252}Cf (the reference standard).

As far as the data requirements are concerned all of these problems have been resolved. There currently is a general overall consensus in the data within an accuracy of 1%. Therefore, the activity in the subject has diminished significantly as there is no longer the drive for commercial application. Furthermore any experiments to achieve a significant improvement in the precision of a measurement are extremely difficult. Despite this apparent satisfaction with the quality of the data, there remain small discrepancies in the values which are probably significant relative to the experimental precision. The resolution of these discrepancies is important to the clear understanding of the physical processes involved in the fission mechanism.

This review will consider firstly, the basic reference data for the measurements of $\bar{\nu}$ and then the problems in the energy dependence of $\bar{\nu}_p$. Finally, the theoretical implications of the measured dependence of $\bar{\nu}_p$ will be discussed.

2. THE REFERENCE STANDARD

The $\bar{\nu}_p$ value for the spontaneous fission of ^{252}Cf has been adopted as the reference standard for all $\bar{\nu}_p$ data since the mid 1960's. ^{252}Cf was

selected as the standard because of its distinct advantages which include a relatively high spontaneous fission rate with respect to its alpha decay rate and because high spontaneous fission rates could be obtained from very small samples with effectively zero fission rate loss within the sample material.

Despite the status of a standard for ^{252}Cf, there has been a long history of disagreement between the experimental determinations. The disagreement in the late sixties and early seventies was essentially a 2 percent discrepancy between the boron pile measurement [1] and the two liquid scintillator measurements of Hopkins and Diven [2] and Asplund-Nilsson et al.[3]

The $MnSO_4$ bath measurements that had been completed at that time[4-6] tended to support the boron pile measurement. At the 1972 IAEA Panel on Neutron Standard Reference Data, a preliminary value from this laboratory[7], obtained using a large liquid scintillator tank, appeared to break the disagreement between the two types of measurements in that the value obtained lay between the two averages. Furthermore, it was apparent that some additional corrections which would reduce the measured values for the two earlier liquid scintillator measurements were required.

The possibility that the discrepancy could be resolved spurred renewed effort to examine in detail all aspects of the different experimental methods. A number of refinements were introduced in the corrections for the liquid scintillator class of measurements. These included improved corrections for delayed gamma rays following fission and the dependence of the neutron energy dependence of the liquid scintillators. Typically the energy dependence was calculated using Monte Carlo methods and then normalised to absolute measurements at specific neutron energies. The major refinements involved the inclusion in the calculations of the variation of the neutron capture gamma ray detection as a function of the neutron energy plus improvements in the experimental techniques. A number of problems were also identified in $MnSO_4$ bath measurements. These included problems with impurities and corrections for sulphur and oxygen.

Most measurements presented at the 1972 Panel have therefore been revised. Two minor corrections were applied to our measurement[8,9] so that the final value was larger by 0.29%. From a re-analysis of the boron pile measurement, Ullo[10] recommended an increase in its value by 0.67%. In 1977, the two early liquid scintillator measurements were revised downwards slightly[9] and it was at about this time that Smith[11] began an extended investigation of the $MnSO_4$ bath technique which has led to a steady increase in the various values obtained using this technique.

Recently, Spencer et al.[12] have published a value of $\bar{\nu}$ for ^{252}Cf of very high precision - of the order of 0.2%. Their value, obtained using the liquid scintillator tank, was in reasonable agreement with a high precision $MnSO_4$ bath determination from Smith and Reeder[18] which was finalised at about the same time. Thus it was proposed in a recent review[13] that, since the most accurate of the liquid scintillator measurements was in reasonable agreement with the most accurate (at that time) $MnSO_4$ bath determination, the discrepancy had finally disappeared. However, the agreement between Spencer and very recent high precision $MnSO_4$ bath measurements has been poor.

Table 1 lists the current status of all accurate measurements of $\bar{\nu}$ for the spontaneous fission ^{252}Cf. The two measurements from NPL, White and Axton (1968)[4] and Axton et al.(1969)[3] have been superseded by Axton and Bardell (1984)[15]. The latest value from the group at the V.G. Khlopin Radium Institute - Aleksandrov et al.(1980)[16] supersedes their earlier published value - Aleksandrov et al.(1975)[17].

The weighted mean of the $MnSO_4$ bath measurements is 3.7563±0.00062. This value is in agreement with the revised boron pile measurement and the recent measurement from Edwards et al.[21]. However, it is clearly in disagreement with the weighted average of all liquid scintillator measurments, namely, 3.7754±0.0059 even after provision is made within the two sets for common errors. The question that arises is whether this disagreement is one between the two techniques - liquid scintillator and $MnSO_4$ bath - or whether there is a more general disagreement. It should be noted that the two liquid scintillator measurements of Boldeman[8] and Zhang and Liu[19] are in agreement with the average of the $MnSO_4$ bath. In fact, there would appear to be a small discrepancy between Boldeman[8] and Spencer et al.[12] since the accuracy of the first measurement for comparison with the second reduces to 0.010. The difference between the two is almost three standard deviations.

Despite these differences, the quality of the data is quite high and the current accuracy of the standard is adequate for all present applications. The present recommended value for the standard derived by Axton (1984)[22] is 3.7661±0.0054.

3. THE THERMAL $\bar{\nu}$ VALUES

The optimum thermal $\bar{\nu}$ values (total neutron emission) along with the other thermal neutron constants - the thermal fission (σ_f) and absorption cross sections (σ_a) and the average neutron emission per absorbed neutrons (η) are typically obtained from a comprehensive evaluation of all 2200

TABLE 1 - $\bar{\nu}$ VALUES FOR SPONTANEOUS FISSION OF ^{252}Cf

EXPERIMENT	VALUE	WEIGHTED MEAN OF GROUP
Liquid Scintillator		
*Asplund-Nilsson et al.(1963)[3]	3.792±0.040	3.7754±0.0059 (with Spencer et al.)
*Hopkins and Diven (1963)[2]	3.777±0.031	
*Boldeman (1974)[8]	3.755±0.016	
Zhang and Liu (1980)[19]	3.754±0.018	3.7600±0.0107 (without Spencer et al.)
Spencer et al.(1982)[12]	3.782±0.007	
Manganese Bath		
White and Axton (1968)[4]	superseded	
Axton et al.(1969)[5]	superseded	
†De Volpi and Porges (1970)[6]	3.747±0.019	
Aleksandrov et al.(1975)[17]	superseded	3.7563±0.0062
Bozorgmanesh (1977)[20]	3.774±0.023	
Aleksandrov et al.(1980)[16]	3.758±0.015	
Smith and Reeder (1984)[18]	3.767±0.011	
Axton and Bardell (1984)[15]	3.7509±0.0107	
Boron Pile		
‡Colvin and Sowerby (1965)[1]	3.739±0.021	
Edwards et al.(1982)[21]	3.761±0.029	
Evaluation		
Axton (1984)[22]	3.7661∓0.0054	

*Revised by Boldeman (1977)[9]

†Revised by Smith (1977)[11]

‡Revised by Ullo (1977)[10]

ms^{-1} point data and Maxwellian averaged data for the principal fissile nuclei. These constants are related by the equation

$$\eta = \bar{\nu}/(1+\alpha) \qquad (1)$$

where α is the capture to fission ratio.

Historically the 2200 ms^{-1} values have been plagued by inconsistencies. The most serious was the so-called $\bar{\nu}$ - η discrepancy. Effectively the $\bar{\nu}$ values derived from pre 1975 measurements of the ratio of $\bar{\nu}_p$ for thermal neutron fission to the standard ^{252}Cf and the absolute value for this standard disagrees with the $\bar{\nu}_p$ values derived from η measurement according to equation (1) especially those for ^{235}U and ^{233}U where the η measurements had the highest precision. Use of the ratio measurements from Gwin et al[23] for ^{235}U gave good agreement, however this agreement was less satisfactory if the absolute value for ^{252}Cf from the same group, Spencer et al.[12] was used.

The $\bar{\nu}_p$ ratio value for ^{235}U from Gwin et al. differed by almost 1% from the average for ^{235}U from pre 1975 data although the data for ^{239}Pu were in excellent agreement. A possible explanation for the discrepancy suggested by Smith [24] was an error in the correction factior in $\bar{\nu}_p$ measurements for the foil thickness. This was investigated by Boldeman and Frehaut[25] who found that the correction factors required were slightly larger than had been used. Consequently, the difference between the Gwin et al. value for ^{235}U and that of previous measurements was reduced to about 0.6%. This difference was slightly larger than that desirable but is probably acceptable.

Recently Axton[22] has made a comprehensive intercomparison of the 2200 ms^{-1} values in which all modern corrections have been incorporated. Table II lists the recommended output values from this study.

4. ENERGY DEPENDENCE OF $\bar{\nu}_p$

For the purposes of this review, the energy dependence of $\bar{\nu}_p$ can be considered for three classes of fission - (a) above barrier fission (4.1) (b) sub barrier fission (4.2) (c) resonance fission. Above barrier fission is considered in some detail, some comments are presented on sub barrier fission which resonance fission has been left entirely to another review.

4.1 Above Barrier Fission

The key questions that have been considered over the years are the systemmatic behaviour of $\bar{\nu}_p$ (E_n) curves as a function of the mass number and fine structure in the $\bar{\nu}_p$ (E_n) dependence at low energy. A major review of $\bar{\nu}_p$ (E_n) data was carried out by Manero and Konshin[2] in 1972. This review is still widely referred to since a great deal of the data was measured before 1972. However, some of the recommendations from this review must be treated with caution as most measurements of relatively

TABLE 11 The results of the calculation are shown below.

			Uncertainty
$\bar{\nu}_T$	^{233}U	2.488	.006
	^{235}U	2.427	.005
	^{239}Pu	2.876	.007
	^{241}Pu	2.937	.007
	^{252}Cf	3.766	.005
σ_a	^{233}U	574.1 b	1.8 b
	^{235}U	681.5 b	1.7 b
	^{239}Pu	1017.7 b	3.8 b
	^{241}Pu	1378.9 b	12.7 b
σ_f	^{233}U	531.9 b	2.4 b
	^{235}U	584.7 b	1.7 b
	^{239}Pu	748.3 b	2.4 b
	^{241}Pu	1018.0 b	10.0 b
σ_γ	^{233}U	42.2 b	1.8 b
	^{235}U	96.8 b	1.8 b
	^{239}Pu	269.4 b	3.4 b
	^{241}Pu	360.9 b	5.6 b
$\bar{\nu}_T$ ratios	$^{233}U/^{252}Cf$	.6607	.0015
	$^{235}U/^{252}Cf$	.6445	.0012
	$^{239}Pu/^{252}Cf$	.7637	.0016
	$^{241}Pu/^{252}Cf$	.7800	.0017
η	^{233}U	2.305	.0063
	^{235}U	2.083	.0055
	^{239}Pu	2.115	.0069
	^{241}Pu	2.169	.0083
$1 + \alpha$	^{233}U	1.079	.004
	^{235}U	1.166	.003
	^{239}Pu	1.360	.005
	^{241}Pu	1.355	.006
σ_a	SULPHUR	.525 b	.129 b

high precision included in the review have been revised (some on several occasions) and because the treatment of complementary data [e.g variations of the average fission fragment kinetic energy data with neutron energy] was not always consistent.

In this review the three key cases of the energy dependence of $\bar{\nu}_p$ will be examined in detail since it is only for these three cases that the data are sufficiently accurate to draw meaningful conclusions.

4.1.1 ^{233}U

The review of Manero and Konshin produced a significant minimum at about 200 keV neutron energy for the $\bar{\nu}_p$ dependence of ^{233}U. The ENDF/BV review also showed significant structure as can be seen in Figure 1. A recent measurement of high precision of the $\bar{\nu}_p$ (E_n) dependence for ^{233}U by

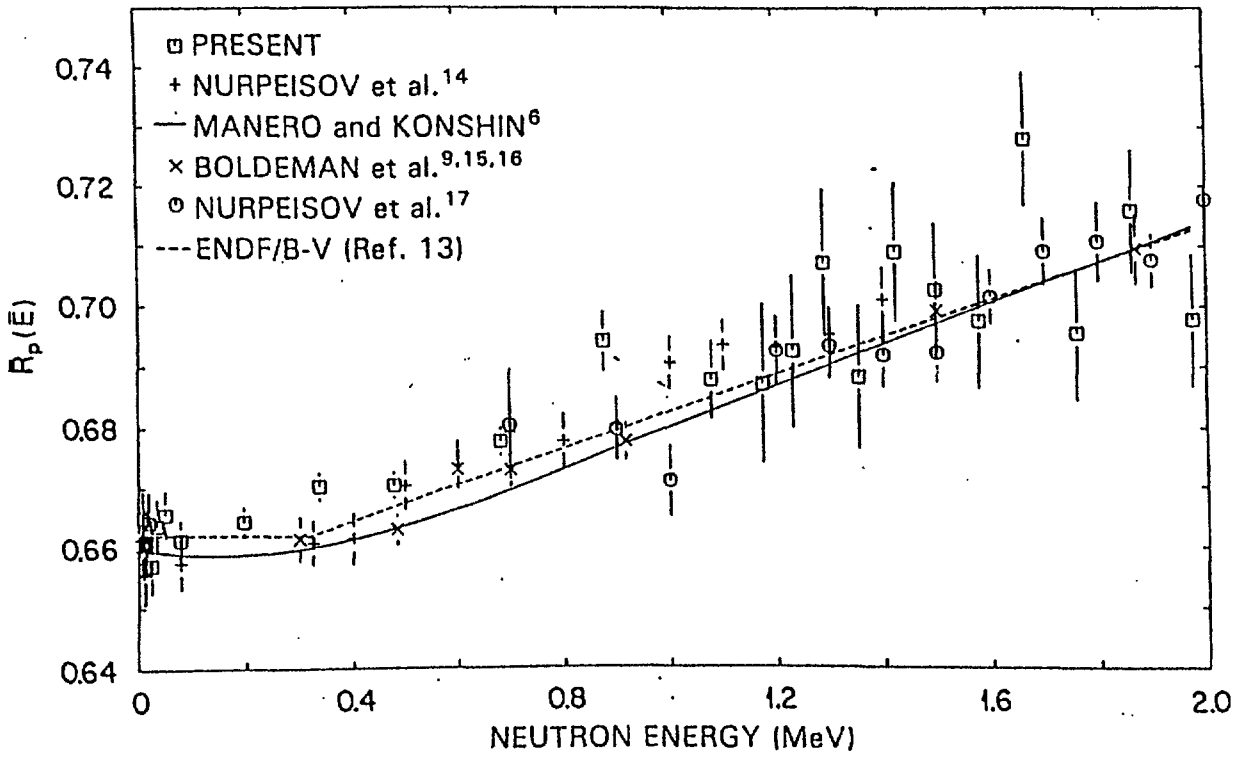

Fig. 1 Plot of $\bar{R}_p(\bar{E})(^{233}U)$ for the interval of 0 to 2.0 MeV. The value of $\bar{R}_p(\bar{E})$ is plotted at the midpoint of the energy interval $\bar{E}$ of the averaging process. (Taken from Ref.28. References in figure are also from Ref.28).

Gwin et al. failed to find any significant structure whatsoever. It is of value therefore to examine the experimental origins for the structure.

The total energy in the fission process appears either as fission fragment kinetic energy or as excitation of the fission fragments. The excited fission fragments lose their energies by neutron emission and eventually gamma ray emission when there is insufficient energy for an additional neutron. The high spin of the fragments modifies this simple picture somewhat as the neutron cannot always carry sufficient angular momentum and the existence of the yrast line favours some additional gamma ray release.

Traditionally it has been assumed that increased excitation in the fission process due to increased incident neutron energy has gone into the excitation of the fission fragments at scission and therefore caused increased neutron emission. Furthermore, it has been assumed that the mass distribution does not change with modest variation in excitation. Therefore, the average fission fragment kinetic energy should be constant with neutron energy and the value of $\bar{\nu}_p$ should increase linearly with energy. Therefore, if any structure should appear in $\bar{E}_K$ (E_n) then complementary behaviour should be seen in $\bar{\nu}_p$ (E_n).

Figure 2 shows a comparison of the variation of the average fission fragment kinetic energy for ^{233}U as a function of neutron energy. The

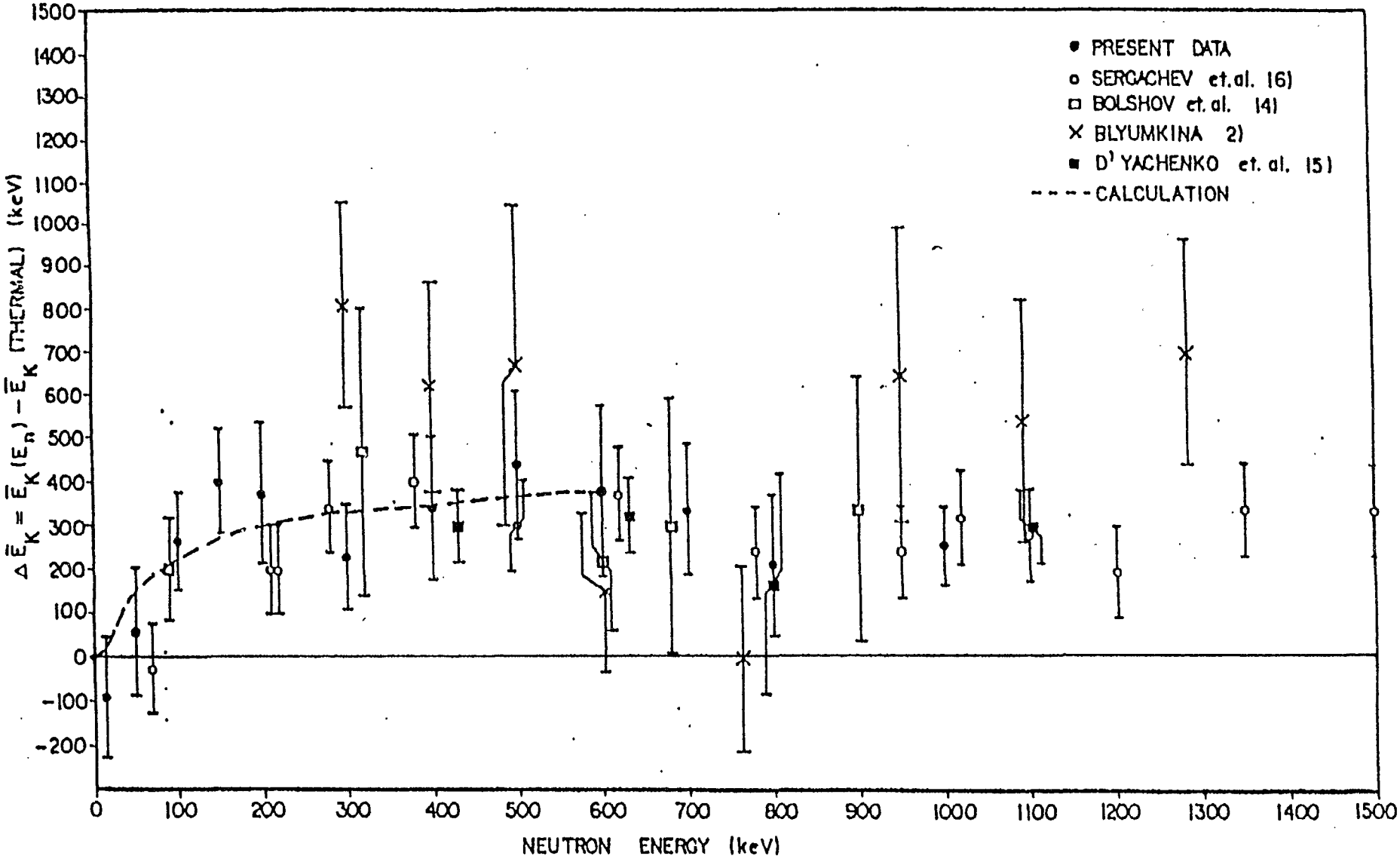

Fig. 2 Average total kinetic energy data for ^{233}U, $\Delta\bar{E}_K = \bar{E}_K(E_n) - \bar{E}_K(\text{thermal})$.
(Taken from Ref.27).

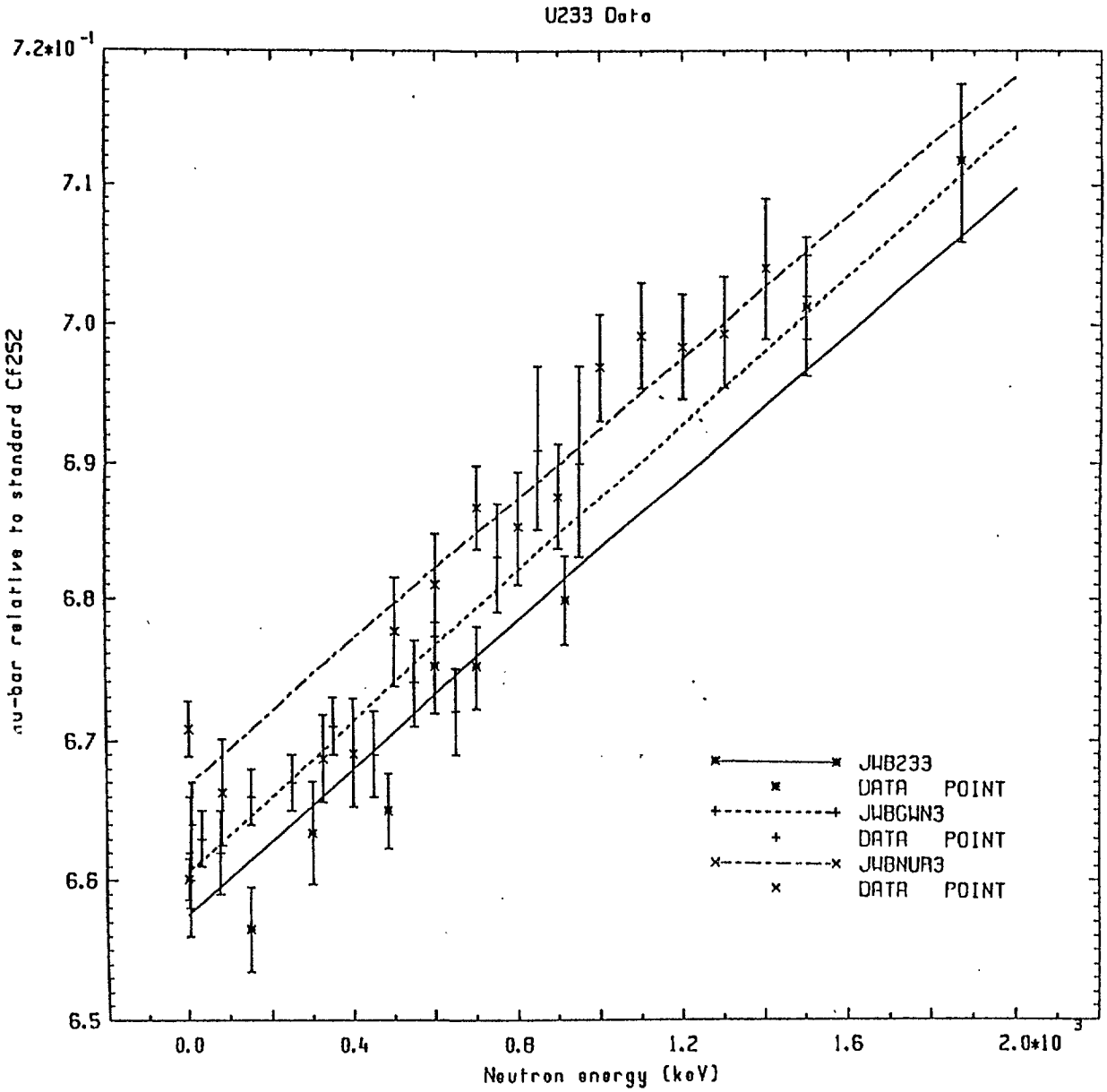

Fig.3

different data sets are generally in excellent agreement and show that $\bar{E}_K$ rises between thermal energies and 150 keV and then remains substantially flat from 150 keV to at least 2 MeV. From the energy balance considerations, the kinetic energy data suggest that $\bar{\nu}_p$ (E_n) should be linear above 200 keV and that these should occur a minimum in the vicinity of 150 keV.

Most of the pre 1980 experimental data for $\bar{\nu}_p$ (E_n) are consistent with the dependence derived from the kinetic energy data. However, none of the data sets specifically confirm this behaviour in their own right. The most that could be said of the combined data was that some structure could be needed because a linear fit to the data appeared to be somewhat different from the thermal value. For example, a linear fit to the higher

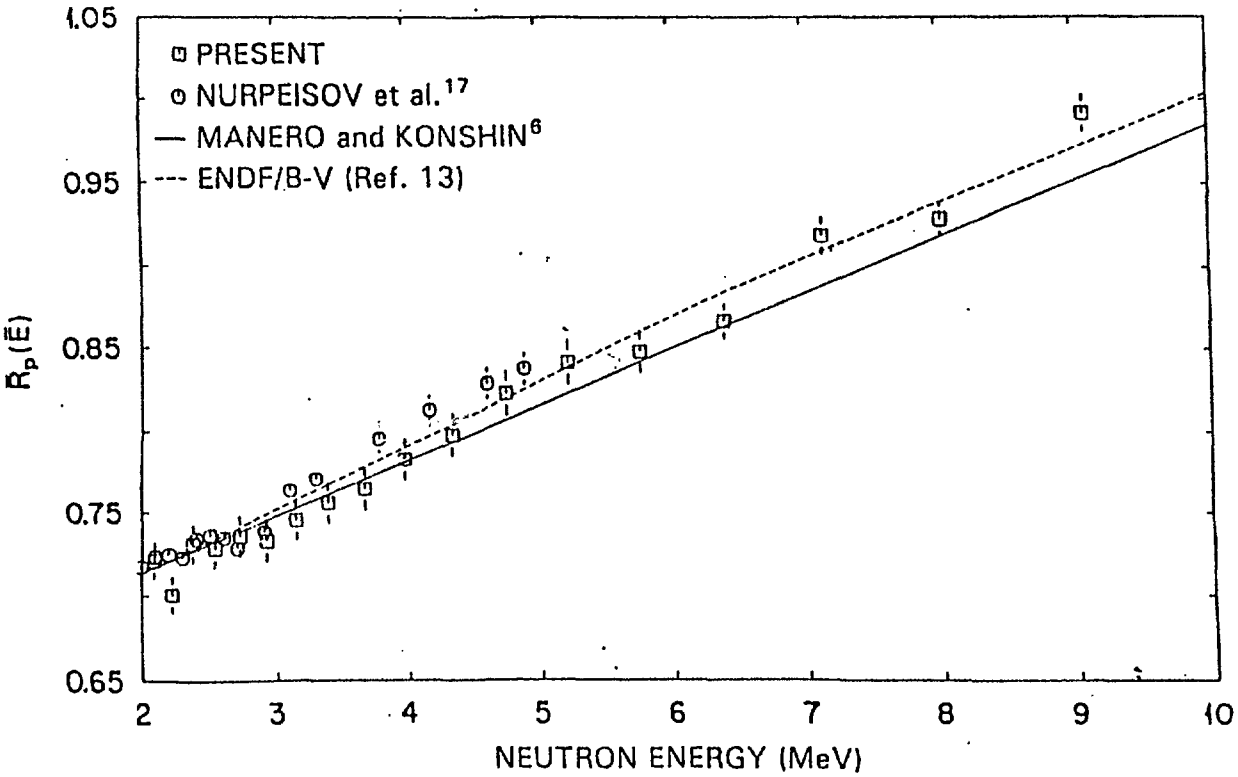

Fig. 4. Plot of $\bar{R}_p(\bar{E})(^{233}U)$ for the interval of 2.0 to 10.0 MeV. The value of $\bar{R}_p(\bar{E})$ is plotted at the midpoint of the energy interval $\bar{E}$ of the averaging process.

energy data from Boldeman et al.[27] gives a zero energy intercept 0.8% less than the thermal value from the same experiment.

The recent data from Gwin et al.[28] on the contrary show no evidence of any fine structure at all and are consistent with a linear dependence. Since this measurement was performed on ORELA, all data measurements were made in the one experiment thereby reducing some of the possibilities for systemmatic error. The data from Gwin et al., Nurpeisov et al.[29,30] and that from Walsh and Boldeman are compared in Figure 3. The shape of the two data sets are not entirely inconsistent although a minimum at about 150 keV would be a better representation of the Walsh and Boldeman data. Equally the data from Nurpeisov et al.is better represented by a minimum at 150 keV but is not statistically inconsistent with the shape derived by Gwin et al. The principal difference between the data sets of Gwin et al. and Boldeman et al. is a systematic difference of 0.48% between the absolute values with the Gwin et al. data being the higher.

The data for the energy region above 2 MeV are less controversial possibly because there are fewer measurements there and high precision is difficult to achieve. Figure 4 taken from the paper by Gwin et al.[28] shows the trend in this region.

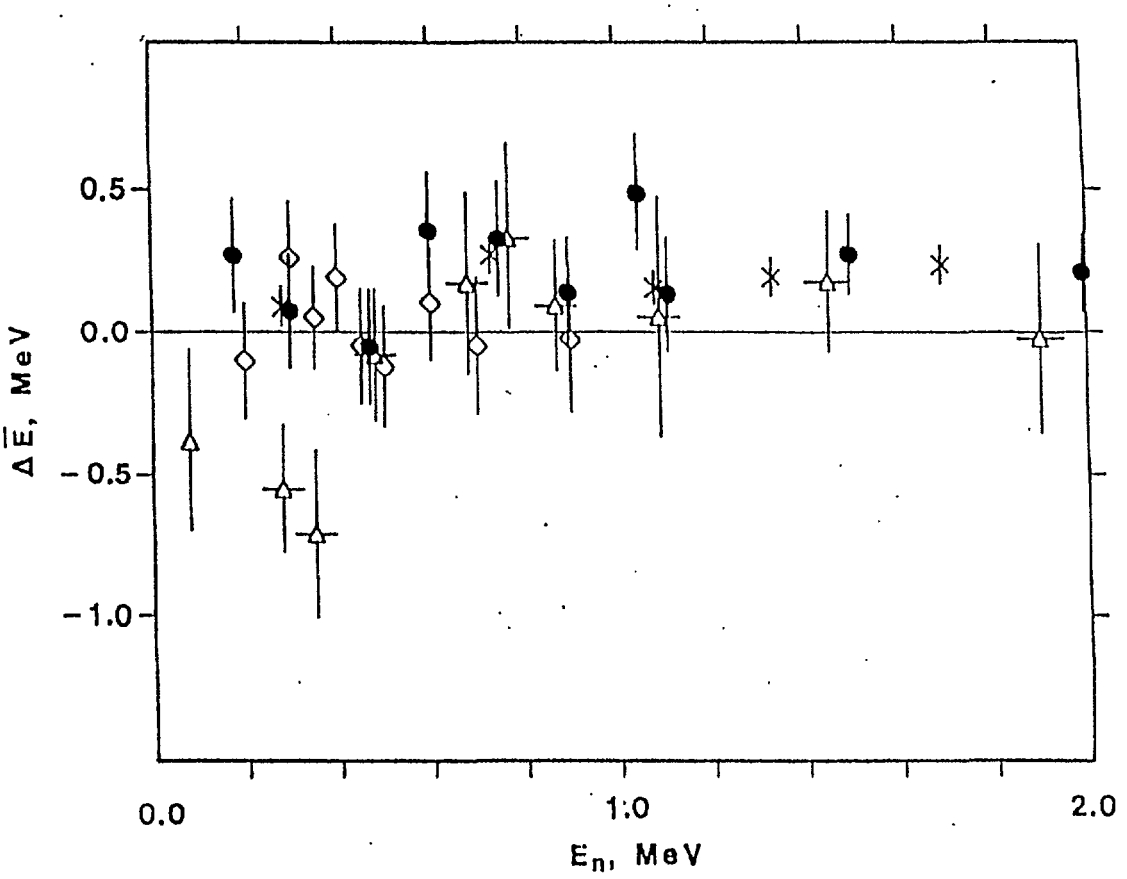

Fig. 5. Average fission fragment kinetic energy data for ^{235}U (taken from Ref.32).

4.1.2 ^{235}U

For ^{235}U, the Manero and Konshin review showed a great deal of structure with a major peak slightly below 400 keV a minimum at 600 keV and other structures at higher energy. Much of the structure that appeared in this review arose from a selective use of complementary data. In particular, the average kinetic energy data from Blyumkina et al[31] showed a very large minimum at 400 keV and when translated through conservation into a $\bar{\nu}_p$ dependence produced a peak with a deviation of about 3 percent. However, other average kinetic energy data which did not show this trend were not included in the review.

The average kinetic energy data for ^{235}U are shown in Figure 5 (taken from Meadows and Budtz-Jorgensen)[32]. All data sets apart from Blyumkina et al. show very little structure and would therefore suggest little structure in $\bar{\nu}_p$ (E_n). The recent measurement for ^{235}U from Gwin et al.[28] is shown in Figure 6 with several of the earlier $\bar{\nu}_p$ (E_n) studies from other experiments[33,34]. The strongest feature of the data from Gwin et al. is a minimum in $\bar{\nu}_p$ (E_n) at about 40 keV neutron energy. There are no other measurements of $\bar{\nu}_p$ (E_n) with which this structure could be compared and neither for that matter have the kinetic energy measurements addressed

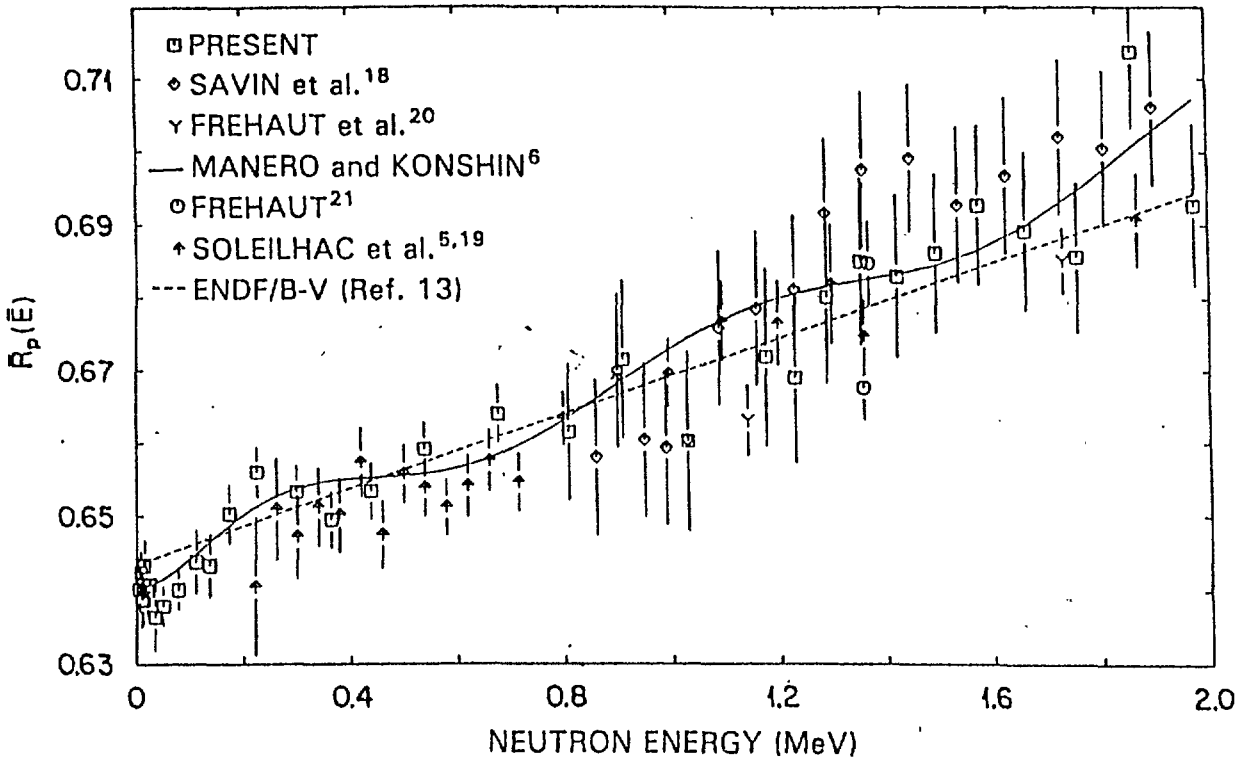

Fig. 6. Plot of $\bar{R}_p(\bar{E})(^{235}U)$ for the interval of 0 to 2.0 MeV. The value of $\bar{R}_p(\bar{E})$ is plotted at the midpoint of the energy interval $\bar{E}$ of the averaging process. (Taken from Ref.28)

this energy region. However, measurements of the variation of the fission fragment anisotropy for neutron fission of ^{235}U (see Musgrove et al.[35] for a comparison) show at this energy sideways peaking which is extremely difficult to explain with standard models. The minimum at 40 keV tends to intensify a small peak at about 250 keV above which the $\bar{\nu}_p$ (E_n) dependence appears to be substantially flat for 200 keV or so. This trend is not dissimilar from that seen in the revised data from the Soleilhac et al.[33] and Boldeman and Walsh data as revised in reference 34. However there is a systematic difference of about 0.5 % between the data from Gwin et al. and the combined data from the other two data measurements (Figure 7).

Figure 8 taken from Gwin et al.[28] presents the $\bar{\nu}_p$ (E_n) data above 2 MeV. Gwin et al. note that their values are systematically 0.5% greater than those of Soleilhac et al.[33] reflecting the trend at lower energies. However, these data are systematically lower than that of Savin[36] by approximately 1%.

4.1.3 ^{239}Pu

Whereas the average fission fragment kinetic energy for ^{233}U and ^{235}U apart from small structures for ^{233}U are essentially constant from thermal to about 4 MeV, the data for ^{239}Pu show a marked decrease with excitation (ref.37 and other ref. therein). This decrease in $\bar{E}_K$ with energy would

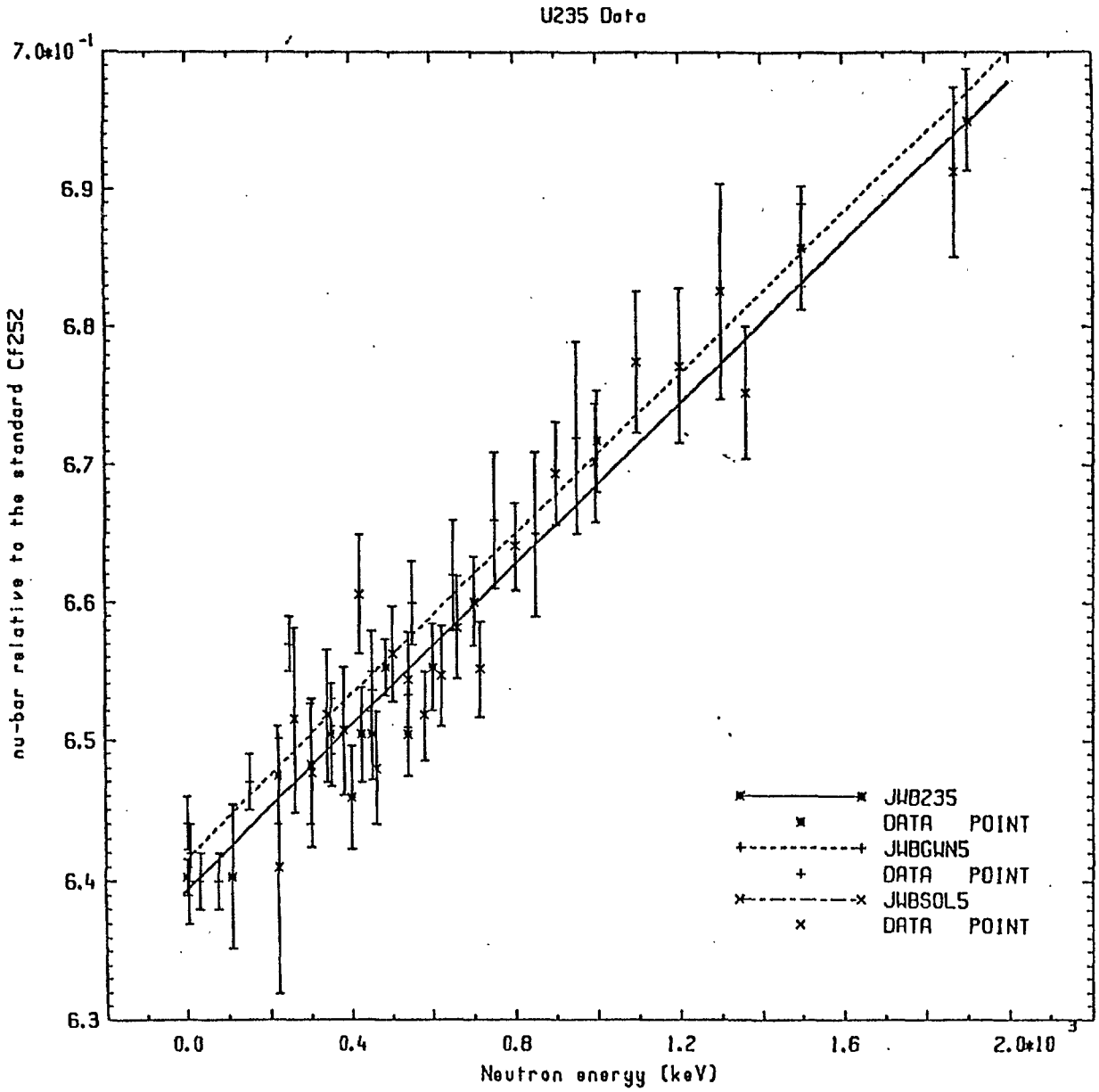

Fig.7. Direct comparison of data from Ref.28,33,34.

not suggest any structure in $\bar{\nu}_p$ (E_n) though complementarity, however, it would be expected to have an effect on the magnitude of the $d\bar{\nu}_p/dE_n$. However superimposed on the steady decrease in $\bar{E}_K$ with energy are a number of step like structures (Figure 9). If there were complementarity between $\bar{\nu}_p$ (E_n) and $\bar{E}_K$ (E_n) then these steps should give rise to peaks in $\bar{\nu}_p$ (E_n). On the contrary this type of behaviour has not been seen in most of the data sets. Figure 10 from Gwin et al.[28] shows a comparison of some of the data sets below 2 MeV. The reference numbers in the figure are those of Gwin et al.

Figure 11 also from Gwin et al. shows a comparison of the data above 2 MeV. Gwin et al. note a general agreement between the data sets but also draw attention to a 0.5 percent systematic disagreement between their

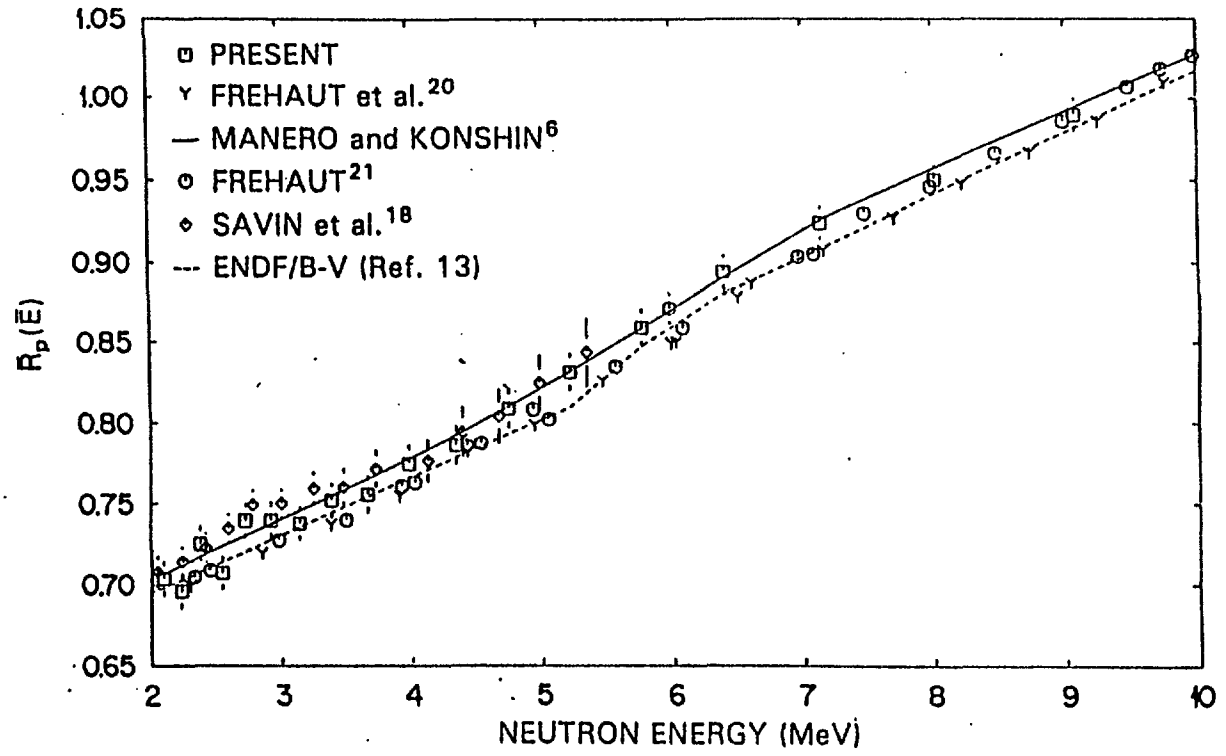

Fig.8 . Plot of $\bar{R}_p(\bar{E})(^{235}U)$ for the interval of 2.0 to 10.0 MeV. The value of $\bar{R}_p(\bar{E})$ is plotted at the midpoint of the energy interval $\bar{E}$ of the averaging process. (Taken from Ref.28).

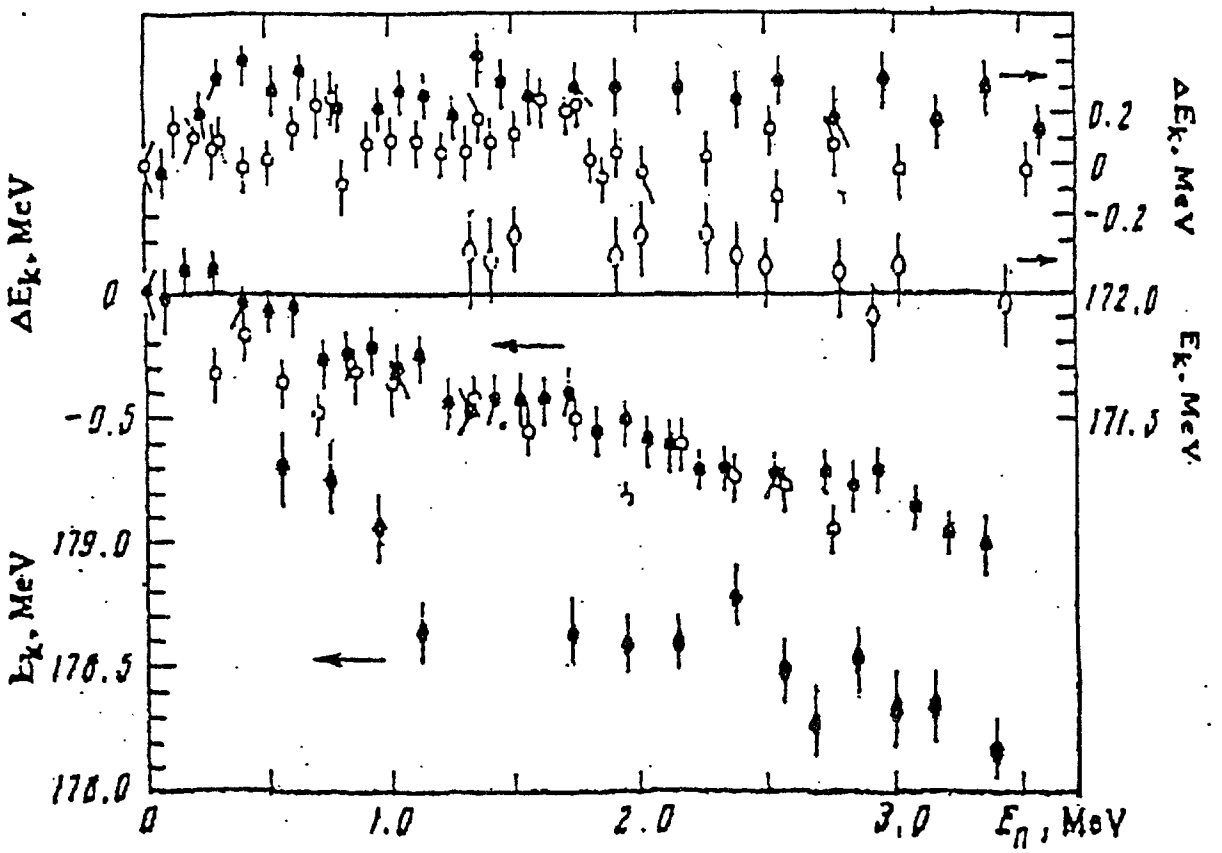

Fig.9. Mean fragment kinetic energy as a function of the energy of the fission-producing neutrons: a - the isotopes ^{233}U(●), ^{235}U (○), ^{238}U (◇); b - the isotopes ^{239}Pu(●), ^{241}Pu (○), and ^{242}Pu (◇).

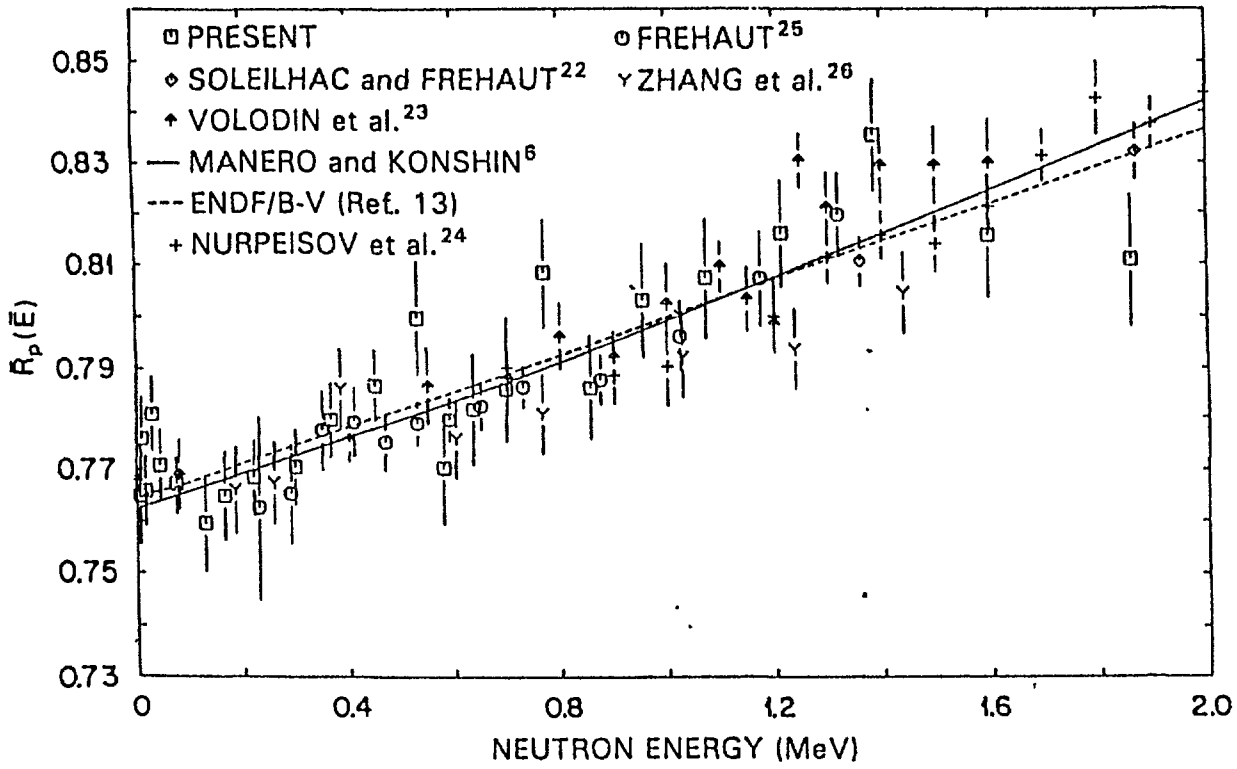

Fig. 10 .Plot of $\bar{R}_p(\bar{E})(^{239}Pu)$ for the interval of 0 to 2.0 MeV. The value of $\bar{R}_p(\bar{E})$ is plotted at the midpoint of the energy interval $\bar{E}$ of the averaging process. (Taken from Ref.28).

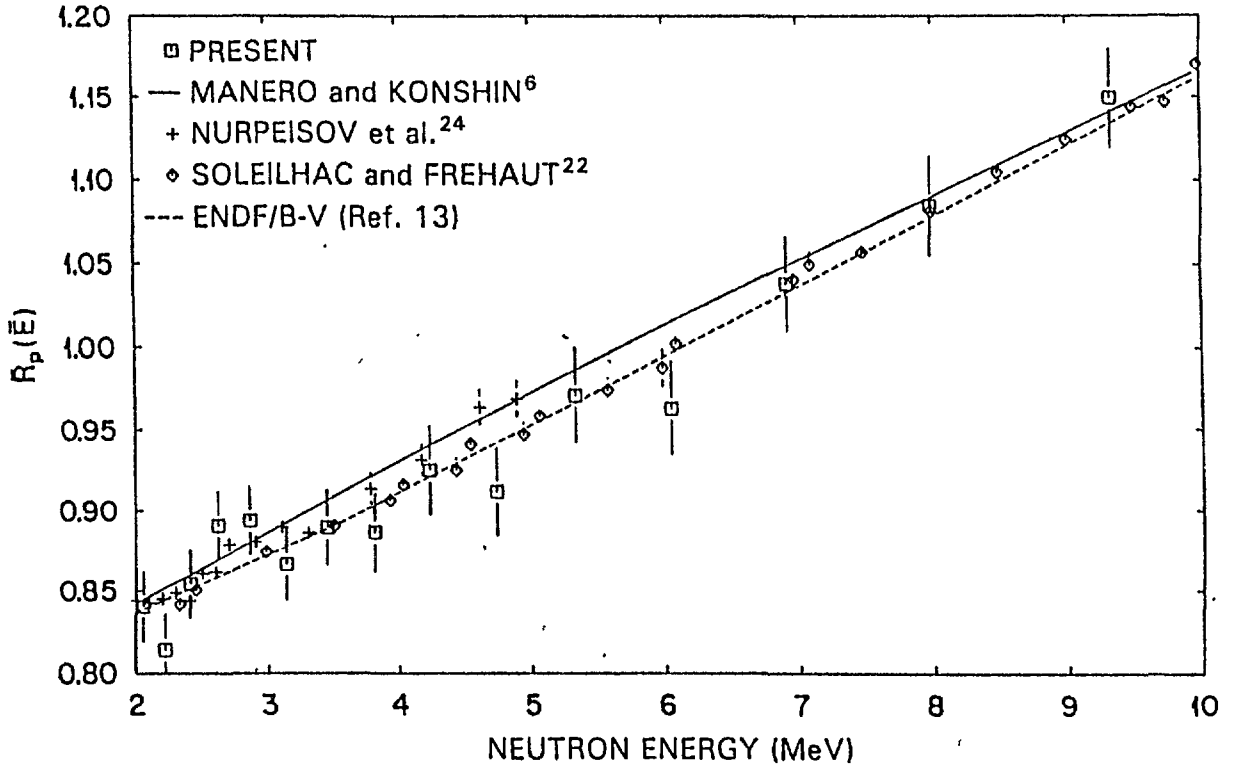

Fig. 11 ,Plot of $\bar{R}_p(\bar{E})(^{239}Pu)$ for the interval of 2.0 to 10.0 MeV. The value of $\bar{R}_p(\bar{E})$ is plotted at the midpoint of the energy interval $\bar{E}$ of the averaging process. (Taken from Ref.28).

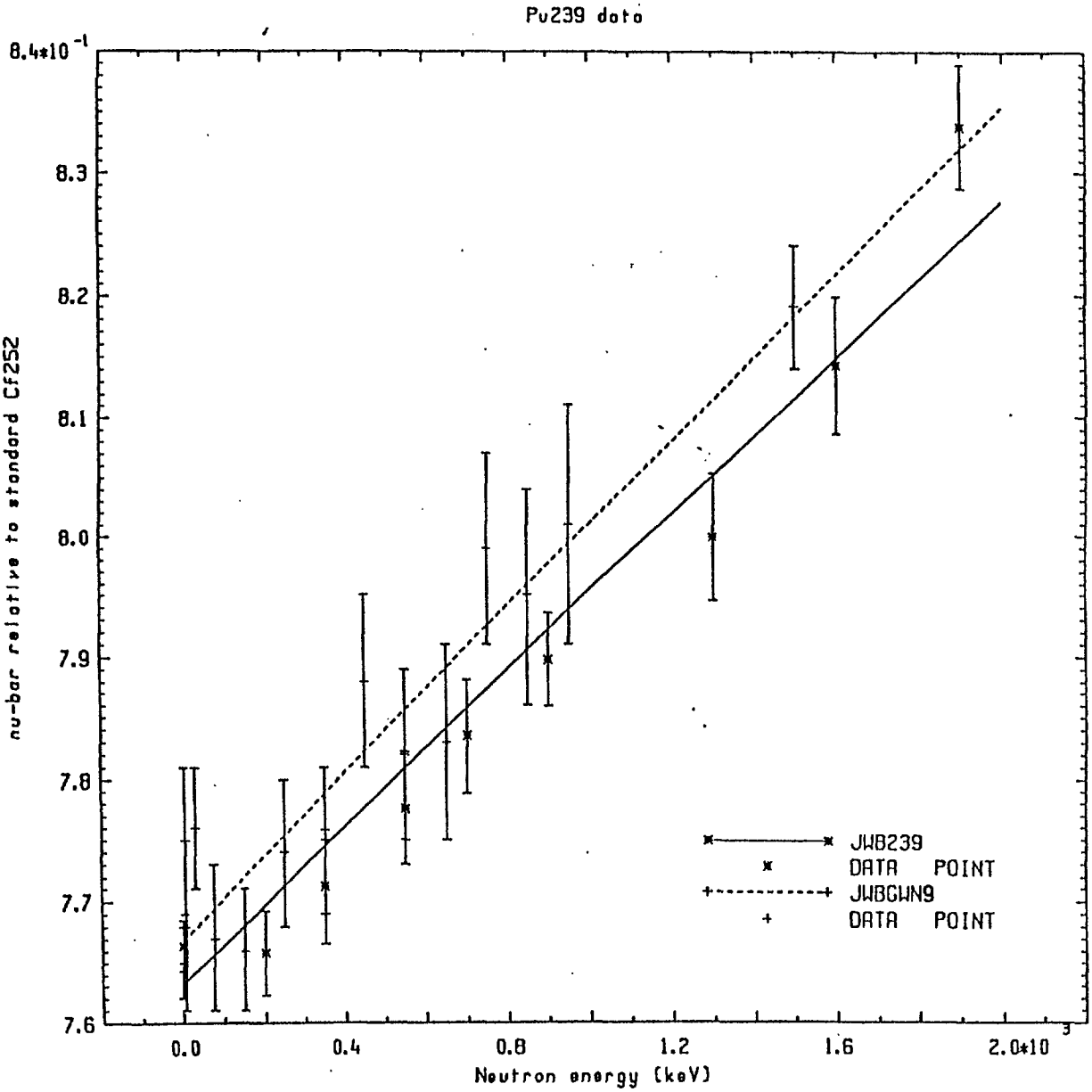

Fig. 12. Direct comparison of data from Ref.28 and 38.

data and that of Soleilhac et al.[33]. In Figure 12, a direct comparison is made of the data from Gwin and that from Walsh and Boldeman[38] which were not included in Figure 10. The systematic difference noted before is obvious in this intercomparison.

4.1.4 Implications

The most worrying aspect of the data for the three isotopes discussed above is a universal discrepancy of about 0.5 percent between the data from Gwin et al. and the data from the French and Australian groups. One possibility that has been suggested already is the effect of foil thickness on $\bar{\nu}_p$ measurements. The measurements of Gwin et al. used very

thin evaporated targets whereas the other two groups used thicker targets. The data however, from the French and Australian groups have been corrected for this effect.

It could be argued that these corrections were assessed assuming uniform deposits and if in fact the deposits were non uniform in thickness then the corrections would be larger. Visual inspection of the deposits, however, suggested that this was not the case. Furthermore, the thicknesses of the fission targets used in the Australian and French data sets varied by factors of at least 2. The fact that the discrepancy is always of the order of 0.5% effectively rules out this possibility. The origin of this discrepancy is therefore not understood.

The measurements by Gwin et al. have considerable advantages relative to other measurements in identifying any fine structure since they used a white source and effectively all measurements were made simultaneously. The conclusions to be drawn from the measurements by Gwin et al. are that the $\bar{\nu}_p$ (E_n) dependences of ^{233}U and ^{239}Pu show no structure whereas that for ^{235}U showed a significant minimum at 40 keV.

The shape of the energy dependences derived is the other experiments are not inconsistent with the trends observed by Gwin et al. although there is a preference in some of the ^{233}U data sets for some structure. If it is assumed that the energy dependence observed by Gwin et al. reflect the truth then the $\bar{\nu}_p$ (E_n) data do not have complementarity with the $\bar{E}_K$ (E_n) data.

The structures observed in the $\bar{E}_K$ (E_n) dependence for ^{233}U and the effective absence of structure in the data for ^{235}U can be readily understood. Blyumkina et al.[31] suggested that the collective energy at the saddle point was weakly coupled to the nuclear degrees of freedcom at scission and thus appeared in the kinetic energy of the fission fragments. Although their analysis of the data was based on inaccurate fission barrier data that existed at that time, a later quantitative analysis by Boldeman et al.[27] confirmed the details of the $\bar{E}_K$ (E_n) dependence. Since $\bar{\nu}_p$ (E_n) no longer shows complementary behaviour to $\bar{E}_K$ (E_n) there are clearly other factors that have not been identified which are influencing the shape of $\bar{\nu}_p$ (E_n).

4.2 Sub Barrier Fission

Measurements of $\bar{\nu}_p$ (E_n) have been carried out for a number of even-even nuclei. However, it is in the two cases of ^{232}Th and ^{230}Th where there has been the greatest activity and where the accuracy has been sufficient to reveal extremely complicated behaviour.

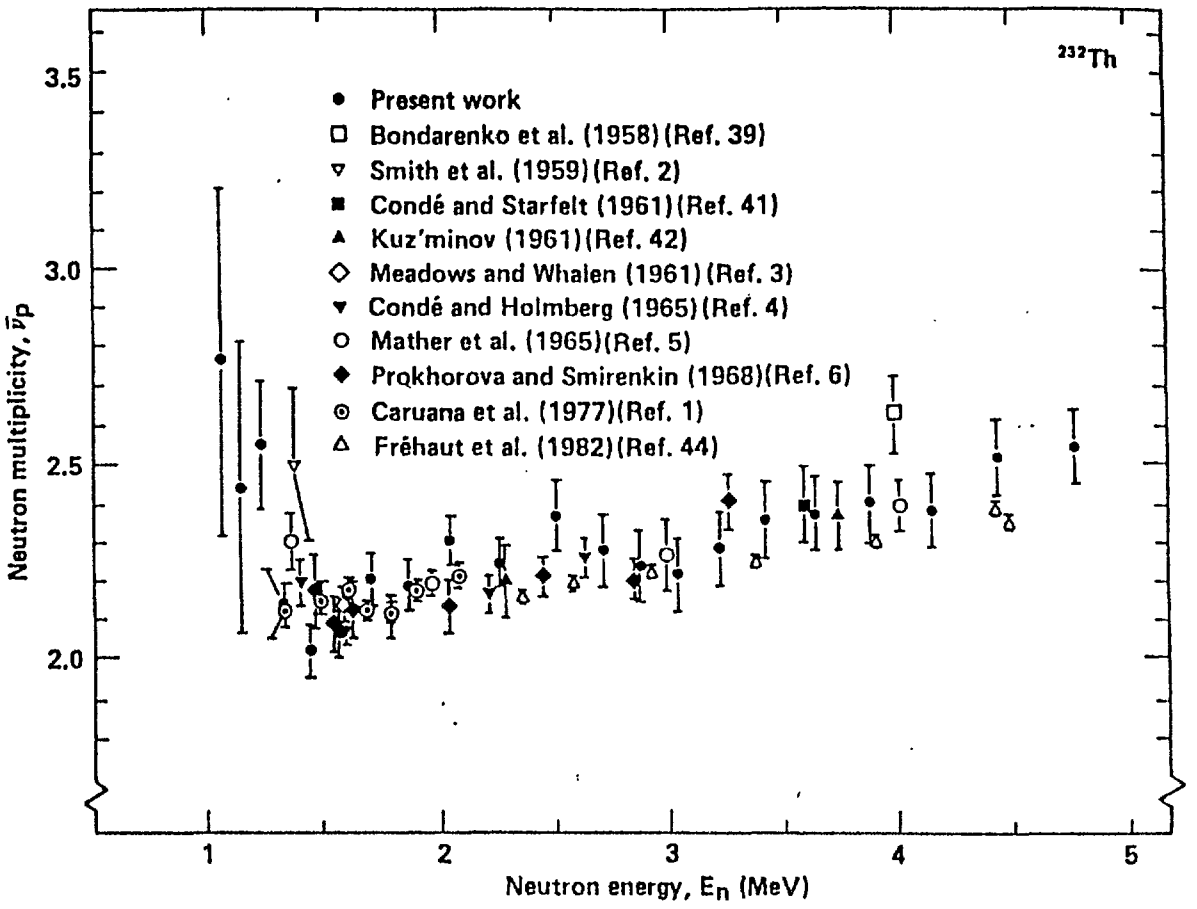

Fig. 13 Measured fission neutron multiplicity results from the present experiment compared with published results from other sources near the (n,f) threshold. All data have been normalized to $^{252}Cf(sf)\bar{\nu}_p = 3.757$. Data references are specified in the text. (Taken from Ref.43).

The study of neutron fission of the thorium nuclei has been extremely controversial since Moller and Nix[38] first predicted that if asymmetric distortions were included in the calculation of the potential energy surfaces then the first barriers would have a triple humped shape. The numerous resonances seen in the sub barrier high resolution neutron fission cross sections of ^{230}Th and ^{232}Th by Blons et al.[39,40] were readily identified as vibrational resonances in the third well of the tripled humped barrier. Although there has been a great deal of disagreement regarding the analytical details[39,48] all analyses agree with this explanation for the combined fission cross section data and fission fragment angular distributions. It might be expected that the $\bar{\nu}_p(E_n)$ and $\bar{E}_K(E_n)$ dependence would show interesting behaviour in this sub barrier region.

Figure 13 taken from Ref.43 presents a comparison of most of the experimental determination of $\bar{\nu}_p(E_n)$ for ^{232}Th. The combined data sets show a dramatic increase in $\bar{\nu}_p$ at energies below 1.5 MeV with the minimum being in the vicinity of 1.5 MeV. The most precise measurements of the $\bar{\nu}_p$

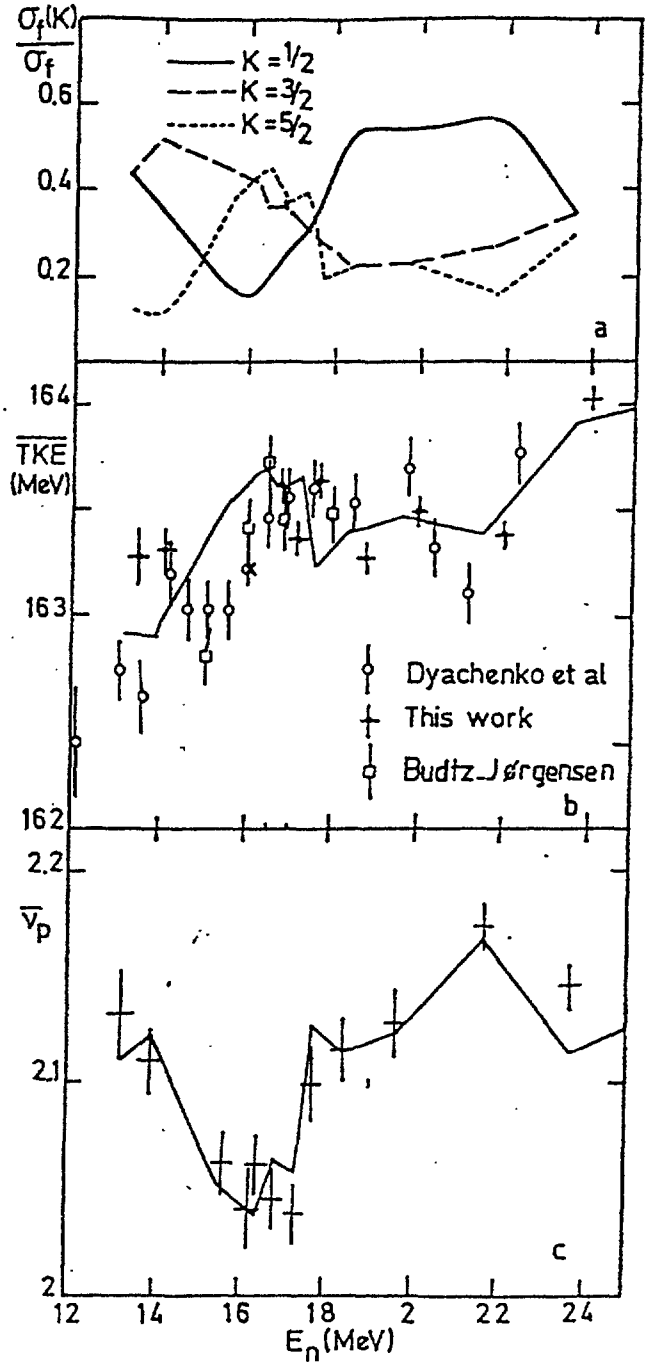

Fig. 14 *Fission de* $^{232}Th + n$
a) contribution relative des différentes sections efficaces de fission partielles à la section efficace de fission totale.
b) comparaison des valeurs de l'énergie $\overline{TKE}$ *obtenues dans ce travail, celui de Dyachenko [4] et de Budtz-Jørgensen [12]. Le trait plein correspond au calcul effectué avec les hypothèses formulées dans le texte.*
c) valeurs expérimentales du nombre $\bar{\nu}_p$ *de neutrons émis par fission en fonction de l'énergie des neutrons incidents. La ligne en trait plein correspond à un ajustement à l'aide des contributions relatives* σ_f^K *de a).* (Taken from Ref:44).

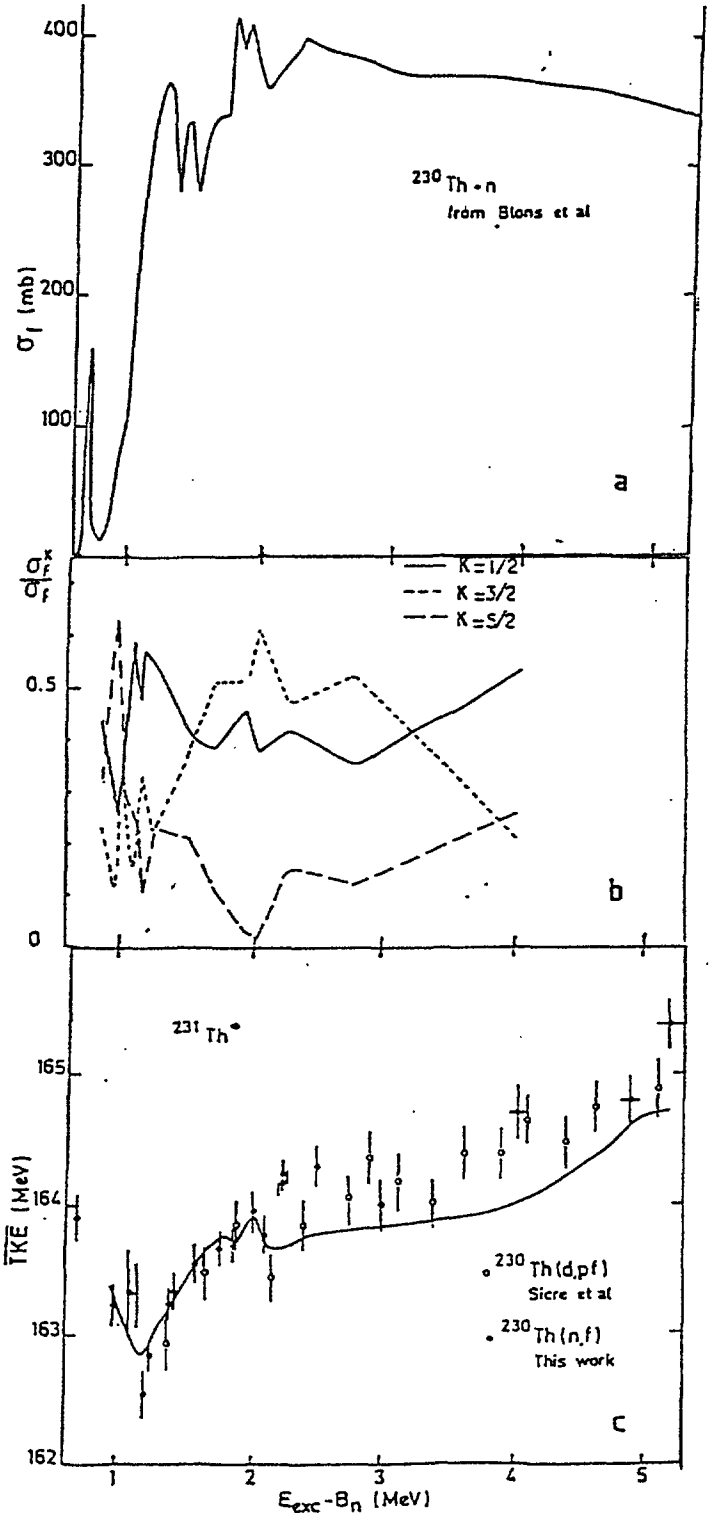

Fig.15 Fission de $^{231}Th^*$
a) section efficace de fission ^{230}Th + n (d'après [7])
b) contribution relative des différentes sections efficaces de fission partielles
c) valeurs expérimentales de l'énergie $\overline{TKE}$. La courbe en trait plein correspond à un calcul effectué avec les équations du texte.

(E_n) dependence by Trochon et al.[44] which are not plotted in Figure 13 are shown in Figure 14. This data set shows the same general trend seen in Figure 13 but shows a great deal more structure. In particular, there is a significant minimum at 1.7 MeV. Also shown in Figure 14 are the average fission fragment kinetic energy data from Trochon et al, Dyachenko et al.[45] and Budtz-Jorgensen[46] together with an analysis [42] of the relative partial fission cross sections contributing to the neutron fission cross section as derived by a triple humped fission barrier analysis.

The $\bar{E}_K$ (E_n) data from these three groups also show a great deal of structure but the detailed agreement is not particularly good. The Trochon et al. data for example show moderate variations but do not show the great deviation in $\bar{E}_K$ (E_n) seen at low energy in the Dyachenko work and the one low energy point from Budtz-Jorgensen and Meadows. The $\bar{\nu}_p$ (E_n) and $\bar{E}_K$ (E_n) dependences show in general complementary trends. However, despite the difficulties inherent in a detailed comparison because of the detailed disagreement in the three kinetic energy data sets it seem unlikely that $\bar{\nu}_p$ (E_n) and $\bar{E}_K$ (E_n) are complementary in detail and perhaps this is consistent with the findings from neutron fission of ^{233}U, ^{235}U and ^{239}Pu.

Trochon et al. have derived the K channel dependences for $\bar{\nu}_p$ (E_n) assuming the partial cross sections plotted in Figure 14. For the three values of K considered the $\bar{\nu}_p$ (E_n) dependences are given by:

$$\bar{\nu}_p\ (K = 1/2) = 0.0915\ E_n + 2$$
$$\bar{\nu}_p\ (K = 3/2) = 0.0915\ E_n + 2.06$$
$$\bar{\nu}_p\ (K = 5/2) = 0.0915\ E_n + 1.7$$

Effectively the Q value for each fission channel is found to be different.

This fact can be readily understood. The fission through all three K channels is sub barrier. The barrier shapes themselves are all triple humped resulting from a mass asymmetric minimum energy pathway to scission. The potential energy surfaces for each K channel will not necessarily be the same. Therefore the mass asymmetry will vary for each channel and therefore the effective Q will be different. Such an analysis suggests as Trochon et al. have pointed out a rapid descent from saddle point to scission.

The fission fragment kinetic energy data for neutron fission of ^{230}Th are shown in Figure 15 together with the fission cross section and a K

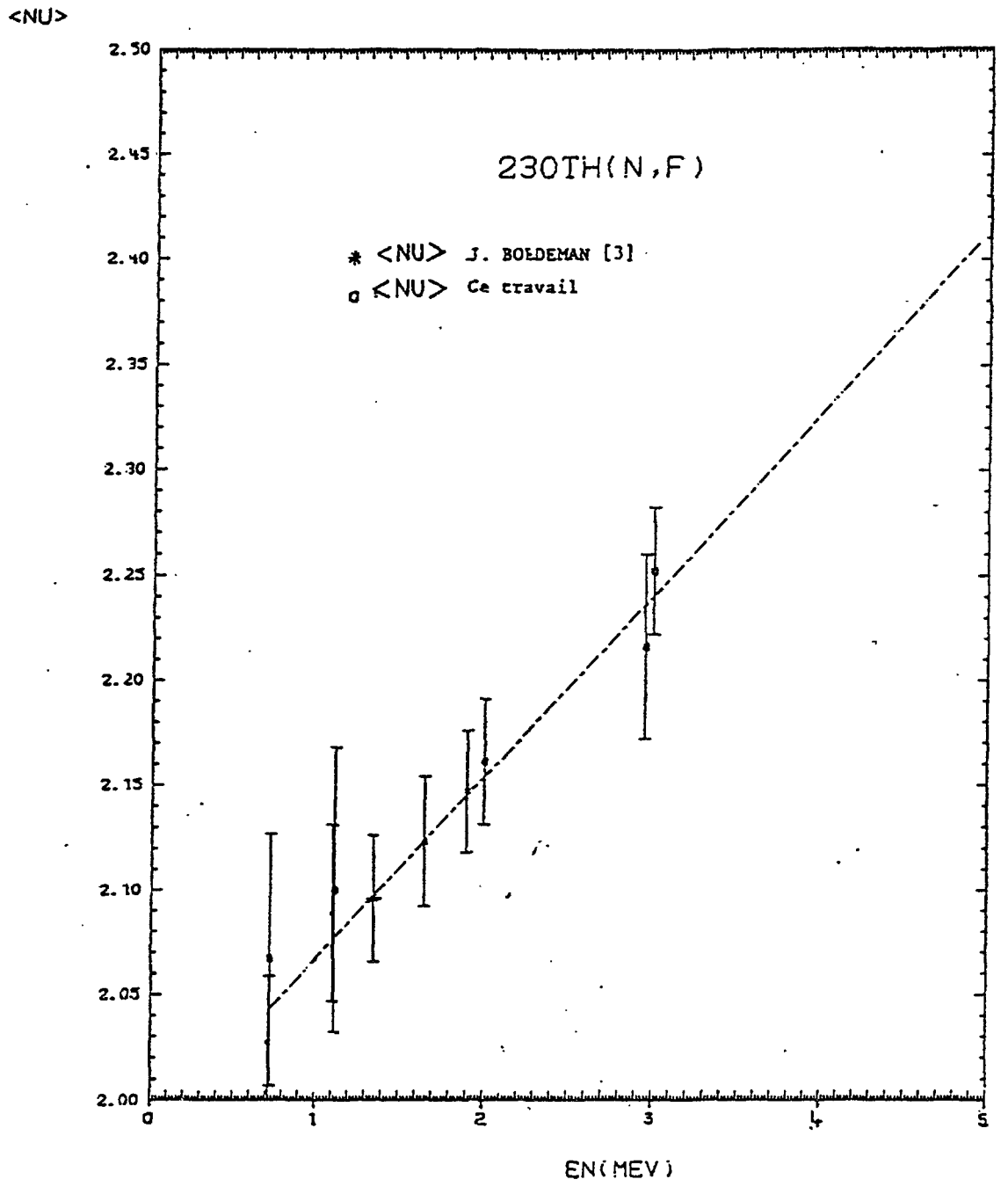

Fig.16.
Valeurs expérimentales du nombre moyen $\bar{\nu}$ de neutrons émis par fission induite sur ^{230}Th. La courbe en pointillée est le résultat d'un lissage par moindres carrés.

channel analysis of the fission cross section. The data from Trochon et al. show considerable structure. This is supported by data from Sicre et al. for the ^{230}Th (d,pf) reaction[47]. On the other hand the two measurements of $\bar{\nu}_p$ (E_n) for ^{230}Th[48,49] reveal a linear dependence (Figure 16). The different behaviour between ^{230}Th and ^{232}Th is not understood.

REFERENCES

1. D.M.Colvin and M.G.Sowerby (1965). Proc. IAEA Symp. Physics and Chemistry in Fission, Salzburg, Vol.2, p.25.
2. J.C.Hopkins and B.C.Diven (1963). Nucl. Phys. 48, p.433.
3. I.Asplund-Nilsson, H.Condé and N.Starfelt (1963). Nucl. Sci. and Eng. 16, p.124.
4. P.H.White and E.J.Axton (1968). J. Nucl. Energy, 22, p.73.
5. E.J.Axton, A.G.Bardell and B.N.Aubric (1969). J. Nucl. Energy 23, p.457.
6. A.De Volpi and K.G.Porges (1970). Phys. Rev. C1, p.683.
7. J.W.Boldeman (1972). Proc. IAEA Panel on Neutron Standard Reference Data, Vienna, p.291.
8. J.W.Boldeman (1974). Nucl. Sci. and Eng. 55, p.188.
9. J.W.Boldeman (1977). NBS Special Publication 493, p.182.
10. J.J.Ullo (1977). Proc. ^{252}Cf Workshop, Brookhaven National Laboratory, 6 December.
11. J.R.Smith (1977). Proc. ^{252}Cf Workshop, Brookhaven National Laboratory, 6 December.
12. R.R.Spencer, R.Gwin and R.Ingle (1982). Nucl. Sci. and Eng. 80, p.603.
13. W.P.Poenitz and G.de Saussure (1984). Prog. in Nucl. Energy 13, p.129.
14. J.W.Boldeman, M.G.Hines, J.P.Fallon and I.Delaney (1984). Proc. 6th ESARDA Symp. Safeguards and Nuclear Materials Management, Venice, p.285.
15. E.J.Axton and A.G.Bardell (1984). Metrologia.
16. B.M.Aleksandrov, E.V.Korolev, Ya M.Kramarovsky, G.E.Lozhkromoev, V.G.Matyukhenov, K.A.Petryhak, A.G.Prusakov, A.V.Sorkina and Eh.A.Shlyamin (1980). Proc. 1980 Kiev Conf. Vol.4, p.119.
17. B.M.Aleksandrov, et al. (1975). Proc. 1975 Kiev Conf. Vol.5, p.166.
18. J.R.Smith and S.D.Reeder (1984). EPRI-NP-3436.
19. H.Q.Zhang and Z.H.Liu (1980). Chin. J. Nucl. Phys. 2, p.29.
20. H.Bozorgmanesh (1977). Thesis, University of Michegan.
21. G.Edwards, D.J.S.Findlay and E.W.Lees (1982). Ann. Nucl. Energy 9, p.127.
22. E.J.Axton (1984). Europe;an Appl. Res. Rept. - Nucl. Sci. Technol. 5, p.609.
23. R.Gwin, R.R.Spencer and R.W.Ingle (1984). Nucl. Sci. and Eng. 87, p.381.

24. J.R.Smith (1979). EPRI NP-1098.
25. J.W.Boldeman and J.Frehaut (1980). Nucl. Sci. and Eng. 76, p.49.
26. F.Manero and V.A.Konshin (1972). At. Energy Review 10, p.637.
27. J.W.Boldeman, W.K.Bertram and R.L.Walsh (1976). Nucl. Phys. A265, p.337.
28. R.Gwin, R.R.Spencer and R.W.Ingle (1986). Nucl. Sci. and Eng. 94, p.365.
29. B.Nurpeisov, V.G.Nesterov, L.I.Prokhorova and G.N.Smirenkin (1973). Sov. J. At. En. 34, p.491.
30. B.Nurpeisov, K.E.Volodin, V.G.Nesterov, L.I.Prokhorova, G.N.Smirenkin and Ju.N.Turchin (1975). Sov. J. At. En. 39, p.199.
31. Yu Blyumkina, I.I.Bondarenko, V.F.Kurznetsov, V.G.Nesterov, V.N.Okolovitch, G.N.Smirenkin and L.N.Usachev (1964). Nucl. Phys. 52, p.648.
32. J.W.Meadows and C.Budtz-Jorgensen (1982). Proc. Int. Conf. on Nucl. Data for Science and Technology, Antwerp, p.740.
33. M.Solielhac, J.Frehaut, J.Gauriau and G.Mosinski (1970). Proc. Conf. on Nuclear Data for Reactors, Helsinki, Vol.2. p.145.
34. J.W.Boldeman, J.Frehaut and R.L.Walsh (1977). Nucl. Sci. and Eng. 63, p.430.
35. A.R.del Musgrove, J.W.Boldeman, J.L.Cook, D.W.Lang, E.K.Rose, R.L.Walsh, J.Caruana and J.Mathur (1981). J. of Physics G. Nucl. Phys. 7, p.549.
36. M.V.Savin, Ju.A.Klohlov, A.E.Savejen and I.N.Paramonova (1972). J. YF 16, p.6.
37. V.G.Vorob'eva, N.P.Dyachenko, n.P.Kolosov, B.D.Kuzminov and A.I.Sergachev (1974). Sov. J. Nucl. Phys. 19, p.489.
38. P.Möller and J.R.Nix (1973). 3rd IAEA Conf. Physics and Chemistry of Fission, Rochester, Vol.1, p.103.
39. J.Blons, C.Mazur and D.Paya (1975). Phys. Rev. Lett. 35, p.1749.
40. J.Blons, C.Mazur, D.Paya, M.Ribrag and H.Weigmann (1978). Phys. Rev. Lett. 41, p.1282.
41. J.W.Boldeman, D.Gogny, A.R.del Musgrove and R.L.Walsh (1980). Phys. Rev. 22C, p.627.
42. H.Abou Yehia, J.Jary, J.Trochon, J.W.Boldeman and A.R.del Musgrove. (1979). Proc. Int. Conf. Neutron Cross Sections for Technology, Knoxville, p.469.
43. R.E.Howe (1984). Nucl. Sci. and Eng. 86, p.157.
44. J.Trochon, J.Frehaut, Y.Pramal, G.Simon and J.W.Boldeman (1982). Proc. Int. Conf. on Nuclear Data for Science and Technology, Antwerp, p.733.

45. N.Dyachenko, B.O.Kuzminov, V.F.Mitrofanof and A.I.Sergachef (1977). Sov. J. of Nucl. Phys. 26, p.365.

46. C.Budtz-Jorgensen and J.Meadows (1982). Lecture Notes in Physics, 158, p.111.

FISSION ENERGETICS AND PROMPT NEUTRON EMISSION

H. Märten, A. Ruben, and D. Seeliger
Technische Universität Dresden, GDR

Abstract: Energy partition in nuclear fission is studied as function of mass asymmetry A_1/A_2 in the framework of a scission point model (two-spheroid model TSM) including semi-empirical, temperature-dependent shell correction energies $\delta W(A)$. Average total kinetic energies $\overline{TKE}(A_1/A_2)$ calculated within TSM agree with experimental data. Based on average excitation energies of the fragments $\overline{E}_i^*(A)$ neutron multiplicities $\bar{\nu}(A)$ are deduced. The TSM, which is applicable to any fission reactions in the (Th-Cf) region for excitation energies of the fissioning nucleus lower than about 30 MeV, reproduces known trends of experimental data on $\overline{TKE}$ and $\bar{\nu}$.

1. Introduction

The energy balance in fission is one of the outstanding problems in fission theory. The question is, how the total available energy, i.e. the sum of energy release $\bar{Q}(A_1/A_2)$ and the excitation energy of the compound nucleus E_c, is distributed on both complementary fragments. The kinds of fragment energies are the kinetic energies $\bar{E}_{k,i}(A)$, which can be measured directly, and the excitation energies $\overline{E}_i^*(A)$, which can be deduced from experimental data on $\bar{\nu}(A)$ as well as average total γ-ray energy $\bar{E}_\gamma(A)$ (i.e. in an asymptotic manner). The knowledge of the different kinds of fragment energies is an essential precondition for the calculation of fission neutron characteristics (multiplicities, energy spectra, double-differential energy and angular distributions) in the framework of a complex statistical model-approach to prompt fission neutron emission.[1]

2. Two-Spheroid Model (TSM)

The TSM, which has firstly been described in Ref. 2 (preliminary version), is a simple scission point model based on a general energy balance:

$$\overline{Q}\left[\frac{A_1}{A_2}\right] + E_c = \underbrace{E_{pre} + E_{coul}}_{\overline{TKE}\left[\frac{A_1}{A_2}\right]} + \overbrace{\underbrace{E_{def}^{(1)} + E_{def}^{(2)} + E_{dis} + E_h}_{\overline{E^*}\left[\frac{A_1}{A_2}\right]}}^{F} + \overbrace{E_{int}^{(1)}+E_{int}^{(2)}}^{} \qquad (1)$$

E_{pre} - pre-scission kinetic energy,
E_{coul} - Coulomb potential energy at scission,
$E_{def}^{(i)}$ - deformation energy of fragment i at scission,
E_{dis} - intrinsic excitation energy at scission due to dissipation between second-saddle point of fission barrier and scission point,
$E_{int}^{(i)}$ - intrinsic excitation of fragment i at scission,
E_h - intrinsic excitation energy ("heat") at the second-saddle point,
F - potential energy at scission for given mass asymmetry.

According to Terrell[3] we describe the fissioning system with two spheroidically shaped fragments nearly touching at the scission point. The nuclear forces between the fragments cause a small distance d ~ 1.4 fm at the place of contact (cf. Ref. 4).
The deformation energy $E_{def}^{(i)}$ is assumed to be quadratic in radius change with reference to a spherical nucleus with radius $R^{(i)}$:

$$E_{def}^{(i)} = \alpha^{(i)} (D^{(i)}-R^{(i)})^2 \qquad (2)$$

($D^{(i)}$ - major semi-axis of spheroid i). $\alpha^{(i)}$ is the deformability parameter related to the stiffness parameter $C_2^{(i)}$ as[5]

$$C_2^{(i)} = \frac{5}{2\pi} \alpha^{(i)} R^{(i)2} \qquad (3)$$

V_{coul} is assumed to be the Coulomb interaction energy of two charges $Z^{(i)}e$ effectively located at the centres of the fragments, i.e.

$$V_{coul} = Z^{(1)}Z^{(2)}e^2/(D^{(1)}+D^{(2)}+d) \qquad (4)$$

Minimizing F, i.e. $\partial F/\partial D^{(i)}=0$, one gets a set of equations:

$$E_{def}^{(i)} = \frac{V_{coul}^4}{4\ \alpha^{(i)}\ Z^{(1)2}\ Z^{(2)2}\ e^2} \tag{5}$$

$$E_{def}^{(1)}/E_{def}^{(2)} = \alpha^{(2)}/\alpha^{(1)} \tag{6}$$

The energy parts E_{pre} and E_{dis} are taken from the systematic study by Gönnenwein[6]. Both energies increase with increasing fissility Z^2/A. Finally, the "heat" energy at the second saddle is assumed to be

$$E_h = E_c - E_{f,B} - \Delta_p \tag{7}$$

with the constraint $E_h>0$. E_h vanishes in the case of spontaneous and threshold fission. The dependence of the pairing energy Δ_p on excitation energy is described by the approach of Kristiak[7].
On principle, the deformability parameter α can be described in the framework of the liquid-drop model (LDM). However, nuclear stiffness is strongly influenced by shell effects. In order to deduce effective shell correction energies $\delta W(A)$ for fragments with typical deformations at scission the equations given above have been applied to well-known fission reactions ($^{252}Cf(sf)$, $^{235}U(n_{th},f)$ a.o.) to determine the deformability parameter $\alpha(A)$. Based on the semi-empirical relation[5]

$$\alpha(A) = \alpha_{LDM}(A)\ \frac{K-\delta W(A)}{K+\delta W(A)} \tag{8}$$

with K=8MeV the parameter α is related to the corresponding LDM value. Eq. (8) has been used to derive sets of semi-empirical shell correction energies $\delta W(A)$. Both E_h and E_{dis} determine the temperature τ at scission. Assuming $\tau^{(1)}=\tau^{(2)}$, the intrinsic excitation energies $E_{int}^{(i)}$ of the complementary fragments can be calculated on the basis of the Fermi-gas model approach, namely:

$$E_{int}^{(i)}(A) = a^{(i)}(A)\ \tau^{(i)2} \tag{9}$$

(a - level density parameter). Due to the temperature τ at scission, the shell effects are diminished. Taking into account the relations[8]

$$\delta W(A,\tau) = \delta W(A,\tau=0)\ \frac{t^2\ \sinh^2 t}{\cosh\ t}, \qquad (10)$$

$$t = 2\pi^2\tau/\ \omega, \quad \omega \sim A^{-1/3}, \qquad (11)$$

shell correction energies at zero temperature can be obtained (cf. Fig. 1).

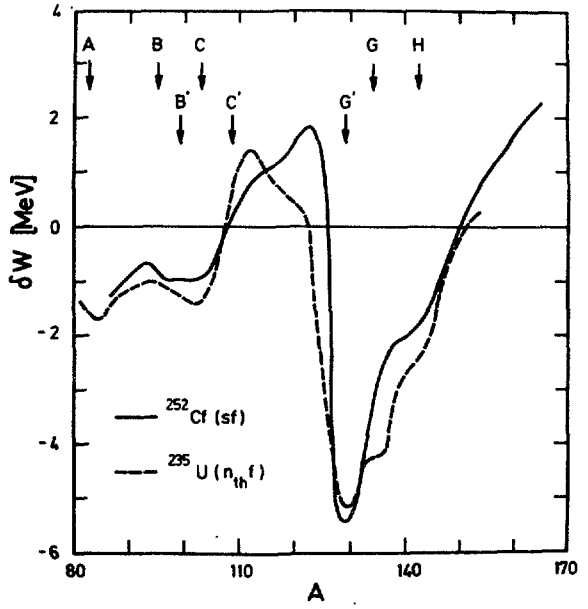

Fig. 1
Zero-temperature shell correction energies as deduced within the TSM for the fission reactions specified. The letters correspond to closed-shell regions (cf. Ref. 4).

As shown in Fig. 1, the shell correction energies for fragments in very different fission reactions are quite similar. Therefore, it seems to be justified to use even these parameter sets for the application of the TSM to any fission reaction (including interpolation).
The fragment energies of interest are $\overline{E^*}(A)$ and $\overline{TKE}(A_1/A_2)$. They are obtained using

$$\overline{E}^{*(i)}(A) = E^{(i)}_{def}(A) + E^{(i)}_{int}(A), \qquad (12)$$

$$\overline{TKE}(A_1/A_2) = E_{coul} + E_{pre}. \qquad (13)$$

According to energy balance of fragment de-excitation due to the evaporation of neutrons (multiplicity $\bar{\nu}$) and γ-ray emission (average total energy $\bar{E}_\gamma$), we have

$$\overline{E}^*(A) = \bar{\nu}(A)\ (\bar{B}_n(A) + \bar{\varepsilon}(A)) + \bar{E}_\gamma(A), \qquad (14)$$

where $\bar{B}_n(A)$ is the neutron binding energy averaged over the neutron cascade and the distribution in charge number Z, and $\bar{\varepsilon}(A)$ is the average neutron emission energy in the centre-of-mass

system approximated by the relation[9]

$$\bar{\varepsilon}(A) = \frac{4}{3} (\bar{E}^*(A)/a(A))^{1/2} \qquad (15)$$

The average γ-ray emission energy is given by

$$\bar{E}_\gamma = (6.6867 - 0.15578\ Z_{FN}^2/A_{FN})\ \bar{\nu} + (0.11127\ Z_{FN}^2/A_{FN} - 2.2408), \qquad (16)$$

where Z_{FN} and A_{FN} are mass and charge number of the fissioning nucleus, respectively.

The neutron yield curves for $^{252}Cf(sf)$ and $^{235}U(n_{th},f)$ are shown in the Figs. 2 and 3.

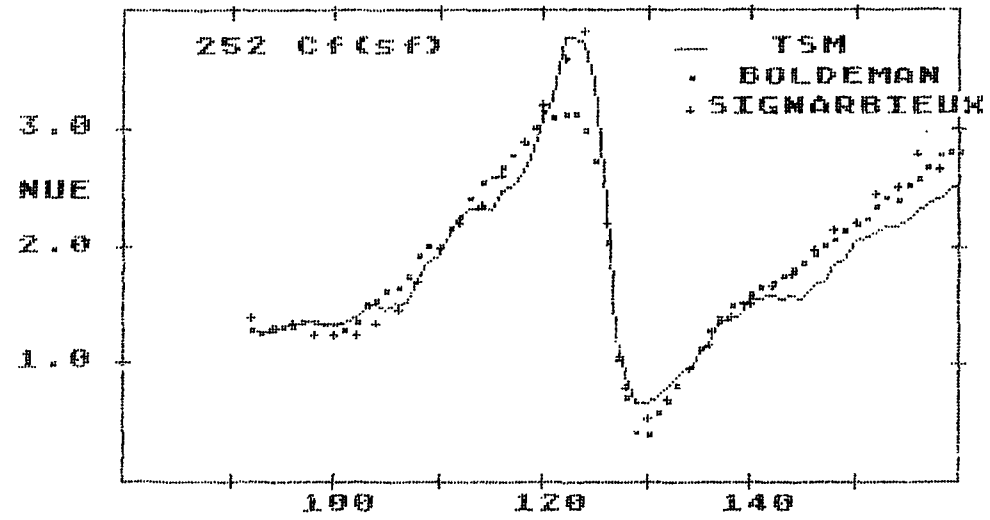

Fig. 2 Neutron multiplicity $\bar{\nu}(A)$ for $^{252}Cf(sf)$. Calculated values (TSM) are compared with experimental data of Boldeman et al.[10] and Signarbieux et al.[11]

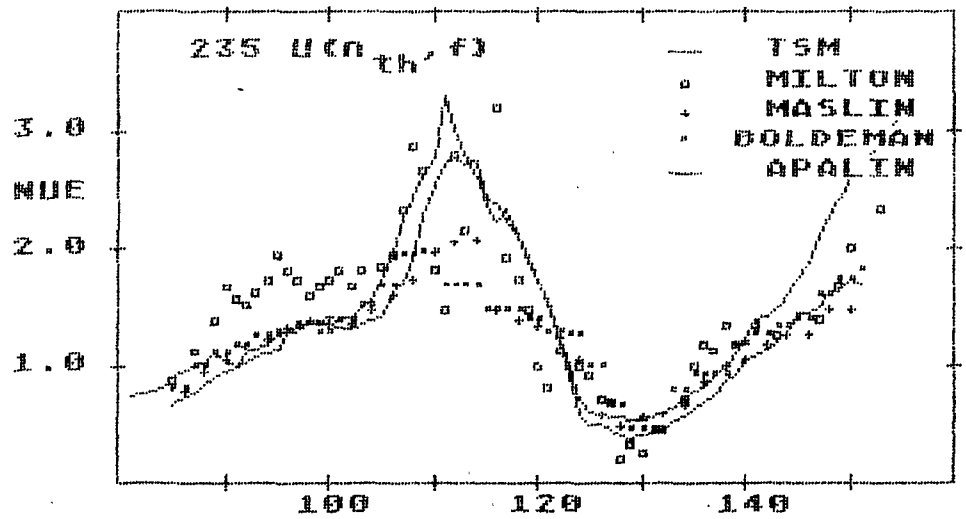

Fig. 3 Neutron multiplicity $\bar{\nu}(A)$ for thermal-neutron induced fission of ^{235}U. Calculated values are compared with experimental data of Milton et al.[12], Maslin et al.[13], Boldeman et al.[14], and Apalin et al.[15]

3. Energy Partition as Function of Incidence Energy

At first, the temperature dependence of $\delta W(A)$ and its influence on fission characteristics should be described:

i) As lower δW, in particular with negative sign, as higher α, i.e. as lower E_{def}. Therefore, $\overline{E}^{*}$ rises strongly with increasing E_c (or incidence energy) in regions with very low δW, in particular around A=132 (double-magic fragment). The excitation energy of complementary fragment do not change remarkably. In general, the well-known saw-tooth curve $\overline{\nu}(A)$ becomes less pronounced with increasing E_c.

ii) The value $\tilde{\alpha} = (1/\alpha^{(1)} + 1/\alpha^{(2)})^{-1}$ can be interpreted as total deformability of the fissioning system at scission. Changes of $\tilde{\alpha}$ with E_c cause corresponding changes in $\overline{TKE}$. Hence, $\overline{TKE}$ is diminished (enhanced) with increasing E_c for fragment pairs with (negative-)positive-sign $\tilde{\alpha}$.

iii) The change of τ with increasing incidence energy is also influenced by the second-barrier height in relation to the first one as well as pairing effects. If we consider total energy parameter changes, i.e. values averaged over A taking into account the fragment yield P(A), the dependence $P(A,E_c)$ may be important (cf. Fig. 5-7).

A typical example of energy partition changes is shown in Fig. 4. Obviously, the fragment pair including the double-magic fragment

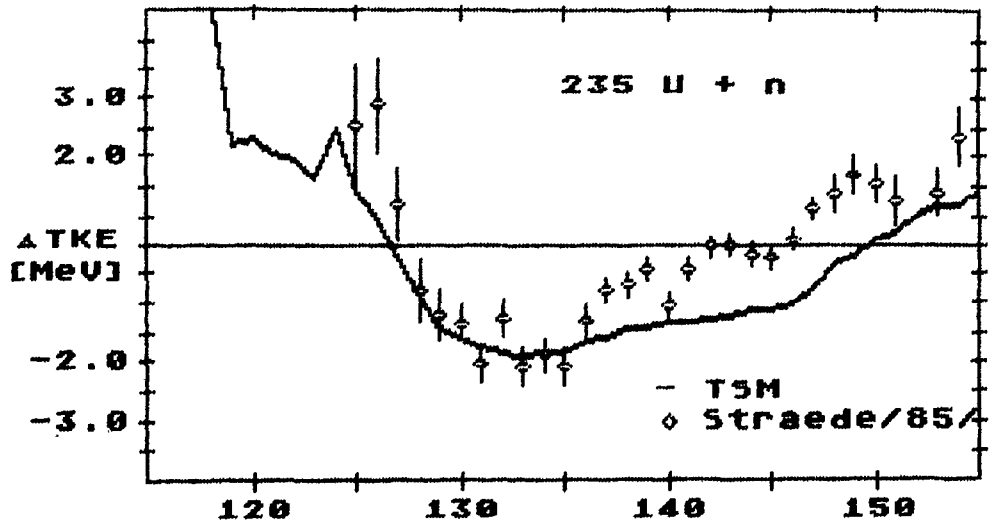

Fig. 4 $\overline{TKE}$-difference $\Delta TKE = \overline{TKE}(E_i=5MeV) - \overline{TKE}(E_i=0MeV)$ for neutron-induced fission of ^{235}U at different incidence energies E_i. TSM results are compared with experimental data[16].

Fig. 5
TKE as function of incidence energy in neutron induced fission of ^{232}Th (experimental data - Refs. 17,18)

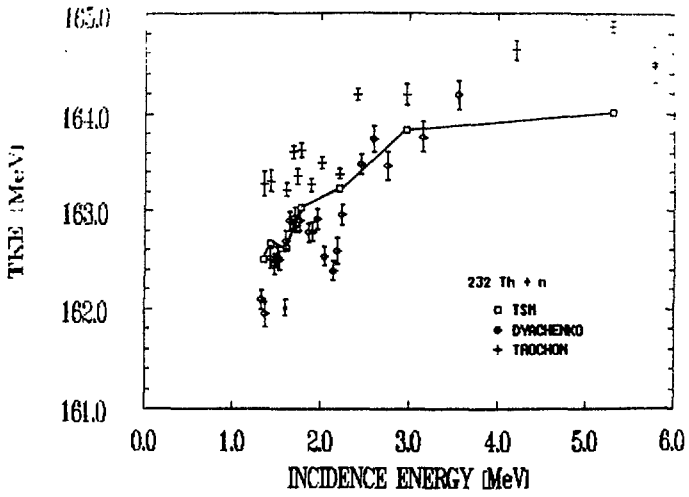

Fig. 6
TKE as function of E_i for neutron induced fission of ^{235}U (experimental data - Ref. 16,19,20)

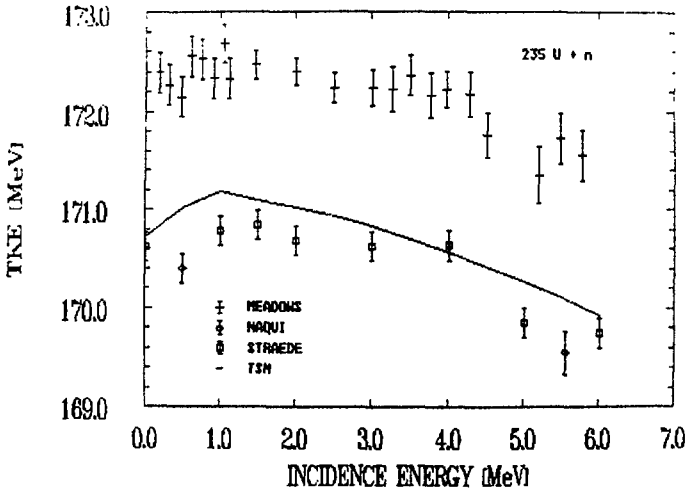

Fig. 7
TKE as function of E_i for neutron induced fission of ^{239}Pu (experimental data - Ref. 21)

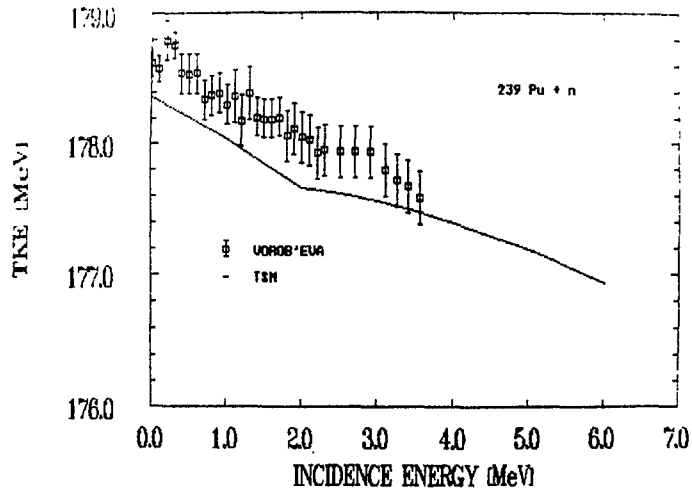

at A ~ 132 has an rather low effective deformability α, which rises with increasing E_c. In this case, $\overline{TKE}$ increases. The opposite behaviour is observed in the case of nearly symmetric and very asymmetric fission.

As shown in the figures, the TSM is successful in describing the energy partition in fission. The main trends of fragment energies with changing E_c are reproduced. In particular, the opposite behaviour of $\overline{TKE}$ as function of E_i for the cases ^{232}Th, ^{235}U, and ^{239}Pu fission induced by fast neutrons can be explained. Even here, the height of the second saddle in relation to the total barrier height, which corresponds to the fission threshold, is of high importance for the influence of pairing effects.

4. Neutron Multiplicities as Function of Incidence Energy

The main part of incidence energy is transformed into excitation energy of the fission fragments resulting in an increase of $\bar{\nu}$ with incidence energy. However, the results discussed in chapter 3 show that certain changes of $\overline{TKE}$ must result in opposite influences on $\bar{\nu}$ (energy balance, cf. Eq. 1).
Some results of calculations in the framework of the TSM are shown in the figures 8-10. The $\bar{\nu}$ data for neutron-induced fission of ^{237}Np confirm item (i) of chapter 3. Here, the experimental data are reproduced by the TSM within experimental uncertainties.

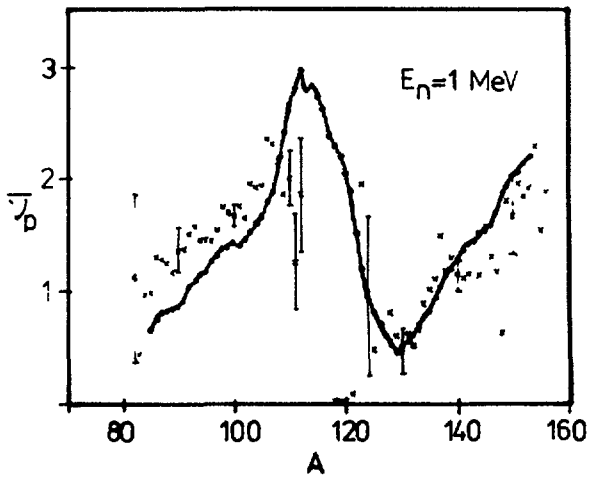

Fig. 8
Average number of prompt neutrons from neutron-induced fission of ^{237}Np as function of fragment mass number for 1.0 MeV incidence energy. TSM results (curve) are compared with experimental data[22].

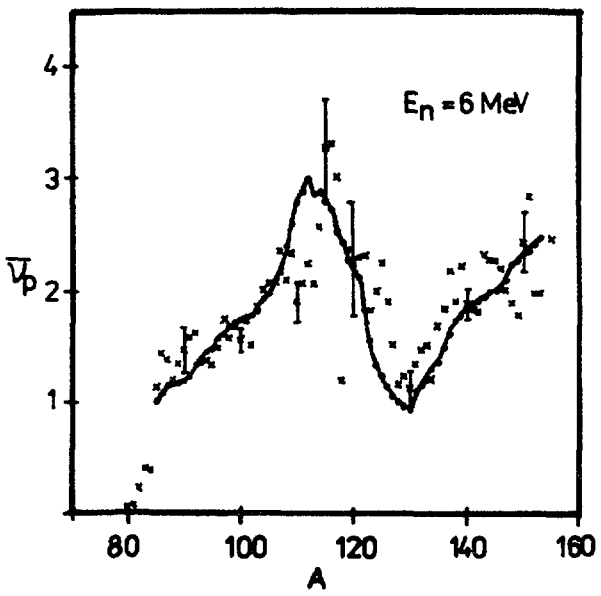

Fig. 9
The same as for Fig. 8, but for 6.0 MeV incidence energy.

In the case of multiple-chance fission, in particular (n,xnf), the calculation has to be done for all possible chances. Each chance has the weight $\sigma_{f,x}/\sigma_{f,tot}$ (σ_f - fission cross section). Including pre-fission neutrons, the total number of fission neutrons is given by

$$\bar{\nu}(E_i) = \sum_x \frac{\sigma_{f,x}(E_i)}{\sigma_{f,tot}(E_i)} (\bar{\nu}_x(E_i) + x), \qquad (17)$$

$$\bar{\nu}_x = \sum P_x(A)\ \bar{\nu}_x(A). \qquad (18)$$

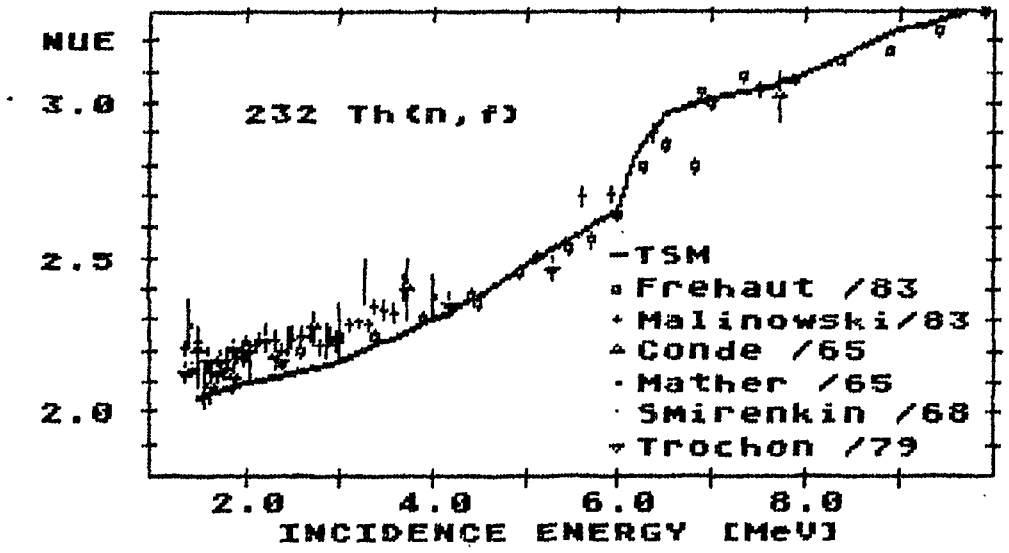

Fig. 10 Total number of neutrons from neutron induced fission of ^{232}Th as function of incidence energy. TSM results are compared with experimental data[23-27,18].

An example is shown in Fig. 10 (preliminary calculation). In the case of ^{232}Th fission induced by neutrons, $\bar{\nu}$ changes drastically at the second-chance fission threshold. The experimental data show the same trend. The agreement of TSM calculation with the experimental data of Frehaut et al.[23] is remarkably good in the whole energy range considered, whereas the TSM underestimates the measured data of other authors in the threshold region (2 - 3.5 MeV).

5. Summary

The TSM as a scission point model with semi-empirical, temperature-dependent shell correction energies for deformed fragments at scission is successful in describing the main features of energy partition in fission as function of mass asymmetry. The diminution of shell effects due to scission point temperature, which depends on the dissipated energy as well as incidence energy (influenced by pairing effects), causes considerable changes of fragment energies as function of E_c (or E_i). It is emphasized, that the average features of energy partition in fission as function of mass asymmetry are described. Channel effects appearing at fission threshold especially are not taken into account. However, they could be considered approximatively by using effective values for the fission barrier and, thus, simulating collective transition states.
The results of TSM calculations are the necessary precondition for the application of complex statistical fission neutron theories for calculations of energy and angular distributions[1,2].

REFERENCES

1 H. Märten, Proc. IAEA Advisory Group Meeting on Nuclear Theory for Fast Neutron Nuclear Data Evaluation, Beijing, 1987, IAEA-TECDOC-483 (Vienna, 1988) 148

2 H. Märten et al., Proc. IAEA Advisory Group Meeting on Properties of Neutron Sources, Leningrad, 1986, IAEA-TECDOC-410 (Vienna, 1987) 153

3 J. Terrell, Proc. IAEA Symp. on Physics and Chemistry of Fission, Salzburg, 1965 (Vienna, 1965) Vol. II, p. 3

4 B.D. Wilkins et al., Phys. Rev. C14 (1976) 1832
5 M. Kildir, N.K. Aras, Phys. Rev. C25 (1982) 365
6 F. Gönnenwein et al., Proc. XVIIth Int. Symp. on Nucl. Phys. - Nuclear Reactions -, Gaussig (GDR), 1987, ZfK-646 (1988) 129
7 J. Kristiak, Proc. 5th Int. Symp. on Neutron Induced Reactions, Smolenice, 1988, in print
8 A. Bohr and B.R. Mottelson, Nuclear Structure (Benjamin, New York, 1975) Vol. II
9 D.G. Madland and J.R. Nix, Nucl. Sci. Eng. 81 (1982) 213
10 R.L. Walsh and J.W. Boldeman, Nucl. Phys. A276 (1977) 189
11 C. Signarbieux et al., J. Phys. 33 (1972) 8
12 J.C.D. Milton and J.S. Fraser, loc. cit. (3), p. 39
13 E.E. Maslin et al., Phys. Rev. 164 (1967) 1520
14 J.W. Boldeman et al., Aust. J. Phys. 24 (1971) 821
15 V.F. Apalin et al., Nucl. Phys. 71 (1965) 553
16 C.A. Straede, Thesis, CBNM Geel, 1985
17 N.P. Dyachenko et al., Yad. Const. 1/40 (1981) 3
18 J. Trochon et al., Nucl. Phys. A318 (1979) 63
19 J.W. Meadows and C. Budtz-Joergensen, ANL/NDM-64 (1982)
20 A.A. Naqui et al., Phys. Rev. C29 (1984) 885
21 V.G. Vorobeva et al., INDC-128/G+Sp (1979)
22 R. Müller et al., Report KFK-3220 (1981)
23 J. Frehaut et al., Proc. Int. Conf. on Nucl. Data for Sci. and Technology, Antwerpen, 1982, D. Reidel Publ. Comp. (1983) 78
24 V.V. Malinovski et al., At. En. 54 (1983) 205
25 H. Conde et al., Arkiv Phys. 29 (1965) 33
26 D.S. Mather et al., Nucl. Phys. 66 (1965) 149
27 L.I. Prochorova, G.N. Smirenkin et al., Yad. Fiz. 7 (1968) 579

KINETIC ENERGIES OF FRAGMENTS AND AVERAGE NUMBER OF PROMPT NEUTRONS IN NEUTRON-INDUCED FISSION OF THORIUM-232

A.A.Goverdovsky, B.D.Kuzminov, V.F.Mitrovanov,
A.I.Sergachev
Instutute of Physics and Power Engineering,
Obninsk, USSR

Abstract

In this work there is carried out an analysis of the correspondence between the changes of the kinetic energy of fragments and the average number of prompt neutrons near a barrier of fission and near the (n, n'f) reaction threshold in the neutron - induced fission of thorium-232.

A number of the works /1-3/ is devoted to the investigations of the kinetic energy of fragments $\bar{E}_k$ in fission of ^{232}Th and the correlation of changins $\bar{E}_k$ and $\bar{\nu}_p$. Unfortunately, the realistic model for explaining a peculiar energy dependence $\bar{E}_k$ is not developed. The investigation results of the kinetic energy of fragments in fission of uranium isotopes with excitation energy close to a fission barrier show the systematic decrease of the kinetic energy of fragments in nuclear fission via vibrational resonances /6/. However, there are no sufficiently reliable data, how this decrease of $\bar{E}_k$ is reflected in $\bar{\nu}$.

In the Fig.1 are given the available measurement results for $\bar{E}_k$ and $\bar{\nu}$ in neutron-induced fission of ^{232}Th. If we direct our attention to the wide resonances close to the energies of E_n = 1.65 MeV and 2.2 MeV, then, by analogy with the case for uranium isotopes one can ascertain a decrease of the kinetic energy of fragments in fission through these resonances.
If this conclusion is valid, then it should not be expected a good agreement of the $\bar{E}_k$ measurement results obtained by the different authors, since a value of the mentioned decrease $\bar{E}_k$ depends upon the relative fraction of recorded fission events through vibrational resonance, i.e., the angular distribution of fragments being born in fission through vibrational resonance, the geometric conditions of fragment recording, the neutron energy resolution and etc.

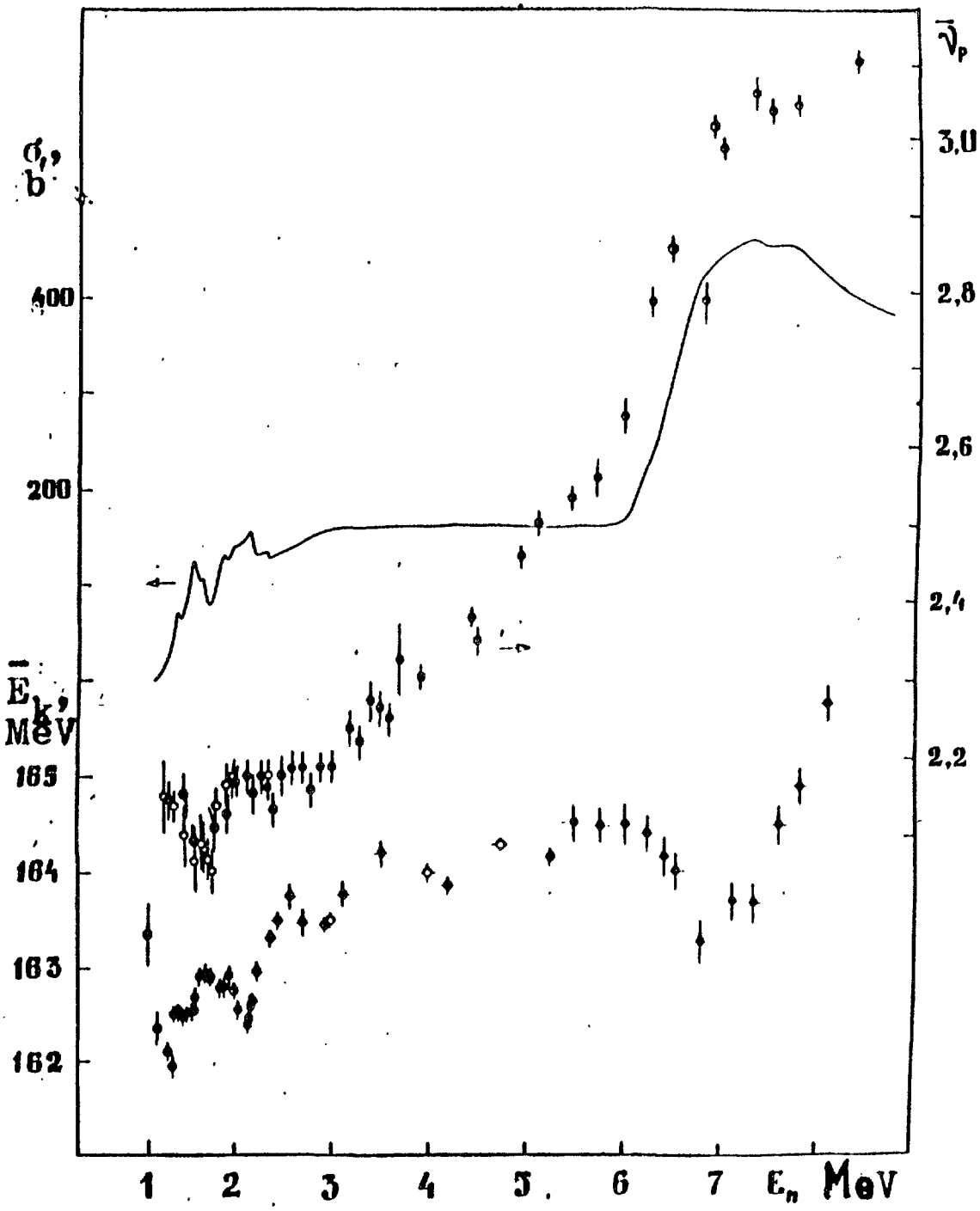

Fig.1. The experimental results of the ^{232}Th(n, f) reaction investigation.

—— —— The (σ_f) fission cross-section /9/;

$\bar{E}_k$: ● - the present work; ○ - /3/; ◑ - /5/ ;

$\bar{\nu}$: ● - /7/; ○ - /8/; ◉ - /10/.

Nevertheless, at that normalization of results by different authors, which is realized here, there is distinctly revealed the structure in an energy dependence of $\bar{E}_k$.

To solve a problem about the influence of changing $\bar{E}_k$ on an energy dependence of $\bar{\nu}$ it should be proceeded from the energy ba-

lance equation

$$\bar{E}_f + \bar{E}_n + B_n = \bar{E}_k + \bar{\nu}\,\bar{\varepsilon}_n + \bar{E}_\gamma \qquad (1)$$

where

$\bar{E}_f$ is the fission energy averaged over all the methods of fission;

E_n is the energy of neutrons giving rise to nuclear fission;

B_n is the neutron binding energy in a fissioning nucleus;

$\bar{E}_k$ is the average kinetic energy of fission fragments;

$\bar{\nu}$ is the average number of prompt fission neutrons;

ε_n is the average energy expended in emitting one neutron;

$\bar{E}_\gamma$ is the average energy carried away by the prompt gamma-quanta.

The neutron energy change E_n can have influence on all the components of the energy balance equation (1), besides B_n. Therefore, for analyzing a quantitative agreement of the $\bar{E}_k$ and $\Delta\bar{\nu}$ changes in the first turn it is necessary to be sure in a constancy of $\bar{E}_f$. In particular, the changes in $\bar{M}_H$, the average mass number of heavy fission fragments, as E_n is changed, restrict the predicting possiblities of the balance equation since these are followed by changes in $\bar{E}_f$, which do not surrender to a quantitative assessment due to a scanty information about the changes in charges.

In the neutron-induced fission of ^{232}Th, $\bar{M}_H$ is left to be constant within the limits of measurement errors $\pm$ 0.1 at $E_n < 2.5$ MeV. Suppose, that in this region of neutron energies $\bar{E}_f$ is left invariable.

In this case

$$\frac{d\bar{\nu}}{dE_n} = \frac{1}{\varepsilon_n}\left(1 - \frac{d\bar{E}_n}{dE_n} - \bar{\nu}\,\frac{d\varepsilon_n}{dE_n} - \frac{d\bar{E}_\gamma}{dE_n}\right).$$

Taking into consideration that

$$\varepsilon_n = 8 \text{ MeV}, \quad \bar{\nu}\,\frac{d\varepsilon_n}{dE_n} \approx 0.05, \quad \frac{d\bar{E}_\gamma}{dE_n} = 0.1$$

it can be carried out the evaluations of an expected value of $\frac{d\bar{\nu}}{dE_n}$ proceeding from the experimental data on changing $\bar{E}_k$. In the Table 1 are given the results of an analysis.

Table 1

No,No	E_n(MeV)	Note	Results of comparison
1.	1.3 - 1.7	M_H = const	The experimental and calculational results are agreed.
2.	1.7 - 2.2	M_H = const	- " -
3.	2.2 - 2.7	M_H = const	It is existed only the qualitative agreement between experimental and calculational results.
4.	3.0 - 6.0	M_H is decreased $\bar{E}_k$ const	$d\bar{\nu}/dE_n$ =0.146 1/MeV
5.	6.0 - 7.0	The (n,n'f)	It is existed only the qualitative agreement.
6.	7.0 - 9.0	The maximum contribution of the (n,n'f) reaction	- " -

When considering an energy dependence of $\bar{\nu}$ in the range neutron energies where the (n, n'f) reaction takes place, the following circumstances must be kept in mind:

1. The exitation energy of a fissioning nucleus above the fission barrier after previous emitting a neutron is distributed in accordance with the scheme shown in the Fig.2, i.e., the average energy of excitation is close to a value of $\frac{E_n - B_f}{2}$.

2. The number of neutrons emitted in the (n,n'f) reaction in the vicinity of a thereshold of this reaction is more that in the (n,f) reaction at the same neutron energy E_n.

Indeed, taking into consideration that $\bar{\nu}$ and $\frac{d\bar{\nu}}{dE_n} = \alpha$ at the singular excitation energy of the A+1 and A nuclei are equal, it can be obtained

$$\bar{\nu}_A - \bar{\nu}_{A+1} = 1 - \alpha (E_n + B_n - E^*)$$

where

$E^* = E_n - \frac{E_n - B_f}{2}$ is the excitation energy of the A fissioning nucleus.

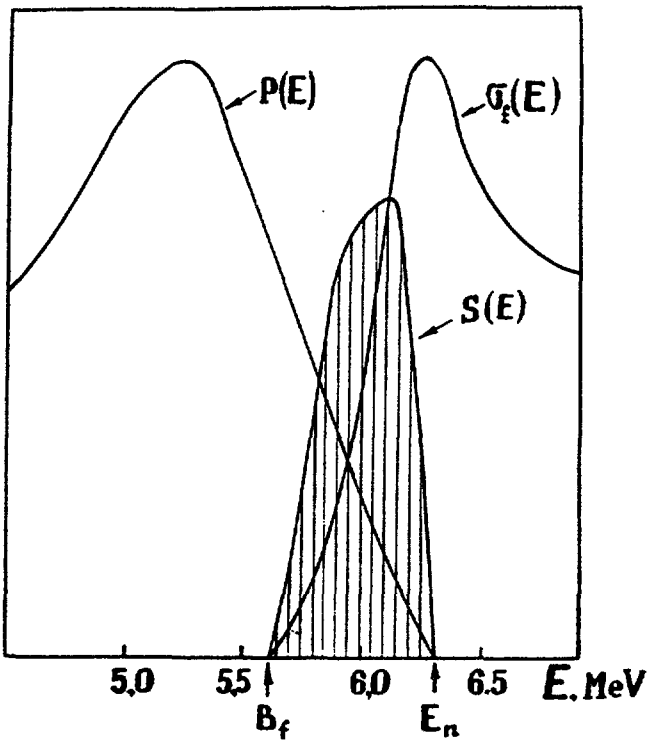

Fig.2. The scheme of forming the S(E) daughter fissioning nucleus excitation spectrum in the (n, n'f) process: $\sigma_f(E)$ is the fission cross-section in the range of the second fissility chance;
P(E) is the spectrum of emission neutron in the process of (n, n'f).

From this it is obtained

$$\bar{\nu}_A - \bar{\nu}_{A+1} = 1 - \alpha\left(B_n + \frac{E_n - B_f}{2}\right).$$

3. When the (n,n'f) reaction is available the velocity of increasing this reaction cross-section is also reflected to an energy dependence of $\bar{\nu}$.

Taking into cosideration the mentioned above assumptions and the costancy of kinetic energy of fragments it can be obtained the following expression for the rate of changing $\bar{\nu}$,

$$\frac{d\bar{\nu}}{dE_n} = \alpha\left(1 - \frac{\beta}{2}\right) + \frac{d\beta}{dE_n}\quad 1 - \alpha\left(\frac{E_n - B_f}{2} + B_n\right)$$

where

$$\beta = \frac{\sigma(n, n'f)}{\sigma_f}$$

Addressing to the Fig.1, it can be noted that an increase of the rate growing $\bar{\nu}$ in the neutron energy range of 6 ÷ 7 MeV can be explained by a contribution of the (n, n'f) reaction.

REFERENCES

1. A.I.Sergachev: Jadernaja Fizica.7, 778(1968).
2. N.P.Djachenko: ZfK - 410, 97(1980).
3. Y.H.Abon: CEA - N - 2134, NEANDC(E) 212/L, 87.
4. J.Caruana: Nucl. Phys. A285, 217(1977).
5. W.Holubarsch: Nucl. Phys. A171, 631(1971).
6. A.A.Goverdovsky: Jadernaja Fizica, 46 , 706(1987).
7. V.V.Malinovsky: Atomnaja Energija, 54 , 209(1983).
8. J.Trochon: 10-th Europ. Conf. on Phys. and Chem. of Complex Nucl. Reactions (1981).
9. J.W.Behrens: Nucl. Sci. Eng. 81, 512(1982).
10. J.Frehaut: Bruyeres-le-Chatel, CEA-N-2284, 71(1982).

ν(m*) MEASUREMENT FOR THERMAL NEUTRON-INDUCED FISSION OF ^{233}U AND ^{235}U BY DOUBLE-VELOCITY DOUBLE-ENERGY METHOD

Y. Nakagome
Research Reactor Institute, Kyoto University
Kumatori-cho, Sennan-gun, Osaka 590-04, Japan

I. Kanno
Japan Atomic Energy Research Institute
Tokai-mura, Naka-gun, Ibaraki 319-11, Japan

I. Kimura
Department of Nuclear Engineering, Kyoto University
Yoshidahonmachi, Sakyo-ku, Kyoto 606, Japan

Abstract

Number of prompt neutrons as a function of individual fragment mass ν(m*) was measured for the thermal neutron-induced fission of ^{233}U and ^{235}U. By measuring the velocities and energies of two fission fragments simultaneously, preneutron-emission fragment mass m* and postneutron-emission fragment mass m were obtained. ν(m*) was deduced by subtracing m from m*. The fragment velocity was measured by a time-of-flight (TOF) method, and the start time was detected by a very thin plastic scintillator film detector. A silicon surface barrier detector was used to measure the fragment energy, which was also used as a stop detector of the TOF. The result of ν(m*) for ^{233}U(n,f) was in agreement with other data in the heavy fragment region, but was 20 to 50% larger than those in the light one. ν(m*) for ^{235}U(n,f) showed a factor of 1.5 to 2 larger in the light fragment region and smaller in the heavy one than the other data. With the energy balance equation, the total kinetic energy was estimated using the ν(m*)-value and was in good agreement with the experimental result. Also using the energy balance equation, the ν(m*)-values were calculated by assuming the thermal equilibrium at the scission point. These values were quite different from the experimental results in both cases.

INTRODUCTION

For the study of the shape and excitation energy of a fission fragment, it is important to know the number of prompt neutrons as a function of the individual preneutron-emission (initial) fragment mass ν(m*). Average total number of prompt neutrons are reported by many authors[1], but the data of ν(m*) are little.

A measurement method of $\nu(m^*)$ is classified in 'direct' and 'indirect' measurement methods. The direct measurement method is of measuring the velocities of both fission fragments and the emitted-neutrons simultaneously. The neutrons are generally detected by using a large liquid scintillator tank[2,3]. Whereas the indirect measurement method is of determining $\nu(m^*)$ from the mass difference between the initial and the postneutron-emission (final) fragment mass numbers. These fragment masses are obtained by measuring the velocities and the kinetic energies of both fragments. The velocity of the fragment is usually measured by the time-of-flight (TOF) method[4] and the energy is detected by an ionization chamber or a silicon surface barrier detector (SSB).

Stein[5] carried out the measurement of the velocities of both fragments and the energy of one fragment of ^{252}Cf spontaneous fission (double-velocity single-energy method) and derived $\nu(m^*)$. Schmitt et al.[6] obtained $\nu(m^*)$ for ^{252}Cf by single-velocity double-energy method. Andritsopoulos[7] measured first $\nu(m^*)$ for the thermal neutron-induced fission of ^{235}U by double-velocity double-energy method. In their experiments, some ingenious devices were used to get the start signal of the TOF. Patin et al.[8] carried out the double-velocity double-energy measurement for $^{233}U(d,pf)$ and Mueller et al.[9] for fast neutron-induced fission of ^{235}U, who used the neutrons produced by charged particle reactions. In these cases the trigger pulses of an accelerator were used as the TOF start signals.

We developed the double-velocity double-energy measurement system for fission fragments using thin film detectors (TFD) as start time detectors of TOF[10].

In this paper, we describe the results of $\nu(m^*)$ for the thermal neutron-induced fission of ^{233}U and ^{235}U with this measurement system.

PRINCIPLE OF $\nu(m^*)$ DETERMINATION

In the fission phenomena, the mass and the momentum are conserved as

$$m_1^* + m_2^* = M \tag{1}$$

$$m_1^* v_1^* = m_2^* v_2^* \ , \tag{2}$$

where the asterisk means the quantities of initial fragment, m_i^* and v_i^* (i=1,2) are the mass and the velocity of the fragment respectively, and

M is the fissioning nucleus mass. From Eqs.(1) and (2), the initial fragment mass is given by

$$m_i^* = \frac{v_i^*}{v_i^* + v_j^*} M \qquad (i=1,2 \quad j=3-i). \tag{3}$$

The velocity measured experimentally, v_i, is that of the final fragment because the neutrons are emitted from the initial fragment within about 10^{-14} s after scission. Assuming the neutrons are emitted isotropically, the averaged fragment velocity does not change before and after the neutron emission, namely

$$v_i^* = v_i. \tag{4}$$

The relation between the velocity and the kinetic energy E of the final fission fragment is given by

$$E_i = \frac{1}{2} m_i v_i^2. \tag{5}$$

In this experiment SSBs were used for measuring the fragment kinetic energy. Then the following relationship between the energy and the pulse height[11] is given as

$$E_i = (a + a'm_i)x_i + b + b'm_i, \tag{6}$$

where x_i is the pulse height, a, a', b and b' are energy calibration constants. By using Eqs.(5) and (6), the final fragment mass is obtained as

$$m_i = \frac{ax_i + b}{v_i^2/2 - a'x_i - b'}. \tag{7}$$

The number of emitted-neutrons are determined by subtracting Eq.(7) from Eq.(3),

$$\nu(m_i^*) = m_i^* - m_i. \tag{8}$$

EXPERIMENT

Apparatus

The experiments of double-velocity double-energy measurement for the thermal neutron-induced fission of ^{233}U and ^{235}U were carried out at the super mirror neutron guide tube facility of the Kyoto University Reactor (KUR)[12]. The experimental arrangement is shown in Fig.1. The neutrons were guided by the facility at distance of 11.7 m from the KUR core. The thermal neutron was collimated to 1 cm x 7 cm by a beam slit made of LiF, and the flux at the uranium target position was 5 x 10^7 n/cm^2s.

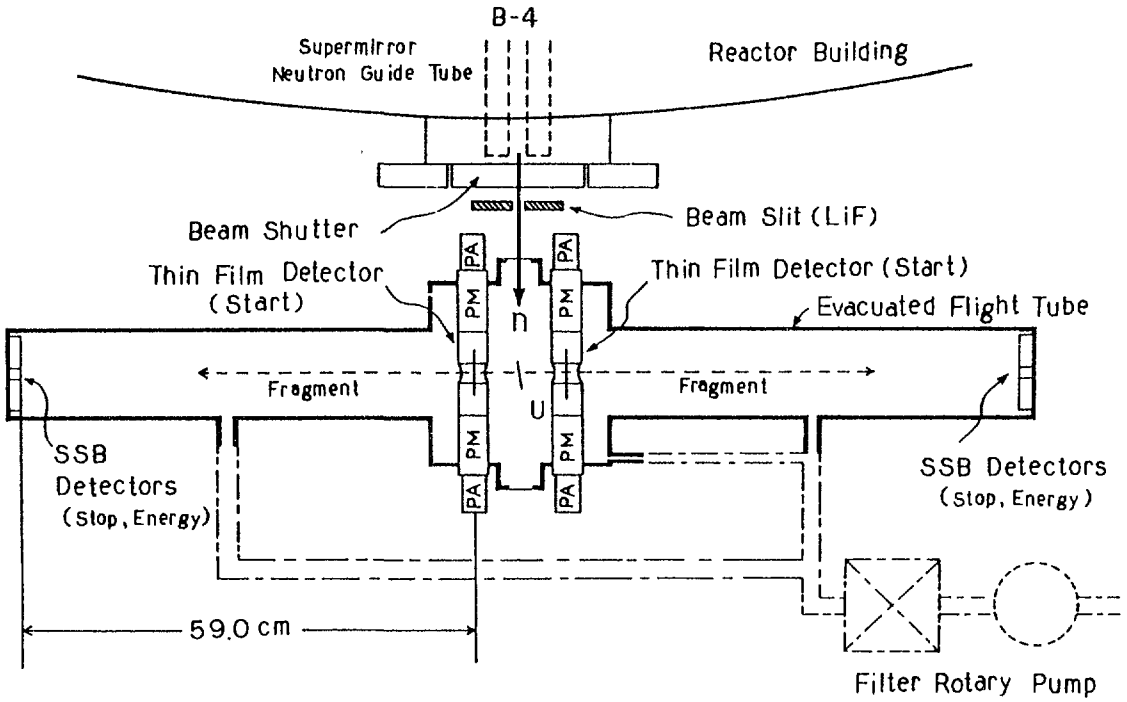

Fig. 1 Experimental arrangement for double-velocity double-energy measurement

The fragment velocity was obtained by a time-of-flight (TOF) method. The flight path was 59 cm. To obtain the start time of the fragment, very thin plastic scintillator film detectors (TFDs) were used. On each end of the flight tubes, three SSBs (ORTEC F-series detectors) were mounted to detect the stop time and also to measure the fragment kinetic energy. TFDs, SSBs and a uranium target were installed in a evacuated chamber and two flight tubes. The vacuum was kept at about 10^{-4} Torr.

The uranium target was made from a very thin nitrocellulose film in which organic uranium compound was dissolved. The diameter of the target was 8 mm and the thickness was 7 $\mu gU\text{-}233/cm^2$ or 9 $\mu gU\text{-}235/cm^2$,

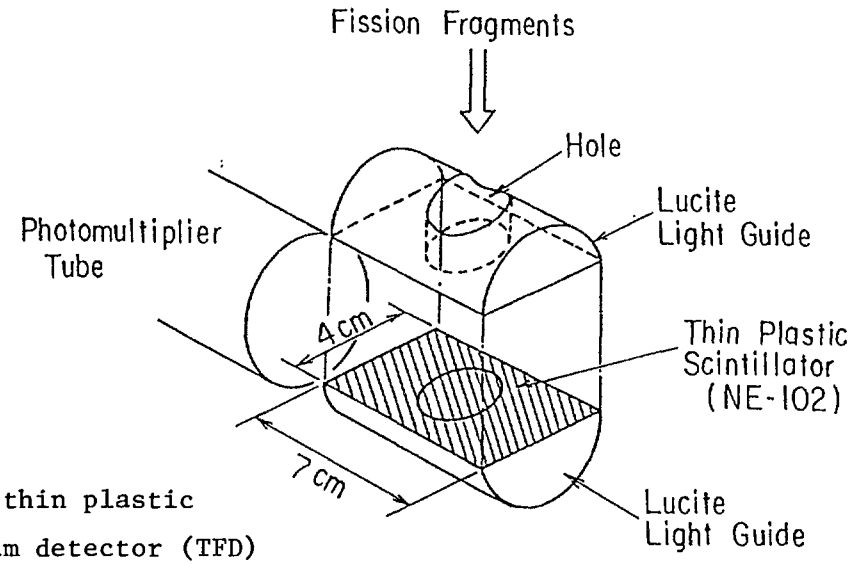

Fig. 2 Illustration of thin plastic scintillator film detector (TFD)

which was determined by counting the number of fission events. The enrichment of ^{233}U was 99.47% and that of ^{235}U 90%.

The TFD illustrated in Fig.2 was placed at 3 cm apart from the uranium target on each fragment path. TFD has been developed by Muga et al.[13] and we have established a fabrication technique of thinner (less than $\sim 50\ \mu g/cm^2$) TFD. The characteristics of TFD have been reported elsewhere[14,15]. The TFD used consists of a thin plastic scintillator film (NE-102), two lucite light guides and photomultipliers. The film whose thickness was $20\ \mu g/cm^2$ was sandwiched in two hemicylindrical light guides. The thickness of the film was determined by measuring the energy loss of α-particles of ^{252}Cf in the film. A hole of 1 cm diameter was bored in the light guide for the fission fragments passing through the film.

The electronics of the double-velocity double-energy measurement system is shown in Fig.3. The timing signal, start or stop signal, was fed into a time-to-amplitude converter (TAC) through a timing amplifier and a constant fraction discriminator (CFD). Only coincided four signals, two TAC signals and two energy ones, were taken by the Multi Parameter Data Aquisition System[16]. The data were accumulated in 1024 channels for each parameter and stored on a floppy disk event by event.

Energy and Time Calibrations

1. Energy Calibration

In the case of measuring the energy of a heavy ion like fission fragment by using an SSB, it is necessary to consider the pulse height defect (Eq.(6)). In accordance with the method proposed by Schmitt et

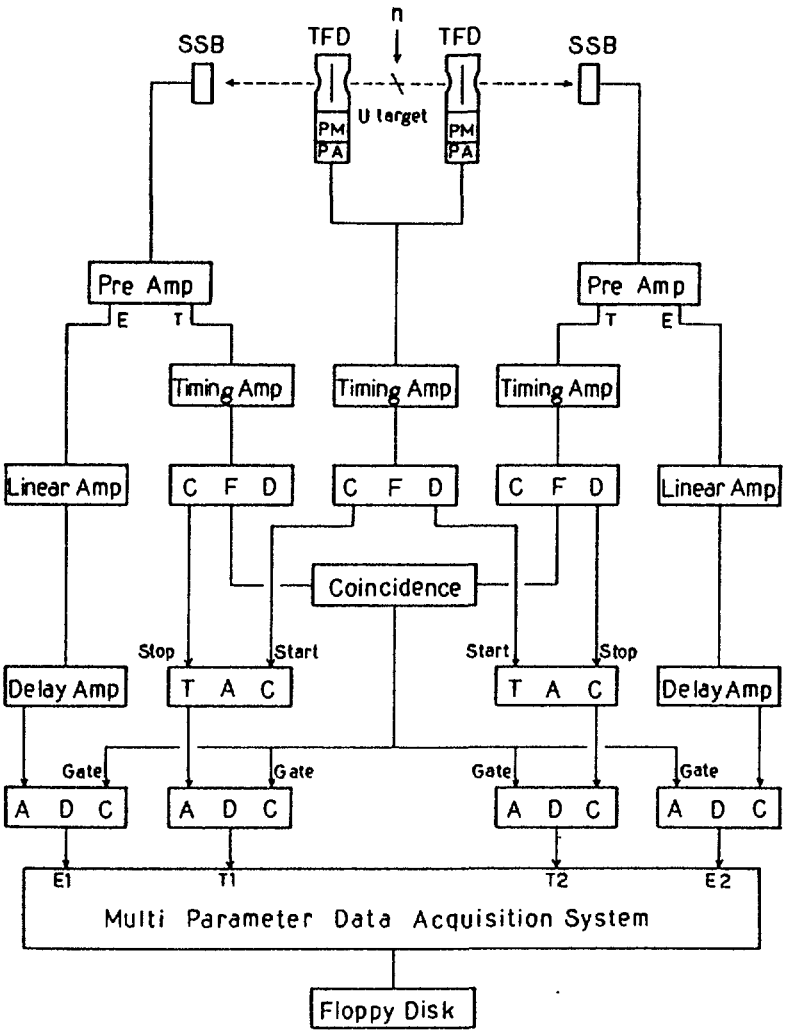

Fig. 3 Block diagram of electronic circuit for double-velocity double-energy measurement

TFD : Thin film detector
SSB : Silicon surface barrier detector
PM : Photomultiplier
PA and Pre Amp : Preamplifier
Timing Amp : Timing amplifier
CFD : Constant fraction discriminator
Linear Amp : Linear amplifier
Delay Amp : Delay amplifier
Coincidence : Coincidence circuit
TAC : Time to amplitude converter
ADC : Analog to digital converter

al.[11], we carried out energy calibration for SSBs with spontaneous fission fragments of ^{252}Cf.

2. Time Calibration

The relation between the pulse height X, which is the output of TAC, and the flight time T is given as

$$T = AX + B, \tag{9}$$

where A and B are the constants. The measurements of the flight time of the light fragments of ^{252}Cf were carried out with different length flight paths L_1 and L_2 to determine A and B. Assigning the pulse heights of TAC as $\bar{X}_1$ and $\bar{X}_2$ which correspond to the averaged pulse heights for L_1 and L_2, respectively, we obtain the relations as

$$\frac{L_1}{\bar{v}} = A\bar{X}_1 + B, \tag{10}$$

$$\frac{L_2}{\bar{v}} = A\bar{X}_2 + B, \tag{11}$$

where $\bar{v}$ is the average velocity of the light fragments of ^{252}Cf. With Eqs.(10) and (11), B is determined as

$$B = \frac{A(L_1\bar{X}_2 - L_2\bar{X}_1)}{L_2 - L_1} . \tag{12}$$

In order to estimate A, we measured another flight time of the light fragments of ^{252}Cf, $\bar{X}_3$, with L_1 employing a delay line. Designating the delay time due to the delay line cable by T_d, the following relation is obtained:

$$\frac{L_1}{v} + T_d = A\bar{X}_3 + B. \tag{13}$$

From Eqs.(10) and (13), A is determined as

$$A = \frac{T_d}{\bar{X}_3 - \bar{X}_1} . \tag{14}$$

The delay line of 5 m was used in our measurement. The T_d was measured with a time calibrator (ORTEC model 462) and was determined 26.302 ns.

Time Resolution

The time resolution of the TFD-SSB system was determined by the following method using 6.118 MeV α-particles of ^{252}Cf. A TFD of 200

$\mu g/cm^2$ thickness was used because a very thin TFD was insensitive to low energy α-particles.

1. Measurement of TOF Spectrum of α-particles

The TOF spectrum of the α-particles of ^{252}Cf was measured with a flight path of 29.5 cm. The full width at half maximum (FWHM) of the time spectrum was found to be

$$\Delta t = 1.33 \times 10^{-10} \text{ (s)}. \tag{15}$$

2. Estimation of Energy Spread of α-particles

The energy spread ΔE_a of the α-particles of ^{252}Cf after passing through the TFD was calculated by the Bethe's formula. This spread was caused by the uncertainty of the scintillator film thickness and was estimated to be 4 keV.

3. Calculation of Time Resolution

The relation between the energy resolution and the time resolution is as follows:

$$\left|\frac{\Delta E_a}{E_a}\right| = 2\left|\frac{\Delta v_a}{v_a}\right| = 2\left|\frac{\Delta t_a}{t_a}\right| , \tag{16}$$

where E_a, v_a and t_a are the energy, velocity and flight time of the α-particle, respectively. t_a is calculated as

$$t_a = \frac{L}{(2E_a / m_a)^{\frac{1}{2}}} , \tag{17}$$

where L is a flight path and m_a is the mass of α-particle.
The time resolution is given as

$$\Delta t = [(\Delta t_a)^2 + (\Delta t_s)^2]^{\frac{1}{2}} , \tag{18}$$

where Δt_a and Δt_s are the time resolution attributed to the uncertainty of energy loss in a scintillator film and the time resolution of this system, respectively. The Δt_a is calculated using Eqs.(16) and (17) and determined to be $\Delta t_a = 0.00561$ ns. With this value and Eq.(18), Δt_s is calculated as

$$\Delta t_s = 1.329 \times 10^{-10} \fallingdotseq 1.33 \times 10^{-10} \text{ (s)}. \tag{19}$$

Correction

In the measurement, the fragments lose energy in the uranium target and in the thin plastic scintillator film. The energy loss of the fragment was calculated by using the Bethe's formula for each fragment.

In the case of using SSBs as timing detectors, it is well known that the arriving time is delayed for some nano-seconds by so-called plasma delay. Former researchers fit the plasma delay to a second order polynomial function of mass and energy[8,9] as

$$t_d = t_d\,(m,\ E). \tag{20}$$

The authors followed the way proposed by Mueller et al.[9] They adjusted the time delay so that the calculated velocity satisfies the equations

$$E_i^* = E_i \frac{m_i^*}{m_i}\ , \tag{21}$$

$$m_i = m_i^* - \bar{\nu}(m_i^*). \tag{22}$$

In our calculation, the averaged neutron emission number $\bar{\nu}(m_i^*)$ was taken from the work of Apalin et al.[2]

RESULTS AND DISCUSSION

A typical fragment TOF spectrum for $^{233}U(n,f)$ is shown in Fig.4. The peak in the lower channel corresponds to the light fragment group and its mean flight time is 40.97 ns. The mean flight time of the heavy fragment group is 60.51 ns. In Fig.5, a typical fragment energy spectrum for $^{233}U(n,f)$ is shown. The peak in the higher channel corresponds to the light fragment group and its energy is about 101 MeV.

The mean values and errors concerning fragment mass, kinetic energy and velocity are listed in Table 1. The values of the present results agree well with other works within the errors.

For $^{233}U(n,f)$, the number of prompt neutrons as a function of initial fragment mass is shown in Fig.6. $\nu(m^*)$ is indicated with a solid circle and the total number of prompt neutrons as a function of heavy fragment mass with an open circle. The result of Apalin et al.[2]

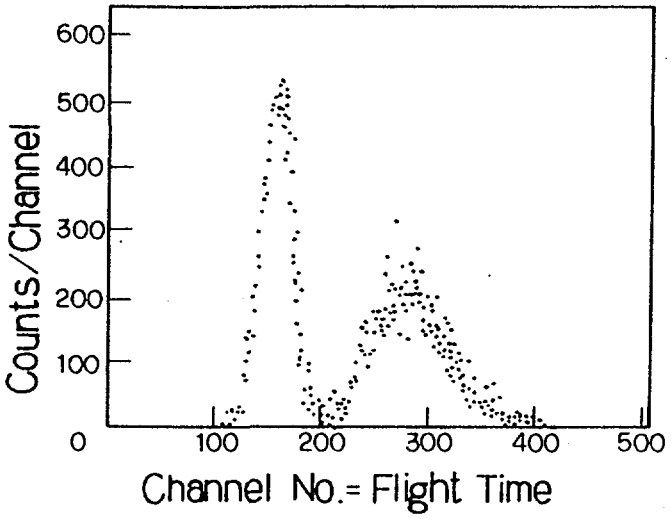

Fig. 4 Typical fragment Time-of-flight spectrum for $^{233}U(n,f)$

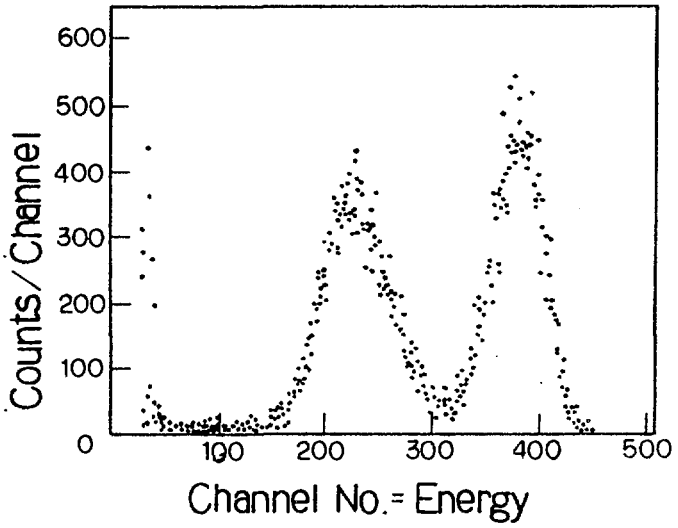

Fig. 5 Typical fragment kinetic energy spectrum for $^{233}U(n,f)$

and of Milton et al.[3] are also plotted, which were obtained by 'direct' measurement methods. Present result is close to the data of Milton et al. in the heavy fragment region, while in the mass region of 100 - 110, the result is close to the data of Apalin et al. In the light fragment region the result disagrees with the other data and is 20 to 50% larger than the data of Apalin et al. The $\nu(m^*)$-values are listed in Table 1.

For $^{235}U(n,f)$, the present result of $\nu(m^*)$ is shown in Fig.7. In the light fragment region, our result is approximately a factor of 1.5 to 2 larger than the other data. On the contrary, it is a factor of 1.5 to 2 smaller than those in the heavy fragment region. The $\nu(m^*)$-values are also listed in Table 1.

Table 1. Mean values and standard deviations of the initial fragment mass, velocity, energy and average number of prompt neutrons for the thermal neutron-induced fission of ^{233}U and ^{235}U.

	$^{233}U(n,f)$		$^{235}U(n,f)$		
	Present	Milton and Fraser[4]	Present	Milton and Fraser[4]	Andritsopoulos [7]
$\langle m_L^* \rangle$ (amu)	94.36±0.23	94.57±0.10	95.93±0.23	96.08±0.10	95.87±0.07
$\sigma(m_L^*)$ (amu)	6.21	5.85	6.26	5.77	6.3
$\langle m_H^* \rangle$ (amu)	139.64±0.23	139.43±0.10	140.07±0.23	139.92±0.10	139.87±0.07
$\sigma(m_H^*)$ (amu)	6.21	5.85	6.26	5.77	6.3
$\langle V_L^* \rangle$ (cm/ns)	1.44	1.442	1.423	1.409	1.415
$\sigma(V_L^*)$ (cm/ns)	0.072	0.068	0.075	0.062	0.051
$\langle V_H^* \rangle$ (cm/ns)	0.975	0.963	0.977	0.966	0.97
$\sigma(V_H^*)$ (cm/ns)	0.073	0.070	0.073	0.071	0.086
$\langle E_L^* \rangle$ (MeV)	101.38±0.72	99.9±1.0	100.55±0.71	99.8±1.0	99.08±0.07
$\sigma(E_L^*)$ (MeV)	5.95	6.2	6.57	6.0	5.9
$\langle E_H^* \rangle$ (MeV)	68.78±0.34	67.9±0.7	69.25±0.34	68.4±0.7	68.190±0.10
$\sigma(E_H^*)$ (MeV)	7.48	7.3	7.73	7.5	8.7
$\langle E_K^* \rangle$ (MeV)	170.16±0.80	167.8±1.7	169.80±0.79	168.3±1.7	167.45±0.2
$\sigma(E_K^*)$ (MeV)	10.65	11.2	11.59	11.41	14.2
$\bar{\nu}(m_L^*)$	1.68±0.69	1.40	1.94±0.69	1.19	1.16±0.09
$\bar{\nu}(m_H^*)$	0.85±0.72	1.03	0.89±0.72	1.23	1.27±0.09

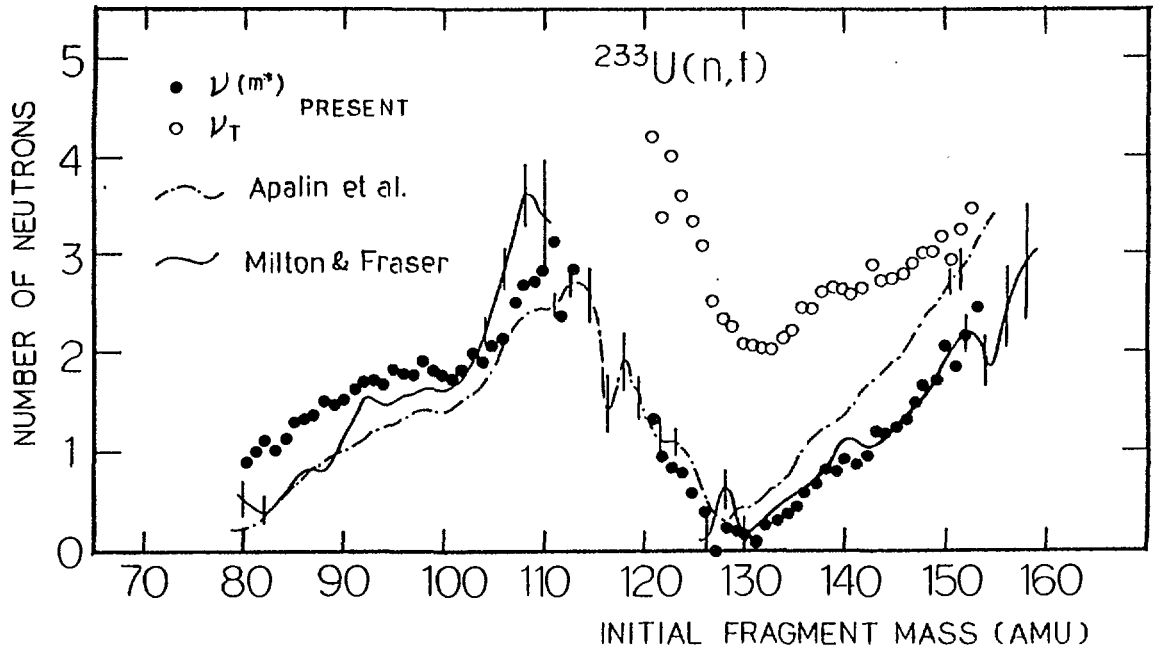

Fig. 6 Prompt neutron distribution $\nu(m^*)$ for thermal neutron-induced fission of ^{233}U

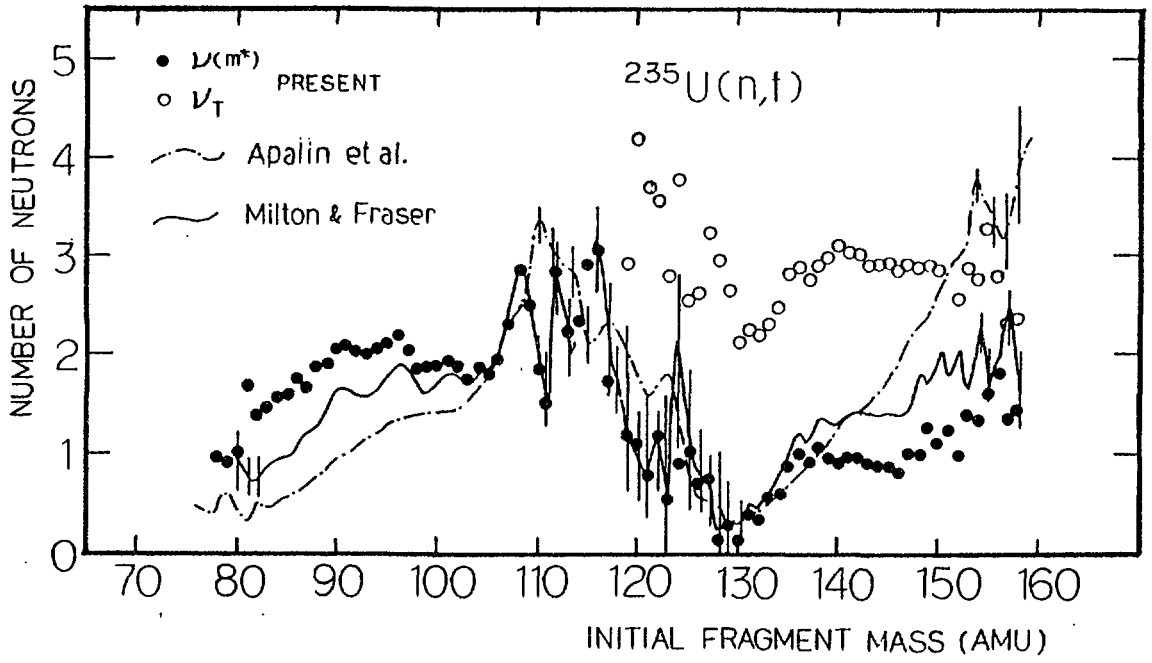

Fig. 7 Prompt neutron distribution for thermal neutron-induced fission of ^{235}U

Using the $\nu(m^*)$-value, we can estimate the total kinetic energy E_k^* from the energy balance equation

$$E_k^* = E_R - \nu(m_1^*)(\overline{E}_{B1} + \overline{E}_{n1}) - \nu(m_2^*)(\overline{E}_{B2} + \overline{E}_{n2}) - \overline{E}_\gamma,$$

where E_R is the total energy released, $\overline{E}_{Bi}$ (i=1,2) the mean binding

energy of neutron, $\overline{E}_{ni}$ the emitted neutron kinetic energy, and $\overline{E}_\gamma$ is the total γ-ray energy emitted by the two fragments. Assuming that the quantities of $\overline{E}_{ni}$ and $\overline{E}_\gamma$ are independent of fragment mass, we used the value $\overline{E}_{ni}$ = 1.2 MeV and $\overline{E}_\gamma$ = 7.5 MeV for ^{233}U and ^{235}U. E_R was calculated with the most probable fission fragment which was estimated by the following empirical formula proposed by Unik et al.[17]

$$\frac{Z}{M} = \frac{Z_L - \frac{1}{2}}{m_L^*} = \frac{Z_H + \frac{1}{2}}{m_H^*} ,$$

where Z and M are the charge and mass numbers of fissioning nucleus, Z_L and Z_H are the most probable charge numbers of light fragment m_L^* and heavy fragment m_H^*, respectively.

The estimated total kinetic energy and the measured one in this experiment are shown in Fig.8 (a) for ^{233}U and (b) for ^{235}U. The agreement between these values is good.

We tried to calculate the $\nu(m^*)$-value with the above energy balance equation by assuming that the thermal equilibrium could be achieved at the scission point between the two fragments. $\nu(m^*_i)$ may be calculated as

$$\nu(m_i^*) = \frac{(m_i^* / M)(E_R - E_k^* - \overline{E}_\gamma)}{(\overline{E}_{Bi} + \overline{E}_{ni})} .$$

In the calculation, the experimental value of E_k^* was used, and the results of $\nu(m^*)$ are shown as an open square in Fig.9 (a) for ^{233}U and (b) for ^{235}U. In both cases, the $\nu(m^*)$-values are quite different from the experimental results. In these calculations we did not consider the deformation of fission fragments.

CONCLUSIONS

The number of prompt neutrons as a function of initial fragment mass $\nu(m^*)$ was measured by using the double-velocity double-energy method for the thermal neutron-induced fission of ^{233}U and ^{235}U. The $\nu(m^*)$ distribution obtained for $^{233}U(n,f)$ was in agreement with the result of Milton et al. in the heavy fragment region, but disagreed with the results of Milton et al. and Apalin et al. in the light fragment region. Especially, the $\nu(m^*)$ in the light fragment region was 20 to 50% larger than the data of Apalin et al.

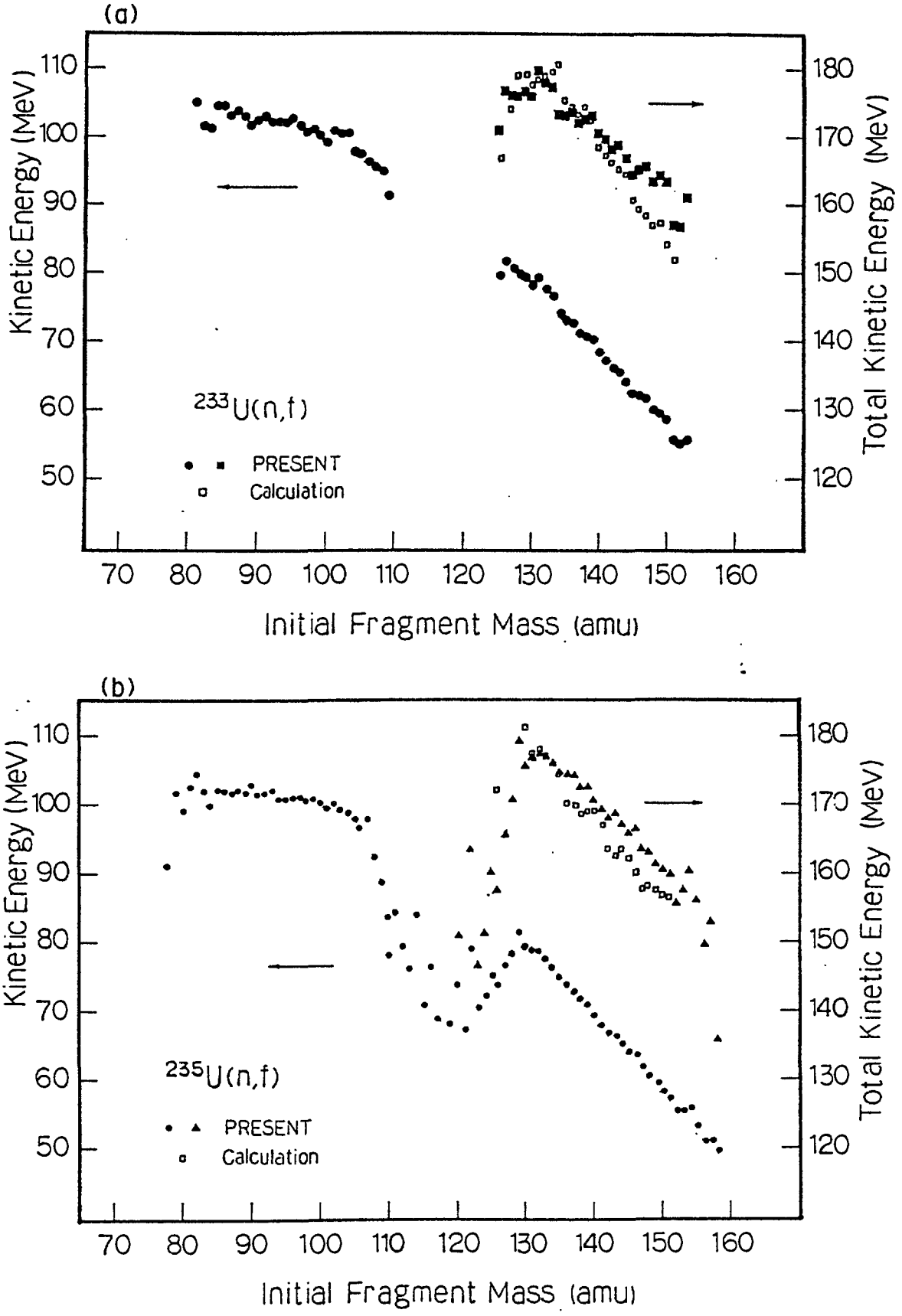

Fig. 8 Kinetic energy distribution of fragment for thermal neutron-induced fission of (a): ^{233}U and (b): ^{235}U.

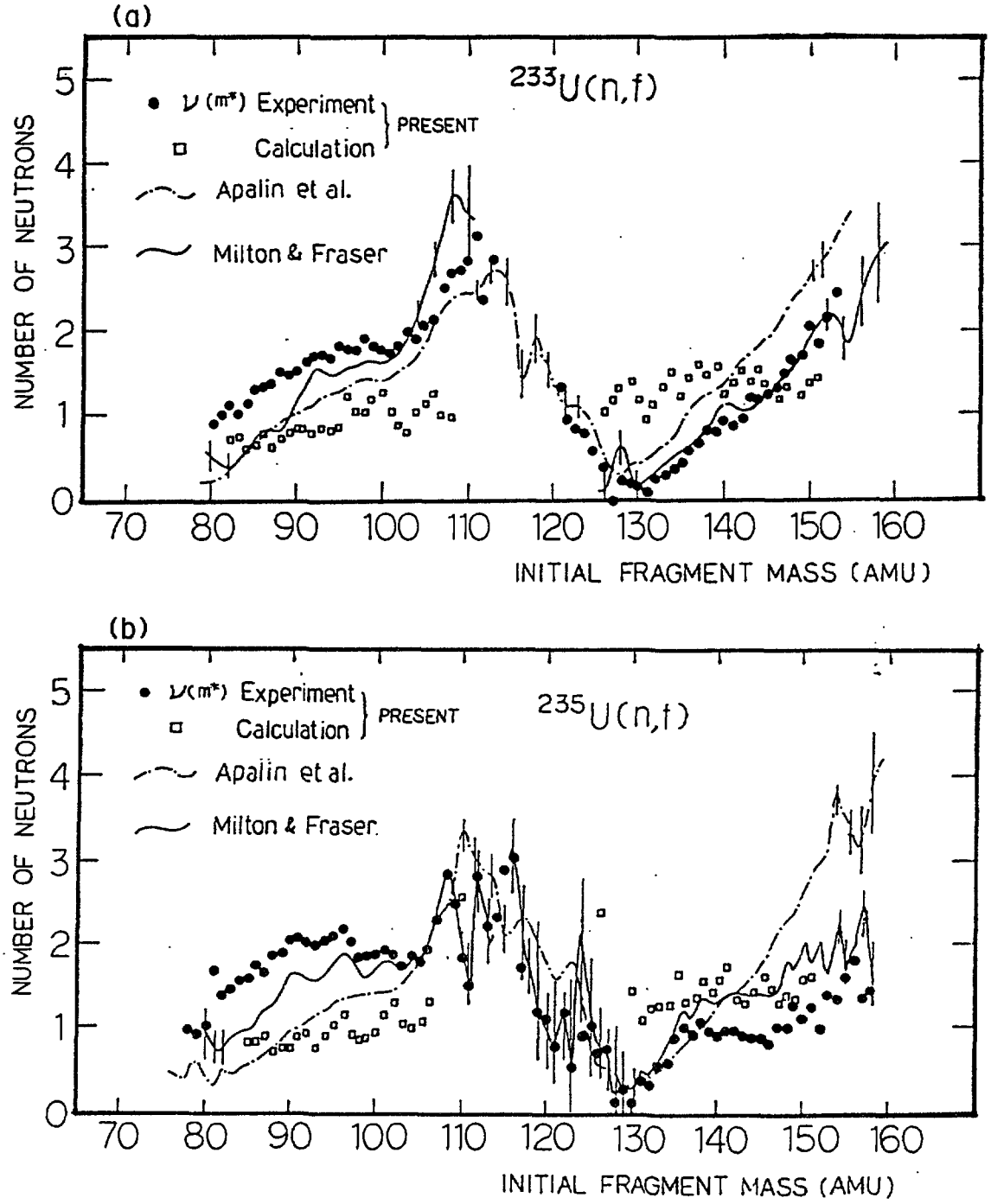

Fig. 9 Comparison of experimental results with calculated results of $\nu(m^*)$ for (a): ^{233}U and (b): ^{235}U(n,f)

The result of $\nu(m^*)$ for ^{235}U(n,f) disagreed with the other data. Our result was a factor of 1.5 to 2 larger in the light fragment region and a factor of 1.5 to 2 smaller in the heavy fragment region than the other data.

The total kinetic energies for ^{233}U and ^{235}U(n,f) measured in these experiments were in good agreement with the estimated values which were calculated with the energy balance equation by using the present $\nu(m^*)$-values.

The calculated $\nu(m^*)$-values by assuming the thermal equilibrium at the scission point were quite different from the experimental results. Since the nucleus like fission fragment is deformed, we have to consider the effect of deformation in these $\nu(m^*)$ calculations.

REFERENCES

1. S.F. Maghabghab and D.I. Garber, "Neutron Cross Sections" Vol.1., BNL-325 Third Edition (1973).
2. V.F. Apalin Yu.N. Gritsyuk, I.E. Kutikov, V.I. Lebedev and L.A. Mikaelian, Nucl. Phys., 71, 553 (1965).
3. J.C.D. Milton and J.S. Fraser, Proc. Symp. Physics and Chemistry of Fission, Vol.2, p.39 (1965) IAEA.
4. J.C.D. Milton and J.S. Fraser, Can. J. Phys., 40, 1626 (1960).
5. W.E. Stein, Proc. Symp. Physics and Chemistry of Fission, Vol.1, p.491 (1965) IAEA.
6. H.W. Schmitt, R.W. Lide and F. Pleasonton, Nucl. Instr. Methods, 63, 237 (1968).
7. G. Andritsopoulos, Nucl. Phys., A94, 537 (1967).
8. Y. Patin, S. Cierjacks, J. Lackar, J. Sigaud, G. Haouat and F. Cocu, Nucl. Instr. Methods, 160, 471 (1979).
9. R. Mueller, A.A. Naqvi, F. Kaeppeler and F. Dickmann, Phys. Rev., C29, 885 (1984).
10. I. Kanno, Y. Nakagome and I. Kimura, J. Nucl. Sci. Tech., 25, 111 (1988).
11. H.W. Schmitt, W.H. Gibson, J.H. Neiler, F.J. Walter and T.D. Thomas, Proc. Symp. Physics and Chemistry of Fission, Vol.1, p.531 (1965) IAEA.
12. T. Akiyoshi, T. Ebisawa, T. Kawai, F. Yoshida, M. Ono, S. Mitani, T. Kobayashi and S. Okamoto, Proc. 1985 Seminar Nucl. Data, JAERI-M-86-080, p.380 (1986).
13. M.L. Muga, D.J. Burnsed, W.E. Steeger and H.E. Taylor, Nucl. Instr. Methods, 83, 135 (1970).
14. I. Kanno and Y. Nakagome, ibid., A244, 551 (1986).
15. I. Kanno and Y. Nakagome, ibid., A251, 108 (1986).
16. S. Uehara, T. Seo, H. Iimura and S. Yamada, Ann. Rep. Res. Reactor Inst., Kyoto Univ., 18, 178 (1985).
17. J. Unik, J. Gindler, L. Glendenin, K. Flynn, A. Gorski and R. Sjoblom, Proc. Symp. Physics and Chemistry of Fission, Vol.2, p.19 (1974) IAEA.

NEUTRON MULTIPLICITY DISTRIBUTION IN FAST NEUTRON-INDUCED FISSION

J. FREHAUT
Centre d'Etudes de Bruyères-le-Châtel
Service de Physique et Techniques Nucléaires
B.P. 12 - 91680 Bruyères-le-Châtel

INTRODUCTION

Although $\bar{\nu}_p$, the average number of prompt neutrons emitted per fission, has been measured for a large number of isotopes over a wide range of incident neutron energies, the information on multiplicity distributions remains scarce. This is because multiplicity distribution measurements require higher statistics and favourable experimental conditions to minimize the related corrections. These conditions are more generally fulfilled for spontaneous and thermal fission.

First of all, a high efficiency neutron detector is needed. The large Gd-loaded liquid scintillator with a typical efficiency of 80 to 85 % is the adequate detector [1].

The counterpart of a high efficiency for fission neutrons is also a high efficiency for incident neutrons scattered by the fission chamber or passing through the shielding. This background neutron component increases with incident neutron energy and flux. This component can be accurately measured and subtracted from the experimental data, but the resulting corrected multiplicity distributions present spurious oscillations increasing with the background rate. The oscillations could be in principle removed using the a priori information we have on the smoothness of the distributions, but the corresponding mathematical formalism remains to be developed.

The only published experimental data for neutron multiplicity distributions in fast neutron-induced fission have been obtained in our laboratory [2] and concern our early measurements on ^{235}U, ^{238}U and ^{239}Pu in the incident neutron energy range between 1 and 15 MeV.

The background was relatively low but the measurements lenghty. Our subsequent measurements in the same energy range for ^{232}Th, ^{237}Np, ^{240}Pu and ^{241}Pu were made with a more intense incident neutron source, but only the variance of the distributions could be extracted from the data.

FITS TO THE MULTIPLICITY DISTRIBUTIONS

A polynonial fit to our experimental data [2] for ^{235}U, ^{238}U, and ^{239}Pu has been made recently by Zucker and Holden [3]. The fits provide the dis-

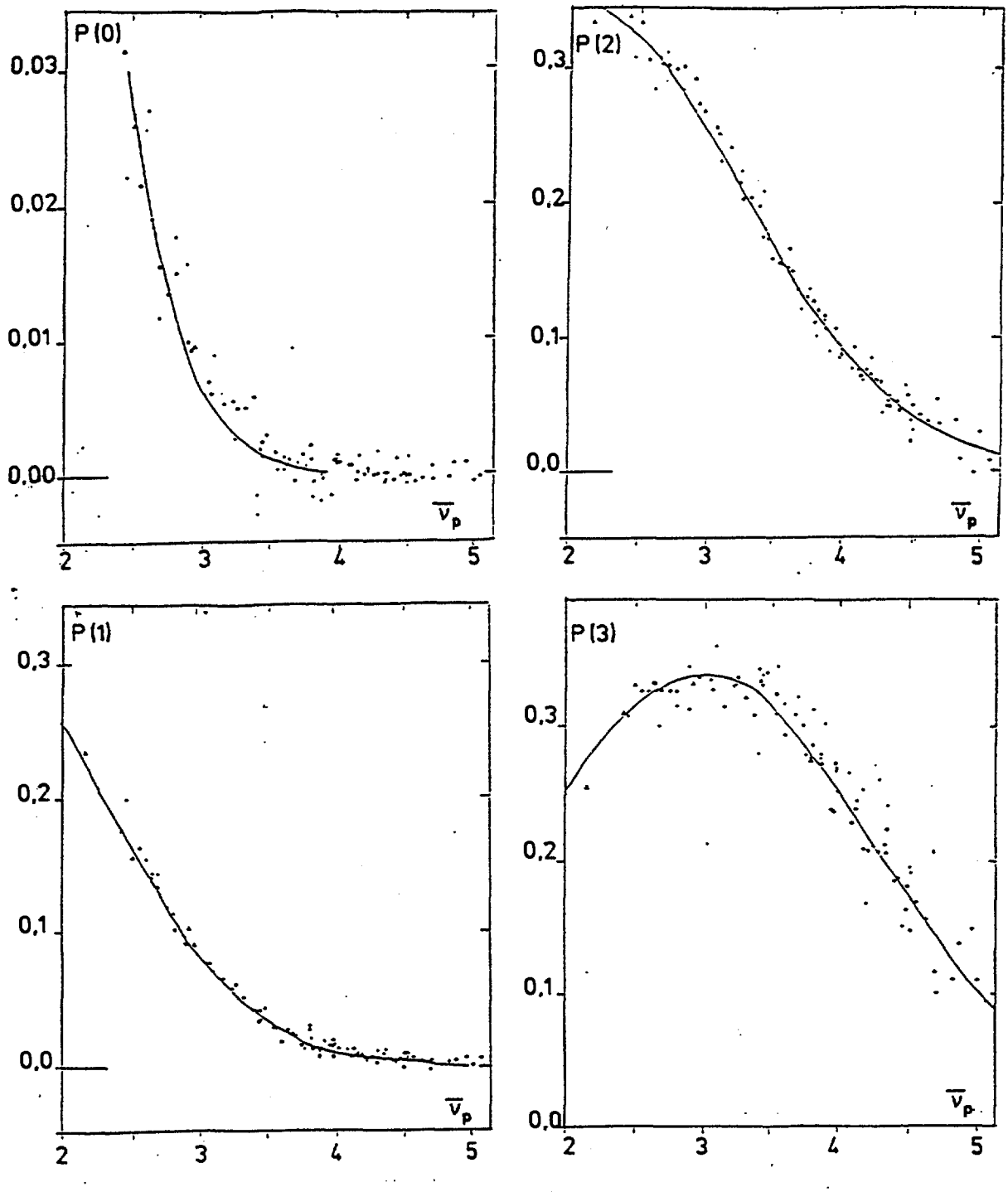

Fig. 1 : Gaussian fit to experimental P (ν) data as a function of $\bar{\nu}_p$ for ν = 0, 1, 2 and 3.

tributions P (ν) and the average neutron number $\bar{\nu}_p$ as a function of incident neutron energy for each nucleus.

We have pointed out in [2] that, within the uncertainties, the P (ν) distributions for the three nuclei were independent of the fissioning nucleus and only related to the average value $\bar{\nu}_p$ of neutrons emitted per fission. We have fitted the data using gaussian distributions :

$$P(\nu) = \frac{K}{\sigma\sqrt{2\pi}} \quad e^{-\frac{1}{2}\left(\frac{\bar{\nu}_p - \nu}{\sigma}\right)^2}$$

where K and σ are considered as adjustable parameters. The results are plotted in figs. 1 and 2, and the set of parameters is given in table I.

Table I : σ et K parameters fitting the experimental P (ν) distributions as a function of $\bar{\nu}_p$.

ν	0	1	2	3	4	5	6	> 7
σ	0.94	1.13	1.22	1.295	1.16	1.222	1.226	1.235
K	2.827	1.073	1.075	1.095	0.953	0.958	1.048	1.000

We believe than these fits of the P (ν) distributions can be used for all the Uranium and Plutonium isotopes. They are also probably valid for ^{237}Np and Americium isotopes. They are not valid for Thorium isotopes. This statement comes out from an analysis of our complete experimental data set and is supported by the analysis of the distribution variances presented in the next paragraph.

ENERGY DEPENDENCE OF P (ν) DISTRIBUTION VARIANCES

The variance σ^2 of the P (ν) distributions for ^{232} Th, ^{235}U and ^{237}Np [4] is plotted as a function of the incident neutron energy in fig 3. Below the second chance fission threshold, σ^2 is a linear function of the excitation energy of the fissioning nucleus. Since in the second chance fission reaction a part of the incident energy is taken away by the neutron emitted prior to fission, the fissioning nucleus has less excitation. The plateaus appearing around 6-8 MeV in fig. 3 are thus understandable.

Since $\bar{\nu}_p$ is also a linear function of the neutron incident energy, the variance σ^2 is a linear function of $\bar{\nu}_p$ below the second chance fission threshold. The corresponding data are plotted in fig. 4 for all the isotopes we have investigated. Within the uncertainties (spread of data points), the data for all isotopes but ^{232}Th are represented by a single line of equation $\sigma^2 = 0.21\ \bar{\nu}_p + 0.75$.

The variances for ^{232}Th are about 0.1 below this line, the difference between the two sets appearing clearly in the region $\bar{\nu}_p \gtrsim 2.4$. The line of equation $\sigma^2 = 0.17\ \bar{\nu}_p + 0.75$ drawn through the Th data results from the semi-theoretical analysis presented below.

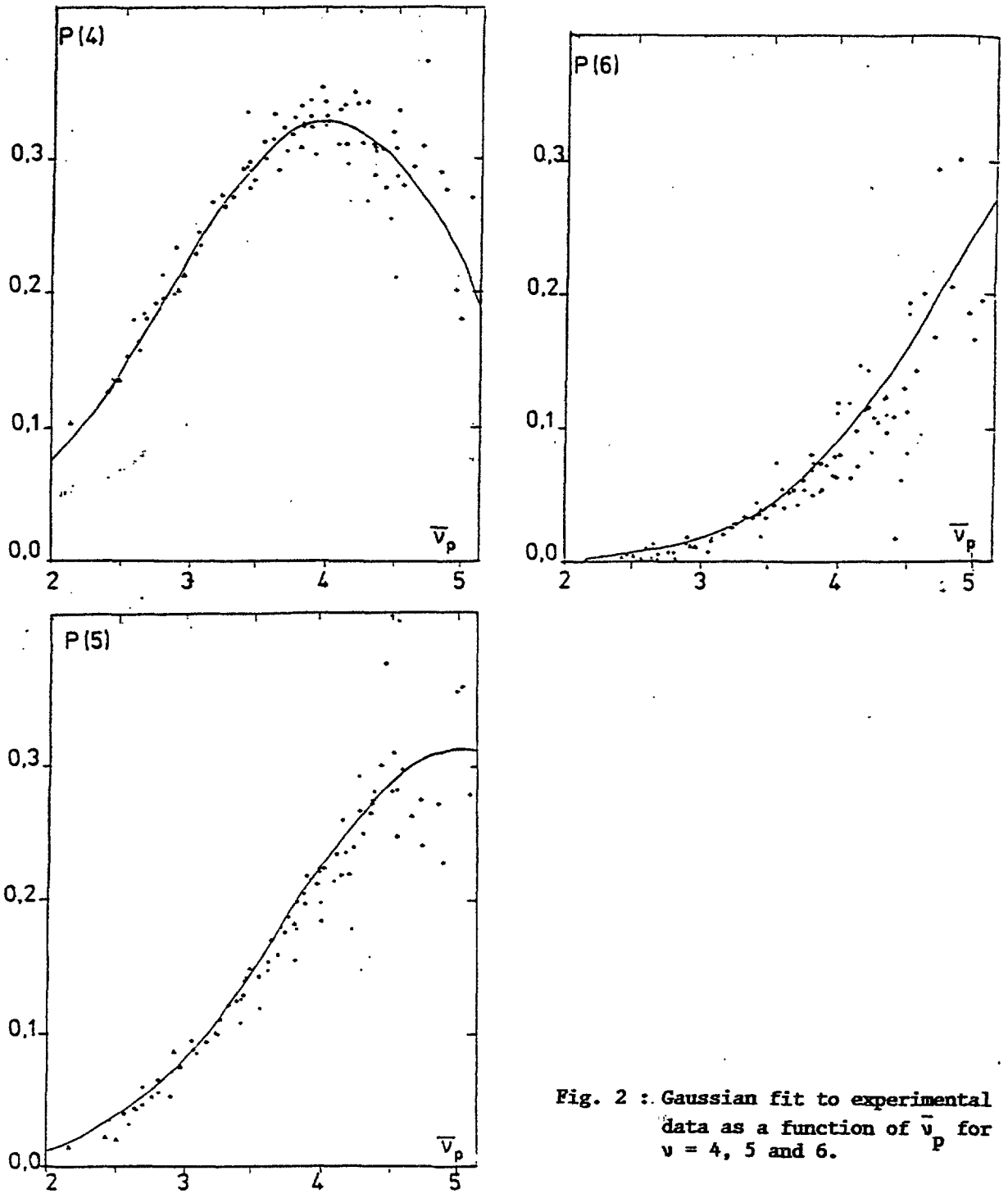

Fig. 2 : Gaussian fit to experimental data as a function of $\bar{\nu}_p$ for ν = 4, 5 and 6.

PHYSICS OF FISSION NEUTRON VARIANCES

Three main processes can contribute to the variance of the P (ν) distributions :

- the excitation energy distribution,
- the neutron kinetic energy distribution,
- the neutron - gamma competition.

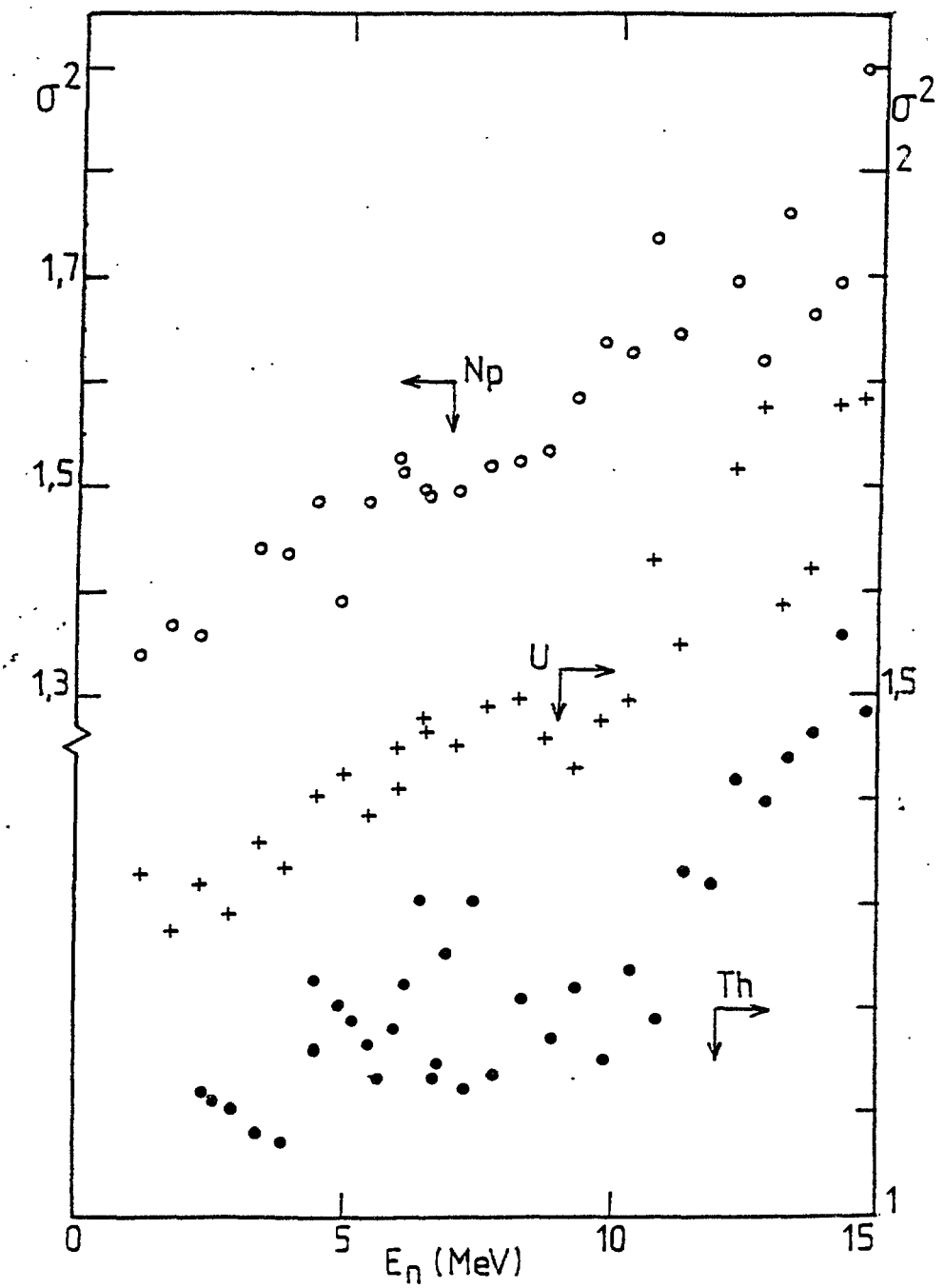

Fig. 3 : Energy dependence of the variance of the P (ν) distributions for ^{232}Th, ^{235}U and ^{237}Np neutron induced fission.

We will evaluate each component and show how the variance behaviour can be accounted for.

- **Excitation energy distribution**

We assume that the total fragment kinetic energy probability distribution $P_k(E_k)$, with its variance σ_k^2, is equivalent to the total excitation energy probability distribution. We assume furthermore that $\bar{\nu}$ is a linear

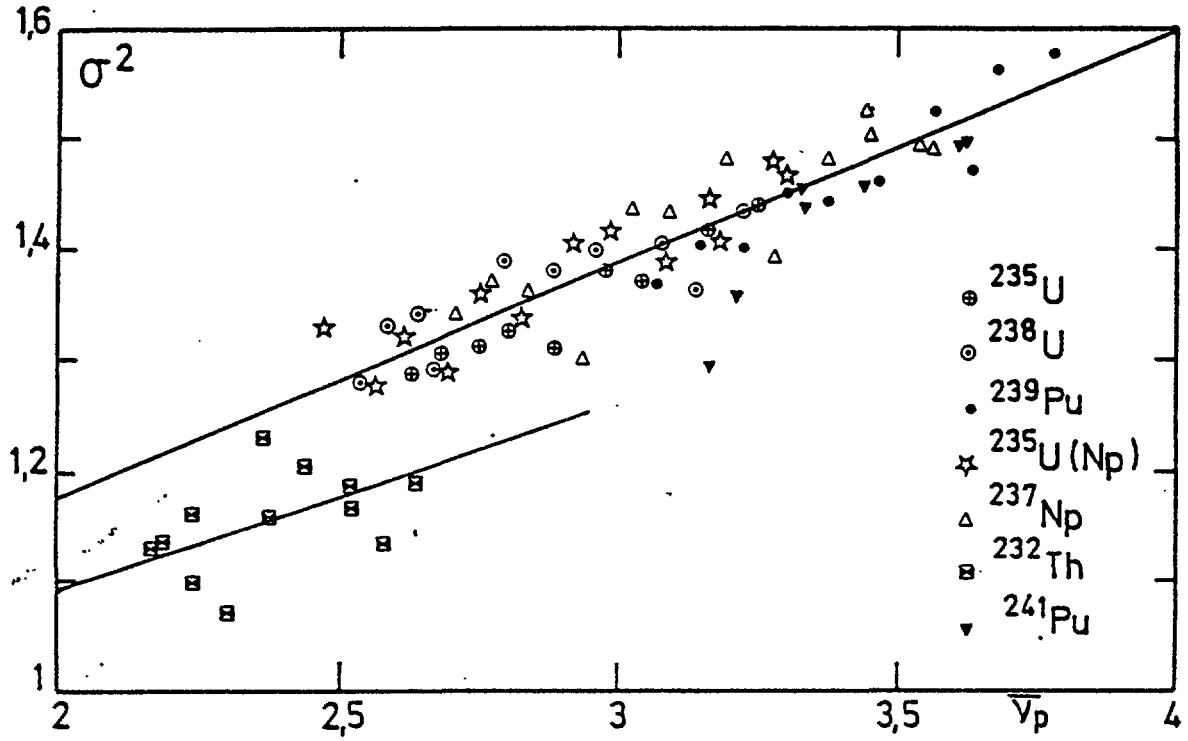

Fig. 4 : Variance of the P (ν) distributions as a function of $\bar{\nu}_p$.

The upper line of equation $\sigma^2 = 0.21\ \bar{\nu}_p + 0.75$ is a fit to all experimental data but ^{232}Th.

The lower line of equation $\sigma^2 = 0.17\ \bar{\nu}_p + 0.75$ represents the ^{232}Th data and is derived from a calculation presented in the text.

function of E_k [5] as well as the variance of the corresponding distribution (ν, E_k) :

$$\bar{\nu}\ (E_k) = a\ E_k + b$$

$$\sigma^2_\nu\ (E_k) = c\ E_k + d$$

The observed P (ν) distribution is :

$$P\ (\nu) = \int_{E_k} \mathcal{P}(\nu, E_k)\ P_k(E_k)\ dE_k$$

It can be shown straightforwardly that :

$$\bar{\nu}_p = \Sigma\ \nu\ P\ (\nu) = \bar{\nu}\ (\bar{E}_k) = a\ \bar{E}_k + b$$

The variance of the P (ν) distribution is :

$$\sigma^2_\nu = \langle\ \nu^2\ \rangle - \bar{\nu}_p^{\,2} = \int_{E_k} P_k(E_k)\ dE_k \sum_\nu\ \nu^2 \mathcal{P}(\nu, E_k) - \bar{\nu}^2(\bar{E}_k)$$

$$= \sigma_\nu^2 (\bar{E}_k) + \int_{E_k} P_k (E_k)\, d E_k \left[\bar{\nu}^2 (E_k) - \bar{\nu}^2 (\bar{E}_k) \right]$$

$$= \sigma_\nu^2 (\bar{E}_k) + a^2 \int_{E_k} P_k (E_k)\, dE_k \, (E_k^2 - \bar{E}_k^2)$$

$$\boxed{\sigma_\nu^2 = \sigma_\nu^2 (\bar{E}_k) + a^2 \sigma_k^2}$$

The term $a^2 \sigma_k^2$ is the contribution to the variance of the excitation energy distribution, whereas $\sigma_\nu^2 (\bar{E}_k)$ contains the other contributions.

$a^{-1} = \frac{dE_k}{d\nu}$ has been experimentally determined [5] to be 13 MeV/neutron for ^{252}Cf. We will assume this value to be valid also for other nuclei.

• **Neutron kinetic energy distribution**

Assuming a Maxwell law for the energy distribution of the fission neutrons

$$P_1 (E) = \frac{2 \sqrt{E}}{\sqrt{\pi}\, T^{3/2}} \exp - \left(\frac{E}{T}\right)$$

with an average energy $\bar{E}_1 = \frac{3}{2} T$ and a variance $\sigma_1^2 = \frac{2}{3} \bar{E}_1^2$, the spectrum for n neutrons emitted is :

$$P_n(E) = \frac{E^{\frac{3}{2} n - 1} \exp -(E/T)}{T^{\frac{3}{2} n} \, \Gamma(\frac{3}{2} n)}$$

with an average energy $\bar{E}_n = n \bar{E}_1$ and a variance $\sigma_n^2 = n \sigma_1^2$

The spectrum corresponding to a distribution D(n) of neutrons, with a variance σ_ν^2 and an average value $\bar{\nu}_p$ is :

$$\mathcal{P}(E) = \sum_n D(n)\, P_n (E)$$

The average energy of the spectrum is $\bar{E}_D = \bar{\nu}_p \bar{E}_1$ and the variance is :

$$\sigma_D^2 = \sum_n D_n \int_E E^2 P_n(E)\, dE - \bar{E}_D^2$$

The integral is equal to $\sigma_n^2 + \bar{E}_n^2$

$$\sigma_D^2 = \sum_n D_n \left(\frac{2}{3} n \bar{E}_1^2 + n^2 \bar{E}_1^2\right) - \bar{\nu}_p^2 \bar{E}_1^2$$

$$\boxed{\sigma_D^2 = \bar{E}_1^2 \left(\frac{2}{3} \bar{\nu}_p + \sigma_\nu^2\right)}$$

The contribution to σ_ν^2 is $\left(\frac{\partial \nu}{\partial E}\right)^2 \sigma_D^2$

$\left(\frac{\partial \nu}{\partial E}\right)^{-1}$ is the energy necessary to emit a fission neutron, i.e. the sum of the binding energy and the center of mass kinetic energy. We will use the value of 6.7 MeV derived by Terrell [6].

• **Neutron-gamma competition**

The competition between gamma-ray and neutron emission introduces an increase of the neutron variance equal to the variance σ_γ^2 of the total gamma energy spectrum as shown in a separate paper [7].

The σ_γ^2 variances have been derived as a function of $\bar{\nu}_p$ in ref. [7]. The corresponding data are :

* from experimental data

- ^{235}U : $\sigma_\gamma^2 = 3.61\ \bar{\nu}_p + 5.12$ $(MeV)^2$
- ^{237}Np : $\sigma_\gamma^2 = 3.37\ \bar{\nu}_p + 3.78$ $(MeV)^2$
- ^{232}Th : $\sigma_\gamma^2 = 2.44\ \bar{\nu}_p + 6.11$ $(MeV)^2$
- ^{252}Cf : $\sigma_\nu^2 = 13\ MeV^2$

* from evaluated data

$\sigma_\gamma^2 = 2\ \beta\ \bar{E}_\gamma$, where β is the single γ-quantum average energy and $\bar{E}_\gamma$ the total average γ-ray energy :

- ^{233}U : $\bar{E}_\gamma = 0.92\ \bar{\nu}_p + 4.4$ (MeV)

  $\beta = 0.145\ \bar{\nu}_p + 0.7$ (MeV)
- ^{239}Pu : $\bar{E}_\gamma = 0.82\ \bar{\nu}_p + 4.4$ (MeV)

  $\beta = 0.117\ \bar{\nu}_p + 0.62$ (MeV)

The contribution to σ_ν^2 is $(\frac{\partial \nu}{\partial E})^2 \sigma_\gamma^2$ where $(\frac{\partial \nu}{\partial E})^{-1}$ = 6.7 MeV as defined previously.

• variance of P (ν) distributions

Summing up the different contributions and solving for σ_ν^2 gives the relation :

$$\sigma_\nu^2 = \frac{(\frac{dE}{d\nu})^2 a^2 \sigma_k^2 + \sigma_\gamma^2 + \frac{2}{3} \bar{\nu}_p \bar{E}_1^2}{(\frac{dE}{d\nu})^2 - \bar{E}_1^2}$$

Following Terrell [6] the average neutron energy can be expressed as a function of $\bar{\nu}_p$:

$$\bar{E}_1 = 0.653\sqrt{\bar{\nu}_p + 1} + 0.74 \quad \text{(MeV)}$$

Taking the σ_k^2 values of ref. [8], σ_ν^2 has been evaluated in table II for the thermal fission of ^{233}U, ^{235}U and ^{239}Pu as well as for the spontaneous fission of ^{252}Cf. The calculated values compare quite well with the experimental data. The contribution to σ_ν^2 of the excitation energy distribution is only on the order of 60 %.

Table II : Comparison of σ_ν^2 experimental data with calculated values and evaluation from a fit to experimental data of fig. 4

	Thermal Fission			^{252}Cf
	^{233}U	^{235}U	^{239}Pu	
σ_ν^2, cal.	1.14	1.20	1.40	1.53
σ_ν^2, exp.	1.191	1.225	1.348	1.60
$\sigma_\nu^2 = 0.21\ \bar{\nu}_p + 0.75$	1.25	1.26	1.36	1.54

• $\bar{\nu}_p$ dependence of σ_ν^2 variances

As the excitation energy increases, the variance σ_k^2 of the fragment kinetic energy distribution remains approximately constant. If we assume also that $\frac{dE_k}{d\nu}$ and $\frac{dE}{d\nu}$ remain constant, it turns out that the increase of σ_ν^2 is only related to the neutron-gamma competition and the energy spectrum of the emitted neutron.

By derivation of σ_ν^2 relative to $\bar{\nu}_p$ we obtain :

$$\frac{\partial(\sigma_\nu^2)}{\partial \bar{\nu}_p} = \frac{\frac{\partial(\sigma_\gamma^2)}{\partial \bar{\nu}_p} + \frac{2}{3}\bar{E}_1^2 + \frac{0.653\,\bar{E}_1}{\sqrt{\bar{\nu}_p + 1}}\left(\frac{2}{3}\bar{\nu}_p + \sigma_\nu^2\right)}{\left(\frac{dE}{d\nu}\right)^2 - \bar{E}_1^2}$$

The first term corresponds to the neutron-gamma competition effect, and the sum of the other terms to the neutron energy spectrum effect. They are respectively quoted as $\Delta\gamma$ and $\Delta\nu$ in Table III, which presents as a function of $\bar{\nu}_p$ the calculated slopes $\frac{\partial(\sigma_\nu^2)}{\partial \bar{\nu}_p}$ for ^{235}U, ^{237}Np and ^{232}Th.

Table III : Slope at different $\bar{\nu}_p$ values of the $\bar{\nu}_p$ dependence of the σ_ν^2 variance.

		^{235}U		^{237}Np		^{232}Th	
$\bar{\nu}_p$	$\Delta\nu$	$\Delta\gamma$	$\Delta\nu + \Delta\gamma$	$\Delta\gamma$	$\Delta\nu + \Delta\gamma$	$\Delta\gamma$	$\Delta\nu + \Delta\gamma$
2	.098	.091	.189	.085	.183	.061	.159
2.5	.111	.091	.202	.085	.197	.061	.172
3	.124	.092	.216	.086	.210	.062	.186
3.5	.137	.092	.229	.086	.223	.062	.199
4	.150	.093	.243	.087	.237	.063	.213

In the region of interest corresponding to $2.5 \lesssim \bar{\nu}_p < 3.7$ in fig. 4, the slopes calculated for ^{235}U and ^{237}Np are very near the value of 0.21 fitted to the experimental data. The slope calculated is nearly a linear function of $\bar{\nu}_p$ and suggests a quadratic dependence of σ_ν^2 with $\bar{\nu}_p$. Nevertheless the divergence between the quadratic and the fitted linear shapes is very small and far below the experimental uncertainties. The neutron-gamma competition represents about 40 % of the slope.

In the case of ^{232}Th the neutron-gamma competition is reduced and the calculated slope is lower. In the region of interest, $2 \lesssim \bar{\nu}_p \lesssim 2.7$, one obtains a slope of about 0.17. Using the same constant value of 0.75 as for other nuclei, one obtains the line of equation $\sigma^2_\nu = 0.17\ \bar{\nu}_p + 0.75$ drawn in fig. 4 which seems to be a good representation of the data.

CONCLUSION

The magnitude of the fission neutron multiplicity distribution variances can be fairly well calculated on the basis of simple physical arguments.

The main contributions to be taken into account are :

- the distribution of excitation energy
- the energy spectrum of the emitted neutrons
- the neutron-gamma competition

The energy dependence of the variances is also quite well reproduced. In particular the difference observed between ^{232}Th and other investigated nuclei is due to a large extent to a difference in the neutron-gamma competition.

The plateaus appearing in fig. 3 above the second chance fission threshold can be quantitatively interpreted as a decrease of the neutron-gamma competition component in the second chance fission [7]. The other components are not appreciably modified. In particular, the variance of the pre-fission neutron spectrum is about the same as the variance of a fission neutron spectrum, so that the part of σ^2_ν corresponding to the neutron total energy spectrum is only sensitive to the total number of neutrons emitted, including the pre-fission neutron.

REFERENCES

1 - J. FREHAUT, Nucl. Inst. Meth. 135 (1976) 511.

2 - M. SOLEILHAC, J. FREHAUT, J. GAURIAU
J. Nucl. Energy 23 (257) 1969.

3 - M. ZUCKER and N. HOLDEN, BNL 38491 (1987).

4 - J. FREHAUT, A. BERTIN, R. BOIS, Proc. Int. Conf. on Nuclear Data for Science and Technology, Antwerp, 1982, P. 78.

[5] H. NIFENECKER et al. Proc. Conf. on Physics and Chemistry of Fission, Rochester, 1973, Vol II, p. 117.

[6] J. TERRELL, Phys. Rev. 113 (1959) 527.

[7] J. FREHAUT, "Neutron-gamma competition in fission", these proceedings

[8] J. P. Unik et al. Proc. Conf. on Physics and Chemistry of Fission, Rochester, 1973, Vol II, p. 19.

NEUTRON MULTIPLICITY OF U-238 SPONTANEOUS FISSION

Huang Shengnian, Chen Jinggui and Han Hongyin
Institute of Atomic Energy
Beijing, China

INTRODUCTION

The spontaneous fission process of U-238 has been widely investigated since its discovery in 1940. Up to now, however, due to the long half-life some aspects remain to be studied in more details. The neutron multiplicity of spontaneous fission of even-even plutonium and curium nuclides have been measured by several groups[1]. The P(ν) distribution obtained could be described by Gaussian curves approximately. It turns out that the widths of these Gaussian curves are almost the same for all even-even plutonium and curium nuclides[2]. It is interesting to see what would be the width of the prompt neutron number distribution for U-238 spontaneous fission. In 1971 Conde et al.[3] measured the $\bar{\nu}$ of U-236 and U-238 spontaneous fission, but in their paper no P(ν) data was given. In present work the P(ν) distribution of U-238 spontaneous fission was measured by using a large liquid scintillation neutron detector.

EXPERIMENTAL EQUIPMENT

1. The fission chamber

Since the U-238 spontaneous fission decay constant is very small, in order to get sufficient counting rate we have to use a multiplate ionization chamber to detect the fission fragments. The size of the plates was ϕ45 mm, source spot ϕ35 mm. The thickness of the uranium layers was about 1 mg/cm^2. The number of the plates was 100. The distance between the electrodes was 3.5 mm. The total length of the chamber is 38 cm. The chamber was filled with CH_4 gas of 2.5 atm. The interference of the α pulses was eliminated by setting a suitable bias.

2. The liquid scintillator

The neutron detector is a liquid scintilllation tank with a central channel of ϕ65 mm. The diameter of the spherical tank is 600 mm. 118 liters of the scintillation solution were filled in the detector. Six photomultipliers were used to record the scintillation light. The output pulses from the anodes of all six photomultipliers were summed up. The fission chamber was put in the central channel of the detector. The neutron detection efficiency of the liquid scintillator η was determined through the standard $\bar{\nu}$ value of Pu-240 spontaneous fission($\bar{\nu}$ = 2.154). The value of $\eta = 0.691 \pm 0.011$ was obtained.

3. The electronics

The data acquisition system includes a coincidence circuit,a multievent analyzer and a multichannel pulse-height analyzer. The coincidence circuit will give an output signal only if both the pulses from the fission chamber and the neutron detector (i.e., the pulse induced by the prompt γ-rays and scattering of fission neutrons in the scintillator) come simultaneously. The resolution time of the coincidence was 100 ns. After each coincidence event a gate of 30 μs was opened immediately. For the background measurement after 100 μs the gate was opened once again. The neutron pulses passing through the gate were fed into the multievent analyzer (MEA). The amplitude of MEA output signal is proportional to the number of the pulses from the neutron detector coming during the 30 μs gate time. Finally the signals from the multievent analyzer were fed into and analyzed by the MCA.

MEASUREMENT

The life time of the fission spectrum neutrons in the scintillator was determined in a separate experiment. It was shown that more than

95 percent neutrons were captured during the period of 30 μs. This is the reason for selecting the gate length of 30 microseconds.

We used the $\bar{\nu}$ of Pu-240 as the standard to determine the efficiency η of the neutron detector. So during the experiment the Pu-240 fission and the U-238 fission were measured alternately. The counting rate of the U-238 fission chamber was about 0.3/min. The measurement lasted more than 200 hours, in which 160 hours were used for the U-238 fission. Altogether 3144 spontaneous fission events of U-238 were acummulated.

RESULT

The data were treated according to the routine method in $\bar{\nu}$ and P(ν) experiments. The background is low (only 0.066 pulses per gate). Some additional corrections were made, for example, the position effect arising from the length difference between two fission chambers.

The data were shown in Table 1. The finally obtained P(ν) distribution was listed in Table 2 and plotted in Figure 1. From the figure

Table 1. The data obtained from measurement

n	0	1	2	3	4	5	total
N_n	504	1206	1043	292	41	4	3144
N_n (background)	26353	17335	582	26	4	0	283300

Table 2. The P(ν) distribution of U-238 spontaneous fission

P(0)	P(1)	P(2)	P(3)	P(4)	P(5)	$\bar{\nu}$	$\langle\nu^2\rangle-\langle\nu\rangle^2$
0.048 ±0.011	0.232 ±0.030	0.479 ±0.033	0.202 ±0.029	0.033 ±0.016	0.006 ±0.006	1.96 ±0.05	0.808 ±0.148

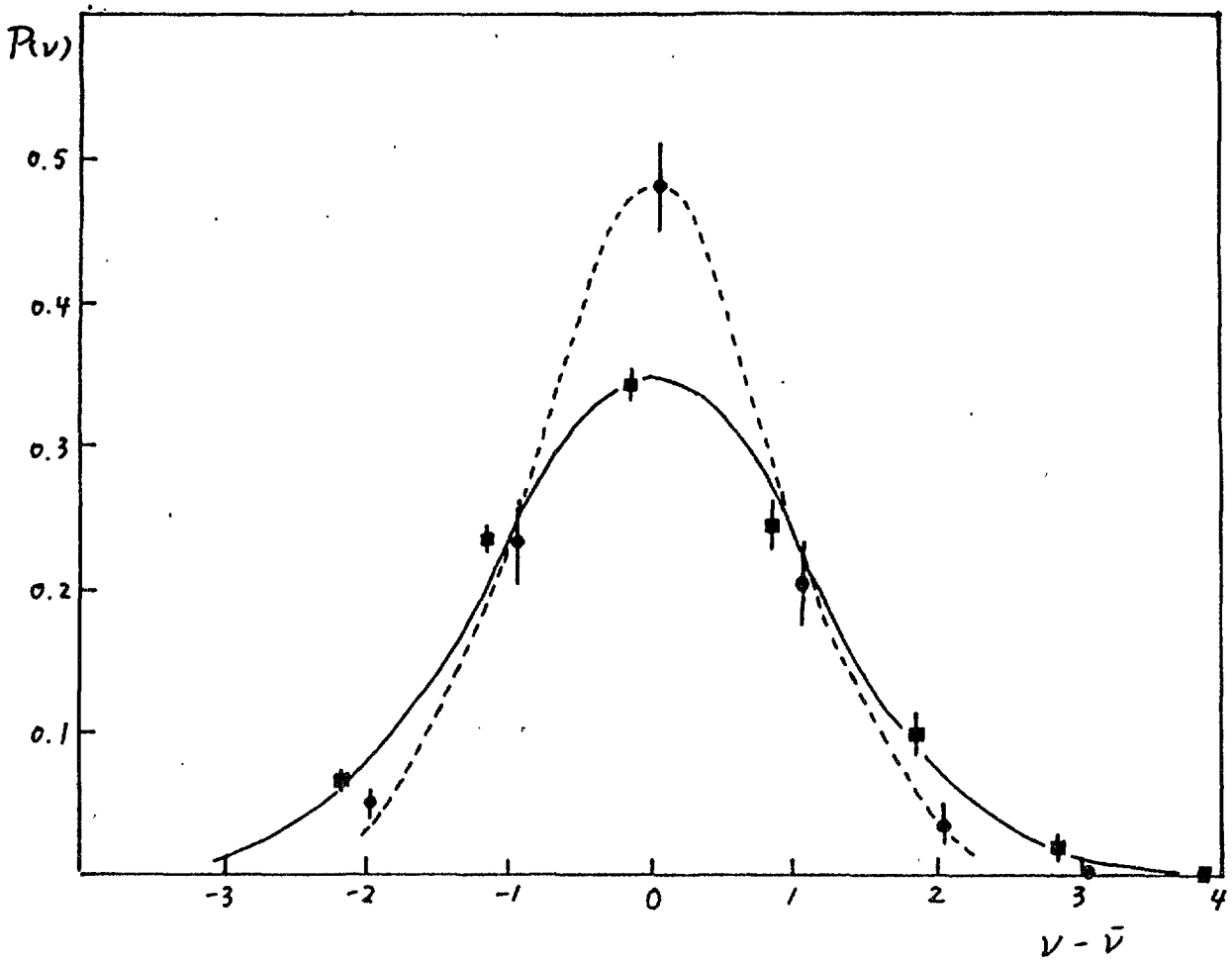

Fig.1 The P(ν) distribution of U-238 spontaneous fission compared with that of Pu-240

♦ Uranium-238; ♦ Plutonium-240.

Table 3. Popeko's result

P(0)	P(1)	P(2)	P(3)	P(4)	P(5)	$\bar{\nu}$	$\langle\nu^2\rangle-\langle\nu\rangle^2$
0.052 ±0.010	0.277 ±0.030	0.366 ±0.035	0.247 ±0.030	0.050 ±0.010	0.008 ±0.003	1.99	1.00 ±0.06

one can see that the experimental points of U-238 P(ν) can be fitted by a Gaussian curve. For comparison the Pu-240 P(ν) values were also shown in the same figure. Due to the poor statistics the uncertainty of the U-238 data is large. But still, one can conclude that the width of the U-238 P(ν) distribution is obviously narrower than that of Pu-240.

A value of $\sigma_\nu = 0.90 \pm 0.09$ was obtained for U-238 spontaneous fission while for Pu-240 and all other Pu and Cm isotopes the width is nearly the same arround 1.15.

DISCUSSION

We completed the above work in 1972 and the result was published in "Acta Physica Sinica",Vol.23,446(1974)(in Chinese). Two years latter, Popeko et al. gave their result on the same topic[4]. The P(ν) distribution of U-238 spontaneous fission given in their paper is similar in width with those of even-even Pu and Cm isotopes and differs from ours. Their numerical data are listed in Table 3.

In 1984, Holden[5] performed an evaluation on P(ν) distributions for various actinides. In his evaluation for U-238 spontaneous fission our data and Popeko's result were simply averaged. After analyzing the experimental details of Popeko's work, however, we found some noteworthy points. Actually, their P(ν) distribution was deduced from the data obtained in four separate runs. The neutron detection efficiency was different in different runs. The detector they used was a set of He-3 thermal neutron counters embeded in paraffin block. The overall efficiency varies from 0.216 to 0.383. Their last run,i.e. the one of best statistics, was performed without the coincidence with fission event. In this run they used a metallic uranium block instead of a fission chamber. In such case one can not obtain the full information of the neutron multiplicity. Among their first three runs,two of them were statistically insufficient for getting correct P(ν) values, in addition,the neutron detection efficiency was too low for these two runs. It seems that the third run is the most reliable one of their experiment.

Recently, we performed a simple calculation to deduce the P(ν) values from their row data set (Table 4). The results of first three runs were shown in Table 5. As can be seen, indeed,the first and second runs

Table 4 The original data of Popeko's experiment

Run	N	η	0	1	2	3	4	5
1	4750	0.216±0.006	3029	1400	294	27	0	0
2	8800	0.264±0.002	5113	2907	702	75	3	0
3	42682	0.383±0.002	18209	17522	5945	906	95	7
4	-----	0.264±0.002	-----	-----	20644	2391	163	16

Table 5 Neutron multiplicity deduced from Popeko's separate runs

Run	P(0)	P(1)	P(2)	P(3)	P(4)	P(5)	$\bar{\nu}$	$\langle\nu^2\rangle-\langle\nu\rangle^2$
1	0.112	0.324	0.000	0.564			2.016	1.34
2	0.116	0.207	0.350	0.257	0.070		1.96	1.21
3	0.051	0.251	0.434	0.204	0.040	0.020	1.99	0.999

can not give right distributions, and the result from third run is in good agreement with our data.

REFERENCES

1. See Manero F. and Konshin V.A., At.En.Rev.,10,637(1972).
2. Terrell J., Phys.Rev.,127,880(1962).
3. Conde H. et al., Jour.Nucl.Energy,25,331(1971).
4. Popeko A.G. et al., Soviet J.Nucl.Phys.,24,473(1976).
5. Holden N.E. et al.,IAEA Consultants' Meeting on "Nuclear Standard Reference Data", Nov.1984.

NEUTRON GAMMA COMPETITION IN FAST FISSION

J. FREHAUT
Centre d'Etudes de Bruyères-le-Châtel
Service de Physique et Techniques Nucléaires
B.P. 12 - 91680 Bruyères-le-Châtel

INTRODUCTION

The early analyses of fission fragment desexcitation were based on the statistical evaporation model and assumed that neutron emission was taking place whenever energetically possible. The residual energy after neutron emission was considered to appear as prompt gamma-rays leading to an average gamma energy $\bar{E}_\gamma$ released per fission of the order of 4 to 5 MeV [1]

Since it was experimentally established that $\bar{E}_\gamma$ was rather of the order of 7 to 8 MeV, the competition between gamma-ray and neutron emission in the last stage of fragment desexcitation has been put forward to explain the difference.

More recent data reviewed by Nifenecker [2] showed that for individual fragments $\bar{E}_\gamma$ as well as $\bar{n}_\gamma$, the number of gamma quanta, present the same saw-tooth shape as $\bar{\nu}_p$ when plotted as a function of fragment mass. From these data a linear relation between $\bar{E}_\gamma$ and $\bar{\nu}_p$ was derived, in which the constant term was 4 MeV, i.e. the statistical prediction for $\bar{E}_\gamma$. The increase of $\bar{E}_\gamma$ and $\bar{n}$ with $\bar{\nu}_p$ was thus interpreted as an increase of the average fragment angular momentum with excitation energy [2].

In the present paper we analyse the data we have obtained on the distribution of the gamma-ray energy per fission, as well as on the average energy $\bar{E}_\gamma$, for the neutron induced fission of several isotopes, in the energy range up to 15 MeV. The data on $\bar{E}_\gamma$ have already been published [3].

EXCITATION ENERGY DEPENDENCE OF $\bar{E}_\gamma$

The measurement of $\bar{E}_\gamma$ was made at the same time as $\bar{\nu}_p$, using the large Gd-loaded liquid scintillator technique [4].

$\bar{E}_\gamma$ is proportional to the area of the prompt pulse detected in the scintillator in coincidence with a fission fragment. A small correction ($\lesssim$ 5 %) is to be applied to account for the contribution of the energy released by the slowing down of the emitted fission neutron. Each fission chamber used contained a ^{252}Cf deposit in order to calibrate the $\bar{\nu}_p$ and $\bar{E}_\gamma$ data. Furthermore the detector has a high detection efficiency and the statistics was large enough to obtain information on the total gamma-ray spectrum.

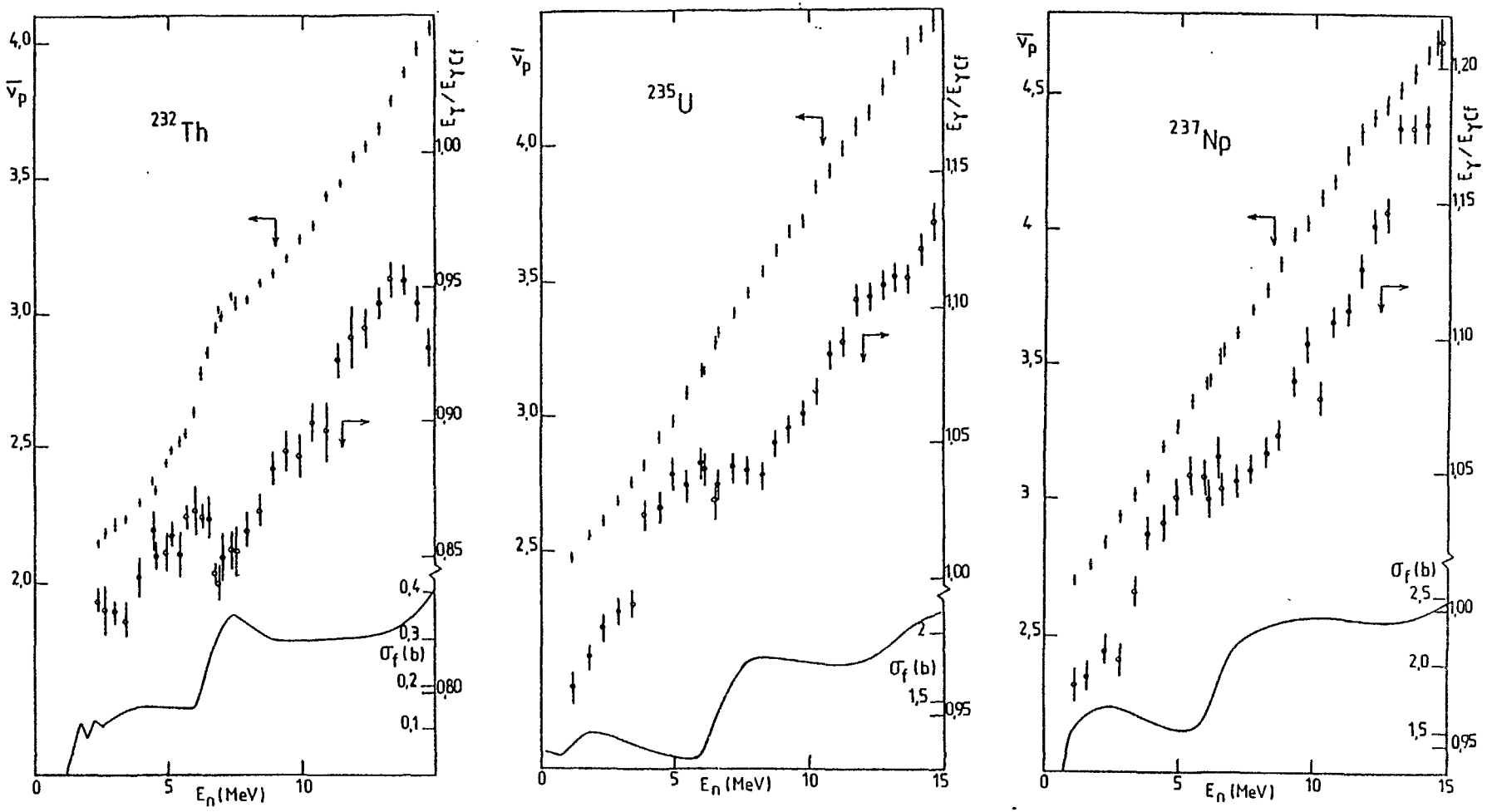

Fig. 1 : $\bar{\nu}_p$, $\bar{E}_\gamma$ and σ_f as a function of incident energy for the neutron induced fission of ^{232}Th, ^{235}U and ^{237}Np. $\bar{E}_\gamma$ is given relative to the corresponding $\bar{E}_{\gamma Cf}$ value for the ^{252}Cf spontaneous fission.

The $\bar{E}_\gamma$ data obtained for ^{232}Th, ^{235}U and ^{237}Np [3] are plotted in fig.1 as a function of the incident neutron energy E_n. Below the second chance fission threshold $\bar{E}_\gamma$ is proportionnal to E_n. In the (n,n'f) reaction, a neutron is emitted prior to fission, without competition with gamma emission. The resulting nucleus will undergo fission with less excitation energy and therefore $\bar{E}_\gamma$ will be lower. The plateaus appearing in fig.1 above the second chance fission threshold can thus be qualitatively understood. A similar behaviour is observed just above the third chance fission threshold.

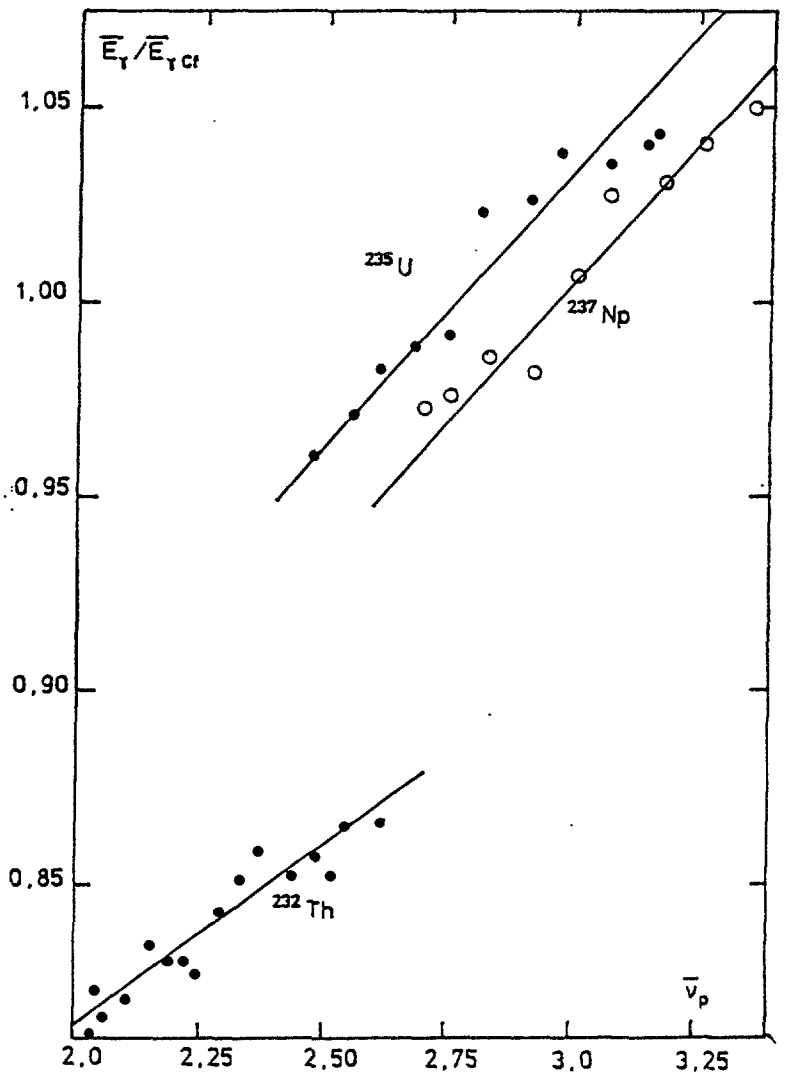

Fig. 2 : $\bar{E}_\gamma$ as a function of $\bar{\nu}_p$ for ^{232}Th, ^{235}U, ^{237}Np. $\bar{E}_\gamma$ is given relative to $\bar{E}_{\gamma Cf}$, the gamma energy released in the ^{252}Cf spontaneous fission.

Since $\bar{\nu}_p$ is also a linear function of incident neutron energy below the second chance fission threshold, we can derive in this energy range a linear relation between $\bar{E}_\gamma$ and $\bar{\nu}_p$. The corresponding data are plotted in fig.2.

The fits to the data give :

$$^{235}U : \frac{\bar{E}_\gamma}{\bar{E}_{\gamma Cf}} = (0.139 \pm 0.010)\ \bar{\nu}_p + (0.619 \pm 0.030)$$

$$^{237}Np : \frac{\bar{E}_\gamma}{\bar{E}_{\gamma Cf}} = (0.1275 \pm 0.011)\ \bar{\nu}_p + (0.623 \pm 0.028)$$

$$^{232}Th : \frac{\bar{E}_\gamma}{\bar{E}_{\gamma Cf}} = (0.090 \pm 0.010)\ \bar{\nu}_p + (0.635 \pm 0.030)$$

The constant term is practically the same for the three nuclei and equal to 4.4 MeV if we assume a value of 7 MeV for $\bar{E}_{\gamma Cf}$. It is the value predicted by the statistical theory, assuming no neutron-gamma competition [1] . Here again, the linear dependence of $\bar{E}_\gamma$ with $\bar{\nu}_p$ can be interpreted in terms of a linear increase of the average spin of the fragments with energy. However, as we will see later, more information can be derived from the experimental data, leading to a different interpretation.

We have also obtained $\bar{E}_\gamma$ data for ^{241}Pu, but with a poor accuracy (fig.3). Assuming the constant term to be 0.63 we have derived :

$$\frac{\bar{E}_\gamma}{\bar{E}_{\gamma Cf}} = (0.112 \pm 0.012)\ \bar{\nu}_p + 0.63$$

From the experimental data on $\bar{\nu}_p$ and $\bar{E}_\gamma$ we can derive the relative contribution of first and second chance fission. For the first chance fission the measured quantities $\bar{E}_{\gamma 1}$ and $\bar{\nu}_1$ are related by the relation $\bar{E}_{\gamma 1} = a\ \bar{\nu}_1 + b$ as discussed previously. In the second chance fission the gamma ray energy is $\bar{E}_{\gamma 2}$ and the number of emitted neutrons is $\bar{\nu}_2 + 1$, $\bar{\nu}_2$ being the real number of fission neutrons. If α is the proportion of second chance fission, then the quantities measured are :

$$\bar{\nu}_m = (1 - \alpha)\ \bar{\nu}_1 + \alpha\ (1 + \bar{\nu}_2)$$

$$\bar{E}_{\gamma m} = (1 - \alpha)\ \bar{E}_{\gamma 1} + \alpha\ \bar{E}_{\gamma 2}$$

If we assume that the same relation holds for $\bar{E}_{\gamma 2}$ and $\bar{E}_{\gamma 1}$, i.e. that $\bar{E}_{\gamma 2} = a\ \bar{\nu}_2 + b$, then we obtain straightforwardly :

$$\alpha = \bar{\nu}_m - \frac{\bar{E}_{\gamma m} - b}{a}$$

Fig. 4 shows that realistic first and second chance fission cross sections can be derived below the third chance fission threshold for ^{235}U and ^{237}Np.

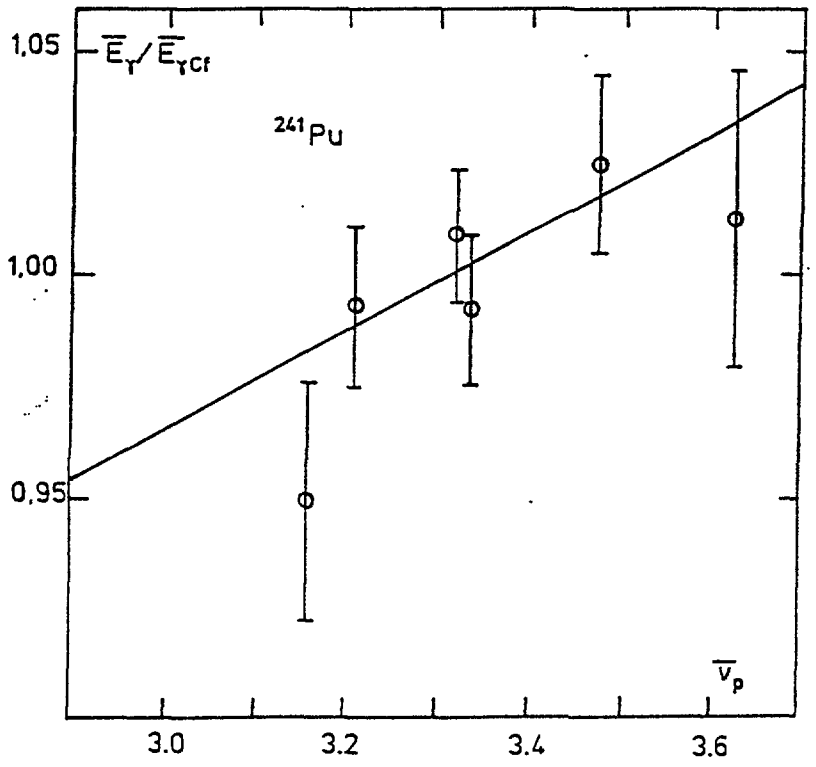

Fig. 3 : $\bar{E}_\gamma$, normalized to ^{252}Cf, as a function of $\bar{\nu}_p$ for ^{241}Pu.

In the case of ^{232}Th the situation is more complicated. The (n,2n) reaction is strongly competing with the (n,n'f) reaction. The emission of a second neutron is about 10 times more probable than fission. It seems that we observe an excess of gamma energy, which could result from the reaction (n,n'γf), with a cross section of the order of 100 mb.

FISSION GAMMA-RAY ENERGY SPECTRUM

The experimental spectra measured in the large liquid scintillator detector are quite broad (fig.5), but they were confirmed by a measurement of the total fission gamma-ray energy spectrum of ^{252}Cf made by J. Lachkar in our laboratory (1971, unpublished) using a large volume INa pit detector (fig.6).

Since the single quantum spectrum is also known, information about the distribution of the number of quanta can be obtained by comparing the two spectra.

The single quantum spectrum can be approximated by the relation :

$$P_1(E) = \frac{e^{-\frac{E}{\beta}}}{\beta}, \text{ where } \beta \text{ is the quantum average energy.}$$

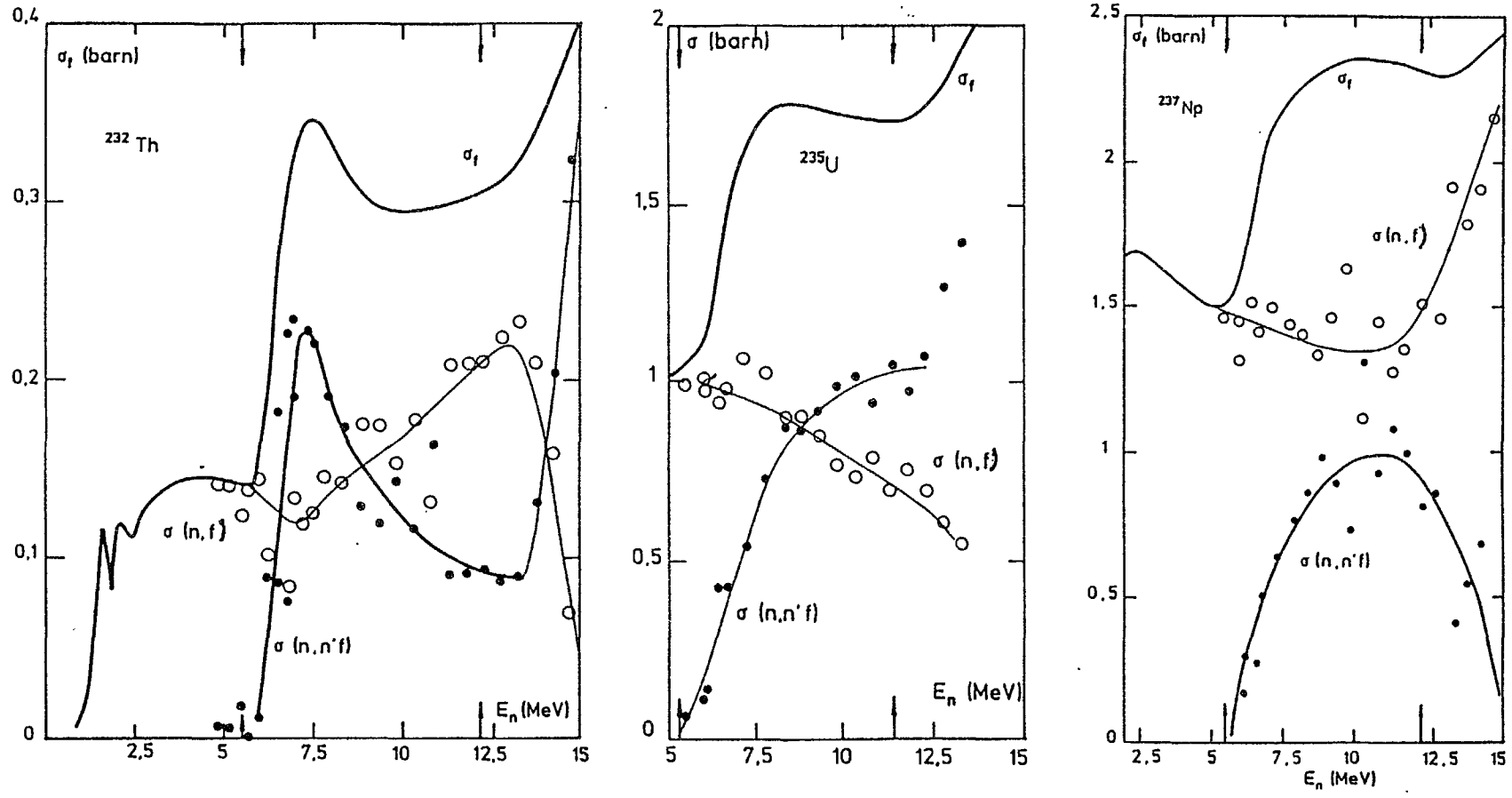

Fig. 4 : Relative contribution to σ_f of first and second chance fission deduced from $\bar{E}_\gamma$ and $\bar{\nu}_p$ measurements for ^{232}Th, ^{235}U and ^{237}Np. The arrows on energy scales indicate the second and third chance fission thresholds.

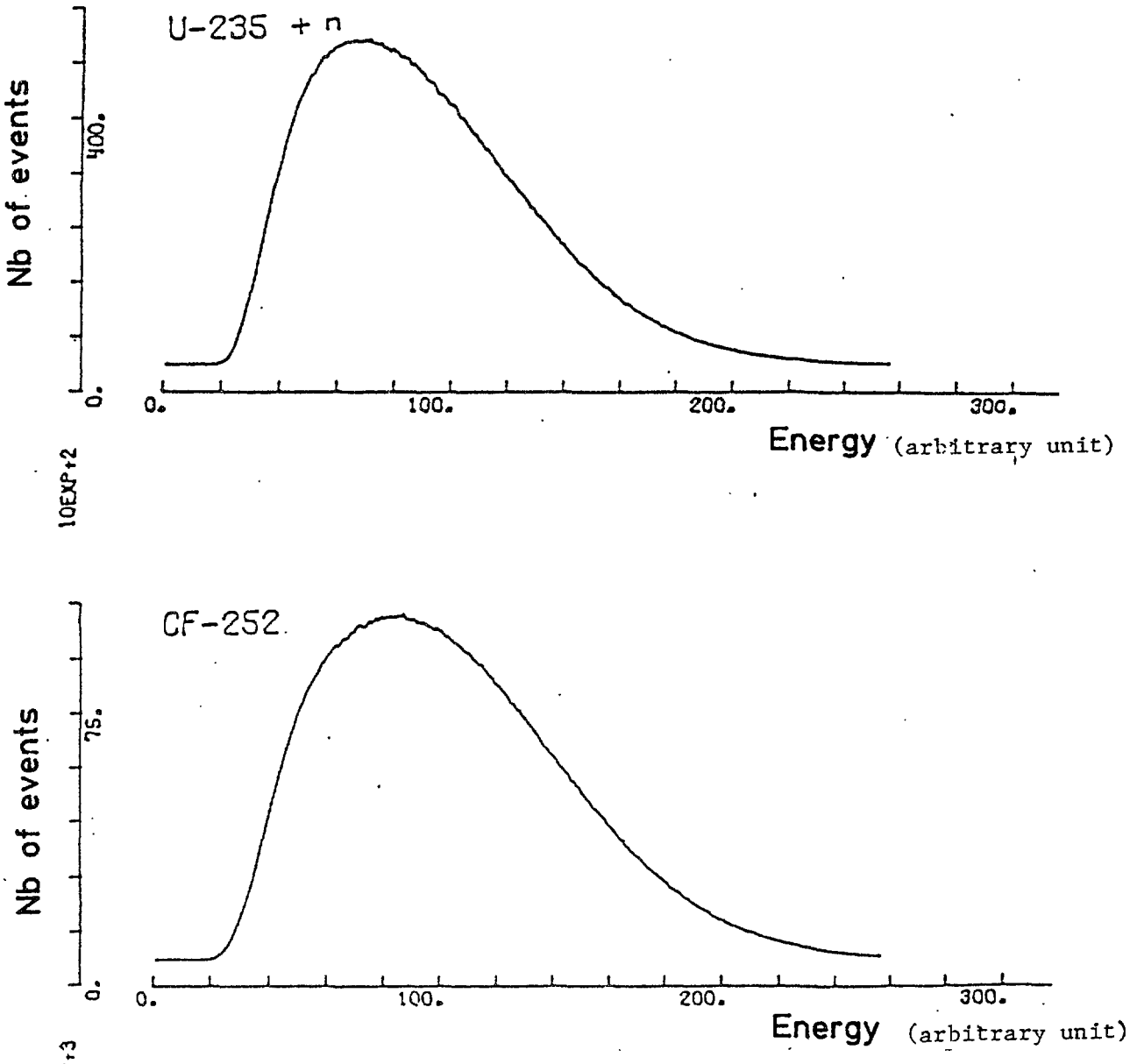

Fig. 5 : Experimental gamma ray spectra obtained with the large Gd-loaded liquid scintillator for the thermal fission of ^{235}U and the spontaneous fission of ^{252}Cf. The scales are relative and different for the two spectra.

When n quanta are emitted, the resulting spectrum is :

$$P_n(E) = \frac{E^{n-1}}{(n-1)!\ \beta^{n-1}}\ P_1(E)$$

with an average energy of $n\beta$.

For a distribution D(n) of the number of quanta the distribution is :

$$\mathcal{P}(E) = \sum_n D(n)\ P_n(E)$$

with an average number of quanta : $\bar{n} = \sum_n n\, D(n)$ and an average γ-ray energy per fission : $\bar{E}_\gamma = \bar{n}\beta$.

The experimental curve has been fitted assuming a gaussian shape for D(n) :

$$D(n) = \frac{1}{\sigma\sqrt{2\pi}}\, e^{-\frac{1}{2}\left(\frac{n-\bar{n}}{\sigma}\right)^2}$$

with $\bar{n}$, β and σ as free parameters.

The best fit (fig.6) is obtained for $\bar{n} = 7.4$, $\beta = 0.96$ and $\sigma = 2.6$, leading to $\bar{E}_\gamma = 7.1$ MeV, which compares very well with other experimental data [5].

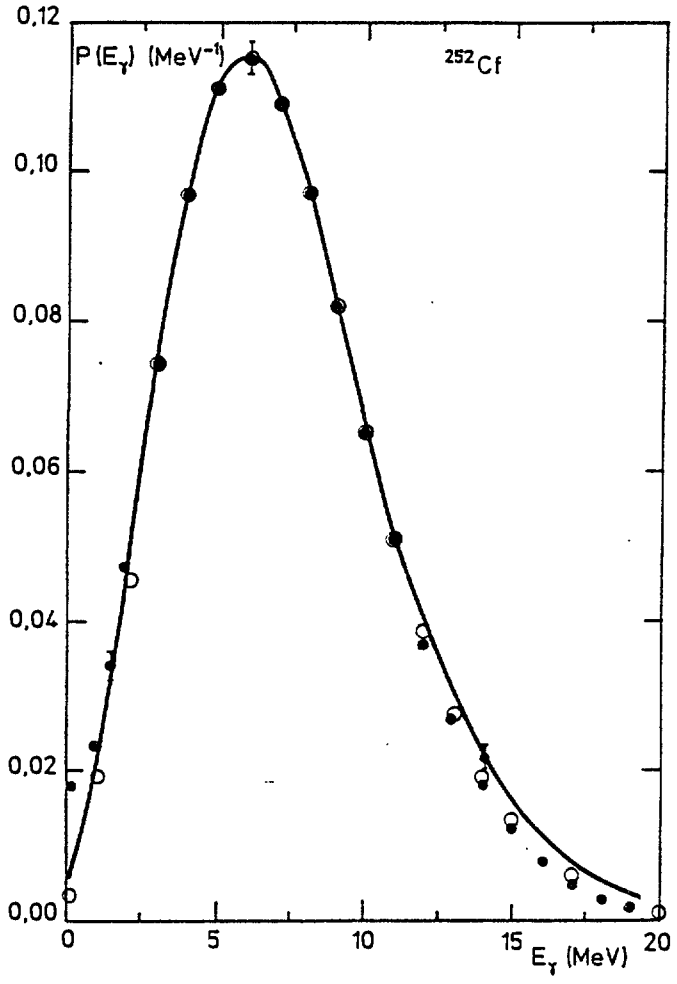

Fig. 6 : Experimental gamma ray spectrum for the spontaneous fission of ^{252}Cf using a NaI detector. Fits to the data (see text) :

● Gauss law for the distribution of the number of quanta.
0 Poisson law for the distribution of the number of quanta.

Since the variance of D(n) is near the average value $\bar{n}$, we have also made a fit using a Poisson distribution :

$$D(n) = \frac{\bar{n}^n}{n!} e^{-\bar{n}}$$

with $\bar{n}$ and β as free parameters.

We obtain also a good fit, particularly at low energy (fig.6) with $\bar{n} = 7.7$ and $\beta = 0.92$ leading to $\bar{E}_\gamma = 7.08$ MeV.

With a Poisson distribution we can furthermore relate simply the average energy $\bar{E}_\gamma$ and the variance σ_γ^2 of the $\mathcal{S}(E)$ distribution to $\bar{n}$ and β :

$$\bar{E}_\gamma = \bar{n}\ \beta$$

$$\sigma_\gamma^2 = 2\ \beta\ \bar{E}_\gamma$$

so that from the experimental data $\bar{E}_\gamma$ and σ_γ^2 available from the liquid scintillator detector we can derive :

$$\beta = \frac{\sigma_\gamma^2}{2\ E_\gamma} \text{ and } \bar{n} = \frac{2\ \bar{E}_\gamma^2}{\sigma_\gamma^2}$$

as a function of excitation energy.

EXCITATION ENERGY DEPENDENCE OF β AND $\bar{n}$

The experimental data for σ_γ^2 below the second chance fission threshold are plotted in fig.7 as a function of $\bar{\nu}_p$ for ^{237}Np, ^{235}U and ^{232}Th. The data for ^{232}Th have been averaged to reduce the dispersion.

Within the uncertainties σ_γ^2 is a linear function of $\bar{\nu}_p$:

$$^{235}\text{U} : \frac{\sigma_\gamma^2}{\sigma_{\gamma Cf}^2} = 0.278\ \bar{\nu}_p + 0.394$$

$$^{237}\text{Np} : \frac{\sigma_\gamma^2}{\sigma_{\gamma Cf}^2} = 0.259\ \bar{\nu}_p + 0.291$$

$$^{232}\text{Th} : \frac{\sigma_\gamma^2}{\sigma_{\gamma Cf}^2} = 0.188\ \bar{\nu}_p + 0.470$$

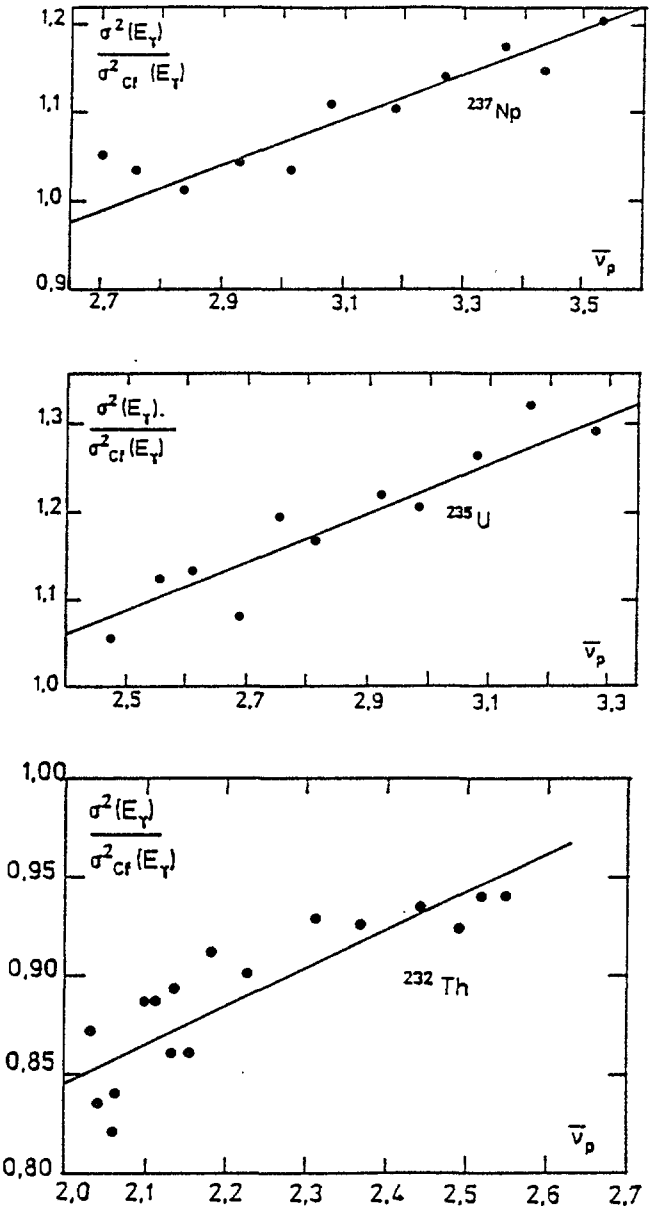

Fig. 7 : Variance of the fission gamma ray spectra as a function of $\bar{\nu}_p$ for ^{232}Th, ^{235}U and ^{237}Np (normalized to ^{252}Cf spontaneous fission).

From these fitted data and the corresponding fits to $\bar{E}_\gamma$ discussed previously we have derived β and $\bar{n}$ as a function of $\bar{\nu}_p$ using the values $\bar{E}_{\gamma Cf}$ = 7.08 MeV and $\sigma^2_{\gamma Cf}$ = 13 MeV^2 derived from our fit to the ^{252}Cf data of fig.6. The results are plotted in fig.8 et 9 for β and n, respectively.

We observe that the average number of quanta $\bar{n}$ remains practically constant, whereas β is increasing almost linearly with $\bar{\nu}_p$.

The relative values of β can be undestood, at least qualitatively, as level density effects if we remember that ^{236}U* is a even-even fissioning nucleus, ^{233}Th* is even-odd, and ^{238}Np* is odd-odd.

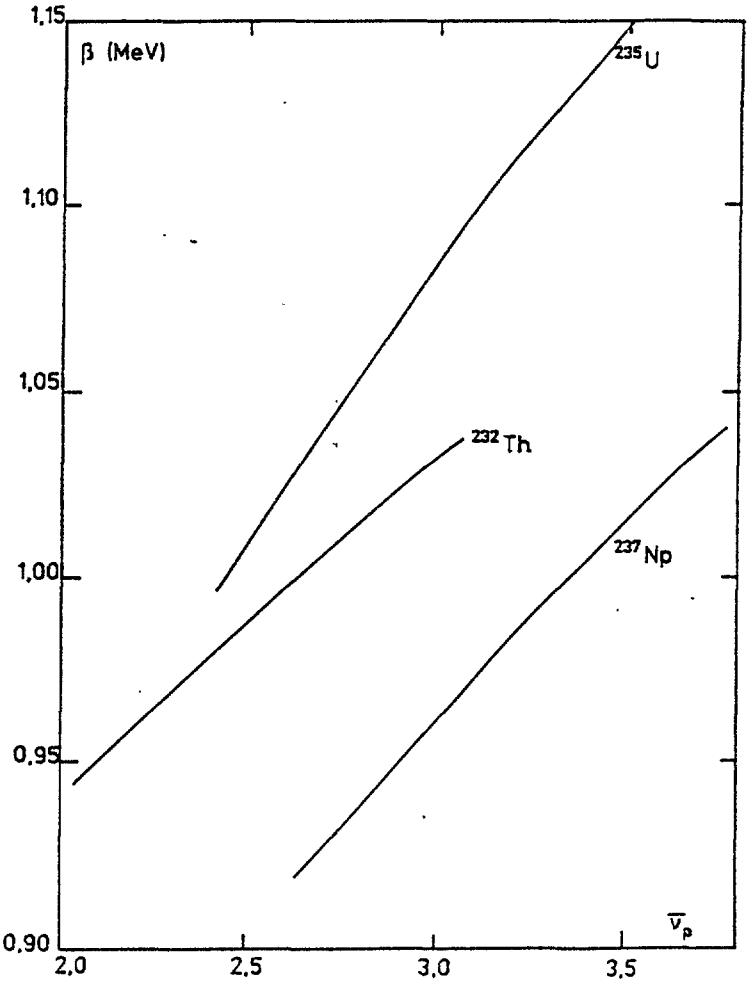

Fig. 8 : Average single fission gamma quantum energy as a function of $\bar{\nu}_p$ for ^{232}Th, ^{235}U and ^{237}Np.

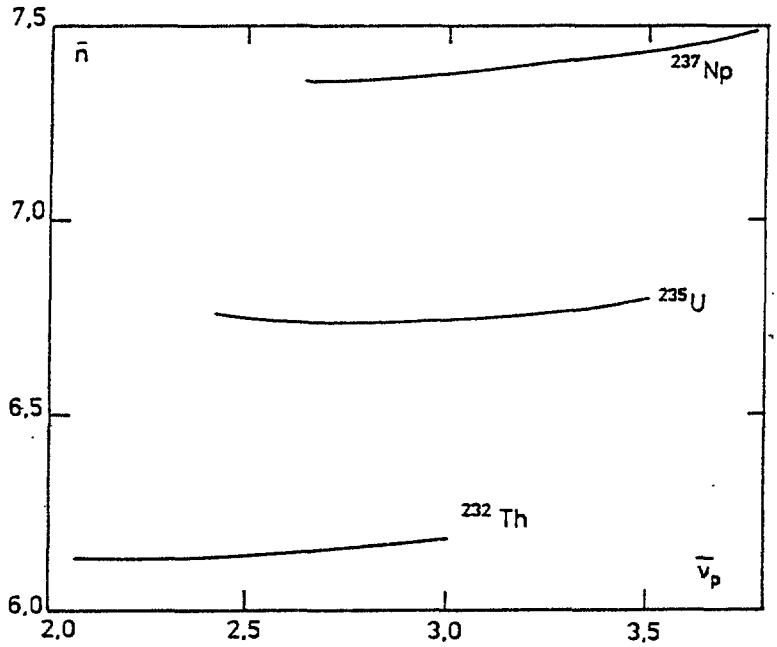

Fig. 9 : Average number of fission gamma quanta as a function of $\bar{\nu}_p$ for ^{232}Th, ^{235}U and ^{237}Np.

The increase of β with excitation energy can be understood in the frame of a larger available phase space allowing a larger number of relatively high energy gamma-rays to be emitted. In that case the quite constant value of $\bar{n}$ would mean that the average fragment angular momentum is not increasing with excitation energy. This interpretation is not in contradiction with the conclusion of an increase of fragment angular momentum with excitation energy derived from the study of the desexcitation of individual fragments. In that latter case, indeed, the average number of gamma quanta is also increasing with excitation energy.

Using the data of ref. [5] for ^{252}Cf we derive from our data for the thermal fission of ^{235}U :

$$\beta = 0.954 \text{ MeV}, \quad \bar{n} = 6.92$$

to be compared to the evaluated data [5] :

$$\beta = 0.97 \text{ MeV and } \bar{n} = 6.89$$

EVALUATION OF β AND $\bar{n}$ FOR OTHER NUCLEI

- **^{233}U and ^{239}Pu**

For these nuclei $\bar{\nu}_p$, $\bar{E}_\gamma$ and $\bar{n}$ are experimentally known for the thermal fission :

	^{233}U	^{239}Pu	Ref
$\bar{\nu}_p$	2.495	2.882	[6]
$\bar{E}_\gamma$, MeV	6.69	6.77	[5]
$\bar{n}$	6.31	7.05	[5]

$$\text{Assuming : } \frac{\bar{E}_\gamma}{\bar{E}_{\gamma Cf}} = a\,\bar{\nu}_p + 4.4 \text{ (MeV)}$$

$$\text{and } \bar{n} = \text{Cst, we can derive } \beta = \frac{\bar{E}_\gamma}{\bar{n}}$$

The results are :

$$^{233}U : \bar{E}_\gamma = 0.92\,\bar{\nu}_p + 4.4 \text{ (MeV)}$$

$$\beta = 0.145\,\bar{\nu}_p + 0.70 \text{ (MeV)}$$

$$^{239}Pu : \quad \bar{E}_\gamma = 0.82\ \bar{\nu}_p + 4.4 \quad (MeV)$$
$$\beta = 0.117\ \bar{\nu}_p + 0.62 \quad (MeV)$$

• **Other nuclei**

In the absence of experimental data, we can use the same formalism, taking the low energy fission values of $\bar{E}_\gamma$ and $\bar{n}$ from the systematics of Hoffman and Hoffman [5] :

$$\bar{E}_\gamma = 0.028\ A + 0.09$$

$$\bar{n} = 0.112\ A - 19.94$$

CONCLUSION

We have taken advantage of the high efficiency to γ-rays of the large Gd-loaded liquid scintillator used in $\bar{\nu}_p$ measurements to derive information about the total prompt γ - ray spectrum in fast neutron induced fission. A careful analysis of the data led to the conclusion that the observed increase of the total average gamma energy $\bar{E}_\gamma$ with excitation energy is due to an increase of the average energy β of the single quanta, the number of quanta $\bar{n}$ remaining about constant. These findings do not support the idea of an increase of the average fragment angular momentum with excitation energy. These results do not contradict the idea of an increase of fragment angular momentum with excitation energy deduced from the study of the desexcitation of individual fragments (mass dependence of $\bar{\nu}_p$, $\bar{E}_\gamma$, $\bar{n}$), since in that case the number of gamma quanta is increasing with the mass correlated fragment excitation energy.

The decrease of $\bar{E}_\gamma$ observed for the second chance fission just results from a lower value of β, since the fissioning nucleus has in that case about 7 MeV less excitation energy than in first chance fission.

REFERENCES

[1] J. TERRELL, Phys. Rev. 113 (1959) 527.

[2] H. NIFENECKER et al., Proc. Conf. on Physics and Chemistry of Fision ROCHESTER, 1973, Vol.II, p.117.

[3] J. FREHAUT, A. BERTIN, R. BOIS, Proc. Conf. on Nuclear Data for Science and Technology, Antwerp, 1982, p.78.

[4] J. FREHAUT, Nucl. Inst. Meth. 135 (1976) 511.

[5] D.C. HOFFMAN and M.H. HOFFMAN, Ann. Rev. Nucl. Sci. 24 (1974) 151.

[6] E.J. AXTON, European Appl. Res. Reports 5 (1984) 609.

NEUTRON AND GAMMA-RAY EMISSION IN Cf-252 TERNARY FISSION

Han Hongyin, Huang Shengnian, Meng Jiangchen,
Bao zongyu and Ye Zongyuan
Institute of Atomic Energy
Beijing, China

Introduction

Although neutron emission from fragments in LRA accompanied fission has been studied in some detail, gamma emission has been very sparsely investigated. Ajitanand[1] measured the γ-yield of Cf-252 ternary fission for different α-particle energies. The result shows a broad maximum in the neighbourhood of E_α = 22 MeV. Considering the linear dependence of $\bar{\nu}$ on E_α, one could guess that the extraordinary behaviour of gamma yield in this energy region might be correlated with some new mode of γ-emission. However, in the experiment of Ajitanand no particle identification was adopted, so the events of ternary fission other than LRA accompanied ones were not excluded and were mixed together. We measured both the neutron and γ-ray yields in the ternary fission of Cf-252, with particle identification, to search for any possible evidence of neutron and γ-ray competition.

Neutron Multiplicity Experiment

In the neutron measurement a platinum backing source with 600 fission/sec was adopted. The diameter of the source spot was 8 mm. In order to distinguish different light charged particles emitted during ternary fission process a ΔE-E telescope was adopted. The ΔE counter was a silicon detector with thickness 55 μm. The E detector was a Si(Li) type one with effective thickness 3 mm. An aluminium absorber (8.1 mg/cm^2 foil) was placed in front of ΔE detector for preventing the fragments and the natural alphas from entering the telescope. The energy of light

charged particles could be derived from the pulse heights of ΔE and E detectors. A surface-barrier type silicon detector was placed close to the source for detecting the fragments of binary fission events. This was needed for giving the veto signal so that neutrons from binary fission will not interfere the correct determination of $\bar{\nu}$ and P(ν) of ternary fission.

A φ600 mm gadolinium-loaded liquid scintillation tank was used to detect the prompt neutrons emitted in the fission events. The construction and principle of operation of this neutron detector had been described elsewhere[2]. The source-telescope assemble was placed in a small vacuum chamber which was located in the center of the neutron detector.

The ΔE and E detectors of the telescope were calibrated by using Am and Cf alpha sources. The total LRA spectrum obtained in present experiment agrees well with previous result[3], this shows the validity of our calibration. The efficiency of the liquid scintillation tank for detection of fission spectrum neutrons was determined via the standard $\bar{\nu}$ value of binary fission of Cf-252 in a separate run.

Pulses from the liquid scintillator were fed into a multievent analyzer[4] whose output pulse height is proportional to the number of input pulses coming within 30 microsecond period after fission occurs. And this output signal, together with pulses from ΔE and E detectors, was sent to a four-parameter data acquisition system[5], though in this case only three parameters were needed. If a binary fission take place before or after a ternary fission event within 30 microseconds (the time duration for slowing down and capture of a neutron in the gadolinium-loaded scintillator), the multievent analyzer will give no output signal. In such way the recorded neutron number of ternary fission will not be perturbed by neutrons from binary fissions.

The measurement lasted 800 hours. In total more than 6×10^4 LRA events and 4800 triton events were obtained.

γ-Emission Experiment

Light charged particles were detected and identified with the ΔE-E telescope in the same way as in above experiment. The prompt γ-rays were recorded by a NaI(Tl) scintillation counter with the crystal size Φ100×100 mm. The Cf-252 source strength was about 10^4 fission/sec, source spot diameter 6 mm, and the backing was a platinum foil of 0.1 mm thick. An aluminium foil was placed in front of telescope to absorb the fission fragments and natural alphas. The angle subtended to the source by the telescope was 35 degrees. The γ detector was located in the opposite side of the source, the angle subtended was 55 degrees. The source-telescope assemble was placed in a vacuum chamber which was evacuated to 10^{-2} torr during measurement. Both the vacuum chamber and the γ detector were shielded by 10 cm thick lead layer. The source,the telescope and the γ detector were located in a same axis.

The signals from ΔE,E and γ detectors were sent to a coincidence circuit. The coincidence circuit can be put on two working regimes: with or without the signal from γ-detector. In double coincidence regime the simultaneous ΔE and E pulses would give an output signal to open the linear gates and the MCA-computer system. Then the ΔE-E twodimensional spectrum of all light charged particles was recorded. In triple coincidence regime the circuit would give output signal only when the ΔE, E give pulses together with the γ detector simultaneously. In this case recorded were the data corresponding to those ternary fission events in which at least one γ-photon was detected. (According to our geometry the probability of detecting two or more photons from one fission event was small and could be taken into account in the correction term.) The ΔE-E spectrum obtained from triple-coincidence events devided by the ΔE-E spectrum from double coincidence events gave out the γ-emission probability for different kinds and different energies of light charged particles. We used the binary fission events as standard, so actually

the ratios of ternary fission γ-photon yields to yield of binary fission were obtained in the experiment.

In order to estimate the influence of any possible angular correlation between γ-photon and light charged particles, we took another run of measurement with the telescope turned to 45 degree direction. The results show no difference in these two cases within experimental accuracy (2 %). In addition, a special run was carried out to determine the background counts in NaI(Tl) detector induced by the fission neutrons.

The ΔE, E detectors were calibrated as in the above experiment, and the γ-detector was calibrated with various γ-sources (Na-24,Cs-137, Mn-54,etc.). The threshold of γ-detector was set at 80 keV.

The double coincidence runs and the triple coincidence runs were accumulated alternately. The measurement lasted 300 hours in total.

Result

The data obtained were analyzed at VAX-11/780 computer. Various kinds of light charged particles were sorted according to the ΔE-E pattern. Some corrections were made including dead time correction, background subtraction, influence of the source backing and aluminium absorber, leakage of neutrons from the central channel of the scintillation tank,etc. In most cases the main source of uncertainty is the statistical error.

Following results were obtained:

(1) The average number of prompt neutrons $\bar{\nu}$ for different fission modes were equal to: 3.757 ± 0.009 for binary fission[6] (used here as standard), 3.13 ± 0.02 for LRA events, 3.09 ± 0.09 for He-3 accompanied fission, 2.95 ± 0.05 for triton events and 3.24 ± 0.07 for proton events. The P(ν) (the probability for emission ν neutrons in a fission event) distributions for binary, LRA and triton accompanied fission modes were given in Fig.1.

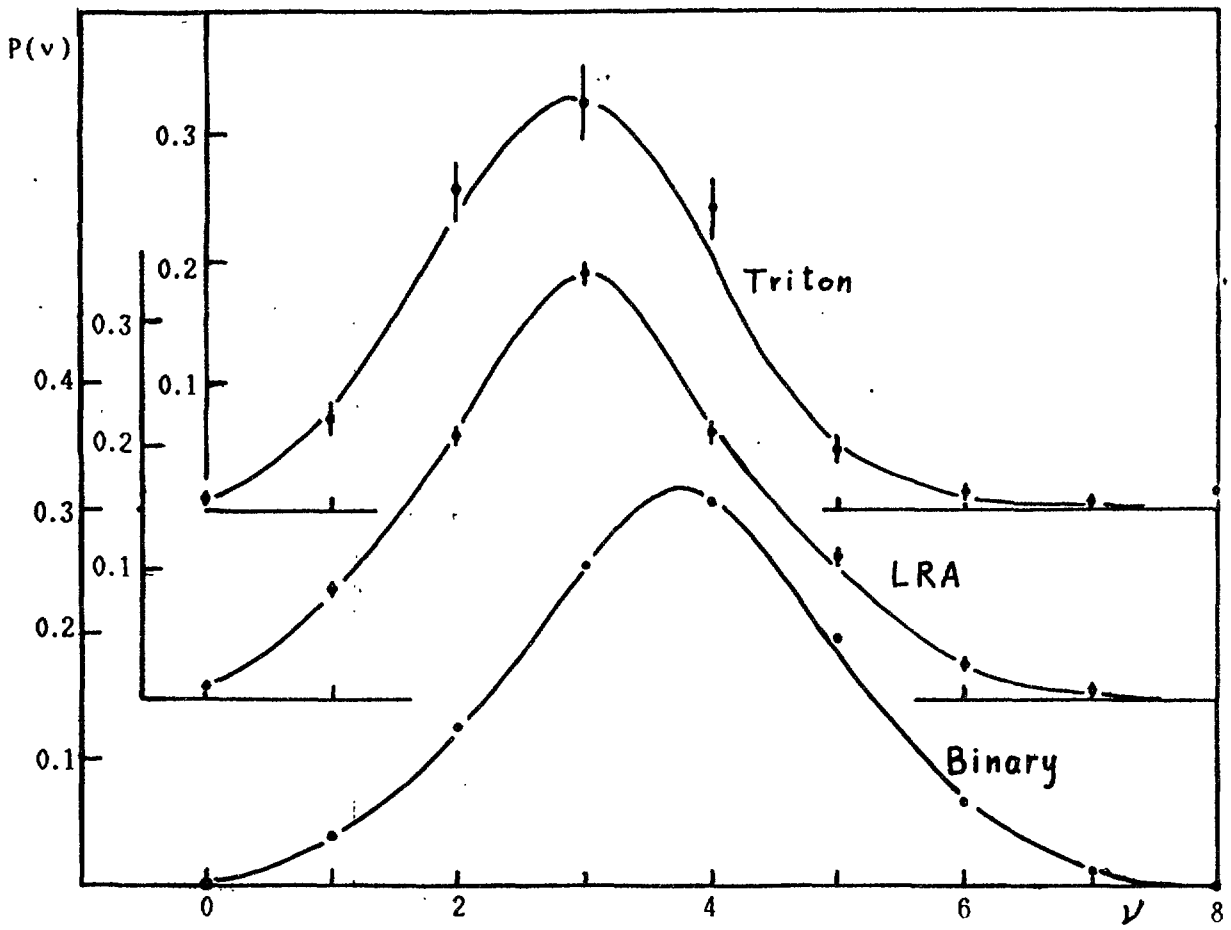

Fig.1 The P(ν) distributions for three modes of Cf-252 spontaneous fission

(2) The dependence of $\bar{\nu}$ on light particle's energy E_α, E_t and E_p was plotted in Figs.2,3 and 4. In the energy ranges E_α>12 MeV, E_t>6 MeV MeV, the data could be fitted by straight lines with following slopes:

$$d\bar{\nu}/dE_\alpha = -0.037 \pm 0.003 \text{ n/MeV} \quad \text{and}$$

$$d\bar{\nu}/dE_t = -0.039 \pm 0.008 \text{ n/MeV},$$

respectively. In proton case the statistical errors were too large and no fit was made.

(3) The average number of prompt γ-photons emitted per fission in triton accompanied events was plotted against triton energy E_t in Fig.5. The corresponding result for LRA events was shown in Fig.6. In these figures exactly given was the ratio K of ternary fission γ-yield to the γ-yield of binary fission. These data show that γ-yield remains nearly constant when E_t lies between 6 MeV and 15 MeV, and when E_α lies bet-

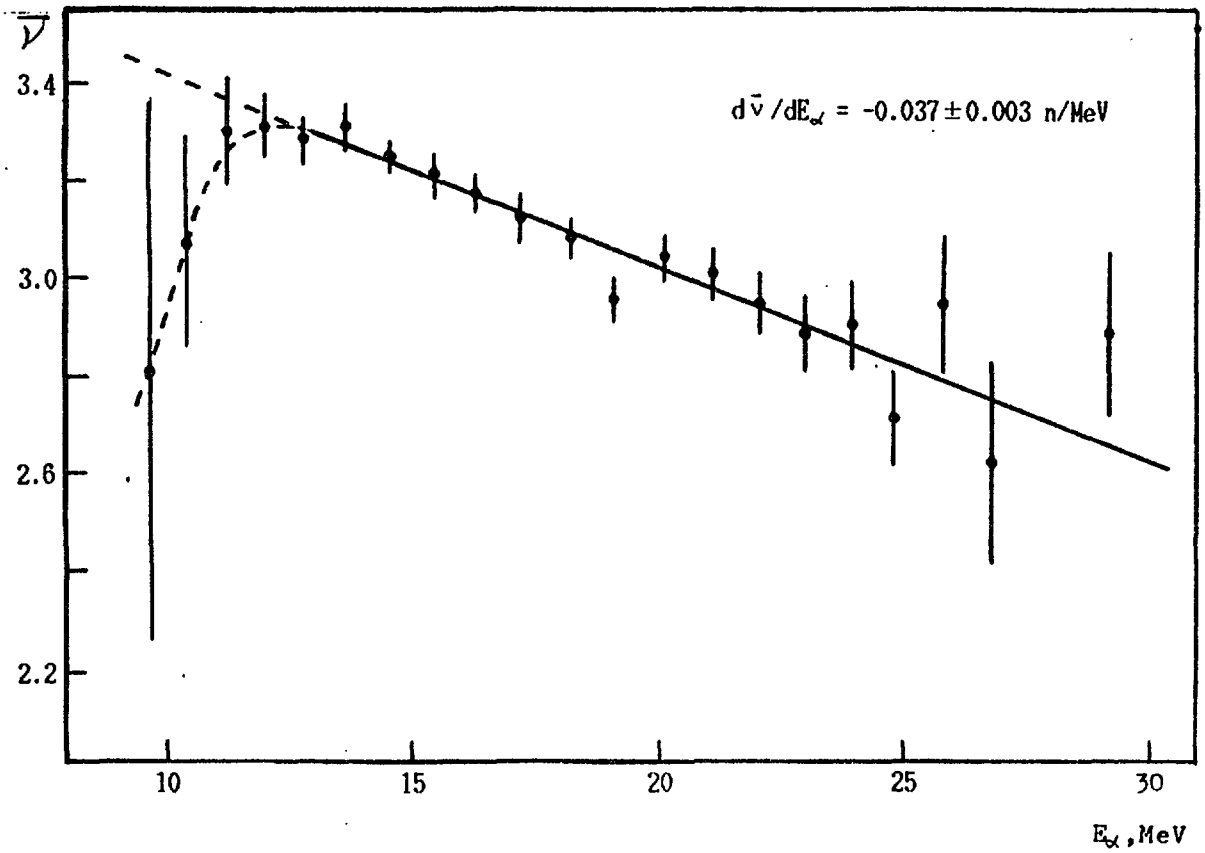

Fig.2 The dependence of $\bar{\nu}$ on alpha-particle's energy

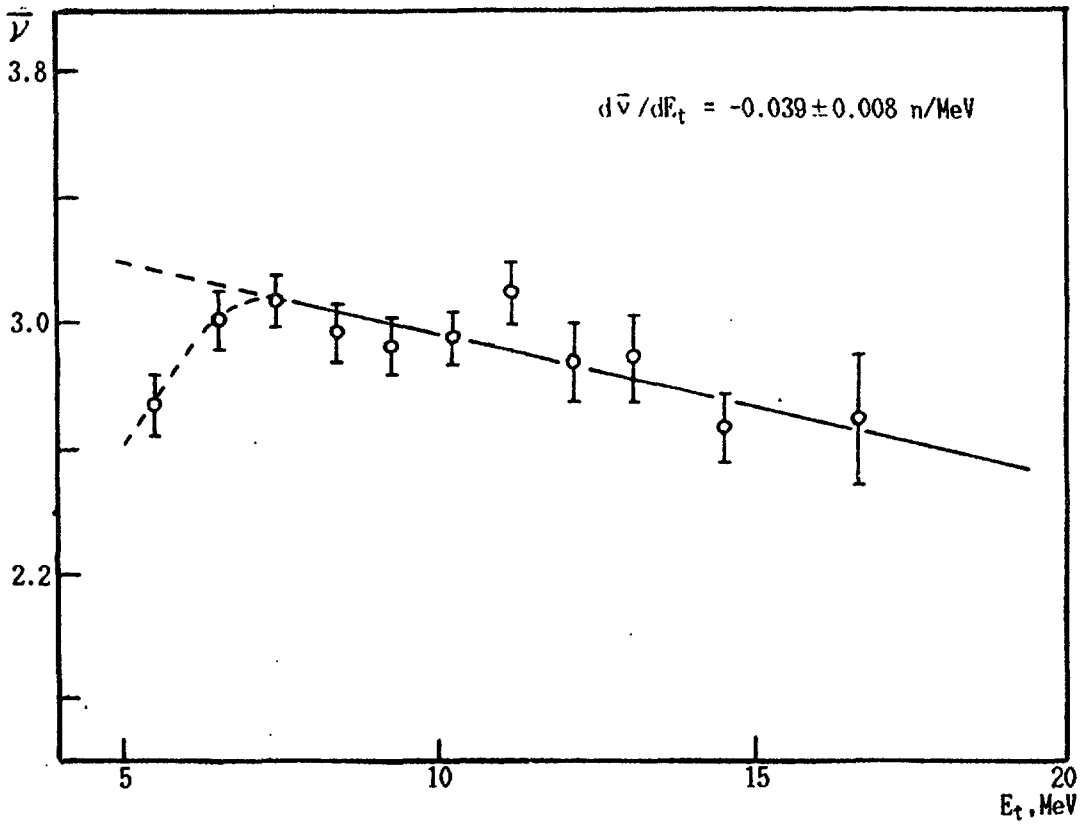

Fig.3 The dependence of $\bar{\nu}$ on triton energy

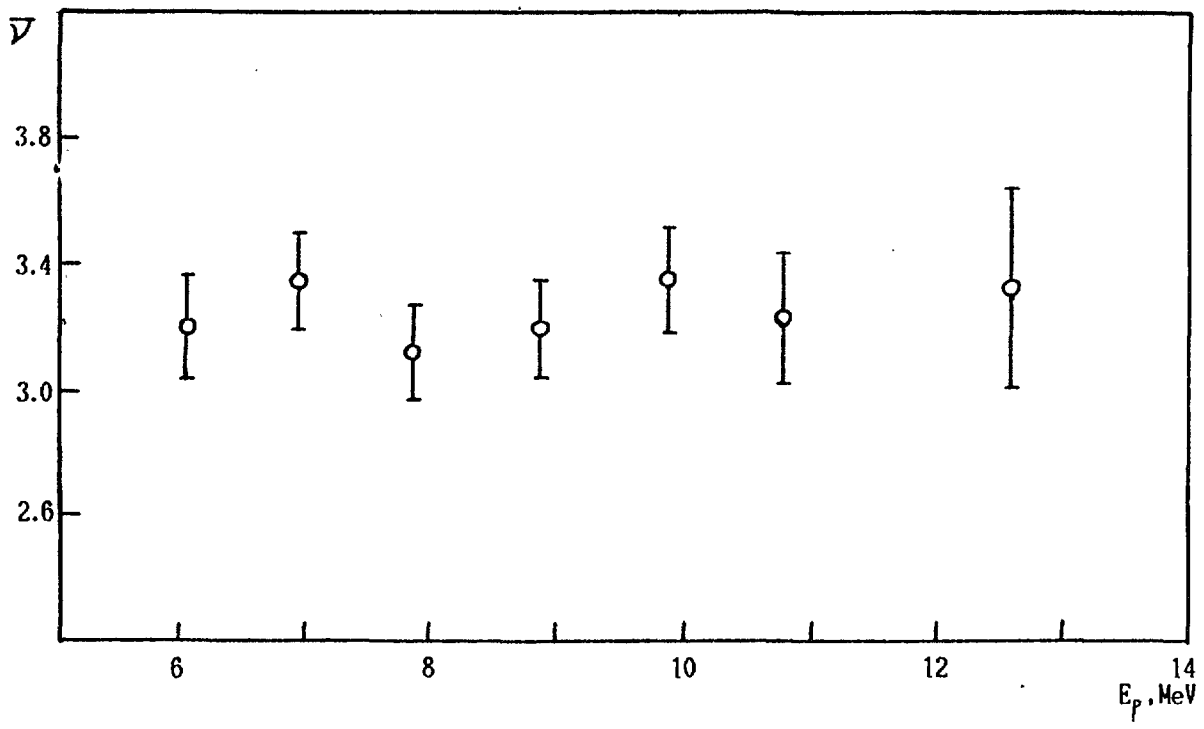

Fig.4 The dependence of $\bar{\nu}$ on proton energy

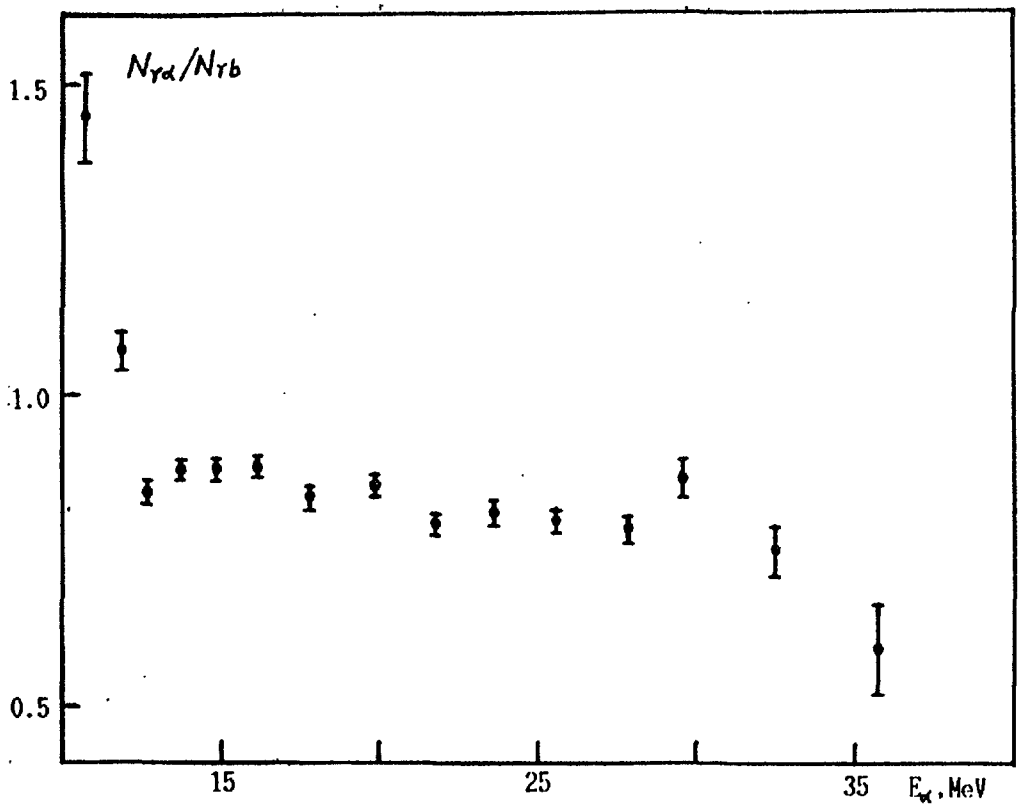

Fig.5 Ratio of the γ-yield in LRA accompanied fission process to that of binary fission $N_{\gamma\alpha}/N_{\gamma b}$ as a function of LRA energy

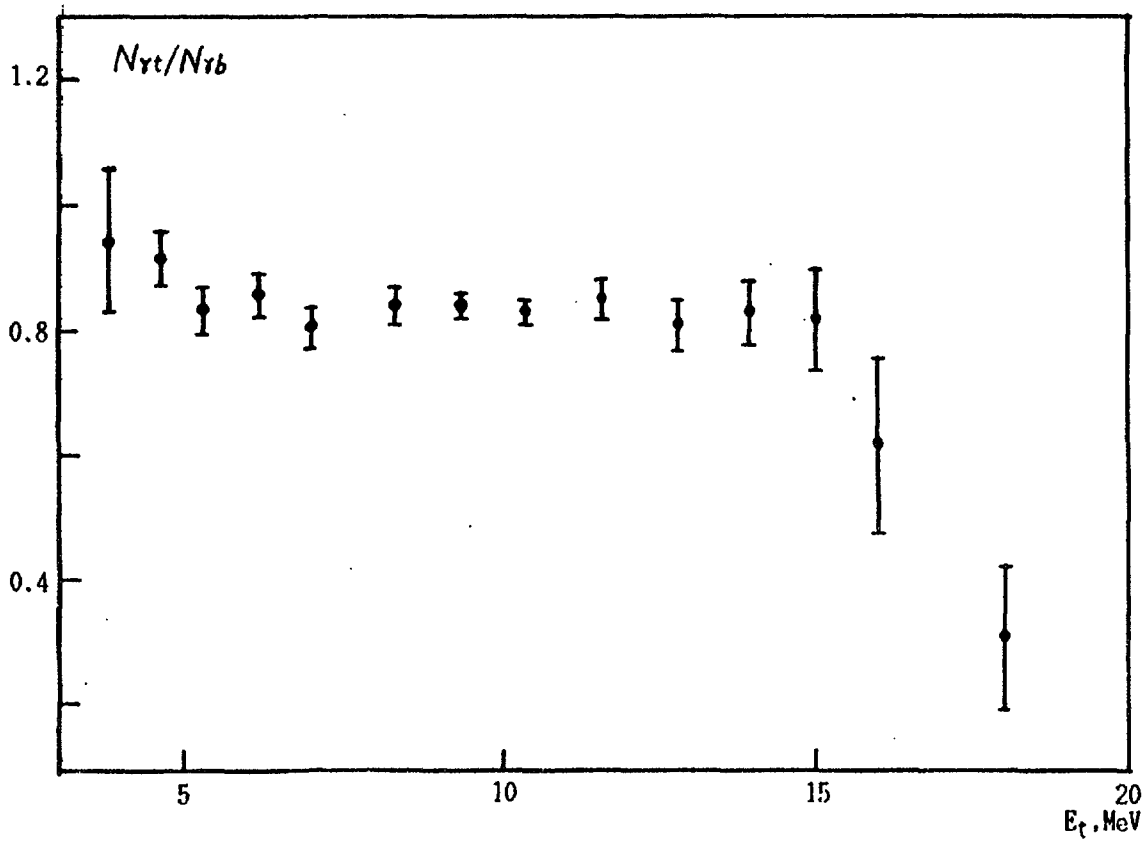

Fig.6 Ratio of the γ-yield in triton accompanied fission process to that of binary fission $N_{\gamma t}/N_{\gamma b}$ as a function of triton energy

ween 10 MeV and 30 MeV. Outside these energy ranges the yield decreases when E_t or E_α increases.

Discussion

In Fig.7 Ajitanand's data were plotted together with our results for comparison. As can be seen in the figure, in energy region E_α<12 MeV the two data sets give opposite trends. Besides, in the neibourhood of 22 MeV in our curve no maximum was found. The last point of Ajitanand's data at 23 MeV, however, agrees with present well. We suppose, the obvious difference in the low energy region might be explained by the fact that in Ajitanand's experiment no particle identification technique had been used. In that case the outgoing charged particles from reactions in

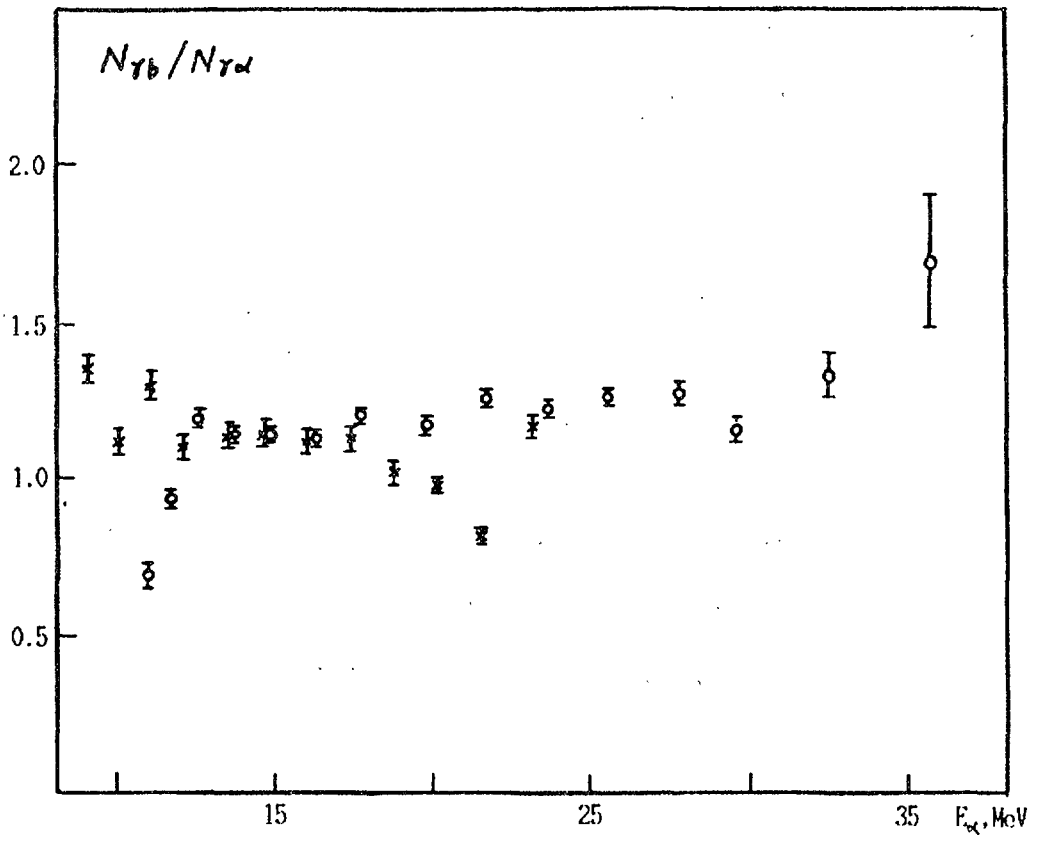

Fig.7 Comparison of Present result with Ajitanand's data

× Ajitanand; o Present work.

aluminium absorber and silicon detector itself induced by fission neutrons may cause false counts in alpha channel which would lead to the extra apparent yield of ternary fission in low energy region.

The behaviour of the neutron and γ emission for E_α>12 MeV and E_t>6 MeV could be explained by the statistical theory. According to this theory, during the deexcitation process the fission fragments will evaporate neutrons as long as they have enough energy. So the prompt γ-rays are emitted only by those fragments which have the remained excitation energy value between zero and neutron binding energy. Thus the fact of independence of γ-yield on E_t or E_α as well as the identity of the slopes $d\bar{\nu}/dE_t$ and $d\bar{\nu}/dE_\alpha$ could be adopted as the evidence of no compe-

tition between the γ and neutron emission. However, the trends of neutron and γ emission in energy region E_t<6 MeV and E_α<12 MeV can't be accounted for by such considerations. As the E_t or E_α decreases, the γ-yield goes up while the $\bar{\nu}$ drops. It can unlikely be attributed to the experimental mistakes. Perhaps there exists some new mechanism of ternary fission? More detailed experimental research, especially in still lower energy region, is needed to clarify this problem.

The authors wish to thank Dr. Zhuang Renjie and Dr. Jiu Zhonghua for preparing the Pt-backing sources, to thank Dr. Liu Zhuhua for providing us multievent analyzer, and Dr. Ding Shenyue and Dr. Xu Jingchen for help and discussion during experiment.

References

1. N.M.Ajitanand, Nucl.Phys.,A133,625(1969)
2. Huang Shengnian et al., Acta Physica Sinica,23,46(1974)
3. W.Loveland, Phys.Rev.,C9,395(1974)
4. Liu Zhuhua, Sci.and Techn.Atom.Energy,No.3,337(1979)
5. Han Hongyin, Nucl.Electronics and Detect.Techn.,4,51(1984)
6. E.Axton, European Appl.Res.Rept.,5,4,609(1984)

$\bar{\nu}_p$ FOR NEUTRON-INDUCED FISSION IN RESONANCE REGION : SPIN AND (N, γ F) REACTION EFFECTS

E. FORT*, J. FREHAUT, H. TELLIER**, P. LONG*
presented by J. FREHAUT
Centre d'Etudes de Bruyères-le-Châtel
Service de Physique et Techniques Nucléaires
B.P. 12 - 91680 Bruyères-le-Châtel

ABSTRACT

The average number of prompt neutrons $\bar{\nu}_p$ emitted per fission event has been evaluated for ^{239}Pu with a special regard to the fluctuations experimerntally observed in the low energy range. These fluctuations are demonstrated to have a significant impact for the applications especially the reactivity coefficient of advanced water reactors. Consequently, the $\bar{\nu}_p$ curve has to be defined in the same fine energy mesh as the fission cross-section for accurate neutron source calculations. In this range formalisms are proposed to calculate $\bar{\nu}_p$ from the resonance parameters, resolved or averaged. Using JEF1 library as a data base the analysis of several thermal, low moderated or fast systems shows a good convergence of the selected microscopic and integral informations.

In the present evaluation the importance of the spin and (n, γf) effects in the generation of dips in the $\bar{\nu}_p$ curve is emphasized. These effects which exist in the low energy range up to about 10 keV lead to a reduction of the effective value of $\bar{\nu}_p$.

Predominant in the epithermal range, the spin effect progressively decreases and the reduction of $\bar{\nu}_p$ is due to the (n, γf) effect only in the keV region.

This paper has been accepted for publication in Nuclear Science and Engineering under the title :

Evaluation of $\bar{\nu}_p$ for ^{239}Pu : impact for applications of the fluctuations at low energy.

* CEN CADARACHE
** CEN SACLAY

COMMENT ON SPIN DEPENDENCE OF $\bar{\nu}_p$ IN THE RESONANCE REGION FOR ^{239}Pu

R.L. Walsh
Australian Nuclear Science and Technology Organisation,
Lucas Heights Research Laboratories,
Australia.

Abstract

The data discrepancy in the spin dependence of $\bar{\nu}_p$ and $\bar{E}_K$ for ^{239}Pu above and below 1eV is discussed in relation to recent multichannel, multilevel cross section analysis of other authors. It is shown that the data discrepancy still exists, but that it is reduced in size.

In reference [1] we reported a data discrepancy concerning the spin dependence of $\bar{\nu}_p$ and $\bar{E}_K$ for $^{239}Pu(n,f)$ in the neutron resonance region. The discrepancy related to data measured above and below 1eV neutron energy. For the region less than 1eV, where the resonances are not resolved, the $\bar{\nu}_p$ and $\bar{E}_K$ data of several authors [2-6] are in good agreement with each other and imply a $\bar{\nu}_p$, $\bar{E}_K$ spin dependence of 2%. (That is, $\bar{\nu}_p(J=0^+)$ exceeds $\bar{\nu}_p(J = 1^+)$ by 2%, with $\bar{E}_K$ displaying the opposite behaviour.) See Figure 1. However, for the energy region above 1eV, where the resonances are resolved, some of the measurements reported a spin dependence of about 3% [2,3], and thus supported the data below 1eV, whilst other measurements found a spin dependence of only 0.25 - 0.5% [7-9]. These results are summarised in Table 1. Reference [1] examined various features of the measurements above and below 1eV, but was unable to resolve the discrepancy.

Of central importance to the findings below 1eV is the change in the $J = 1^+$ fission strength between the prominent $J = 1^+$ resonance at 0.296 eV and thermal energy. The measured charge in $\bar{\nu}_p$ and $\bar{E}_K$ must be increased in value to take account of the fact that the $J = 1^+$ and $J = 0^+$ fission strengths are mixed together. In this way one arrives at the spin dependence between a 'pure' $J = 0^+$ ground state level and a 'pure' $J = 1^+$ level. Reference [1] used values for $J = 1^+$ fission strengths of 92% at $E_n = 0.296$ eV and 45% at thermal energy. This gave an absolute change in $J = 1^+$ fission strength of 47%. These values were calculated [6,10] using a single -level analysis of the isolated $J = 1^+$ resonance at 0.296 eV and with no assumptions as to the resonance parameters of the single $J = 0^+$ bound level [11]. Including consideration of the collective energies of the K bands and their relative availability [6, 12] gave

$$0.025 = \Delta\bar{\nu}_p(0.92 - 0.45) + (\Delta\bar{\nu}_p/1.25)(0.009 - 0.063) \qquad 1.$$

where $\Delta\bar{\nu}_p = \bar{\nu}_p(J = 0^+) - \bar{\nu}_p(J = 1^+)$

0.025 neutrons = measured difference in $\bar{\nu}_p$ between thermal energy and 0.296 eV (from Figure 1), after subtraction of the $(n,\gamma f)$ effect

$\therefore \bar{\nu}_p = 0.059$ neutrons.

This is just the 2% spin dependence mentioned above. (The thermal $\bar{\nu}_p$ value is taken as the recommended value of [13], 2.857 ± 0.010).

TABLE 1
Summary of $\bar{\nu}_p$ and $\bar{E}_K$ data above 1 eV [b]

Quantity measured	Author	Result [a]
$\bar{\nu}_p$	Weinstein *et al.* [5]	$\Delta\bar{\nu}_p \sim 3\%$
$\bar{\nu}_p$	Hockenbury *et al.* [6]	
$\bar{\nu}_p$	Fréhaut and Shackleton [10]	$\Delta\bar{\nu}_p = (0.5 \pm 0.25)\%$
$\bar{\nu}_p$	Weston and Todd [16]	$\Delta\bar{\nu}_p \leq 0.5\%$
$\bar{E}_K$	Wagemans *et al.* [17]	$\Delta\bar{E}_K = -50 \pm 90$ keV
		$\Rightarrow \Delta\bar{\nu}_p = (0.25 \pm 0.45)\%$

[a] $\Delta\bar{\nu}_p = \bar{\nu}_p(J=0^+) - \bar{\nu}_p(J=1^+)$,
$\Delta\bar{E}_K = \bar{E}_K(J=0^+) - \bar{E}_K(J=1^+)$.

[b] The reference numbers in the table are those of Ref [1].

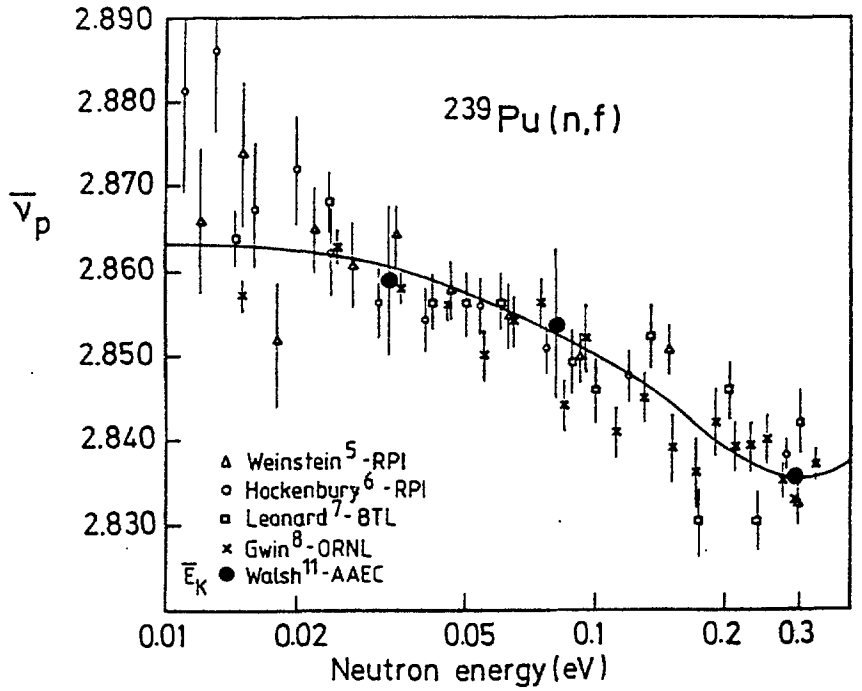

Figure 1 $\bar{\nu}_p$ and $\bar{E}_K$ data below 1 eV. Normalised to $\bar{\nu}_p$ = 3.736 for ^{252}Cf(sf). Taken from Ref. [1]. The reference numbers in the figure are those of [1].

A more sophisticated analysis has been performed by Derrien et al [14]. They carried out a multichannel, multilevel R matrix analysis of the ^{239}Pu neutron cross section up to 1 keV. Four bound levels were used, two of J = 0^+ and two of J = 1^+. These levels were found to be necessary to fit the cross section data at low energy and in between the resonances. This multilevel analysis found values for the J = 1^+ fission strength of 97% at E_n = 0.296 eV and 29%

at thermal energy (reported in [15]). Presumably, interference effects cause the J = 1^+ strength at thermal to be decreased compared with that found in the single level analysis above.

The absolute change in the J = 1^+ fission strength found in the multilevel analysis [14] is thus 68%. A calculation similar to that of equation 1 then gives $\Delta \bar{\nu}_p = 0.041$ neutrons. This represents 1.4% of the thermal $\bar{\nu}_p$ value.

Thus, the multilevel approach reduces the $\bar{\nu}_p$ spin dependence from the 2% of the single level approach to 1.4%. However, this is still significantly larger than the value 0.25 - 0.5% found in references [7 - 9], Table 1. It therefore appears that the discrepancy in the data concerning the spin dependence of $\bar{\nu}_p$ and $\bar{E}_K$ above and below 1 eV still exists, but that it is somewhat reduced in size. This conclusion is at variance with a conclusion of Ref. [15], which reported the data discrepancy to be now removed.

REFERENCES

1. Walsh R.L. and Boldeman J.W., Nucl. Phys. A451 (1986) 113

2. Weinstein S., Reed R., and Block R.C., Proc. 2nd IAEA Symp. on physics and chemistry of fission, Vienna, 1969, p. 477.

3. Hockenbury R.W., Reed R.L., and Block R.C., Proc. 3rd IAEA Symp. on physics and chemistry of fission, Rochester, 1973, vol. 2, p. 502; and private communication to B.R. Leonard Jr.

4. Leonard B.R. Jr., Seppi E.J., and Friesen W.J., report HW-4344.

5. Gwin R., Spencer R.R., Ingle R.W., Todd J.H. and Weaver H., report ORNL/TM-6246 (1978) and Gwin R., Spencer R.R., and Ingle R.W., Nucl. Sci. Eng. 87 (1984) 381.

6. Walsh R.L., Boldeman J.W. and Elcombe M.M., Proc. 4th IAEA Symp. on physics and chemistry of fission, Jülich, 1979, vol. 2, p. 129 and ensuing discussion.

7. Fréhaut J., and Shackleton D., Proc. 3rd IAEA Symp. on physics and chemistry of fission, Rochester, 1973, vol. 2, p. 201.

8. Weston L.W., and Todd J.H., Phys. Rev. C10 (1974) 1402.

9. Wagemans C., Wegener-Penning G., Weigmann H., and Barthelemy R., Proc. 4th IAEA Symp. on physics and chemistry of fission, Jülich, 1979, vol. 2, p. 143.

10. Walsh R.L., Ph.D. thesis (1980), University of Wollongong, Wollongong, NSW, Australia.

11 Vogt E., Phys. Rev 118 (1960) 724.

12 Derrien H., Blons J. and Michaudon A., in Nuclear Data for Reactors (Proc. Conf. Helsinki 1970) Vol. 1, IAEA, Vienna (1971) 481.

13. Boldeman J.W., Proc. Int. Specialists Symp. on neutron standards and applications, Gaithersburg, 1977, NBS SP 493, p. 182.

14. Derrien H., de Saussure G., Perez R.B., Larson N.M. and Macklin R.L., report ORNL/TM-10098, June 1986.

15. Fort E., Fréhaut J., Tellier H. and Long P., Submitted to Nucl. Sci. Eng., 1987.

INTERPRETATION OF FLUCTUATIONS OF ν AND E_γ IN RESONANCES OF $^{235}U(n,f)$

F.-J. Hambsch*, H.-H. Knitter, C. Budtz-Jørgensen**
Commission of the European Communities
Joint Research Center
Central Bureau for Nuclear Measurements
GEEL, BELGIUM

J.P. Theobald
Physikalisches Institut, Technische Hochschule
DARMSTADT, GERMANY

Abstract : Fluctuations of ν and E_γ in resonances of $^{235}U(n,f)$ were measured in earlier experiments. Recently fission fragment mass- and total kinetic energy distributions of $^{235}U(n,f)$ were determined for single isolated resonances, resonance groups and energy bins in the energy range from 0.006 eV to 130 eV in an experiment at GELINA. Fluctuations of the symmetric fission fragment yield and of the asymmetric fragment peak shapes were observed. These fluctuations are interpreted as fluctuations of fission exit channel populations: by the superlong symmetric and the two asymmetric standard I and standard II exit channel populations. Mainly the fluctuations in the standard I and the standard II exit channels cause variations in the average reaction $\langle Q\rangle_{E_i}$-values. Correlated with the fluctuations of the mass yields in the asymmetric mass peaks also strong fluctuations of the total kinetic energy averaged over all fragments $\langle TKE\rangle_{E_i}$ are observed, which are anti-correlated with ν_{E_i}, the number of promptly emitted neutrons. It is explained, contrary to earlier assumptions, why the asymmetric and not the symmetric fission fragment yield fluctuations cause the fluctuations in ν and E_γ from resonance to resonance. It can also be concluded that the ν-fluctuations are not J-dependent.

1.) Introduction

The number of neutrons emitted in the neutron induced fission of $^{235}U(n,f)$, $\nu(E_i)$, was measured in the resonance region by Weinstein et al. (1), Reed et al. (2), Ryabov et al. (3), and by Theobald et al. (4).
Two groups of ν-values were found in these early experiments. The authors interpreted the division of the ν-values into two sets as an indication for a spin dependence and made a spin classification of the observed

---

Present adresses: * Carl Schenck A.G., Darmstadt, Germany
** Danish Space Research Institute, DK-2800 Lyngby

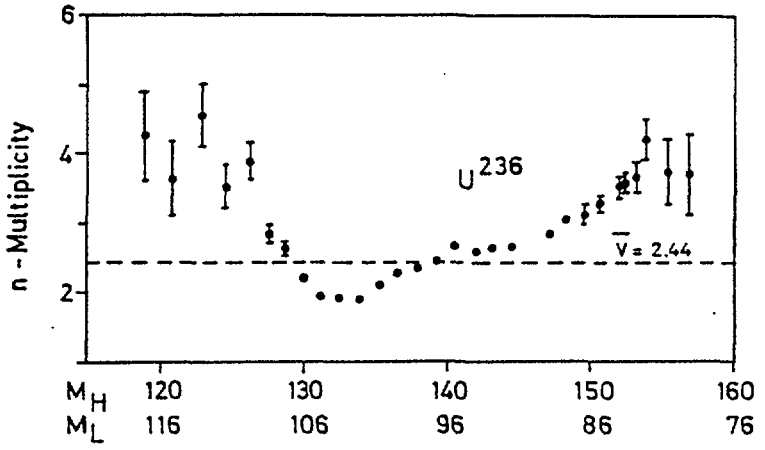

Fig. 1

Number of prompt neutrons versus mass split emitted in the thermal neutron induced fission of ^{235}U.

resonances. The spin determination by the two first authors was based on the assumption that the 8.77 eV and the 19.3 eV resonances have spin 3^- and 4^-, respectively. Moreover it was assumed that the 3^- resonances show the higher ν-values than the 4^- resonances. The two latter authors found, however, smaller ν-values for 3^--resonances than for 4^--resonances. This is in agreement with the theory of Bohr and Wheeler which does not prohibit symmetric fission when passing 4^- saddle point transition states. Symmetric fission yields more prompt neutrons compared to the average as shown in fig. 1 and, hence, fission through 4^--states should show more prompt neutrons. This was the earlier argumentation. The data of fig. 1 are from Apalin et al. (5). The unambiguous spin determination with polarized neutrons and polarized ^{235}U-target nuclei by Keyworth et al. (6) and Moore et al. (7) yielded, however, for both above mentioned resonances the same spin of 4^-! What is now the reason for the ν-fluctuations from resonance to resonance?

2.) Correlation between $Y_{E_i}(M)$ with $\langle TKE \rangle_{E_i}$ and $\langle Q \rangle_{E_i}$

In a recent experiment at GELINA, Hambsch et al. (8,9) measured for the first time complete fission fragment mass and total kinetic energy distributions for single isolated resonances, resonance clusters or energy bins from 0.006 eV to 130 eV incident neutron energy. The mass distributions $Y_{E_i}(M)$ did not only show fluctuations of the valley to peak ratios as expected, but showed also significant changes in the shape of the asymmetric mass peaks. Fig. 2 shows as an example the mass distribution of $^{235}U(n,f)$ measured for thermal neutrons, the difference in

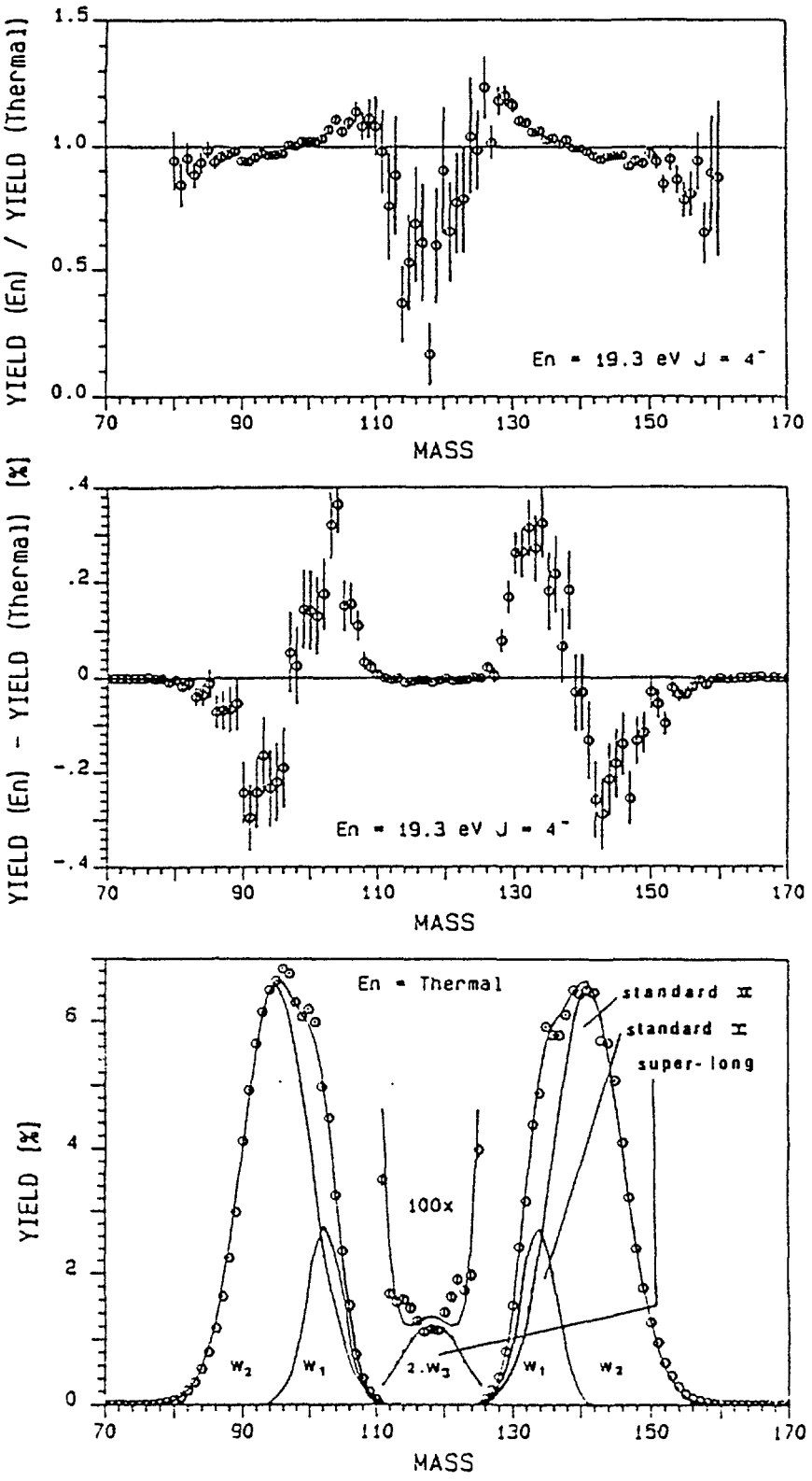

Fig. 2

In the lowest part, the $^{235}U(n,f)$ experimental mass distributions for thermal neutrons and the partial and global mass distributions obtained from the fit are plotted as full lines versus the mass. In the middle and upper part the yield difference and ratio of the mass distributions measured in the 19.3 eV resonance and for thermal neutrons are plotted respectively.

absolute scale of the yields measured for fission in the 19.3 eV resonance and for thermal neutrons,as well as the ratio between both mass distributions.

This figure shows mass yield fluctuations in the resonance region of $^{235}U(n,f)$. The set of three Gaussian distributions which are indicated by full lines in fig. 2 composes the whole mass distribution. They were obtained by a least squares fit through the experimental points and give a good general description for the whole mass distribution.

Three fission paths in ^{236}U were predicted by Brosa et al.(10,11). According to Knitter et al. (12,13) each Gaussian can be interpreted as mass distribution from one of the three fission paths. The Gaussians, representing the partial mass distributions, are indicated in fig. 2 with the corresponding names of the fission paths. The W_i are the populations of the fission paths. The superlong, the standard I and standard II fission paths for thermal neutrons are populated by (0.069 ± 0.013)%, (18.22 ± 0.28)% and by (81.50 ± 0.43)%, respectively. The population of the superlong symmetric path fluctuates from resonance to resonance up to 200 %, whereas the populations of the standard I and standard II paths vary up to 20%. On absolute scale these latter yield fluctuations of the asymmetric mass peak shape are much larger than those of the symmetric fission region.

Fig. 3 shows the number of events as function of neutron energy, the relative ratios of the standard I /standard II path populations, the relative total kinetic energies averaged over all fragments <TKE> and the relative ν-values as measured by Howe et al. (14). In order to obtain a correct comparison the same energy bins as in the experiment of Howe et al. were selected also for the evaluation of the present experiment. The fluctuations in <TKE> go up to 450 keV. Since the average total kinetic energy TKE(M) is mass split dependent, a correlation between the fluctuations W_1/W_2 of the mass distribution and the <TKE>-values is observed. The correlation diagram between the two quantities is shown in fig. 4. A correlation coefficient of r = (0.81 ± 0.05) demonstrates the clear correlation. Also the Q-value is mass split dependent. Therefore, when the mass distribution changes, also the Q-value averaged over all mass splits, <Q>, will change. The <Q>-values for the observed mass distributions were calculated. The Q-values were taken from Möller et al. (15), where for each mass split the maximum possible Q-value was used. In fig. 4 the <Q>-value changes are plotted versus the <TKE> variations. It is clearly seen, that the changes of <TKE> are positively correlated with changes of <Q>. The correlation coefficient was determined to be r = (0.87 ± 0.03).

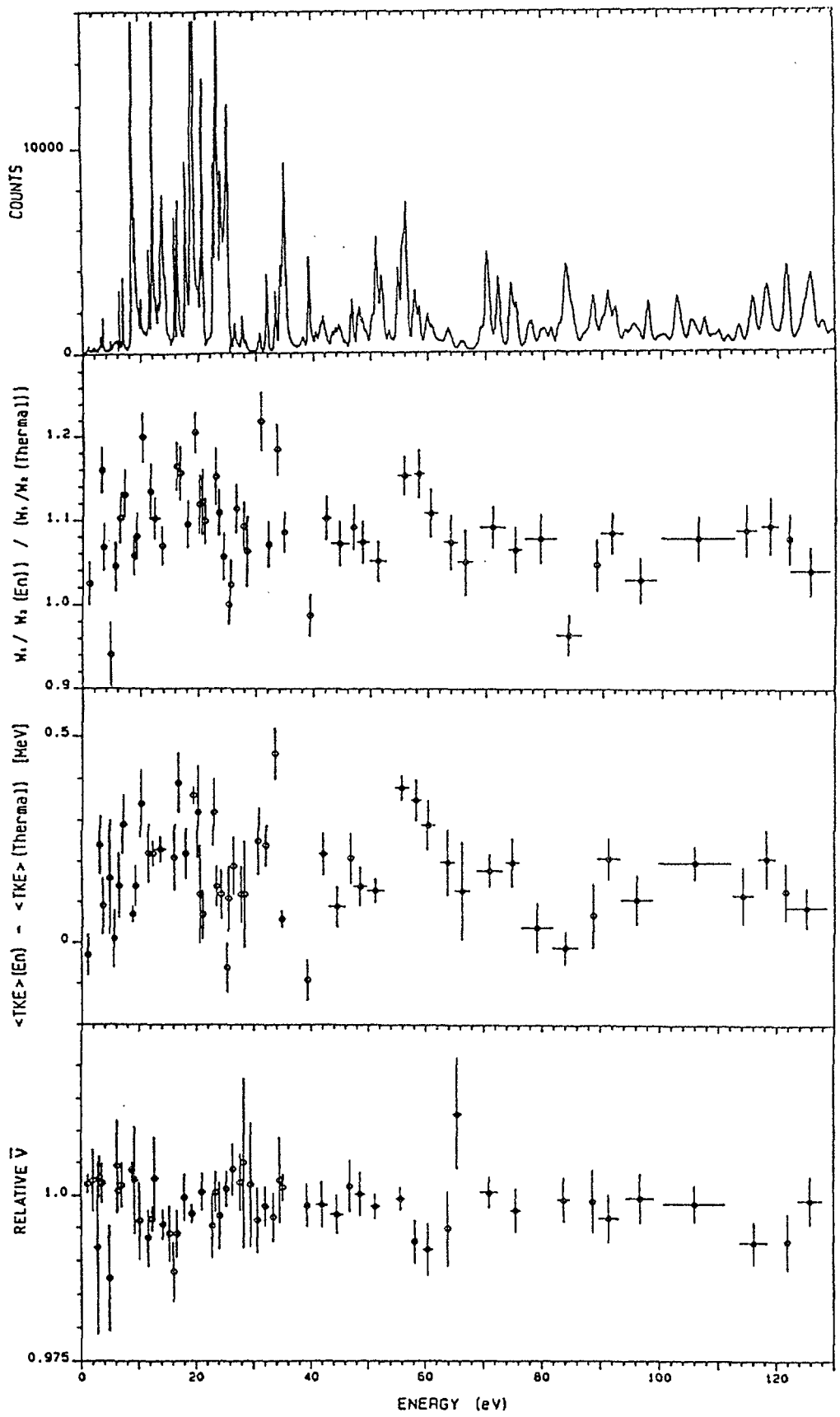

Fig. 3

The neutron time-of-flight spectrum, the relative ratio of the standard I/standard II fission mode populations, the <TKE>-fluctuations with respect to the thermal value and the relative ν-values of Howe et al. are plotted versus the incident neutron energy.

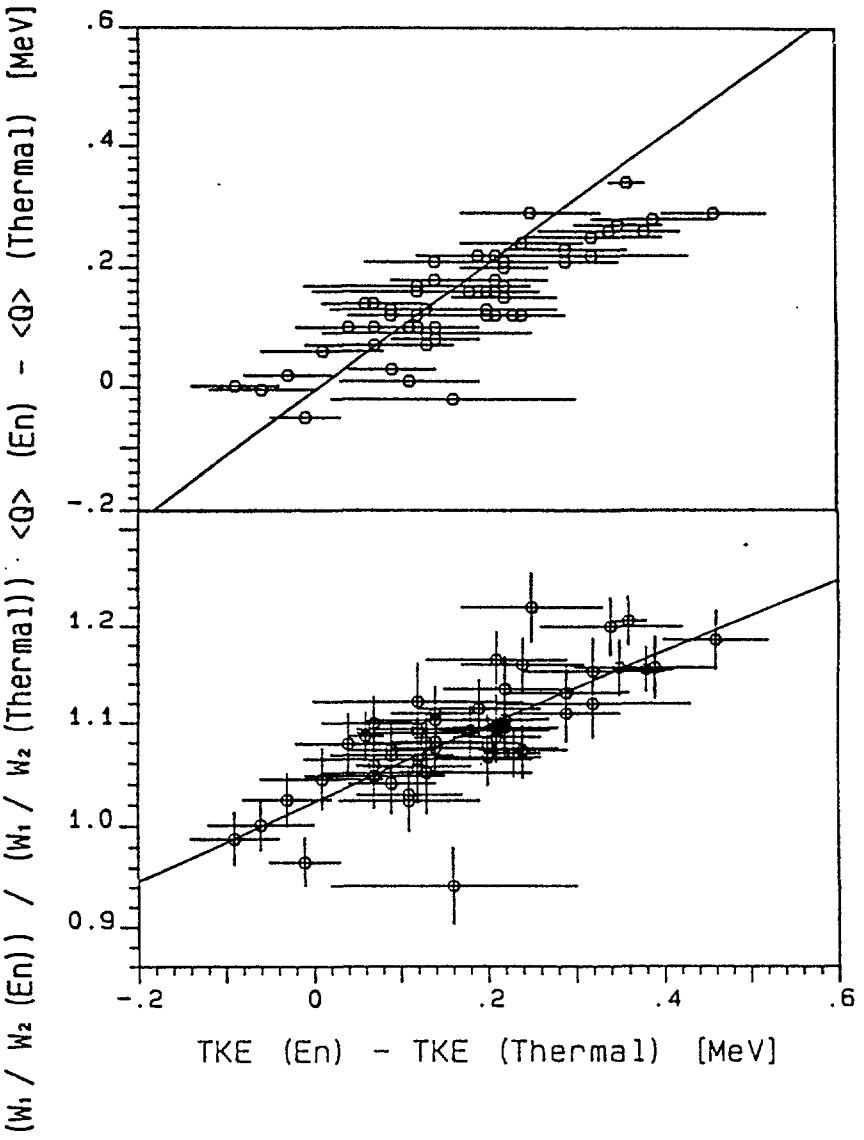

Fig. 4

Correlation diagram of the relative population ratios of the standard I and standard II fission paths and the relative average $\langle Q \rangle_{E_i}$-values are plotted with respect to the relative total kinetic energies $\langle TKE \rangle_{E_i}$.

3.) Correlation of ν with $\langle TKE \rangle_{E_i}$ and $Y_{E_i}(M)$

An anticorrelation between the ν-values of Howe et al. (14) and the present $\langle TKE \rangle_{E_i}$ values is observed as shown in fig. 3. Below 40 eV neutron energy this anticorrelation between the two quantities is most clearly visible. The correlation coefficient of $r = (-0.40 \pm 0.13)$, calculated according to Bevington (16) and Fisher (17) using the statistical weights of the input data, confirms this anti-correlation if 43 comparable values of the presented energy range are used. If one limits the comparison to the data below 40 eV, then even a correlation coefficient of $r = (-0.69 \pm$

0.11) is obtained. A significance test of the correlation coefficients, the Students t-test, gave for both cases 99% and 99.9 % probability for the existence of an anticorrelation between the ν and <TKE>-fluctuations. The same evaluation was done with the ν-data of Reed (2) and Fréhaut et al. (18). The correlation coefficients are $r = (-0.43 \pm 0.18)$ for 21 data points and $r = (-0.25 \pm 0.20)$ for 19 data points of the above-mentioned data-sets, respectively. Therefore the anticorrelation between the fluctuations of ν and <TKE> is established.

The mass-split dependence of ν as given in fig. 1 shows high values for ν compared to the average for symmetric mass splits. This mass split dependence of ν led in the past to the search for a connection between the ν - fluctuations and the resonance spins J. In the region of symmetric masses, where the fission channel theory of Bohr expects differences in the mass yields between the transition states with different J, particularly many neutrons are emitted. With variations of the symmetric mass yield correlated changes of ν-values are expected. However, the present measurement has shown that also the mass-asymmetric yields vary from resonance to resonance, and their absolute changes are much larger than those in the symmetric mass region. This can be seen from the difference spectrum given in the middle part of fig. 2. Moreover, the changes of the asymmetric mass distribution with resonance energy cause predominantly the variation of the reaction <Q>-value, which is observed together with a correlated change of <TKE>. Therefore the difference energy between <Q> and <TKE> which is available for other processes, varies much less than <TKE>. Also drastic relative changes in the symmetric fission yield cannot cause the observed fluctuations in ν , because of their small contributions on an absolute scale.

The explanation for the fluctuations of ν with resonance energy is given by the mass split dependence of ν as shown in fig. 1 and by the fluctuations of the asymmetric mass peak yields as seen in the middle part of fig. 2. The neutron multiplicity in the mass split range 129/107 to 138/98 is below the average and for more asymmetric splits above the average. These are the mass split ranges where the yields increase and decrease, respectively, when <TKE> increases with respect to the thermal value. The net effect is an effective reduction of ν which explaines the observed anticorrelation. A correlation between ν and the spin J can be excluded.

4.) The fluctuations of E_γ

The average energy released by promptly emitted γ-rays for $^{235}U(n,f)$, E_γ, was measured in the resonance region together with ν in experiments by

Reed(2) and Fréhaut et al. (18). An anticorrelation between E_γ and ν was expected since it was assumed that the energy available for both processes stayed constant. The measurements of Fréhaut et al. showed fluctuations with resonances, however the uncertainties were too large to draw conclusions for a (ν-E_γ) anticorrelation. The measurements of Reed yielded an unexpected correlation between ν and E_γ.

The γ-multiplicity and the γ-energy as function of mass split were measured by Pleasonton et al. (19). The mass-split dependence of both quantities shows qualitatively a very similar behaviour as the neutron multiplicity does. Therefore, the same arguments as were used in the previous section for the explanation of the ν-fluctuations are valid for the explanation of the E_γ-fluctuations. Hence, ν and E_γ should be positively correlated, and therefore, the E_γ fluctuations should be also anti-correlated with the <TKE>-fluctuations of the present experiment. The correlation coefficients between the E_γ and <TKE>-fluctuations of $r = (-0.11 \pm 0.27)$ for 14 and $r = (-0.28 \pm 0.19)$ for 24 comparable values of Reed and of Fréhaut et al., respectively, do however not allow a definite conclusion about the correlation of E_γ with the other fission parameters.

5.) Conclusions

From the present measurement it can be concluded that the fluctuations of the average number of neutrons, ν, originate from the fluctuations in the populations of the standard I and standard II exit channels, which compose the asymmetric mass peak. Since no spin dependence for the asymmetric mass yield fluctuations is observed also the ν-fluctuations are not J-dependent.

A correlation instead of an anticorrelation is expected between ν and E_γ.

The question, why the mass yields show fluctuations, can be answered with the following : Each of the Brosa exit channels must possess one or more accessible nuclear states. If the matrix elements between the compound state and these states are small and Gaussian distributed, the partial fission widths $\Gamma_{f,i}$ will be X^2_n-distributed, like it is normally the case for Γ_f. Therefore the branching ratios

$$R_i = \frac{\Gamma_{f,i}}{\sum_i \Gamma_{f,i}} \quad with \quad \Gamma_f = \sum_i \Gamma_{f,i}$$

will fluctuate. The number of degrees of freedom n per exit channel should then reduce compared to the number of degrees of freedom of the total fission width Γ_f.

References

1) S. Weinstein, R.L. Reed and R.C. Block
Proc. of Symposium on Physics and Chemistry
of Fission, I.A.E.A., Vienna, (1964) page 477

2) R.L. Reed
Ph. D.-thesis, Rensselaer Polytechnic Institute, Troy,
New York, 1973

3) Yu. v. Ryabov, So Don Sik, N. Chikov and N. Yaneva
Sov. J. Nucl. Phys. 14, 519 (1972)

4) J.P. Theobald, J.A. Wartena, and R. Werz
J. Nucl. Energy, 27, 435(1973)

5) V.F. Apalin, Yu. V. Gritsyuk, I.E. Kutikov, V.I. Lebedev, and L. A. Mekaelian
Nucl. Phys. 71,553(1965)

6) G.A. Keyworth, C.E. Olsen, J.D. Moses, J.W.T. Dabbs, and N.W. Hill
Conf. on Nucl. Cross Sections and Technology
Washington D.C., USA, 1975
NBS - Special Publication 425, 576 (1975)

7) M.S. Moore, J.D. Moses, G.A. Keyworth, J.W.T. Dabbs, and N.W. Hill
Phys. Rev. C18, 1328 (1978)

8) F.-J. Hambsch
Ph.-D. thesis, CBNM Geel, Belgium (1987)

9) F.-J. Hambsch, H.-H. Knitter, C. Budtz-Jørgensen, and J.P. Theobald,
to be published

10) U. Brosa, S. Grossmann, and A. Müller
Proc. of XVIth Intern. Symp. on Nuclear Physics,
Gaussig/Dresden (1986)

11) U. Brosa, S. Grossmann, and A. Müller
Z. Naturforsch. 41a, 1341 (1986)

12) H.-H. Knitter, F.-J. Hambsch, C.Budtz-Jørgensen, and J.P. Theobald
Z. Naturforsch. 42a, 786 (1987)

13) H.-H. Knitter, F.-J. Hambsch, C.Budtz-Jørgensen, and J.P. Theobald
Proc. of Intern. Conf. on Neutron Physics,
Kiew, SU, 21st-25th Sept. 1987, to be published

14) R.E. Howe, T.W. Phillips, and C. D. Bowman
Phys. Rev. C13, 195 (1976)

15) P. Möller, and R. Nix
Atomic Data Tables 26, 165 (1981)

16) P.R. Bevington
Data Reduction and Error Analysis for the Physical Science
Mc. Graw Hill, New York (1969)

17) R.A. Fisher
Statistical Methods for Research Workers
Oliver and Boyd, Edinburg (1958)

18) J. Fréhaut, and D. Shakleton
Proc. of Symposium on Physics and Chemistry of Fission, IAEA,
Rochester (1973) p. 201

19) F. Pleasonton, R.L. Ferguson, and H. W. Schmitt
Phys. Rev. C6, 1023 (1972)

MASS DISTRIBUTION STRUCTURES AS A FUNCTION OF EXCITATION ENERGY OF THE ^{252}Cf SPONTANEOUS FISSION FRAGMENTS

I.D. Alkhazov, A.V. Kuznetsov, S.S. Kovalenko,
B.F. Petrov, V.I. Shpakov
Khlopin Radium Institute,
Leningrad 197022, USSR

Abstract: Structures with a period of 5 amu were found in the fragment mass distributions in the ^{252}Cf spontaneous fission. The structures were observed for both the maximal and minimal fragment excitation energies as well as for the most asymmetric excitation energy partition between the fragments.

(^{252}Cf, spontaneous fission, neutron multiplicities, mass distributions, fragment excitation energy)

Partial multiplicities of neutrons emitted in spontaneous fission of ^{252}Cf by meach of complementary fragments were simultaneously measured by means of a set-up comprising a combination of two large liquid scintillators. The fragment kinetic energies were also measured using silicon SB-detectors. Scintillator tanks were separated one from another by a combined shield to avoid their mutual influence /1/.

The initial two-dimensional distribution $P(\nu_1,\nu_2)$ of neutrons emitted by both complementary fragments were reconstructed as a function of the fragment mass A and total kinetic energy with corrections for background, time resolution and neutron detection efficiency introduced. Finite mass and energy resolution of the fragment registration was allowed for /2/.

To perform the $P(\nu_1,\nu_2)$ distribution unfloding a method of statistical regularization was employed using prior information on the initial distribution momenta /3/. The $P(\nu_1,\nu_2)$ distributions

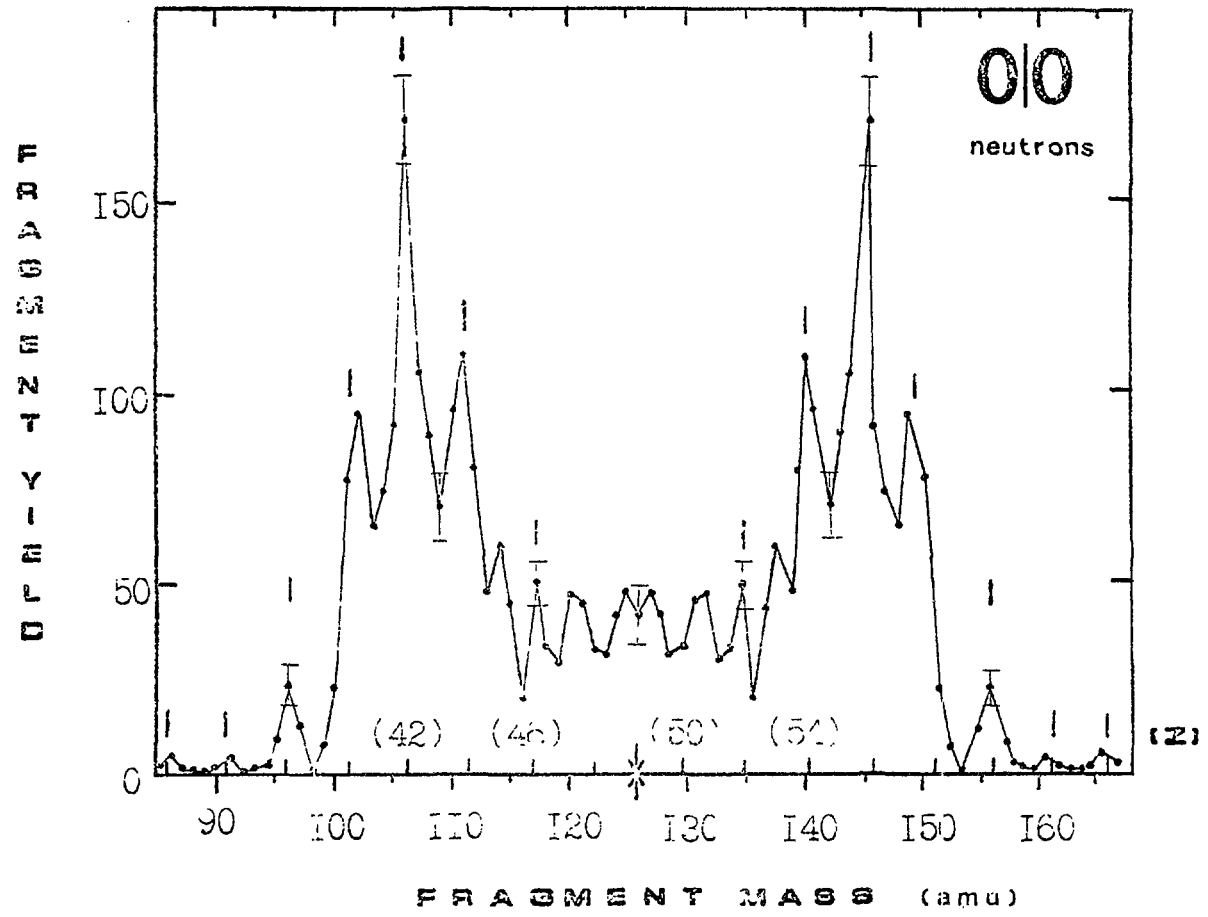

Fig.1 Preneutron mass distribution of the fission fragments in the case when no neutrons are emitted

for various A were then converted into preneutron mass distributions of fragments emitted fixed numbers of neutrons - $Y_A(\nu_1, \nu_2)$. (Figures ν_1 and ν_2 in this case denote the numbers of neutrons emitted by a fragment with mass A and by its complement with mass 252 - A).

Fig.1 presents such a mass distribution $Y_A(0,0)$ for the case when no neutrons are emitted. The main features of this distribution are a narrow peak at the mass A = 145 corresponding to the neutron deformed shell N = 88, and besides a pronounced structure with a period of about 5 amu. The peaks of this structure correspond to even fragment charges and are connected with the proton pairing effects. Values of the most probable charges as a function

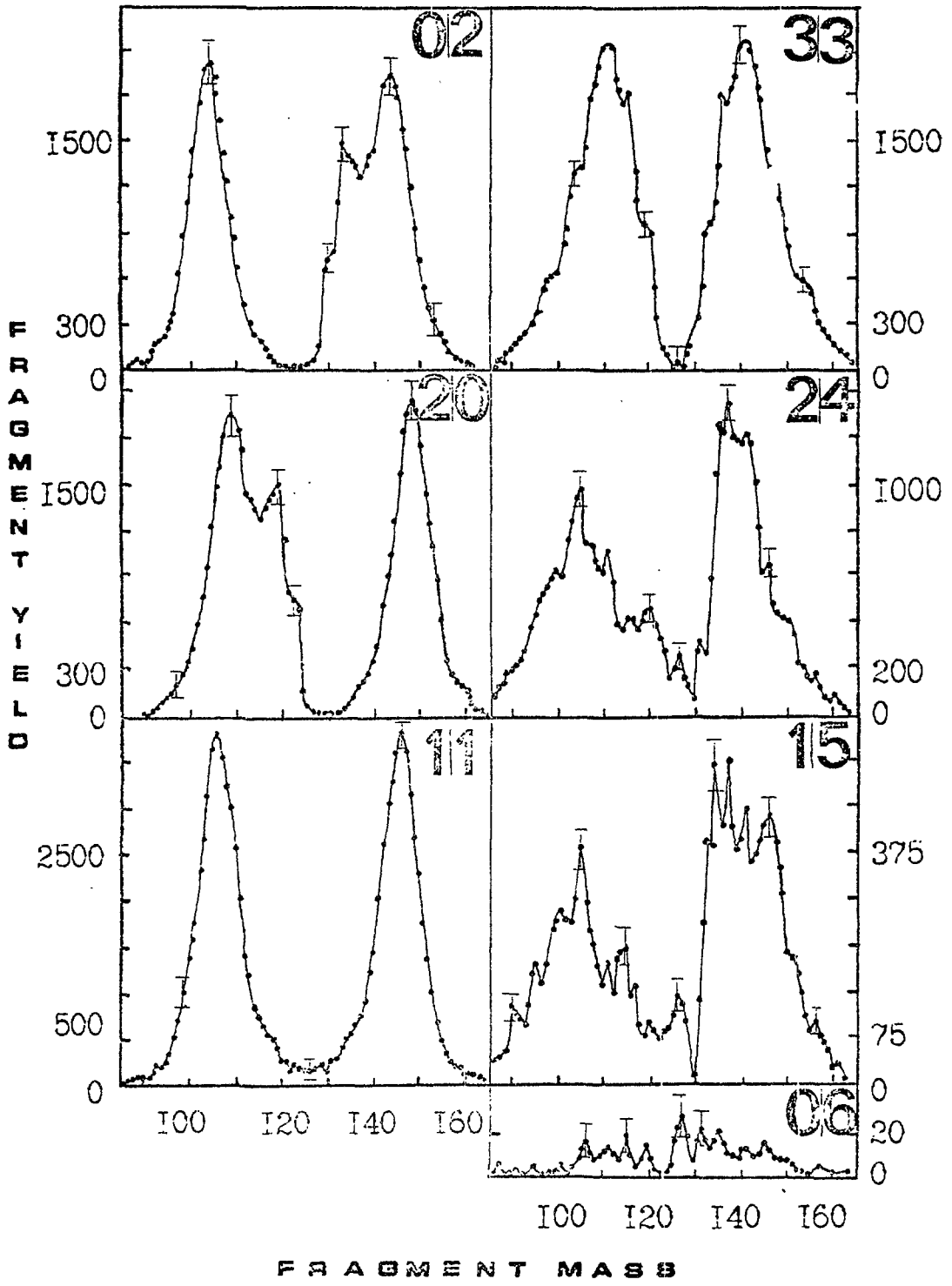

Fig.2 Partial fragment mass distributions in the cases when $\nu_{total} = 2$ and $\nu_{total} = 6$

of fragment mass for the ^{252}Cf spontaneous fission were taken from /4/. Such shell and even-odd charge structures which are characteristic for cold compact fission and vanish with the fragment excitation increase are found in a number of works /5-8/ and can be regarded as established.

Fig.2 presents preneutron mass distributions for various combinations of (ν_A, ν_{252-A}) at $\nu_{total} = 2$ and 6. It can be seen that the even-odd charge structure disappears at $\nu_{total} = 2$ and at the same time a new shell peak arises at A = 132 together with that at A = 145, which corresponds to the double magic shell (Z=50, N=82). In the case of $\nu_{total} = 6$ structures with the period of 5 amu appear again being the more pronounced the more asymmetric is excitation energy partition between the fragments (cf. the cases (3,3), (2,4), (1,5).

Existence of structures similar to those at the cold compact fission at the fragment excitation energy over 60 MeV (which is equivalent to the emission of 6 neutrons or more) suggests that strongly deformed configurations can be "cold" in the scission point and the final fragment excitation energy is conditioned by their deformation energy.

The possibility of strongly deformed cold fission was proposed by Hasse /9/ proceedings from the fact experimentally observed by Nifenecker et al. /10/ that covariance of the number of neutrons emitted by complementary fragments for fixed A is reduced to zero both at maximal and minimal values of TKE. A similar experimental fact was also obtained in our measurements (see Fig.3). According to Nifeneckers calculations /10/, the zero value of $Cov(\nu_1, \nu_2)$ corresponds to zero variance of the fragment excitation energy which means reducing to zero of free energy and consequently the intrinsic excitation in the scission point.

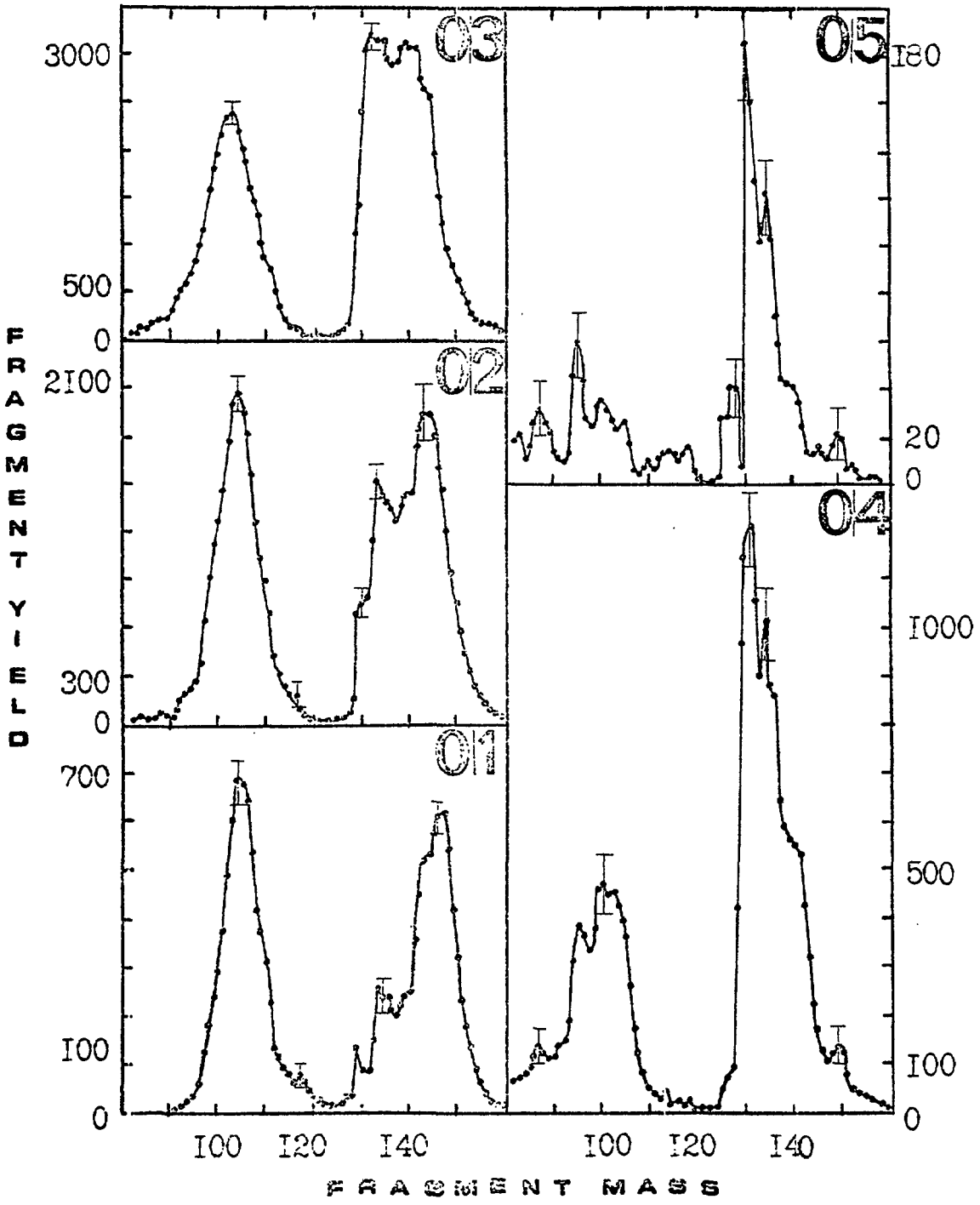

Fig.3 Momenta of multiplicity distributions of neutrons emitted by the complementary fragments with the mass A = 108-144 amu as a function of TKE

(a) data from this work (b) data from /10/

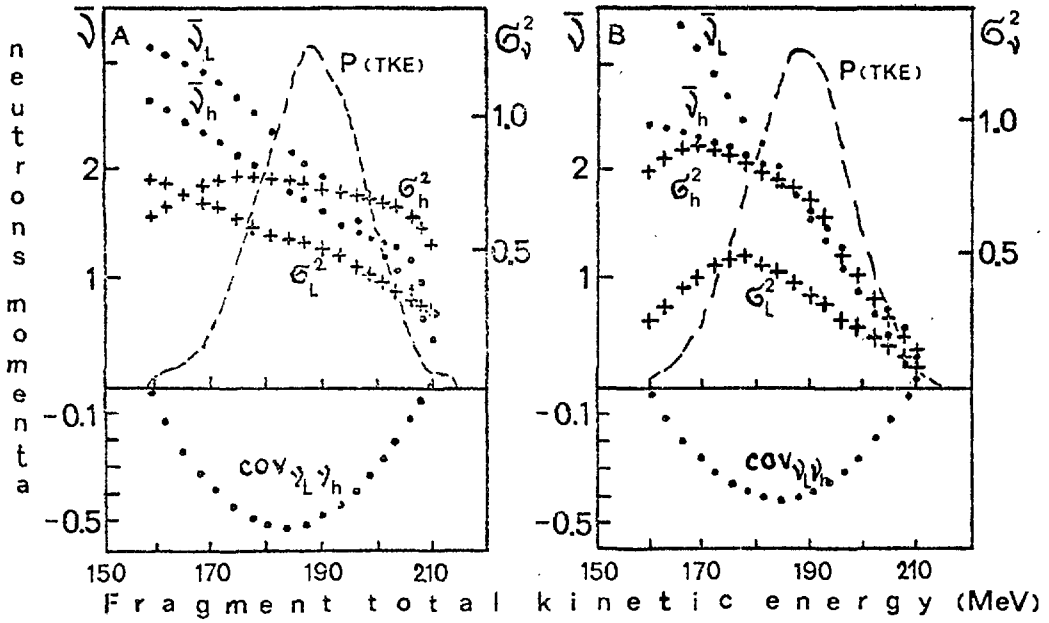

Fig.4 Preneutron fragment mass distributions for fixed compact configuration of one fragment ($\nu_1 = 0$)

Hower, on the basis of our results it can be proposed that cold deformed fission is conditioned rather by deformation of one fragment than by deformation of the whole system. If one fixes a compact configuration of one fragment with mass A ($\nu_1 = 0$) and considers the behaviour of mass distributions with the other fragment deformation (i.e. the number of neutrons emitted) (Fig.4), it can be seen that at the very asymmetric deformation (for example, the case (0,4)) the even-odd charge structure appears at a rather modest deformation or excitation energy, that is at $\nu_{total} = 4$, which is close to $\bar{\nu}$ (^{252}Cf) = 3.75.

The data obtained suggest that there can be two types of cold scission configurations:

1. With small deformations of both fragments and with minimal values of total excitation energy-cold compact fission;

2. With large fragment deformations and/or total excitation energies, being more pronounced as both the excitation energy and the asymmetry of its partition between fragments are higher.

REFERENCES

1. I.D.Alkhazov et al. In Proc. of 6th All-Union Conf. on Neutron Physics, Kiev, USSR, 1983. Moscow, ZNIIatominform, 1984, v.1, p.32.
2. I.D.Alkhazov et al. Sov. Nucl. Phys. 47, 1214 (1988).
3. I.D.Alkhazov et al. In Proc. of the XV Internat. Symp. on Nucl. Physics: Nucl. Fission. Gaussig, GDR, 1985, p.168.
4. UCRL - 9883.
5. G.Barreau et al. In Proc. of Internat. Conf. on Nucl. Data for Basic, and Appl. Sci., Santa Fe, USA, 1985, p.409.
6. J.P.Theobald. In Proc. of Internat. Conf. on Nucl. Data for Sci. and Technology, Antwerp, Belgium, 1982, p.719.
7. R.L.Walsh. Ref. 6, p.357.
8. G.Mariolopoulos et al. Nucl. Phys. A361, 213 (1981).
9. R.W.Hasse. Preprint GSI, Darmschtadt, FRG, 1987, GSI-87-24.
10. H.Nifenecker et al. In Proc. of Internat. Conf. on Physics and Chemistry of Fission. Rochester, USA, 1973, v.2, p.117.

SESSION 2:

ENERGY SPECTRUM OF FISSION-NEUTRONS

Chairman:

D. Seeliger

(TU Dresden, GDR)

Fission Spectrum Measurement of ^{232}Th and ^{238}U for 2 MeV Neutrons

M.Baba, H.Wakabayashi, M.Ishikawa, N.Nakashima*,
N.Ito and N.Hirakawa
Department of Nuclear Engineering, Tohoku University
Aramaki, Aoba, Sendai 980, Japan

Abstract

Prompt fission neutron spectrum for 2-MeV neutron induced fission was measured for ^{232}Th and ^{238}U using a time-of-flight technique and solid samples as fission source. The fission neutron spectra were obtained from 2 MeV to 10 MeV for Th and to 12 MeV for U. The parameters for Maxwellian and Watt type distribution functions that fitted the experimental spectra were deduced using a least squares technique, whereas neither of them interprets all-over the experimental spectrum. The Maxwellian temperatures obtained by the fitting were in agreement with those expected from the number of prompt neutrons per fission according to Terrell or Howerton & Doyas's formula.

Typical results are shown as well for double-differential neutron emission spectra of thorium and uranium for 14.1 MeV neutrons. These data, especially at backward angle, will be useful in test of models for neutron emission in multiple-chance fission.

Introduction

The prompt fission neutron spectrum in the neutron induced fission is of importance as the basis for applied purposes and model calculation of neutron emission in fission. However, previous experimental data are limited in number and quality, especially for fissionable nuclei. These data, most of them were taken until the beginning of the '70th, reported only restricted energy range of fission neutrons with insufficient experimental accuracy.

For measurement of fission neutron spectra over wide range of emission energy, a neutron spectrometer is required to have sufficient energy resolution and gamma-ray rejection capability. Recent neutron time-of-flight (T-O-F) spectrometer equipped with updated neutron detectors and electronics is expected to have potentials for application to fission spectrum measurement.

In this study, we have carried out the measurements of prompt fission neutron spectrum of ^{232}Th and ^{238}U for 2 MeV incident neutrons, using a T-O-F technique and solid samples. This paper describes the experimental techniques and data analyses as well as the results of fission spectrum in comparison

with evaluated values. The spectrum parameters are given for Maxwellian and Watt type distribution function.

There described are as well the measurement of double-differential neutron emission spectra of thorium and uranium for 14 MeV neutrons.

Experimental Apparatus

The measurements were performed using Tohoku University Dynamitron T-O-F spectrometer /1,2/ and relatively long flight path of 3.2 and 3.9 m for ^{232}Th and ^{238}U, respectively. Cares were taken for signal to background ratio, timing resolution, and for determination of detector efficiency and energy-scale of the spectrometer.

As the fission source, we adopted solid cylinder samples of elemental thorium and uranium, 2cm in dia. and 5 cm long, since the measurement using a fission chamber appeared unpractical because of limited number of fissioning atoms containable in the chamber, and of perturbation caused by chamber structure. The use of solid samples prevents to discriminate scattered neutrons from fission neutrons and to obtain the spectrum information below the incident energy because of overwhelming scattered neutrons.

Therefore, the incident energy was set at 2 MeV as that low acceptably but above the region of resonance structure in fission cross section, where a peculiar fission mode is observed.

The primary neutrons were produced via the T(p,n) reaction using a tritium -loaded titanium target. The 4.5 MV Dynamitron accelerator provided pulsed proton beam, about 1.5ns duration at 2 MHz repetition rate, and average beam current 4 to 6 micro-amps. The energy spread was about 50 to 70 keV in FWHM. The T-O-F spectrum of source neutrons was free from spurious components due to dark current and/or parasitic reactions down to 10^{-3} times of primary neutrons peak.

Figure 1 illustrates the experimental setup.

The fission samples were placed about 10 cm from the neutron producing target suspended by a remotely-controlled sample changer.

The neutron detector was housed in a massive hydrogenous shield with a tight collimation to reduce time-dependent backgrounds. The detector was a NE213 scintillator, 14 cm in dia. and 10 cm thick, coupled to a 5" dia. Hamamatsu R1250 photomultiplier (P.M) tube via a acrylic light pipe; the P.M tube was connected to a P.M base with special potential gradient to maintain timing-resolution over a wide range of neutron energy /3/.

The detector was incorporated with two separate zero-crossing pulse-shape discriminators (PSD) with pulse-height dynamic range of 400, to reject gamma-

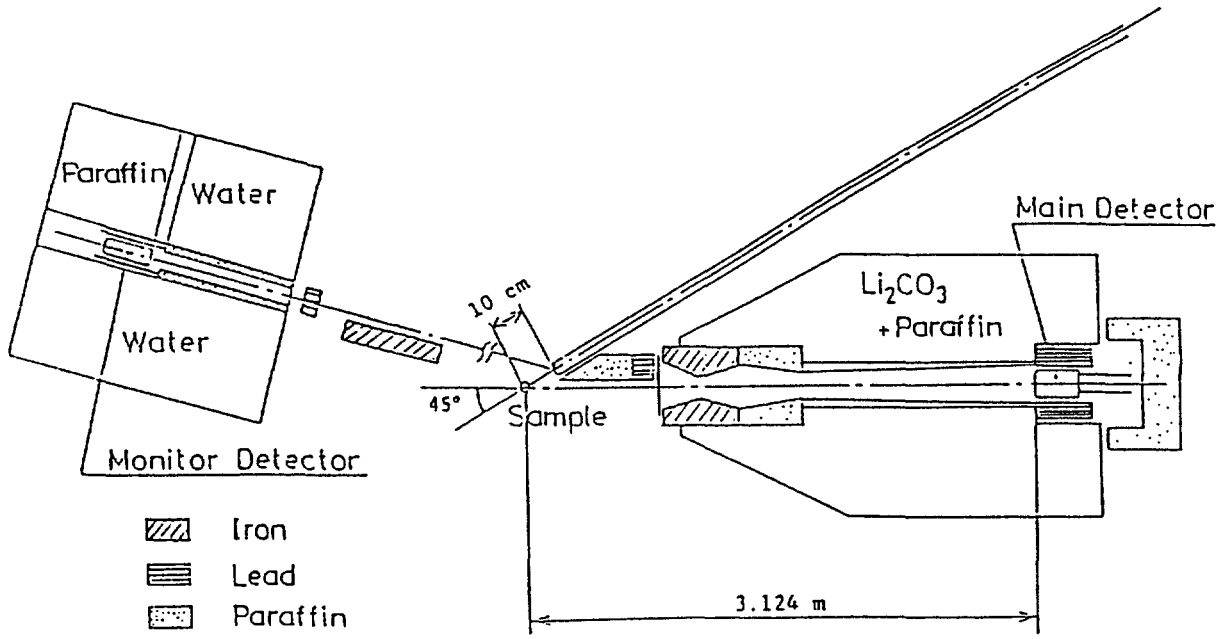

Fig.1. Experimental setup for fission spectrum meaurement.

rays backgrounds. The biases of the PSDs were set at 0.3 or 0.6 and 2 MeV proton. The higher bias eliminates most of the events caused by neutron interaction with carbon in the scintillator, and leads to a smooth detector efficiency curve /4/ and reliable PSD performance. The PSDs had been adjusted so as to cover all the neutron signals up to 18 MeV.

The relative efficiency of the detector was determined on the basis of Monte-carlo calculation /5/, and measurements of fission neutrons from ^{252}Cf and of hydrogen-scattered neutron yields at 14 and 18 MeV. Two measurements approved the calculated results except for the region near the bias, where calculation dose not necessarily represent actual detector performance. The efficiency near the bias was determined from the measurement of ^{252}Cf neutrons assuming NBS spectrum /6/ for Cf neutrons. The uncertainty of the efficiency curve is believed to be within 5 %.

A smaller NE213 scintillator monitored the spectrum and intensity of the source neutrons and provided the normalization of sample-in run to sample-out run.

The electronics block diagram is illustrated in Fig.2. The five data, i.e., two sets of T-O-F and PSD spectrum for each bias and monitor spectrum, were stored simultaneously in a multichannel pulse-height analyzer. Simultaneous data storage with two separate systems provided monitoring of the system reliability.

The energy-scale of the T-O-F spectrometer was determined from the measured flight path length and time width of the analyzer calibrated using ORTEC 462 time calibrator. This energy-scale was checked experimentally by

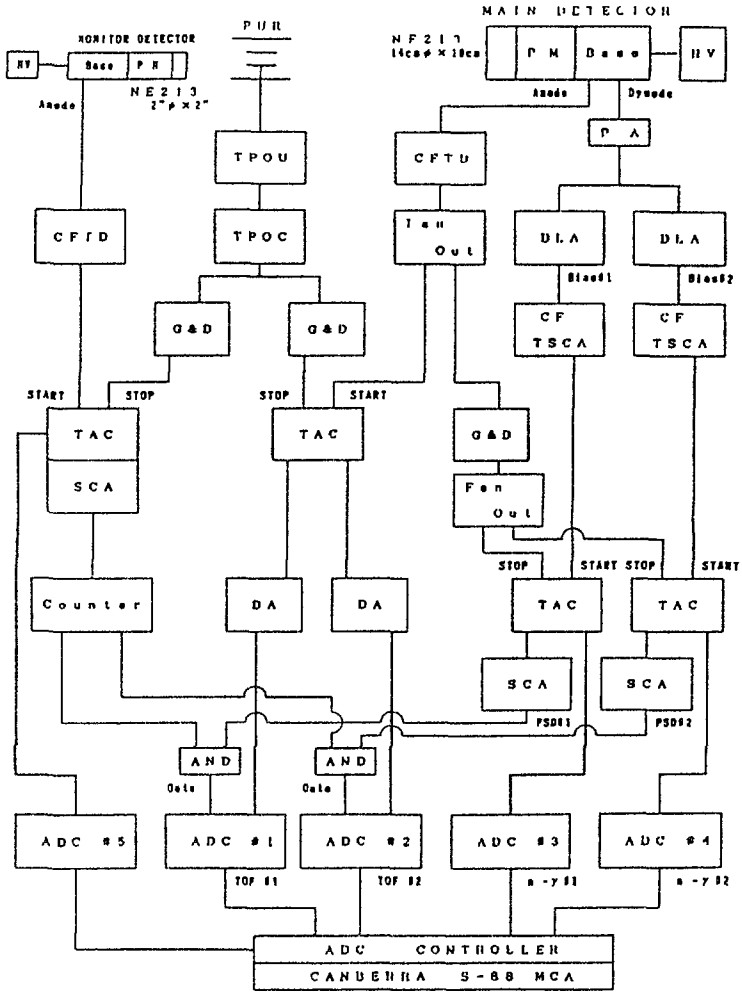

Fig.2. Electronics block diagram for fission spectrum measurement.

observing the T-O-F spectrum from the (d,n) reaction on a thin LiF target which produced several neutron peaks corresponding to excitation energy of residual nuclei. The neutron energies calculated by kinematics agreed within 1 % with those expected from the energy-scale. In addition, neutron transmission experiment for resonance structure of carbon and iron approved the validity of the procedure of energy-scale determination.

Measurements

The measurements were performed at laboratory emission angle of 135° to minimize the scattered neutron backgrounds. The data were taken in cyclic manner for samples of thorium or uranium, sample-out and lead sample in one to two hours interval checking the reproducibility of the counting system. The lead data were used to inspect the sample-dependent backgrounds and peak shape of elastically-scattered neutrons.

The overall timing resolution, determined from the width of prompt gamma-ray peak, was 1.6 to 1.8 ns.

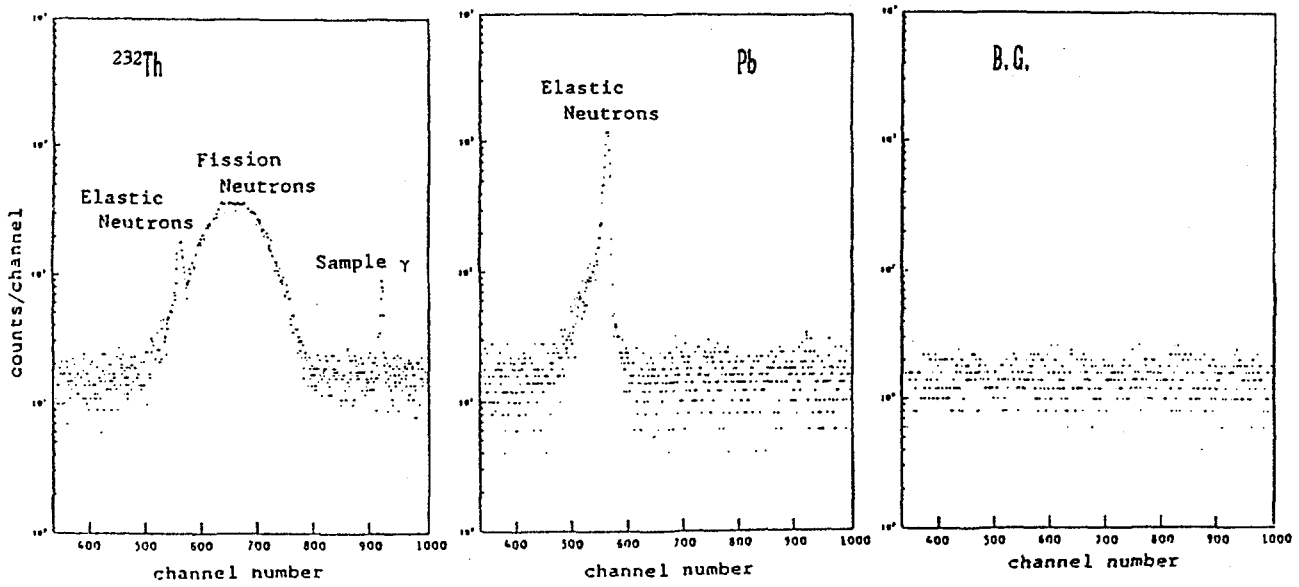

Fig.3. Time-of-flight spectra for thorium, lead and sample-out.

Figure 3 shows the resulting T-O-F spectra by high bias system for Th run. The spectra for lead and sample-out revealed flat distribution of backgrounds and no significant contribution of sample-dependent ones in the region of fission neutrons. Therefore, the background for samples could be assumed to be flat with a level determined by the counts at the region below detector bias.

Data Analyses

For derivation of fission spectrum, the data by high-bias system were used because of much better signal to background ratio. The data by low-bias system were in qualitative agreement with those by high-bias system.

The cumulative T-O-F data were corrected for backgrounds and detector efficiency, then were converted into energy spectra. The data were corrected further for the effects of 1) neutron multiple-scattering in the sample, 2) tail of elastically-scattered neutrons, 3) finite time-resolution of the T-O-F spectrometer, and for 4) time-shift due to detector thickness.

The effect of multiple-scattering was evaluated using Monte-carlo and analytic calculations. The calculations showed that multiple-scattering distorted very little, lower than a few %, the shape of fission spectrum so long as concerned above 2 MeV. This is mainly due to steeply rising spectrum shape with decreasing neutron energy.

The tail of the elastic peak was subracted by using the data of lead.

The effects 3) and 4) were also minor owing to sufficiently good energy resolution of the present spectrometer.

The results of fission spectrum were fitted by the least squares technique with the Maxwellian and Watt type distribution function in the form

$$N_M(E) = C_m.SQR(E).\exp(-E/T_m), \quad \text{and}$$
$$N_W(E) = C_w.\exp(-E/A).\sinh(BE), \quad \text{respectively,}$$

where, E and Tm is the neuron energy and Maxwellian temperature, respectively, and Cm, Cw, A, B are the constants.

Results and Discussion

In Fig.4 and 5, are shown the results of fitting the experimental fission spectra with Maxwell and Watt type function. The fitting was performed in the energy region only above 2 MeV; this procedure did not necessarily provide proper normalization for each spectrum and is appropriate for shape comparison alone.

Figure 3 and 4 indicate, in both cases of Th and U, that the Maxwellian distribution tends to deviate upward above 7 or 8 MeV, and Watt function shows reverse trend, while the experimental spectrum are not so definitive at highest energy region. Such features have been reported by Johansson & Holmqvist for 0.5 MeV neutron induced fission of ^{235}U /7/. The overprediction of high energy neutrons by Maxwellian spectrum is well known for ^{252}Cf fission spectrum; the present observation is consistent with the fact.

The parameters obtained by the fitting are following:

^{232}Th; Tm=1.26, A=0.96, B=2.17

^{238}U; Tm=1.25, A=0.97, B=2.17,

the uncertainties of the parameters are the order of a few %. The present values of Maxwellian temperature are overlapped within experimental uncertainty with that by Batchelor et al. (Tm=1.26 MeV) for Th at 3 MeV /8/, and that by Barnard et al. (Tm=1.29+0.03 MeV) for U at 2 MeV incident energy /9/. They are also compared with that predicted by Terrell/10/ or Howerton & Doyas's /11/ formula on relation of Maxwellian temperature Tm or mean energy of fission neutrons versus number of prompt neutrons per fission. The present Tm is in good agreement with the prediction for Th but is smaller by 4.5 % for U.

Then, the experimental fission spectra are compared with the evaluations by JENDL-2, 3T** and ENDF/B-IV in Fig.6 & 7. In the comparison, the spectra are normalized each other between 2 and 6 MeV. The Maxwellian spectra adopted in ENDF/B-IV are harder again in both cases of Th and U. The Watt spectrum for Th by JENDL-2 and Madland-Nix model/12/ calculation for U by JENDL-3T/13/, provide better presentation of the experimental data.

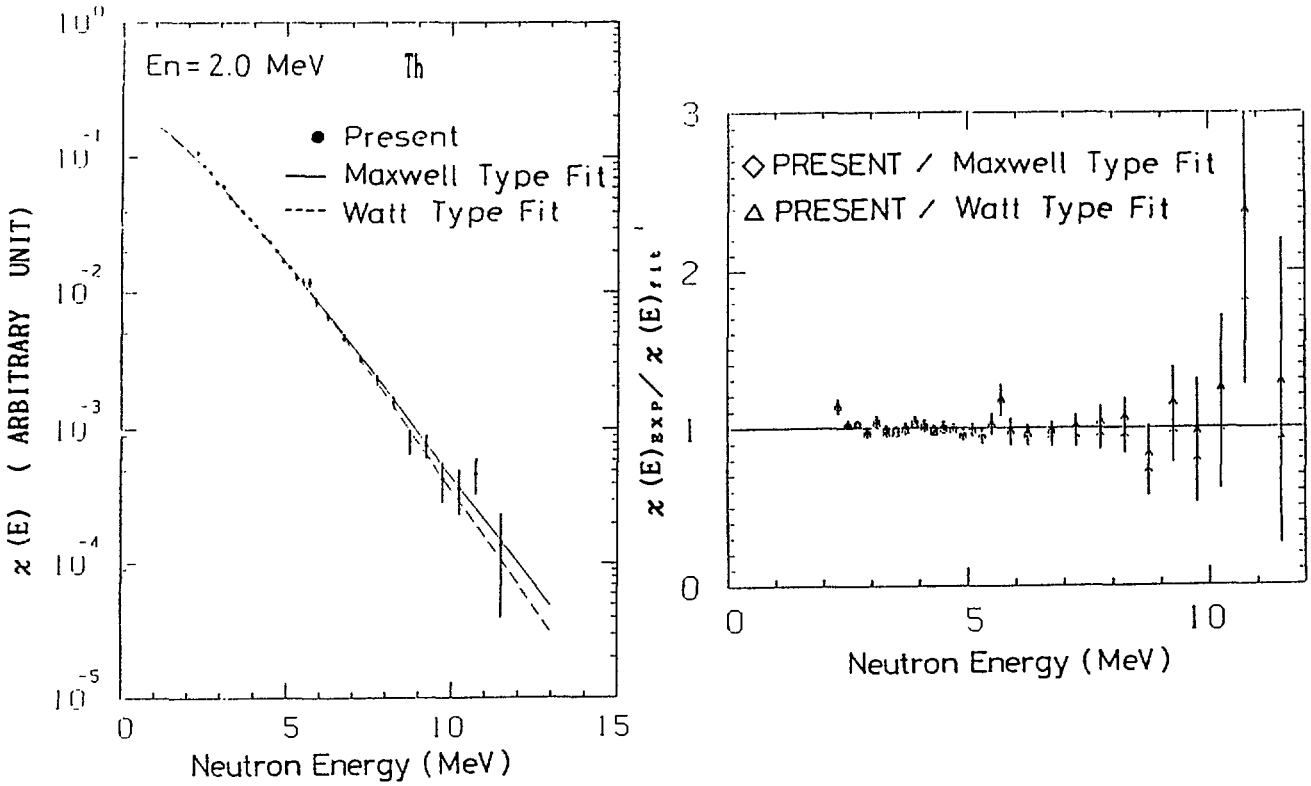

Fig.4. Th-232 prompt fission neutron spectrum compared with the Maxwellian and Watt type functions fitted to the experimental spectrum.

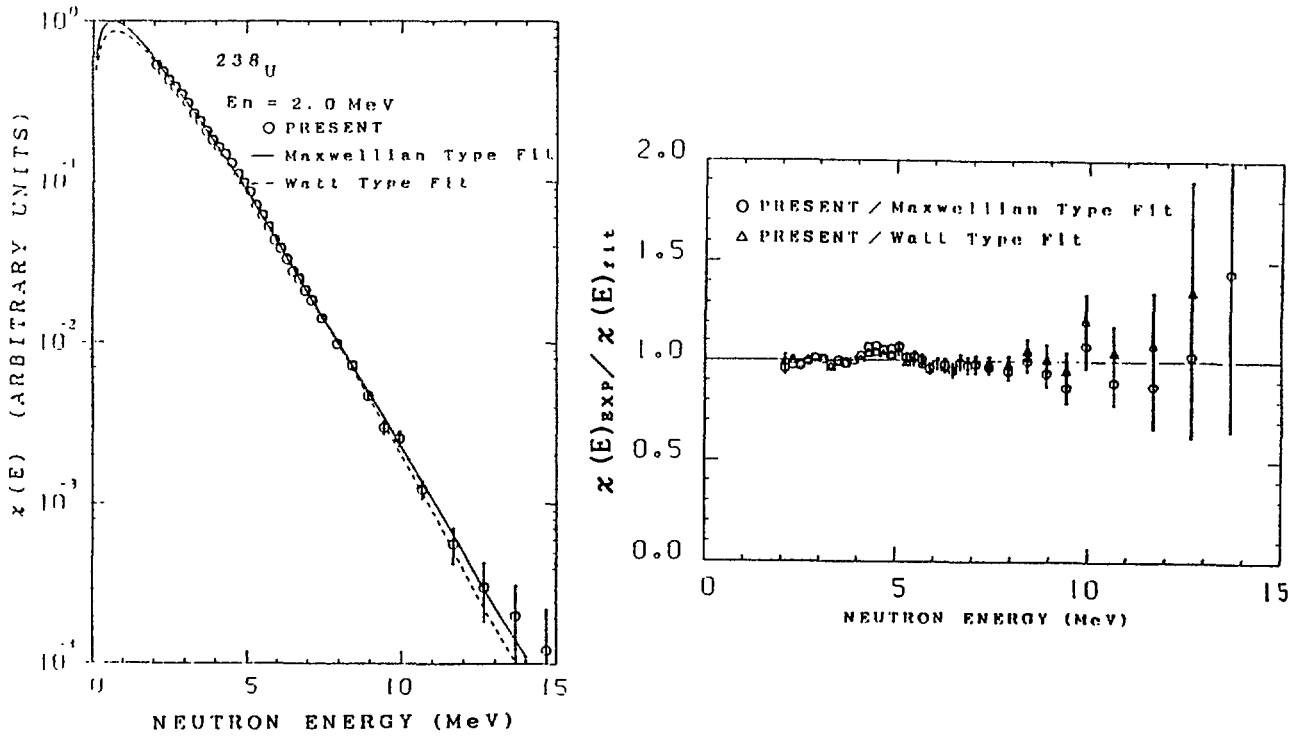

Fig.5. U-238 prompt fission neutron spectrum compared with the Maxwellian and Watt type functions fitted to the experimental spectrum.

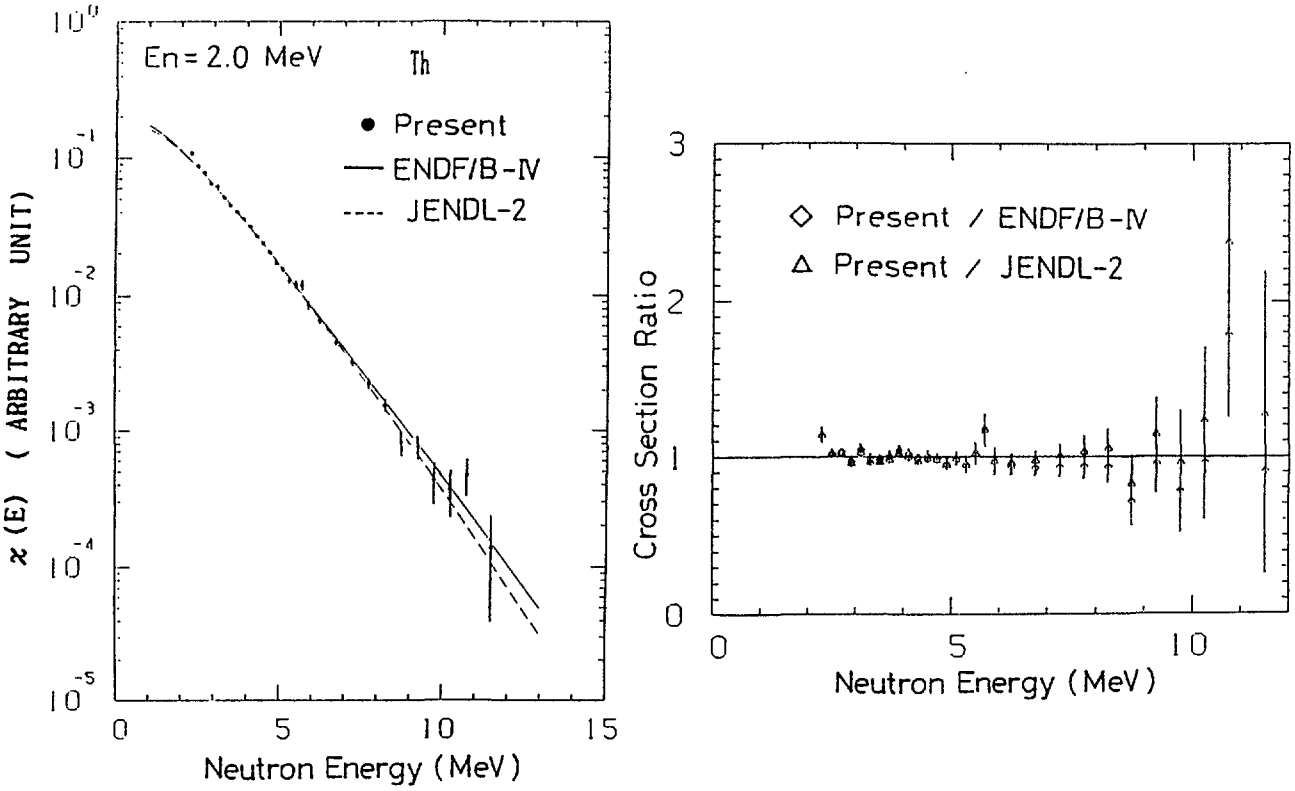

Fig.6. Th-232 prompt fission neutron spectrum compared with evaluations.

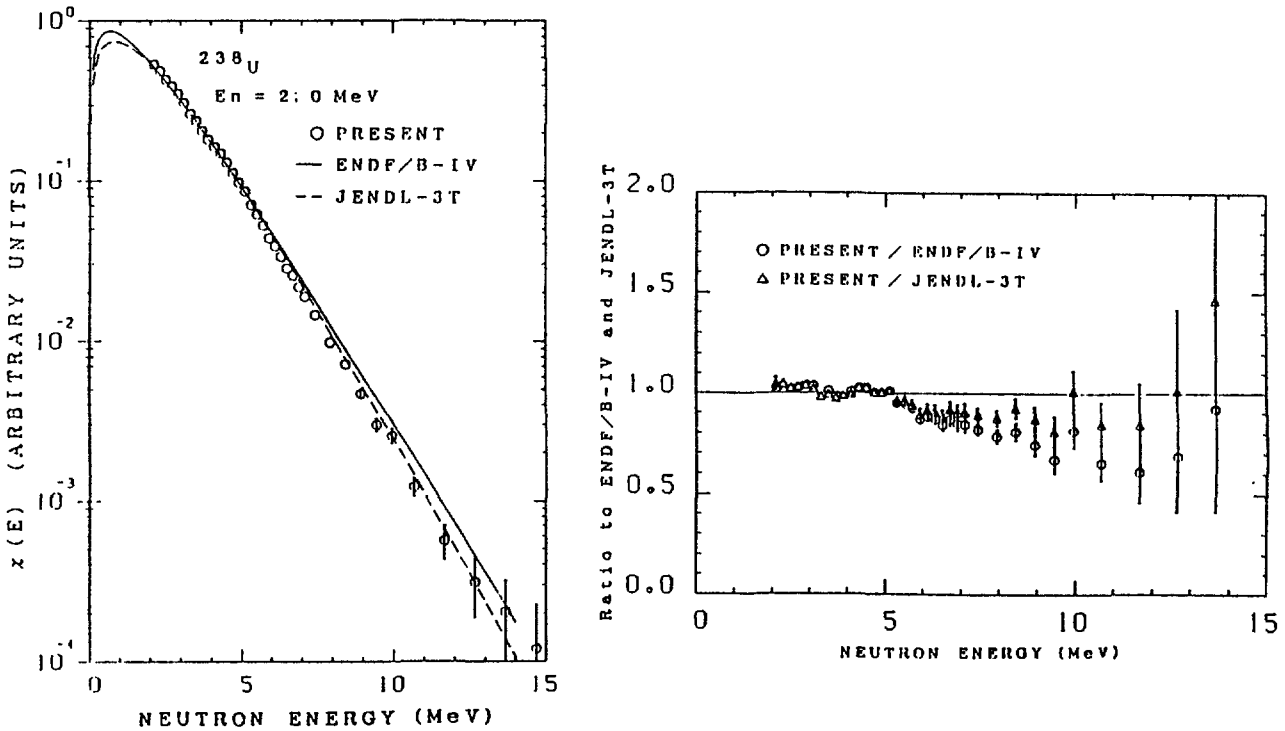

Fig.7. U-238 prompt fission neutron spectrum compared with the evaluations.

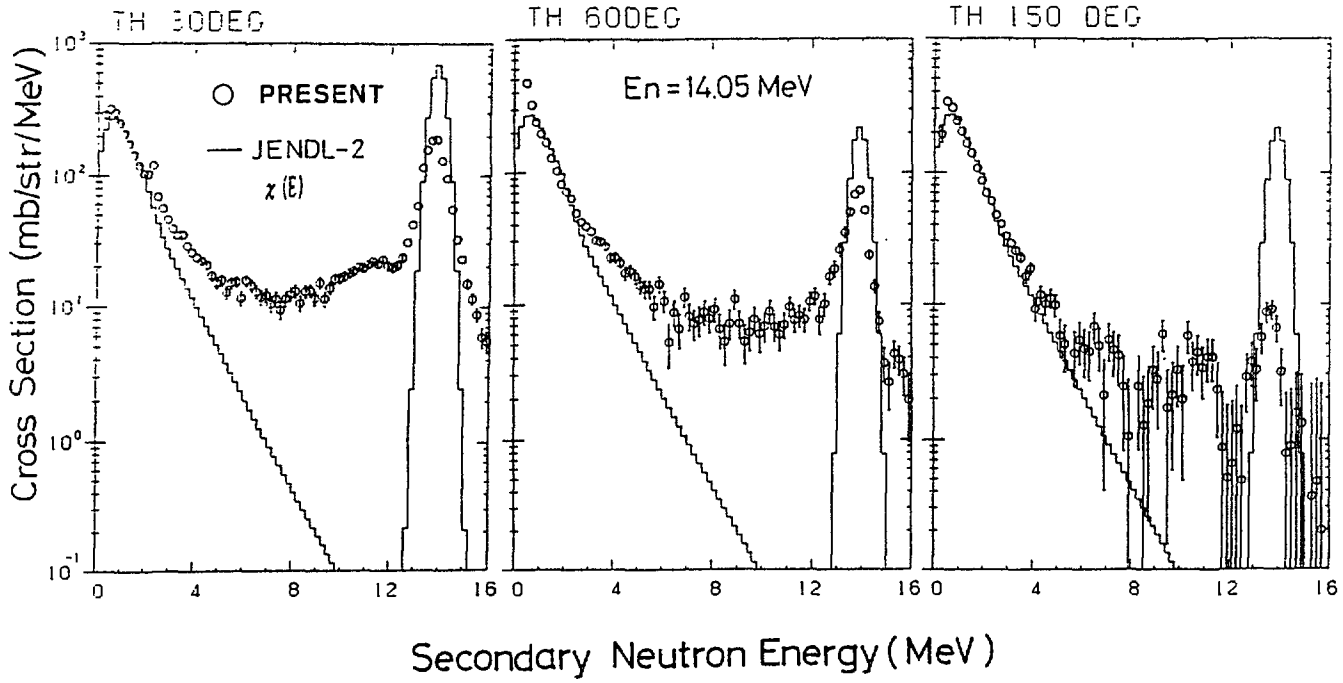

Fig.8. Double-differential neutron emission spectra of Th-232 for 14 MeV neutrons.

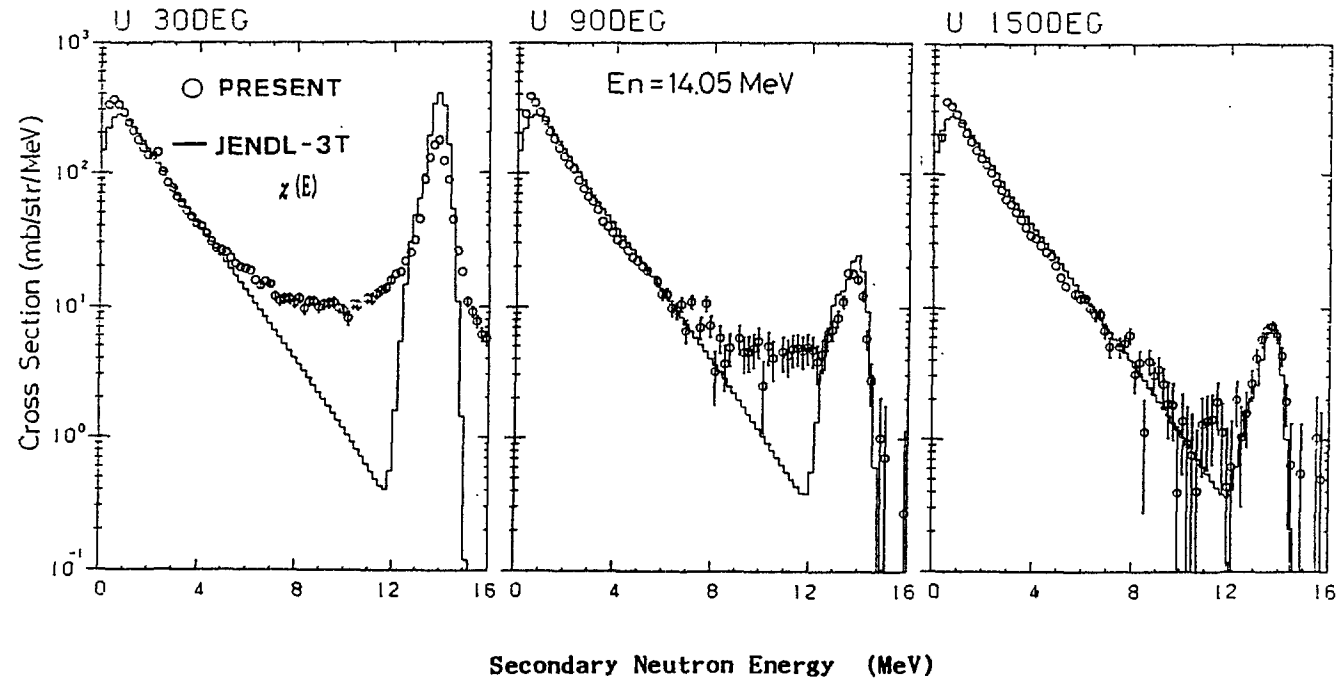

Fig.9. Double-differential neutron emission spectra of U-238 for 14 MeV neutrons.

The present data, however, were obtained at the fixed observation angle; therefore, the effect of angle dependence of the spectrum should be taken into consideration for more detailed discussion.

14 MeV Double-differential Neutron Emission Spectra of Thorium and uranium

Here briefly introduced are the double-differential neutron emission spectra of thorium and uranium for 14.1 MeV incident neutrons.

The measurements were performed similarly with above described experiment except that the primary neutrons were obtained via the T(d,n) reaction at 97.5° emission angle and the flight path was longer, 5 to 6m. Experimental details are described in ref.1 and 2.

Figure 8 and 9 show typical results.

Emission neutrons above about 5 MeV are strongly angle dependent because of pre-equilibrium emission mechanism. At backward angle, they are disappearing and emission spectra look close to the fission spectrum, while they still contain neutrons from low-lying levels and non-fission process of (n,Xn) reaction. Therefore, the backward data will be useful to extract fission spectrum information including multiple-chance fission, via a comparison with theoretical model calculations /14/. Data analyses are now in progress.

Summary

We have measured the prompt fission neutron spectrum of ^{232}Th and ^{238}U for 2-MeV neutron induced fission and obtained spectrum parameters for Maxwellian and Watt type distribution function. Both of them do not provide overall reproduction of experimental spectra. The deviation from the experiment show similar trend as in the cases of neutron induced fission of ^{235}U and spontaneous fission of ^{252}Cf.

For more detailed discussion, refinement of experimental data at high energy region and the check of angle dependence of fission spectrum are desired.

The 14 MeV neutron emission data, especially those at backward angle, will be used for test of the model for neutron emission in multiple-chance fission.

References

1. M.Baba; JAERI-M 86-029 pp.119
2. S.Chiba et al.; J.Nucl.Sci.Technol.,22(10) 1 (1985)
3. M.Baba et al.; NETU 47 110 (1986), (Dep. Nucl. Eng., Tohoku Univ.)
4. M.Drosg et al.; Nucl.Instr.Meth.,176 477 (1980)
5. V.Verbinski et al.; Nucl.Instr.Meth.,65 8 (1968)

6. J.A.Grundl & Eisenhauer; Proc. Conf. "Nucl. Data for Sci. Technol.,", NBS special publication 325 vol.2 pp.250
7. P.I.Johansson & B.Holmqvist; Nucl.Sci.Eng.,62 695 (1977)
8. R.Batchlor et al.; Nucl.Phys.,71 228 (1965)
9. E.Barnard et al.; Nucl.Phys.,71 228 (1965)
10. J.Terrell; Phys.Rev.,127 880 (1962)
11. R.J.Howerton & R.J.Doyas; Nucl.Sci.Engi.,46 414 (1971)
12. D.G.Madland & J.R.Nix; Nucl.Sci.Eng.,81 213 (1982)
13. JENDL compilation group (Nuclear Data Center, JAERI), private communication
14. D.Seeliger; presented at the consultant meeting

---

* Present address; Japan Atomic Energy research Institute

** JENDL-3T is a temporary file for testing the evaluated data for JENDL-3. The data in JENDL-3T will be partly revised in JENDL-3.

ENERGY AND ANGULAR DISTRIBUTION OF NEUTRON EMISSION IN THE SPONTANEOUS FISSION OF ^{252}CF

H. Märten, D. Richter, D. Seeliger,
Technical University, Dresden, GDR

W. Neubert,
Central Institute of Nuclear Research, Rossendorf, GDR,

A. Lajtai,
Central Institute for Physics, Budapest, Hungary

Abstract: A new experimental method has been applied to measure the double-differential emission probability of Cf fission neutrons between 100 keV and 10 MeV. The neutron-fragment correlation experiment has been based on neutron time-of-flight spectroscopy combined with a direction-sensitive method of fragment spectroscopy. The angular distributions obtained cover the whole range from 0 to π. Results are presented and discussed in comparison with previous data.

1. Introduction

Fundamental studies of fission neutron emission including the clarification of mechanisms require the precise measurement of emission probabilities $N(E,\Theta)$, i.e. depending on both LS energy E and emission angle Θ with reference to the light-fragment direction.[1] These provide the basis for the further developement of theoretical models for calculating fission neutron spectra.[2] Compared with previous measurements[3], i.e. fragment spectroscopy for a fixed solid angle and consecutive measurement of neutron spectra at selected neutron detector positions, the method used in this work relies on a direction-sensitive spectroscopy of the fission fragments to measure the whole distribution $N(E,\Theta)$ by the use of one or two neutron detectors at fixed positions simultaneously. In this way, systematic experimental uncertainties are avoided. First applications, in particular a measurement of anisotropy of ^{252}Cf(sf) neutron emission, have been presented elsewhere.[4,5] A similar method based on a gridded ion chamber (twin arrangement) has been recently developed at CBNM Geel.[6]

2. Experimental method

As represented schematically in the figs. 1 and 2, a position-sensitive parallel-plate avalanche counter[7] PPAC(PS) has been used for the measurement of fragment direction. The fast timing signal from a single PPAC located close to the fission sample S defines the fission time and , therefore, serves as the input pulse for the measurement of time-of-flight TOF of neutrons as well as fission fragments.

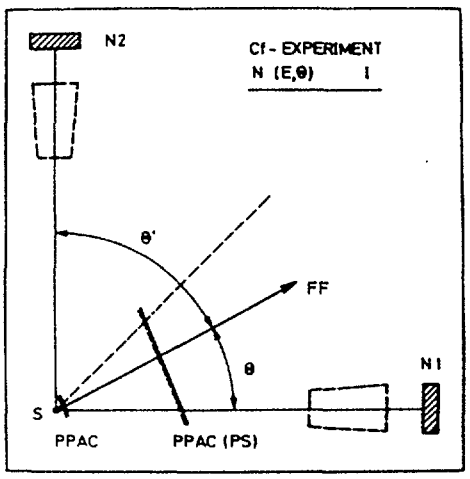

Fig. 1 Experimental arrangement of fragment detectors (PPAC, PPAC(PS)) as well as neutron detectors (N1, N2) for the $\pi/4$-geometry of fragment (FF) direction measurement (Variant I). The shadow cones for measuring the background of scattered neutrons are indicated.

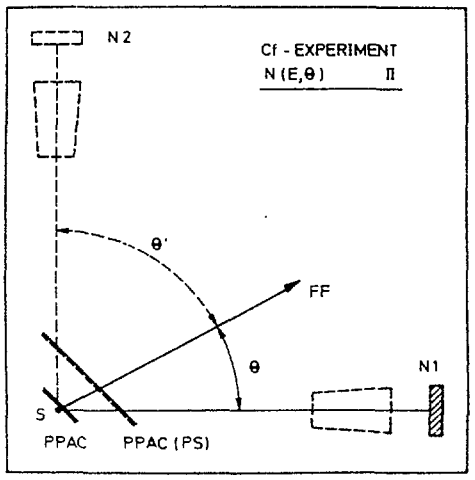

Fig. 2 As for figure 2, but for the $\pi/2$-geometry of fragment direction measurement (variant II).

The multi-parameter data acquisition (position amplitude, fragment TOF, neutron TOF for two neutron detectors) has been realized on the basis of a computer-microcomputer system with magnetic disc and 2D colour display. A typical two-dimensional fragment spectrum is represented in fig. 3 showing two banana-shaped regions, which correspond to the heavy and the light fragment groups, as well as resolved position peaks corresponding to the segments of the PPAC(PS). The distinction between the fragment groups has to be based on a subdividing line obviously depending on position.

The two experimental variants represented in the figs. 1 and 2 have been applied in two experiments characterized in table 1.

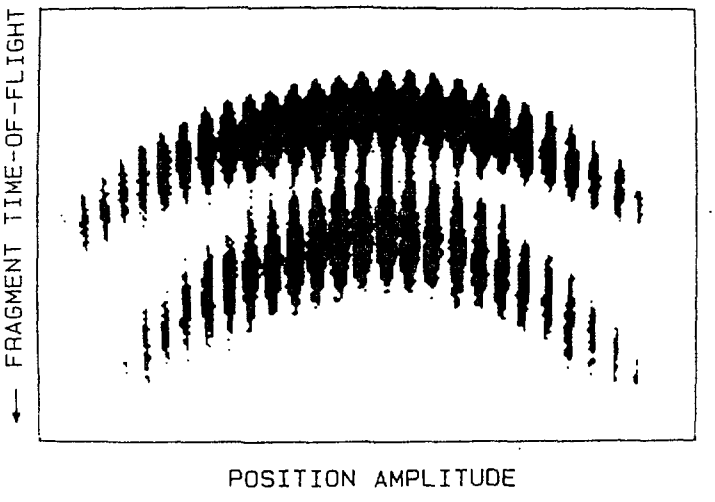

Fig. 3 Two-dimensional representation of a non-correlated fragment spectrum. The black regions include channels with more than 100 counts.

The $N(E,\Theta)$ data analysis includes the following procedures:

i) off-line generation of two-dimensional (neutron TOF, position) spectra for both neutron detectors and for selected fragment groups using a data sorting code,

ii) subtraction of the background components depending on E and Θ after their normalization (random background, spectrum of scattered neutrons from the shadow cone measurement, delayed-γ-ray spectrum in the case of Li glass detectors),

iii) computing the correlated position spectra for eligible neutron energy bins ΔE (corresponding to a certain neutron TOF scale bin) and the following unfolding, which yields the peak areas A_i corresponding to the angle Θ_i of neutron emission (i - PPAC(PS) segment number),

iv) calculation of the neutron emission probability according to

$$N_i(\bar{E},\Theta_i) = A_i \cdot \left[N_{FF} \cdot \bar{\nu} \cdot g_i \cdot \varepsilon(\bar{E}) \cdot \Delta\Omega_n \cdot \Delta E \right]^{-1}, \qquad (1)$$

where N_{FF} -number of counted fragment signals (PPAC(PS)), $\varepsilon(\bar{E})$ - neutron detection efficiency stated

Table 1 Synopsis of two different experiments

Item	Experiment 1	Experiment 2
neutron energy range	100 keV - 2 MeV	1 MeV - 10 MeV (18 MeV in polar direction)
PPAC-PPAC(PS) arrangement	$\pi/2$-geometry (fig. 2)	$\pi/4$-geometry (fig. 1)
angular resolution (fragments)	4.0 deg	1.8 deg
neutron detector type	NE 912 (6-Li glass scintillator)	NE 213 (liquid organic scintillator)
neutron detector size	4.5 cm in diam. 0.95 cm thickness	12.7 cm in diam. 3.8 cm thickness
photomultiplier	56 AVP	XP 2040
flight path	35 cm	1.6 m
time resolution (FWHM γ-peak)	2.55 ns	1.45 ns
background suppression	amplitude discrimination	pulse shape discrimination
additional background measurements	shadow cone arrangement (scattered-neutron background) NE 913 (7-Li det.) measurement (delayed-γ-ray background)	shadow cone arrangement (scattered-neutron background)

for the energy bin average $\overline{E}$, $\overline{\nu}$ - average number of neutrons per fission, g_i - geometrical efficiency of fragment detection (see below), $\Delta\Omega_n$ - solid angle of neutron detection.

Non-correlated fragment spectra have to be measured additionally in order to deduce the geometrical efficiency g_i of the PPAC(PS) segments, which was found to be equal to the solid angle of fragment detection in a given PPAC(PS) strip. The total sum over all g_i has been normalized to 1. (cf. equ. 1).

In addition to the data correction for the different background components as already discussed, the emission probabilities obtained have been corrected for energy resolution and energy bin width, for angular resolution, for accidental coincidences, and dead time losses.

3. Results and discussion

Both variants of $N(E,\Theta)$ measurements described in section 2 have been applied to spontaneous fission of ^{252}Cf. The source of about 10^4 fissions per second strength was a 5mm diameter, thin layer on a 0.15 mm thick Ta backing. The two variants characterized by different angular resolutions (cf. table 1) correspond to the typical anisotropies in the energy ranges covered. The variant-I arrangement (with the better angular resolution) was employed to measure $N(E,\Theta)$ at medium and high energy, i.e. at high emission anisotropy. In addition, a special diaphragm has been used to reduce the out-of-plane deviation of fragment detection for the PPAC(PS) segments corresponding to polar directions (Θ = 0 and 180 deg) and, hence, to guarantee a sufficiently good angular resolution for the polar regions.[8] The results of the experiments, which have been concentrated for 5 deg bins (120 angle points originally), are represented in the figs. 4 and 5. They can be characterized as follows:

i) For the lowest energy analysed (100 keV), the angular distribution was found to be nearly isotropic (anisotropy ratio 1.1 ± 0.1).

ii) The anisotropy increases as E increases. At 10 MeV, the anisotropy ratio is close to 100.

iii) In agreement with the results of the Geel group[6], the measured polar/equatorial anisotropy ratio is considerably higher than previous data[3,9] at energies higher than 4 MeV.[5] Specifically the precision of $N(E,\Theta)$ measurements in the equatorial direction (90 deg) in the case of low emission probabilities and at high energy is of considerable importance for

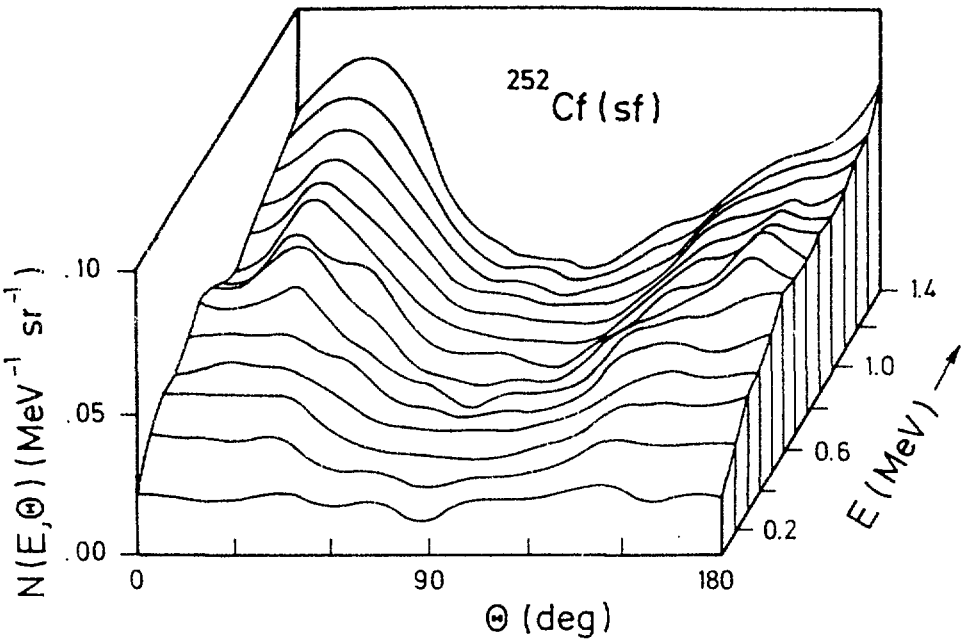

Fig. 4 Angular distributions of $^{252}Cf(sf)$ neutrons at low energy (E = 0.1(0.1)1.4 MeV) deduced from a variant II measurement with NE 912 scintillators (6-Li glass).

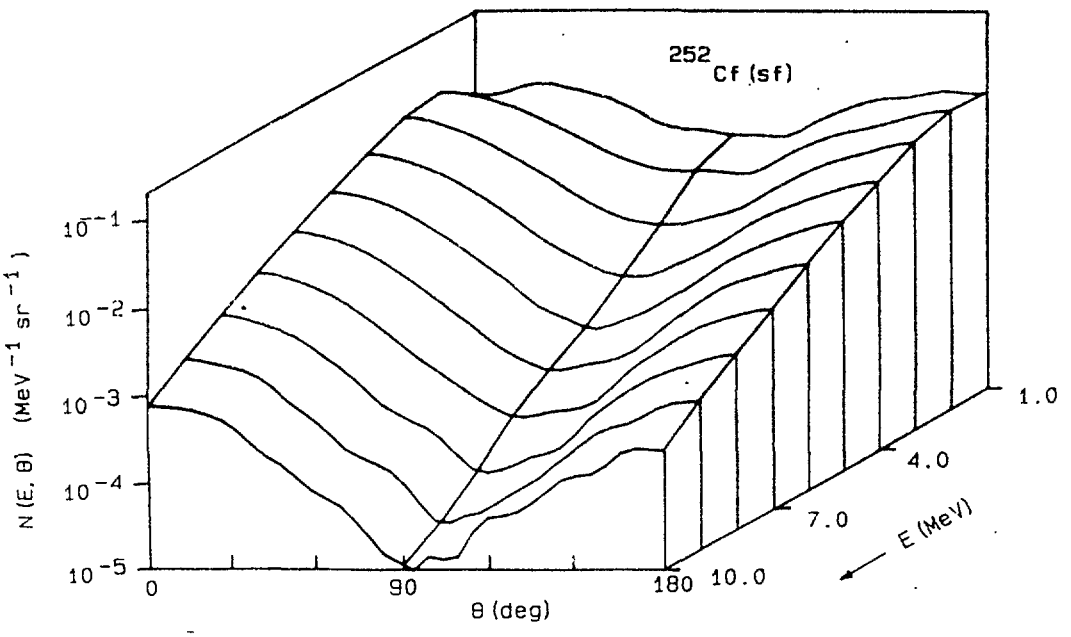

Fig. 5 Plot of N(E,Θ) of $^{252}Cf(sf)$ neutrons in the MeV range (results of a variant I measurement with NE 213 scintillators).

studying emission mechanisms. The efficient background suppression applied in this work was an essential precondition to avoid systematic errors.

iv) A significant N(E,Θ) valley appears in the polar region at Θ close to 0 deg and E ≈ 0.95 MeV. It has to

be attributed to neutron emission from the light-fragment group. The position of this valley ($E \approx 0.95$ MeV corresponds to the average light-fragment kinetic energy E_f per nucleon) indicates a kinematic effect due to neutron evaporation from fully accelerated fragments.[2] An equivalent appearance hasn't been found for heavy-fragment neutron emission ($\overline{E}_f \approx 0.56$ MeV) but some indications of structures. The 1 MeV angular distribution is represented in fig. 6.

v) The kinematics of neutron emission from the fully accelerated fragments is the main reason for the differences of both polar spectra. The differential energy distribution at 0.deg is considerably higher than the 180-deg spectrum for $E > 1.5$ MeV (cf. the different E_f values mentioned in item iv).

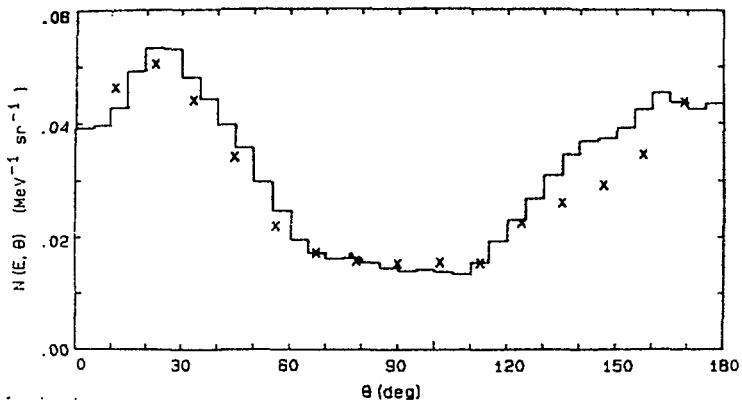

Fig. 6 The angular distribution of 252-Cf(sf)-neutrons at E = 1 MeV (histogram - experimental data of this work, crosses - ref. 3).

4. Conclusion

The experimental method presented enables the precise measurement of double-differential emission probabilities $N(E,\theta)$ of fission neutrons. The measured data on $^{252}Cf(sf)$ neutron emission cover a wide energy range extending from 100 keV (first measurement below 0.5 MeV) to 10 MeV (to 18 MeV in polar direction). The new method is suitable for measuring the full angular distribution with a rather high angle point density simultaneously. Specifically, the shape of the Cf neutron angular distributions in the 0.3 - 1.4 MeV range has been deduced with high accuracy (including the whole polar region, cf. fig. 6), enabling essential conclusions to be reached on theoretical approaches[10].

References

1 H. Märten, D. Neumann, D. Seeliger, Proc. IAEA Consultants' Meeting on the U-235 Fast-Neutron Fission Cross-Section and the Cf-252 Fission Neutron Spectrum, Smolenice (CSSR),1983, INDC(NDS)-146/L(1983)199

2 H. Märten, D. Richter, D. Seeliger, and W. Neubert, Proc. Int. Conf. on Nucl. Phys. - Nucl. Fission, Gaussig (GDR), 1985, ZfK-592(1986)1

3 H. R. Bowman, S. G. Thompson, J. C. D. Milton, and W. J. Swiatecki, Phys. Rev. 126(1962)2120

4 H. Märten, D. Richter, D. Seeliger, W. D. Fromm, and W. Neubert, Proc. Int. Conf. on Nucl. Data for Basic and Applied Science, Santa Fe (USA), 1985, Radiation Effects 93(1986)41

5 D. Seeliger, H. Märten, D. Richter, and W. Neubert, submitted to Yad. Fiz.

6 C. Budtz-Jørgensen and H. H. Knitter, loc. cit. (4), Radiation Effects 93(1986)5

7 W. Neubert, A. A. Kotov, L. N. Andronenko, A. I. Iljin, G. G. Kovshevny, L. A. Vaishnene, and S. S. Volkov, Nucl. Instr. Meth. A 204(1983)453

8 H. Märten, D. Richter, D. Seeliger, W. Neubert, and A. Lajtai, Proc. IAEA Advisory Group Meeting on Neutron Source Properties, Leningrad (USSR), 1986

9 C. J. Bishop, I. Halpern, R. W. Shaw, Jr., and R. Vandenbosch, Nucl. Phys. A 198(1972)161

10 H. Märten, A. Ruben, and D. Seeliger, invited paper to this conference

THE NEUTRON SPECTRUM FROM NEUTRON-INDUCED FISSION OF ^{232}Th

H. Märten, D. Richter, A. Ruben and D. Seeliger
Technische Universität Dresden, Sektion Physik, WB Kernphysik
G.N. Lovchikova, S.E. Sukhikh, and A.M. Trufanov
Institute for Physics and Power Engineering, Obninsk, USSR

The prompt neutron spectrum from ^{232}Th fission induced by 7.3-MeV neutrons has been measured at the Rossendorf tandem facility by the use of a multi-plate fission chamber in conjunction with the three-dimensional-data analysis of neutron time-of-flight, scintillator (NE 213) light output, and pulse shape amplitude (n/γ-discrimination). This type of neutron spectroscopy enables a accurate particle discrimination without detector efficiency losses and the application of the sliding bias method based on a two-dimensional efficiency matrix as a function of neutron energy and bias (Monte Carlo calculation). The final spectrum obtained with reference to a ^{252}Cf(sf) neutron spectrum measurement is shown in fig. 1 in comparision with the calculation in the framework of the generalized Madland-Nix model (GMNM) /1/. This statistical-model approach to prompt fission neutron emission is combined with a scission-point model (TSM) /2/ to describe the energy partition (excitation energy, kinetic energy) in fission. In the case of multiple-chance fission reactions (as at 7.3-MeV incidence energy), the theoretical analysis is done for all possible chances. The neutron spectrum from ^{232}Th fission by 7.3-MeV neutrons (fig. 1) is not influenced by pre-fission neutrons above 1 MeV neutron energy. The GMNM (adjusted on the basis of the ^{252}Cf(sf) standard spectrum /1/) describes the measured Th spectrum without any further adjustements. The effect of multiple-chance fission on the average energy of fission neutrons $\bar{E}$ is shown in fig. 2 in comparision with few experimental points.

The experimental and theoretical investigation of Th fission neutron emission has shown that GMNM-TSM provides the basis for the consistent description of fission neutron data in a wide range of fissioning nuclei.

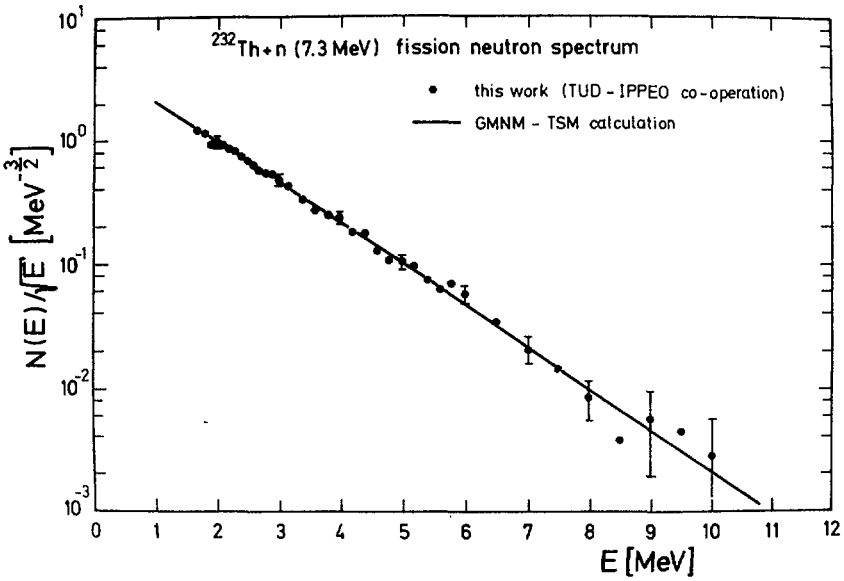

Fig. 1 The ^{232}Th fission neutron spectrum at 7.3-MeV incidence energy

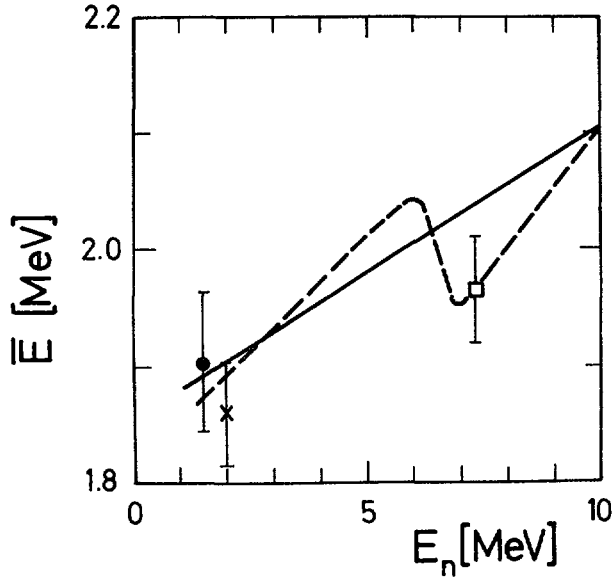

Fig. 2 The average eneregy of the neutron spectrum from ^{232}Th fission as a function of incidence energy E_n (∘ - /3/, x - /4/, □ - this work, ——— ENDF/B-IV, --- GMNM-TSM)

REFERENCES

/1/ Märten, H. and Seeliger, D.; Nucl. Sci. Eng. 93 (1986) 370
Märten, H. et al.; Proc. Int Conf. Neutron Physics, Kiev, 1987 (Moskau, 1988) Vol. 3, p. 49

/2/ Märten, H. et al.; Proc. Int. Conf. Nucl. Phys., Gaussig, 1987 (in press)

/3/ Sukhikh, S.E. et al.; Yad. Const. 3 (1986) 34

/4/ Hirakawa, N. et al.; Radiation Effects 93 (1986) 229

DIFFERENTIAL NEUTRON-EMISSION CROSS-SECTIONS OF ^{238}U BOMBARDED WITH 14 MEV NEUTRONS

T. Elfruth, T. Hehl, H. Kalka, H. Märten, A. Ruben,
D. Seeliger, K. Seidel, and S. Unholzer
Technische Universität Dresden, Sektion Physik, WB Kernphysik

Neutron-emission cross-sections of ^{238}U are needed for fission and fusion (hybrid) reactor calculations. The accuracy achieved in previous experiments doesn't meet actual requirements. A new measurement based on an improved time-of-flight spectrometer /2/ at the pulsed neutron generator /3/ of the Technical University shall contribute to enhance the accuracy.

The angle-integrated emission spectrum is shown in Fig. 1. Contributions to the spectrum arise from neutron scattering in the precompound and in the compound nucleus stage, from (n,2n), (n,3n) and fission neutrons. The theoretical analysis of neutron emission spectra should account for all competing reaction channels. This is illustrated for the present case in the following scheme:

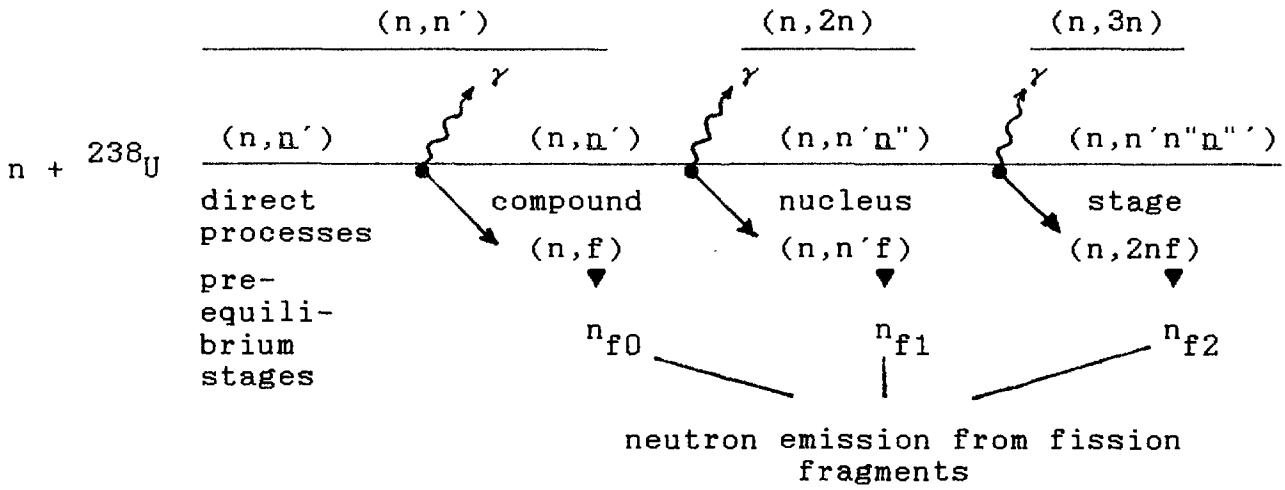

The (n,n') contributions were calculated using the code EXIFON /4/ taking into account statistical one- and two-step direct single-particle as well as collective interactions (statistical multi-step direct processes). Further, statistical multi-step compound processes are considered by solving the master equation for pre-equilibrium and equilibrium emission in a closed manner. The strength of the other channels and the spectra of the second and third neutrons in (n,2n) and (n,3n) reactions, respectively, were calculated by the use of the extended Hauser-Feshbach code

STAPRE /5/ including fission channel. The spectral shapes of fission neutrons were calculated in the framework of GMNM formalism /6/ for all possible fission channels. Here, neutron evaporation from fully accelerated fission fragments has been assumed as the predominant emission mechanism. The GMNM concept includes the dependence of fission neutron spectra on fragment mass number. The fragment energy distribution was calculated in the framework of a scission point model including semi-empirical, temperature-dependent shell energies (Two-Spheroid Model) /7/. As a first step of the theoretical analysis, all calculations have been performed with model parameters representing the mean behaviour of nuclei. Non of the model parameters was adjusted. The agreement of the calculated total spectrum with the angle-integrated experimental neutron spectrum is good (Fig. 1).

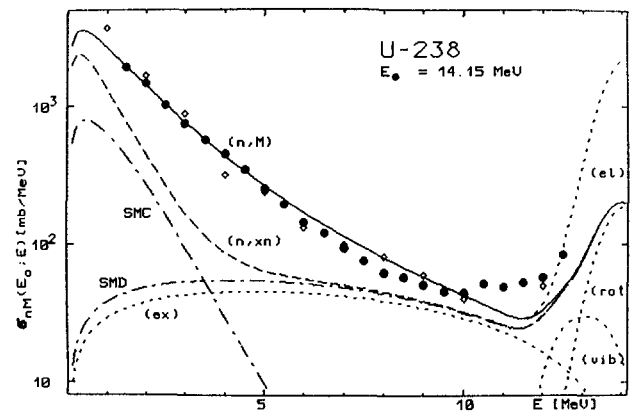

Fig. 1
Angle-integrated neutron emission spectrum from ^{238}U at 14.1 MeV neutron incidence energy. Experimental data of the present work (●) and from Ref. /8/ (◇) are compared with the calculated spectrum composed of the contributions indicated. The (n,n′) component consists of direct collective (vib, rot), direct single-particle (ex), direct multi-step processes (all together SMD) and statistical multi-step compound (SMC) contributions. The dashed line shows the spectrum including all (n,xn)-processes. (n,M) denotes the full spectrum including post-fission neutron distributions.

References

/1/ World Request List for Nuclear Data, IAEA, Vienna, 1981, INDC(SEC)-78/URSF

/2/ Dietz, V. et al., Annual Report 1980, ZfK-443(1981)196

/3/ Helfer, H. et al., Annual Report 1983, ZfK-539(1984)126

/4/ Kalka, H. et al., Proc. Int. Conf. Nucl. Phys., Gaussig, 1987, ZfK-646(1988)24

/5/ Uhl, M. and B. Strohmaier, Report IRK-76 (1976)

/6/ Märten, H. and D. Seeliger, Nucl. Sci. Eng. 93(1986)370

/7/ Märten, H. et al., Proc. IAEA Advisory Group Meeting on Properties of Neutron Sources, Leningrad, 1986, IAEA-TECDOC 410 (IAEA, Vienna) 153

/8/ Kammerdiener, J.L., Ph. D. Thesis, University of California, 1972, UCRL-51232

NEW EVALUATION OF OUR ABSOLUTE MEASUREMENTS OF ^{252}Cf PROMT FISSION NEUTRON SPECTRUM IN THE LOW ENERGY RANGE

A.Lajtai
Central Research Institut for Physics
Budapest, Hungary

P.P.Dyachenko, E.A.Seregina, V.N.Kononov
Institute of Physics and Power Engineering
Obninsk, USSR

Abstract

Low energy californium neutron spectrum data have been determined utilizing new, refined neutron detector efficiency values. The efficiency of the neutron detector - a 0.95 cm thick NE-912 glass detector - was determined independently by using a 0.0835 cm thin glass detector as a reference, the efficiency of the latter being determined by a Monte-Carlo calculation.

The more precise repetition of this calculation taking into occount the effects of all constituent elements resulted in more accurate efficiency data. The use of these new values in determining the efficiency of the thick neutron detector leads to quite considerable changes in data compared with those of the earlier evaluations.

The paper contains the new efficiency data for the thick ^{6}Li glass detector and the californium neutron spectrum evaluated by them. This spectrum can be well described by the complex evaporation model spectrum calculated by Märten.

The energy spectrum of prompt neutrons from spontaneous fission of ^{252}Cf serves as IAEA proposed standard. Correct measurement of the spectrum required a presice knowledge of the efficiencies of the neutron detectors.

Some years ago we measured the californium fission neutron spectrum in the range 25 keV - 1.22 MeV by the time-of-flight method /1/. Our data were included in Mannhard's evaluated spectra /2/. However, there was some inconsistency between our data and those of Blinov et al. /3/ and of Poenitz et al. /4/ in the energy range 125-315 keV in view of which some data in this range were excluded from Mannhard's evaluation.

Table I.

E (KeV)	N(E)	ERRORS	N(E)/MAXW (T=1.42)	EFFICIENCY (%)	ERROR
25	3.53	0.48	1.14	1.748	0.079
35	2.87	0.46	0.79	1.609	0.051
45	4.406	0.48	1.075	1.505	0.044
55	4.20	0.45	0.934	1.444	0.043
65	4.435	0.44	0.913	1.389	0.040
70	4.962	0.45	0.958	1.318	0.039
85	4.834	0.43	0.883	1.305	0.038
95	5.64	0.41	0.981	1.331	0.039
105	5.688	0.39	0.948	1.341	0.039
115	6.402	0.47	1.028	1.388	0.074
125	7.032	0.47	1.089	1.459	0.079
135	6.786	0.45	1.018	1.558	0.085
145	6.495	0.42	0.947	1.672	0.091
155	7.308	0.46	1.038	1.860	0.101
165	7.14	0.44	0.99	2.103	0.114
175	7.546	0.45	1.023	2.473	0.134
185	7.545	0.44	1.002	2.919	0.158
195	7.914	0.46	1.031	3.523	0.192
205	7.674	0.44	0.979	4.264	0.226
215	8.587	0.49	1.08	5.256	0.213
225	7.354	0.43	0.911	5.887	0.321
235	7.695	0.44	0.939	6.580	0.356
245	7.749	0.45	0.933	6.641	0.360
255	7.391	0.43	0.879	6.211	0.337
265	8.167	0.47	0.959	5.497	0.230
275	8.918	0.52	1.035	4.900	0.263
285	8.907	0.53	1.022	4.257	0.230
295	8.798	0.51	1.000	3.635	0.198
305	8.538	0.50	0.961	3.208	0.174
315	8.551	0.50	0.954	2.904	0.158
325	8.984	0.53	0.994	2.585	0.141
335	8.771	0.52	0.962	2.343	0.128
345	8.454	0.50	0.92	2.147	0.117
355	8.831	0.53	0.954	1.981	0.108
365	9.357	0.56	1.004	1.848	0.101
375	9.404	0.56	1.003	1.745	0.095
385	9.075	0.55	0.962	1.679	0.091
395	9.192	0.55	0.97	1.565	0.085
410	9.577	0.56	1.001	1.495	0.080
430	9.888	0.59	1.024	1.375	0.075
450	9.393	0.55	0.964	1.313	0.071
470	9.712	0.62	0.989	1.114	0.061
490	9.362	0.56	0.947	1.001	0.054
510	9.697	0.57	0.975	0.902	0.049
530	9.889	0.60	0.989	0.844	0.046
550	9.770	0.58	0.976	0.762	0.041
570	9.711	0.58	0.963	0.736	0.041
590	9.667	0.59	0.955	0.726	0.039
610	9.982	0.61	0.985	0.684	0.037
630	9.938	0.61	0.978	0.657	0.035
650	10.02	0.63	0.985	0.633	0.035
670	9.983	0.62	0.98	0.623	0.034
690	9.924	0.65	0.974	0.605	0.033
710	10.296	0.64	1.011	0.562	0.031
735	10.467	0.65	1.028	0.540	0.029
765	10.509	0.63	1.033	0.526	0.027
795	10.032	0.62	0.988	0.543	0.030
825	9.881	0.62	0.976	0.544	0.030
855	9.97	0.63	0.988	0.538	0.029
885	10.013	0.62	0.996	0.531	0.029
915	9.768	0.62	0.974	0.531	0.029
945	9.755	0.62	0.978	0.530	0.029
975	9.597	0.59	0.969	0.533	0.029
1005	9.516	0.59	0.966	0.535	0.030
1020	9.401	0.59	0.958	0.529	0.030
1060	9.864	0.61	1.014	0.528	0.029
1100	9.822	0.62	1.019	0.510	0.028
1140	9.985	0.62	1.046	0.515	0.028
1180	9.486	0.59	1.005	0.512	0.028
1220	9.820	0.60	1.053	0.511	0.028

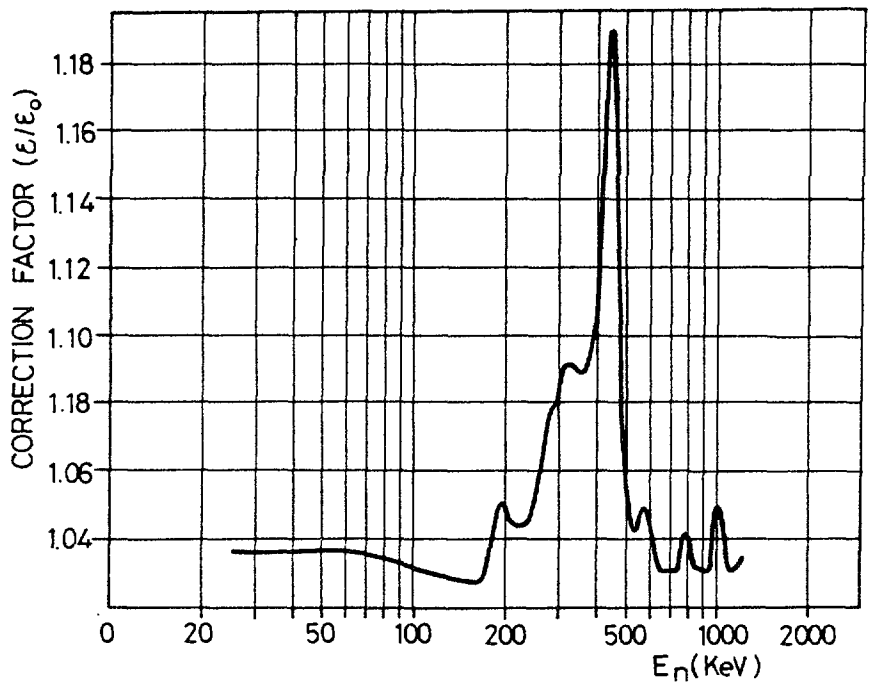

Fig.1 Efficiency correction factors for thin ^{6}Li glass detector (Monte Carlo calc.)

A 0.95 cm glass scintillator was used in our time-of-flight integral neutron spectrum measurement for detecting neutrons. Hower, due to multiple scattering the efficiency of detectors of such thickness cannot be obtained directly from the elementary $^{6}Li(n,\alpha)$ cross section values. Therefore an independent measurement /5/ was performed to determine the absolute efficiency values of our NE-912 glass detector. For this purpose, (0.0835 cm) NE-908 glass scintillator served as a standard detector; its efficiency was determined by Monte-Carlo calculations.

Detailed analyses have revealed errors in several energy values in the earlier MC efficiency calculation. The results of the new, more detailed MN calculations were performed at the Institute of Physics and Power Engineering, Obninsk /6/ the corraction factors are shown in Fig.1. They express the multiple scattering efficiency effects relative to the efficiencies for the pure $^{6}Li(n,\alpha)$ reactions.

The increase of efficiency in the energy range 20-150 keV is small (3-3.5 %) but at higher energies it can extend to 18 %, as is the case at 440 keV due to the scattering resonance of oxygen.

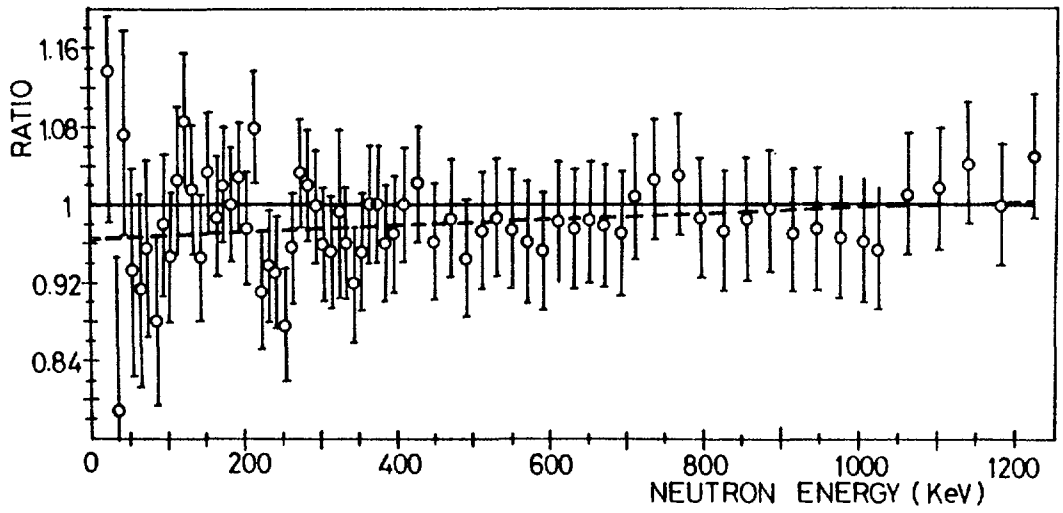

Fig.2 Ratio of californium neutron spectrum to a Maxwelliam distribution with temperature of 1.42 MeV Dasned line is Märten's calculation /10/.

These results agree with those of Allen et al. /7/, of Poenitz et al. /8/ and of Lamaze et al. /9/ at those energies for which they made calculations. In these new calculations all constituents of the NE 908 thin glass detector ^{6}Li, ^{7}Li,Si,O.Al,Mg,C are included and the results show 1-10 % deviations from the earlier ones.

The changes in the standard efficiency values obviously influence the efficiency of the thick NE 912 glass detector and therefore, in turn, affect the evaluation of the fission neutron energy spectrum. The energy dependence of the energy spectra of neutrons and the efficiencies of the thick NE-912 glass detector with their estimated errors are shown in Table 1.

Comparison of the measured energy spectra with a Maxwell-distribution of T=1.42 parameter can be seen in Fig.2. The results of Märten's /10/ complex evaporation model calculation using a β =0.1 anisotropy value are shown by a dashed line. It can be seen that the measured spectrum - with the exception of some points - agrees well the calculation.

References

1. A.Lajtai et al.: INDC (NDS)-146, 177 (1983)
2. W.Mannhard: IAEA-TECDOC-410, 158 (1987)
3. M.V.Blinov et al.: Nuclear Data for Science and Technology, Proc.Int.Conf.Antwerp 479 (1983)
4. W.P.Poenitz, T.Tamura: Nuclear Data for Science and Technology, Proc.Int.Conf.Antwerp 465 (1983)
5. V.N.Kononov et al.: Nucl.Instr.Meth. A234 361 (1985)
6. A.A.Androsenko et al.: Report FEI-1777 (1986)
7. B.J.Allen et al.: Phys.Rev. C8 1504 (1973)
8. W.Poenitz, J.W.Meadows: Neutron Standard Reference Data, IAEA Vienna 95 (1974)
9. G.P.Lamaze et al.: Nucl.Sci.Eng. 68 183 (1987)
10. H.Märten et al.: Report INDC(GDR)-28 (1984)

Simultaneous Investigation of Fission Fragments and Neutrons in ^{252}Cf (SF)

C. Budtz-Jørgensen and H.-H. Knitter
Commission of the European Communities
Joint Research Centre
Central Bureau for Nuclear Measurements, Geel, Belgium

A B S T R A C T

The gridded twin ionization chamber developed at CBNM is used to measure the kinetic energy-, mass- and angular distributions of the fission fragments of the spontaneous fission of ^{252}Cf. Together with a neutron time-of-flight detector this experimental arrangement permits to measure the correlations between neutron emission, fragment angle, mass and energy of the fission fragments. Without neutron coincidences $40 \cdot 10^6$ fission events were recorded which are evaluated to give mass-, total kinetic energy- and the variance distributions in a broad mass range from mass 67 to 185. About $3 \cdot 10^6$ fission events were recorded in coincidence with a neutron detected in the time-of-flight detector. Angular distributions in the CM-system revealed isotropy in the whole fission neutron energy range. This permits the conclusion that fission neutrons are emitted from the fully accelerated fragments and that the hitherto assumed scission neutron component of 15 to 20 % is much smaller, as can be determined from the uncertainty of the second Legendre polynomial coefficient. The average number of neutrons was determined as function of fragment mass and TKE. The mass range for $\bar{\nu}(A)$ was extended beyond that of earlier measurements and revealed two new sawteeth near masses 80 and 176. The slopes and end points of $\bar{\nu}(TKE)$ were also determined for each fragment mass. The fragment centre-of-mass fission neutron spectra were determined as function of fragment mass and TKE. These spectra permitted the evaluation of the average neutron energy $\bar{\eta}(A,TKE)$ the nuclear temperature $T(A,TKE)$ and the λ-factor from the cascade evaporation model. These quantities permitted the evaluation of the level density parameter $a(A)$ in the mass range from 90 to 169.

1. INTRODUCTION

Nuclear fission has been a longstanding theme of scientific investigation and here the spontaneous fission of ^{252}Cf gives a relatively easy opportunity to study the correlations between neutron emission and fission

fragment parameters. The measurement of such correlations can contribute to a better understanding of the fission process. For ^{252}Cf much more effort than for other nuclei was devoted to the measurement and interpretation of the prompt fission neutron spectrum, because this spectrum is also used as a neutron spectrum shape standard. Several attempts /1,2/ have recently been made to give a theoretical description of the prompt fission neutron spectrum of ^{252}Cf. These models are based on the assumption that the mechanism of neutron emission is the evaporation from the fully accelerated fragments. However, the comprehensive measurements of Bowman et al. 3) of the prompt neutron anisotropy have led to the conclusion that a fraction (~10-20 %) of the total number of fission neutrons is emitted isotropically in the laboratory frame of reference. In spite of many further investigations the knowledge of the so-called scission neutron emission is poor and partially contradictory. Therefore it is of much interest for the basic understanding of the neutron emission process, not only to measure precisely the integral prompt fission neutron spectrum, but to also obtain in multi-dimensional measurements the correlations between the neutron emission and the different fission fragment parameters.

With the recent advent of the socalled multi modal fission theories together with the random neck-rupture process as formulated by Brosa et al./4/ such measurements have gained further importance. Not only do these theories explain many experimental results in fission but they predict also hitherto unobserved features including some which are specific for neutron emission in fission (5).

2. EXPERIMENTAL METHOD

The present multiparameter measurement of the ^{252}Cf prompt neutron spectrum, $N(E_n,\Theta_n,A,TKE)$ has been performed at CBNM. The experimental set-up is shown in fig.1. Fission fragment detection is made using the gridded ion chamber developed at our laboratory with which fission fragment angle θ, kinetic energy, and mass can be determined simultaneously. This chamber has been described in detail in refs. /6,7/ and only some essential points will be given here. The fission fragment kinetic energies (E_L, E_H) are determined using the anode pulses from the twin chamber. The energy resolution for fission fragment detection is $<$ 0.6 MeV /7/, which means that the detector contribution to the mass resolution is $<$ 0.5 u. This is a factor of 2 to 3 better than achievable with Si detectors conventionally used as fission fragment spectrometers.

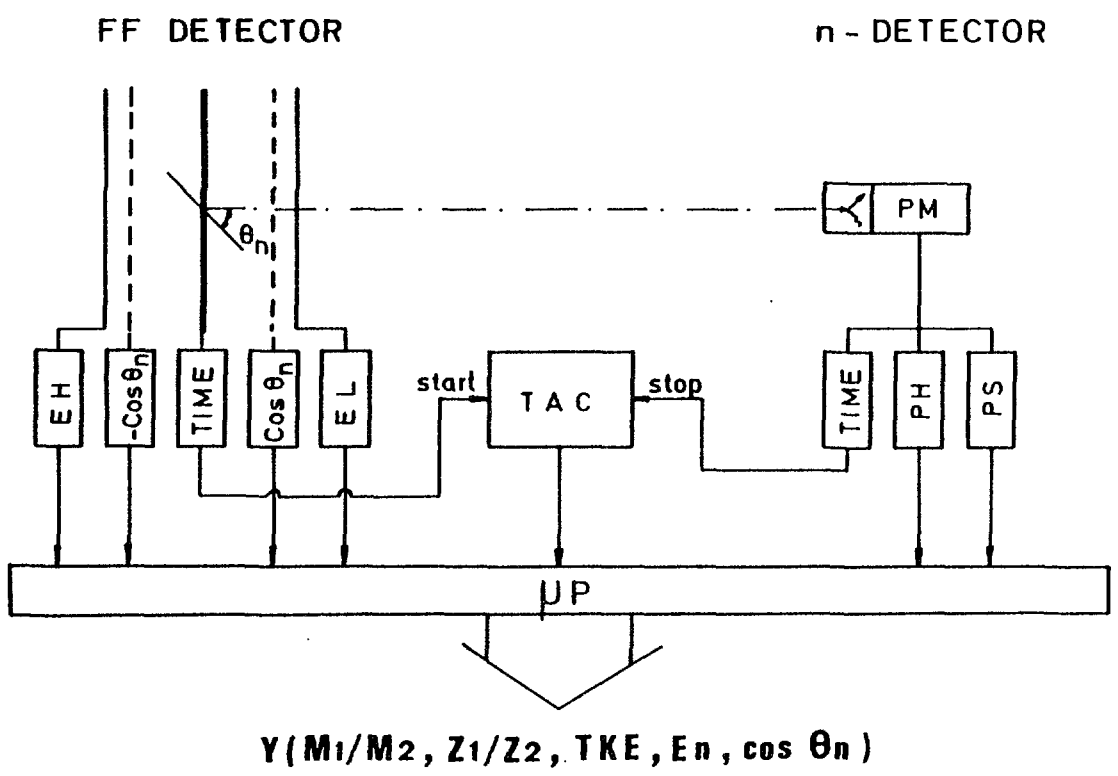

Figure 1.
Experimental set-up.

The fragment angle information is determined as cosine of the angle θ between the normal of the electrodes and the path of the fission fragments. The cosθ resolution is ~ 0.05. For timing the pulses from the common cathode are used giving a resolution ⟨ 0.7 ns FWHM together with the neutron detector. The neutron detector, a 4" x 1" NE 213 scintillator, is located on the axis of the ionization chamber. The distance between the ^{252}Cf-source and the neutron detector was 0.51 m. Both, the pulse height and the pulse shape for n/γ discrimination are recorded. Neutron energies are determined using conventional time-of-flight technique. All 7 parameters are digitized, each allocated 8192 channels, and stored sequentially on tape for off-line analysis. A ^{252}Cf source prepared by vacuum evaporation onto a 120 μg cm^{-2} thick Ni-foil is mounted in the chamber. The source activity is $\sim 3.10^2$ fiss·s^{-1}, yielding a fragment-neutron coincidence rate of 1 s^{-1}.

3. EXPERIMENTAL RESULTS AND ANALYSIS.

The experimental set-up shown in fig. 1 allowed for each event the determination of the fragment energies, the neutron energy and its emission angle. The observed fragment energies were converted to

preneutron energies and the preneutron fragment masses were calculated using well known techniques /8/. The correction for neutron emission was made respectively using the neutron multiplicities as function of mass and total kinetic energy determined in the present experiment, see section 3.2.2. The fragment energies were corrected for fragment recoil due to neutron emission using the procedures discussed in /9/. Thus in total each fission event is characterized by 6 quantities: fragment energies $E_{L,H}$, fragment masses $A_{L,H}$ neutron energy E_n and emission angle Θ_n.

3.1) Results in the Laboratory Reference System.

A ^{252}Cf (SF) mass-yield measurement based on 4.10^7 fission events recorded with the above set-up, however without demanding coincidences with the neutron detector, is shown in fig. 2 together with the average total kinetic energy and the square root of the variance as function of fragment mass. Good agreement with published distributions is observed for the mass yields. The yield enhancement in far-out asymmetric fission ($A_H \geq 176$), which was recently seen by Barreau et al. /10/ is confirmed in our measurement as well as the fluctuations of the TKE(A) and the σ(TKE) for fragments in this region.
These experimental results were recently discussed by U. Brosa et al. /11/ within the multi modal fission model. The data suggest the existence of no less than four distinct fission channels for ^{252}Cf (SF). Theoretical least square fits to the distributions as outlined in /12/ are presently underway at CBNM.
The evaluation of the ^{252}Cf fission neutron fragment correlations is based on a database of $3 \cdot 10^6$ recorded coincidences. Fig. 3 displays the neutron TOF spectrum integrated over all fragments but uncorrected for the neutron detector efficiency.

The advantage of having a weak source is seen here since the influence of accidental coincidences ($\sim 1 \cdot 10^{-3} \cdot ns^{-1} \cdot h^{-1}$) can be completely neglected. It is especially gratifying that no background events were detected to the left of the gamma peak, a consequence of the near 100 % efficiency of the ionization chamber. This means that the analysis can be extended to very high neutron energies, where scission neutrons might play a role /2/.
The mass integrated prompt fission neutron spectrum of ^{252}Cf(SF) was evaluated in some detail. For the present evaluation the neutron detection efficiency, which is needed to obtain the spectrum shape, was calculated using the Monte Carlo code from the thorough detector efficiency investigation of Dietze and Klein /13/. This code calculates the absolute

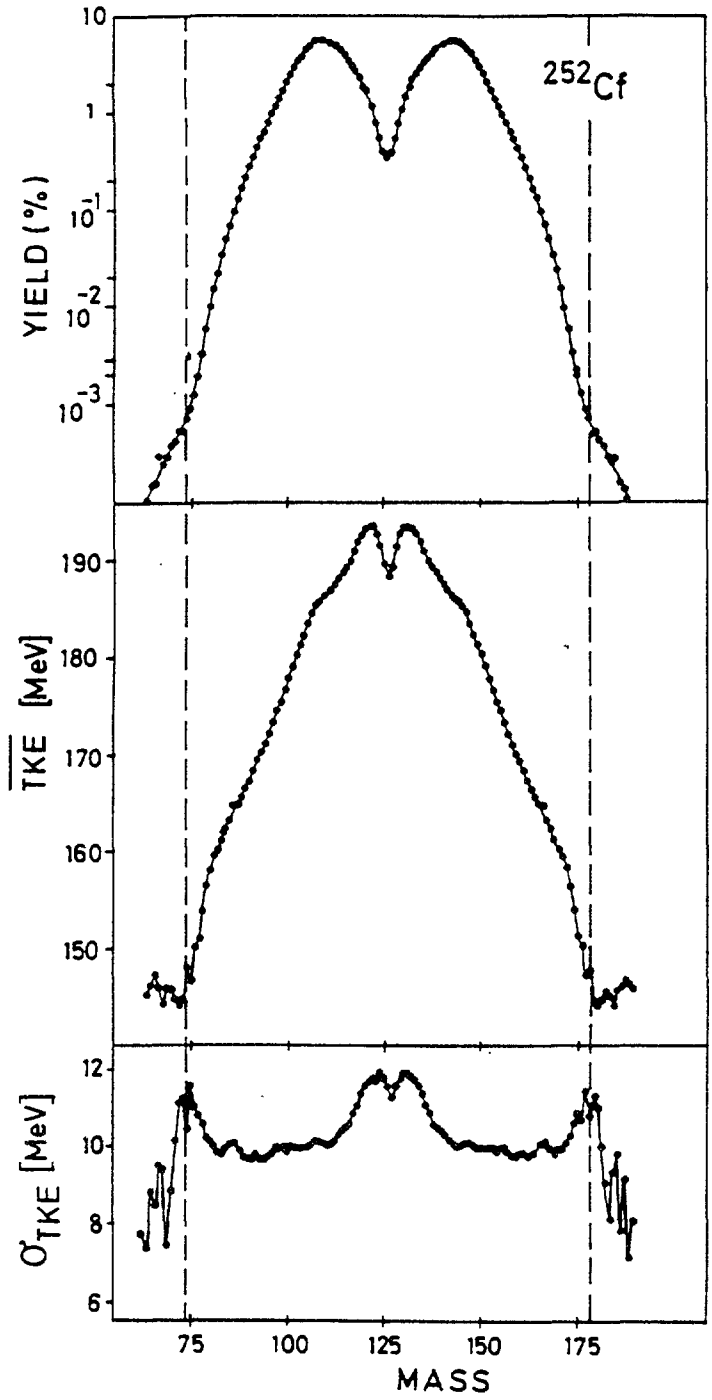

Figure 2

The fission fragment yield, the average total kinetic energy and the square root of the variance of the total kinetic energy distributions are plotted versus the fragment mass for the spontaneous fission of ^{252}Cf.

neutron detection efficiency for a given pulse height threshold. The spontaneous fission process is not only accompanied by neutrons but also by γ-rays which might be detected by the neutron detector. Most of the γ-emission happens at the instant of fission and up to a few ns later. In this time range fall also the high energy neutrons which are emitted with a very low intensity. Therefore the very high energy region of the neutron

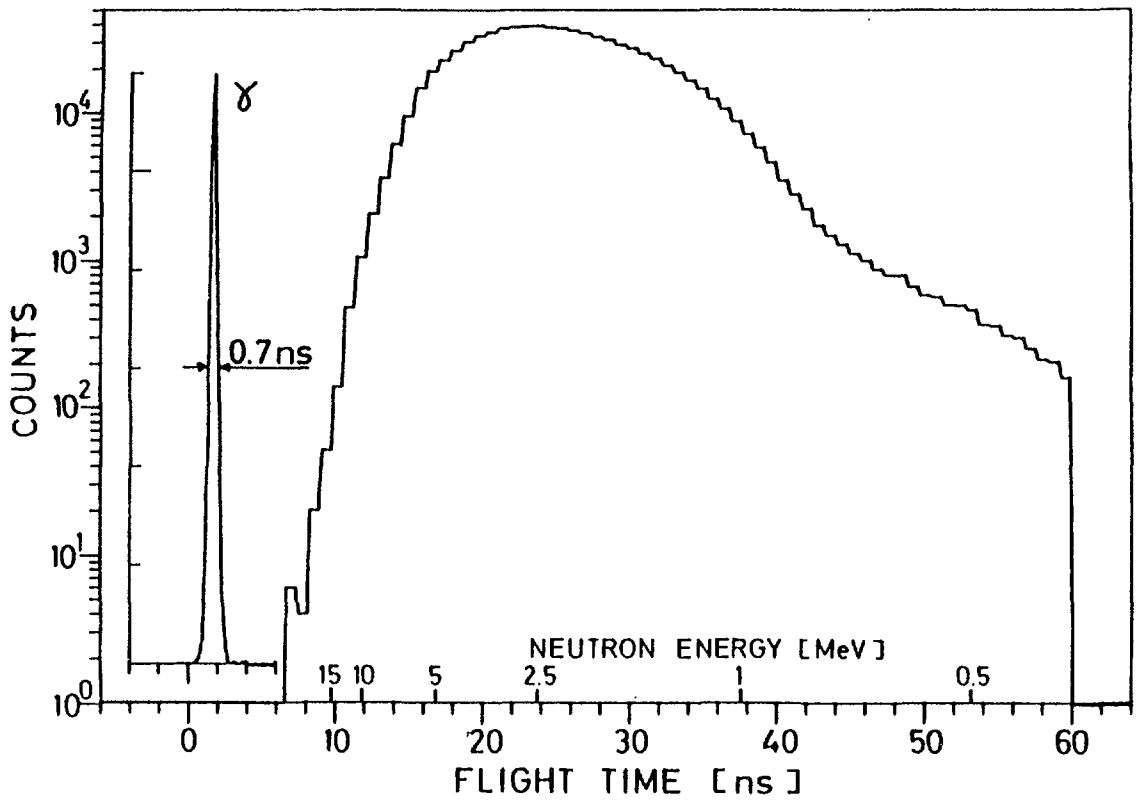

Figure 3
Fission neutron time-of-flight spectrum.

spectrum is most sensitive to false events induced by γ-rays. The pulse shape circuit employed in the present set-up was not able to give a clean discrimination between γ- and neutron events for pulse heights corresponding to a proton recoil energy smaller than 2 MeV. Therefore several neutron time-of-flight spectra with different pulse height thresholds in the neutron detector were selected from the same raw experimental data. Absolute detector efficiency curves were calculated for the same pulse height thresholds. In this way one obtains for each of the selected detector thresholds a neutron spectrum. These spectra are automatically normalized with respect to each other by the absolute detector efficiency calculations. Therefore, in overlapping energy ranges and where the measurements are not disturbed by γ-events, the spectra must coincide with each other. This was observed and a single neutron energy spectrum was composed containing at low neutron energies the data from a spectrum with a low threshold of 0.5 MeV and at higher neutron energies from a spectrum with a threshold of 2 MeV. The data above 14 MeV were obtained using a detector threshold of 7.2 MeV where the pulse shape discrimination could eliminate γ-ray events completely. This spectrum divided by $\sqrt{E}$ is plotted in fig. 4 logarithmically versus the incident neutron energy. The full line in fig. 4 represents the result of a least

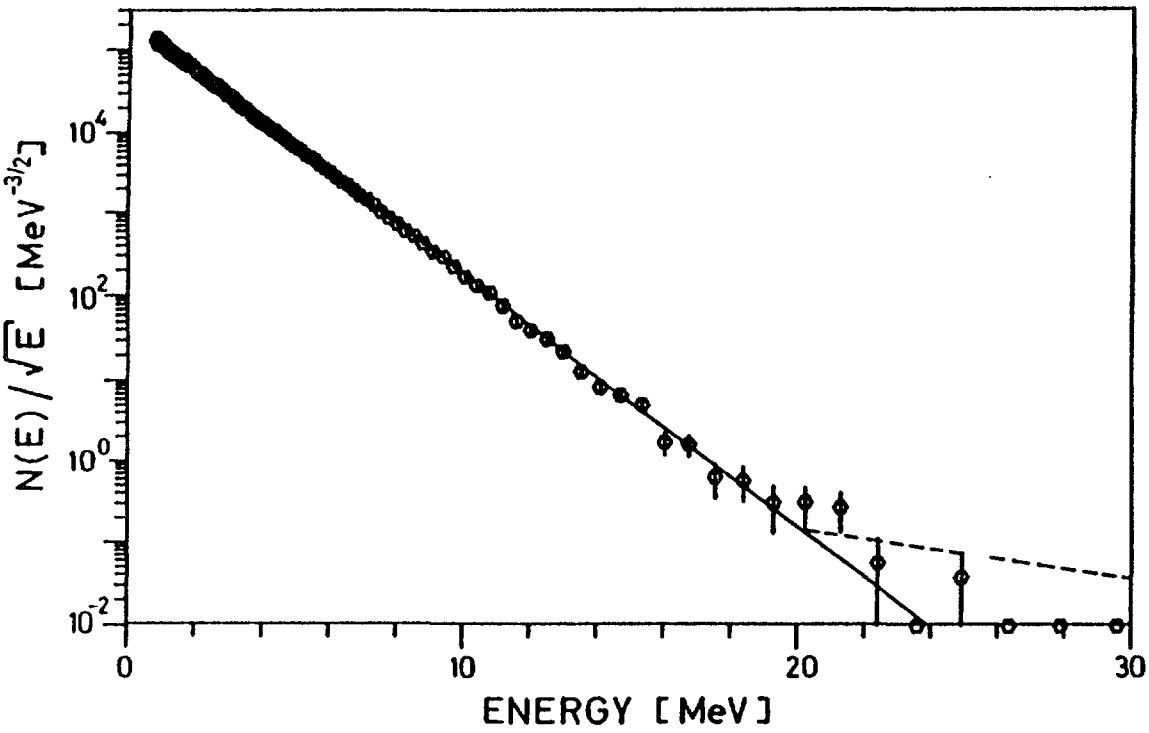

Figure 4

Fission neutron energy spectrum divided by the square root of the neutron energy versus the neutron energy.

squares fit through the experimental data with a Maxwellian energy distribution. The temperature parameter obtained by the fit is T=1.41 ± 0.03 MeV. The error is essentially determined by the rather short flight path of 0.51 m. The neutron energy spectrum shows no major deviations from the Maxwell distribution in the neutron energy range from 0.5 MeV to 20 MeV. The deviations from the Maxwell distribution are in general less than 5 % in the above energy range. The results do not confirm the large excess of neutrons above 20 MeV found by Märten et al. /14,15/. However with the present counting statistics some deviations from the Maxwellian shape cannot be excluded here. The points plotted at the 10^{-2} line contain zero events.

The measured fragment-neutron angular distributions integrated over all fragments versus the neutron energy are shown in a bi-parametric representation in fig. 5. The present data agree fairly well with the results of Bowman et al. /3/ below 4 MeV. However, at higher neutron energies our data are much more anisotropic with intensity ratios N(90°)/N(0°) more than one order of magnitude smaller than those of Bowman above 8 MeV. These findings were first reported by us in ref. /16/ and have been confirmed by H. Märten et al. /17/. The comparison between the present angular anisotropy measurements as function of fission neutron energy and those of Bowman et al. /3/ is made in fig. 6. The full line in

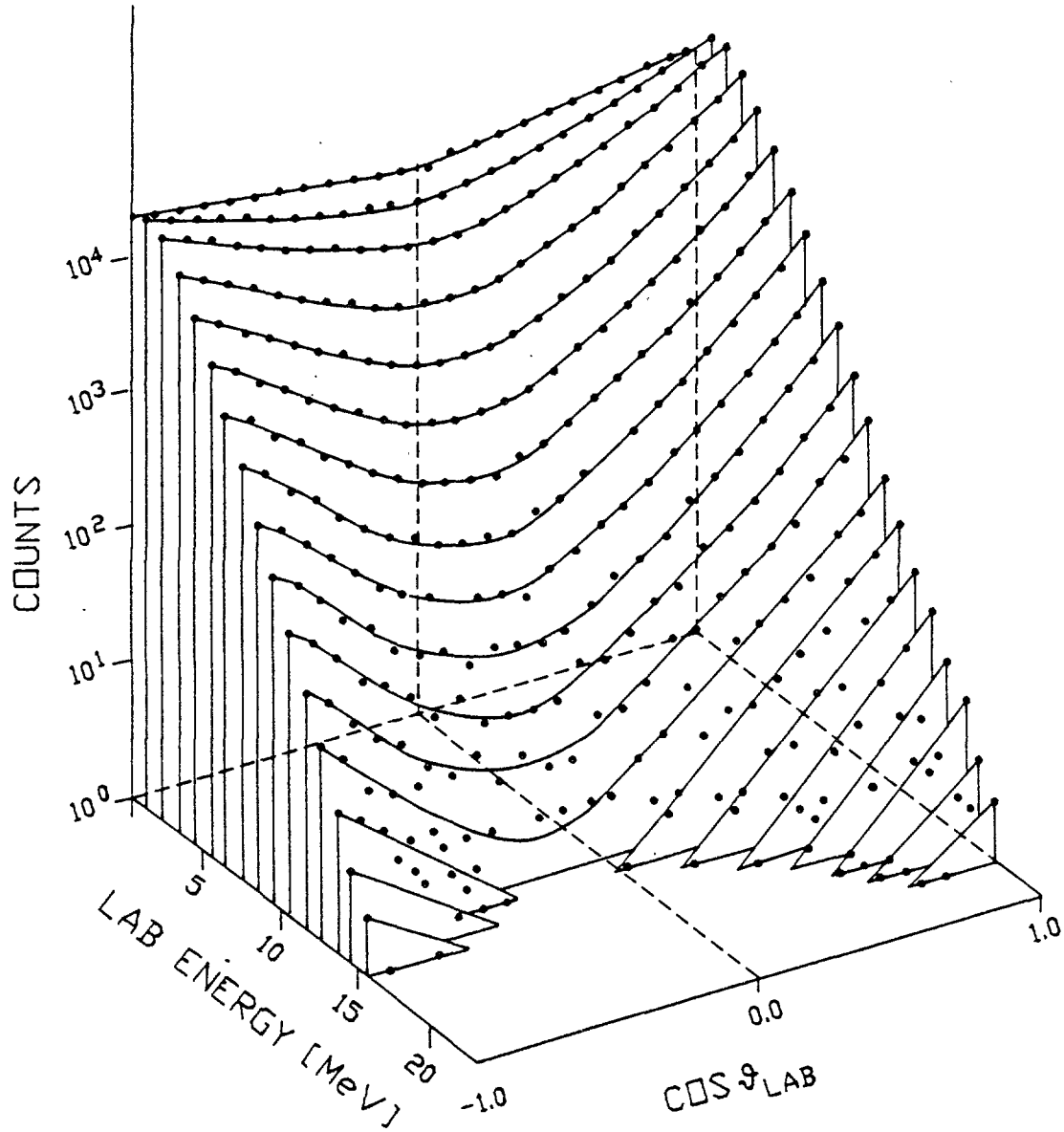

Figure 5
Fission neutron yield versus the laboratory neutron energy and versus the cosine of the angle between the directions of movement of the light fragment and the neutron.

fig. 6 represents calculations of the angular anisotropy as function of the neutron energy with the assumption that all neutrons are emitted from the fully accelerated fragments. The according equations and the needed numerical values were taken from Terrell /18/. The energy dependence of the present N(90°)/N(0°) intensity ratio is in agreement with the assumption that all neutrons are emitted from the fully accelerated fragments.

3.2. Results in the Fragment Center of Mass System.

From the results discussed in the previous section it can be concluded that the major part of the ^{252}Cf fission neutrons are emitted from the

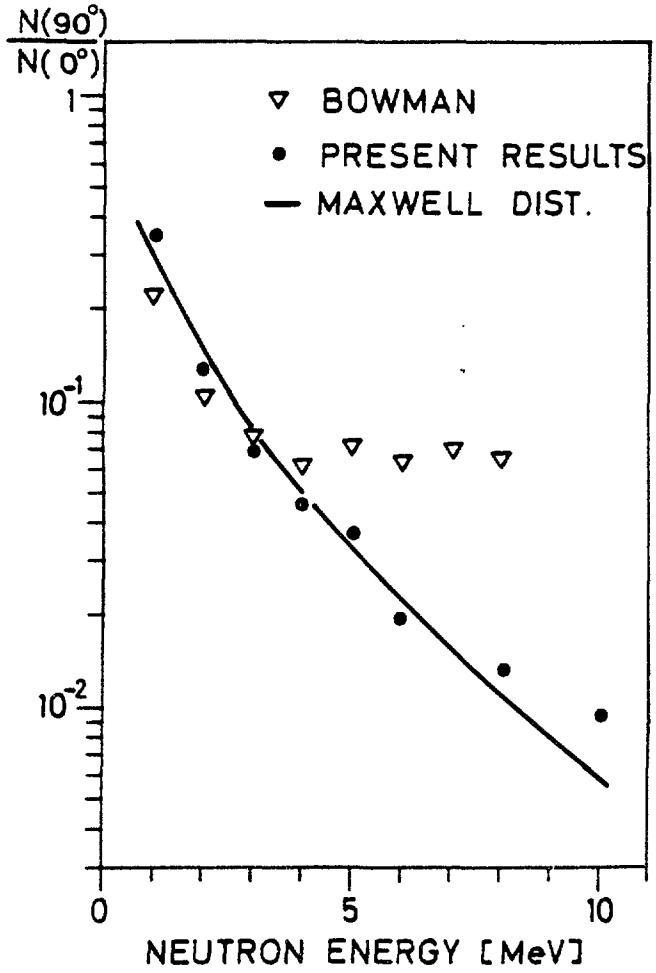

Figure 6

Fission neutron intensity ratio N(90°)/N1(0°) is plotted versus the fission neutron energy. The full line represents this ratio calculated with the assumption of neutron evaporation from the fully accelerated fragments.

fully accelerated fragments. The complete experimental determination of all kinematic parameters as described in section 2 allows then to deduce the neutron spectra in the center-of-mass system of the fission fragment. However, this transformation is not straightforward, because at each laboratory angle only the sum of contributions from the two fragments is observed. Thus in estimating the number and energy spectrum from one fragment one must subtract an initially unknown contribution from the other. Fortunately this correction is small as it will be shown in the following . Fig 7 depicts the kinematic situation of neutron evaporation from the moving fragments. In the first approximation it is assumed that only neutrons from the fragments flying into the hemisphere facing the neutron detector are detected. The neutron center-of-mass velocity V_{CM} is then given by the observed laboratory-system quantities :

$$V_{CM}^2 = V_{F_1}^2 + V_{LAB}^2 - 2V_{F_1} \cdot V_{LAB} \cdot \cos\Theta_{LAB} \qquad [1]$$

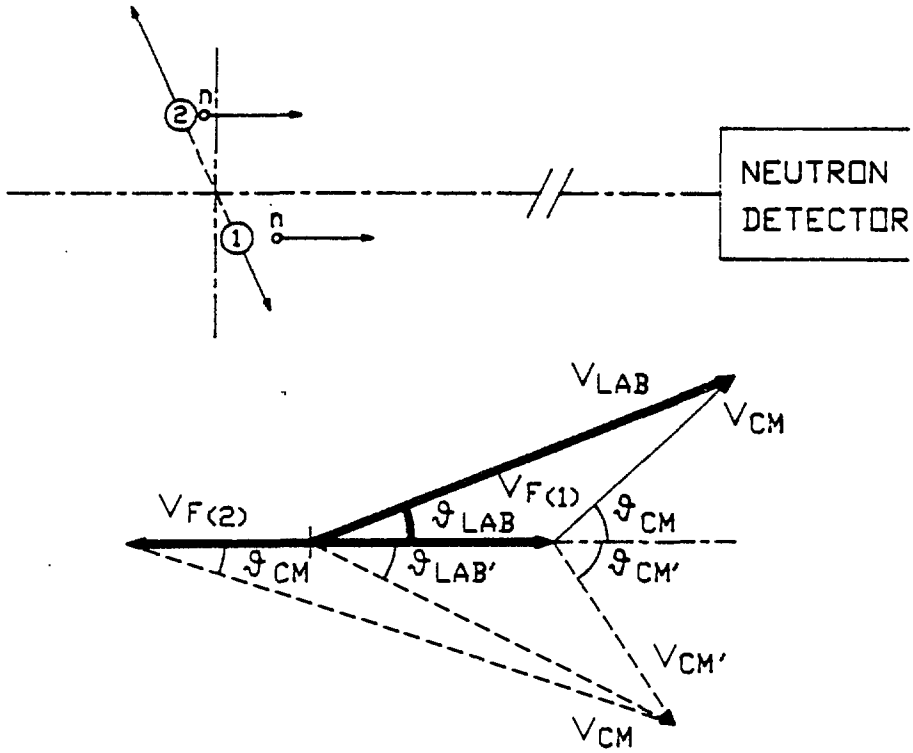

$$V_{CM}^2 = V_F^2 + V_{LAB}^2 - 2 \cdot V_F \cdot V_{LAB} \cdot \cos \vartheta_{LAB}$$

$$\cos \vartheta_{CM} = (V_{LAB} \cdot \cos \vartheta_{LAB} - V_F) / V_{CM}$$

$$\cos \vartheta_{CM} \geq 0 \Longrightarrow \begin{cases} V_{LAB} \geq V_F / \cos \vartheta_{LAB} \\ En \geq 0.3 \text{ MeV} \end{cases}$$

Figure 7
Representation of neutron emission from the fully accelerated fragments and the transformation diagram to the fragment centre-of-mass system. Thick vectors and angle with thick indication are known from the experiment.

$$\cos \Theta_{CM} = (V_{LAB} \cdot \cos \Theta_{LAB} - V_{F_1}) / V_{CM} \qquad [2]$$

where V_{F_1}, V_{LAB} are the fragment and the neutron laboratory velocities respectively, and Θ_{CM}, Θ_{LAB} are the neutron emission angles in the center-of-mass and laboratory system, respectively. Since neutron emission in the center-of-mass system is symmetric about Θ_{CM}= 90° /18/ the following analysis will be restricted to the case : $0° \leq \Theta_{CM} \leq 90°$. This condition implies that only those events for which:

$$V_{LAB} \geq V_{F_1} / \cos \Theta_{LAB} \qquad [3]$$

will be included in the analysis. Neutrons for which equation [3] is observed must have been emitted with laboratory energies which are larger than the minimum fragment energy per nucleon. The applied neutron detector threshold of 0.3 MeV did therefore insure that all wanted neutrons were taken into account. The data were analyzed event by event and from equations [1],[2] the multiparameter distribution N ($E_{L,H}$, $A_{L,H}$, E_{CM}, cos Θ_{CM}) could be generated.

In the next step this distribution was used to determine the desturbing contribution from the complementary fragment. Such an event is illustrated by dashed lines in fig. 7. Obviously only neutrons emitted with high center-of-mass energies from the complementary fragment can be detected and due to the exponentially decaying evaporation spectrum their number will be low. This can be seen from fig. 8 where the number of coincidences versus mass A are compared respectively for fragments emitted towards and away from the neutron detector. The contribution from the complementary fragment is for most fragments only a few percent, however in some mass regions e.g. A ~ 130, where the neutron multiplicity is much lower than for the complementary fragment the correction is significant. In the following all the discussed distributions have been corrected for the contribution from the complementary fragment.

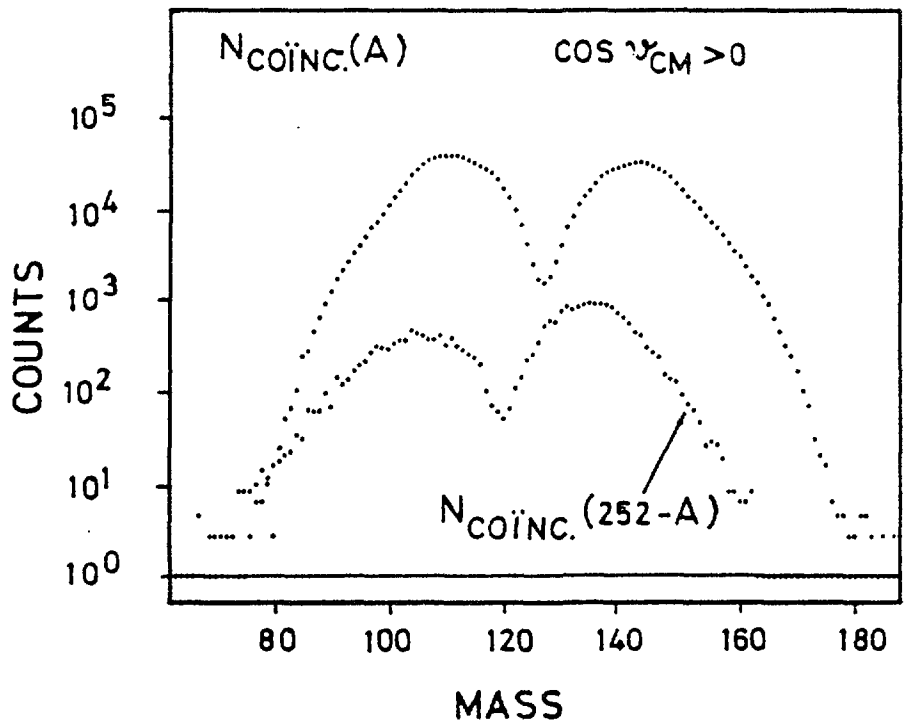

Figure 8

Fission neutron yield for $\cos\Theta_{CM} > 0$ versus fragment mass A. The lower curve shows the yield which is due to neutrons from the complementary fragment.

3.2.1 Angular Distributions in the Center-of-Mass-System.

Using the procedures discussed above the angular distributions of the fission neutrons in the center-of-mass-system of the flying fragment were evaluated. Fig. 9 is a biparametric plot of the mass integrated angular

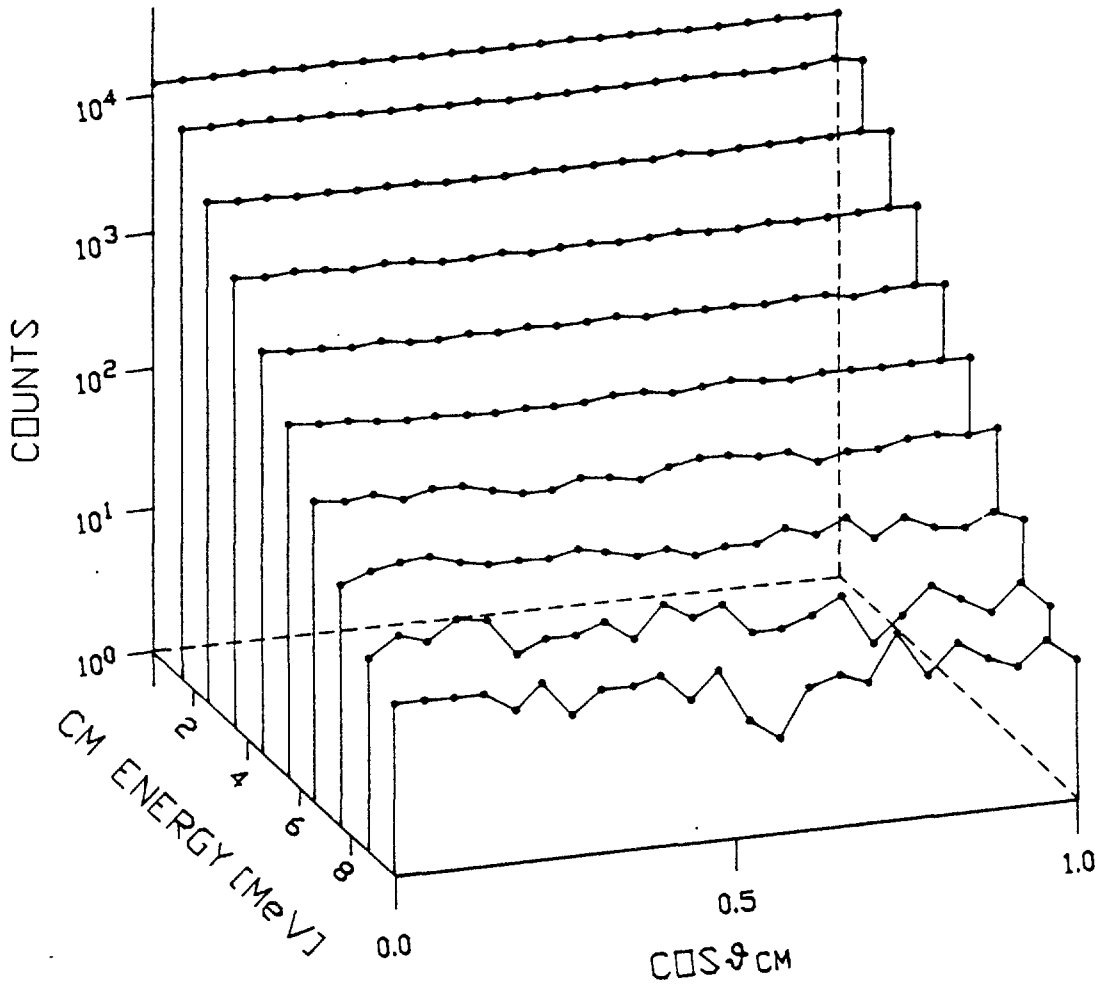

Figure 9
Fission neutron angular distribution $0 \leq \cos\Theta_{CM} \leq 1$ as function of fragment center-of-mass fission neutron energy.

distributions in the $\cos\Theta_{CM}$ interval [0,1] and for neutron energy intervals of 1.0 MeV. Fig. 10 displays the angular distribution $W(\cos\Theta_{CM})$ integrated over all neutron energies and normalized such that

$$\int_0^1 W(\cos\Theta_{CM})\, d\cos\Theta_{CM} = 1 \qquad [4]$$

To our knowledge the present experiment is the first direct measurement of the ^{252}Cf fission neutron center-of-mass angular distributions. Obviously our results show that the neutrons are emitted isotropically in the

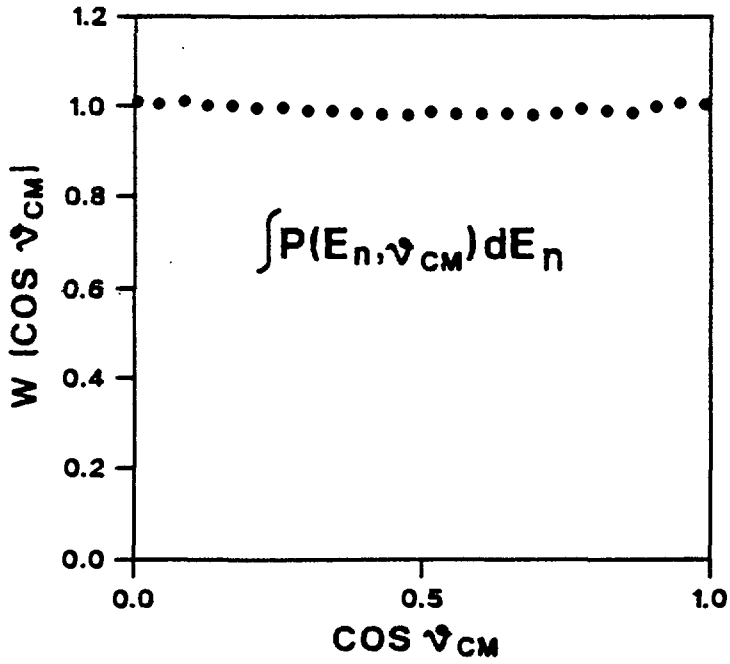

Figure 10
Fission neutron angular distribution in the fragment center-of-mass system integrated over all neutron energies.

center-of-mass system. An analysis of the data in fig. 10 yields for the angular distributions :

$$W(cos\Theta_{CM}) = 1 + (0.01 \pm 0.02) \cdot P_2(cos\Theta_{CM}) \qquad [5]$$

where P_2 is the second order Legendre polynom. The center-of-mass anisotropy is an important parameter for theoretical models of the ^{252}Cf fission neutron spectrum as already discussed by Terrell /18/. The present result of isotropy confirms the assumption made in most theoretical descriptions e.g. in the one recently presented by Madland and Nix /1/.

3.2.2. Average Neutron Multiplicity

The average neutron multiplicities $\bar{\nu}$ (A,TKE) as function of fragment mass A and total kinetic energy TKE were calculated from the fission yields versus A,TKE and the neutron fragment coincidence spectra transformed to the fragment center-of-mass system as described in the previous section. The $\bar{\nu}$ (A,TKE) data were normalized to the recently evaluated value $\bar{\nu}_{52}$= 3.7632 /19/, where $\bar{\nu}_{52}$ is the average prompt neutron emission from both fragments. The neutron multiplicity versus mass $\bar{\nu}$(A) is displayed in the lower part of fig.11. Due to the high counting statistics and the low background yields in the present experiment it was possible to extend the $\bar{\nu}$-measurement considerably in the mass range compared to earlier

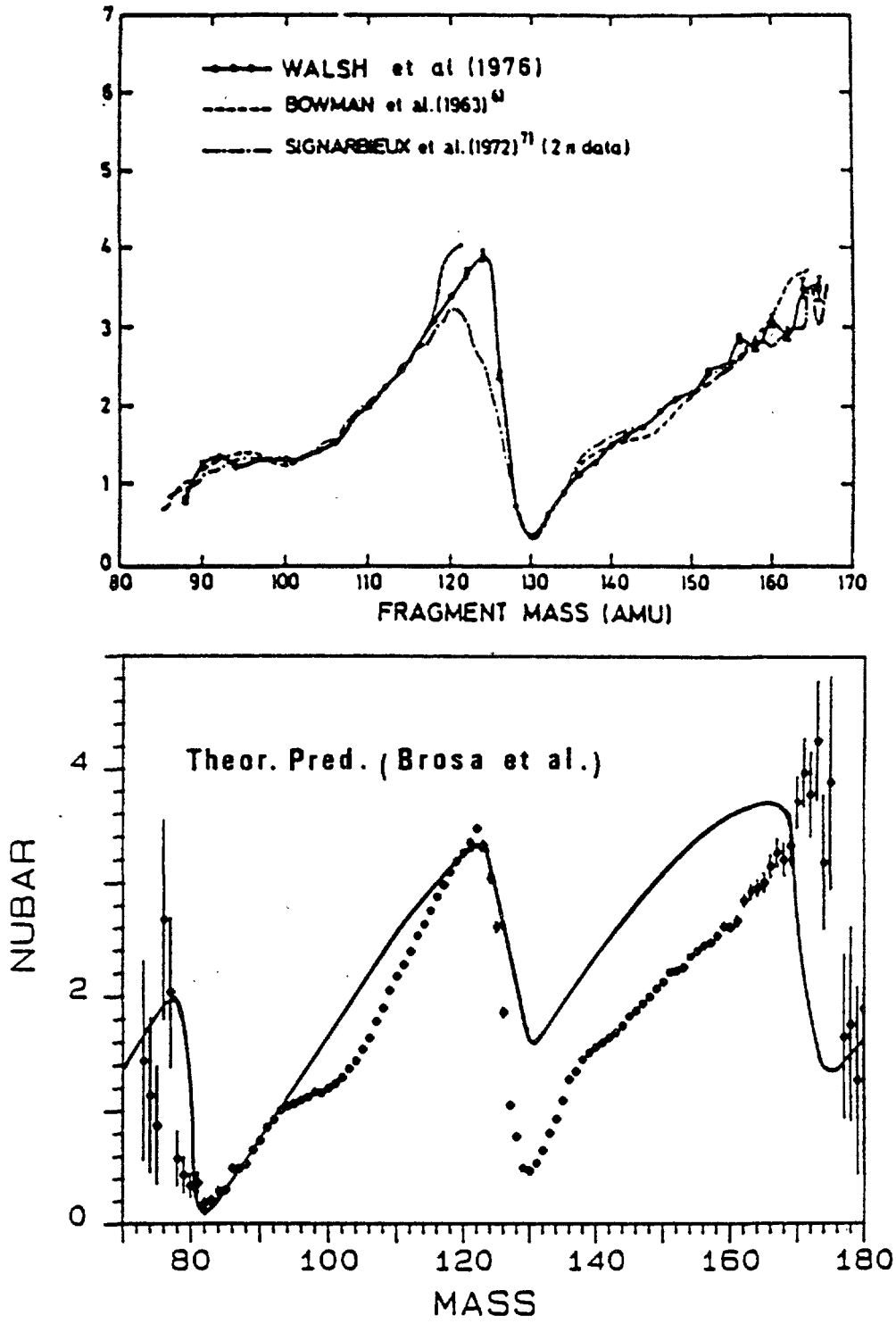

Figure 11

The average neutron multiplicity is plotted versus the fragment mass. The upper part shows data from the literature, the lower part from the present experiment. In the lower part the full line represents the prediction of Brosa /5/.

measurements. Comparison can be made with three previous data sets /3,20,21/ given in the upper-part of fig.11. The general agreement is quite good, however near the peak at A ≃ 120 the data sets scatter by up to 15%. Here the measurements are very sensitive to mass resolution effects and a proper correction for effects of fragment recoil /9/. The present data do not confirm the fine structures in $\bar{\nu}(A)$ seen by Walsh et al. /21/. It is remarkable that the present data show an increase of $\bar{\nu}$ below mass 82 indicating a saw-tooth shape also in the low mass region. At the heavy mass end, above mass 176, a clear decrease of the neutron multiplicity is observed producing even a third saw-tooth. The existence of a triple saw-tooth for ^{252}Cf has recently been predicted by Brosa /5/. This prediction is based on two hypothesis: multi modal fission and scission at random positions on the neck. The very mass-asymmetric fission component discussed in section 3.1.1. and by Brosa et al. /11/ will under these two assumptions produce the saw-tooth structures at A ≃ 82 and ≃ 176. The full line in the lower part of fig. 11 shows the predicted $\bar{\nu}(A)$ shape of Brosa /5/. The qualitative agreement is impressive, although the neutron emission from the heavy fragments is somewhat overestimated.

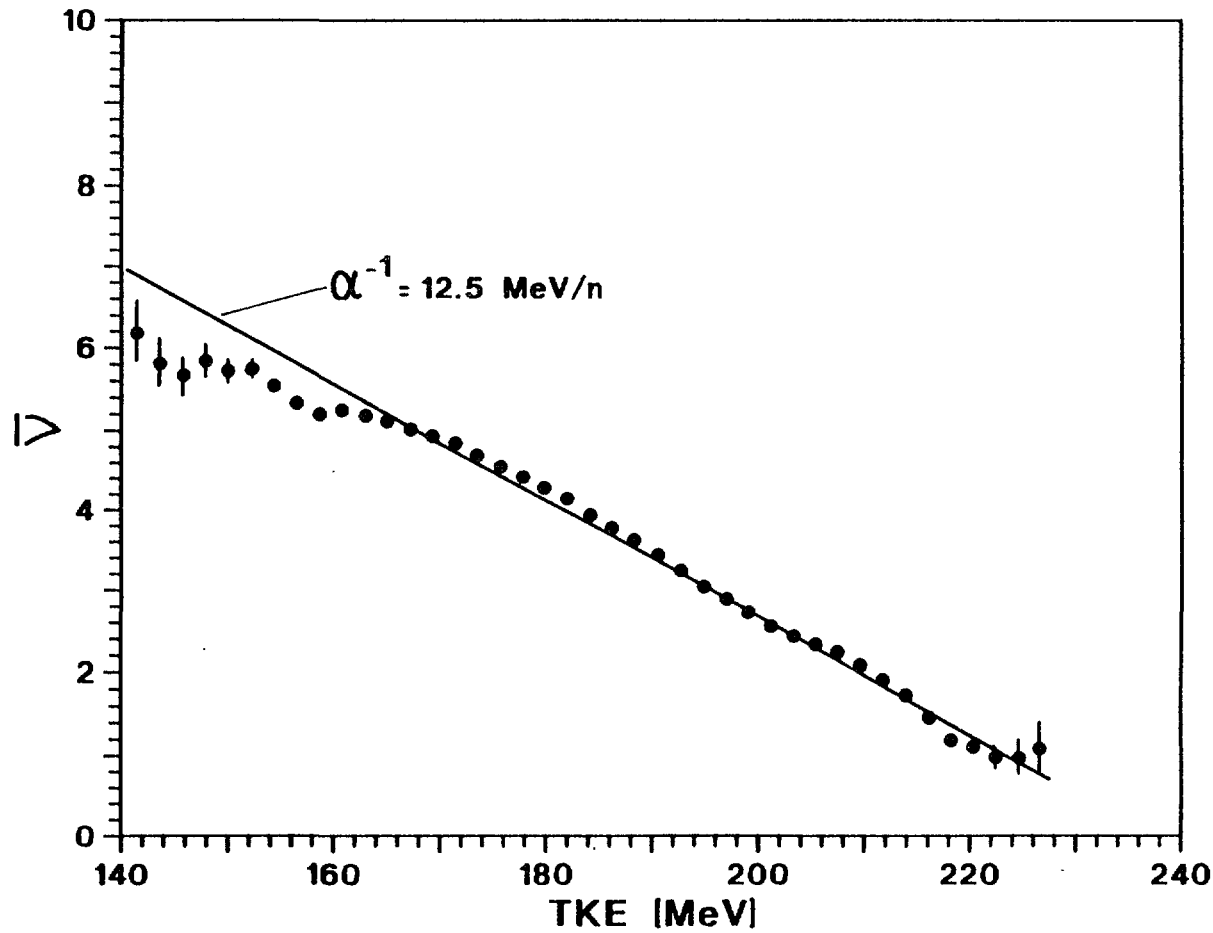

Figure 12

The neutron multiplicity summed over all fragments is plotted versus TKE.

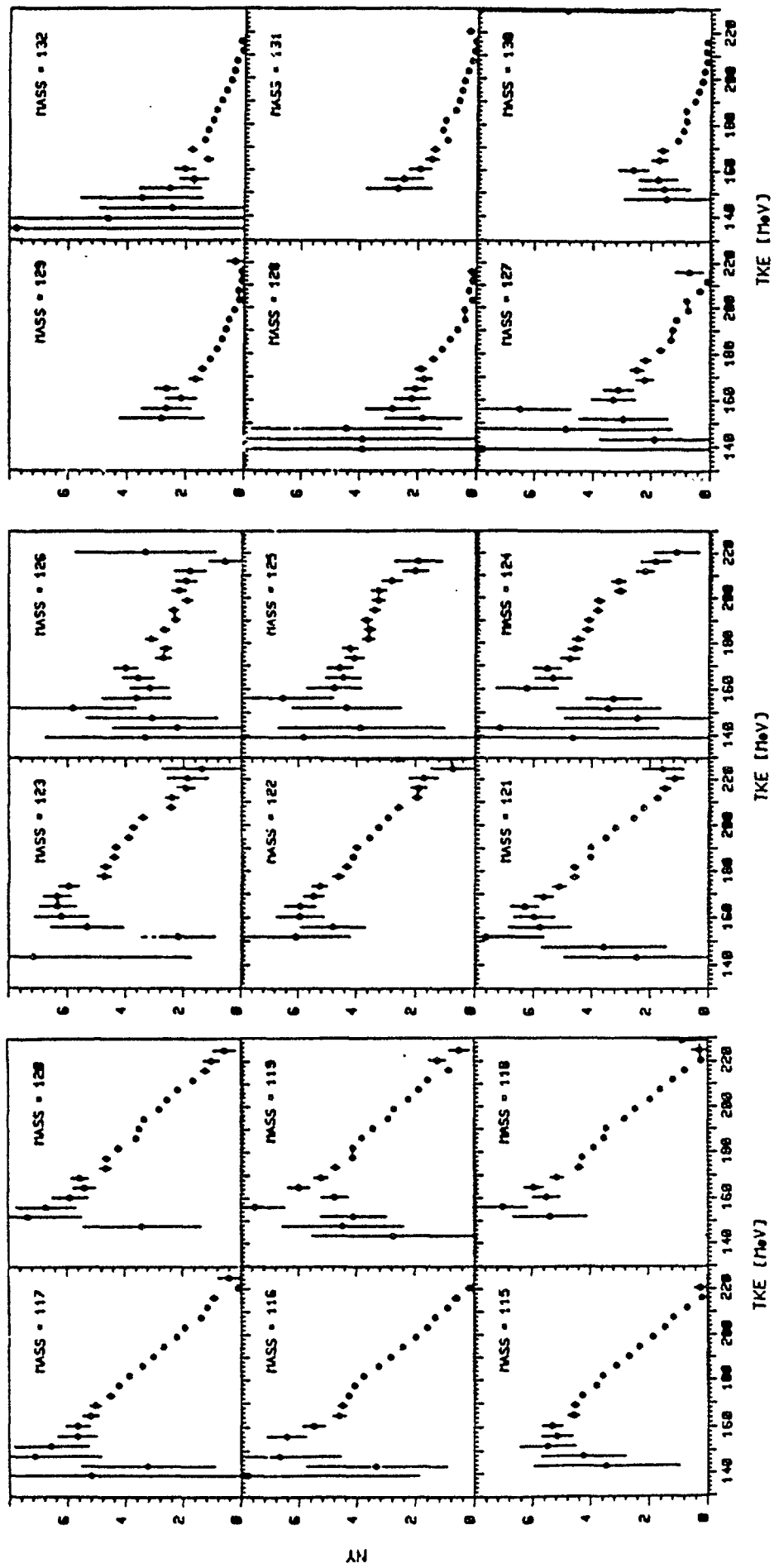

Figure 13
The neutron multiplicity for fragments from mass 117 to 132 is plotted versus TKE.

The variation of the total number of neutrons emitted by both fragments as function of their total kinetic energy, TKE, is displayed in fig. 12 . Also here the high counting statistics allowed an extension of the energy range compared to previous measurements. The variation is nearly linear with a small deviation towards low TKE values. The inverse slope of this $-(\delta\bar{\nu}/\delta TKE)^{-1}$ variation $-(\delta\bar{\nu}/\delta TKE)^{-1}$ is 12.5 MeV/n which compares well with the value of 13.0 MeV/n found by Nifenecker et al. /9/.

The variation of the average number of neutrons for some selected masses, A = 117-130, as function of TKE is shown in fig. 13. Again a near linear dependence is observed. Therefore, the variation of the average number of neutrons as function of TKE can be approximated for each fragment by a straight line. The straight lines are determined by their slope $-(\delta\bar{\nu}/\delta TKE)(A)$ and by their crossing points with the TKE-axis at TKE_{max} (A) where the neutron emission stops. These two quantities were deduced from the plots as shown in fig. 13. The slopes are plotted as function of heavy and light fragment mass in fig. 14, for each mass split on top of each other. The slope of $\bar{\nu}$ with TKE is a measure of the deformability of that part of the pre-scission shape from which the fragment with mass number A was produced. This can be read from equation [6]

$$\frac{\delta E_x}{\delta D} \approx \frac{\delta \nu}{\delta D} = \frac{\delta \nu}{\delta TKE}(A) \cdot \frac{TKE^2}{Z_1 \cdot Z_2 \cdot e^2} \qquad [6]$$

where E_X is the energy stored in the part of the pre-scission configuration which corresponds to the potential fragment of mass A. The distance between the fragment charge centers at scission is represented by D. Fig. 14 is consistent with the picture of a pre-scission configuration which has a hard heavy head with mass around 130 u and a hard light head of mass around 80 u, whereas the rest of the nucleons form the neck. This scission configuration would correspond to the standard fission mode, which is the most frequent one, as proposed by Brosa et al. /11/. In fig. 15 the TKE_{max} values are plotted as function of heavy and light fragment mass. It is clearly shown, that the fragments of one mass split in general do not stop with neutron emission at the same TKE-value.

A rather recent measurement of Zakharova et al. /22/ revealed remarkable structures in $\bar{\nu}(A)$ for fragment TKE values below 140 MeV. However, these results are not confirmed by the present analysis of $\bar{\nu}(A,TKE)$ which is based on 6-8 times better counting statistics than the Zakharova measurement. The present data show even at the lowest TKE values a smooth saw-tooth shape for $\bar{\nu}(A)$. However, below TKE of 140 MeV the results of ref. /22/ display relative yields which are typically 10^2 times larger

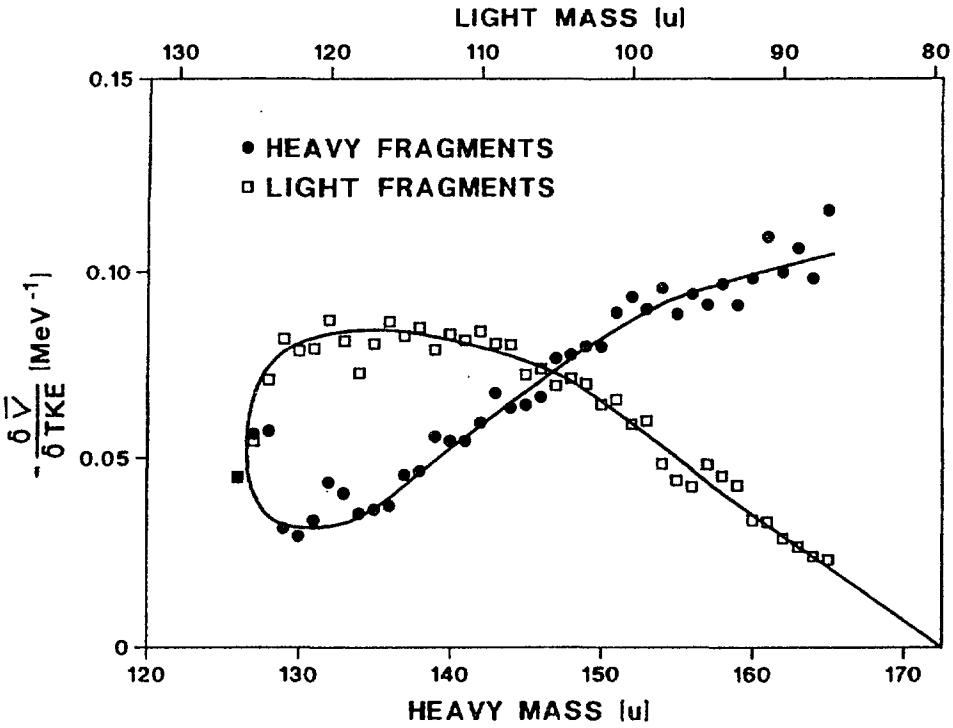

Figure 14

The slopes of the neutron multiplicities with TKE are plotted versus the light and heavy fragment mass.

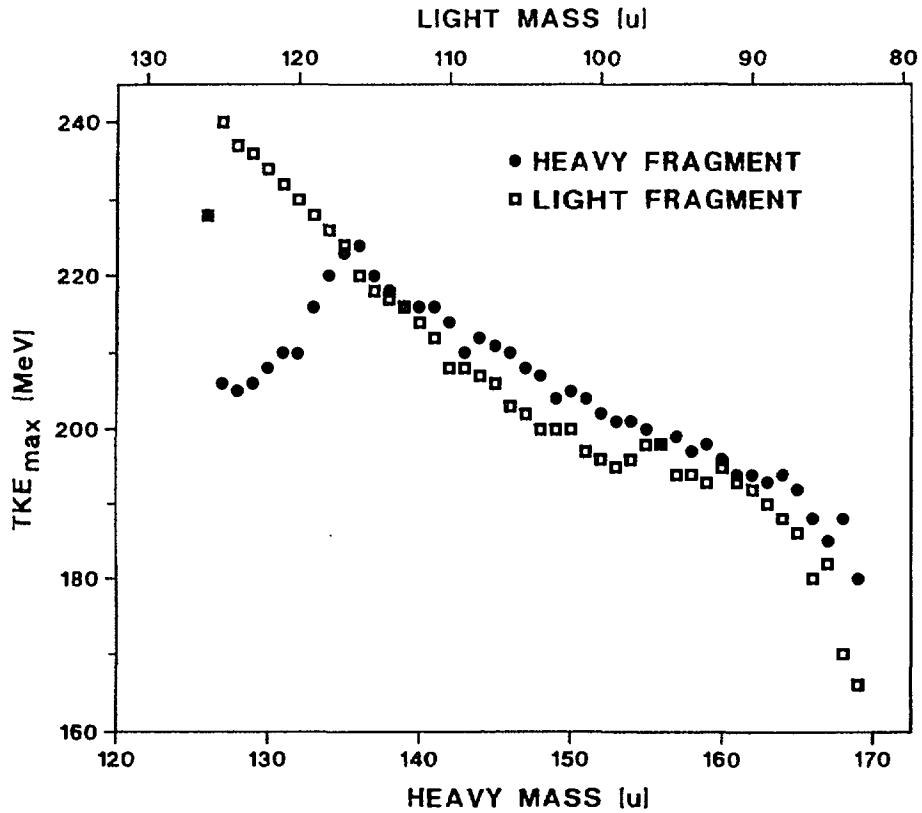

Figure 15

The total kinetic energies where the neutron emission stops are plotted versus the heavy and light fission fragment masses.

than the present ones. This suggests that the low energy results of ref. /22/ are influenced strongly by low energy failing effects produced by the fragment detector and that the observed structures are of experimental origin.

3.2.3. The Fission Neutron Spectrum in the Center-of-Mass System

The neutron energy η in the center-of-mass system of the fragment was evaluated event by event using the procedures described in the beginning of section 3.2.. Fig. 16 displays the η spectrum integrated over all fragments. According to standard nuclear evaporation theory the center-of-mass neutron energy spectrum corresponding to a fixed residual nuclear temperature T is given approximately by V.F. Weisskopf /23/

$$\Phi(\eta) = \frac{\eta}{T} \exp(-\eta/T) \qquad [7]$$

The evaporation spectum for neutrons emitted in a cascade process is slightly modified and Le Couteur and Lang /24/ obtained :

$$\Phi(\eta) = const. \cdot \eta^{\lambda} \cdot \exp(-\eta/T_{eff}) \qquad [8]$$

where λ is close to 5/11 and the effective temperature is T_{eff} = 11/12·T. If there is a distribution of initial energies the spectrum will have the same form as equation [8] but with a decreased value of λ /24/. The

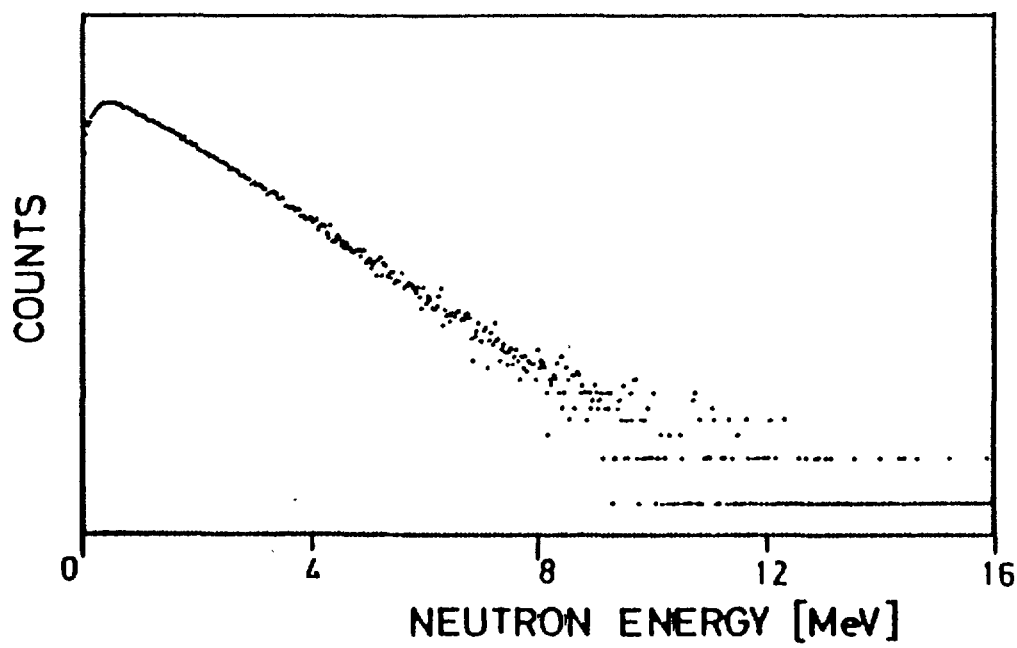

Figure 16
Integral fission neutron spectrum in the fragment center-of-mass reference system.

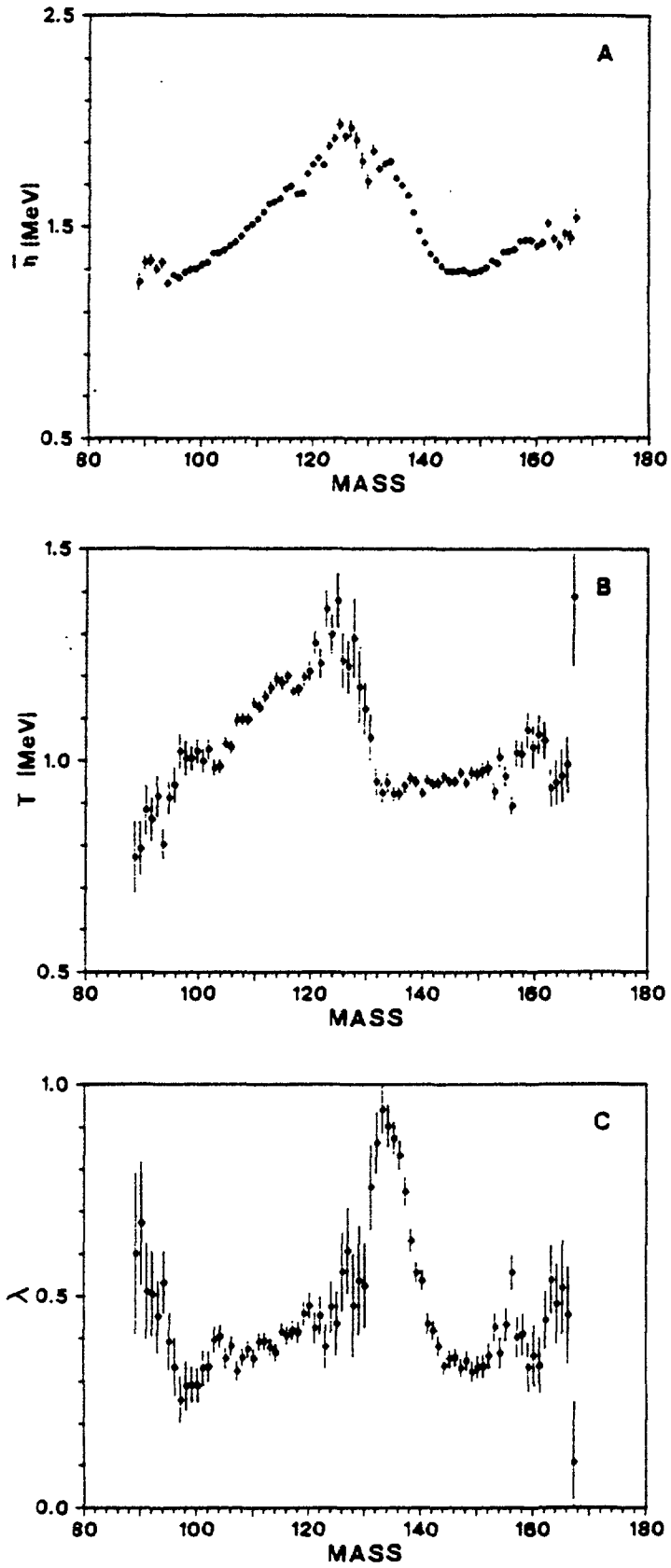

Figure 17

The average fission neutron energy, the nuclear temperature and the cascade neutron emission coefficient are plotted versus the fragment mass.

parameters λ, T of equation [8] were then treated by us as free parameters to be determined from the experimental η-distributions. For the integrated spectrum the values λ = 0.38 and T = 1.07 MeV gave the best description. The accordingly calculated spectrum is shown on fig. 16 as the full line. The neutron spectrum belonging to each mass A was evaluated and T (A) and λ (A) were determined using equation [8].

Fig. 17 a displays the average energy $\bar{\eta}$ as function of A. The results agree fairly well with the data of Bowman et al. /3/ who were the first to note the surprising fact that, whereas the saw-tooth function $\bar{\nu}(A)$ is very asymmetric with respect to mass 126, the energy $\bar{\eta}(A)$ is nearly symmetric. In particular fragments around mass 120, emitting on average more than three neutrons, and fragments around mass 132 which emit less than one, nevertheless evaporate their neutrons with very nearly equal average energies. However, contrary to Bowman et al. /3/ we find that the shape of the evaporation spectra is mass dependent. This can be seen from fig. 15 b and c where the nuclear temperature T and the exponent λ are plotted as function of A. The λ values scatter around a value of 0.4,a value close to the exponent of the cascade evaporation spectrum of Le Couteur /24/. However, around the double shell closure, A = 132, a pronounced peak with a peak value close to 1.0 is visible. This means that neutrons here are evaporated with spectra close to the Weisskopf spectrum, equation [7]. This is not surprising since the average neutron multiplicities for these fragments are smaller than one and cascade effects play therefore a small role.

The derived nuclear temperatures do reproduce a saw-tooth behaviour although less pronounced than for $\bar{\nu}(A)$.

Bowman et al. /3/ did already point out that the combined data of the number $\bar{\nu}$ and the neutron evaporation spectra contain a considerable amount of informations on the fission fragment nuclear level densities. Lang /25/ did later extract the level density parameter for ^{252}Cf (SF) fission fragments using the database of ref. /3/. The improved experimental conditions and high counting statistics of the present data justify a reevaluation of these parameters. According to the Fermi gas model the excitation energy E_X of the neutron evaporating fragment is related to the nuclear temperature T by :

$$E_x = a \cdot T^2 \qquad [9]$$

The excitation energy of the nascent fragment is estimated by:

$$E_x(A, TKE) = \nu(A, TKE)\left|B_n(A,Z) + \eta(A,TKE)\right| + E_\gamma(A,TKE) \qquad [10]$$

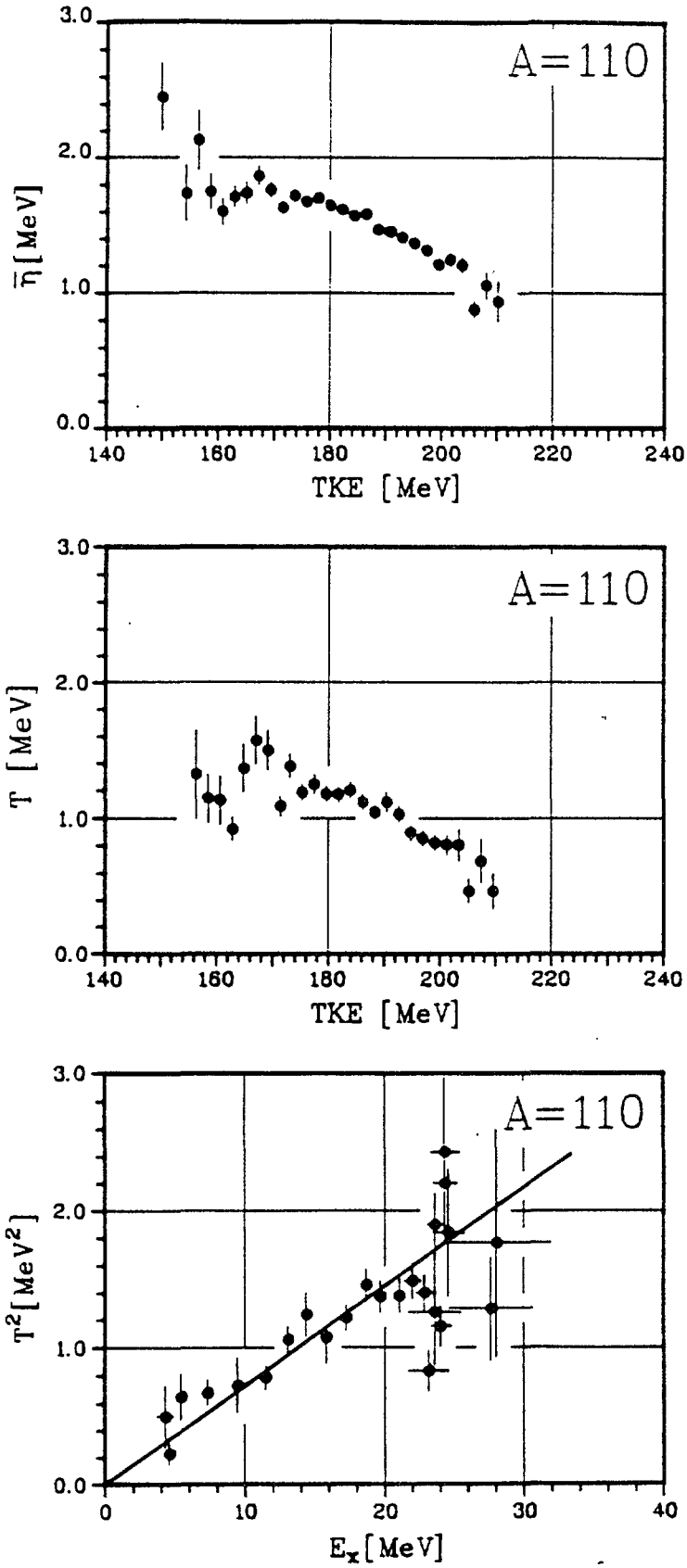

Figure 18

The average fission neutron energy and the nuclear temperature are plotted versus the total kinetic energy for the fragment with mass 110. In the lowest part of the figure the square of the temperature is plotted versus the fragment excitation energy.

Here $\bar{\nu}$ (A,TKE), $\bar{\eta}$(A,TKE) and E_γ(A,TKE) are the average number of neutrons, their average energy and the total energy carried away by γ rays from a fragment with mass A and total kinetic energy TKE, respectively. B_n(A,Z) is the average binding energy of a neutron in a nucleus with mass A and most probable charge Z.

The average neutron energy $\bar{\eta}$(A,TKE) and the nuclear temperatures T(A,TKE) were determined as previously described from the neutron spectra belonging to each mass and TKE. The TKE dependence of these quantities are exemplified for mass A = 110 in the two upper plots of fig. 18. The excitation energies E_x(A,TKE) were determined using equation [10]. Here the neutron binding energies B_n(A,Z) were calculated from the mass tables of Möller and Nix /26/. The average γ-energy was estimated by $E_\gamma = \frac{1}{2} B_n$.

In the lower part of fig 18 the square of the temperature, T^2, has been plotted versus E_x. A near linear dependence is observed and the level density parameter a was determined according to equation [9].

The level density parameter a obtained from the present data is shown in fig. 19 as function of A. For comparison the full line in fig. 19 represents the experimental relation

$$a = A/C \qquad 11$$

for C = 10 MeV. It is obvious that this relation gives a rather poor description of the level density parameters, especially in the mass range A = 120 to 150. Our data agree well with the evaluation of Lang/25/ although the latter results have much larger uncertainties. Both data sets show that shell effects have a dominant influence on the level densities and that the simple relation of equation [11] which has been assumed in the most recent theoretical models /1,27/ for the neutron evaporation spectrum is very approximative.

4. CONCLUSIONS

The present work demonstrates that the overwhelming part of neutrons is emitted from the fully accelerated fragments. The scission component is negligibly small up to 10 MeV neutron energy in the CM-system, as can be deduced from the angular distributions shown in fig. 9.

The mass range for the experimental values of the average number of neutrons as function of mass, $\bar{\nu}$(A), was extended considerably. Two new sawteeth were discovered near the fragment masses 80 and 176. This $\bar{\nu}$(A)-curve can be understood by the multi modal fission model and scission at random positions in the neck as proposed by Brosa et al. /5,11/.

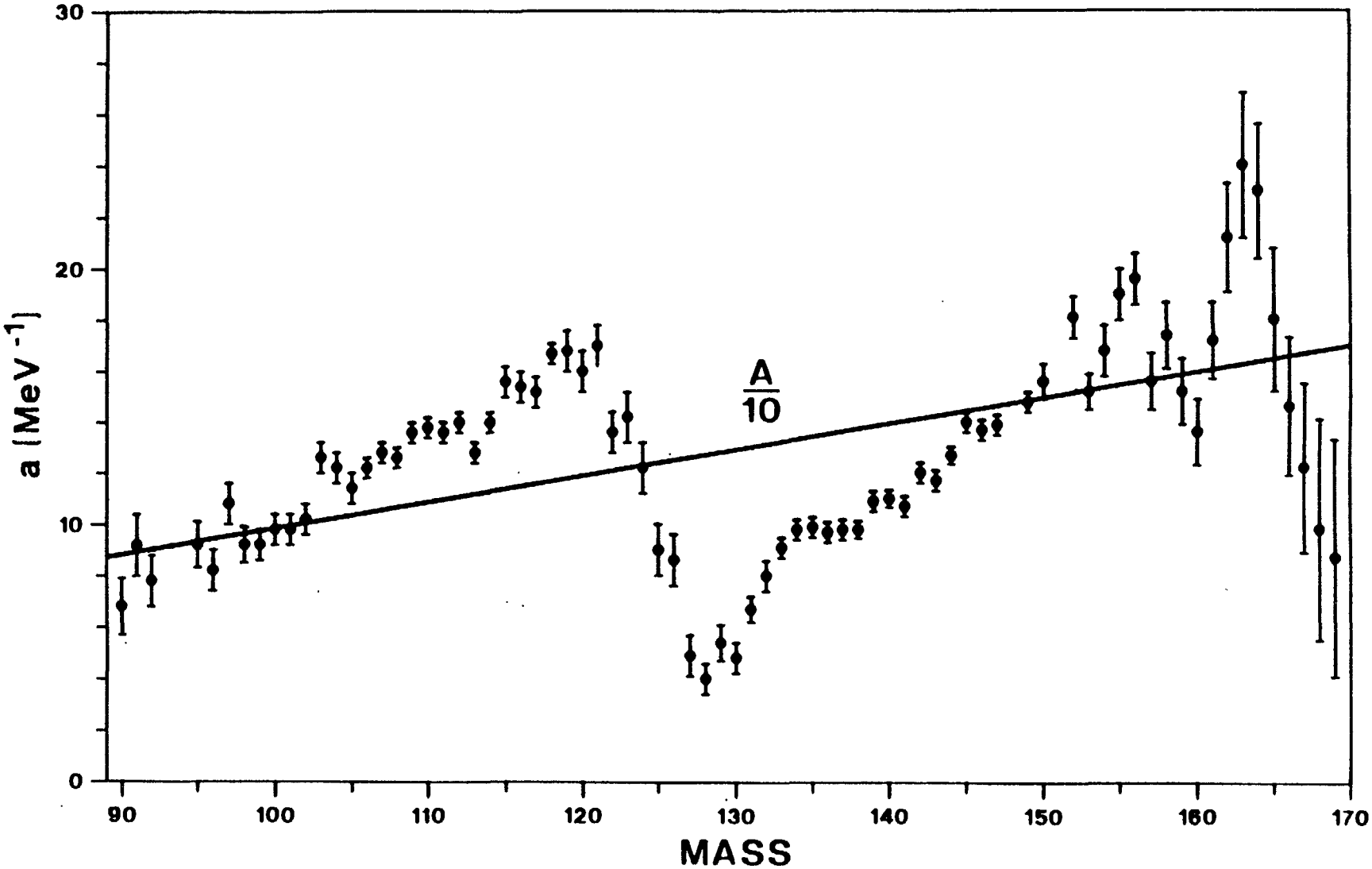

Figure 19

The level density parameter is plotted versus the fragment mass. The full line represents the curve a = A/10.

The $\bar{\nu}$-dependence on TKE for the fragment with mass A gives new information about the deformability of that part of the pre-scission shape which forms the fragment of mass A after scission.

The neutron spectra in the CM-system, measured as function of fragment mass and TKE, yielded values for the average neutron energy $\bar{\eta}(A,TKE)$ and of the nuclear temperature T(A,TKE). These informations together with $\bar{\nu}(A,TKE)$ were used to determine the level density parameter a(A) in the fragment mass range $90 \leq A \leq 165$.

The use of realistic level densities in theoretical calculations of the fission neutron spectrum instead of applying crude approximations like a = A/10 or similar expressions would certainly improve the results.

References

1. D.C. Madland and J.R. Nix
   Nucl. Sci. Eng. 81, 213 (1982)
2. H. Märten, D. Neumann, and D. Seeliger
   Proc. IAEA Consultants' Meeting on the ^{235}U Fast Neutron Fission Cross-Section and the ^{252}Cf Fission Neutron Spectrum, Smolenice, March 1983, INDC(NDS) - 146, P. 195 (1983)
3. H.R. Bowman, S.G. Thompson, J.C.D. Milton, and W.J. Swiatecki
   Phys. Rev. 126, 2120 (1962).
4. U. Brosa, S. Grossman, and A. Müller
   Z. Phys., 325A, 241 (1986)
5. U. Brosa
   to be published by Phys. Rev. C
6. H.-H. Knitter, and C. Budtz-Jørgensen
   Proc. of the Int. Conf. on Nuclear Cross Sections for Technology, Knoxville, U.S.A., Oct. 1979, NBS Spec. Publ. 594, p. 947 (1980)
7. C.Budtz-Jørgensen, H.-H. Knitter, Ch. Strade, F.-J. Hambsch, and R. Vogt
   Nucl. Instr. Meth. 258A, 209 (1987)
8. Ch. Straede, C.Budtz-Jørgensen, and H.-H. Knitter
   Nucl. Phys. 462A, 85(1987)
9. H.Nifenecker, C. Signarbieux, R. Babinet, and J. Poiton
   3rd IAEA Symp. on the Physics and Chemistry of Fission, Rochester, 1973, Vol. 2, p. 117
10. G. Barreau, W. Sicre, F. Caïtucoli, M. Asghar, T.P. Doan, B. Leroux, G. Martinez, and T. Benfoughal
    Nucl. Phys. 432A, 411(1985).

11. U. Brosa, S. Grossman, and A. Müller
Z. Naturforsch. 41a, 1141 (1986)

12. H.-H. Knitter, F.-J. Hambsch, C. Budtz-Jørgensen, and J.P. Theobald
Z. Naturforschung, 42a, 786 (1987)

13. G. Dietze, and H. Klein
Bericht ND-22, Physikalisch Technische Bundesanstalt, Braunschweig, Germany, (1982).

14. H. Märten, D. Seeliger, and B. Strobinski
Proc. Int. Con. on Nuclear Data for Science and Technology, Antwerp, Sept. 1982, D. Reidel Publishing Company, NL, page 488

15. H. Märten, and D. Seeliger
Proc. IAEA Advisory Group Meeting on Nuclear Standard Reference DATA, Geel, Nov. 1984, IAEA-TECDOC-335, page 255, Vienna (1985)

16. C. Budtz-Jørgensen, and H.-H. Knitter
Proc. Int. Conf. on Nuclear Data for Basic and Applied Science, Santa Fe, USA (1985), Radiat. Eff.93, 5(1986).

17. H. Märten, D. Richter, D. Seeliger, W.D. From, W. Neubert, and A. Lajtai
Nucl. Instr. Meth. 264A, 375 (1988)

18. J. Terrell
Phys. Rev. 127, 880 (1962).

19. E.J. Axton
IAEA-TECDOC-335, p.214 (1984)

20. C. Signerbieux, J. Potton, M. Ribrag, and J. Matuszek
Phys. Lett. 39B,503 (1972)

21. R.L. Walsh, and J.W. Boldeman
Nucl. Phys. A276, 189 (1977)

22. V.P. Zakharova, and D.K. Ryazanov
Sov.J. Nucl. Phys. 30, 19 (1979).

23. V.F. Weisskopf
Phys. Rev. 52, 295 (1937)

24. K.J. Le Couteur and D.W. Lang
Nuclear Physics 13, 32 (1959)

25. D.W. Lang
Nucl. Phys. 53 113 (1964)

26. P. Möller, and J.R. Nix
Atomic Data Tables 26, 165 (1981)

27. H. Märten, and D. Seeliger
Nucl. Sci. Eng. 93,370 (1986)

EMISSION ENERGY SPECTRA OF NEUTRONS FROM SPONTANEOUS FISSION FRAGMENTS.

C.I.Batenkov, A.B.Blinov, M.V.Blinov, S.N.Smirnov

V.G.Khlopin Radium Institute, Leningrad, USSR

ABSTRACT

Multiparameter precision measuremente of differential energy spectra of ^{252}Cf spontaneous fission neutrons have been carried out for different masses, kinetic energies and excitation energies of the fragments at different emissionangles. These data have been analysed on the assumption of the evaporation model. The dependence of the average neutron energies have been studied for different masses and the fragments' total kinetic energies. Average energies of the neutrons emitted by spontaneous fission fragments have been compared with those of the neutrons from nuclear reactions.

INTRODUCTION

The shape of the emission spectra of fission neutrons is determined first of all by the stage of fission in which the emission takes place. Conventionally it is possible to distinguish several stages: the emission from the fissioning nucleus (descent from the barrier to the scission point, during scission of the nucleus), neutron emission in the process of acceleration of the fragments, at establishing their equilibrium shape and the emission at the last stage by cascade evaporation from equilibrium heated fragments. The emission spectra from excited nuclei fragments are connected both with the individual properties of the corresponding nuclei and with their excitation energy. The contribution of these components is determined by measuring and analyzing neutrons' angular and energy distributions and correlation of them with the mass A, the kinetic energy E_k and the excitation energy of the fragments E*.

The available in literature /1-5/ information on the dependence of the average energies of the spectra $\bar{E}_n$ on A and E_k is incomplete and insufficiently precise. Theoretical calculations weredone only for the dependence $\bar{E}_n$ (A) /6-7/.

In the given work multiparameter measurements have been carried out of the dependence of ^{252}Cf spontaneous fission neutrons' emission spectra on the mass, the kinetic energy and the excitation energy of the fragments.

METHOD AND APPARATUS

Measurements were carried out using a multiparameter spectrometer of spontaneous fission neutrons.

The fission source was made of high-purity ^{252}Cf by the vacuum self-transfer method on an aluminium oxide film 50 $\mu g/cm^2$ thick. The diameter of the active spot was 3 mm, the intensity of the source, 10^5 fiss/s.

The elecrons knocked out by fission fragments from the aluminium oxide film were registered by means of a detector based on a microchannel plate (MCP). Such a detector enabled to register all the fission events and gave a time reference to the moment of fission with precision better than 100 ps.

The fragments moving within the limits of a small solid angle were registered by two detectors on the base of MCP located diametrically opposite on the same axis with the source at a distance 9 cm from it. The velocity and the energy of the fragments after emission of the neutrons were determined by the time-of-flight method.

The neutron energy was also determined by the time-of-flight method. A stilben crystal 50x30 mm with a photoelectric multiplier FEU-30 was used as a neutron detector.

The efficiency was determined directly and continuously in the course of the experiment. Due to use of the detector with a full registration of the fission fragments it was possible simultaneously with a differential by angle neutron spectrum to accumulate an integral one the shape of which is an international standard. Such a method enabled to determine precisely the efficiency of the neutron detector in the low energy region and to exclude the influence of

the threshold's instability on its determination. For neutron energies lower 8 MeV the threshold by recoil protons was established equal 0,15 MeV, and for E_n over 8 MeV-1 MeV. This enabled to obtain the ratio effect/background not worse than 10 for the neutron energy range 0,3-15 MeV.

Neutrons and γ-quanta were separated by the pulse shape. The suppression coefficient at the threshold 0,5 MeV was equal 10^4 and at the threshold 0,15 MeV it equalled 10^2. The variance determined by the half-width of the γ-quanta distribution was 0,37 nsec for the whole energy range.

The energy calibration and the resolution of the neutron channel were checked by measuring the cross-section of neutron absorption by a carbon sample.

The value of neutron scattering on closely situated construction elements is an important characteristic that influences the correctness of measurements. For it to be excluded all the construction elements were made as small as possible: the thickness of the vacuum chamber was 0,3 mm, the thickness of the MCP, 0,5 mm. This enabled to reduce the contribution of the scattering and absorption effects to a value less 2 %.

The neutron spectra measurements were duplicated on three flight bases: 37.5, 75.0, 150.0 cm; besides, in order to increase the reliability of the measurements two neutron detectors arranged collinearly were used simultaneously. The measurements were done for angles 2, 6, 15, 30, 45, 60, 75, 90 degrees. The angular resolution was 2,6° and 11° in different experiments.

The treatment of the measurements consisted of two stages. During the first one carried out on line with a computer, the mass A, the kinetic energy E, the velocity of the fragment V_f and the time of flight of the neutron T, were determined. An accumulation was done of a matrix of fragment-fragment coincidenses on the N_f (M, E, I) coordinates, where I is the number of the detector, a matrix of fragment-fragment-neutron coincidenses on the N_n (T, A, E, I) coordinates and a matrix of velocities V_f (A, E, I). For each event are given: a compensation of the time-amplitude dependence of the time "zero", a correction of the fragments

energies taking into account the effect of neutron recoil. As a result of the treatment the neutron spectra were presented as a distribution of the neutron flux density

$$\rho(v,\varphi) = T^3 \cdot n/(R \cdot \varepsilon \cdot L^3),$$

where L is the distance of a neutron flight,
R - the number of registered fragments,
n - the number of registered neutrons,
ε - the efficiency of the neutron detector,
v - the velocity of a neutron.

RESULTS AND DISCUSSION

To obtain the emission spectra one must know precisely the velocity of the emitting source. This enables to find out what part of neutrons is emitted from a fully accelenated of fragment. For this purpose the yields and the spectra of the neutrons emitted from the fragments at angles 0 and 90° on the L. s. to the direction of their movement were compared. The yields of the neutrons measured at the angle of 90° and the ones calculated for the angle 90° from the experimental data at the angle of 0°, differ by 7 % in supposition that this effect is connected with the so called "scission neutrons". The average number of these neutrons is about 3 % of the total number which is somewhat less that the value previously obtained /8/ and coincides with the results of out measurements /9, 10/ carried out by a different method of registrating the fragments.

Analogous comparisons of the yields and spectra of the neutrons for 0° and 90° were carried out also for separate groups of fragments. In Fig. 1 a dependence is presented of the difference of the neutron yield (0-90) on the total kinetic energy of the fragments E_K for all the masses, and in Fig. 2 the same kind of dependence on the fragments' masses for all the E_k, as the number of the "scission" neutrons (v') isotropic in the l. s. The experimental neutron yields at the angle 90° are somewhat greater than the calculated ones for 0°, however the difference does not exceed substantiously the systematic error of the measurement. The obtai-

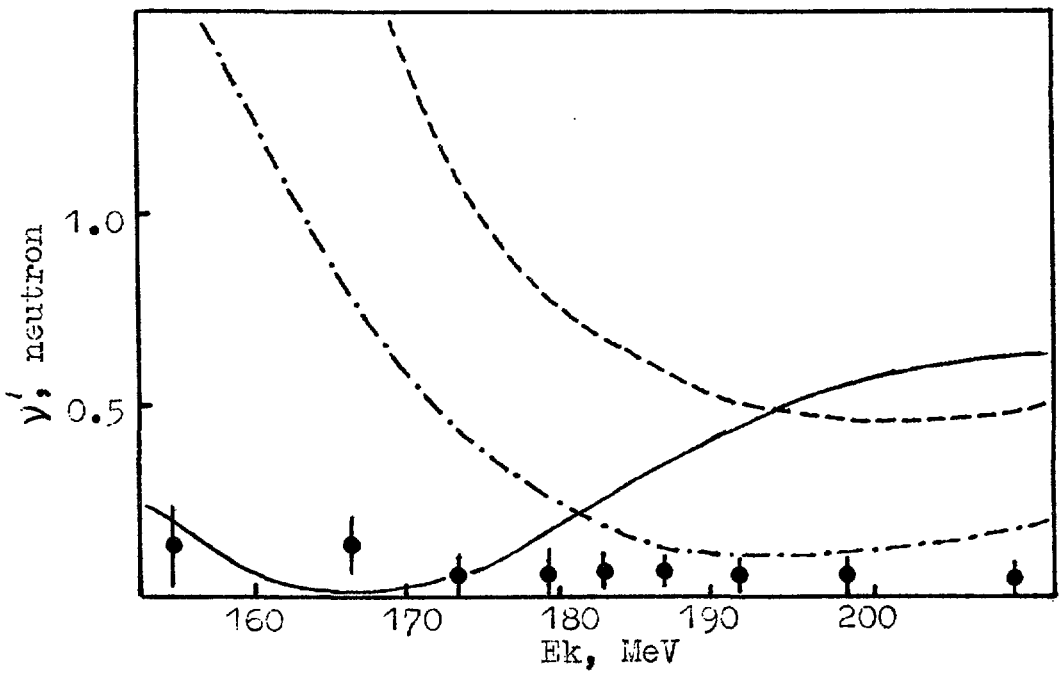

Fig. 1. The number of the "scission" neutrons in dependence on the fragment's mass (A) for a sum of E_k;
the data of works: ---- /2/, -·- /3/, —— /11/,
the data of this work: ●

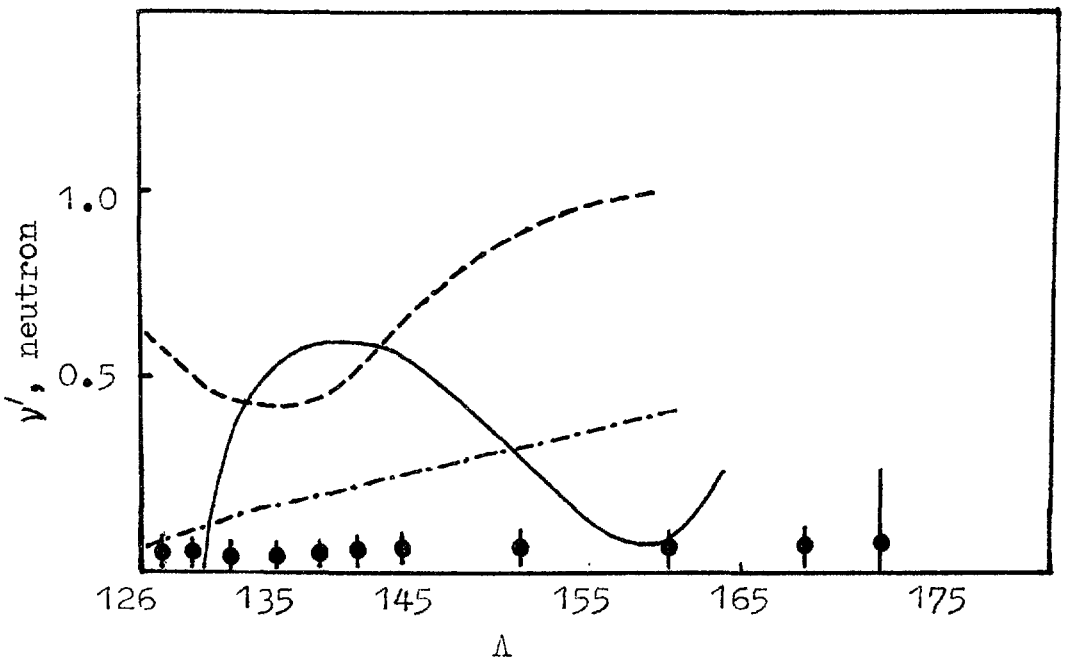

Fig. 2. The number of the "scission" neutrons in dependence on the total kinetic energy (E_k) for the sum of fragments' masses;
the data of works: ---- /2/, -·- /3/, —— /11/,
the data of this work: ●

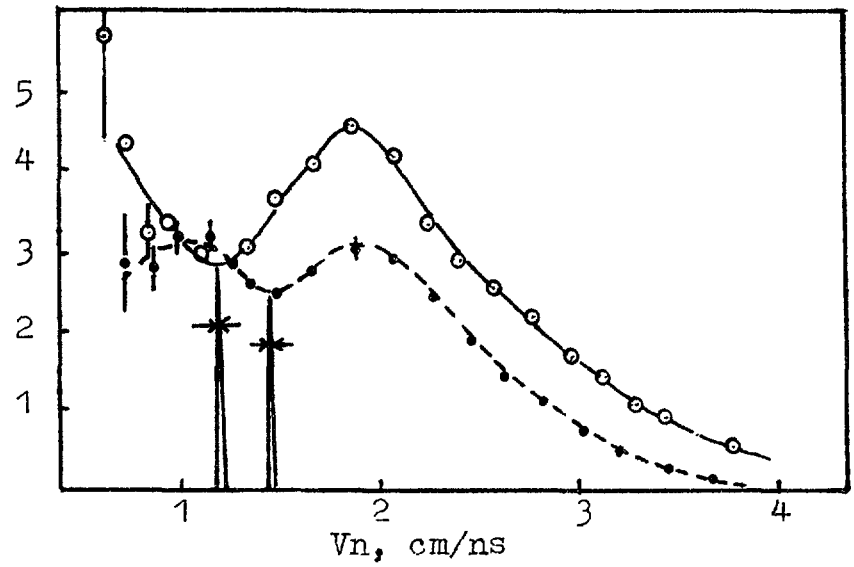

Fig. 3. The spectrum of the neutrons emitted at the angle 5°,
● M = 98±5 m.u., EK = 175±5 MeV, V = 1.44 cm/nsec,
○ M = 117±5 m.u., EK = 175±5 MeV, V = 1.22 cm/nsec;
the arrows show the variance of the neutron's velosity.

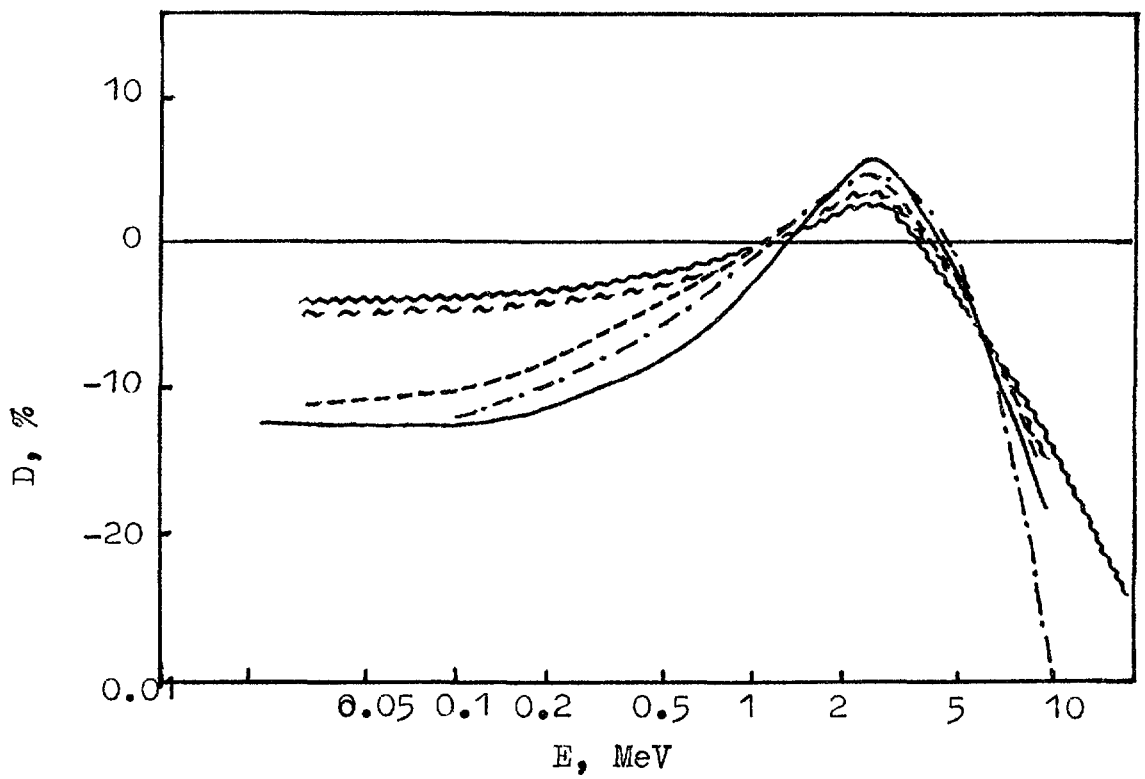

Fig. 4. Deviation of the integral spectra from the Maxwell distibution (T = 1.42 MeV);
the data of works: xxxx /13/, ---- /21/, -·- /22/, ~~~ /23/, ____ this work.

ned data differ considerably from the results of other studies /2, 3, 11/. The difference of the results is connected with the fact that in the given work a neutron spectrometer of high energy resolution in a wide energy range was used, the neutron detector's efficiency was carefully determined directly in the course of the experiment, with accounting of the influence of neutron recoil in each registered event (it influences most strongly on comparison of the spectra at 0° and 90°, where with a wrong accounting of the recoil effect, the errors for separate groups of fragments may reach 100 %), as well as with other characteristics of the setup, the conditions of measurements and with introducing a number of different corrections: for time resolution of the neutron and fragment channels, for recoil from the neutrons uncorrelated with the angle, for real collimation, etc.

We carried out /12/ determination of the average velocity of the fragments at which a neutron emission takes place immediately by the irregularity of the spectrum's shape connected both with the kinematic effect and with the emission spectrum. The results of the measurements showed a good agreement of these velocities with the maximum velocities determined by the Coulomb interaction of the fragments (Fig. 3).

A comparison was also done of the integral spectrum measured by the direct method and the one calculated using the data of neutron spectra in the c.m.s. of the fragments, obtained from measurements at small angles and in supposition that neutron emission takes place only within the limits of evaporation from fully accelerated fragments.

It is worth mentioning that in the energy range 1-10 MeV the integral spectrum (Fig. 4) obtained by us /10, 14/ goes close enough to the evaluation of /13/. In the low energy range our integral spectrum is somewhat lower than the data of direct measurements. The difference in the low energy range may be connected with the influece of the anisotropic effect in the c.m.s., caused by the fragment's angular momentum as well as with presence of a small share of nonevaporation neutrons. Variation of the anisotropic coefficient in the form $1+\beta P_2(\cos\varphi)$, with experimental spectra at an

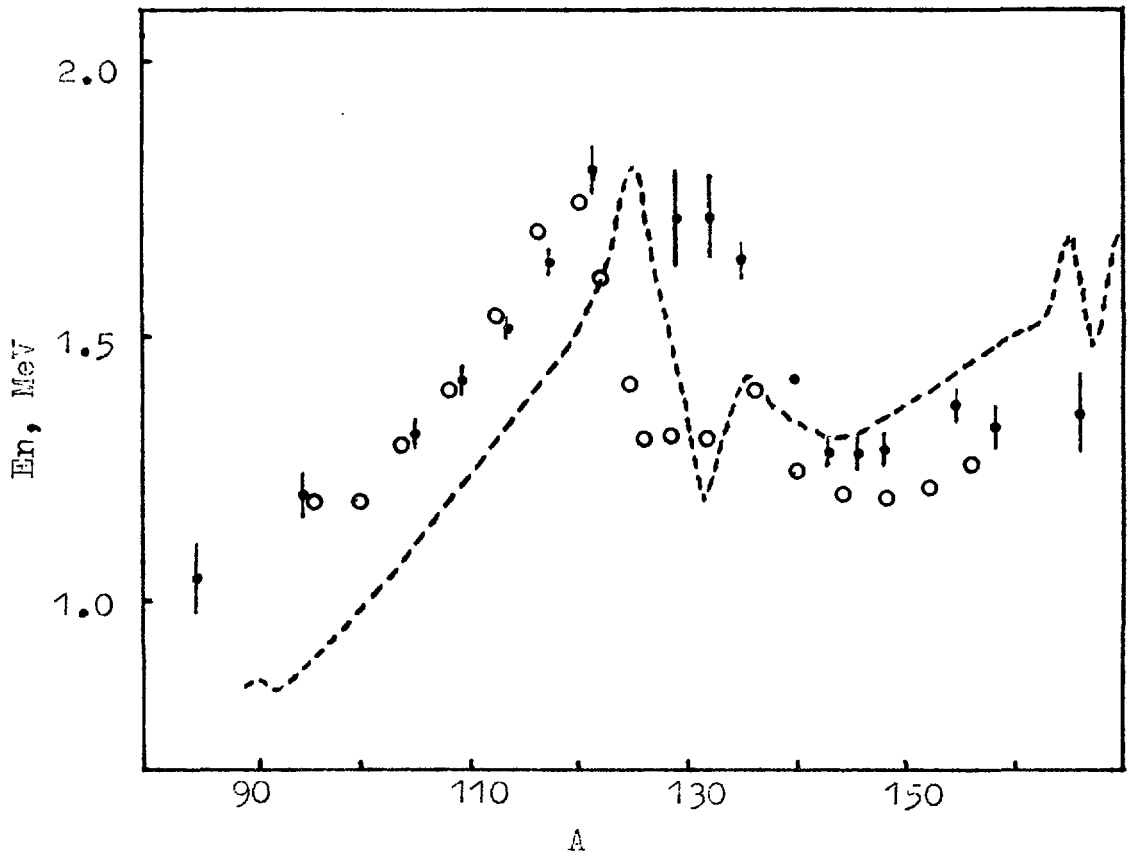

Fig. 5. Average neutron energy in the center-of-mass system of a fragment, in dependence on the fragment's mass (A), for a sum of E_k;
o - calculation of work /7/, ---- data of work /4/,
● - data of this work.

angle 0° in the l. s. being used as basic data, does not allow to get a complete agreement of the integral spectra in the low energy range ($\beta_{opt.} = 0.04$). Introducing neutrons of nonevaporation character (about 3 % of the total number) can account for the discrepancy of the spectra.

In connection with the fact that not less that 97 % of the neutrons are emitted within the scope of the evaporation model, a possibility arises to analyze neutron emission spectra for certain masses and excitation energies of the fragments with the aim of studying the densities of nuclei's levels, determining the cross-sections of the reverse process and other statistical characteristics for neutron-rich nuclei of the fragments.

In Fig. 5 the dependences are presented of the average energies of the neutrons on the fragment's mass summed

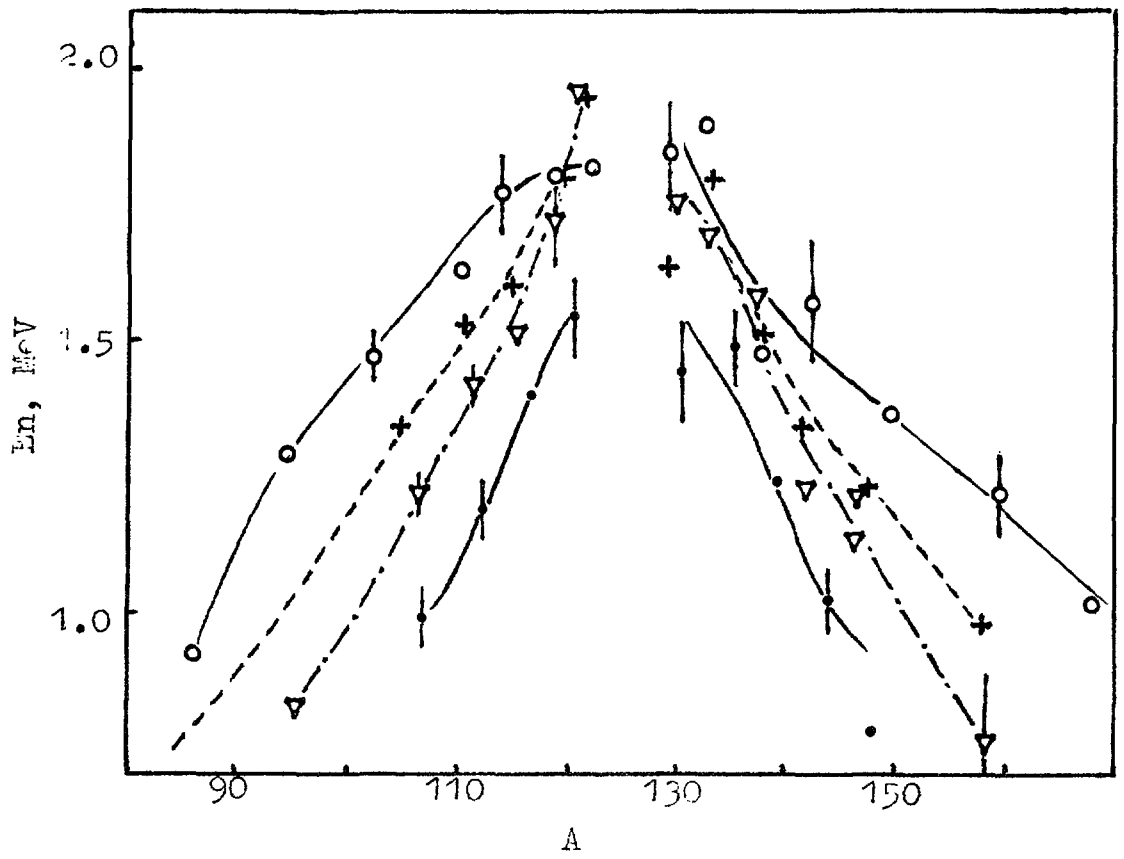

Fig. 6. Average neutron energy (E_n) in the center-of-mass system of a fragment as the function of the mass (A) for fixed intervals of EK,
○ - EK = 175±5, ✱ - EK = 186±5,
● - EK = 200±5, □ - EK = 192±5 MeV.

over all the kinetic energies, as well as analogous data from an experimental /4/ and a theoretical /21/ works. Excluding the mass region of 130, quite a satisfactory agreement with the theoretical calculation is observed.

The results of measurements of differential emission spectra of neutrons in the C. M. S. are presented in Fig. 6, where average neutron energies are shown in dependence on the mass for different total kinetic energies of the fragments. A strong variation of the average energy is observed for different E_k (respectively, different excitation energies). Especially strong variation is observed in the mass ranges 145-170 and 100-110 a.m.u. In analyzing neutron emission spectra one should know, if there is an emission of neutrons from the fragments heated up to maximum temperatures, or, as the authors of /15/ assumed, the neutrons

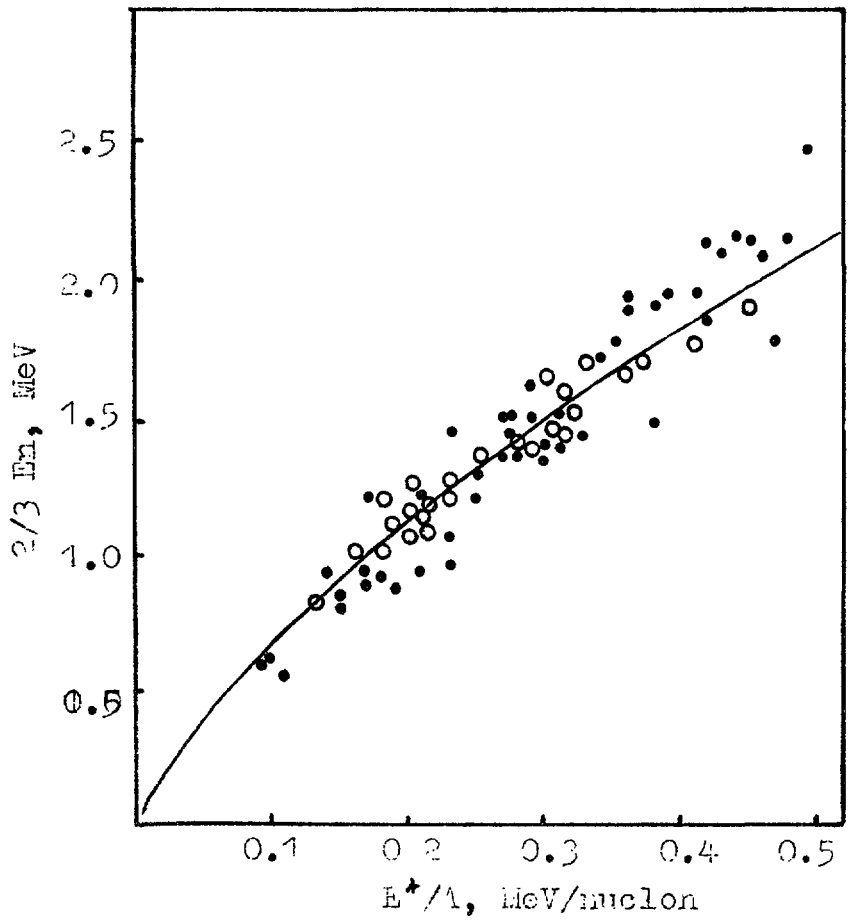

Fig. 7. Average neutron energy in dependence on the ratio of the average thermal energy of excitation E of the emitting nuclei to the mass number (A), o - the data on reactions (p,n), (n,2n), (n,n'), (α,n) from works /17-19/, —— - data systematics presented in work /16/ on reactions (HI,xn),

* - the data of this work (the average energy for A in the region of the closed shell 125-135 is excluded from the comparison).

are emitted in the process of dissipation of the collective deformation energy into thermal energy of excitation, which strongly depends on the viscosity of the fragment's nuclear matter. One of the ways to find it out is to compare the fragments' temperature at which neutron emission takes place with the temperature of the nuclei excited in different nuclear reactions at the same full excitation energies. In Fig. 7 a dependence is shown of the average energy of the neutrons from different fragments of ^{252}Cf spontaneous

fission on the excitation energy of the fragment (after emission of the first neutron). Here the data are also presented from the reactions (nn), (n2n) (pn) (αn) and from heavy-ion interactions /16-19/ for equilibrium part of the spectra. One can see that there is a satisfactory agreement in a broad energy range between two groups of data for nuclei distant from the closed shell (A = 132). Comparison of the data for these magic nuclei is hindered due to almost complete absence of information for them. The obtained agreement of the spectra's average energies points to the neutron emission's taking place after the end of the process of dissipation and accumulation by the fragment of the full internal energy of excitation. Using the said dependence E_n (A, E_k), as well as the obtained in this experiment dependence $\bar{J}$(A, E_k), the parameter of the levels' density (a) was determined by means of the thermodynamic relation for several intervals of values of the total kinetic energy of the fragments. Fig. 8 presents the dependence a/A(A). It is worth paying attention to the fact that in the region of magic nuclei A = 130-135 a low value of a/A is observed at great E_k (the excitation energy is low), and a gradual increase of a/A with a decrease of E_k (an increase of the excitation energy). This gives evidence of a gradual destruction of the shell effects and points to the magic fragment's getting a gradually increasing (and, in the end, a considerable) share of the total excitation energy possible already in the scission point. If the excitation energy in the scission point were small for A = 130-135 at all the values of E_k, no considerable variations of the value of a/A would be observed. The dependence a/A(A) at different excitation energies for fragments had not been studied before. Note, that in the mass region 95-120 and 150-170 the value of a/A for different E_k does not change within the limits of experimental errors.

In Fig. 8 there are also presented the results of calculations /20/ that take account of the contribution of vibrational and rotational excitations into the levels' density. Excluding the near-magic region, the agreement with our experimental data is good enough.

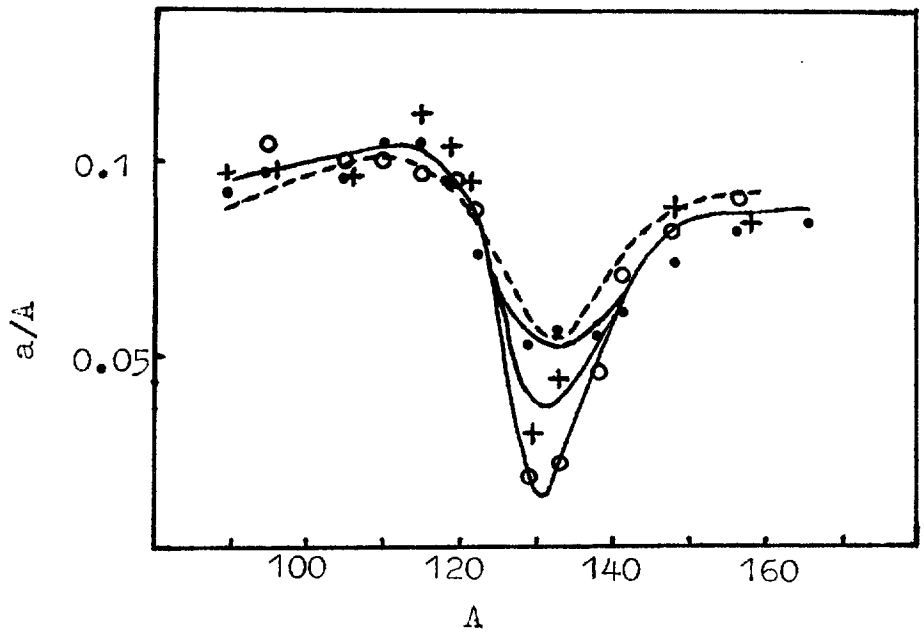

Fig. 8. The density parameter of the levels (a) as a function of the fragment's mass for definite EK,
---- - calculation of work /20/,
● - EK = 177±5 MeV, * - EK = 186±5 MeV, O - EK = = 196±5 MeV.

Processing of the experimental data continues in order to obtain new information about the fission process and the statistical properties of excited fragments.

REFERENCES

1. H. R. Bowman et al., Phys. Pew., 1962, v. 126, p. 2120.
2. V. M. Piksaikin et al., Yad. Fiz., 1977, v. 25, p. 723.
3. E. A. Seregina et al, Yad. Fiz., 1985, v. 42, p. 1337.
4. C. Budtz-Jorgensen, H. Knitter, Proc. of the XY Int. Simp. on Nucl. Phys. (Gaussig 1985), ZFK-592, 1986.
5. H. Marten et al, Proc. IAEA Cons., Meeting on the CF-252 fission neutron spectrum (Smolenice 1983), Report INDC (NDS)-146/L (1983), p. 199.
6. D. W. Lang, Nucl. Phys, 1964, 53, 113.
7. W. A. Rubchenya, B. F. Gerasimenko, Atomnaya Energia, 1985, v. 59, N 5, p. 335-339.

8. O. I; Batenkov, M. V. Blinov, V. A. Vitenko, Phis. and Chem. of Fission (Vienna, 1980), p. 267.

9. O. I. Batenkov et al, Nejtronnaya Fizika, Kiev, 1984. Part 1, p. 344.

10. O. I. Batenkov et al., Properties of neutron sources (Proc. of the Meeting, IAEA Leningrad 1986), IAEA-Tecdoc-410, p. 201 (1986).

11. Y. S. Zamjatin, D. K. Ryazanov, Yad. Fiz., 1979, v. 29, p. 595.

12. O. I. Batenkow et al, Nejtronnaya Fizika., Kiev, 1984, Part. 1, p. 339.

13. W. Mannhart, Loc. Cit. (10), p. 158-171.

14. O. I. Batenkov et al., Loc. Cit. (4), p. 25.

15. V. M. Adamov et al., Phys. Lett., 448 4, (1973), 331.

16. S. A. Karamyan, Yad. Fiz., 1984, v. 40, 2, p. 347-356.

17. O. A. Salnikov et al, Yad. Fiz., 1970, v. 12, N 6, p. 1132-1142.

18. G. N. Lovchikova et al, Yad. Fiz., 1981, v. 33, N 1, p. 41-47.

19. B. V. Zhuravlev et al, Nejtr. Fiz., Kiev, 1984, Part 3, p. 267-271.

20. A. V. Ignatyuk et al, Yad. Fiz., 1979, v. 29, p. 875.

21. B. F. Gerasimenko, V. A. Rubcheya, Loc. Cit. (10), p. 410.

22. D. J. Madland, R. J. Labauve, Report, LA-UR-84-129, 1984.

23. H. Marten, D. Richter, D. Seeliger, Loc. Cit. (4), p. 1.

WHAT CAN BE LEARNT ABOUT NEUTRON EMISSION MECHANISM IN FISSION FROM HEAVY ION INDUCED FISSION STUDIES

S.S. Kapoor
Bhabha Atomic Research Centre
Bombay 400 085.

Introduction

During the early sixties, several groups of workers (1-4) had carried out detailed investigations of prompt neutron emission in fission by studying fragment-neutron angular correlations in spontaneous fission of ^{252}Cf and in thermal fission of fissile nuclei. In these studies the comparison of the observed neutron anisotropy with that calculated for neutron emission from the fully accelerated fission fragments showed that a small fraction of about 10% neutrons is not emitted from the moving fragments. These neutrons which are not emitted from moving fragments but emitted isotropically in the laboratory system have been usually referred to in literature as scission neutrons or prescission neutrons. Three types of mechanisms of emission of these so called scission neutrons have been suggested: (i) these may be emitted during the neck snapping process, (ii) these may be evaporated from the fissioning nucleus in its descent from saddle to scission (4), as the fissioning nucleus is expected to become increasingly excited if part of the decrease in the potential energy of the system is converted into internal excitation energy, (iii) these may be emitted from the excited fragments during the acceleration period of the fragments. It is possible that all these mechanisms may be contributing to the emission of prescission neutrons to some extent. However the existence of a significant fraction of scission neutrons in low energy fission concluded in the earlier work is not yet established by further studies. Nevertheless, it is important to further investigate quantitatively the number and spectrum of these scission neutrons for two reasons: Firstly for a good theoretical description of the fission neutron spectra, the scission neutron component, if present, should not be neglected. Secondly, from the measured number of scission neutrons per fission, one may hope to learn about the strength of

energy dissipation in fission which governs the saddle to scission time and the fraction of the decrease in potential energy which gets converted into excitation energy provided mechanism (ii) is the principal source of prescission neutron emission. The second point has been investigated in detail in the recent years through the study of neutron emission in heavy-ion induced fission. In this paper, we present a review of some of the recent results on neutron emission in heay ion induced fission, with the hope that results of some of these investigations will provide important clues to the question relating to scission neutrons in low energy fission as well.

Data on neutron emission in Heavy Ion induced fission

In the recent years, fission fragment-neutron angular correlations have been measured for the case of heavy ion induced fission for a variety of target-projectile combinations and bombarding energies as given in Table I. The observed neutron spectra in coincidence with the fission fragments can be fitted to those calculated with the assumption of three possible types of neutron sources:

(i) non-equlibrium emission from a moving source

(ii) Emission from the energy equilibrated moving composite

(or compound) system and (iii) emission from the moving fragments. The information about the contribution of non-equilibrium component and also the temperature and the source velocity associated with it can be deduced from measurements of neutrons in coincidence with the evaporation residues. In most cases of medium energy heavy ion induced fission, the contributionfromnon-equilibrium neutron emission is foundto be rather small and the bulk of the neutrons are found to originate from statistical de-excitation of either the energy equilibrated compound system or the fission fragments. In this paper we shall discuss the results on evaporated neutron yields originating from cases (ii) & (iii) mentioned above.

TABLE I

Heavy Ion Induced Reactions where fragment-neutron angular correlations are measured

S.n.	Projectile-target system	Compound nucleus	E_x (Mev)	X	α	α_{BG}	Ref.
1.	207 MeV $^{16}O + ^{142}Nd$	^{158}Er	140	0.61	.797	0.770	8
2.	180 MeV $^{24}Mg + ^{134}Ba$	^{158}Er	115	0.61	.696	0.770	8
3.	180 MeV $^{32}S + ^{126}Ti$	^{158}Er	93	0.61	.595	0.770	8
4.	216 MeV $^{50}T + ^{108}Pd$	^{158}Er	72	0.61	.367	0.770	8
5.	107-121MeV $^{18}O + ^{150}Sm$	^{168}Yb	78-91	0.60	.786	0.760	6
6.	109-123MeV $^{19}F + ^{159}Tb$	^{178}W	79-90	0.64	.786	0.795	7
7.	103-133MeV $^{19}F + ^{159}Tm$	^{188}Pt	69-67	0.67	.798	0.818	7
8.	168 MeV $^{28}Si + ^{164}Er$	^{192}Pb	68	0.70	.708	0.837	6
9.	132-163MeV $^{28}Si + ^{170}Er$	^{198}Pb	52-80	0.70	.717	0.837	7
10.	94-134 MeV $^{19}F + ^{181}Ta$	^{200}Pb	54-90	0.70	.810	0.837	6
11.	158 MeV $^{30}S + ^{170}Er$	^{200}Po	70	0.70	.700	0.837	6
12.	94-123MeV $^{18}O + ^{192}OS$	^{210}Po	54-83	0.71	.829	0.843	6
13.	92-122MeV $^{16}O + ^{197}Au$	^{213}Af	48-76	0.74	.850	0.860	6
14.	103-137MeV $^{19}F + ^{232}Th$	^{251}Fy	51-85	.83	.850	0.899	6
15.	192 MeV $^{12}C + ^{175}Lu$	^{187}Iy	164	0.66	.558	0.811	13
16.	316 MeV $^{40}Ar + ^{141}Pr$	^{181}Iy	164	0.68	.784	0.825	13
17.	220 MeV $^{20}Ne + ^{165}Ho$	^{185}Ir	164	0.66	.872	0.811	12

X - Fissibility parameter

α - Mass-asymmetry in the entrance channel

α_{BG}- Mass-asymmetry of Businaro-Gallone peak calculated by the analytical expression given by A. Abe (KEK preprint 86-26, June 1986)

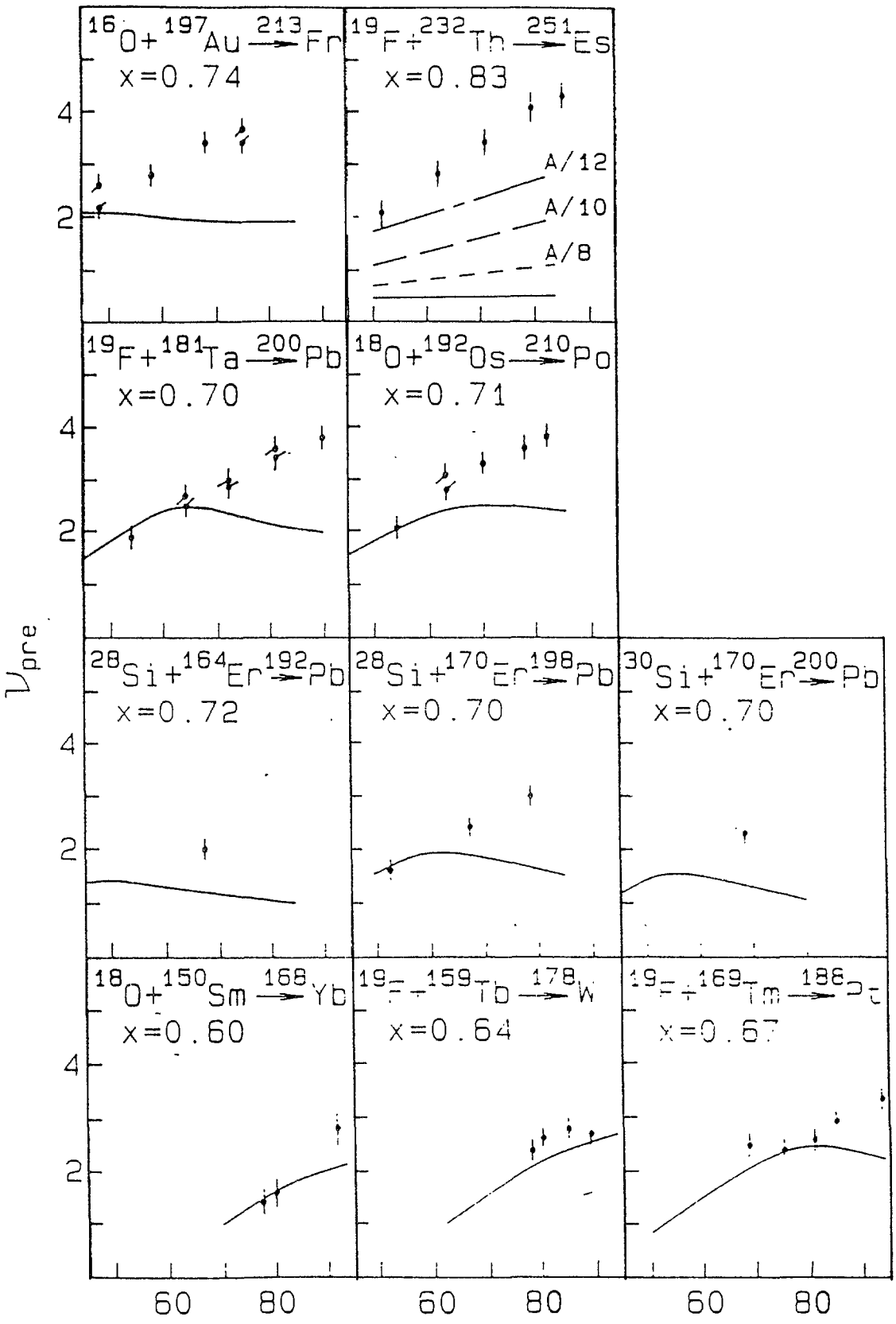

Fig.1. $\bar{\nu}_{pre}$ versus E_x for various systems deduced by Newton and coworkers (from ref.7).

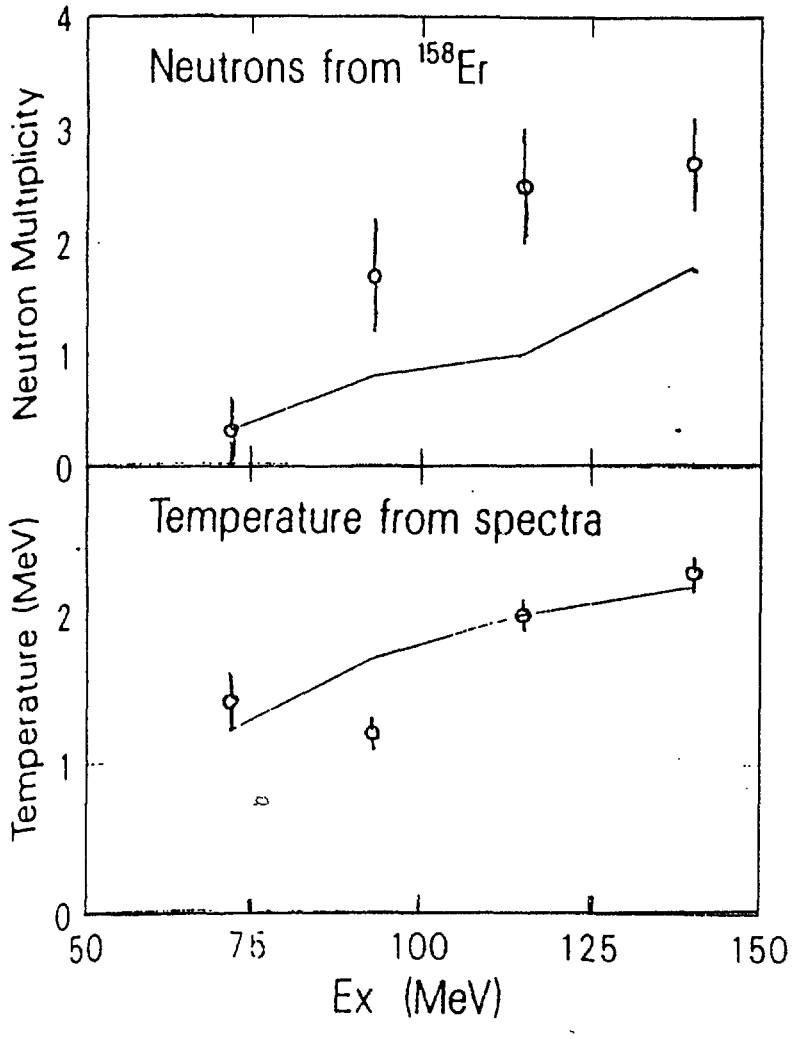

Fig.2. $\overline{\nu}_{pre}$ versus E_x for various systems leading to ^{158}Er deduced by Gavron et al (from ref.6).

Fig.1 shows the experimentally deduced values of the average number of evaporated prefission neutrons $\overline{\nu}_{pre}$ versus compound nucleus excitation energy E_x for various systems together with the results of the statistical model calculations from the recent work of Newton and coworkers (6,7). A similar comparison between the experimental and statistical model calculation values of prefission neutronsfor the case of compound system ^{158}Er formed at different excitation energies taken from the work of Gavron et al (8-10) is shown in Fig.2. Earlier similar studies at higher excitation energies have also been carried out (11,12) and these results are given in Table II. It can be seen from Figs.1 and 2 and Table II that the dominant feature of all the above studies is that the neutrons are evaporated prior to fission with multiplicities which are significantly larger than those given by the statistical model calculations. The two

TABLE II

Comparison of $\alpha\,\bar{\nu}_{pre}$(expt) with those calculated by statistical model for the cases of heavy ion reactions (data from ref.13)

S.No.	Projectile-target system	C.N	E_x (Mev)	X	$\alpha\,\bar{\nu}_{pre}$(expt)	$\bar{\nu}_{pre}$(statistical model
1	$^{141}_{59}Pr$ + 316 MeV $^{40}_{18}Ar$	$^{187}_{77}Ir$	164	Ø.558	Ø.77	3.6+Ø.6	1.1
2.	$^{175}_{71}Lu$ + 192 MeV $^{12}_{6}C$	$^{185}_{77}Ir$	164	Ø.872	Ø.77	6.3+Ø.8	4.5
3.	$^{165}_{67}HØ$ + 220 MeV $^{20}_{10}Ne$	$^{181}_{77}Ir$	164	Ø.784	Ø.77	5.6+Ø.5	1.9

crucial parameters which govern the statistical model estimates of $\bar{\nu}_{pre}$ are the fission barrier height B_f, and the ratio a_f/a_n, where a_f and a_n are the level density parameters corresponding to the saddle point configuration and the residual nucleus respectively. These two parameters also govern the fission excitation functions and cannot be treated as independent free parameters, as only those pairs of values of B_f and a_f/a_n can be allowed which simultaneously reproduce the excitation energy dependence of the fission cross-sections. With this condition imposed on the values of B_f and a_f/a_n, it has not been possible to account for the observed values of $\bar{\nu}_{pre}$ on the basis of statistical model calculations of neutron evaporation in competition with fission in the above studies. Considering that neutron evaporation during nuclear dynamics is not included in the statistical model, the above discrepency suggests that a significant number of neutrons are emitted during nuclear dynamics from the point of contact of the target-projectile to the point of acceleration of the fragments to full velocities. The different possible stages of emission of prefission neutrons are summarized in Table III.

It is difficult to disentangle the relative contributions from the various stages shown in Table III. However, since the contributions from different stages are expected to have their

TABLE III

Different possible stages of emission of equilibrium prefission neutrons

S.No.	Stage	Quantities governing neutron emission yield
1.	Formation phase spanning fusion to C.N. stage	Time of formation of C.N. governed by mass-asymmetry in the entrance channel
2.	Neutron emission in competition with fission during de-excitation of C.N.	case 1: usual statistical model ignoring dynamical effects: a_f/a_n, B case 2: Incorporation of dynamical effects, with nuclear dissipation coefficent β, which determines the strength of coupling to collective mode in fission direction, modifies Γ_f and introduces a delay time in building quasi-stationary probability flow over the fission barrier: a_f/a_n, B dissipation strength.
3.	Saddle to scission	Saddle to scission time, the additional exciation energy gained from saddle to scission and the value of a for highly deformed configurations. The first two quantities depend on strength of energy dissipation. This time increases with fissility parameter X.
4.	During scission act	
5.	Scission ot fragment acceleration time	Rate at which fragment deformation energy is converted to excitation energy and a value will determine fragment nuclear temperatures during its acceleration phase.

own characteristic systematic dependence on the parameters of the reaction, it may be possible to draw some qualitative inference about the relative contributions of each process, by suitable choice of entrance channel and compound nucleus parameters.

Neutron Emission during formation phase

Contribution to neutron emission during the compound nucleus formation phase can be inferred by analysing the results on $\overline{\nu}_{pre}$ for a given compound nucleus formed with different mass-asymmetry α in the entrance channel. The time of formation of the compound nucleus with fissibility X greater than the critical point ($X = X_{BG}$) is expected to be governed by the value of α relative to the conditional Businaro-Gallone (BG) peak (13) at the mass-asymmetry α_{BG}. In order to quantitatively relate the compound nucleus formation time with mass-asymmetry, it will be necessary to carry out dynamical calculations of the compound nucleus formation phase which take into account both the potential energy landscape and the energy dissipation. In the absence of any such detailed studies, one can only make some qualitative inferences. One would expect that the time of the compound nucleus formation phase would be larger if $\alpha < \alpha(BG)$ as compared to the case of $\alpha > \alpha(BG)$. Zank et al (12) have assumed that for the cases studied by them, formation time should increase as α decreases. Based on such qualitative comparison of the observed deviations of the prefission multiplicities with the statistical calculations for the three cases involving different mass-asymmetries (Table II), Zank et al (12) have inferred that neutron evaporation during the formation phase is not significant. Although this inference needs more justification by further experimental and theoretical work, we will assume here that the average number of neutrons evaporated during the formation phase is smaller than the observed excess number over the statistical model estimates and there is another principal source or reason for the excess neutrons.

Neutron emission during fragment acceleration

In a realistic analysis of the fission-neutron angular correlation data, one should also take into account neutron

emission from the excited fission fragments during the process of acceleration on their way to achieving final velocities. The neutrons emitted during this phase will be angularly correlated with the fragment velocity vectors on the basis of the instaneous fragment velocities and not by the final velocity of the fully accelerated fragments. This will have the effect of weakening the observed fragment-neutron angular correlations. It has been shown by Hinde et al (6) that if one assumes that the neutrons emitted during the time to reach Ø.82 of their asymptotic velocity are isotropic, and those emitted thereafter are from fully accelerated fragments, the calculated fragment-neutron anisotropy will be the same as that obtained from a more rigorous calculations based on instaneous fragment velocities during neutron emission. Hence, one can simulate the effect of the neutron emission during fragment acceleration phase by allowing in the statistical model calculation an additional component of neutrons emitted during the time the fragments take to reach about Ø.82 of their asymptotic velocity from the scission point. Their results given in Fig.3 show the contribution to neutron emission from this phase. Clearly the observed data can not be explained by the statistical model calculations, even if one takes into account neutron emission during fragment acceleration.

Neutron Emission from pre-saddle and saddle-scission phase

Mechanism of additional neutron emission over the normal statistical model values in the pre-saddle phase has been pointed out and developed by Weidenmuller and co-workers (14-18) which takes into account nuclear dissipation in the dynamics of the fission process based on the earlier work of Kramers (19). It was shown quite earlier by Kramers (19) that energy dissipation increases the fission life time over that calculated by Bohr-wheeler (2Ø) statistical model. This is due to the quasi-stationary diffusion process over the fission barrier. Weidenmuller and co-workders (14-18) have shown that when dissipation is considered, a certain transient time is needed after the formation of compound nucleus for the system to reach its final quasi-stationary values Γ_f^o of the fission width. In other words, starting from a value of zero at the instant of

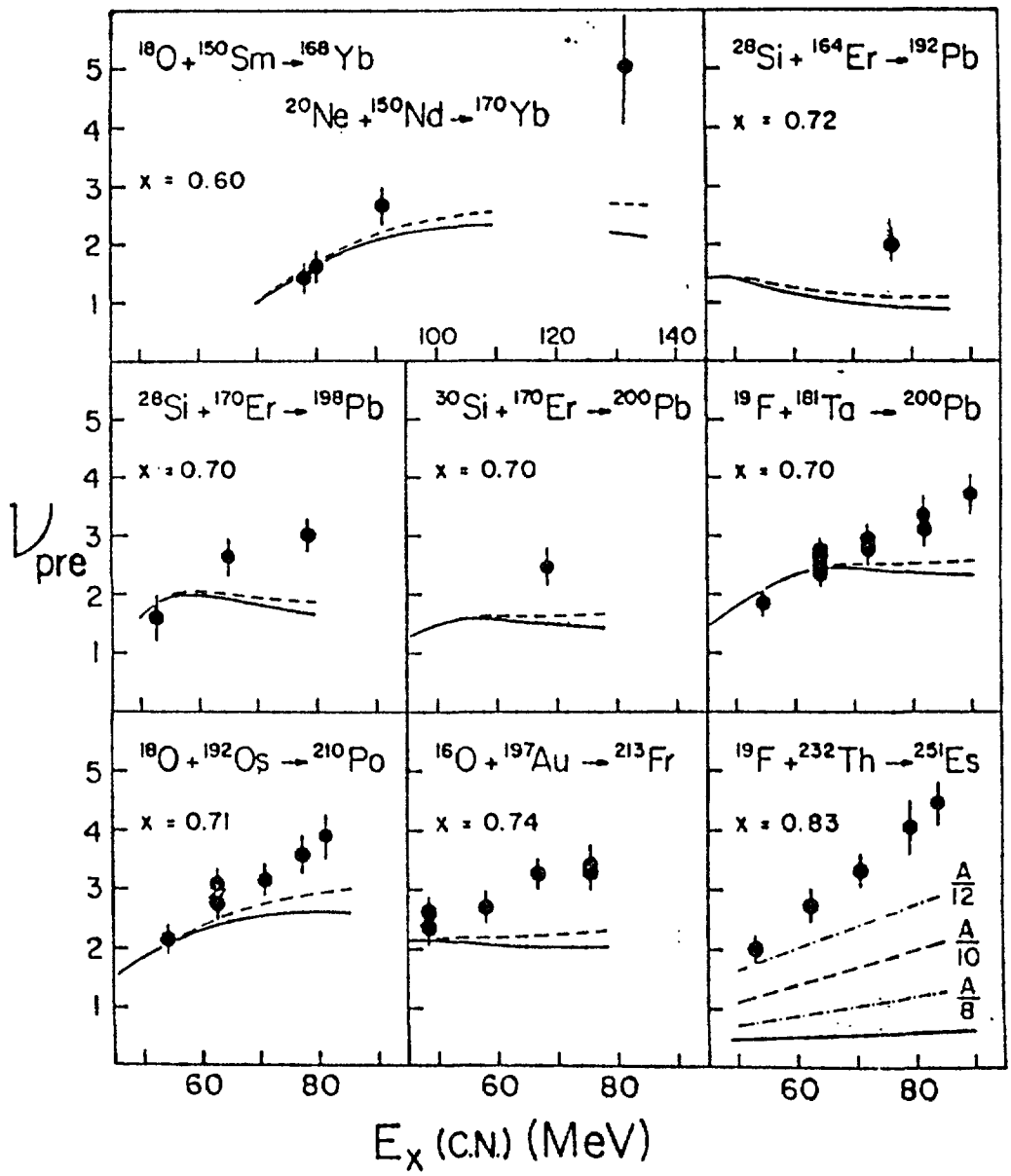

Fig.3. $\bar{\nu}_{pre}$ versus E_x for various systems. The solid curves are results of statistical calculations. The dashed curves include the effect of neutron emission during fragment acceleration.

compound nucleus formation, the fission width Γ_f grows asymptotically to its final value Γ_f^0 with a time period τ_D. One may compare this behaviour to that of charging of a condensor and write $\Gamma_f = \Gamma_f^0 (1-e^{-t/\tau_D})$. This would result in considerably enhanced neutron emission as compared to normal statistical values for the duration of time t upto τ_D. Another way to take into account this mechanism will be to introduce an effective time delay τ_D' in the onset of fission after the formation of the compound nucleus during which only neutron

evaporation can take place. (To account for a given average number of excess neutrons, the value of τ_D required will be larger than τ_D', since in the latter case fission is totally suppressed). Garange et al (18) have calculated the dependence of the transient time τ ($\tau = 3/2\ \tau_D$), where τ is time taken to reach about 90% of the final Γ_f value on the nuclear dissipation coefficient β by solving a multidimensional Fokker-Planck equation. An empirical formula for the transient time τ is given by (18) $\tau = 1.4\ \beta^{-1} \ln (10\ E_f / T) + 1.4 (\beta / T) \times 10^{-42}$ Mev. s^2)s.

For the case of compound nucleus ^{158}Fm formed with $J = 65\ \hbar$, the values of τ are in the range 3-15 x 10^{-21} s for values of β upto 5 x 10^{21} s^{-1}. Also the value of τ is minimum for $\beta \sim 10^{21}$ s^{-1} and increases for both the lower and higher values of β.

The mean time τ required to traverse the distance from the saddle point to the scission point has been calculated by Hoffman and Nix (21)

$$\tau_{ss} = \frac{2}{\omega_0}\left(\left\{1 + \left[\beta/2\omega_0\right]^2\right\}^{1/2} + \frac{\beta}{2\omega_0}\right) R\left[\left(\frac{\Delta V}{T}\right)^{1/2}\right]$$

where

$$R(z) = \int_0^z \exp(y^2)\,dy \int_0^\infty \exp(-x^2)\,dx$$

Here Δ V is the difference in potential energy between the saddle to scission points, and $\Delta\omega_0$ is the frequency of the inverse harmonic oscillator potential that osculates the fission barrier at the saddle point. For ^{158}Fm nucleus the mean saddle to scission times were also calculated and were found to be about (1-5) x 10^{-21} s for the values of β upto 6 x10^{21} s^{-1}.

Gavron et al (8) have also carried out a detailed analysis to deduce the values of β from the measured prefission neutron multiplicities for the four systems (Table I) leading to the compound nucleus ^{158}Fm. As an example of their analysis, we show in Fig. 4 their results for one of the systems $^{24}Mg + ^{134}Ba$. From the results shown in this figure and from similar comparisons made for other systems, Gavron et al (8) infer a value of $\beta \sim 6 \times 10^{-21}$ s for the ^{158}Fm system assuming that β is temperature independent. For this value of β, the

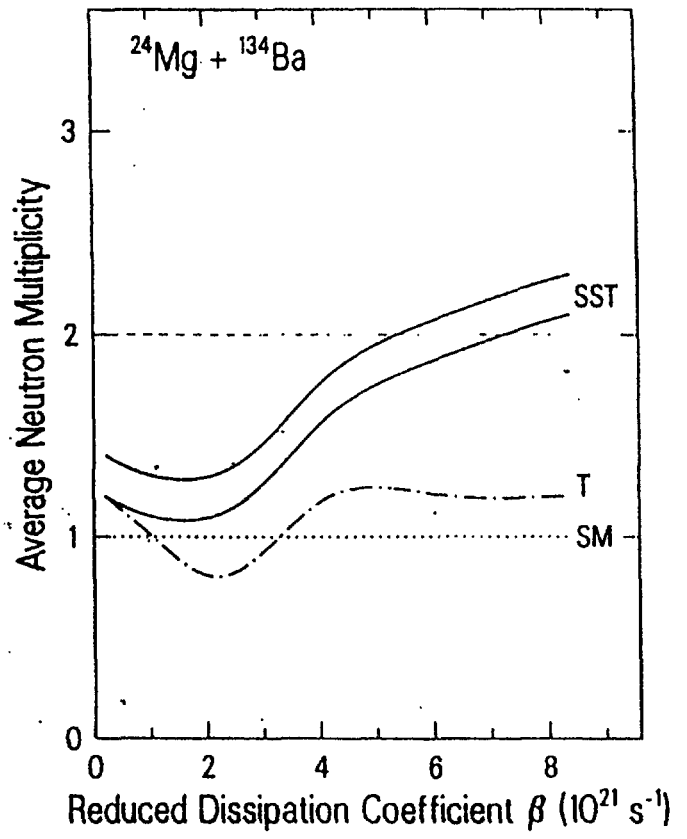

Fig. 4. Comparison of experimental results to model calculations (from ref.8) for the system $^{24}Mg + ^{134}Ba$.

calculated values of average transient time is 10^{-20} s and saddle-to-scission time is 5×10^{-21} s for the ^{158}Er compound nucleus. With the increase in the fissility and therefore mass number A of the fissioning nucleus, the value of γ_{ss} is expected to increase because the difference in the saddle shape and scission shape and therefore ΔV increases with A. Fig.6 taken from ref.7 shows the calculated saddle to scission times for the cases of one-body and two-body dissipation mechanism. The above deduced saddle-to-scission time of 5×10^{-21} s for ^{158}Er (X = 0.61) is consistent with the prediction of the dynamical calculations of Carjan et al (22) for the case of one-body dissipation. The calculated values for the two-body viscosity with η = 0.02 TP which was deduced by Davies et al (23) by fitting the fragment kinetic energy data predict much lower values of γ_{ss} as compared to the above deduced value. The results of Gavron et al (8) therefore point out that motion from saddle to scission is highly overdamped as predicted by the one-body dissipation mechanism.

Hinde et al (6) have reached somewhat similar conclusions based on the analysis of their data for several systems. They could obtain satisfactory fits to their results on ν_{pre} with E_x by allowing for a finite transient time τ_D alone, or by allowing for a finite saddle-to-scission time alone or by a combination of the above two. As expected, the values of τ_D, and τ_{SS} needed to fit the data depend on the value of the level density parameter a_n used. With the level density parameter given by $a_n = A/10$, their values of τ_D and τ_{SS} needed to fit the data are as follows:

(i) $\tau_D = 70 \times 10^{-21}$ s , $\tau_{SS} = 0$ or

(ii) $\tau_D = 0$, $\tau_{SS} = 30 \times 10^{-21}$ s or

(iii) $\tau_D = \tau_{SS} \simeq 20 \times 10^{-21}$ s

Figs. 6 and 7 taken from ref.6 show fits to the data for the case (i) and (ii) Similar fits have also been obtained under assumption (iii).

Of the above three cases, case (i) is unrealistic, since strong dissipation giving a large value of τ_D must also lead to large value of τ_{SS}. The individual values of τ_D and τ_{SS} for a fixed additional time for neutron emission are also expected to be dependent on mass number A, and case (iii) is also an approximation. The value of τ_{SS} deduced for case (ii) is a good measure of the lower limit on the total additional time ($\tau_F + \tau_D + \tau_{SS}$) taken by the nucleus from the point of contact to the point of scission which is available for neutron ν emission. There is a good possibility that the time periods τ_F & τ are not sequential but are concurrent as Γ_f may attain a finite value during the equilibration process of the compound nucleus in its formation phase. The value of τ_F is expected to be in the range of 10^{-21} s - 10^{-20} s depending on the entrance channel mass-asymmetry. Further allowing for the value of τ , one may conclude that the data suggests saddle-to-scission times of about 2-3 x 10^{-20} s for nuclei with X $\simeq$ 0.6-0.7. Comparison of this result with the calculated values shown in Fig.5 again points that the saddle-to-

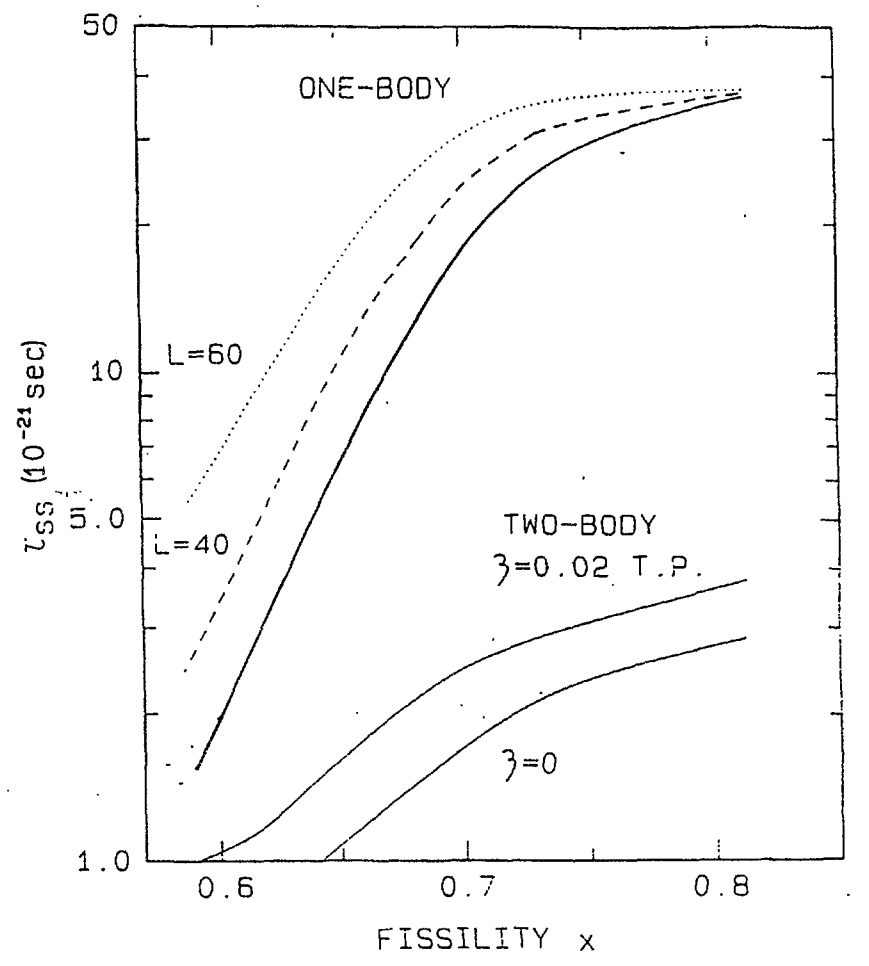

Fig. 5. τ_{ss} time versus Fissility based on calculations (from ref.7).

scission motion is highly dissipative, and the estimated values of τ_{ss} point to one-body dissipation mechanism.

Similar comparisons between the experimental prescission neutron multiplicities and statistical model calculations were carried out by Zank et al (12) for the heavy ion reactions studied by them. In their analysis, the time available from saddle-to-scission is considered as the source of excess neutrons (equivalent to case (ii) of Hinde et al (6)); and this time was calculated as a function of two-body viscosity parameters in the macroscopic model of Davies et al (23). An agreement with the experimental value of $\bar{\nu}_{pre}$ could be achieved only for very large values of the viscosity parameter η = Ø.1 - Ø.15 TP. For the three reactions Pr + Ar, Ho + Ne and Lu + C, they have estimated mean saddle-to-scission times to be very large: about 2.3, 11 and 5 x 10^{-20} s however with large error bars.

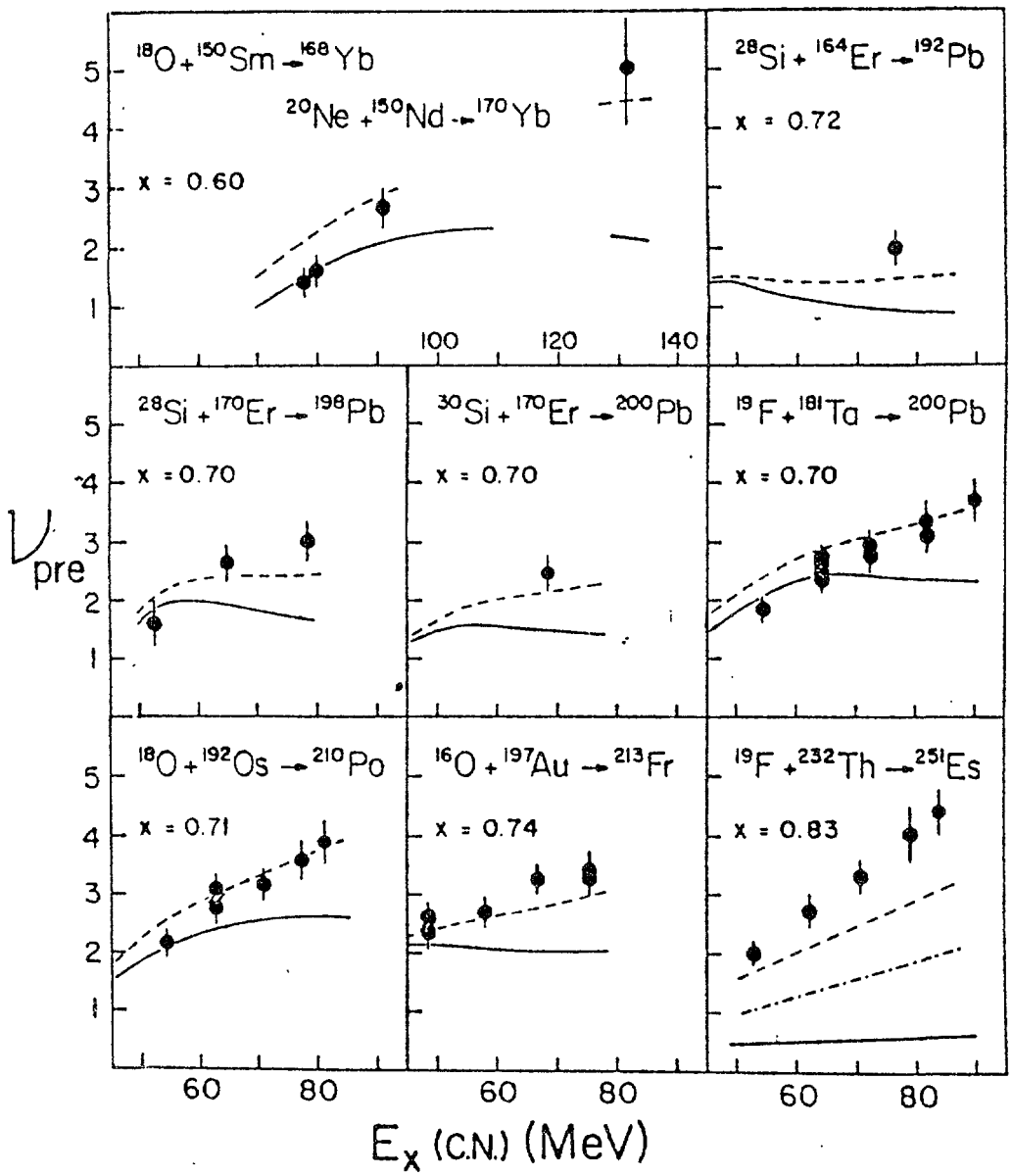

Fig.6. Comparison of $\overline{\nu}_{pre}$ (experimental) with calculated values allowing for neutron evaporation during saddle-to-scission timeof3Ø x1Ø$^{-21}$s (from ref.6) (a_n =A/1Ø).

Main Conclusion

Thus, the various studies of the neutron emission in heavy ion induced fission discussed above lead to the same conclusion that the fission dynamics and in particular the motion from saddle to scission is highly dissipative. If this large strength of energy dissipation was to be accounted by a pure two-body viscosity coefficient η , one would require values of η which are order of magnitude larger than the value of η determined by Davies et al (23) from the analysis of fragment kinetic

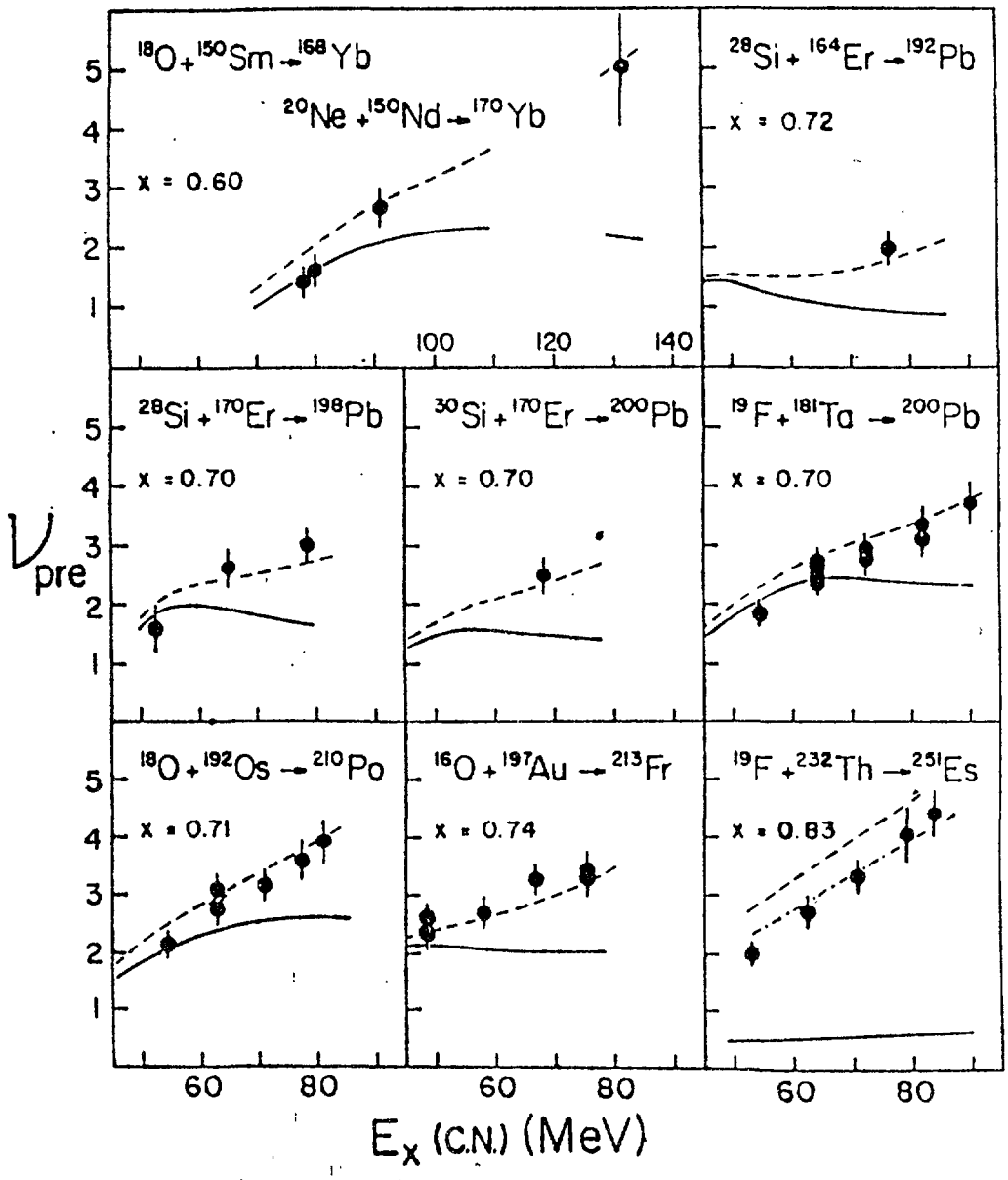

Fig. 7 Same as Fig.3, but allowing a fission delay time of 70×10^{-21} s (from ref.6).

energies. However, the one body dissipation mechanism can account for the large values of the deduced energy dissipation strength. In fact a mixture of relatively small two-body viscosity and a large one-body friction seem to be operative throughout the fission dynamics.

Outlook for low energy fission

The kinetic energy of the nascent fragments at the moment of scission depends on the potential energy difference Δ V between the saddle and scission point and the strength of energy

dissipation. If the strength of energy dissipation is η , the scission point kinetic energy $\bar{E}_{ss}$ has been derived (21) to be

$$\bar{E}_{ss} = T\left[1 + \gamma\left\{\left[1+\gamma^2\right] - \gamma\right\}\right] + \Delta V\left[(1+\gamma^2)^{1/2} - \gamma\right]^{1/2}$$

where $\gamma = \beta/2\omega_0$ where ω_0 is the barrier frequency, and T is the temperature at the scission point. For β = 6 x 10^{21} s^{-1} and ω_0 = 2 x 10^{21} s^{-1} for saddle-to-scission calculation, $\gamma \sim$ 1.5 and $\bar{E}_{ss} \simeq$ Ø.Ø9 Δ V + 1.45 T. Thus for the values of $\beta \sim$ 6 x 10^{21} s^{-1} inferred from the analysis of heavy ion reaction data, one expects that only about 1Ø% of the potential energy drop Δ V would appear as pre-scission excitation energy. The calculation of Δ V is again quite model dependent. According to calculations of Sierk and Nix (24), the values of Δ V are

Δ V $\sim$ 35 Mev for ^{236}U

$\sim$ 5Ø Mev for ^{252}Cf.

One may thus assume that the values of excitation energy plus deformation energy at scission in the low energy fission of ^{236}U and ^{252}Cf are about 32 Mev and 45 Mev respectively. The average temperature at the scission point will depend on the division of this energy into excitation and deformation energies and on the level density parameter a_n applicable to highly deformed saddle-to-scission shapes. To make an estimate of the average number of neutrons which may be emitted from saddle-to-scission transition in the case of spontaneous fission of ^{252}Cf we have calculated this number with the following assumptions (i) excitation energy increases linearly with time during descent to the scission point, (ii) a = A/1Ø . Fig.8 shows the calculated number of neutrons evaporated during descent to the scission point for different excitation energies at the scission point and for various saddle-to-scission times. Thus if the excitation energies at scission are $\sim$ 25-3Ø MeV and saddle-to-scission times are long (> 4 x 10^{-20} s), as can be expected for a highly dissipative motion, a non-negligible number of neutrons can be emitted during this phase. In fact evaporation of the neutrons during the highly dissipative descent of the fissioning nucleus

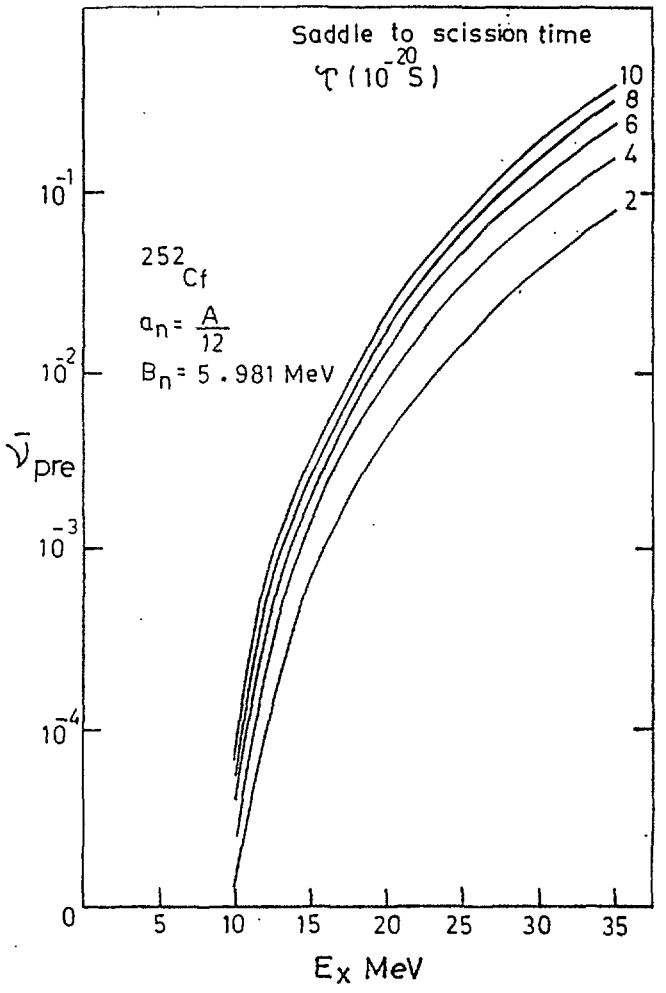

Fig.8. Calculated yield during descent to scission for ^{252}Cf.

from saddle-to-scission, together with neutron evaporation during the fragment acceleration phase is not expected to be a negligible fraction of the total neutron yield in low energy fission. However, this fraction needs to be quantitatively estimated more accurately by further experimental and theoretical work and should be taken into consideration for a good theoretical description of the standard fission neutron spectrum for the case of ^{252}Cf fission.

Stimulating discussions with my colleagues Drs. V.S. Ramamurthy, R.K. Choudhury and A. Chatterjee while working on this paper are gratefully acknowledged.

References

1. H.R. Bowman, et al, Phys. Rev. 126 2120 (1962).

2. K. Skarsvag and K. Bergheim, Nucl. Phys. 45 72, (1963).

3. S.S. Kapoor, R. Ramanna, P.N. Rama Rao, Phys. Rev. 131 283 (1963).

4. For further references, see review article - J.S. Fraser and J.C.D. Milton, Am. Rev. Nucl. Sci. 16 379 (1966).

5. K. Skarsvag, Physica Scripta 7 160 (1973).

6. D.J. Hinde, et al., Nucl. Phys. A452 550 (1986); D.J. Hinde et al., Phys. Rev. Lett. 52, 986 (1984).

7. J.O. Newton et al., Preprint of paper submitted to Nucl. Phys. A, (1987).

8. A. Gavron et al., Phys. Rev. C35, 579 (1987).

9. A. Gavron, et al., Phys. Rev. Lett. 47, 1255 (1981); 48, 835 (E) (1982).

10. A. Gavron et al., Phys. Lett. 176B, 312 (1986)

11. E. Holub et al., Phys. Rev. C28, 252 (1983).

12. W.P. Zank et al., Phys. Rev. C33, 519 (1986).

13. U.L. Businaro and s. Gallone, Nouvo Cimento 629, 1277 (1955); Nouvo Cimento 5, 315 (1957).

14. P. Grange, J.Q. Li and H.A. Weidenmuller, Phys. Lett. 96B, 26 (1980).

15. P. Grange, J.Q. Li and H.A. Weidenmuller, Phys. Rev. C27, 2063 (1983).

16. H.A. Weidenmuller and J.S. Zhang, Phys. Rev. C29, 879 (1984).

17. S. Hassani and P. Grange, Phys. Lett. 137B, 281 (1984).

18. P. Grange et al., Phys. Rev. C34, 2Ø9 (1986).

19. H.A. Kramers, Physica (The Hague) 7, 284 (194Ø).

2Ø. N. Bohr and J.A. Wheeler, Phys. Rev. 56, 426 (1939).

21. H. Hoffman and J.R. Nix, Phys. Lett. 122B, 117 (1983).

22. N. Carjan et al., Nucl. Phys. A452, 381 (1986).

23. K.T.R. Davies et al., Phys. Rev. C13, 2385 (1976).

24. A.J. Sierk and J.R. Nix, Phys. Rev. C21, 982 (198Ø).

Prescission Neutron Emission in thermal neutron fission of ^{235}U

R.K. Choudhury and S.S. Kapoor
Nuclear Physics Division, B.A.R.C., Bombay 400 085

Neutron emission in low energy fission mostly takes place due to evaporation from fully accelerated excited fission fragments. However, on the basis of energy and angular correlations it was concluded in earlier studies that a certain fraction of neutrons of about 10-30% appears to be emitted isotopically in the compound nuclear c.m. frame. This component termed as scission or prescission component ν_{pre}, was reported by Bowman et al[1] in ^{252}Cf fission and by Kapoor et al[2] in thermal neutron induced fission of ^{235}U. Since then, there have been a number of other experiments[3-6] where this fraction has been measured as a function of total kinetic energy of the fragments. Since the total kinetic energy is anticorrelated with the excitation energy of the fragments, measurement of the correlation of ν_{pre} with kinetic energy may throw much light on the emission mechanism of prescission neutrons. As summarised earlier by Märten et al[7], the analysis of various experimental data showed conflicting results on the dependence of ν_{pre} on the total kinetic energy, E_k for the case of ^{252}Cf fission.

We had earlier reported[8] an analysis of prompt neutron anisotropics in thermal neutron fission of ^{235}U as a function of total kinetic energy, E_k of fission fragments. The calculation was prompted by the experimental data of Blinov et al[3], which indicates that the anisotropy initially increases and then saturates at higher total kinetic energies

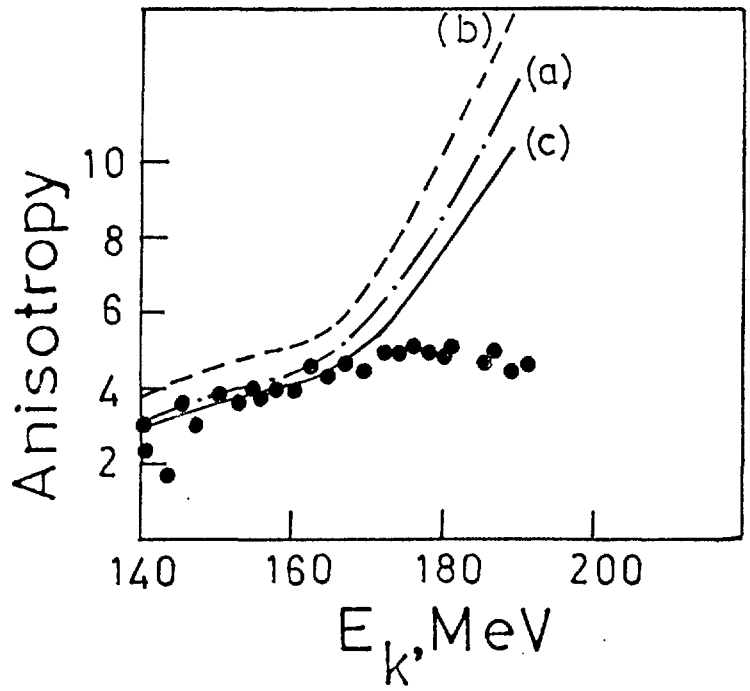

Fig.1. Variation of neutron anisotropy with respect to light fragment direction with total kinetic energy. Experimental results ..., (a) calculation without temperature distribution of fragment for a = A/8, (b) and (c) calculation with temperature distribution for a = A/8 and a = A/12 respectively.

as shown in fig.1. Our calculation based on the assumption that neutron emission takes place solely from fully accelerated fragments, indicated that the anisotropy should increase monotonously with the total kinetic energy. From the comparison of the calculated and experimental anisotropies, the fraction of prescission neutrons as a function of E_k could be deduced for an assumed neutron emission spectrum. It was seen that this fraction increases with E_k, leading to approximately constant value for ν_{pre} of 0.3 neutrons for all E_k values.

The calculation took into account the mass distribution for each E_k value, but the temperature of the fragment was

fixed at the value $T = \sqrt{E_{exc}/a}$, where $E_{exc} = Q - E_k$ and 'a' was the level density parameter given by $a = A/8$. Since during neutron emission, the temperature is gradually reduced, one needs to take a temperature distribution for the fission fragments. Here we show the effect of assuming a temperature distribution for the fragments, on the anisotropy of neutrons as a function of E_k. A linear temperature distribution was assumed for the deexciting fission fragment[2] having a maximum temperature $T_m = \frac{3}{2}\bar{T}$, where $\bar{T}$ is calculated as above from the excitation energy. The present calculation is in the same line as that reported in Ref.8 but for the assumption on the temperature distribution. Fig.1 shows the results of the present calculations along with the experimental data of Blinov et al. It is seen that the calculated anisotropy values are increased if fragments are given a linear temperature distribution as compared to the values for constant temperature. In order to obtain agreement for lower E_k values, the level density parameter is required to be $a = A/12$, instead of $a = A/8$, required without assuming a distribution in temperature, as shown in fig.1.

This result is significant, since it indicates that higher level density of the fragments is required to fit the anisotropy data. At the same time, it is also clear that at high E_k values, the observed anisotropy values cannot be explained by assuming neutron emission from fully accelerated fission fragments alone. The flattening of the anisotropy at high E_k values can be obtained on the basis of a prescission neutron component as explained in Ref.8. Further experimental studies on the neutron anisotropy for specific fragment mass

and total kinetic energies are needed to make better estimates of this pre-scission neutron component, to learn about the neutron emission mechanism in the early stages of the fission process.

THEORY OF PROMPT FISSION NEUTRON EMISSION

H. Märten, A. Ruben, and D. Seeliger
Technische Universität Dresden, GDR

Abstract: Basic requirements to be met for the physically consistent calculation of energy and angular distributions of prompt fission neutrons are summarized. Main emphasis is pointed to an adequate statistical-model approach (SMA) to cascade neutron evaporation from a fragment diversity specified by the occurrence probability $P(\{p_f\})$ as function of a fragment parameter set $\{p_f\}$ ("internal" consistency) as well as to the SMA application to any fission reaction depending on the $P(\{p_f\})$-description as function of the fissioning-nucleus parameters $\{p_{FN}\}$ ("external" consistency).

1. Introduction

A large number of microscopic measurements has shown that the energy spectrum of prompt fission neutrons (PFN) is an evaporation-like distribution phenomenologically described by either a Maxwellian or a Watt spectrum. Most of the observations are consistent with the theoretical concept of neutron emission from highly excited and rapidly moving fragments. However, PFN emission has to be understood as a superposition of different components corresponding to specific mechanisms.[1] In addition to the main one (i.e. cascade evaporation from fully accelerated fragments), the so-called "scission neutron" emission due to rapid nuclear-potential changes close to scission, the neutron emission during fragment acceleration (probably including non-equilibrium effects), and neutron emission from n-unstable light charged particles (^{5}He, ^{6}He*, etc.) after ternary fission can be assumed. The possible role of these secondary mechanisms has been discussed in Refs. 1,2. Several characteristics of secondary neutrons (mostly considered as a central component in the lab. frame of fissioning nucleus) have been derived from experimental PFN data (in particular, the dependence of the emission probability distribution on neutron emission angle) in comparison with statistical-model approaches to the predominant evaporation component. It has been emphasized in Ref. 1 that most of the

contradictions of informations deduced are due to rough ansatzes for the description of PFN spectra in the centre-of-mass system (CMS) of fragments and the neglection of the intricate fragment occurrence probability $P(\langle p_f \rangle)$, i.e. average fragment parameters are used. Furthermore, the CMS spectra have been often adjusted on the basis of the experimental distributions themselves. Several questions appear:

(i) What are the requirements to be met in adequate calculations of PFN characteristics?

(ii) What role do secondary mechanisms play?

(iii) Is their consideration necessary for practical SMA applications to PFN emission at all?

(iv) How can the distribution $P(\langle p_f \rangle)$ be predicted, in particular in the case of induced fission reactions as function of incidence energy?

The questions stated above concern basic problems of PFN and fission theory as well as their practical application.

2. "Internal" consistency of PFN theory

Several attempts have been made to describe PFN energy and angular distributions assuming that all prompt neutrons are evaporated from fully accelerated fragments (SMA).[3-7] These approaches can be classified according to

(i) the ansatz of an evaporation spectrum as function of $\langle p_f \rangle$ (either Hauser-Feshbach or Weisskopf-Ewing or approximative),

(ii) the complexity of $P(\langle p_f \rangle)$ considered.

The physical constraints of a pure SMA have been emphasized in a recent review paper[8]. The importance of the consideration of a complex $P(\langle p_f \rangle)$ distribution for the precise description of PFN emission distributions has been studied in the framework of the cascade evaporation model (CEM)[7,9] indicating certain deviations if neglecting special features of PFN emission. However, the applicability of a SMA is restricted in most cases due to the lack of knowledge of the $P(\langle p_f \rangle)$ distribution. Provided that $P(\langle p_f \rangle)$ is known accurately, the agreement of SMA calculations with experimental data (energy and angular distributions, in particular as function of certain $\langle p_f \rangle$ variables) is a measure of the "internal" physical consistency of the SMA. It should be assumed that any deviations are due to

(i) the influence of secondary-neutron emission as discussed above,

(ii) the non-adequate SMA ansatz (e.g. neglection of PFN characteristics),

(iii) experimental errors (!).

In the case of ^{252}Cf spontaneous fission , $P(\langle p_f \rangle)$ can be deduced from experimental data on neutron and γ-ray emission as function of fragment variables (mass number A, charge number Z, total kinetic energy TKE, excitation energy E^*, angular momentum I) with reliable precision.[7] The CEM considering the whole dependence of PFN emission on A, TKE, and E^*, e.g. $\langle p_f \rangle = \langle A, TKE, E^* \rangle$, as well as on averages $\bar{Z}(A)$ and $\bar{I}(A)$, has recently been used to describe new experimental data[10] on energy and angular distributiopns $N(E,\theta)$ of $^{252}Cf(sf)$ PFN. In particular, the center-of-mass system anisotropy of neutron emission (due to fragment angular momentum) and neutron/γ-competition of de-excitation have been considered.[11] As shown in Appendix A, the parameter-free CEM reproduces the measured data within the experimental as well as theoretical uncertainties. No significant indications of secondary neutrons have been found. The upper limit of their relative yield was estimated to be < 5%. At present, the CEM can obviously be assumed as a "internally" consistent SMA to describe the whole distribution $N(E,\theta)$. In particular, the crucial polar regions at E close to the average fragment kinetic energy per nucleon E_f, i.e. at low center-of-mass frame energy of emitted neutrons, have satisfactorily been reproduced due to the consideration of neutron/γ-competition and reliable choice of the global optical potential.[8,11] Concerning the analysis of $N(E,\theta:\langle p_f \rangle)$ data, a more detailed investigation should provide further informations on PFN emission. The new experimental data obtained by Knitter and Butz-Jorgensen[12], i.e. $N(E,\theta:A,TKE)$, are a comprehensive base for further studies.

The Madland-Nix model (MNM)[5] has widely been used for the description of PFN spectra N(E). It incorporates an approximative spectrum ansatz. Furthermore, the calculations are performed for average fragment parameters $\bar{p}_f$ of both groups in binary fission reactions. The consideration of the spectrum dependence on A has been introduced in the generalized MNM (GMNM)[13], i.e. $\langle p_f \rangle = \langle E^*, A \rangle$, $\overline{TKE}(A_1/A_2)$, $\bar{E}^*(A)$, $\bar{Z}(A)$, $\bar{I}_{total}$. However, some refinements

had to be taken into account to obtain a consistent description of N(E,θ) for any fission reaction, namely the consideration of n/γ-competition (simulated by a low limit T_o of rest-nucleus temperature) as well as semi-empirical level density parametr a(A) instead of the Fermi-gas model approach a∝A.[8,11] Including these modifications, the GMNM provides the basis for a reliable prediction of PFN energy and angular distributions. The a(A) scaling factor considered as well as the limit T_o are handled as model parameters defining the spectrum hardness and the shape of angular distribution at E close to E_f, respectively. Both parameters have been adjusted on the basis of ^{252}Cf(sf) data. They are not changed in case of GMNM applications to any fission reaction. Both the CEM and the GMNM are suitable to describe N(E,θ) for ^{252}Cf(sf) with adequate accuracy, i.e. within experimental as well as theoretical uncertainties (internal consistency). However, their application to any fission reaction requires the knowledge of the relevant P({p_f}) distribution. A reliable prediction of P({p_f}), i.e. the precondition of the "external" consistency of PFN theory, is only possible for applications of the more simple GMNM. In the case of CEM, it can be derived neither from fission theory nor from experimental data with sufficient accuracy and/or completeness. Hence, we'll focus on GMNM discussing possibilities of P({p_f})-prediction for any fission reaction.

3. Prediction of fragment distribution for complex SMA applications

As outlined above, the application of a complex SMA requires the knowledge of P({p_f}:{p_{FN}}), where {p_{FN}} denotes a parameter set of the fissioning nucleus as mass and charge number, excitation energy, angular momentum, etc. Since basic fission theories fail to reproduce this occurence probability with adequate accuracy, the GMNM has been combined with semi-empirical fission theories providing P(A,$\overline{E^*}$(A),$\overline{TKE}$(A_1/A_2) : A_{FN},Z_{FN},E^*_{FN}) for actinide fission (Th - Cf) at E^*_{FN} below about 25 MeV:

(i) two-spheroid model (TSM)[14], i.e. a scission point model including semi-empirical, temperature-dependent shell correction energies, for the prediction of $\overline{E^*}$(A) and $\overline{TKE}$(A_1/A_2) (energy partition as function of mass asymmetry),

(ii) 5-Gaussian approach[15] (justified theoretically[16] as well as experimentally[17]) for the prediction of P(A : A_{FN}, Z_{FN}, E^*_{FN}) (mass yield curve).

In addition, the angular distribution of fragments with reference to incident-beam direction, W(β), which causes a PFN anisotropy with reference to incident-beam direction, is approximated by a

(iii) statistical-model description[18] of W(β : A_{FN}, Z_{FN}, E^*_{FN}) based on the distribution in angular-momentum projection (K) depending on fissioning-nucleus temperature (calculations based on an adjustment to experimental data).

In the case of multiple-chance fission reactions, e.g. (n,xnf) reactions, the fragment occurence probability is predicted for each chance separately. Consequently, the GMNM can be applied to each chance. In our first applications, this has been done for average $\bar{E}^*_{FN}$ for x>0. The weight of each chance, i.e. the partial fission cross sections $\sigma_{f,x}$, as well as the spectra of pre-fission neutrons are calculated within the Hauser-Feshbach model including fission channel (code STAPRE)[19]. In summary, the following scheme should be realized:

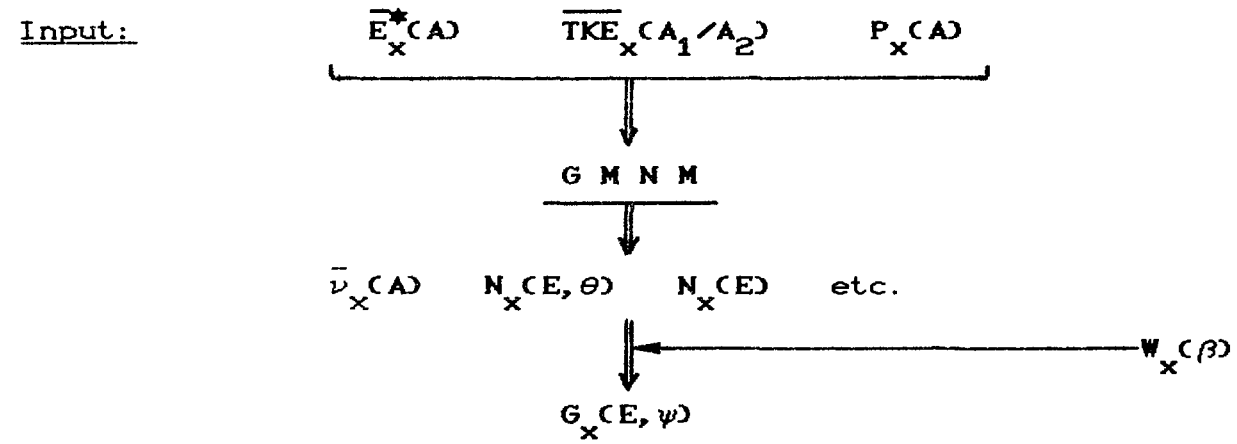

(emission probability with reference to incident particle direction)

Results: Total average number of fission neutrons (including pre-fission and post-fission neutrons):

$$\bar{\nu}_{tot} = \sum_x \frac{\sigma_{f,x}}{\sigma_{f,tot}} (\bar{\nu}_x + x)$$

Cross section of post-fission neutron emission:

$$\sigma(E,\psi) = \sum_x \sigma_{f,x} \bar{\nu}_x G_x(E,\psi)$$

etc.

(For some applications, see Appendix B as well as Refs. 20,21).

The semi-empirical fission theories mentioned above reproduce the following remarkable trends in the dependence of fragment variables on E^*_{FN}:

(i) Due to the diminution of shell effects with increasing scission point temperature (which increases as E^*_{FN} increases), $\bar{E}^*(A)$ and ,consequently, $\bar{\nu}(A)$ changes in a definite manner: The strong saw-tooth behaviour becomes less pronounced with increasing E^*_{FN}. $\bar{E}^*(A)$ shows the strongest rise at A around 132 (double-magic fragment) as a consequence of the diminished stiffness. The TSM reproduces the the energy partition results as measured (cf. Refs. 22,23).[24]

(ii) Position, width, and weight of the 5 Gaussians describing the mass yield curves (two asymmetric "standard" fission paths, one symmetric fission path[16]) have been adjusted on the basis of experimental data as in Ref. 19. The higher E^*_{FN},

- the higher the weight of the symmetric mode,
- the higher the widths.

The relative weights of both asymmetric modes depend on E^*_{FN}. Whereas $\bar{A}_H$ (mass number of the heavy-fragment group) is almost independent on A_{FN} at very low E^*_{FN}, it is remarkably dependent on E^*_{FN} itself.

(iii) The fragment anisotropy decreases with increasing E^*_{FN} (except threshold region where special fission channels are important).

It should be emphasized that experimental fragment occurence probabilities are commonly used for the calculations if they are known with sufficient accuracy. This is necessary in the case of threshold fission specifically. Here, channel effects are considerable. So far, they are not included in the semi-empirical fission theories.

The reliable description of $P(\{p_f\}:\{p_{FN}\})$ is of high importance to predict PFN data for any induced fission reaction ("external" consistency of PFN theory). Some results are shown in Appendix B. So, it becomes possible to study $\bar{\nu}(E^*_{FN})$, $\bar{E}(E^*_{FN})$, and, in particular, the correlation function $E(\bar{\nu})$ (cf. Ref. 25).

As shown in the Appendixes A and B, the shape of PFN spectra is

neither Maxwellian nor Watt type. Whereas $\bar{E}$ increases as E^*_{FN} increases, the shape of the PFN spectrum with reference to Maxwellians corresponding to given $\bar{E}$ is little changed. However, this result is a pure theoretical one. So far, the accuracy of measured PFN spectra is not sufficient to confirm this behaviour found for pure (n,f)-reactions. In the case of multiple-chance fission, remarkable deviations from the approximatively linear increase of $\bar{E}$ and $\bar{\nu}$ with increasing incidence energy appear at higher-order thresholds ($x \geq 1$).[20,25] This is due to the diminished E^*_{FN} for $x \geq 1$ as a consequence of pre-fission neutron emission.

4. Conclusions

(i) PFN energy and angular distributions $N(E,\theta)$ can be well described by a complex SMA based on the assumption that all neutrons are evaporated from fully accelerated fragments characterized by an intricate occurence probability $P(\{p_f\})$ (CEM without free parameter, GMNM based on parameters adjusted for $^{252}Cf(sf)$).

(ii) However, such a SMA should probably simulate emission probability distributions of secondary neutrons (scission neutrons, neutrons emitted during fragment acceleration) to a certain extent. In contrast to previous assumptions (central component[26]), recent theoretical works[27,28] indicate that scission neutrons are preferentially emitted in polar direction. Further, the neutron component during fragment acceleration is strongly influenced by dissipation mechanism (relaxation)[2].

(iii) The TUD concept for calculations of PFN spectra, angular distributions, and multiplicities in any fission reactions relies on a combination of GMNM with semi-empirical fission theories, since basic fission theories fail to reproduce the fragment occurence probability in a complete and sufficiently accurate manner. In spite of this alternative compromise, PFN data are well described/predicted. Especially, multiple-chance fission reactions are considered separately in connection with Hauser-Feshbach theory including fission channel for the calculation of scattered-neutron cross-sections, fission cross-sections, and γ-production cross-sections.

REFERENCES

1 H. Märten et al., Proc. Int. Conf. on Nucl. Phys. - Nuclear Fission -, Gaussig, 1985, ZfK-592 (1986) 1

2 H. Märten, D. Seeliger, J. Phys. G: Nucl. Phys. 14 (1988) 211

3 E. Nardi et al., Phys. Lett. 43B (1973) 259

4 J.C. Brown , F.S. Dietrich, Phys. Rev. C10 (1974) 2545

5 D.G. Madland, J.R.Nix, Nucl. Sci. Eng. 81 (1982) 213

6 B.F. Gerassimenko, V.A. Rubchenya, IAEA-TECDOC-335 (1985) 280

7 H. Märten, D. Seeliger, J. Phys. G: Nucl. Phys. 10 (1984) 349

8 H. Märten, Proc. IAEA Advisory Group Meeting on Nuclear Theory for Fast Neutron Nuclear Data Evaluation, Beijing, 1987, IAEA-TECDOC-483 (Vienna, 1988) 148

9 H. Märten et al., Proc. IAEA Consultants' Meeting on the U-235 Fast-Neutron Fission Cross-Section, and the Cf-252 Fission Neutron Spectrum, Smolenice, 1983, INDC(NDS)-146 L (1983) 199

10 H. Märten et al., Nucl. Instr. Meth. A264 (1988) 375

11 H. Märten et al., Proc. Int. Conf. on Neutron Physics, Kiev, 1987 (Moskow, 1988) Vol. III, p. 49

12 C. Budtz-Jorgensen, H.H. Knitter, Rad. Eff. 93 (1986) 5

13 H. Märten, D. Seeliger, Nucl. Sci. Eng. 93 (1986) 370

14 H. Märten et al., Proc. Int. Conf. on Nuclear Physics, Gaussig, 1986, ZfK-610 (1986) 169

15 D. Lucas, H. Märten, to be published

16 U. Brosa et al., loc. cit. (14), p. 162

17 C.A. Straede, Thesis, CBNM, Geel (1985)

18 J.R. Huizenga, R. Vandenbosch, Nuclear Fission (1973)

19 M. Uhl, Proc. Int. Conf. on Nuclear Physics, Gaussig, 1982, ZfK-491 (1982) 155, and A.V. Ignatyuk et al., Yad. Fiz. 47 (1988) 355

20 T. Elfruth et al., Proc. Int. Symp. on Nuclear Physics - Nuclear Reactions -, Gaussig, 1987, ZfK-646 (1988) 39

21 H. Märten et al., ibid., p. 160

22 J. Trochon et al., Nucl. Phys. A318 (1979) 63

23 H. Yamamoto et al., J. Nucl. Sci. Techn. 16 (1979) 779

24 H. Märten et al., loc. cit. (20), p. 156

25 H. Märten et al., Proc. Int. Conf. on Nucl. Data for Science and Technology, Mito, 1988, ed. by S. Igarasi, JAERI, SAIKON Publ. Comp. (Tokyo, 1988) p. 683

26 H.R. Bowman et al., Phys. Rev. 126 (1963) 2120

27 P. Mädler, Z. Phys. A321 (1985) 343

28 B. Milek et al., Report KFKI-1987-19/A (1987)

29 W. Mannhart, Proc. IAEA Advisory Group Meeting on Properties of Neutron Sources, Leningrad, 1986, IAEA-TECDOC-410 (1987) 194

30 P.I. Johansson et al., NBS Spec. Publ. 425 (1975) 572

APPENDIX A

Selected Results of CEM and GMNM Calculations for 252-Cf(sf) (Check of Internal Consistency)

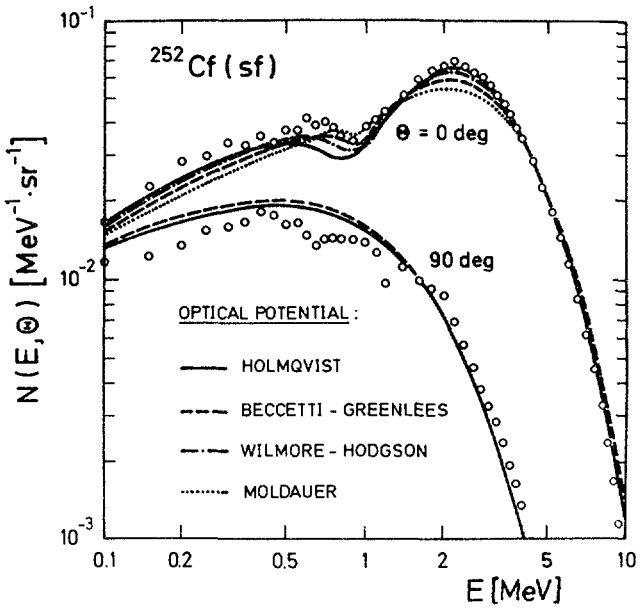

Fig. A1

Differential ^{252}Cf(sf) neutron spectra for polar (θ=0deg) and equatorial direction (θ=90deg). Experimental data (Ref. 10) are compared with CEM calculations based on several optical potentials as indicated.

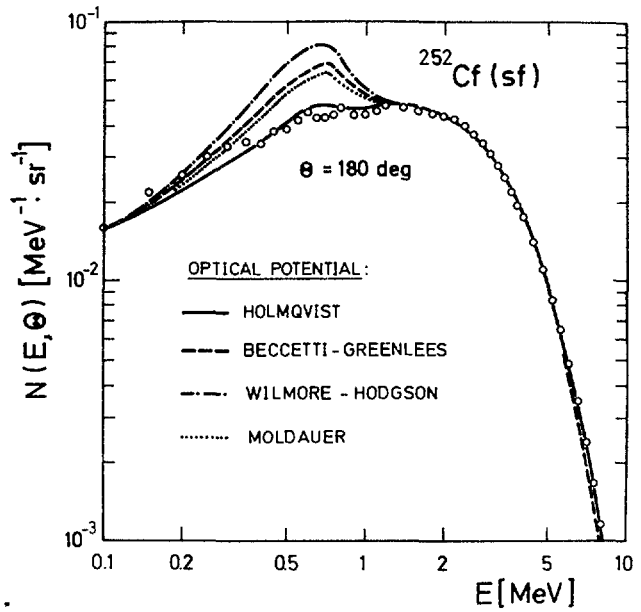

Fig. A2

As for Fig. A1, but for θ=180deg.

Fig. A3

Angular distribution of fission neutrons from 252-Cf(sf) for E=1 MeV (histogram - experimental data from Ref. 10, curves - CEM results for several optical potentials, cf. Fig. A1)

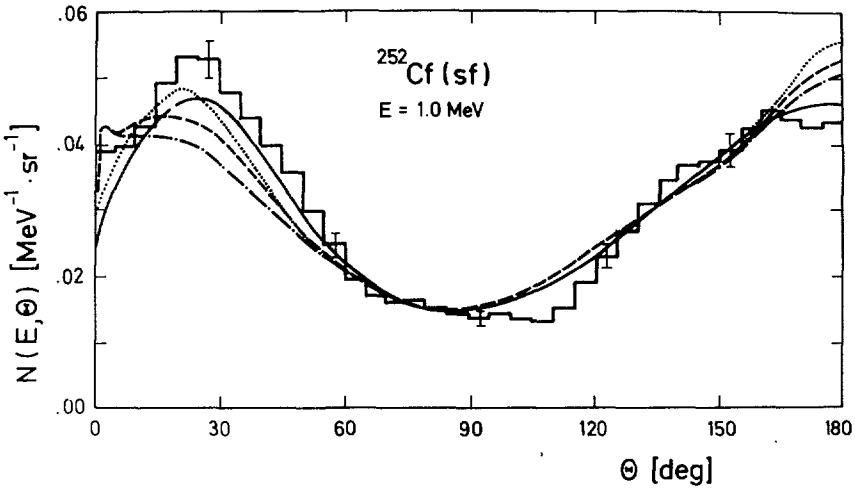

Fig. A4

The same as for Fig. A3, but for E=0.55 MeV. Note that 1 MeV (0.55 MeV) corresponds to the average kinetic energy of the light (heavy) fragment group, i.e. the polar regions in this energy range are determined by low-energy neutron emission in the center-of-mass system.

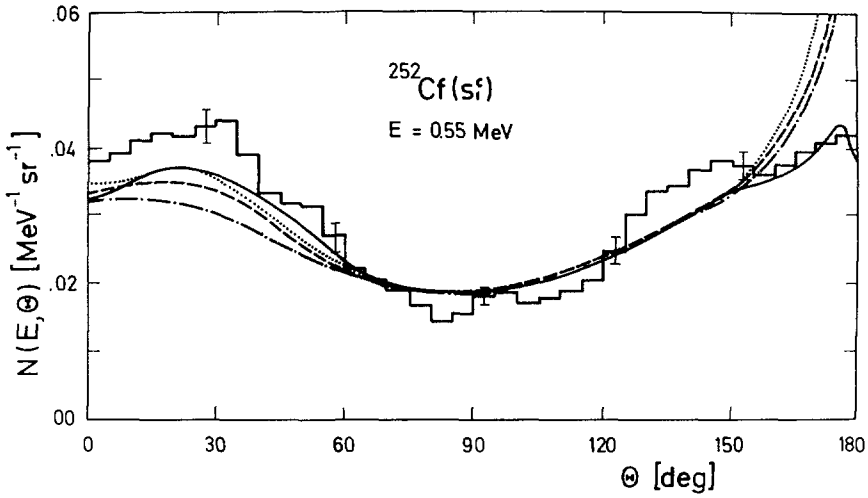

Fig. A5

Total fission neutron spectrum for 252-Cf(sf) represented as ratio R to a Maxwellian with a "temperature" parameter T=1.42 MeV (dots - evaluated data from Ref. 29, cont. line - CEM, dashed line - GMNM)

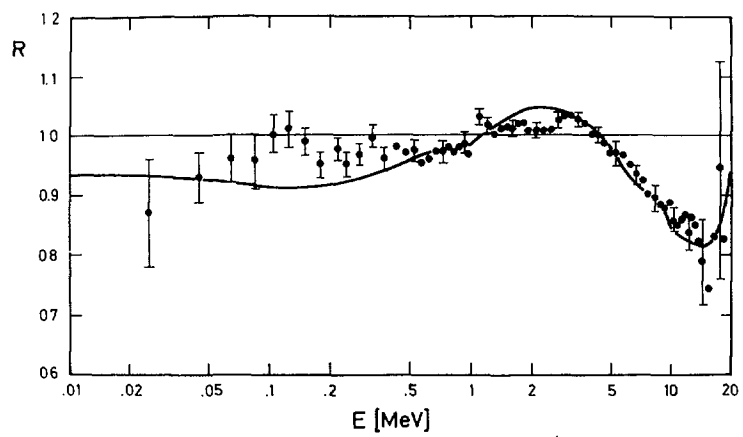

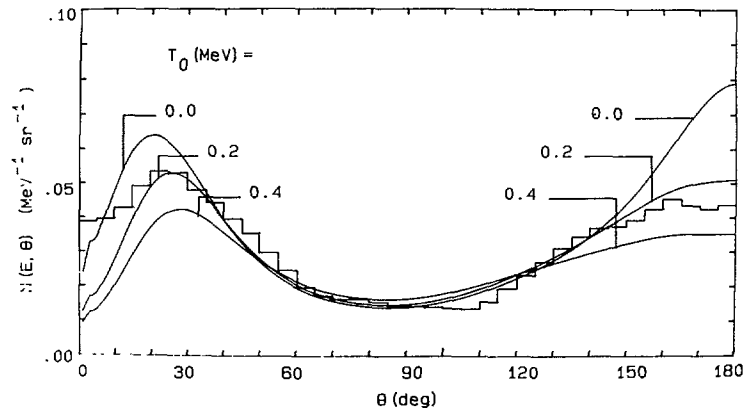

Fig. A6

Cf neutron angular distribution at E=1.0MeV (hostigram - experimental data from Ref. 10, curves - GMNM based on different parameters To, i.e. low limit of rest-nucleus temperature simulating n/γ-competition).

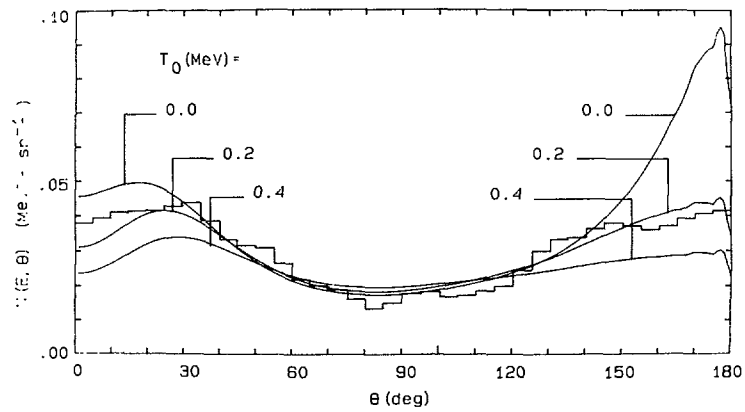

Fig. A7

As for Fig. A6, but for E=0.55MeV

APPENDIX B

GMNM Applications to Induced Fission Reactions

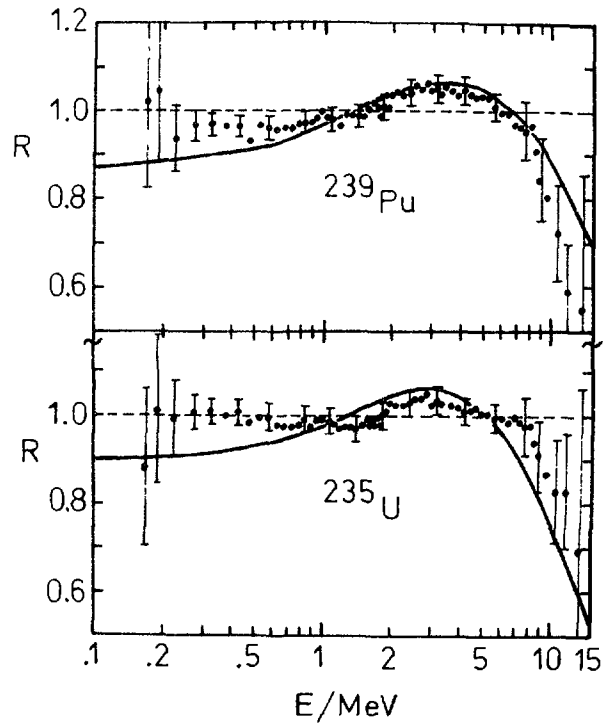

Fig. B1

Ratio of PFN spectra calculaetd in the frame-work of GMNM (curves) to reference Maxwellians with T=1.383MeV and T=1.318MeV for 0.5-MeV neutron induced fission of 239-Pu and 235-U, respectively (dots - experimental data from Ref. 30).

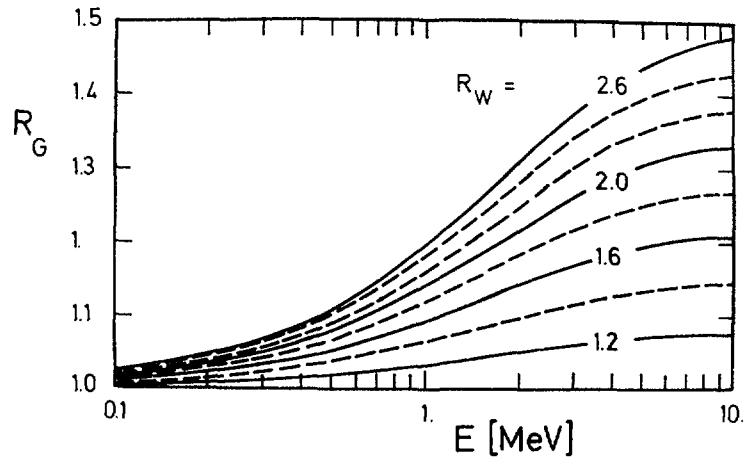

Fig. B2

Anisotropy ratio RG (0deg/90deg) of PFN emission with reference to fragment anisotropy ratio RW (parameter) for actinide fission (average behaviour) (cf. Ref. 30 for experimental data)

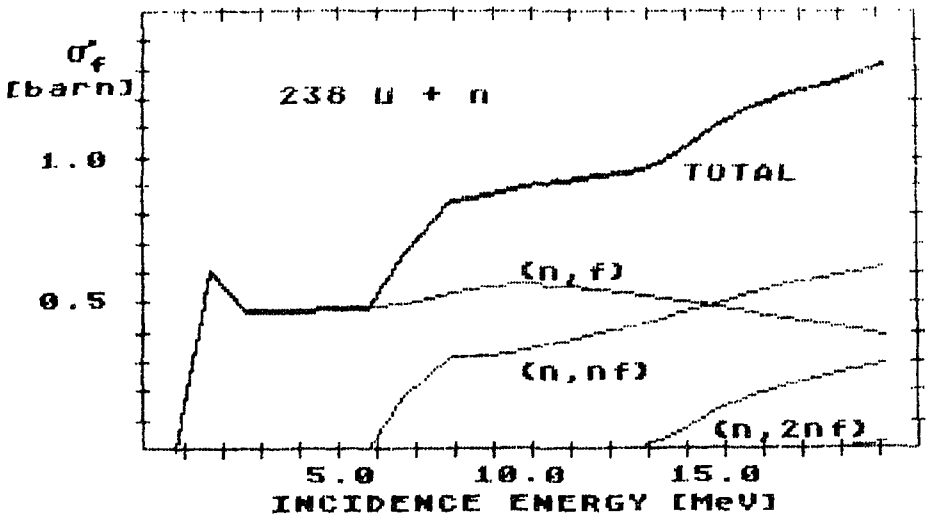

Fig. B3

Fission cross section for neutron induced fission of 238-U as calculated with STAPRE (Ref. 19). In the case of multiple-chance fission, the partial fission cross sections are represented, too.

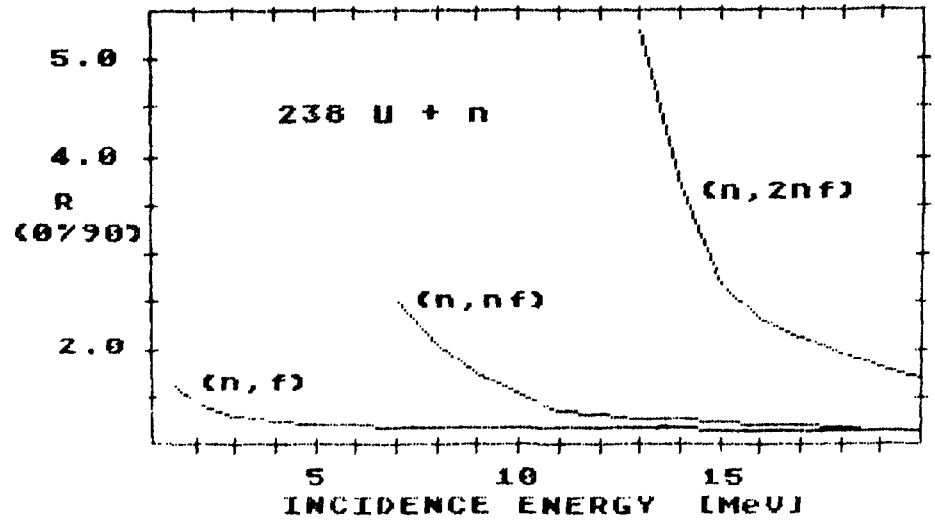

Fig. B4

Fragment anisotropy ratio R(0deg/90deg) for the different chances in the neutron induced fission of 238-U. Curves were deduced from experimental data considering a statistical description of fragment anisotropy in conjunction with the calculated fission cross section shown in Fig. B3, i.e. decomposition of experimental data.

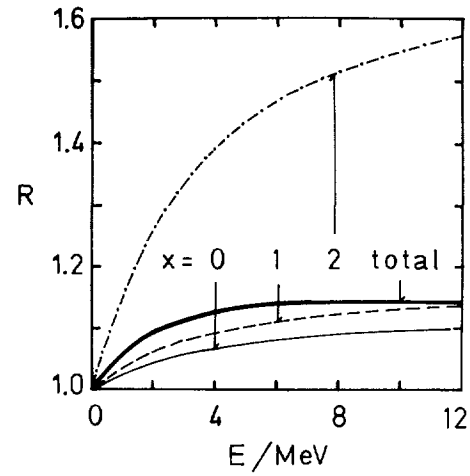

Fig. B5

Partial anisotropies R of PFN emission with reference to incidence beam direction for 238-U fission induced by 14.5 MeV neutrons, i.e. 238-U(n,xnf) with x=0,1,2

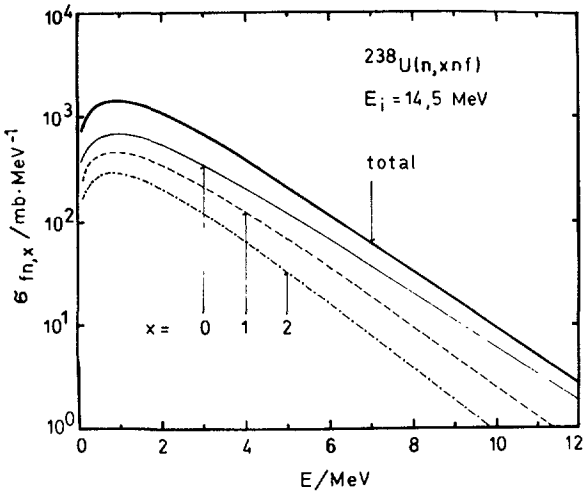

Fig. B6

Partial PFN cross sections for 238-U fission induced by 14.5 MeV neutrons (cf. Ref. 21)

RECENT IMPROVEMENTS IN THE CALCULATION OF PROMPT FISSION NEUTRON SPECTRA: PRELIMINARY RESULTS

David G. Madland, Raphael J. LaBauve, and J. Rayford Nix
Theoretical Division, Los Alamos National Laboratory
Los Alamos, New Mexico 87545

ABSTRACT

We consider three topics in the refinement and improvement of our original calculations of prompt fission neutron spectra. These are an improved calculation of the prompt fission neutron spectrum N(E) from the spontaneous fission of ^{252}Cf, a complete calculation of the prompt fission neutron spectrum matrix N(E,E_n) from the neutron-induced fission of ^{235}U, at incident neutron energies ranging from 0 to 15 MeV, and an assessment of the scission neutron component of the prompt fission neutron spectrum. Preliminary results will be presented and compared with experimental measurements and an evaluation. A suggestion is made for new integral cross section measurements.

I. INTRODUCTION

In this paper we report on initial efforts to refine and improve our original theoretical description of prompt fission neutron spectra and average prompt neutron multiplicities.[1] Although the refinements and improvements performed to date affect both the spectra and multiplicities, our work so far has been on the spectra alone. We consider three topics in the refinement of our original calculations of prompt fission neutron spectra. These are (a) an improved calculation of the *standard* prompt fission neutron spectrum N(E) from the spontaneous fission of ^{252}Cf, (b) a complete example of the incident neutron energy dependence of the prompt fission neutron spectrum N(E) for the neutron-induced fission of ^{235}U, resulting in the prompt fission neutron spectrum matrix N(E,E_n), and (c) an assessment of the scission neutron question arising in prompt fission neutron spectra.

On the first topic, (a), the contributions to N(E) from the *entire* fission-fragment mass and charge distributions are calculated instead of calculating on the basis of a *seven-point approximation* to the peaks of these distributions as has been done in the past. Preliminary results are presented and compared with a measurement, an earlier calculation, and a recent evaluation of the spectrum, as well as recent integral cross section measurements in this field. On the second topic, (b), we use the exact energy-dependent approach from our original work[1] and calculate the entire fission spectrum matrix N(E,E_n), for incident neutron energies in the range 0 MeV$\leq E_n \leq$15 MeV. At the higher incident neutron energies, we use the multiple-chance fission probabilities determined in our original calculation. Results are presented and compared with recent integral cross section measurements in the thermal field, other comparisons with experiments at specific incident neutron energies having been performed earlier. Due to the effort that would be required to experimentally verify a theoretical calculation of the complete fission spectrum matrix N(E,E_n), we instead suggest

that a number of crucial integral cross section measurements be performed. On the third topic, (c), we discuss the experimental evidence for scission neutrons and the most likely physical mechanism for their production. However, at this time we do not calculate the scission-neutron component of N(E) due to lack of *conclusive* evidence for its existence.

In Sec. II we consider the fission spectrum N(E) for the ^{252}Cf(sf) *standard reaction* and in Sec. III we consider the fission spectrum matrix $N(E,E_n)$ for the neutron-induced fission of ^{235}U. We discuss scission neutrons in Sec. IV and our conclusions in Sec. V.

II. IMPROVED CALCULATION OF THE PROMPT FISSION NEUTRON SPECTRUM FROM THE SPONTANEOUS FISSION OF ^{252}Cf.

The prompt fission neutron spectrum N(E) from the spontaneous fission of ^{252}Cf is important due to its use as a *standard* neutron field. In addition, because of extensive experimental studies on this spectrum, it is used as a test case in the development of theoretical models of prompt fission neutron spectra for spontaneous as well as neutron-induced fission. In this paper, a measurement, an earlier calculation, an evaluation, and preliminary results from an improved calculation of N(E) for the ^{252}Cf(sf) reaction are presented and compared. In addition, measured and calculated integral cross sections for the ^{252}Cf(sf) spectrum are also presented and compared.

Our previous calculations[1-5] of the prompt fission neutron spectrum have utilized input parameters based upon *average* values of the fission-fragment mass, charge, and kinetic energy distributions. In particular, values of the average energy release in fission, $\langle E_r \rangle$, and the total average fission-fragment kinetic energy, $\langle E_f^{tot} \rangle$, have been used instead of the specific values occurring from all possible binary mass and charge divisions in fission. Likewise, the calculations of the inverse process to neutron emission, compound nucleus formation, have been restricted to two nuclei: the average central light fragment and the average central heavy fragment. Finally, it was noted that in the vicinity of the average fragments, the average numbers of neutrons emitted from the light and heavy fragments are approximately equal. The spectrum N(E) has therefore been given by the *average* of the spectra calculated from the light and heavy fragments, namely

$$N(E) = \frac{1}{2}\left[N(E,E_f^L,\sigma_c^L) + N(E,E_f^H,\sigma_c^H)\right], \qquad (1)$$

where E is the laboratory neutron energy, E_f^L and E_f^H are the average kinetic energies per nucleon of the light and heavy fragments, respectively, and σ_c^L and σ_c^H are the cross sections for the inverse process in the average light and heavy fragments, respectively.

In the present work, the use of input parameters based upon *average* values of the fission-fragment mass, charge, and kinetic energy distributions is replaced by *direct use, on a point-by-point basis, of the distributions themselves*. Following a description of the refinements to our original calculations, in the next subsection, preliminary results are presented and discussed.

II. A. Refinements in the Model

The energy release E_r for *each binary fission considered* is given by

$$E_r = M(Z_c,A_c) - M_L(Z_L,A_L) - M_H(Z_H,A_H) \ , \qquad (2)$$

where M is a mass excess expressed in MeV and c, L, and H refer to compound fissioning nucleus, light fission fragment, and heavy fission fragment, respectively. Use of Eq. (2) over the fission-fragment mass and charge distributions *replaces* the average value $<E_r>$ obtained using the seven-point approximation given in Ref. 1 and used in Refs. 1-5 (note that in Ref. 2, an exact calculation of $<E_r>$ was also performed). In evaluating Eq. (2), experimental masses from the 1986 Audi-Wapstra mid-stream mass evaluation[6] are used where they exist and otherwise the calculated masses of Möller and Nix.[7]

The total fission-fragment kinetic energy E_f^{tot} for *each binary fission considered* is taken from the experimental results of Schmitt *et al.* ,[8] in which E_f^{tot} is given as a function of heavy fragment mass,

$$E_f^{tot} = E_f^{tot}(A_H) \ , \qquad (3)$$

for all values of A_H observed ($126 \le A_H \le 166$). These $E_f^{tot}(A_H)$ values are themselves averages due to the fission-fragment distributions in charge $P(Z_L)$ and $P(Z_H)$, for fixed values of A_L and A_H, respectively. Recall that the binary fission assumption demands that the sets (A_L,A_H,A_c) and (Z_L,Z_H,Z_c) simultaneously satisfy complementarity. Use of the measurements of E_f^{tot} by Schmitt *et al.*,[8] represented by Eq. (3), *replaces* the average value of the total fission-fragment kinetic energy $<E_f^{tot}>$ used in Refs. 1-5.

The values of E_f^{tot} are used in two ways in the calculation of N(E). The first way is in the calculation of the average kinetic energies per nucleon, E_f^L and E_f^H, of the light and heavy fragments. These are obtained by use of momentum conservation, as before, and are given by

$$E_f^L = (A_H/A_L)(E_f^{tot}/A_c) \ , \text{ and} \qquad (4)$$

$$E_f^H = (A_L/A_H)(E_f^{tot}/A_c) \ . \qquad (5)$$

In all of our previous work these same equations have been used, but they have been evaluated using $<E_f^{tot}>$ instead of E_f^{tot}, the average central light fragment instead of A_L, and the average central heavy fragment instead of A_H.

The values of E_f^{tot} are also used, together with the values of the energy release in fission E_r, to calculate the maximum temperatures T_m of the temperature distributions P(T) representing the corresponding distributions of fission-fragment excitation energy. In the present calculation this is done for *each binary fission considered*, whereas in our previous calculations *one average value* of T_m was used. For spontaneous fission, T_m is now given by

$$T_m = [(E_r - E_f^{tot})/a]^{1/2} , \tag{6}$$

where E_r and E_f^{tot} are given by Eqs. (2) and (3), respectively, and a is the Fermi gas level density parameter

$$a = A_c/(\text{const}) . \tag{7}$$

Previously, the average values $\langle E_r \rangle$ and $\langle E_f^{tot} \rangle$ were used in evaluating Eq. (6).

The compound nucleus cross section σ_c for the inverse process is computed for the two fragments occurring in *each binary fission considered.* Thus, $\sigma_c = \sigma_c(\varepsilon,Z,A)$, ($Z_L$ or Z_H, A_L or A_H), where ε is the center-of-mass neutron energy. The optical-model potential of Becchetti and Greenlees[9] is used on a 100-point grid extending to 40 MeV, as in our earlier work for the *average light and heavy fragments.*

Given the above refinements to calculate the prompt fission neutron spectrum for each pair of complementary points on the fission-fragment mass and charge distributions, it remains to combine the results from all contributing pairs. For a given fragment mass number A, (A_L or A_H), the charge distribution in Z, (Z_L or Z_H), approximates a Gaussian distribution

$$P(Z) = (1/\sqrt{c\pi}\,) \exp[-(Z - Z_p)^2/c] , \tag{8}$$

where the most probable charge Z_p, (Z_p^L or Z_p^H), is obtained using a corrected unchanged charge distribution (UCD) assumption due to Unik *et al.*,[10]

$$(Z_p^L - \tfrac{1}{2})/A_L = (Z_c/A_c) = (Z_p^H + \tfrac{1}{2})/A_H , \tag{9}$$

and where the width parameter, c, is given by

$$c = 2(\sigma^2 + \tfrac{1}{12}) , \tag{10}$$

where σ is the average charge dispersion. A value of $\sigma = 0.40 \pm 0.05$ is used, which was determined in the experiments of Reisdorf *et al.*[11] for the pre-neutron emission charge distribution in the thermal-neutron-induced fission of ^{235}U.

Given the charge distribution P(Z) for each fragment mass number A, the contributions from all fragment masses are summed. This is accomplished by use of weighting factors comprised of (a) the fragment mass yields Y(A), (A_L or A_H), and (b) the average number of prompt neutrons emitted for each fragment mass $\bar{\nu}(A)$, (A_L or A_H). In the present work, the pre-neutron emission experimental fragment-yields of Schmitt *et al.*[8] are used and the average prompt neutron multiplicities measured as a function of fragment mass by Walsh and Boldeman[12] are also used.

Using Eqs. (2)-(10), the expression for the prompt fission neutron spectrum N(E) in the preliminary refined model is given by

$$N(E) = \sum_A \frac{\bar{\nu}(A)}{\bar{\nu}_{tot}} Y(A) \sum_Z P(Z)\, N\left[E, E_F(A), \sigma_c(Z,A), T_m(Z,A)\right] \qquad (11)$$

where $\bar{\nu}_{tot} = \sum_A \bar{\nu}(A)Y(A)$ is the total average prompt neutron multiplicity and the sums occurring are over Z_L and Z_H as well as over A_L and A_H.

II. B. Preliminary Results

The first calculation using the refined model summarized by Eq. (11) is for the spontaneous fission of ^{252}Cf. In this calculation, the fission-fragment mass and charge distributions are represented by 28 fragments:

(a) 14 approximately equispaced fragment masses in the range $88 \leq A \leq 164$, with a spacing of about 6 in mass number, and

(b) 2 isobars per fragment mass, with values of Z that are the nearest integer values above and below the most probable charge Z_p.

The contributions to the prompt neutron spectrum from *each binary fission considered* therefore include:

(a) 28 optical-model calculations of the compound nucleus formation cross section $\sigma_c(Z,A)$ for the inverse process, using Ref. 9,

(b) 14 calculations of the energy release in fission E_r, one for each fragment pair, with values spanning the range $198.061 \text{ MeV} \leq E_r \leq 236.421 \text{ MeV}$,

(c) 7 experimental values[8] of the total fragment kinetic energy E_f^{tot}, each accounting for 2 fragment pairs, spanning the range $165.91 \text{ MeV} \leq E_f^{tot} \leq 195.22 \text{ MeV}$,

(d) 14 calculations of the average kinetic energy per nucleon, one for each pair of isobars, with 7 such pairs for the light fragments having values in the range $0.777 \text{ MeV} \leq E_f^L \leq 1.227 \text{ MeV}$, and 7 such pairs for the heavy fragments having values in the range $0.353 \text{ MeV} \leq E_f^H \leq 0.729 \text{ MeV}$,

(e) 14 calculations of the most probable charge Z_p, one for each pair of iosbars, yielding 7 values of Z_p^L for the light fragments and 7 values of Z_p^H for the heavy fragments,

(f) 7 experimental values[8] of the fragment mass yield Y(A), each accounting for 2 fragment pairs, spanning the range $0.17\% \leq Y(A) \leq 5.55\%$, and

(g) 14 experimental values[12] of the average neutron multiplicity as a function of fragment mass $\nu(A)$, one for each pair of isobars, spanning the range $0.71 \leq \nu(A) \leq 3.89$.

The preliminary results obtained using Eq. (11) with *28 fission fragments* to explicitly represent the total fission-fragment mass and charge distributions are illustrated in Figs. 2-7. For comparison purposes, a calculation of the spectrum reproduced from our earlier work[4] is shown in Fig. 1. The solid curve here shows the spectrum calculated using Eq. (1), for *two averge fragments* from the yield peaks, with a nuclear level-density parameter $a = A_c/(9.15\ \text{MeV})$ obtained in a least-squares adjustment to the experimental spectrum of Poenitz and Tamura.[13] Ratios to the least-squares adjusted Maxwellian spectrum (T_M = 1.429 MeV) were used as the basis for comparison.

In Fig. 2 we show our earlier calculation again, as the dashed curve, together with the present calculation using Eq. (11), as the solid curve. The effects of the refined model calculation

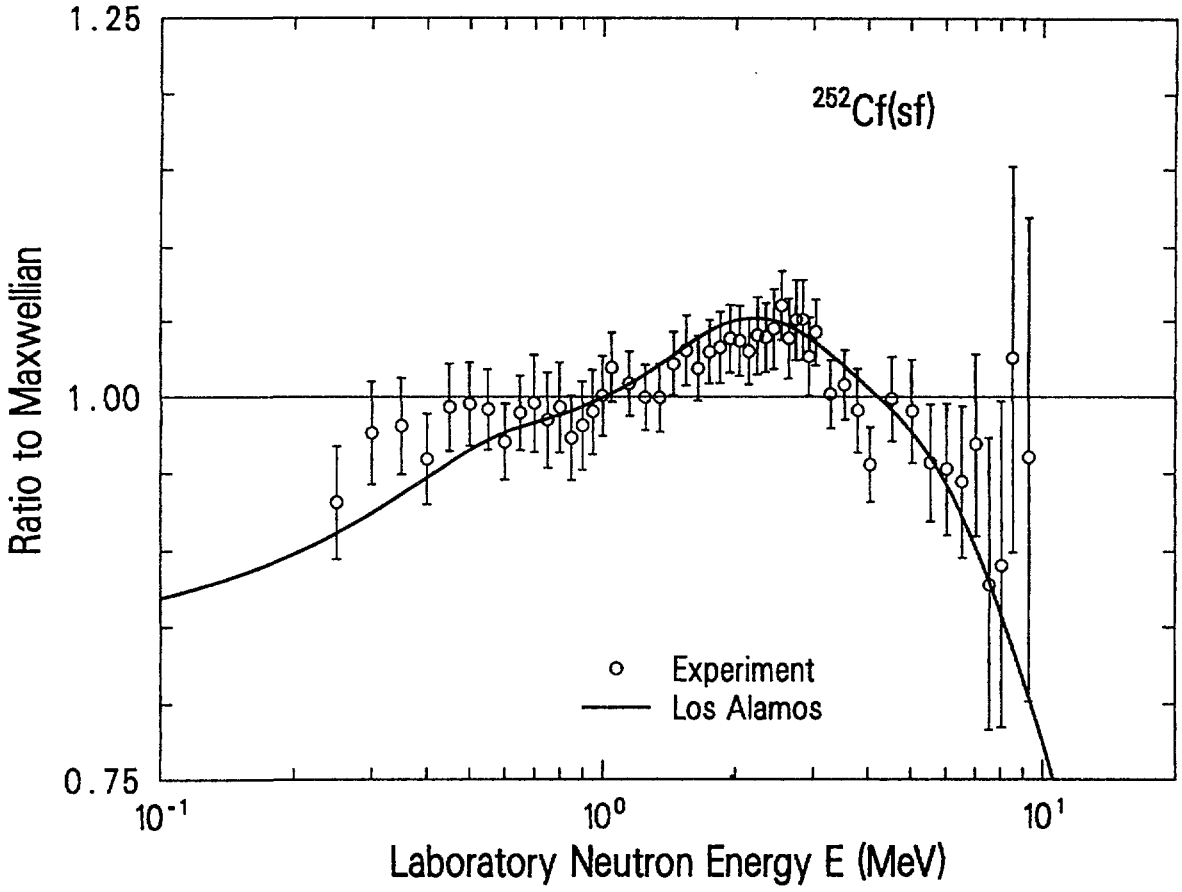

Fig. 1. Ratio of the previous least-squares adjusted Los Alamos spectrum and the experimental spectrum of Poenitz and Tamura (1982) to the least-squares adjusted Maxwellian spectrum, for ^{252}Cf(sf).

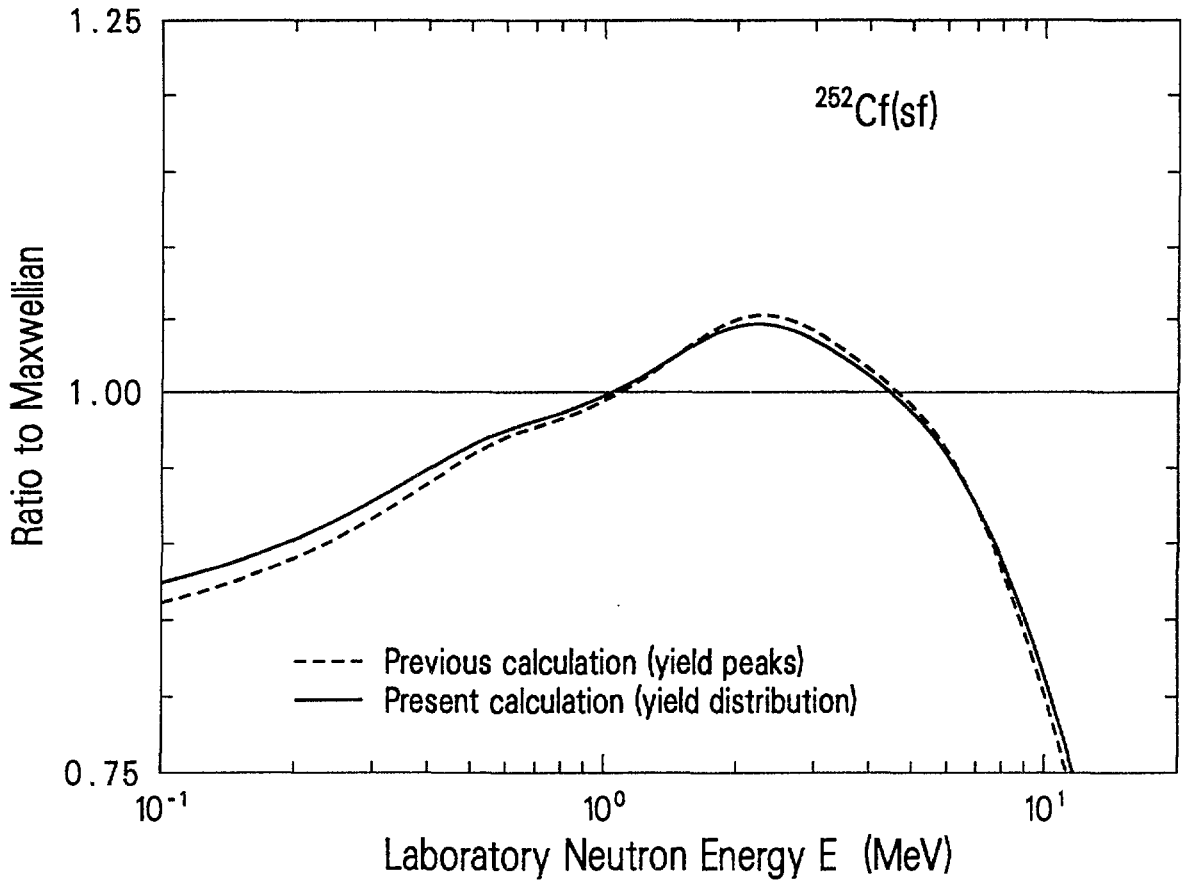

Fig. 2. Ratio of the previous least-squares adjusted Los Alamos spectrum, based on considerations of the *peaks* of the fission-fragment mass and charge distributions, and the present Los Alamos spectrum, based on considerations of the *entire* fission-fragment mass and charge distributions, to a Maxwellian spectrum with T_M = 1.42 MeV. The nuclear level-density parameter in both calculations is given by a = A_c/(9.15 MeV).

compared with the previous model calculation are that the spectrum is increased in the regions below approximately 1.4 MeV and above approximately 8.8 MeV, and is decreased in the region between approximately 1.4 MeV and 8.8 MeV. A comparison of Figs. 1 and 2 clearly shows that these effects are in *exactly the right direction* to give even better agreement with the experiment of Poenitz and Tamura[13] than was obtained in the previous calculation.[4] However, it is equally clear that the refined calculation does not yet exactly reproduce the experiment. Namely, an even larger increase would be possible in the low and high energy regions of the calculated spectrum. Note that the spectra shown in Fig. 2 are both calculated with a level-density parameter, a = A_c/(9.15 MeV), identical to that used in Fig. 1, and also that the reference Maxwellian of Fig. 2 is calculated with T_M = 1.42 MeV.

The present calculation shown in Fig. 2 is compared with a recent evaluation of the spectrum by Mannhart[14] in Fig. 3. The "data" shown are from the "group averages" spectrum obtained by Mannhart. Again, a reference Maxwellian with T_M = 1.42 MeV has been used. The agreement between the present calculation and the evaluated spectrum is not nearly as good as in the case of the experimental spectrum of Poenitz and Tamura.[13] A least-squares adjustment to the level-density parameter was then performed resulting in the value a = A_c/(9.40 MeV), which improved

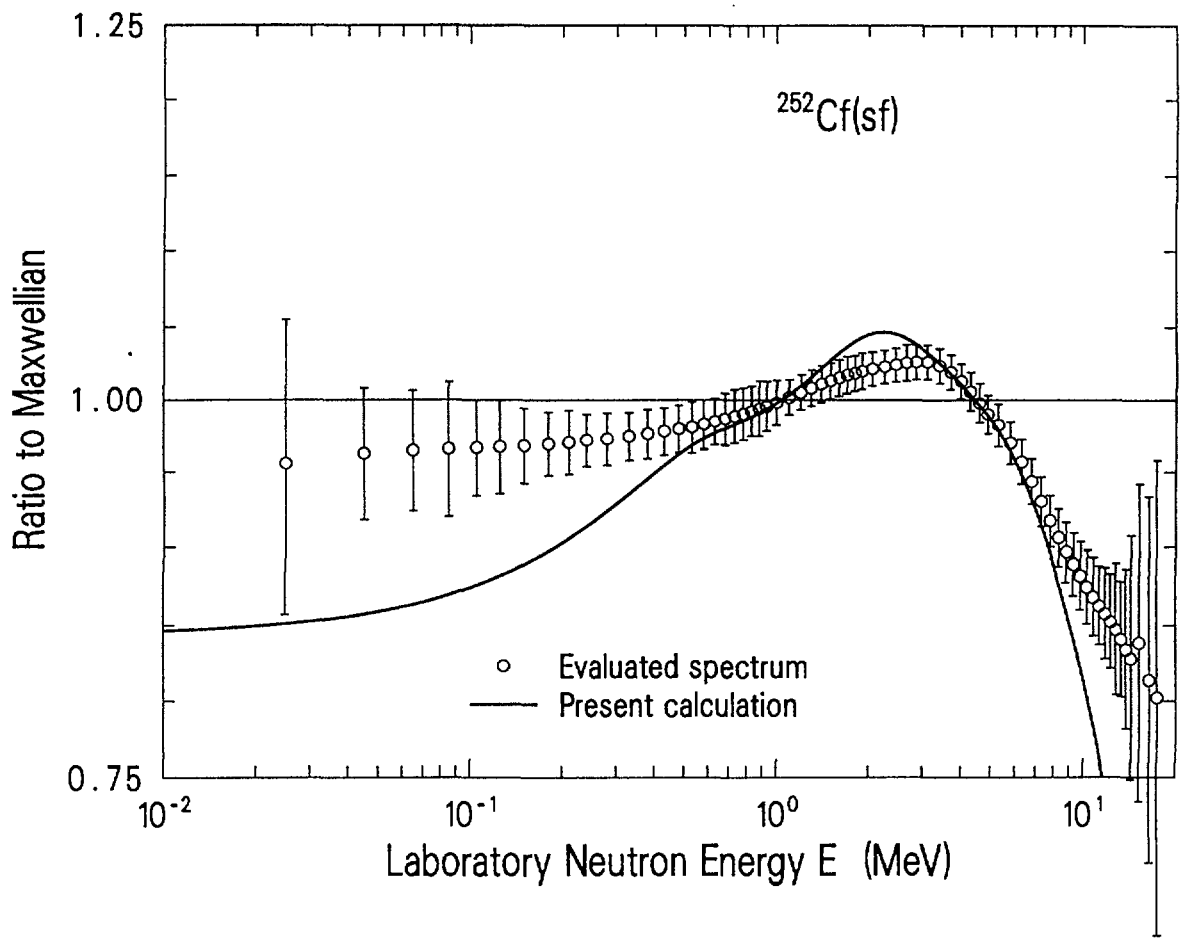

Fig. 3. Ratio of the present Los Alamos spectrum and the evaluated spectrum of Mannhart (1987) to a Maxwellian spectrum with T_M = 1.42 MeV, for ^{252}Cf(sf). The nuclear level-density parameter is given by a = A_c/(9.15 MeV).

the χ^2 approximately by a factor of two. The comparison of this spectrum with the evaluation of Mannhart is shown in Fig. 4 using the same reference Maxwellian spectrum. Although the agreement with the evaluated spectrum is improved, it is again not nearly as good as in the case of the experimental spectrum of Poenitz and Tamura and the unadjusted present calculation.

Comparisons of integral cross sections calculated using these spectra and experimental values are shown in Figs. 5-7. Recall that the integral cross section, $\langle\sigma_i\rangle$, represents the net effect of the pointwise cross section $\sigma_i(E)$ in the presence of the neutron field N(E), and is given by

$$\langle\sigma_i\rangle = \frac{\int_{E_1}^{E_2} \sigma_i(E)N(E)dE}{\int_{E_1}^{E_2} N(E)dE}, \qquad (12)$$

where E is the neutron energy and E_1 and E_2 are the energy limits of the field. A specific reaction with a known cross section and a threshold, at E = E_{th}, serves as a means by which integral

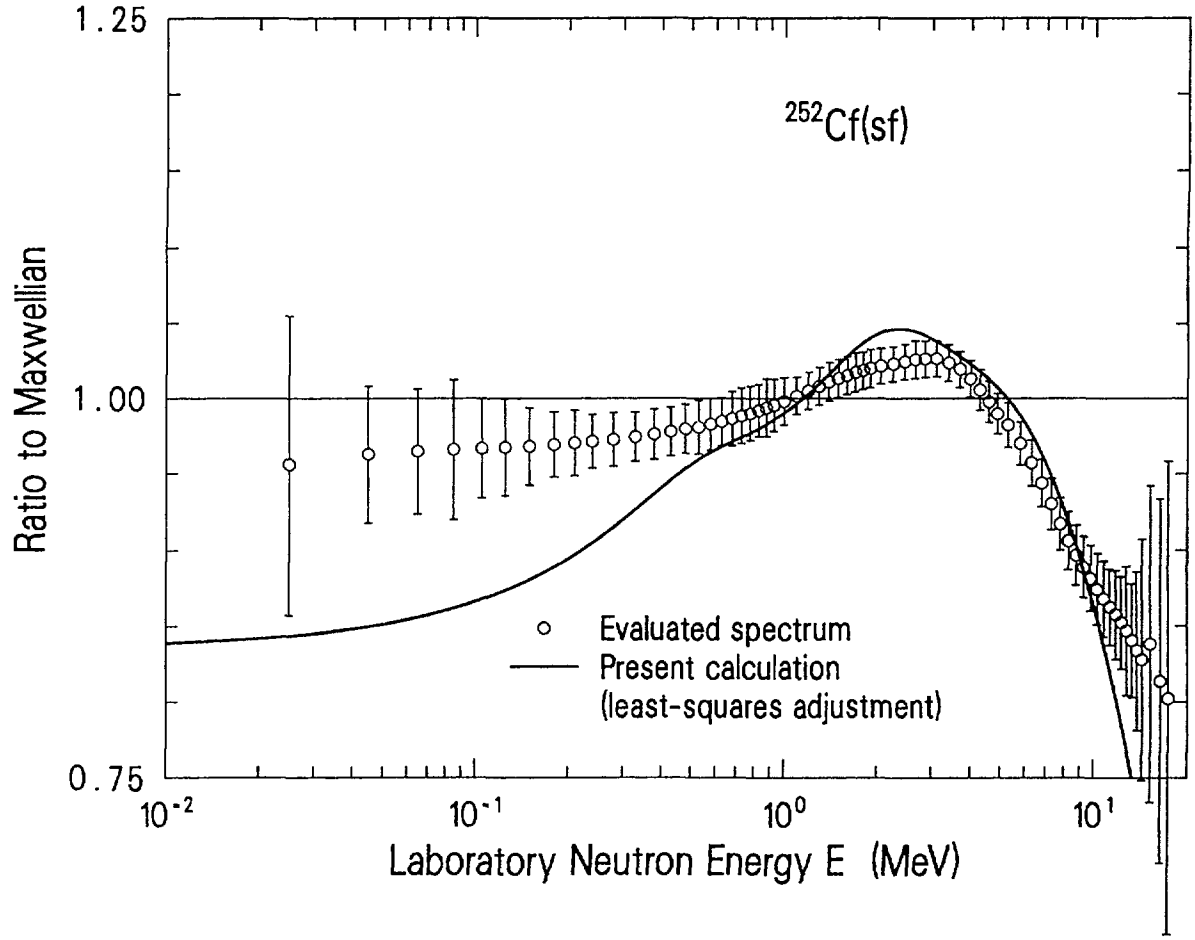

Fig. 4. Ratio of the present least-squares adjusted Los Alamos spectrum and the evaluated spectrum of Mannhart (1987) to a Maxwellian spectrum with T_M = 1.42 MeV, for ^{252}Cf(sf). The adjusted nuclear level-density parameter is given by a = A/(9.40 MeV).

comparisons can be made of different neutron fields for energies $E \geq E_{th}$. For the present calculations, we use ENDF/B-V pointwise cross sections[15] in all cases except for four high threshold reactions (E_{th} > 12 MeV) where we use recent evaluations by Young[16] and measurements by Bayhurst *et al.*[17] and Mannhart and Vonach.[18] We compare our calculated values obtained using Eq. (12) with the experimental integral cross sections measured by Kobayshi *et al.*[19] and Mannhart.[20-22]

The ratios of the calculated integral cross sections using the present spectrum, shown as the solid curve in Figs. 2 and 3, to the corresponding experimental integral cross sections are plotted in Fig. 5 as a function of the threshold energy of the reaction (defined here as the energy at which the integral of the pointwise cross section reaches 0.01% of its total value.) The figure shows that the present spectrum is compatible with the experimental integral cross sections for emitted neutron energies below about 9.5 MeV, but is too soft for higher emitted neutron energies. Similarly, the ratios of the calculated integral cross sections using the present least-squares adjusted spectrum, shown as the solid curve in Fig. 4, to the corresponding experimental integral cross sections are plotted in Fig. 6. This figure shows that the present least-squares adjusted spectrum is also too soft, but only for emitted neutron energies in excess of about 11.5 MeV, compared to 9.5 MeV before. Moreover, the departure from experiment for higher threshold energies is clearly less than

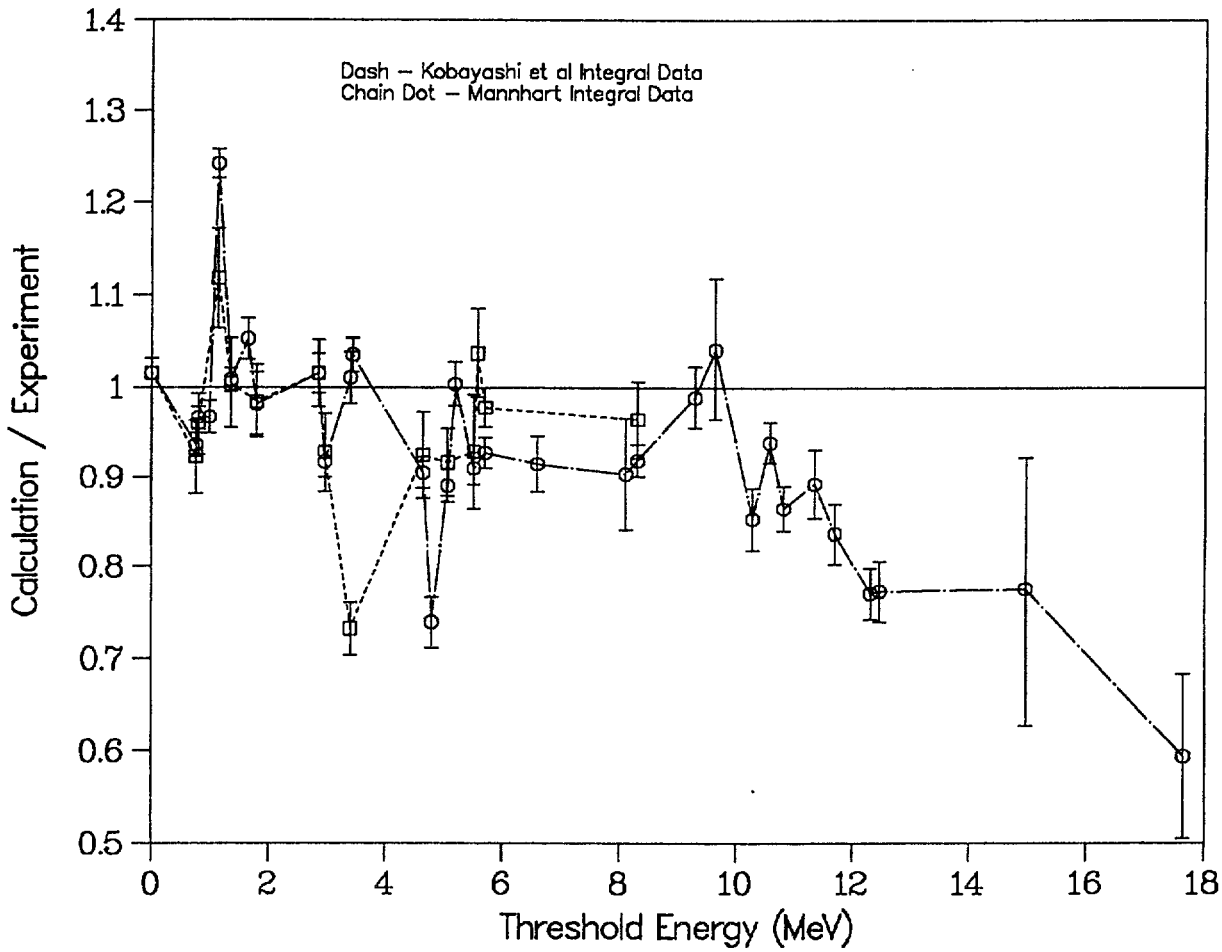

Fig. 5. Ratio of calculated to experimental integral cross sections for the neutron field from the spontaneous fission of ^{252}Cf, as a function of the threshold energy for the reaction. The calculated values are obtained using the present spectrum from Eq. (11) in Eq. (12) together with ENDF/B-V pointwise cross sections, except for four high threshold reactions extending beyond 20 MeV (see text).

before. Thus, the present least-squares adjusted spectrum is compatible with the experimental integral cross sections for emitted neutron energies up to about 11.5 MeV, but is somewhat soft for higher energies. Therefore, further improvement is needed.

Finally, the ratios of the calculated integral cross sections using Mannhart's spline fit[14] to his evaluated spectrum, shown as the points in Figs. 3 and 4, and the corresponding experimental integral cross sections are plotted in Fig. 7 (since the spline fit extends only to 20 MeV, integral cross sections cannot be calculated for reaction thresholds above about 13 MeV.) This figure shows that the spline fit to the evaluated spectrum is compatible with the experimental integral cross sections for emitted neutron energies up to about 12.5 MeV. However, there is clearly a trend in the ratios indicating that the spline fit is increasingly too hard for energies in the range of about 7 to 12 MeV. Thus, the evaluated spectrum may also require some revision in this energy range. Clearly, further work must be done on the prompt fission neutron spectrum for the spontaneous fission of ^{252}Cf, especially if this spectrum is to be used as a *standard* spectrum.

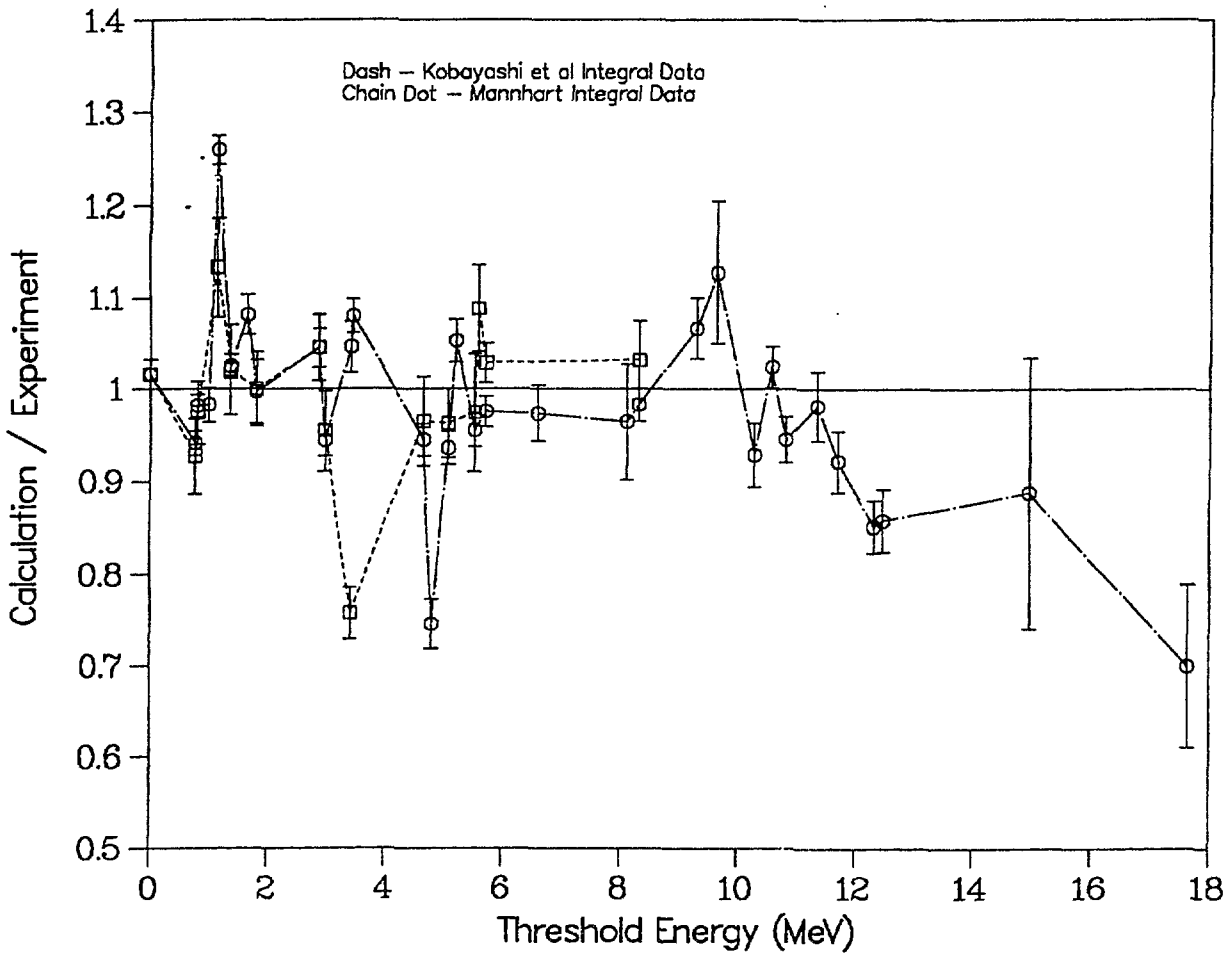

Fig. 6. Ratio of calculated to experimental integral cross sections for the neutron field from the spontaneous fission of ^{252}Cf, as a function of the threshold energy for the reaction. The calculated values are obtained using the present least-squares adjusted spectrum from Eq. (11) in Eq. (12) together with ENDF/B-V pointwise cross sections, except for four high threshold reactions extending beyond 20 MeV (see text).

III. PROMPT FISSION NEUTRON SPECTRUM MATRIX FROM THE NEUTRON-INDUCED FISSION OF ^{235}U

At sufficiently high incident neutron energies, say, above 6 MeV, the excitation energy of the compound nucleus is large enough that fission is possible following the emission of one or more neutrons. Thus, at some excitation energy the first-chance fission (n,f) reaction is in competition with the second-chance fission (n,n'f) reaction, and at some higher excitation energy these two reactions are in competition with each other and with the third-chance fission (n,n'n"f) reaction, and so on. In this section we account for the effects of and competition between multiple-chance fission processes up through third-chance fission in the calculation of N(E). We use the *exact energy-dependent approach from our original work*[1], embodied in Eq. (1), to calculate N(E) for ^{235}U at sixteen incident neutron energies in the range 0 MeV $\leq E_n \leq$ 15 MeV. This yields the prompt fission neutron spectrum matrix $N(E,E_n)$ for the neutron-induced fission of ^{235}U up through third-chance fission. In the following subsections we briefly describe the calculation, but

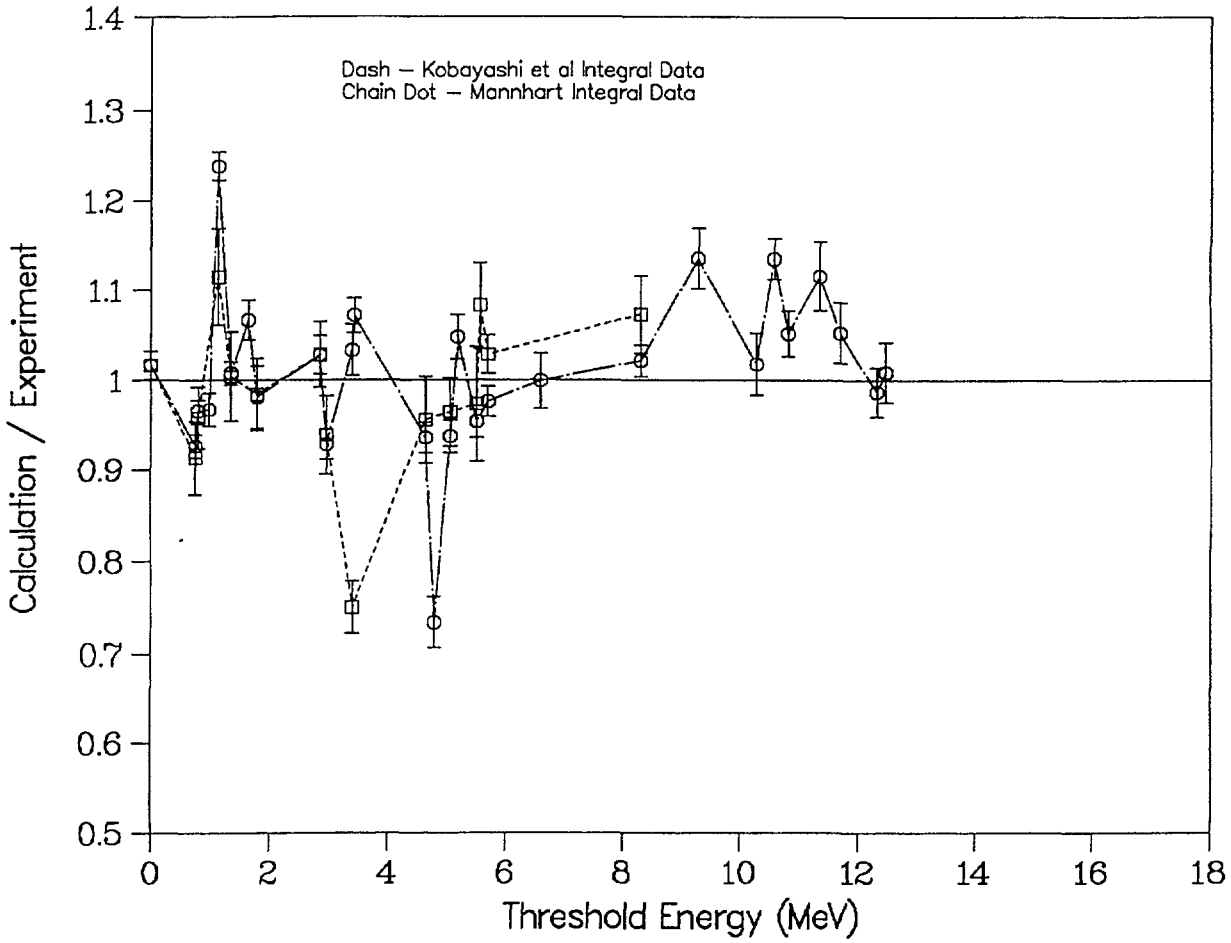

Fig. 7. Ratio of calculated to experimental integral cross sections for the neutron field from the spontaneous fission of ^{252}Cf, as a function of the threshold energy for the reaction. The calculated values are obtained using Mannhart's spline fit to his evaluated spectrum (1987) together with ENDF/B-V pointwise cross sections.

refer the reader to Ref. 1 for details of the formalism as well as comparisons with experiment for certain incident neutron energies. We then examine some properties of the fission spectrum matrix $N(E,E_n)$.

III. A. Description of the Calculation

The main ingredients necessary for the calculation of N(E) when multiple-chance fission occurs are

1. multiple-chance fission probabilities $P_{f_i}^A$,
2. evaporation spectra $\phi_j(E,\sigma_c)$ due to neutron evaporation prior to fission,
3. distributions of excitation energy $D_i(E^*,\sigma_c)$ in the fissioning nuclei, following neutron evaporation, but prior to fission,
4. average prompt neutron multiplicities $\bar{\nu}_{p_i}$ for the fissioning nuclei, and

5. prompt fission neutron spectra $N_i(E)$ for the fissioning nuclei,

where the subscript i refers to first-, second-, or third-chance fission, the subscript j refers to the corresponding neutron evaporation spectra prior to fission, and σ_c is the cross section for the inverse process of compound nucleus formation.

The multiple-chance fission probabilities $P_{f_i}^A$ are obtained using experimental total fission probabilities for excitation energies below the neutron separation energy and by using the ratio of a measured total fission cross section to a calculated compound nucleus cross section above the neutron separation energy. The calculated compound nucleus cross section is obtained using an actinide optical-model potential. The multiple-chance fission probabilities are then unfolded from the total fission probability by expressing the i'th-chance fission probability in terms of the first-chance fission probabilities of the nuclei encountered in reaching i'th-chance fission. This requires the assumption that average fission probabilities are approximately equal to fission probabilities evaluated at average excitation energies, and also requires the distribution of excitation energy $D_i(E^*,\sigma_c)$ in each participating nucleus. Using this approach, one obtains the first-, second-, and third-chance fission probabilities given by Eqs. (45) - (47) of Ref. 1.

The evaporation spectra $\phi_j(E,\sigma_c)$ due to neutron evaporation prior to fission are given by

$$\phi_j(E,\sigma_c) = k(T)\, \sigma_c(E)\, E \exp(-E/T)\,, \tag{13}$$

where k(T) is the temperature dependent normalization constant, $\sigma_c(E)$ is the cross section for the inverse process of compound nucleus formation, T is the residual nuclear temperature, and j indexes the spectra according to the j'th neutron evaporated prior to fission.

The distributions of excitation energy $D_i(E^*,\sigma_c)$ in the fissioning nuclei are given by

$$D_i(E^*,\sigma_c) = c(T)\, \phi(E_m - E^*, \sigma_c)\,, \tag{14}$$

where c(T) is the temperature dependent renormalization constant, E^* is the excitation energy, and E_m its maximum value. Clearly, the distributions of excitation energy, Eq. (14), are complementary to the energy distributions of evaporated neutrons prior to fission, Eq.(13).

The average prompt neutron multiplicities $\bar{\nu}_{p_i}$ for the successive fissioning nuclei in multiple-chance fission are obtained using Eqs. (27) and (33) of Ref. 1. It is important to calculate these $\bar{\nu}_{p_i}$ values accurately as they strongly weight the corresponding prompt fission neutron spectra $N_i(E)$. These spectra are obtained using Eqs. (22) - (28) of Ref. 1., leading to Eq. (1) of the present work.

Using the formalism summarized above, the total prompt fission neutron spectrum due to first-, second-, and third-chance fission events is given in the laboratory system by

$$\begin{aligned} N(E) = \{ & P_{f_1}^A\, \bar{\nu}_{p_1}\, N_1(E) + P_{f_2}^A\, [\phi_1(E) + \bar{\nu}_{p_2}\, N_2(E)] \\ & + P_{f_3}^A\, [\phi_1(E) + \phi_2(E) + \bar{\nu}_{p_3}\, N_3(E)]\} \,/ \\ & [P_{f_1}^A\, \bar{\nu}_{p_1} + P_{f_2}^A\, (1 + \bar{\nu}_{p_2}) + P_{f_3}^A\, (2 + \bar{\nu}_{p_3})]\,, \end{aligned} \tag{15}$$

where E is the energy of the emitted nuetron and A is the mass number of the fissioning compound nucleus. The first term of this equation is the first-chance fission component; the second and third terms are the second-chance fission component; and the fourth, fifth, and sixth terms are the third-chance fission component of the spectrum. The evaluation of Eq. (15) for the n + ^{235}U system, with incident neutron energies in the range 0 MeV ≤ E_n ≤ 15 MeV, is performed using input quantities given and tested in Ref. 1. The resulting fission spectrum matrix $N(E,E_n)$ is discussed next.

III. B. Results

The prompt fission neutron spectrum matrix $N(E,E_n)$ for the n + ^{235}U system is shown in Figs. 8 and 9. In Fig. 9, the ratio matrix

$$R(E,E_n) = \frac{N(E,E_n)}{N(E,0)} \qquad (16)$$

is shown to enhance fine details of $N(E,E_n)$ by renormalization to the thermal spectrum $N(E,0)$.

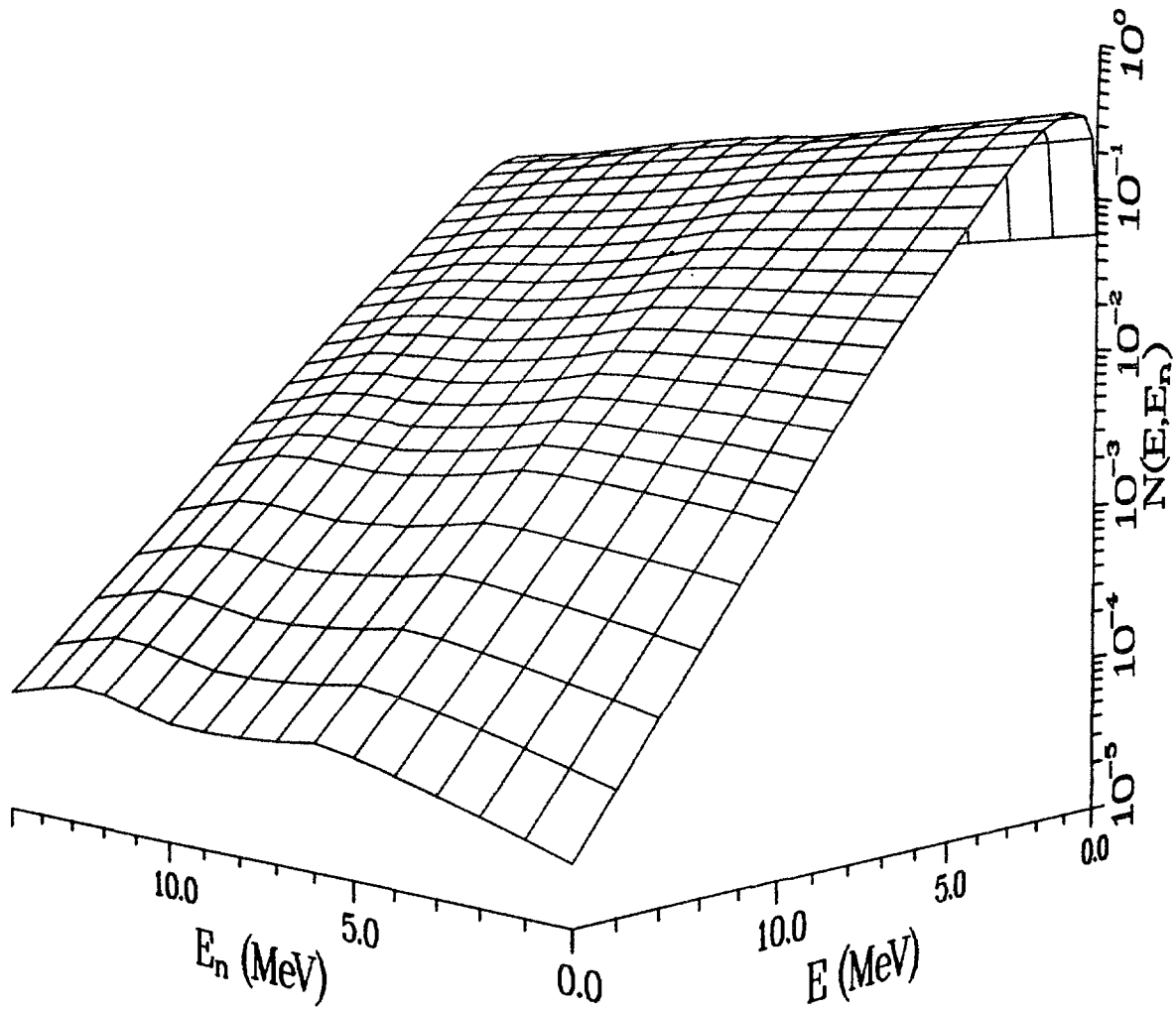

Fig. 8. Prompt fission neutron spectrum matrix $N(E,E_n)$ for the neutron-induced fission of ^{235}U as a function of incident neutron energy E_n and emitted neutron energy E.

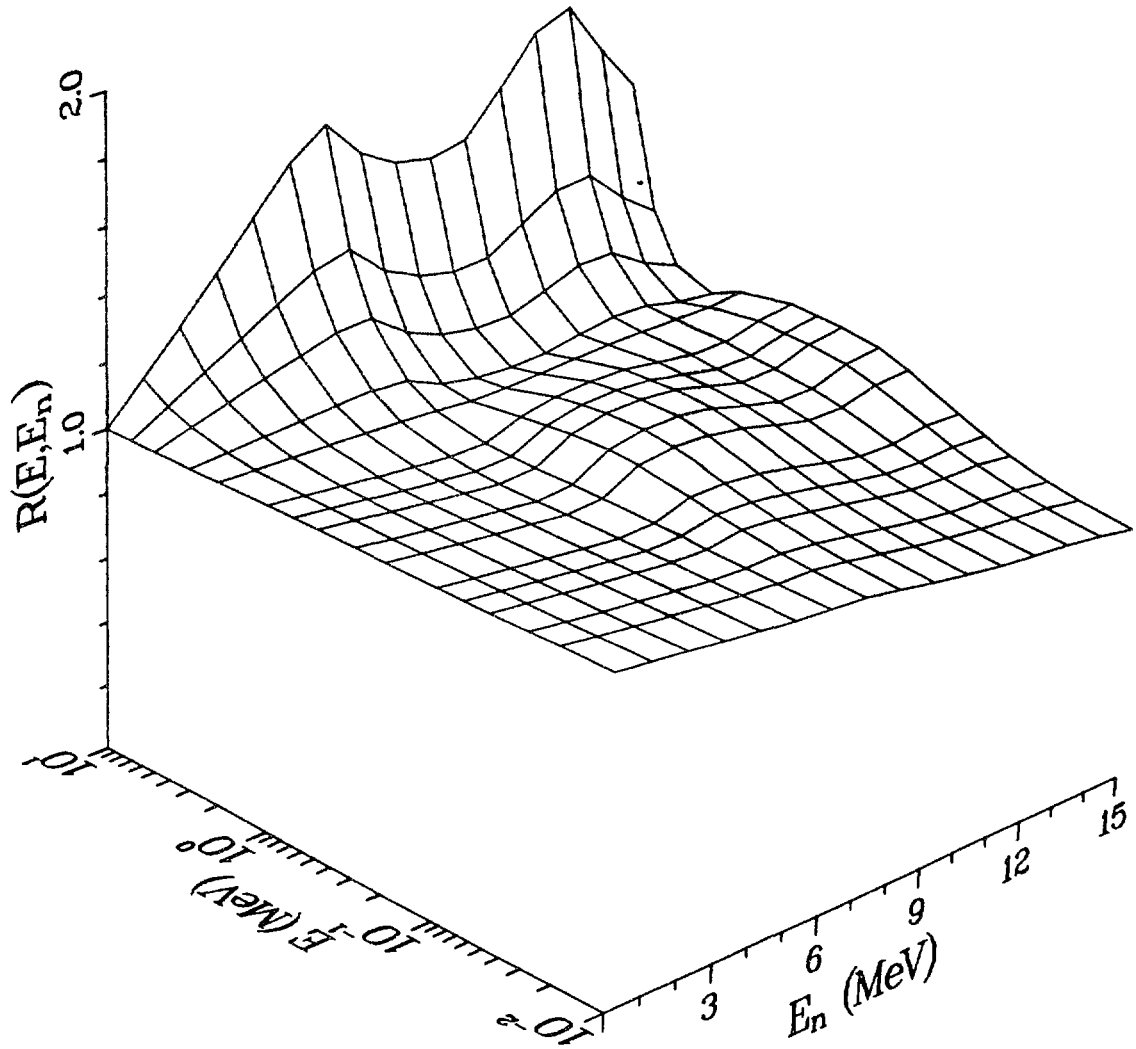

Fig. 9. Prompt fission neutron spectrum ratio matrix $R(E,E_n) = N(E,E_n)/N(E,0)$ corresponding to the matrix shown in Fig. 8.

These two figures clearly illustrate the dependence of the matrix upon incident energy E_n, particularly in the tail regions corresponding to high secondary neutron energy, and in the peak regions corresponding to the most probable secondary neutron energy. In the tail regions, E > ~ 5 MeV, the spectra become harder with increasing E_n. However, as E_n increases beyond about 6 MeV, the tail regions soften somewhat because part of the nuclear excitation energy of the compound fissioning nucleus is dissipated by the emission of a neutron prior to fission. This softening is observed again as E_n increases just beyond 13 MeV, where the threshold for the emission of two neutrons prior to fission occurs. A similar behavior is observed in the peak regions of the spectra, E ~ 1 MeV, except that here the transitions from first-chance to second-chance fission, and second-chance to third-chance fission, are more abrupt than in the tail regions. There are suggestions of a *staircase effect* in the peak regions of the spectra and an *oscillatory effect* in the tail regions of the spectra, with increasing incident neutron energy E_n. Finally, at the lower secondary neutron energies, E < ~ 10 keV, the spectra are softer with increasing incident neutron energy as one expects because each spectrum (or vector) of the matrix is normalized to unity when integrated from zero to infinity.

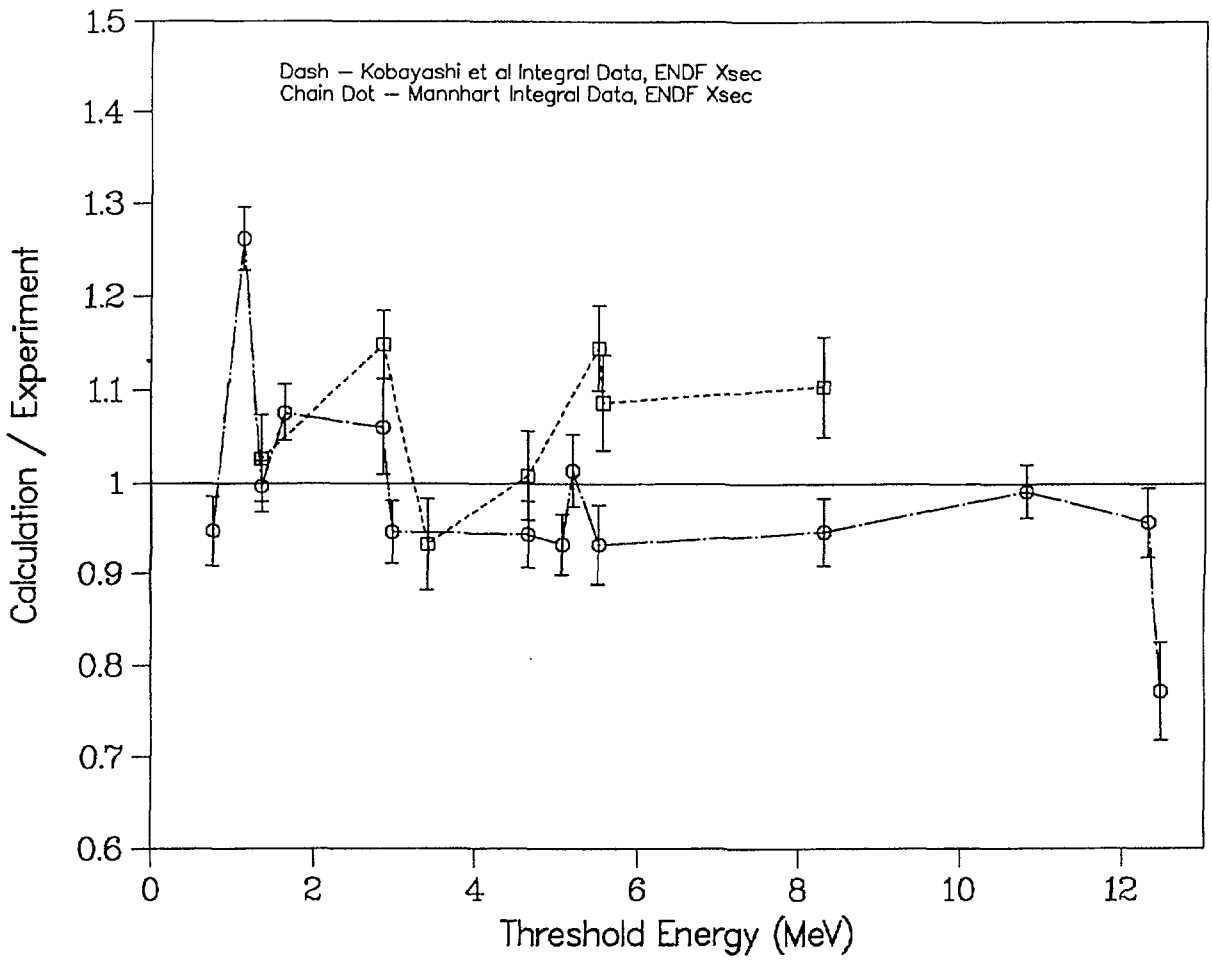

Fig. 10. Ratio of calculated to experimental integral cross section for the neutron field from the thermal-neutron-induced fission of ^{235}U, as a function of the threshold energy of the reaction. The calculated values are obtained using the present spectrum from Eqs. (1) and (15) in Eq. (12) together with ENDF/B-V pointwise cross sections.

We refer the reader to Ref. 1 for comparisons between experiment and various portions of the matrix $N(E,E_n)$ for the n + ^{235}U system that were separately calculated earlier. However, no comprehensive comparisons were made between calculated and experimental integral cross sections for this system in our earlier work. We therefore show such a comparison in Fig. 10 for calculated integral cross sections in the thermal field N(E,0) and corresponding experimental integral cross sections measured by Kobayashi and Kimura[23] and by Mannhart[24]. All of the calculations were performed using ENDF/B-V pointwise cross sections[15] in Eq. (12). The ratios of calculated integral cross sections using the present thermal spectrum to the corresponding experimental integral cross sections are plotted as a function of the threshold energy of the reaction, as before. The figure shows that the present thermal spectrum N(E,0) is compatible with the experimental integral cross sections for emitted neutron energies up to at least 12.5 MeV.

However, few integral cross section measurements have been reported for the n + ^{235}U field at other than thermal energy for the incident neutron inducing the fission. Therefore, in order to study the dependence on incident neutron energy, E_n, we calculate integral cross sections using the fission spectrum matrix $N(E,E_n)$ that we have determined for the n + ^{235}U system. First, we consider fictitious pointwise cross sections consisting of unit step functions at nine values of the

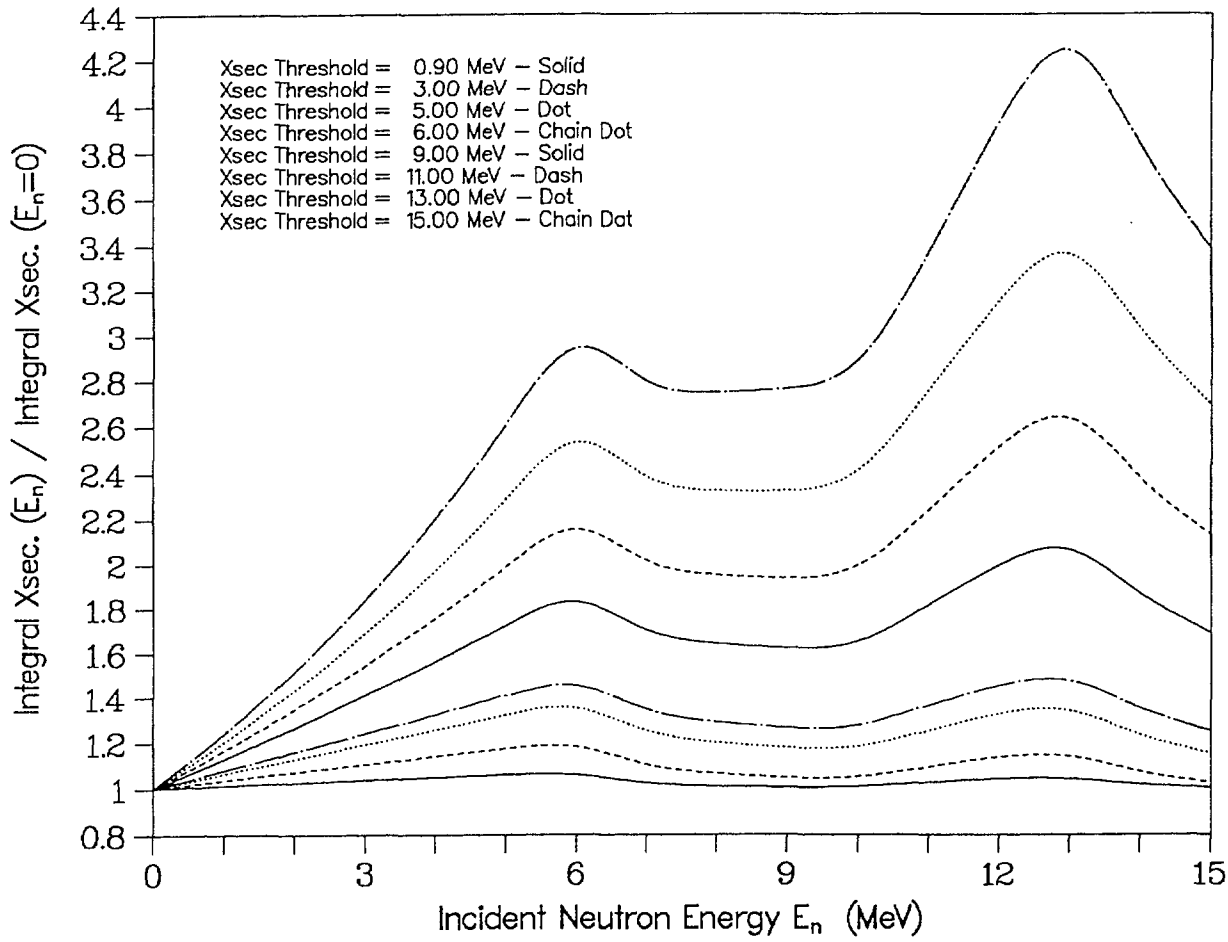

Fig. 11. Ratio of calculated integral cross section for the neutron field $N(E,E_n)$ from the neutron-induced fission of ^{235}U at incident energy E_n to that for incident energy E_n = 0, for eight unit step function cross sections with varying threshold energies.

threshold energy for the reaction (E_{th} = 0,0.9,3,5,6,9,11,13, and 15 MeV). Using the matrix $N(E,E_n)$ in Eq. (12) together with the array of nine step functions yields calculated integral cross sections as a function of the incident neutron energy inducing the fission. The integrated cross sections so obtained represent the net effect of each unit step function cross section in the presence of each energy dependent neutron field $N(E,E_n)$. We form the ratios of the calculated integral cross sections for incident neutron energy E_n to those for incident neutron energy $E_n = 0$ and plot these ratios as a function of E_n in Fig. 11. This figure shows a striking sensitivity to the features of the fission spectrum matrix $N(E,E_n)$ itself, shown in Figs. 8 and 9. In particular, each integral cross section increases with incident neutron energy until the threshold for second-chance fission is crossed, after which it decreases and then gradually increases again until the threshold for third-chance fission is crossed, after which it again decreases. We note that these effects are most pronounced for threshold energies above about 8 MeV. One immediately deduces from Fig. 11 that a crucial test of the calculated fission spectrum matrix $N(E,E_n)$, illustrated in Figs. 8 and 9, might be to measure a high threshold reaction integral cross section at, perhaps, four or five well-chosen incident neutron energies. While this would be a very difficult measurement, it would not be nearly as difficult as a measurement of the fission spectrum matrix itself.

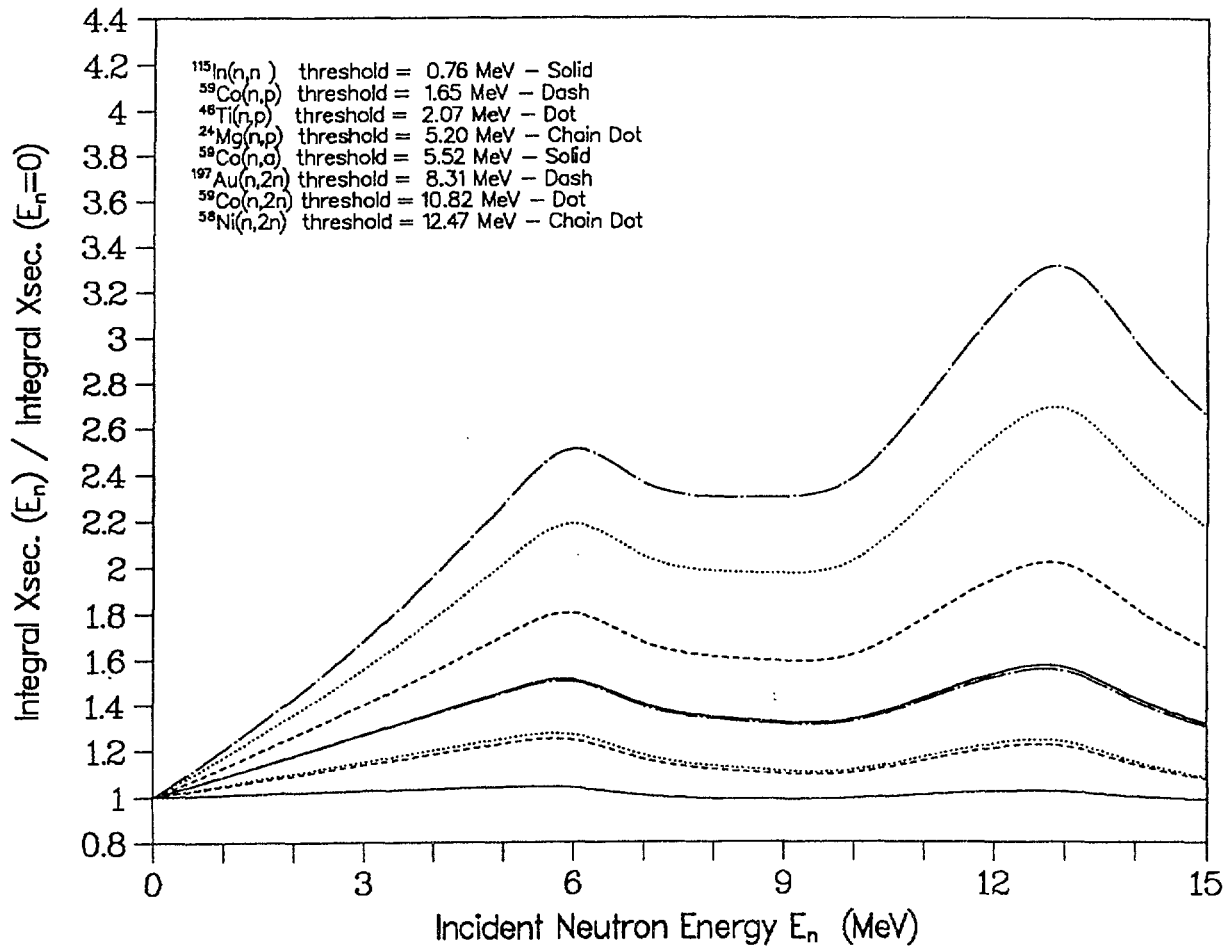

Fig. 12. Identical to Fig. 11 except that eight ENDF/B-V pointwise cross sections with different reaction threshold energies are used.

The suggestion of such a set of integral cross section measurements becomes more significant when real pointwise cross sections for specific reactions are used instead of unit step functions. Figure 12 is identical to Fig. 11 except that eight ENDF/B-V pointwise cross sections have been used in Eq. (12) together with the matrix $N(E,E_n)$. These cross sections span a range of threshold energies from 0.76 MeV to 12.47 MeV. Clearly, the striking sensitivity to the detail of $N(E,E_n)$ is again present for threshold energies above about 8 MeV. Thus, a crucial test of the calculated fission spectrum matrix $N(E,E_n)$ is indeed possible by *measuring the energy dependence of one of the high threshold integral cross sections* plotted in Fig. 12. For this purpose, as well as others, we list the values of the calculated integral cross sections as a function of incident neutron energy in Table I, for six of the reactions shown in Fig. 12, including the four highest threshold reactions.

TABLE I

INTEGRAL CROSS SECTIONS CALCULATED AS A FUNCTION OF THE ENERGY OF THE NEUTRON INDUCING FISSION

Incident Energy E_n (MeV)	Integral Cross Sections					
	$^{115}In(n,n')$	$^{59}Co(n,p)$	$^{59}Co(n,\alpha)$	$^{197}Au(n,2n)$	$^{59}Co(n,2n)$	$^{58}Ni(n,2n)$
0.0	180.1714	1.5176	0.1500	3.3120	0.2001	0.0032
1.0	181.8343	1.5877	0.1632	3.7310	0.2341	0.0039
2.0	183.4242	1.6575	0.1766	4.1737	0.2714	0.0046
3.0	184.9466	1.7269	0.1904	4.6395	0.3119	0.0054
4.0	186.4063	1.7960	0.2045	5.1278	0.3558	0.0063
5.0	187.8076	1.8647	0.2189	5.6381	0.4030	0.0073
6.0	187.2995	1.8903	0.2270	5.9727	0.4375	0.0081
7.0	181.2945	1.7645	0.2107	5.5590	0.4099	0.0076
8.0	178.7848	1.6977	0.2021	5.3492	0.3970	0.0074
9.0	178.1883	1.6689	0.1985	5.2796	0.3945	0.0074
10.0	178.9745	1.6764	0.2005	5.3764	0.4060	0.0077
11.0	181.6871	1.7543	0.2150	5.8896	0.4557	0.0088
12.0	184.2059	1.8361	0.2307	6.4575	0.5119	0.0101
13.0	184.1326	1.8494	0.2353	6.6727	0.5383	0.0107
14.0	180.2874	1.7269	0.2149	6.0416	0.4857	0.0097
15.0	178.3752	1.6361	0.1980	5.4804	0.4351	0.0086
Threshold Energy E_{th} (MeV)	0.76	1.65	5.52	8.31	10.82	12.47

IV. SCISSION NEUTRONS

In our calculations of the prompt fission neutron spectrum, we have neglected any possible contributions from neutrons emitted near the scission point. This is partly for ease of computation and partly because previous studies of scission neutrons have provided no conclusive evidence for their existence.

In some previous experimental studies, the energy and angular distributions of the neutrons observed in the spontaneous fission[25-32] of ^{252}Cf and in the neutron-induced fission[33] of ^{235}U have been decomposed into components arising from isotropic emission from the moving fission fragments and an isotropic component in the laboratory system, which was assumed to arise from scission neutrons. However, the most likely mechanism for the production of scission neutrons--the dynamical ejection of neutrons in the neck region[34-36] by a rapidly rising single-neutron potential--should lead to neutrons that are predominantly emitted at 90° relative to the direction of

the fission fragments[37] rather than isotropically in the laboratory system. Use of such scission-neutron distributions peaked at 90° would yield fewer scission neutrons[37] than the 5.6 to 25 % that were obtained with isotropic scission-neutron distributions.[25-33] The extracted numbers of scission neutrons would also be affected if the slight anisotropy in emission from the moving fragments, which arises from their angular momentum of typically several $\hbar$, were taken into account.[38,39]

Other mechanisms for the emission of scission neutrons have also been considered. One of these is the statistical evaporation of neutrons from fragments near scission before they are fully accelerated,[40] which would lead to angular distributions in the laboratory system that are more nearly isotropic than those corresponding to evaporation from fully accelerated fragments. At the opposite extreme, the propagation throughout the fragments of shock waves resulting from the snapping of an elongated neck could lead to the emission of nearly monoenergetic neutrons in the directions of the moving fragments.[41] Similar catapult mechanisms[42,43] have also been considered within the time-dependent Hartree-Fock approximation.

In addition to the above theoretical uncertainties, more recently measured angular distributions for the spontaneous fission[44,45] of ^{252}Cf disagree significantly with earlier data for laboratory neutron energies greater than about 4 MeV. These new data are consistent with the assumption that all neutrons are emitted from the fully accelerated fragments.[44,45]

Although we feel that the neglect of scission neutrons is at this stage well justified, this topic deserves further theoretical and experimental study since it could reveal important dynamical information concerning neck rupture in fission.

V. CONCLUSIONS

We have considered three topics in the refinement of our original calculations of prompt fission neutron spectra. On the first topic, an improved calculation of the *standard* prompt fission neutron spectrum N(E) from the spontaneous fission of ^{252}Cf, it has been shown that the preliminary calculations using the refined model calculation embodied in Eq. (11) yields *improved agreement* with the experimental spectrum of Poenitz and Tamura[13] and *unsatisfactory agreement* with the evaluated spectrum of Mannhart.[14] The discrepancy probably arises from two sources. On the one hand, the spectrum of Poenitz and Tamura is one of seven experiments used in the Mannhart evaluation. Therefore, the differences between the various experiments making up the evaluation are likely to be at least as large as the difference between the present calculation and the evaluation. On the other hand, the convergence of the refined model calculation with the number of fragments included must be demonstrated. In addition, the physical effects of (a) center-of-mass anisotropy, and (b) explicit gamma-ray deexcitation should both be taken into account.

On the second topic, a complete example of the incident neutron energy dependence of the prompt fission neutron spectrum from the neutron-induced fission of ^{235}U, the matrix $N(E,E_n)$, has been calculated and studied. It has been observed that the surface of this fission spectrum

matrix displays a remarkable sensitivity to the detail of multiple-chance fission. In addition, a strong sensitivity of calculated integral cross sections to this detail has been observed. In fact, a measurement of the energy dependence of high threshold integral cross sections in the energy-dependent neutron field from the n + ^{235}U fission reaction would provide a crucial test on the structure of the matrix N(E,E_n).

On the third topic, an assessment of the scission neutron component of the prompt fission neutron spectrum, the most likely mechanism for the production of scission neutrons has been identified. However, we do not calculate the scission neutron component of N(E) using this mechanism at this time due to the lack of *conclusive* experimental evidence as to its existence.

REFERENCES

1. D. G. Madland and J. R. Nix, Nucl. Sci. Eng. 81, 213 (1982).

2. D. G. Madland and J. R. Nix, "*Calculation of the Prompt Neutron Spectrum and Average Prompt Neutron Multiplicity for the Spontaneous Fission of ^{252}Cf*," Proc. Int. Conf. Nuclear Data for Sci. and Tech., Antwerp, Belgium, 1982 (D. Reidel Pub. Co., Boston, 1983), p. 473.

3. D. G. Madland and J. R. Nix, "*Prompt Fission Neutron Spectra and Average Prompt Neutron Multiplicities*," NEANDC Specialists' Meeting on Yields and Decay Data of Fission Product Nuclides, Brookhaven National Laboratory, Upton, N.Y., 1983, R. E. Chrien and T. W. Burrows, Eds. (BNL 51778, 1984), p. 423.

4. D. G. Madland, R. J. LaBauve, and J. R. Nix, "*Differential and Integral Comparisons of Three Representations of the Prompt Neutron Spectrum for the Spontaneous Fission of ^{252}Cf*," Proc. Advisory Group Mtg. Nuclear Standard Ref. Data, Geel, Belgium, 1984 (IAEA-TECDOC-335, Vienna, 1985), p. 267.

5. D. G. Madland, R. J. LaBauve, and J. R. Nix, "*Comparisons of Four Representations of the Prompt Neutron Spectrum for the Spontaneous Fission of ^{252}Cf*," Proc. Int. Conf. Nuclear Data for Basic and Applied Sci., Santa Fe, N.M., 1985 (Gordon and Breach, N. Y., 1986), Vol. 2, p. 1445.

6. G. Audi and A. H. Wapstra, At. Data Nucl. Data Tables, to be published.

7. P. Möller and J. R. Nix, "*Nuclear Masses from a Unified Macroscopic-Microscopic Model*," At. Data Nucl. Data Tables, in press.

8. H. W. Schmitt, J. H. Neiler, and F. J. Walter, Phys. Rev. 141, 1146 (1966).

9. F. D. Becchetti and G. W. Greenlees, Phys. Rev. 182, 1190 (1969).

10. J. P. Unik *et al.*, "*Fragment Mass and Kinetic Energy Distributions for Fissioning Systems Ranging from Mass 230 to 256*," Proc. Third IAEA Symp. on Physics and Chemistry of Fission, Rochester, N.Y., 1973 (IAEA, Vienna, 1974), Vol. II, p. 19.

11. W. N. Reisdorf *et al.*, Nucl. Phys. A177, 337 (1971).

12. R. L. Walsh and J. W. Boldeman, Nucl. Phys. A276, 189 (1977).

13. W. P. Poenitz and T. Tamura, "*Investigation of the Prompt-Neutron Spectrum for Spontaneously-Fissioning ^{252}Cf*," Proc. Conf. on Nuclear Data for Sci. and Tech., Antwerp, Belgium, 1982 (D. Reidel, Dordrecht, 1983), p. 465.

14. W. Mannhart, "*Evaluation of the Cf-252 Fission Neutron Spectrum Between 0 MeV and 20 MeV,*" Proc. Advisory Group Mtg. Neutron Sources, Leningrad, USSR, 1986 (IAEA-TECDOC-410, Vienna, 1987), p. 158.

15. M. R. Bhat, in "*ENDF/B Summary Documentation,*" Brookhaven National Laboratory report BNL-NCS-17541 (ENDF-201), Brookhaven National Laboratory, July 1979.

16. P.G. Young, "*Calculation and Evaluation of n + ^{169}Tm Reactions from 10^{-5} eV to 30 MeV,*" Los Alamos National Laboratory report Applied Nuclear Science Research and Development Progress Report (in preparation).

17. B. P. Bayhurst *et al.*, Phy. Rev. C 12, 451 (1975).

18. W. Mannhart and H. Vonach, Z. Physik A272, 279 (1975).

19. K. Kobayashi *et al.*, "*Measurement of Average Cross Sections for Some Threshold Reactions of Ti, Cr, and Pb in the Californium-252 Spontaneous Fission Neutron Spectrum Field,*" Annual Reports of the Research Reactor Institute, Kyoto University, Kyoto, Japan, Vol. 17, p. 15, 1984.

20. W. Mannhart, "*Recent Experiments on Cf-252 Spectrum-Averaged Neutron Cross Sections,*" Proc. Fifth ASTM-EUATOM Symposium on Reactor Dosimetry, Geesthacht, Federal Republic of Germany, September 24-28, 1984.

21. W. Mannhart, "*The High Energy Portion of the Cf-252 Neutron Spectrum Deduced from Integral Experiments,*" Proc. Advisory Group Mtg. Neutron Sources, Leningrad, USSR, 1986 (IAEA-TECDOC-410, Vienna, 1987), p. 194.

22. W. Mannhart, "*Californium-252 Spectrum Averaged Neutron Cross-Sections,*" in Handbook on Nuclear Activation Data, International Atomic Energy Agency, Vienna, 1987, Sec. 2-4.

23. K. Kobayashi and Il Kimura, in Proc. Third ASTM-EURATOM Symposium on Reactor Dosimetry, Ispra, Italy, 1979, Vol. 2, p. 1004.

24. W. Mannhart, "*Spectrum-Averaged Neutron Cross Sections Measured in the U-235 Fission-Neutron Field in MOL,*" Proc. Fifth ASTM-EURATOM Symposium on Reactor Dosimetry, Gesthacht, Federal Republic of Germany, September 24-28, 1984.

25. H. R. Bowman, S. G. Thompson, J. C. D. Milton, and W. J. Swiatecki, Phys. Rev. 126, 2120 (1962).

26. M. V. Blinov, N. M. Kazarinov, and I. T. Krisyuk, Yad. Fiz. 16, 1155 (1972).

27. C. J. Bishop, I. Halpern, R. W. Shaw, Jr., and R. Vandenbosch, Nucl. Phys. A198, 161 (1972).

28. Z. Fraenkel, I. Mayk, J. P. Unik, A. J. Gorski, and W. D. Loveland, Phys. Rev. C 12, 1809 (1975).

29. V. M. Piksaikin, P. P. D'yachenko, and L. S. Kutsaeva, Yad. Fiz. 25, 723 (1977).

30. Yu. S. Zamyatnin, D. K. Ryazanov, B. G. Basova, A. D. Rabinovich, and V. A. Korostylev, Yad. Fiz. 29, 595 (1979).

31. P. Riehs, Acta Phys. Austriaca 53, 271 (1981).

32. H. Märten, D. Neumann, and D. Seeliger,"*Theoretical Analysis of the Cf-252 Fission Neutron Spectrum,*" in Proceedings of the IAEA Consultants' Meeting on the U-235 Fast-Neutron Fission Cross-Section, and the Cf-252 Fission Neutron Spectrum, Smolenice, Czechoslovakia, 1983, IAEA Report No. INDC (NDS)-146 (1983), p. 199.

33. S. S. Kapoor, R. Ramanna, and P. N. Rama Rao, Phys. Rev. 131, 283 (1963).

34. R. W. Fuller, Phys. Rev. 126, 684, (1962).

35. I. Halpern, Annu. Rev. Nucl. Sci. 21, 245 (1971).

36. Y. Boneh and Z. Fraenkel, Phys. Rev. C 10, 893 (1974).

37. J. R. Nix, D. G. Madland, and A. J. Sierk, *"Effect of Fission Dynamics on the Spectra and Multiplicities of Prompt Fission Neutrons,"* in Proceedings of the International Conference on Nuclear Data for Basic and Applied Science, Santa Fe, New Mexico, 1985 (Gordon and Breach, New York, 1986), Vol. 1, p. 263.

38. H. Märten, D. Richter, D. Seelinger, and W. Neubert, in Proceedings of the Nuclear Physics Symposium, Gaussig, German Democratic Republic, 1985, to be published.

39. H. Märten, *"Theoretical Description of the Cf-252 Fission Neutron Spectrum,"* in Proceedings of an Advisory Group Meeting on Properties of Neutron Sources, Leningrad, USSR, 1986, IAEA Report No. IAEA-TECDOC-410 (1987), p. 144.

40. G. A. Pik-Pichak, Yad. Phys. 10, 321 (1969).

41. V. S. Stavinsky, Zh. Eksp. Teor. Fiz. 36, 629 (1959).

42. P. Mädler, Z. Phys. A321, 343 (1985).

43. B. Milek, R. Reif, and J. Révai, Phys. Rev. C 37, 1077 (1988).

44. C. Budtz-Jørgenson and H. H. Knitter, Commission of the European Communities, CBNM Geel, Belgium, preprint (no date).

45. C. Budtz-Jørgenson , H. H. Knitter, Ch. Straede, and F. J. Hambsch, in Proceedings of the Workshop on Nuclear Dynamics IV, Copper Mountain, Colorado, 1986, National Technical Information Service Report No. CONF-860270, UC-34C, INC-40007-37 (1986), p. 17.

DIFFERENTIAL AND INTEGRAL CHARACTERISTICS OF PROMPT FISSION NEUTRONS IN THE STATISTICAL THEORY

B. F. Gerasimenko, V. A. Rubchenya
V. G. Khlopin Radium Institute,
Leningrad, USSR

Theoretical investigation of differential and integral characteristics of prompt fission neutrons (PFN) is of great interest, since the comparison of calculated characteristics with experimental data makes it possible to refine the parameters of theoretical models for PFN emission and to reveal the effect of individual fragment properties on these characteristics. One of the most current sources of experimental information about PFN characteristics of low energy fission is spontaneously fissionable ^{252}Cf, whose integral PFN-spectrum is studied the most completely and used as a neutron standard.

The investigations of PFN spectra of low energy fission of nuclei have shown that the main part of PFN is emitted by heated, fully accelerated fragments in accordance with the equilibrium statistics laws /1-8/ and that the nonequilibrium neutron emission rate seems to be less than 10 % of total number of neutrons emitted per fission event /1, 5, 6, 8/.

Numerous calculations of differential and total PFN spectra for the case of ^{252}Cf spontaneous fission have been performed by using of different theoretical models /9-18/, but in many of them a number of factors affecting the complex PFN emission process has been neglected or substantial simplifications have been used roughening the results of the calculations. It has been found at present that the use of Hauser-Feshbach statistical theory is the most consistent and promissing approach to the calculation of both spectra and PFN characteristics. On the basis of this approach a statistical model for calculation of differential PFN characteristics of low energy fission has been proposed /15,, 16/, which was systematically used to calculate the spectra and fission neutron multiplicity distributions /4, 7, 14-17/. In

order to take into account the anisotropy effects arising at PFN emission from fragments the model has been improved. The improvement allowed to evaluate consistently the anisotropy of angular distributions of neutrons from individual fragments (in center-of-mass system (CMS)) of fragments and to take into account its effect on the shape of PFN spectra in laboratory system.

Model

The above mentioned statistical model used is described in detail in /15, 16/. Here we summarize briefly its basic assumptions and its main features only.

It was assumed in the model, that PFN are emitted only from fully accelerated heated fragments. This assumption corresponds to the fact, that the fragment excited state lifetime τ_c and the time of fragment acceleration τ_{acc} relate as $\tau_{acc} \ll \tau_c$ and furthermore that the condition $\tau_{diss} < \tau_{acc}$ is valid as well.

In the latter inequality τ_{diss} is the time of transformation of fragment collective excited state energy to heat energy of fragment. In the model cascade character of PFN emission from fragments is taken thoroughly into account. The fragment excitation energy distribution, fragment spin-, fragment kinetic energy distributions were taken into account as well as the fragment charge and mass distributions. The fragment shape was assumed to be spherical, the angular anisotropy of PFN emission in CMS of fragment in primary version of the model was neglegted. For the level density of excited fragment the Fermi-gas model expression /19/ is used. This expression takes into account shell structure of fragments and pair correlations in them. Neutron binding energy in a fragment was calculated according to /20/. The neutron transmission coeffecients and analogous coefficients for γ-radiation are calculated by using of optical model and of photoabsorbtion cross-sections of dipole γ-quanta respectively. The optical model parameters were taken from /21/, for photoabsorbtion cross-section the Lorenz form with parameters from /22, 23/ is used. Fragment spin distribution parameter are chosen in the same way as in /16/. The initial

distribution $Po(E^*, A, Z)$ of excitation energy E^* of the primary fragment (A, Z) is assumed to be Gaussian with parameters specified according to /16/.

As mentioned above, the hypothesis of isotropic neutron emission in CMS covers no more than 90-95 % of total number of PFN per fission. The remaining part of PFN showing itself as an increased neutron yield in the low energy region (in laboratory system of coordinates (LSC)) is considered as a non-statistical component of PFN. As it has been shown in /24/, the CMS angular distribution of particle of kinetic energy emitted from excited nucleus must be anisotropic if both the particle and the nucleus have their anqular moments different from zero. Then in the first order of approximation, as it has been shown in /24/, the angular distribution of emitted particle is proportional to $(1 + b\cos^2\theta_{CMS})$, where θ_{CMS} is the particle emission angle in CMS relative to a specified direction in space, "b" is anisotropy parameter. In /24/ quasi-classical evaluation of "b" was made as well. As the calculation in /17/ has shown, the above mentioned semiempirical account of anisotropy of neutron CMS-angular distributions improves the agreement of calculated ^{252}Cf PFN integral spectrum with experimental one in the region of low energy of neutrons. Therefore the consistent account of anisotropy of CMS-angular distribution of PFN on the basis of statistical Hauser-Feshbach theory would facilitate the more precise evaluation of non-statistical component in PFN emission. For these reasons we improved the model described in /16/ by taking into consideration the angular dependence in the expression for CMS-double differential spectrum of PFN. The proper results of /25, 26/ were used. Now the expression for CMS double differential spectrum of a neutron emitted at angle θ_{CMS} to the fission axis from a fragment of mass number A, charge Z and of kinetic energy E_k with averaging over excitation energy E^* and spin of the fragment includes the expansion into Legendre polynomials $P_k(\cos\theta_{CMS})$:

$$\frac{d^2N(\varepsilon,\theta_{CMS}, A, Z, E_k)}{d\, d\theta_{CMS}} \propto \int dE^* \sum_J P(E^*, J, A, Z, E_k) \sum_{K'} R_{k'}(E^*, J, A, Z, \varepsilon) P_k(\cos\theta_{CMS}) \quad (1)$$

where K' = 0, 2, 4,... and

$$R_{K'}(E^*, J, A, Z, \varepsilon) = \frac{\sum_{I',l,j} \rho(E^* - \varepsilon - B_n, A-1, Z, I') \times}{\Gamma_n^t(A, Z, E^*, J) + \frac{\times T_{lj}(\varepsilon)\eta_{K'}(j, I', J)}{+\Gamma_\gamma^t(A, Z, E^*, J)}} \quad (2)$$

Here, as in /15, 16/, $P(E^*, J, A, Z, E_k)$ is the fragment excitation energy- and spin distribution; I' is the spin of residual nucleus $(A-1, Z)$; $\rho(E^*, J, A, Z)$ is the level density in nucleus (A, Z) with excitation energy E^* and spin J; $T_{lj}(\varepsilon)$ is the transmission coefficients of a neutron of CMS-energy ε, of orbital moment l and of total moment j; Γ_n^t and Γ_γ^t are the total neutron and the total radiation widths, respectively; the coefficients $\eta_{K'}(j, I', J)$ can be expressed in terms of the Clebsh-Gordan coefficients of vectorial addition of moments $\vec{j}$, $\vec{I}'$, $\vec{J}$ /27/ with $\vec{j} = \vec{l} + \vec{S}$, $\vec{J} = \vec{I}' + \vec{j}$; $\vec{S}$ is the neutron spin. The values of $P(E^*, J, A, Z)$, (E^*, J, A, Z), $T_{lj}(\varepsilon)$, Γ_n^t and Γ_γ^t are calculated in the same manner as in the works /15, 16/, and the averaging over fragment kinetic energy E_k is performed similarly to /16/.

Results and discussion

To calculate PFN differential and integral characteristics following to the statistical model described in /15, 16/, the code "SCØFIN" /28/ was developed and adapt for BESM-6 computer. The spectra of PFN and the PFN multiplicity distributions for individual fragments of ^{252}Cf spontaneous fission were calculated. The comparison of calculated spectra of individual fragment and integral PFN spectrum with experimental ones has been performed in /3, 4, 7, 14-17/. The comparison showed, that the model reproduces adequately both the mean energies and the shape of experimental spectra. Calculated CMS spectra of neutrons averaged over E_k had close temperatures and were approximately similar, which agreed with experimental results /1/.

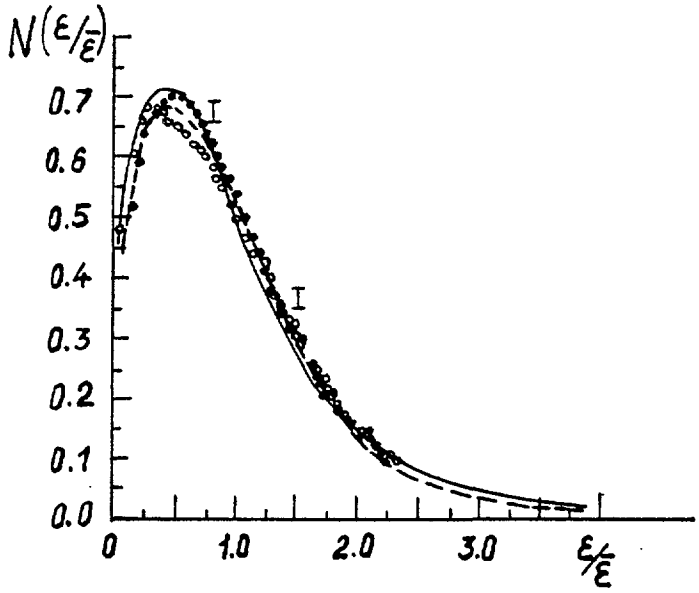

Fig. 1. Calculated and experimental spectra of PFN from ^{136}I fragment of ^{252}Cf spontaneous fission at different values of kinetic energy E_k of the pair.

• - experiment /29/, E_k = 172 MeV;
∘ - experiment /29/, E_k = 208 MeV;
——— - calculation (this work), E_k = 172 MeV;
— — — - calculation (this work), E_k = 208 MeV.

Subsequent experiments /4, 5, 29/ have shown that with the growth of difference in the value of excitation energy of fragments with a definite mass the shape of CMS spectra of these fragments deviates from "standard" one, particularly in the region of low CMS energies of neutrons $\varepsilon \lesssim \bar{\varepsilon}$. This was observed, for example, for fragments greatly differing in kinetic energy. Our more detailed calculations of CMS spectra of PFN from such fragments confirmed the above-mentioned deviation within the limits of input data uncertainty. Fig. 1 shows an example of calculated CMS spectra of neutrons from the ^{136}I fragment compared with the experimental data of /29/. The spectra are shown for two values of total kinetic energy E_k of fragments: 172 and 208 MeV. In calculations corresponding values of $\bar{E}^*$ were determined within the framework of the model /15, 16/ using the values of $\bar{\nu}$ and $\bar{\varepsilon}$ for this fragment from the work /29/. The values of dispersions $\sigma^2_{E^*}(A, E_k)$ were taken from /30/. It is seen from the Fig. 1 that in the region of neutron energies

$\varepsilon \lesssim \bar{\varepsilon}$ experimental spectra differ from one another; corresponding calculated spectra agree, in the main, with experimental ones within the limits of error. Some discrepancy between calculated and experimental spectra in the region $\varepsilon < 0.5\bar{\varepsilon}$ taking into consideration the sensitivity of calculations to the accuracy of input data /15/ seems to be connected with the uncertainty in the E^* and $\sigma^2_{E^*}$ values.

Another PFN characteristic important for understanding of the fission neutron emission mechanism is the multiplicity distribution of PFN from individual fragments. In contrast to the data on spectra the experimental data on multiplicity distributions of PFN from individual fragments of low energy fission, in particular of ^{252}Cf fission, are few in number: in this respect we can mention the well-known work /30/ and the works /31, 32/. The data of /31, 32/ give the possibility to compare the calculated multiplicity distributions of prompt neutrons from individual fragments of ^{252}Cf spontaneous fission obtained using the statistical model /15, 16/ with experimental ones. This is of particular interest considering that within the framework of most other theoretical models /11, 13/ used for calculation of fission neutron spectra consecutive calculation of multiplicity distributions of PFN from individual fragments has been unsuccessful. The experimental data presented in /31, 32/ make it possible to evaluate dispersions $\sigma^2_{E^*}(A)$ of excitation energy distributions for a number of ^{252}Cf spontaneous fission fragments and to obtain mean values of $\bar{\nu}(A)$ for these fragments. We have made calculations according to the statistical model /15, 16/ of multiplicity distributions for PFN from individual fragments using the evaluated dispersions $\sigma^2_{E^*}(A)$ and the values of $\bar{\nu}(A)$ taken from /31, 32/. Fig. 2 shows calculated multiplicity distributions $P_A(\nu)$ of prompt neutrons from several most probable fragments (^{108}Mo, ^{112}Ru, ^{144}Ba, ^{140}Xe) of ^{252}Cf spontaneous fission. For compactness of representation the distributions are given in the form of accumulated probability F_A $(0 \leq \nu \leq K)$; F_A $(0 \leq \nu \leq K) = \sum_{\nu=0}^{K} P_A(\nu)$, $K \leq \nu_{max}(A)$; $\nu_{max}(A)$ - maximum number of neutrons from the

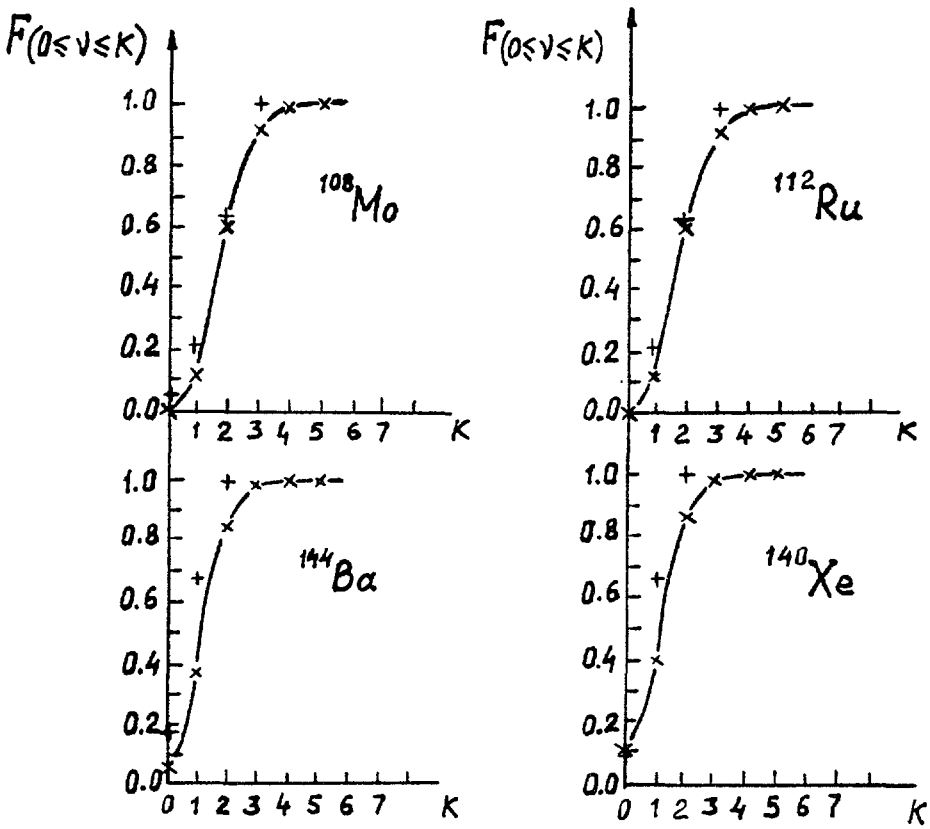

Fig. 2. Calculated multiplicity distributions of PFN from individual fragments of ^{252}Cf spontaneous fission. The distributions are given in the form of accumulated probability F_A $(0 \leq \nu \leq K)$,

$$F_A\ (0 \leq \nu \leq K) = \sum_{\nu=0}^{K} P_A(\nu).$$

x - calculation from the statistical model (this work);

+ - binomial distribution with the parameters obtained with the values of $\bar{\nu}(A)$ and $\sigma_\nu^2(A)$ of calculated distributions.

fragment with mass number A obtained during the calculation. For comparison in the same Fig. the binomial distributions are shown with parameters derived from $\bar{\nu}_{calc.}(A)$ and $\sigma^2_{\nu_{calc.}}(A)$ of calculated $P_A(\nu)$ distributions. As it is seen from Fig. 2, calculated multiplicity distributions are not approximated by binomial ones. Fig. 3 gives the comparison of dispersions $\sigma^2_{\nu_{calc.}}(A)$ of calculated PFN

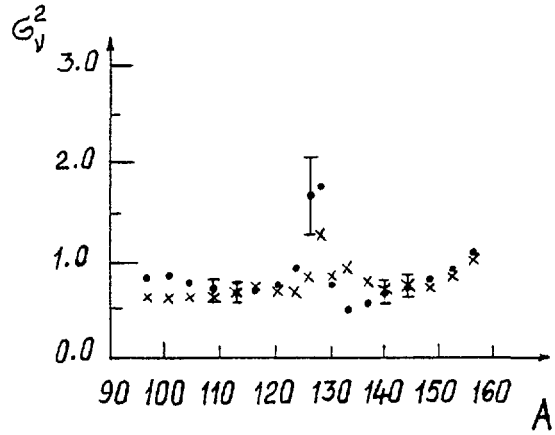

Fig. 3. Disperssion $\sigma_\nu^2(A)$ of the number of neutrons emitted from individual fragments of ^{252}Cf spontaneous fission.

• - evaluation according to the data of /31, 32/;
x - calculation from the statistical model (this work).

multiplicity distributions for a number of ^{252}Cf spontaneous fission fragments with corresponding experimental data from /31, 32/. It can be seen from Fig. 3 that the calculated values of $\sigma^2_{\nu_{calc.}}(A)$ are in good agreement with experimental ones. The values of $\bar{\nu}(A)$ taken from /31, 32/ are also well reproduced in calculations. It should be noted that CMS spectra of neutrons that we have calculated using the values of $\sigma^2_{E*}(A)$ and $\bar{\nu}(A)$ from /31, 32/ differ insignicantly from analogous spectra calculated earlier in /15/. This means that using the statistical model described in /15, 16/ one can described consistently the spectra and multiplicity distributions of PFN from individual fragments.

The problem of anisotropy value of PFN angular distributions in CMS of fragments and that of evaluation of its effect on differential and integral PFN spectra are of particular interest in studying the PFN emission mechanism. The authors calculated spectra and angular distributions of PFN from individual fragments of ^{252}Cf spontaneous fission with allowance for angular anisotropy of neutron emission in CMS of fragments using the exp essions (1) and (2). Spin values of primary fragments were taken according to the results of /33, 34/, other parameters of the model were chosen as in /15, 16/. The calculations have shown that the

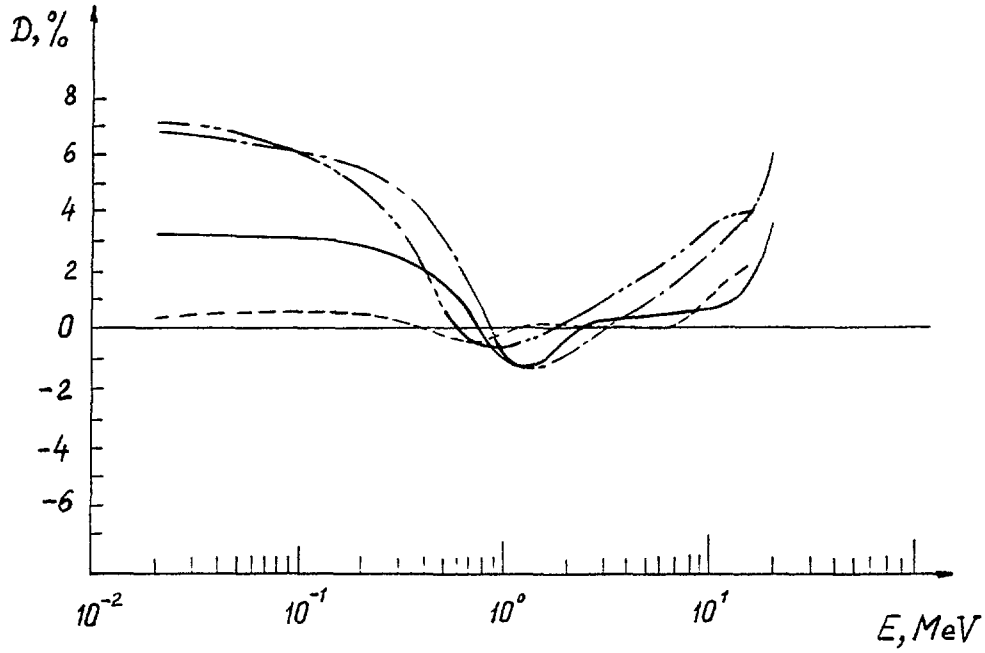

Fig. 4. Calculated LS – spectra of PFN from the fragments ^{108}Mo and ^{144}Ba of ^{252}Cf spontaneous fission obtained taking into account anisotropy of PFN emission in CMS of fragment.

The spectra are presented as a ratio to corresponding calculated LS – spectra obtained neglecting anisotropy of PFN emission in CMS of fragment.

——— ^{108}Mo
– – – – ^{144}Ba
} b = b(E);
——·—— ^{108}Mo, b = 0.1;
——··—— ^{144}Ba, b = 0.1.

anisotropy coefficient b for PFN angular distributions in CMS of fragments depends substantially on the neutron energy and the mode of fission. Mean values $\bar{b}$ of calculated anisotropy coefficients satisfy the condition $\bar{b} \leqslant 0.07$ which agrees with the latest experimental evaluations /35/. Fig. 4 shows calculated LS - spectra of PFN from ^{108}Mo and ^{144}Ba fragments pertaining to the group of most probable fragments of ^{252}Cf spontaneous fission. LS - spectra are obtained from CMS - spectra calculated taking into account the angular anisotropy depending on CMS neutron energy according to (1) and (2). In Fig. 4 LS - spectra are presented as a ratio to LS - spectra obtained on the base of

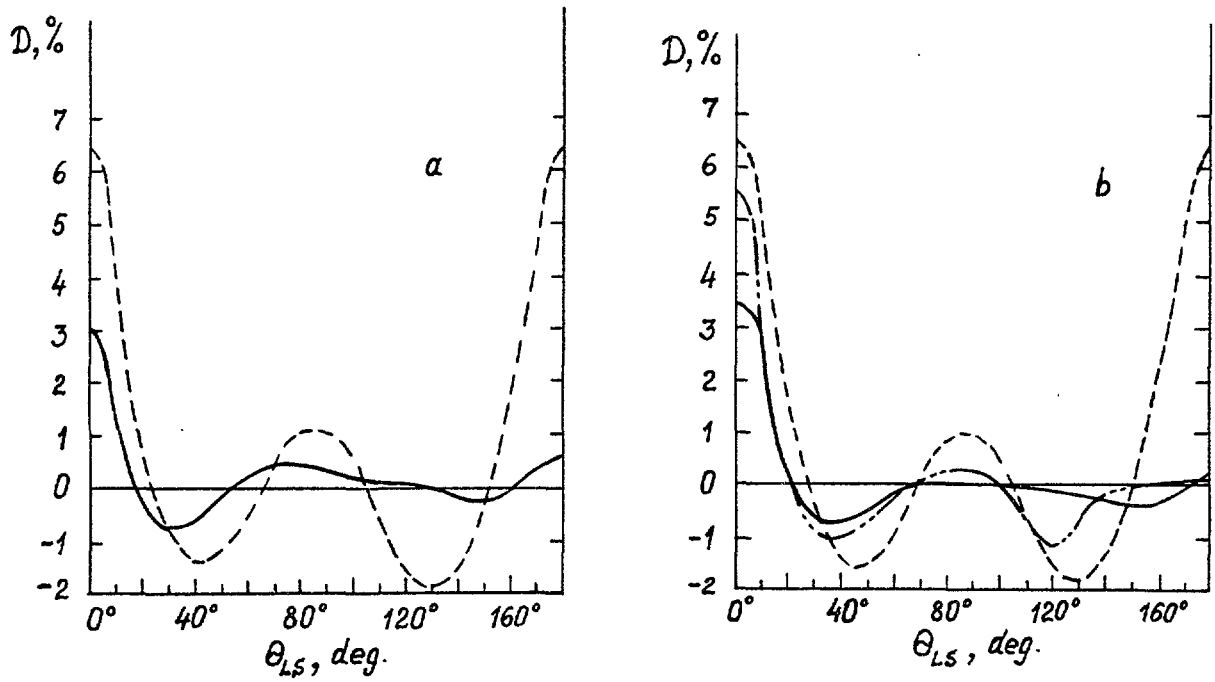

Fig. 5. a). Calculated angular LS distributions of PFN from ^{108}Mo, ^{144}Ba pair of fragments of ^{252}Cf spontaneous fission obtained taking in account PFN emission anisotropy in CMS. The angular distributions are presented in the form of ratio to corresponding angular LS distributions, isotropic in CMS of fragment.

——— - angular distribution calculated with $b = b(\mathcal{E})$;

– – – – - angular distribution calculated with $b = 0.1$.

b). Calculated angular LS distributions of PFN of the first cascade ($\nu = 1$) from pairs of fragments of ^{252}Cf spontaneous fission corresponding to different mode of fission obtained taking accout of PFN emission anisotropy in CMS of fragments.

——..—— ^{96}Sr, ^{156}Nd
———— ^{108}Mo, ^{144}Ba } $b = b(\mathcal{E})$;
– – – – ^{108}Mo, ^{144}Ba, $b = 0.1$

CMS spectra calculated with the statistical model /15, 16/ ignoring the anisotropy of PFN emission in CMS of fragments. The initial spin of fragments is assumed to be equal to $8\hbar$. It is seen from Fig. 4 that the effect of anisotropy on LS - spectra shows up mainly as an increase of neutron yield in the region of low ($E \leqslant 0.5$ MeV) and high ($E \geqslant 15$ MeV) LS energies. It is also seen that the said effect is greater for a light fragment than for a heavy one. For comparison the same Fig. shows analogous calculated spectra but obtained with the use of the current phenomenological approximation of anisotropy coefficients: b = 0.1. From the comparison of these results it follows that the neglect of the dependence of anisotropy coefficients on neutron energy and on fragment mass leads to a overestimation of CMS anisotropy effect on the behaviour of LS - spectra in the said regions of LS energy of neutrons.

Fig. 5a depicts angular LS distributions of prompt neutrons from the same pair of fragments as in Fig. 4 calculated with (1) and (2). The form of representation of distributions is the same as in Fig. 4. As it is seen from Fig. 5a, consistent account of the anisotropy of neutron angular distributions in CMS of fragments leads to the increase of neutron yield in LS at small angles. It can be seen from Fig. 5a that these results differ somewhat from analogous ones obtained with the approximation b = 0.1.

Fig. 5b presents calculated angular LS distributions of the first cascade neutrons ($\nu = 1$) from the pairs of neutrons corresponding to different modes of fission. The angular distributions are calculated with account of CMS anisotropy according to the expressions (1) and (2). The calculation is performed with the same value J of initial spin of fragments (J = 8). One can see that the account of neutron emission anisotropy in CMS of fragments according to (1) and (2) causes the increase of neutron emission at small LS - angles with growing fission asymmetry.

Summarizing the above results one can conclude that for a more accurate statistical description of PFN spectra from fragments of low energy fission the dependence of PFN emission anisotropy in CMS on the neutron energy and fragment parameters should be taken into account during

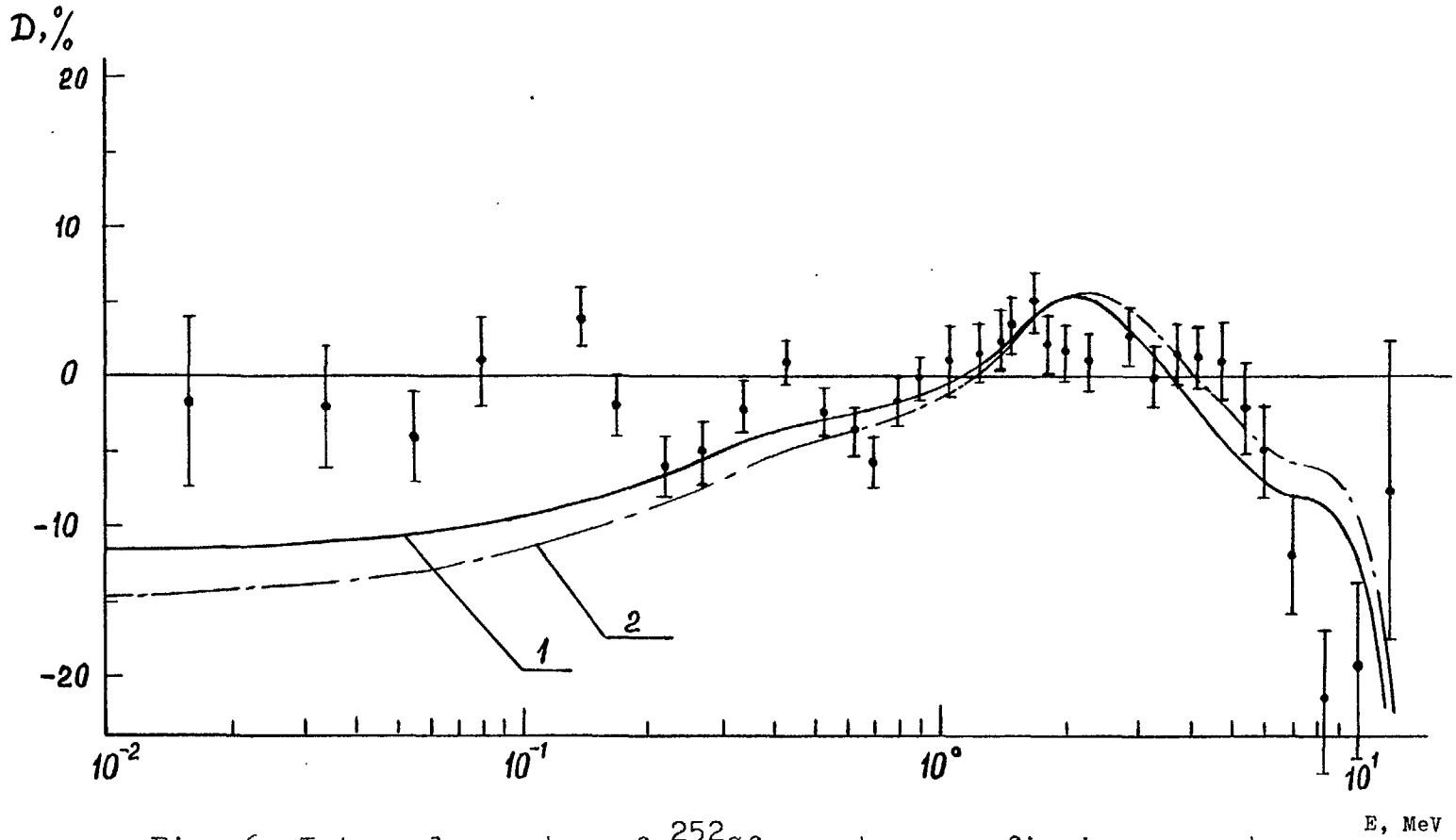

Fig. 6. Integral spectra of ^{252}Cf spontaneous fission prompt neutrons with reference to Maxwellian spectrum with T = 1.42 MeV.

1 - calculation /17/; values of $\bar{\nu}(A)$ and $\sigma^2_{E*}(A)$ were taken from /30/ and /36/ respectively (see text);

2 - calculation (this work); values of $\bar{\nu}(A)$ and $\sigma^2_{E*}(A)$ were taken from /31, 32/ (see text);

I● - experiment /37/.

calculations. From the results presented here it follows also that the problem of a more accurate estimation of the effect of angular CMS anisotropy of PFN emission on the results of PFN integral spectrum calculation is closely connected with that of calculated result uncertainty arising from the uncertainty in available experimental data used as input data for calculation. Fig. 6 shows two integral PFN spectra of ^{252}Cf spontaneous fission calculated using the statistical model /15, 16/ neglecting PFN emission anisotropy in CMS of fragments. The spectra are presented as a relation D to the Maxwellian spectrum with T = = 1.42 MeV. These spectra are obtained for two sets of input data differing only by the values of $\bar{\nu}(A)$ and $\sigma^2_{E*}(A)$. In Fig. 6 the spectrum denoted by 1 is calculated in /17/ using the data for $\bar{\nu}(A)$ and $\sigma^2_{E*}(A)$ taken from the works /31, 32/. As can be seen from Fig. 6, the uncertainty of calculated results in the integral spectrum low energy region of interest reaches 25 % of estimated D value. The said uncertainty gives the ideas of the order of magnitude of the deviation of calculated integral spectrum which should be caused by consideration of CMS anisotropy in this region of energies in order that this deviation could be perceptible on the background of uncertainties in the results of integral spectrum calculation.

Conclusion

The discussion of PFN differential and integral characteristics calculated with the statistical model /15, 16/ based on Hauser-Feshbach theory shows that this model provides a means for most complete and consistent account of principal features of a complex statistical process of PFN emission from fragments in low energy fission. The statistical model makes it possible to describe well enough different PFN characteristics: spectra, multiplicity distributions, angular distributions of PFN from individual fragments and integral characteristics.

The inclusion in this model of consistent calculation of PFN angular characteristic anisotropy in CMS of fragments gives the possibility to separate more completely the sta-

tistical component in PFN spectra, to determine better the relation between anisotropy and individual characteristics of fragments and to evaluate more exactly the effect of PFN emission angular anisotropy in CMS of fragments on differential and integral PFN spectra.

References

1. H. R. Bowman, S. G. Thompson, J. C. D. Milton, W. Swiatecki. - Phys. Rev., 1962, v. 126, p. 2120-2136.
2. D. W. Lang. - Nucl. Phys., 1964, v. 53, p. 113-127.
3. O. I. Batenkov, M. V. Blinov, G. S. Boykov et al. - Proc. IAEA Consultants' Meeting on the U-235 fast-neutron fission cross-section and the Cf-252 fission neutron spectrum. Vienna: IAEA, 1983, p. 161-173.
4. O. I. Batenkov, A. B. Blinov, M. V. Blinov, B. F. Gerasimenko, V. A. Rubchenya, S. M. Smirnov. - Nejtronnaya Fizika. Ch. I. M., 1984, S. 344-349.
5. E. A. Seregina, P. P. Dyachenko. - Preprint FEI-1625, 1984, 23 p.
6. O. I. Batenkov, A. B. Blinov, M. V. Blinov, S. M. Smirnov. - Nejtronnaya Fizika. Ch. I, M., 1984, S. 339-343.
7. Gerasimenko B. F., V. A. Rubchenya. - Proc. IAEA Advisory Group Meeting on Nuclear Standard Reference Data. IAEA-TECDOC-335. Vienna, 1985, p. 280.
8. V. A. Rubchenya. - Preprint RI-28, 1974, 14 p.
9. V. P. Zommer, A. E. Savel'ev, S. V. Zhikhareva. - Atomnaya Energiya, 1967, t. 23, vyp. 4, S. 327-333.
10. J. Brown, F. Dietrich. - Phys. Rev., 1984, v. 10C, p. 2545-2549.
11. D. Madland, J. Nix. - Nucl. Sci. Eng., 1982, v. 81, p. 213-271.
12. H. Märten, D. Neumann, D. Sceliger. - Proc. IAEA Consultant's Meeting on the U-235 fast-neutron cross-section and the Cf-252 fission neutron spectrum. Vienna: IAEA, 1983, p. 199-212.
13. H. Märten, D. Seeliger. - Proc. IAEA Advisory Group Meeting on Nuclear Standard Reference Data. IAEA-TECDOC-335. Vienna, 1985, p. 255-267.

14. B. F. Gerasimenko, V. A. Rubchenya. - Nejtronnaya Fizika. Ch. I. M., 1984, S. 349-353.
15. B. F. Gerasimenko, V. A. Rubchenya. - Preprint RI-183, 1984, 20 p.
16. B. F. Gerasimenko, V. A. Rubchenya. - Atomnaya Energiya, 1985, t. 59, vyp. 5, s. 335-339.
17. B. F. Gerasimenko, V. A. Rubchenya. - Proc. IAEA Advisory Group Meeting on properties of neutron sources. IAEA-TECDOC-410. Vienna, 1987, p. 208-112.
18. H. Märten. - Proc. IAEA Advisory Group Meeting on properties of neutron sources. IAEA-TECDOC-410. Vienna, 1987, p. 144-152.
19. A. V. Ignatyuk, G. N. Smirenkin, A. S. Tishin. - Yadernaya Fisika, 1975, t. 21, p. 485-490.
20. W. Myers, W. Swiatecki. - Nucl. Phys., 1966, v. 81, p. 1-60.
21. F. Becchetti, G. Greenleess. - Phys. Rev., 1969, v. 182, p. 1190-1209.
22. S. M. Zakharova, V. S. Stavinskii, Yu. H. Shubin. - Yadernye konstanty. Vyp. 7, 1971, p. 5-26.
23. P. Oliva, D. Prosperi. - Nuovo Cimento, 1967, v. ILB, p. 161-184.
24. T. Ericson, V. Strutinski. - Nucl. Phys., 1958, v. 8, p. 284-293.
25. L. Wolfenstein. - Phys. Rev., 1951, v. 82, p. 690-696.
26. J. Blatt, L. C. Biedenharn. - Revs. Mod. Phys., 1952, v. 24, p. 258-272.
27. E. Sheldon, P. Gantenbein. - J. Appl. Math. Phys., 1967, v. 18, p. 397-433.
28. B. F. Gerasimenko, V. A. Rubchenya. - Byulleten' Tsentra dannykh LIYAF, vyp. 12, L, 1986, p. 3-29.
29. E. A. Seregina, P. P. Dyachenko, A. A. Seregin. - Yadernaya Fizika, 1986, t. 43, s. 1092-1099.
30. H. Nifenecker, C. Signarbieux, R. Babinet, J. Poitou. - Proc. IAEA Symposium on Physics and Chemistry of Fission. Vienna, 1974, v. 2, p. 117-178.
31. I. D. Alkhazov, A. V. Daniel, V. D. Dmitriev. - Nejtronnaya Fizika. Ch. I. M., 1984, s. 324-328.

32. I. D. Alkhazov, V. D. Dmitriev, A. V. Kuznetsov et al. - Proc. XV-th Intern. Symp. on Nuclear Physics. Nuclear Fission. ZfK-592, 1986, p. 29-34.
33. J. Wilhelmy, E. Cheifetz, R. Jared et al. - Phys. Rev., 1972, v. 5C, p. 2041-2060.
34. T. Datta, S. Dange et al. - Z. Phys., 1986, v. A324, p. 81-85.
35. O. I. Batenkov, A. B. Blinov, M. V. Blinov, S. N. Smirnov. - Proc. IAEA Advisory Group Meeting on properties of neutron sources. IAEA-TECDOC-410, Vienna, 1987, p. 201-207.
36. V. M. Piksaykin, P. P. Dyachenko, L. K. Kutsaeva. - Yadernaya Fizika, 1977, t. 25, s. 723-731.
37. M. V. Blinov, G. S. Boykov, V. A. Vitenko. - Preprint RI-191, 1985, 51 p.

CALCULATION OF FISSION NEUTRON SPECTRUM WITH INCORPORATION OF PRE-ACCELERATION NEUTRON EMISSION

*R.L. Walsh and G. Chircu**

Australian Nuclear Science and Technology Organisation,
Lucas Heights Research Laboratories,
Menai NSW 2234, Australia.

Abstract

We have incorporated a component of pre-acceleration neutron emission into our calculation of the fission neutron spectrum of ^{252}Cf using the spin-dependent Madland-Nix Model. The calculation now gives good agreement with the data in the low energy region below 0.5 MeV.

1. INTRODUCTION

For many years, the existence of a 'scission' component in the neutron emission from fission has been assumed. These scission neutrons are emitted near the moment of snapping of the neck forming the two fragments, and have an angular distribution which is isotropic in the laboratory system. The experimental results indicated that, for ^{252}Cf(sf), 5-10% of the total neutrons are scission neutrons [1-5] and for ^{235}U(n,f), 10-15% [6-8].

Recent data [9-12] have found little or no evidence for scission neutrons. The results could be explained by assuming all neutron emission to be from fully accelerated fragments [10-12] or by including as well a small component of 'pre-acceleration' neutron emission, that is, neutrons emitted before the fragments have attained their full velocities [9].

This work examines the effect on the fission neutron spectrum (FNS) of ^{252}Cf of incorporation of a component of pre-acceleration neutron emission. In particular, the work attempts to fit the low energy FNS data for ^{252}Cf below 0.5MeV, using the Madland-Nix Model [13]. Hitherto, only the Complex Cascade Evaporation Model [14,15] and Hauser-Feshbach type models [16] had been able to satisfactorily reproduce these low energy data.

2. CALCULATION OF FNS WITH NO PRE-ACCELERATION NEUTRONS

We assume that all the neutron emission occurs from fully accelerated fragments and calculate the FNS for ^{252}Cf using the Madland-Nix Model (MNM) [13]. Furthermore, we have extended the MNM formalism to take account of the spin of the fission fragment (β = 0.1) [17,18]. The nuclear level density parameter 'a' was chosen by chi - square minimisation with respect to the evaluated data points of Mannhart [19]. This gave a = A/(9.3 MeV) and a chi-square value of 3.8 per degree of freedom. Our calculation and the Mannhart data are shown in Figure 1, relative to a Maxwellian spectrum with TM = 1.42. (The continuous line includes fragment spin, the dashed line neglects fragment spin.)

---

*University of Wollongong, Wollongong NSW 2500, Australia.

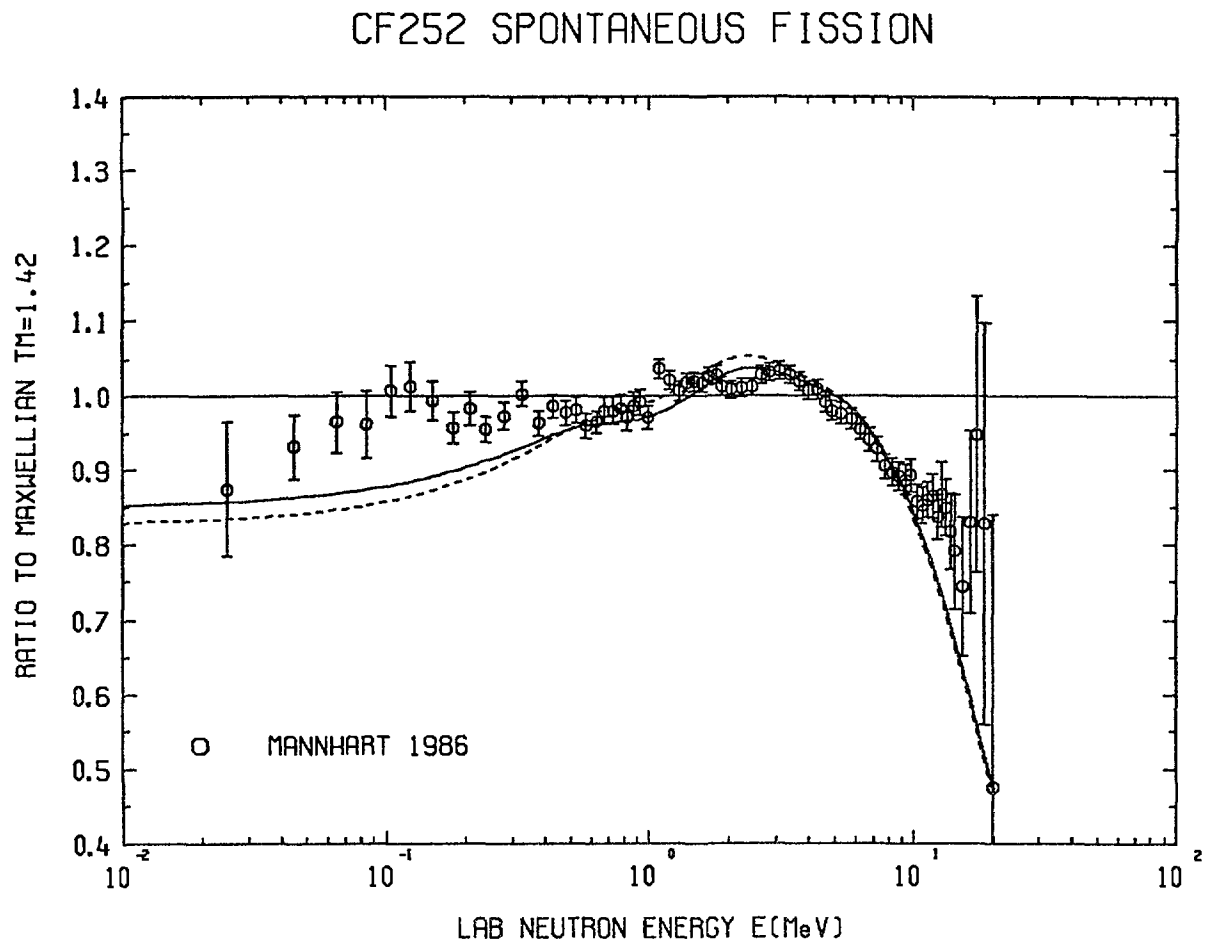

Figure 1 Fission neutron spectrum (FNS) for ^{252}Cf(sf) calculated using spin-dependent Madland Nix Model (MNM). Nuclear level density a = A/(9.3 MeV). Fission energy release E_R = 218.886 MeV. Continuous line includes fragment spin (β = 0.1); dashed line neglects fragment spin. From [18]. Evaluated data points of Mannhart [19] also shown. χ^2 = 3.8 per degree of freedom.

Above 0.5 MeV there is good agreement between the calculation and the data. Below 0.5 MeV the calculation is some 10% below the data. It is interesting to ask whether inclusion of pre-acceleration neutrons might improve this agreement at low energy. Several authors have discussed the effect of these neutrons on the FNS for ^{252}Cf [15] and the possibility of their improving agreement between theory and data at low energies. [16,20]

3. CALCULATION OF FNS WITH INCORPORATION OF PRE-ACCELERATION NEUTRONS

i. Following Riehs [9], we have extended the (spin included) MNM by assuming that 13.2% of the total neutrons are emitted when the fragments have attained a fraction b_v = 0.2 of their final velocity. The pre-acceleration neutrons are assumed to have an evaporation energy spectrum in the CMS and the fragment spin is included. The FNS thus calculated for ^{252}Cf is shown by the continuous line in Figure 2. The value of a is a = A/(9.3 MeV), as for Figure 1. The dashed line shows the FNS without

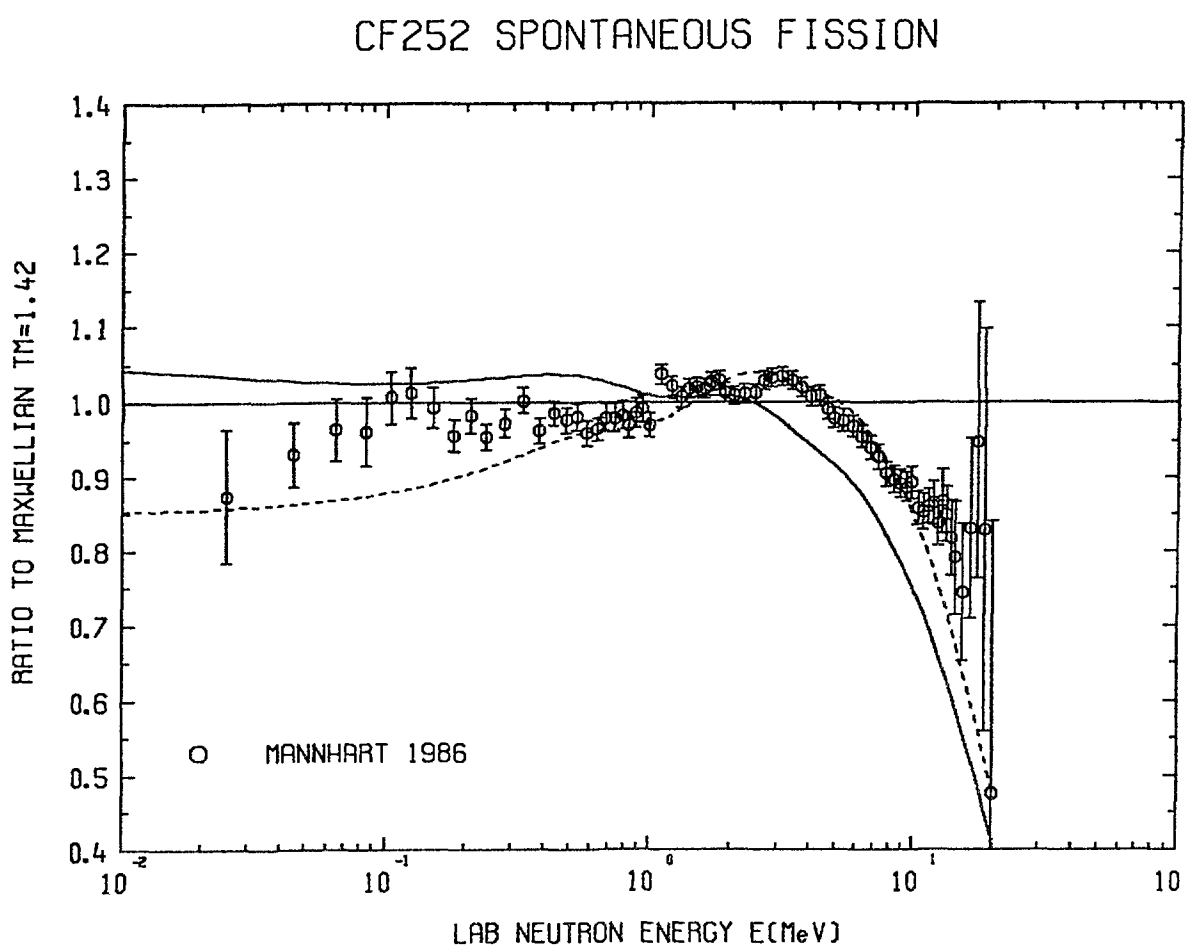

Figure 2. Fission neutron spectrum calculated with incorporation of pre-acceleration neutrons (à la Riehs [9]). Pre-acceleration component = 13.2%, b_v = 0.2, shown by continuous line. Dashed line shows FNS without pre-acceleration neutrons (same as continuous line in Fig. 1). Other parameters as for Fig. 1.

pre-acceleration neutrons (but with fragment spin included). It is seen that the inclusion of pre-acceleration neutrons has 'overshot' the low energy data by about 7% and produces 5-10% worse agreement with the data above 3 MeV. However the flat shape of the data below 0.5 MeV is now better reproduced.

ii. We next try to get the best fit possible by simultaneous variation of the parameters b_v and a to find a minimum in chi-square. This was done assuming the arbitrary values of 5% and 10% for the relative pre-acceleration component. The resulting parameter values found were b_v=0.5, a = A/(9.8 MeV), and 10% for the pre-acceleration component. The resulting FNS curve is shown by the continuous line in Figure 3. The value of χ^2_{min} is 1.2 per degree of freedom. The agreement with the data below 0.5 MeV is now good. At the same time, the agreement with the data above 0.5 MeV (of Figure 1) has been maintained. (The dashed curve shows the calculated FNS for a = A/(9.8 MeV) but with no pre-acceleration neutrons incorporated.) The above results have been presented in ref. [21].

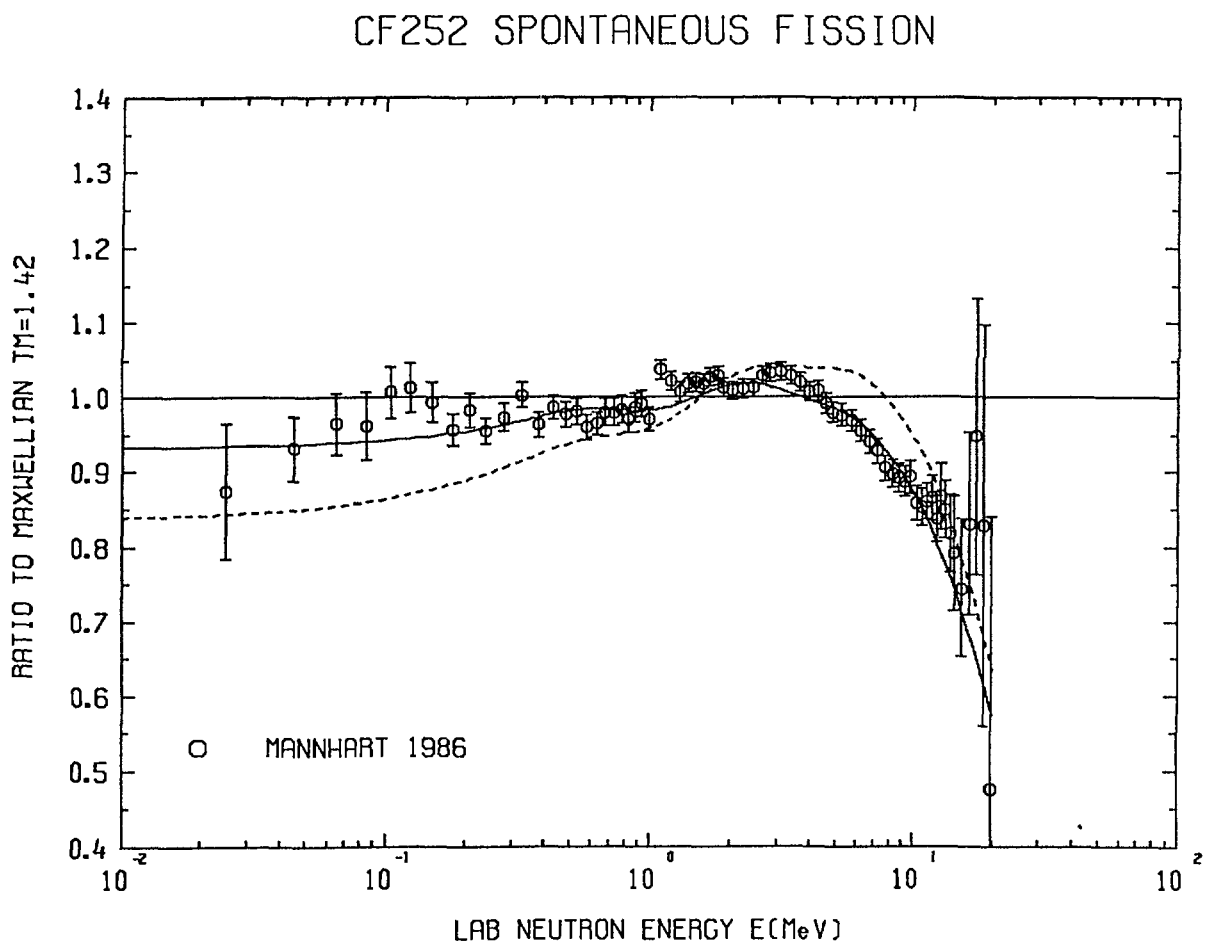

Figure 3. Fission Neutron Spectrum calculated with incorporation of pre-acceleration neutrons - continuous line shows best fit obtained by simultaneous variation of b_v and a to find minimum in χ^2. Pre-acceleration component = 10%, b_v = 0.5, a = A/(9.8 MeV). χ^2 = 1.2 per degree of freedom. Dashed line shows FNS for a = A/(9.8 MeV) but without pre-acceleration neutrons.

4. DISCUSSION

The assumption that the pre-acceleration neutrons are all emitted at a fixed point in time is most probably an oversimplification. A distribution of emission times during the acceleration stage would be a truer picture. The authors of the Complex Cascade Evaporation Model (CEM) have also considered such a distribution in their calculation of the FNS [15]. However, the simplified, fixed-time version presented in the present work serves to show that calculations of the FNS for ^{252}Cf using the Madland-Nix Model can reproduce the flat behaviour of the evaluated data [19] below 0.5MeV, whilst at the same time maintaining a perfectly reasonable value for the nuclear level density parameter (a = A/(9.8 MeV)). Hitherto, only the CEM [14] and Hauser-Feshbach type models [16] for the FNS were able to reproduce the low energy data. (The fragment spin is included in all three models.)

Incorporation of pre-acceleration neutrons in calculation of the FNS for neutron induced fission of thorium, uranium and plutonium isotopes is presently underway.

5. REFERENCES.

1. Bowman H.R. et al., Phys. Rev. 126 (1962) 2120.
2. Cheifetz E. and Fraenkel Z., Phys. Rev. Lett. 21 (1968) 36.
3. Bishop C.J. et al., Nucl. Phys. A198 (1972) 161.
4. Fraenkel Z. et al., Phys. Rev. C12 (1975) 1809.
5. Ward D. et al., Nucl. Phys. A403 (1983) 189.
6. Kapoor S.S. et al., Phys. Rev. 131 (1963) 283.
7. Skarsvag K. and Borgheim K., Nucl. Phys. 45 (1963) 72.
8. Milton J.C.D. and Fraser J.S., Proc. IAEA Symp. Physics and Chemistry of Fission, Salzburg, Austria, 1965, Vol. 2, p. 39.
9. Riehs P., Acta Physica Austriaca 53 (1981) 271.
10. Märten H. et al., Proc. Int. Conf. Nucl. Data, Santa Fe, USA, May 1985, Vol. 1, p. 377.
11. Budtz - Jorgensen C. and Knitter H. - H., ibid, Vol. 1, p. 341.
12. Batenkov O.I. et al., Proc., IAEA Group Meeting on Neutron Sources, Leningrad, U.S.S.R., June 1986, p. 201.
13. Madland D.G. and Nix J.R., Nucl. Sci. Eng. 81 (1982) 213.
14. Märten H. and Seeliger D., Proc. Int. Conf. Nucl. Standard Ref. Data, Geel, Belgium, 1984, p.255. Also J. Phys. G10 (1984) 349.
15. Märten H. et al., Proc. XV Int. Symp Nucl. Phys., Gaussig, GDR, Nov. 1985, p.1.
16. Gerasimenko B.F. and Rubchenya V.A., loc. cit (12), p. 208.
17. Walsh R.L., Report NEANDC(E) 241/L, INDC(FR) 70/L (1987)
18. Walsh R.L. and Chircu G., Proc. Int. Conf. Neutron Physics, Kiev, U.S.S.R., September 1987.
19. Mannhart W., loc. cit. (12), p. 158.
20. Blinov M.V. et al., Report INDC(CCP) - 238 (1984).
21. Walsh R.L. and Chircu G., Proc. 12th AINSE Nucl. Phys. Conf., Sydney, Australia, January 1988.

Status of the Cf-252 fission neutron spectrum evaluation with regard to recent experiments

W. Mannhart
Physikalisch-Technische Bundesanstalt
Braunschweig, FRG

Abstract:

A summary of the present status and future development of the evaluation of the neutron spectrum of spontaneous fission of Cf-252 is given. The experimental data base has been critically analysed to identify new and revised experiments. Both theoretical and semi-empirical descriptions of this neutron spectrum are discussed and reviewed.

1. Introduction

The increased number of recent efforts to determine the neutron spectrum of spontaneous fission of Cf-252, both experimentally and with theoretical models, has formed a sound basis for a new evaluation of this spectrum. Based on this evaluation, the Cf-252 neutron spectrum is now established as an internationally accepted reference standard for metrological applications.

In the present paper the status of the evaluation and possible future extensions are summarized. The essential steps of the present evaluation are reviewed and a direct comparison between input and output of the evaluation is made. The actual status of the experimental data base is discussed with the aim of updating the evaluation in the future. Recent trends and improvements in the theoretical description of this important neutron spectrum are briefly summarized. Finally, a recent attempt to approximate the spectrum with a simple Watt distribution is annotated and reviewed.

2.1 Existing evaluation

This work is fully documented elsewhere [1]. The numerical data have been released and are available from the Nuclear Data Centers.

Besides the numerical figures of the spectrum, it was the aim of the evaluation to generate a complete uncertainty file, reflecting present knowledge of this important reference neutron spectrum and indispensable for any application purposes. This requirement conflicted with the documentation of many of the experiments, especially the older ones. A second aspect to be considered was the recent identification of possible error sources in time-of-flight experiments (see [2], for example) which showed a few effects and corrections that are essential for obtaining reliable results. These were:

(1) The definition of an accurate neutron energy scale.
(2) The proper correction for the time resolution of the neutron detector.
(3) The correction for non-isotropic detection losses in the fission fragment detector.
(4) The correction for uncorrelated stop signals in the electronic circuit.

It has been demonstrated that neglecting the last two corrections in particular can result in strong changes of the shape of the measured neutron spectrum. In the light of all these circumstances, only such experiments could be included in the evaluation process for which, due to sufficently detailed documentation, a full examination of the above-mentioned corrections was possible. Unfortunately, this resulted in a great reduction of the number of experiments that could be used. It was chiefly the more recent experiments which passed this selection process. These experiments with the energy range they cover are listed in Table 1.

All the input data of the evaluation were point data at discrete neutron energies, thus the problem of different energy bins in different experiments was avoided. In such cases where this reduction has not been performed by the authors, appropriate corrections for the energy bin width and the time resolution were applied to the data. For each experimental data set, an uncertainty covariance matrix was generated. Before this was done, the individual energy scale uncertainty was transformed into a spectral amplitude uncertainty and was taken into account in the uncertainty propagation procedure.

Table 1: Experiments taken as a basis for the evaluation

Authors	Energy range of the experiment
Poenitz/Tamura [2]	0.25 MeV - 9.25 MeV
Blinov et al. [3]	42 keV - 11.36 MeV
Boldeman et al. [4] (Lithium glass)	124 keV - 2.66 MeV
Boldeman et al. [4] (Plastic scintillator)	1.05 MeV - 14.25 MeV
Lajtai et al. [5]	25 keV - 1.22 MeV
Böttger et al. [6]	2.00 MeV - 14.00 MeV
Märten et al. [7]	8.89 MeV - 19.77 MeV

The first step of the evaluation was intended to preserve as much of the individual structure of each experimental data set as possible, and particularly to avoid any artificial smoothing process. An appropriate energy grid with 70 grid-point energies was therefore established, dependent on the density of the data points available and on the necessity to adequately represent the structure of the spectrum over the whole energy range. Each experimental data point was transformed to its neighbouring energy grid point with a slope determined from a preliminary fit to each experimental data set with a Maxwellian distribution. As the shifts between the experimental energies and the grid energies were only small ones, the original structure of each data set was essentially preserved.

The evaluation was carried out, at grid energies with generalized least-squares methods, i. e., only the statistical uncertainty components were reduced, whereas the systematic components and their correlations influenced the data adjustment process in its entirety. Between 40 keV and 14 MeV the evaluation is based on at least two (or more) experiments overlapping in their energy range. Above 14 MeV neutron energy, the evaluation is dominated by a single data set [7]. However, this set overlaps between 9 MeV and 14 MeV with other experiments, so the weight of its contribution to the evaluation process is fairly reduced.

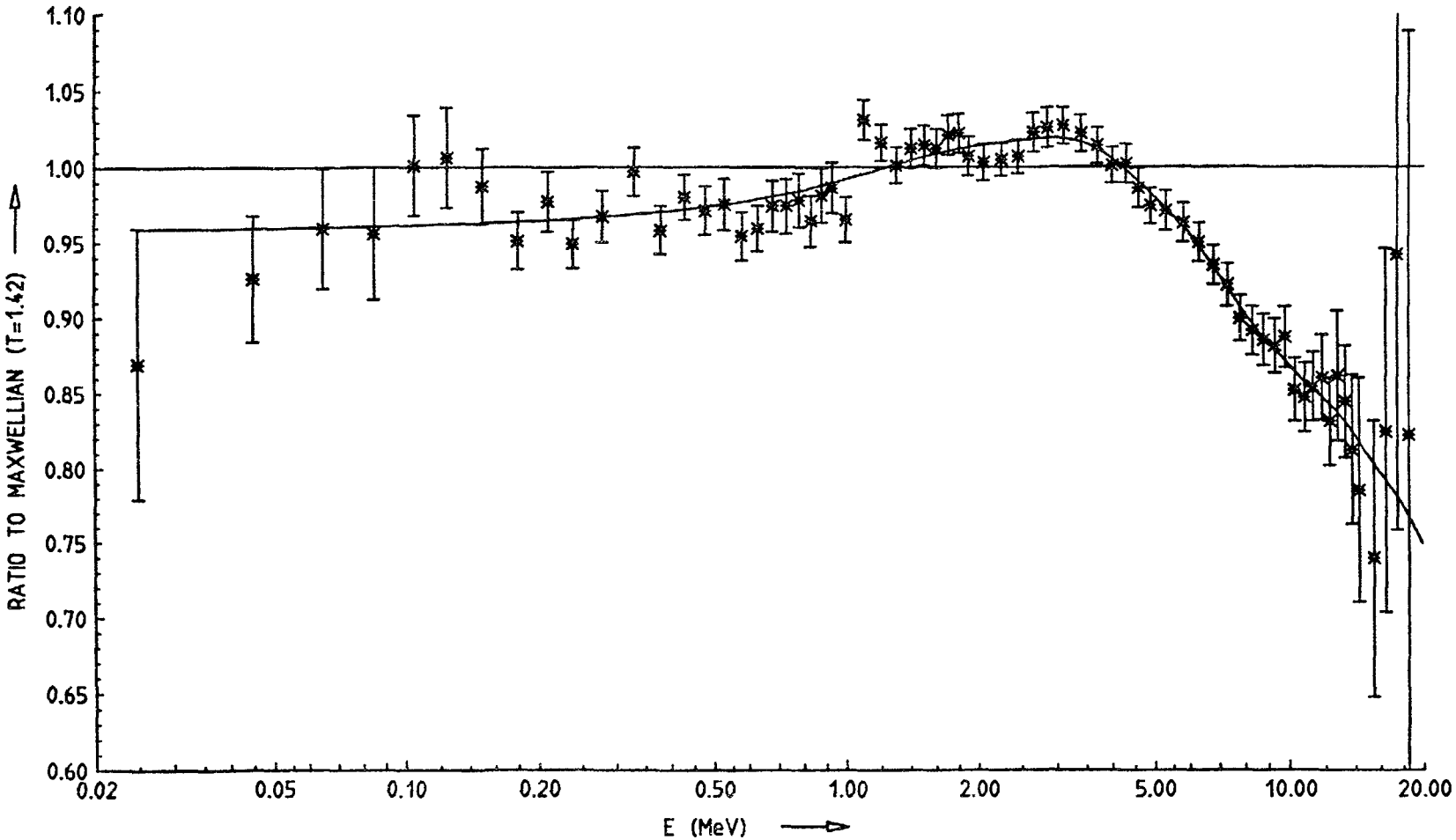

Fig. 1: Evaluated data of the Cf-252 neutron spectrum. For graphical representation, the data were scaled relative to a Maxwellian with T = 1.42 MeV. The point data with error bars are from the "point-wise" evaluation procedure. The solid line represents the smoothed "continuous" evaluation, the final result.

Some of the experimental data were measured as shape data. In such cases an additional normalization factor was derived from the evaluation procedure. The individual factors were close to unity and are listed elsewhere [1].

The evaluation resulted in a chi-square per degree of freedom of nearly unity and indicated no real inconsistencies between the various experiments. The result of this "point-wise" evaluation is shown in Fig. 1. The data are plotted relative to a Maxwellian distribution with T = 1.42 MeV to compensate for the large dynamic range of this neutron spectrum. However, it should be mentioned that the evaluation has been carried out with the absolute data, i. e. without any scaling. Each evaluated data point is given with a corresponding error bar representing one standard deviation (1 σ). These uncertainties obtained from the evaluation process reflect the present experimental knowledge of this neutron spectrum. The evaluated point data obtained without any smoothing procedure allowed the examination of possible structures in the neutron spectrum. A careful inspection showed no structure which significantly exceeded the 3 σ-level. This has also been confirmed by a weighted spline fit to the data. The result of this fit, shown as solid line in Fig. 1, represents the final "continuous" evaluation result. The spline interpolation procedure has not been used for a further uncertainty reduction.

Due to the fact that the present ENDF formats are not suitable for representing a spline interpolation, the numerical data of the spline fit were given in a form allowing the conventional ENDF interpolation rules to be applied. The uncertainty covariance matrix of the evaluated neutron spectrum exhibits a special structure due to the fact that the secondary condition of the spectrum integral is unity. This has automatically been taken into account in the evaluation procedure. The relative standard deviations derived from this matrix are ≤ 2 % between 0.2 MeV and 9.5 MeV and ≤ 5 % between 45 keV and 13.3 MeV.

2.2 Comparison with input data

In the Figs. 2 - 8 the result of the evaluation is shown in comparison with the experimental data sets used as input for the

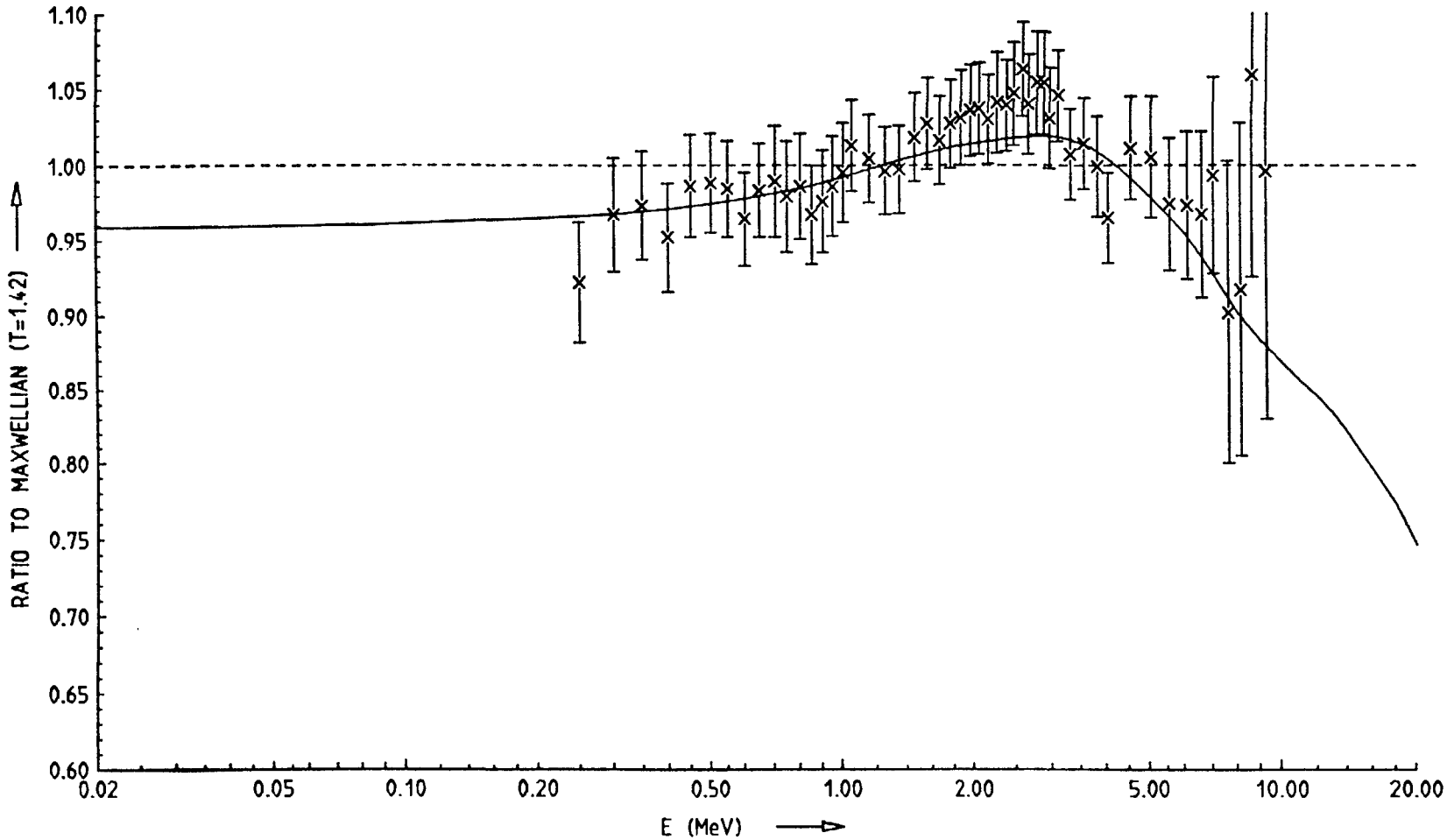

Fig. 2: Experimental data of Poenitz and Tamura [2] in comparison with the evaluation (solid line).

evaluation procedure. In the original documentation of this evaluation [1] no such direct comparison was made in the form of graphs.

With the same scaling as in Fig. 1, the experimental data of Poenitz and Tamura [2] are shown in Fig. 2. Only the error bars of the experimental data are given. The final evaluated neutron spectrum is represented by the solid line. The evaluated spectrum describes very well the trend of these experimental data. But it should be borne in mind that the evaluated spectrum is a general result based on more than one experiment, and it would therefore be unrealistic to expect optimum agreement with a single data set.

The agreement with the data set of Blinov et al. [3] is shown in Fig. 3. The experiment of Boldeman et al. [4] consisted of two separate data sets. The low-energy data of this experiment shown in Fig. 4 were measured with a lithium glass neutron detector, whereas the high energy data shown in Fig. 5 are based on a plastic scintillator used as a neutron detector. In Fig. 4 several enhanced data points can be seen, resulting from an incomplete correction of the broad $^{6}Li(n,\alpha)$ resonance at 240 keV. These data were disregarded in the evaluation process. A second experimental data sets also obtained with a lithium glass detector is shown in Fig. 6. In the figure, the original data of Lajtai et al. [5] are shown as triangles with error bars. These data have been revised very recently (see chapter 2.3.2) and the modified data are indicated in Fig. 6 by dots.

When the data sets of Böttger et al. [6] and Märten et al. [7] shown in Fig. 7 and Fig. 8, respectively, are compared with the evaluation, we see that the evaluation tends towards a decrease of Böttger's data above 5 MeV and an increase of Märten's data above 8 MeV. This trend is also supported by the data shown in Figs. 2 and 3, and reflects the attempt of the evaluation to compromise between overlapping experiments. The influence of such a procedure on an individual data set is governed to a great extend by the degree of correlation between the data.

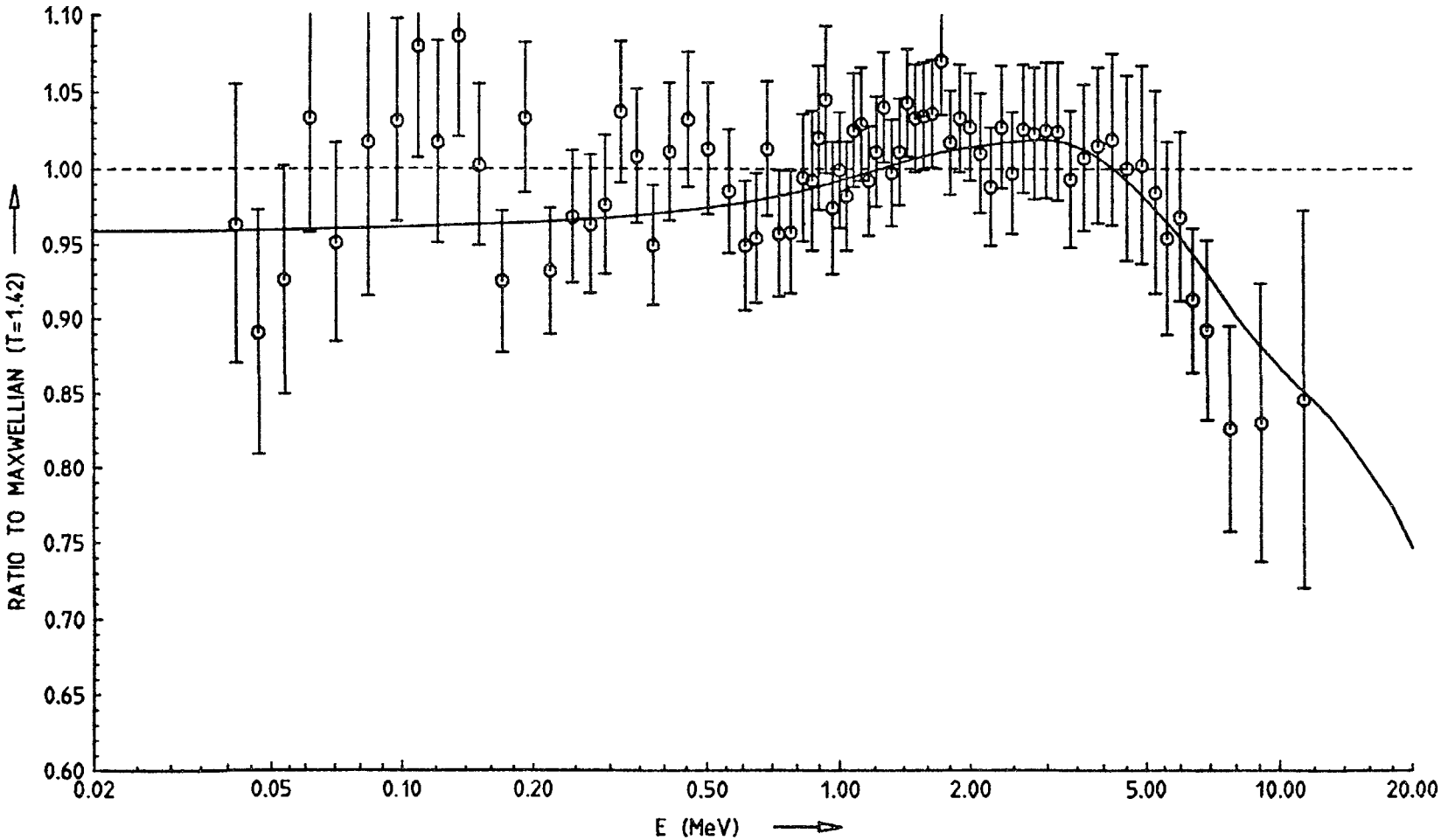

Fig. 3: Experimental data of Blinov et al. [3] in comparison with the evaluation.

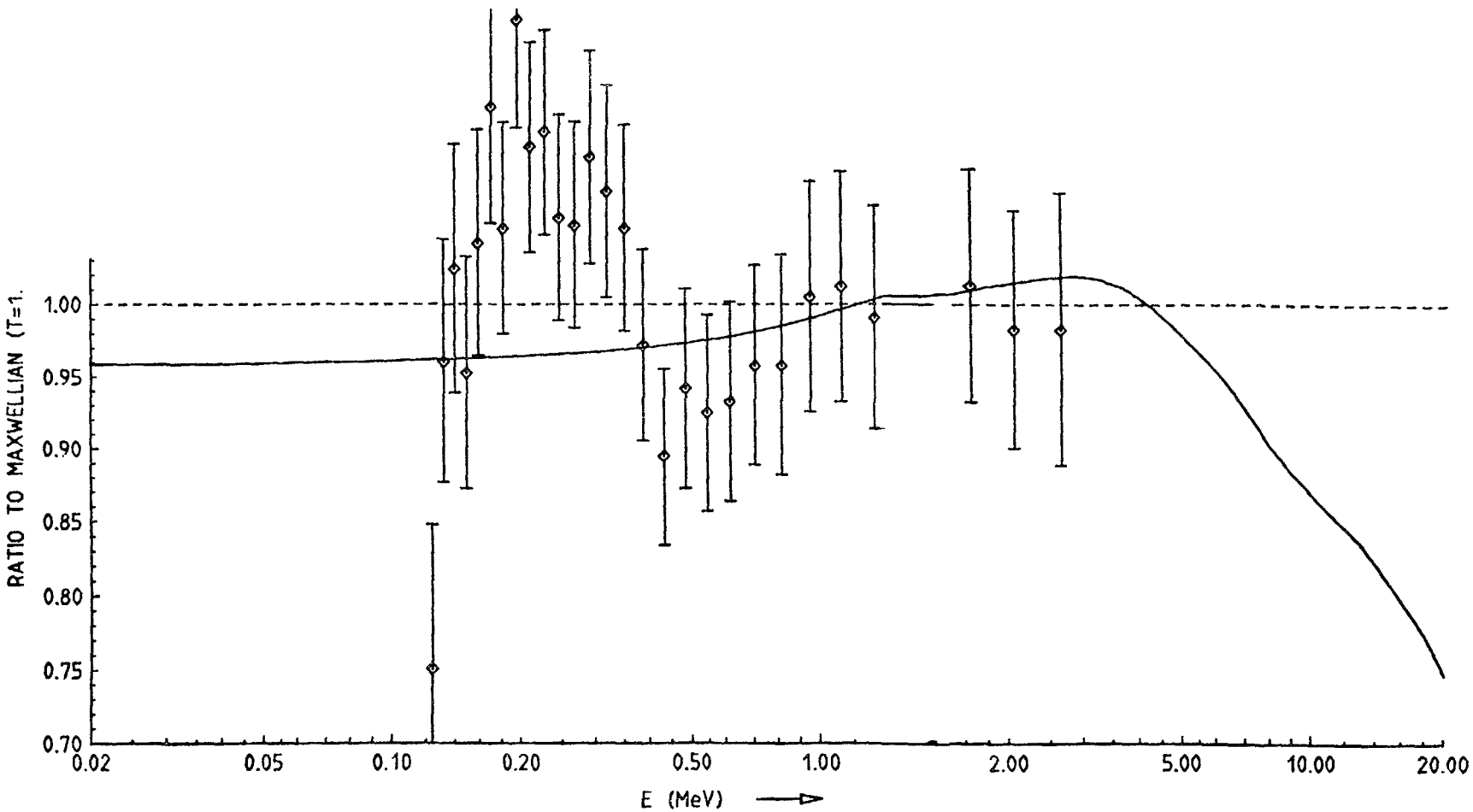

Fig. 4: Experimental data of Boldeman et al. [4] obtained with a lithium glass detector in comparison with the evaluation.

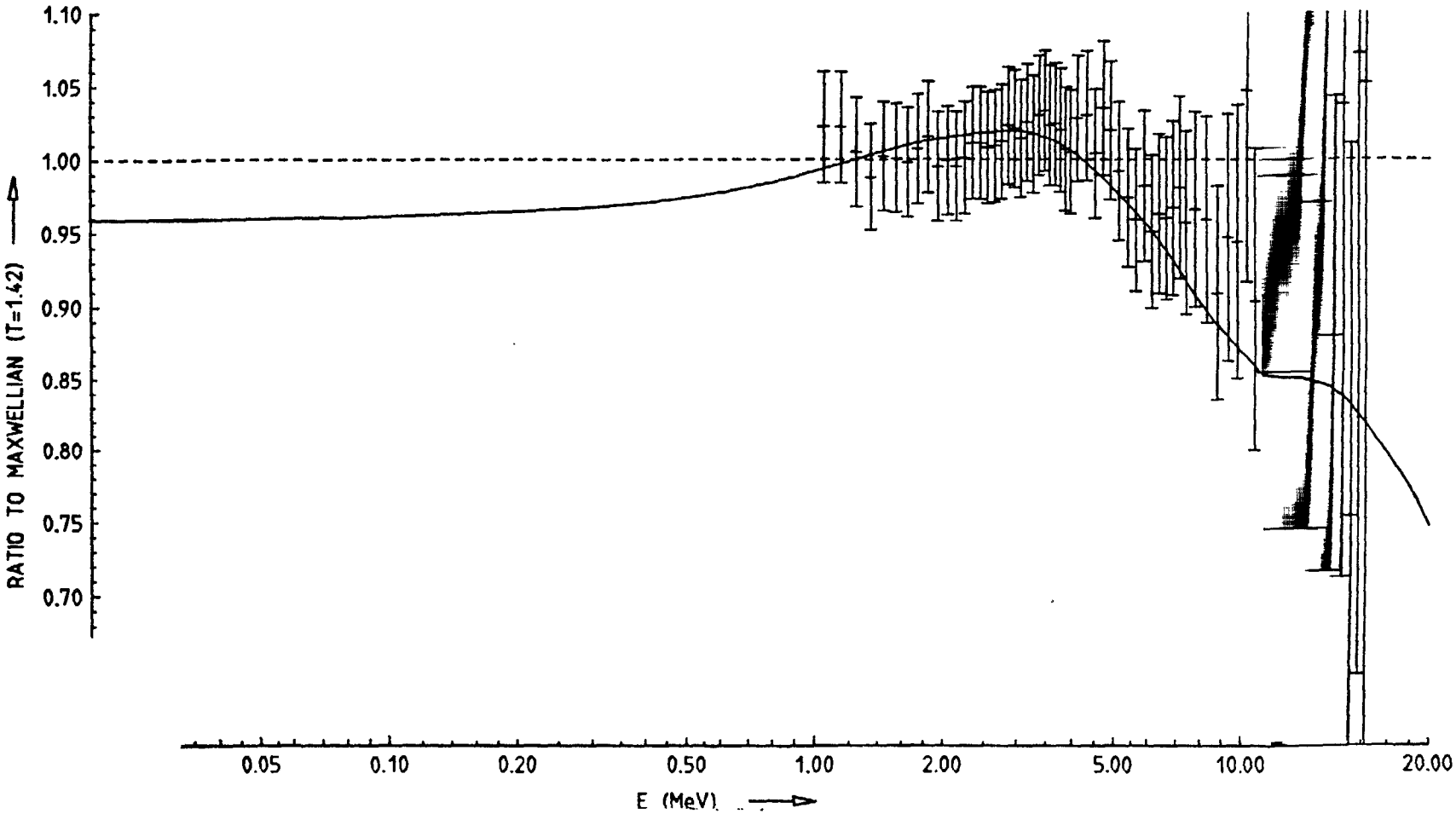

imental data of Boldeman et al. [4] obtained with a plastic scintillator in h the evaluation.

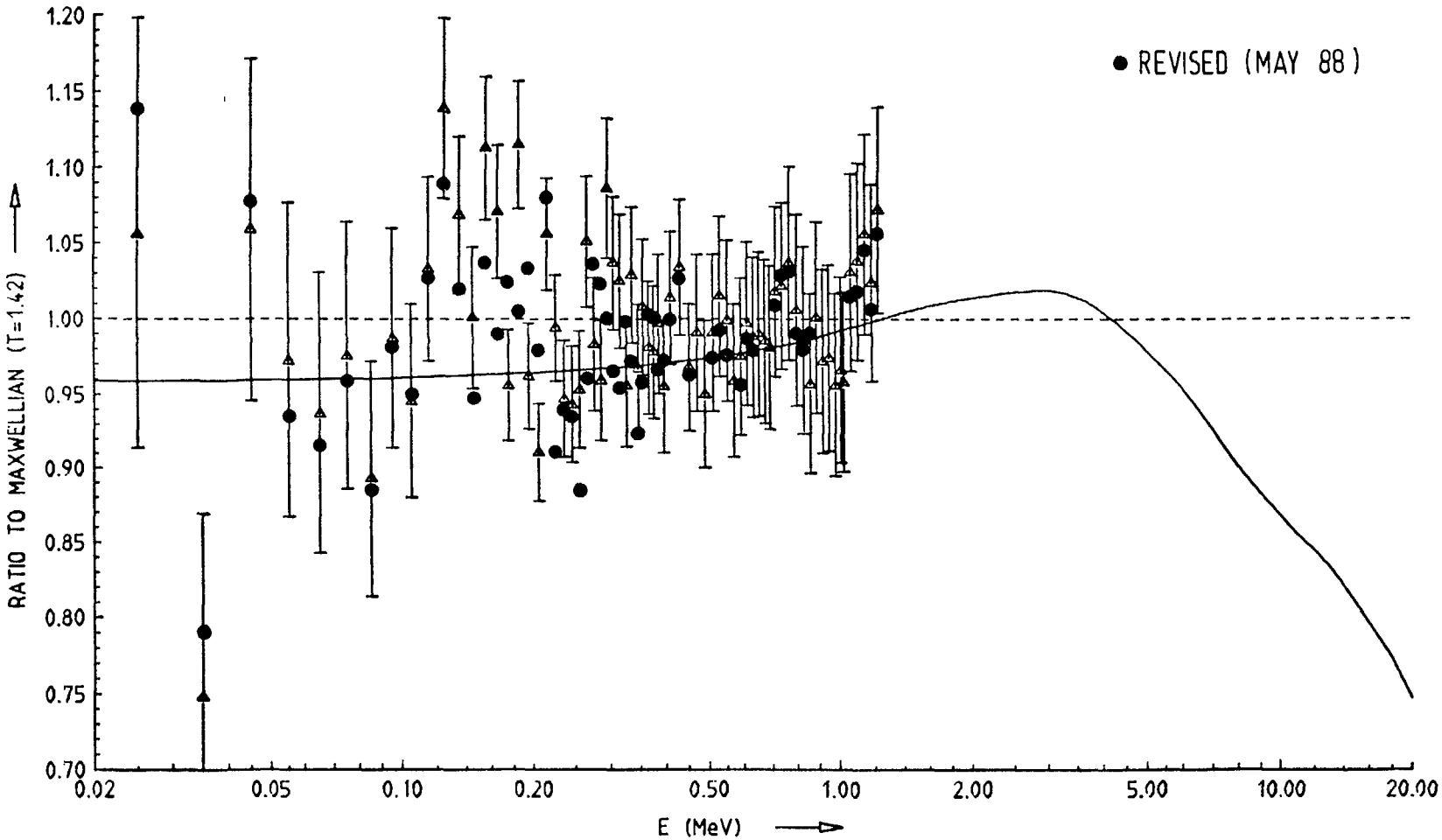

Fig. 6: Experimental data of Lajtai et al. [5] in comparison with the evaluation. The original experimental data are shown as triangles. The recently revised data are represented by dots.

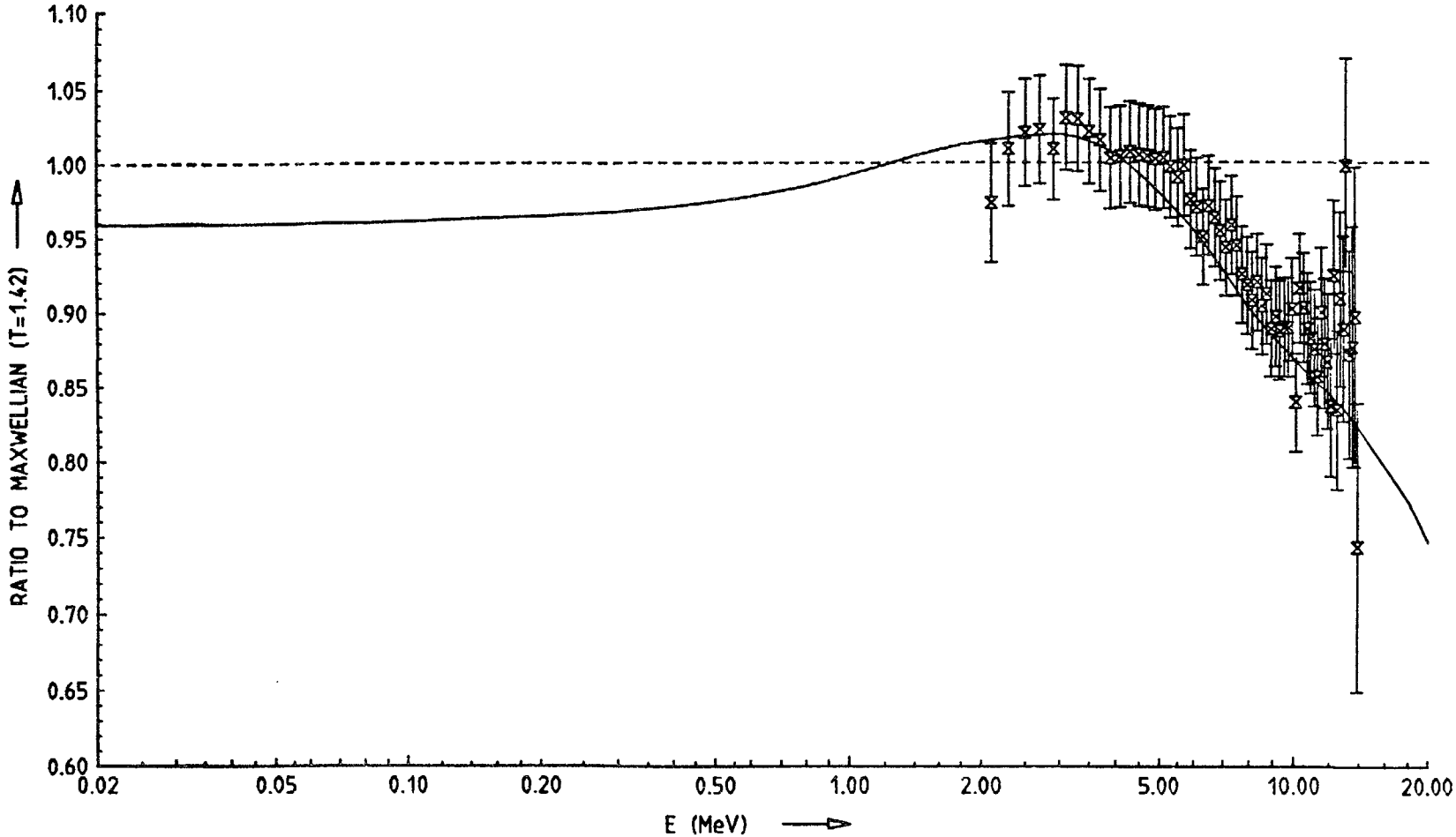

Fig. 7: Experimental data of Böttger et al. [6] in comparison with the evaluation.

2.3 Future perspectives of the evaluation

2.3.1 Integral data

Besides the high-resolution time-of-flight experiments already used in the evaluation, there is another class of broad energy range experiments, namely the integral responses of threshold neutron activation detectors in the Cf-252 neutron field. From data on these, information on the neutron spectrum can be derived with unfolding methods. This has already been done in a previous work [8]. The information obtained from such integral experiments is not very sensitive as regards low neutron energies (< 1 MeV) but it provides valuable data on the shape of the Cf-252 neutron spectrum at higher neutron energies.

The result of the unfolding procedure is shown in Fig. 9. The representation in Fig. 9 is somewhat different compared with the previous figures. The result is normalized up to 6 MeV to the same Maxwellian (T = 1.42 MeV) as used in Figs. 1 - 8, but above 6 MeV the normalization changes and follows the exponential correction term (see also chapter 2.4) of the NBS segment fit [30]. For comparison, the curve of the "continuous" evaluation of chapter 2.1 is shown in Fig. 9 as a broken line. Within the uncertainties, there is remarkable agreement between the unfolded and evaluated data, which suggests that both evaluation methods could be combined. However, there are also arguments against this which will be briefly reviewed.

The Cf-252 neutron spectrum and particularly its higher energy portion, assumed that both are sufficiently well defined, is very useful for a test of differential (energy-dependent) cross section data. This is demonstrated in Table 2. For the various neutron reactions listed in column 1 the integral responses in a Cf-252 neutron field are given. The calculated values in column 2 were obtained with the evaluated neutron spectrum and cross section data from ENDF/B-V or from other sources if indicated by additional references [9 - 17]. Compared with the high precision experimental data shown in column 3, these data allow conclusions on the suitability of differential cross section sets for application purposes to be drawn. The data quoted in the

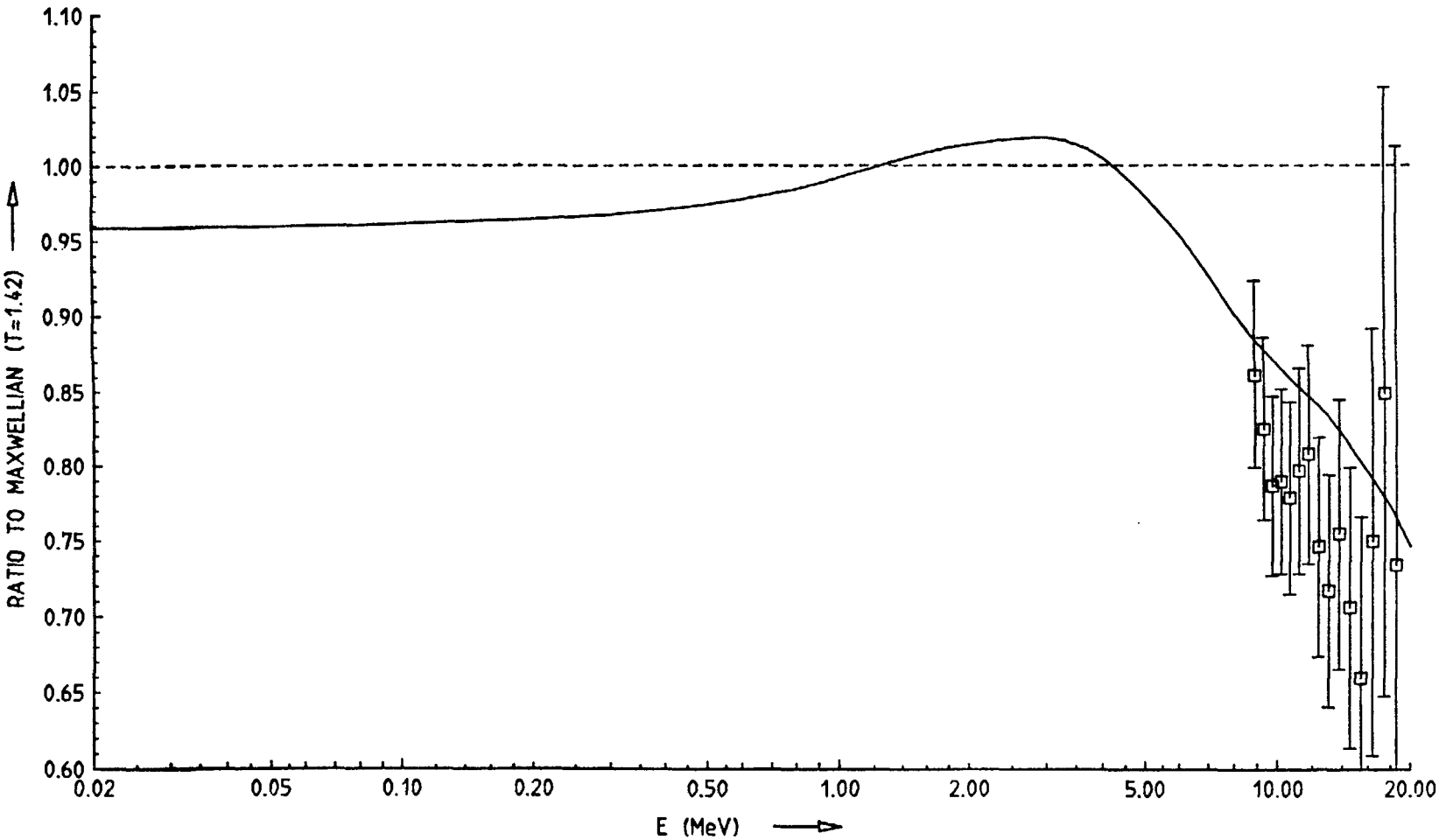

Fig. 8: Experimental data of Märten et al. [7] in comparison with the evaluation.

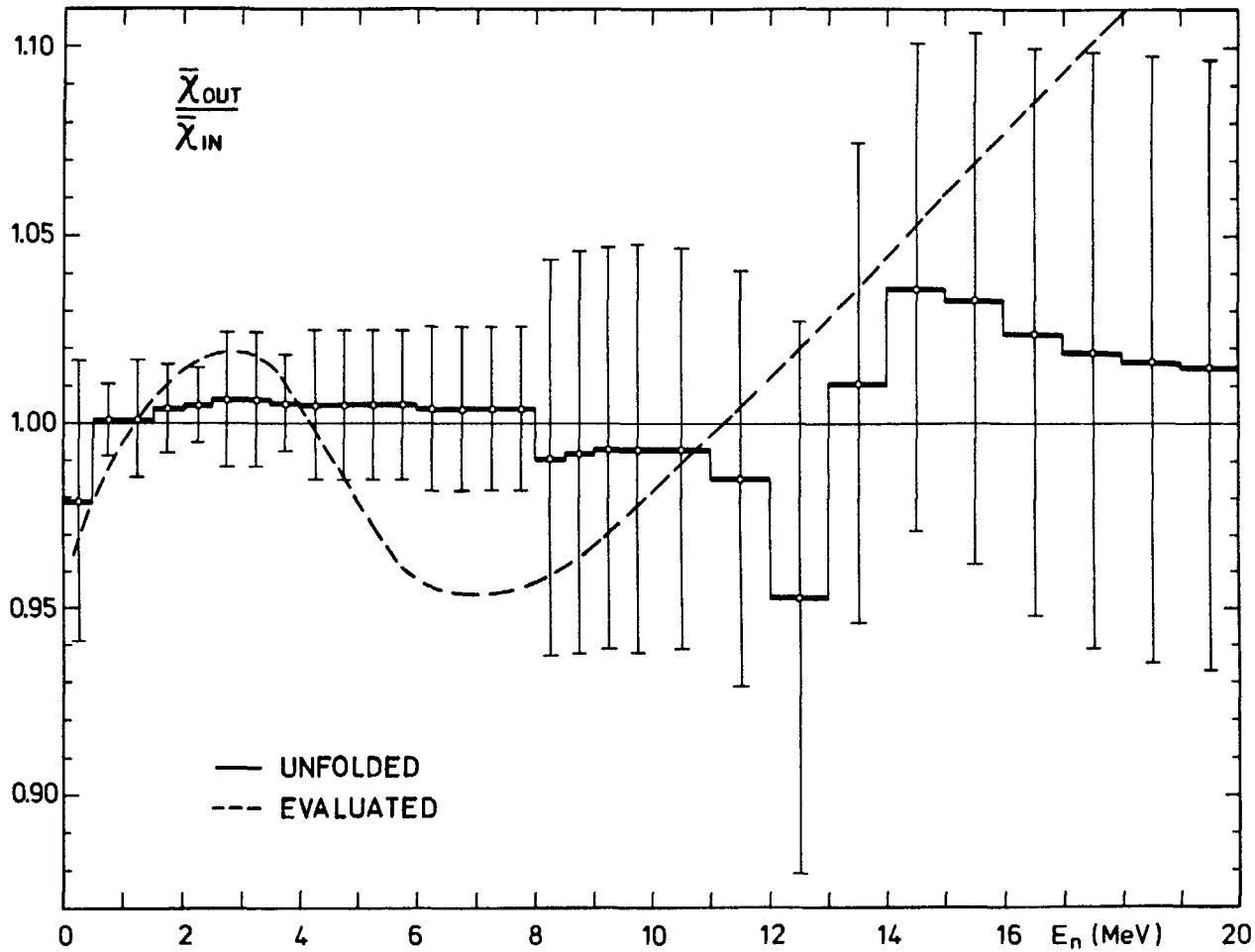

Fig. 9: Result of the Cf-252 neutron spectrum obtained from a spectrum-unfolding procedure based on integral data in comparison with that obtained from the evaluation. The error bars appertain to the unfolded result. The scaling differs partly from that of Figs. 1 - 8 (see text).

Table 2: Cf-252 spectrum-averaged neutron cross sections (in millibarn). The calculated data were obtained with the evaluated spectrum and σ (E) data from ENDF/B-V or from other sources when indicated. The experimental data were taken from various experiments and have been evaluated [18]. The C/E values marked (*) indicate problematic cases.

REACTION	CALCULATION		EXPERIMENT	RSD	C/E	
F-19(N,2N)	1.714E-2*	[9]	1.613E-2	3.40	1.063	
MG-24(N,P)	2.101E+0	[10]	1.998E+0	2.42	1.052	
AL-27(N,P)	5.027E+0		4.885E+0	2.14	1.029	
AL-27(N,A)	1.034E+0		1.017E+0	1.47	1.017	
	9.886E-1	[11]			0.972	
S-32(N,P)	7.591E+1		7.262E+1	3.50	1.045	
TI-46(N,P)	1.317E+1		1.409E+1	1.76	0.935	
TI-47(N,P)	1.933E+1	[12]	1.929E+1	1.66	1.002	
	2.406E+1				1.247	*
TI-48(N,P)	4.002E-1		4.251E-1	1.89	0.941	
V-51(N,P)	6.638E-1	[13]	6.493E-1	1.95	1.022	
V-51(N,A)	3.878E-2	[14]	3.904E-2	2.22	0.993	
MN-55(N,2N)	4.623E-1		4.079E-1	2.34	1.133	*
FE-54(N,P)	8.790E+1		8.692E+1	1.34	1.011	
FE-56(N,P)	1.374E+0		1.466E+0	1.77	0.937	
NI-58(N,P)	1.134E+2		1.176E+2	1.30	0.964	
NI-58(N,2N)	9.048E-3	[15]	8.961E-3	3.59	1.010	
	8.103E-3				0.904	*
CO-59(N,P)	1.699E+0	[16]	1.692E+0	2.49	1.004	
CO-59(N,A)	2.110E-1		2.220E-1	1.86	0.950	
CO-59(N,2N)	4.266E-1		4.055E-1	2.52	1.052	
CU-63(N,G)	9.673E+0		1.045E+1	3.24	0.926	
CU-63(N,A)	6.581E-1	[17]	6.893E-1	1.98	0.955	
	7.383E-1				1.071	
CU-63(N,2N)	2.082E-1	[10]	1.845E-1	3.98	1.128	*
CU-65(N,2N)	6.766E-1		6.587E-1	2.24	1.027	
ZN-64(N,P)	3.913E+1	[10]	4.063E+1	1.64	0.963	
ZR-90(N,2N)	2.196E-1	[10]	2.212E-1	2.90	0.993	
IN-115(N,G)	1.217E+2		1.257E+2	2.23	0.968	
IN-115(N,N')	1.834E+2		1.976E+2	1.37	0.928	
I-127(N,2N)	2.349E+0		2.071E+0	2.75	1.134	*
AU-197(N,G)	7.619E+1		7.686E+1	1.59	0.991	
AU-197(N,2N)	5.648E+0		5.511E+0	1.83	1.025	
U-235(N,F)	1.237E+3		1.210E+3	1.20	1.022	
NP-237(N,F)	1.360E+3		1.361E+3	1.58	0.999	
U-238(N,F)	3.158E+2		3.257E+2	1.63	0.970	
PU-239(N,F)	1.794E+3		1.812E+3	1.37	0.990	

RSD : RELATIVE STANDARD DEVIATION IN %

*Read as 1.714×10^{-2}

"experiment" column were obtained from various experimental sources and have been evaluated from these data [18]. The C/E values of the last column of Table 2 indicate problematic cases, and in cases where more than one cross section set is available, allow a differentiation to be made between the data. Due to the existing experimental correlations between differential cross section data of various reactions, the above mentioned integral testing procedure would be handicapped if integral cross section data were part of the neutron spectrum evaluation. With regard to this and also to the fact that there is no real lack of suitable time-of-flight data in the neutron spectrum evaluation, it has been decided for the time being to avoid the inclusion of integral data in the evaluation.

2.3.2 Revised experiments

Two of the experiments included in the spectrum evaluation have meanwhile been revised.

In the case of the data of Lajtai et al. [5], the Monte Carlo calculations defining the neutron detector efficiency have been repeated with refined methods [19]. The resulting changes of the neutron spectrum values are shown in Fig. 6.

For the PTB neutron spectrum experiment [6], the neutron detector efficiency has been modified. The efficiency was readjusted with a common normalization factor of 0.975 [20], i. e., all spectrum values of Fig. 7 must to be increased by 2.5 %.

2.3.3 Other experiments to be included in the evaluation

Other experiments, chiefly for the high-energy portion of the neutron spectrum, have recently been published.

The experiment of Märten et al. [21] consists of two data sets. To investigate the validity of the correction for non-isotropic fission fragment losses, this experiment has been performed with the neutron detector in two positions at angles relative to the perpendicular of the fission deposit layer. The data obtained at

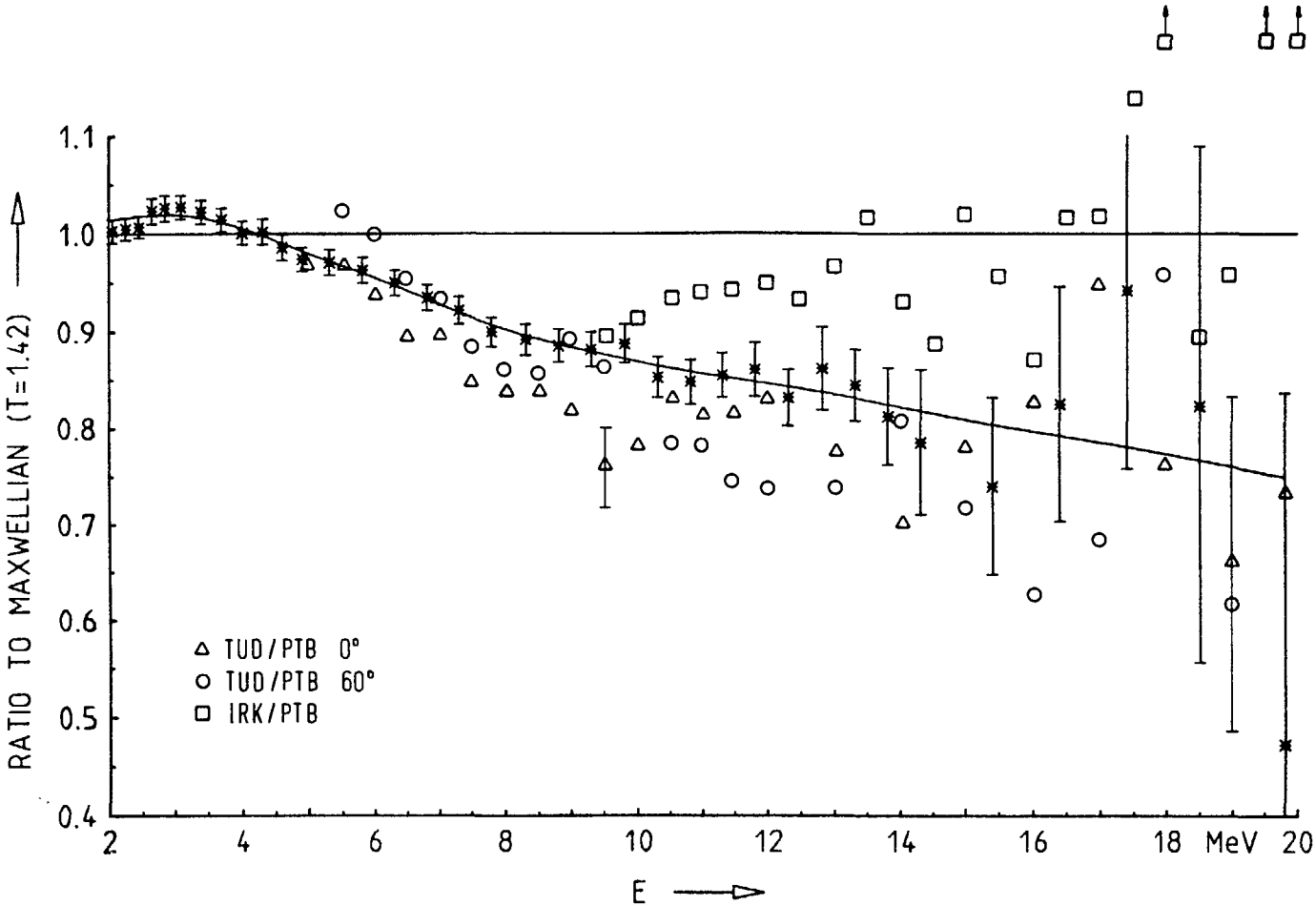

Fig. 10: Data of recent high energy experiments in comparison with the "point-wise" (crosses with error bars) and "continuous" (solid line) evaluation. The data of Märten et al. [21] (see text) are given as triangles and open circles. Only at 9.5 MeV and 19 MeV are two representative error bars shown for the data measured at zero degrees. The data of Chalupka et al. [22] are represented by squares without error bars.

angles of 0 and 60 degrees are shown in Fig. 10. These data are in accordance with an earlier experiment [7] and confirm the deviation of the high-energy part of the spectrum from a Maxwellian.

A second experiment performed by Chalupka et al. [22] also devoted to the high-energy portion of the spectrum, produced some controversial results. These data (also shown in Fig. 10) show a tendency to approach the shape of a Maxwellian with T = 1.42 MeV at high neutron energies. This is in contradiction to other experiments and also to the information obtained from integral experiments [8, 23, 24]. It is not yet clear how a future evaluation can contribute to the solution of this problem and another independent experiment would be highly desirable.

The description of a new low energy experiment [25] has recently been published, but as yet the numerical data are not available. A further experiment to be considered is the simultaneous investigation of fission fragments and neutrons by Butz-Jørgenson and Knitter [26]. This detailed experiment of neutron and fission fragment angular distributions also produced integrated neutron spectrum data between 0.5 MeV and 20 MeV. With a flight path of only 51 cm in this experiment, it remains questionable whether the high-energy data are of sufficiently good quality to be included in a forthcoming new evaluation.

2.4 Comparison with theoretical models

It is beyond the scope of this work to give a review of all the recently developed theories for describing the neutron spectrum of Cf-252. The interested reader is referred to a very comprehensive recent review by Märten [27]. Only two representative models (where detailed numerical values are available) are compared in Fig. 11 with the present evaluation. The model (M-N) of Madland and Nix [27] is based on the nuclear evaporation theory and has been developed to describe fission neutron spectra and other parameters of various fissioning nuclei. When applied in the case of Cf-252, the level density parameter of this model was adjusted by a fit to the experimental data of Poenitz and Tamura [2]. The

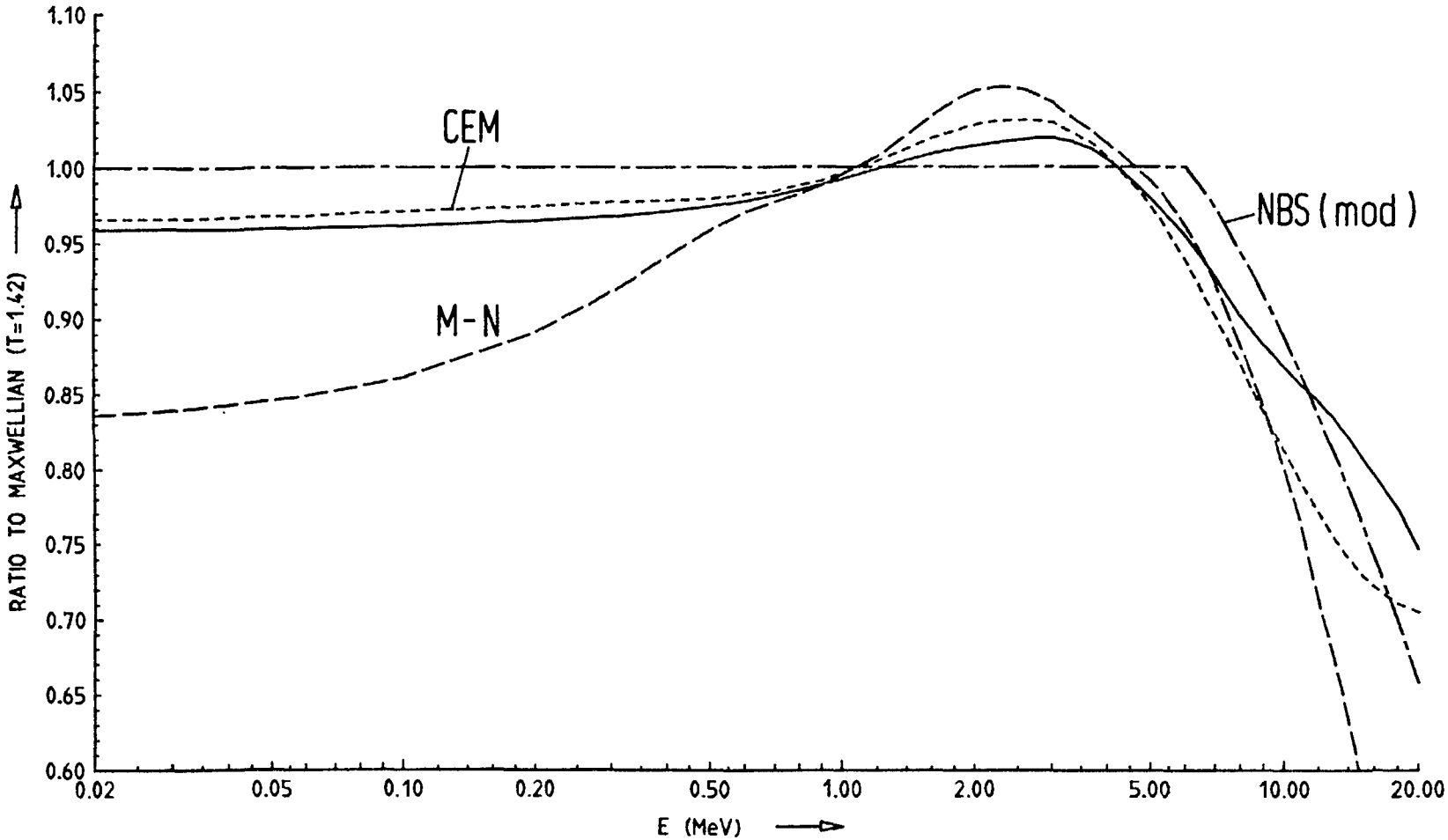

Fig. 11: Comparison of the evaluated neutron spectrum (solid line) with results obtained from theoretical models. The data of the cascade evaporation model (CEM) of Märten and Seeliger [28] and of the Madland and Nix (M-N) theory [27] are shown. In addition, a slightly modified version of an earlier National Bureau of Standards (NBS) evaluation is shown.

cascade evaporation model (CEM) of Märten and Seeliger [28] is free of adjustable parameters. The version shown in Fig. 11 is that obtained with an anisotropy parameter of $\beta = 0.1$. Besides the theoretical models, the shape of an earlier evaluation [30] performed in 1975 at the National Bureau of Standards (NBS) is also shown in Fig. 11. The segment correction functions below 6 MeV in this work have not been taken into account here. However, it is quite remarkable how well this old evaluation is in accordance in its trend with recent theories and the present evaluation.

Between 0.5 MeV and 8 MeV, there are only minor differences between the evaluation and the theoretical models shown in Fig. 11. At high and low neutron energies the general picture changes. Considering that the relative uncertainties of the theories are of the order of 10 - 30 %, the agreement of the cascade evaporation model (CEM) [28] with the evaluation of within 2 % below 8 MeV and within 5 % above 8 MeV, is quite remarkable. Apart from its importance for cross-section data testing (see chapter 2.3.1), the high-energy tail of the neutron spectrum is very sensitive in its theoretical description and thus also useful to test of the theoretical model.

Many of the theoretical models have meanwhile been modified and refined. The recent improvement of the model of Madland and Nix [31] by replacing the prior averages with detailed fission-fragment mass and charge distributions only weakly influenced the result of this theory at high and low neutron energies. Another attempt to extend the Madland and Nix model to include the fission fragment spin and take into account possible pre-accelerated neutrons [32] should be noted.

The neutron spectrum results obtained with the Hauser-Feshbach theory represent the most general theoretical description but require an enormous amount of detailed input information. Only simplified versions of this theory have been attempted to date [33]. The resulting numerical data strongly depend on what is assumed for the neutron emission anisotropy in the center-of-mass system of the fission fragments. When this effect is neglected, the theoretical result is similar to that of Madland and Nix [31]

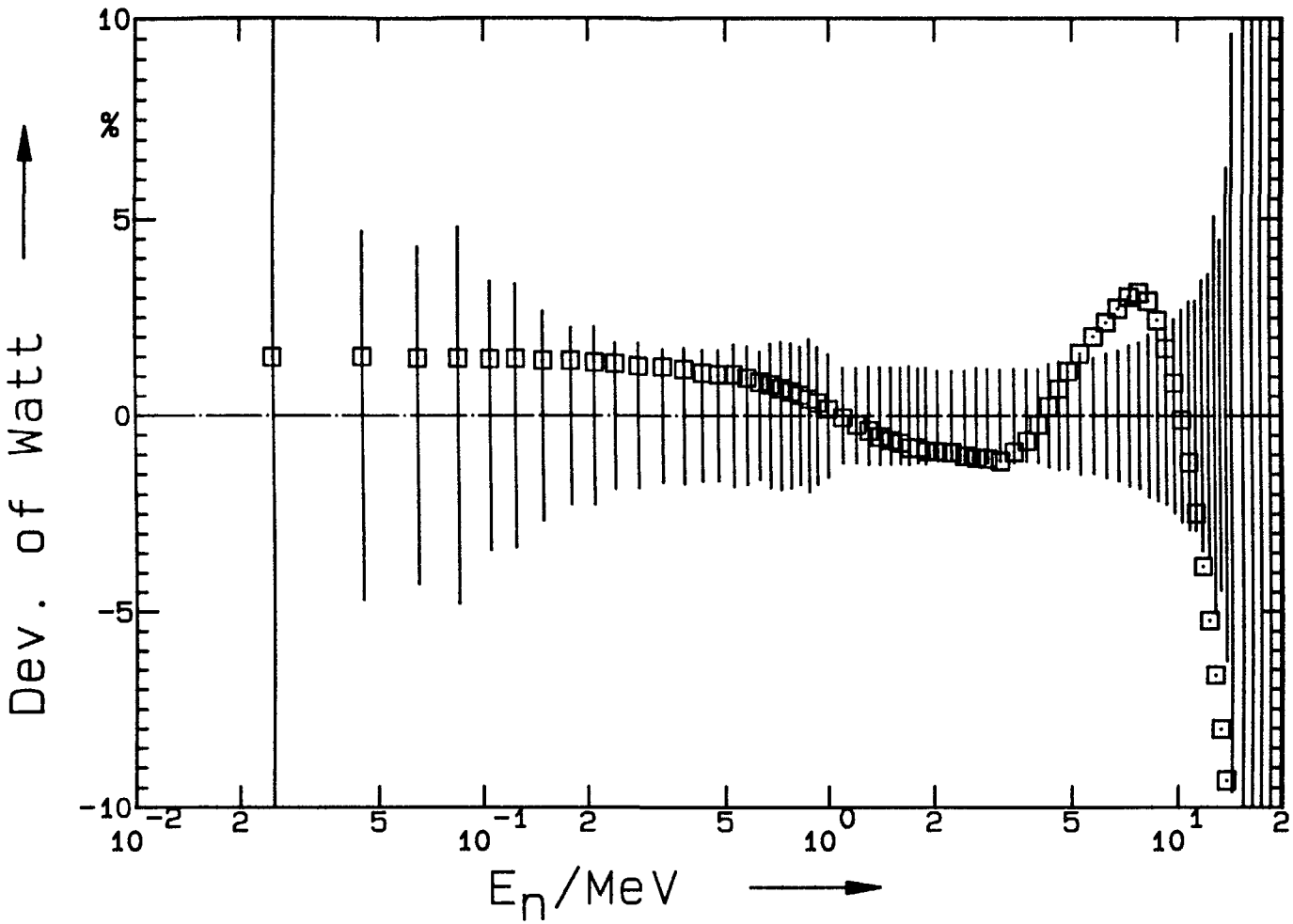

Fig. 12: Result obtained from the fit of a Watt distribution to the evaluated point data neglecting to the data correlations. The deviations of this Watt distribution from the data of the "continuous" evaluation shown with error bars are plotted.

and shows unsatisfactory agreement with the evaluated spectrum for high and low neutron energies.

The recent availability of detailed experimental data on neutron-fission-fragment correlations and angular distributions [26, 34, 35] has opened up new vistas for the theoretical models. A comparison of these data with that derived from the models has led to a better understanding of the neutron emission mechanism and has guaranteed a higher quality of the integrated neutron spectrum due to the improved details in the theory. The first steps in this direction were quite promising. The results obtained by Märten et al. [35] with the extended cascade evaporation model (CEM), and also with a generalized version of the Madland and Nix model, approximate the evaluated neutron spectrum very closely. In both cases the differential neutron spectra, $N(E,\theta)$, were part of the theoretical description.

3. Approximation of the spectrum with a Watt distribution

Fröhner [36] recently investigated the possibility of describing the Cf-252 neutron spectrum with a simple 'macroscopic' model. He studied the suitability of a few models and concluded that a Watt distribution is sufficient to describe the neutron spectrum fairly well. On the assumption that the neutron evaporation spectrum in the center-of-mass system of the fissioning nucleus is represented by a Maxwellian distribution, the transformation to the laboratory system ends in such a Watt distribution.

Independent of the existing evaluation [1], Fröhner performed his own analysis of the experimental data base available. He applied the necessary corrections to the data and, where necessary, estimated the total uncertainties. His data base is essentially identical with that of Table 1, but contains a few additional experiments which were not part of the present evaluation. The fit of a Watt distribution to Fröhner's data base resulted in the following parameters:

$$T_W = 1.175 \pm 0.005 \text{ MeV and } E_W = 0.359 \pm 0.009 \text{ MeV} \quad (1)$$

with a correlation coefficient of

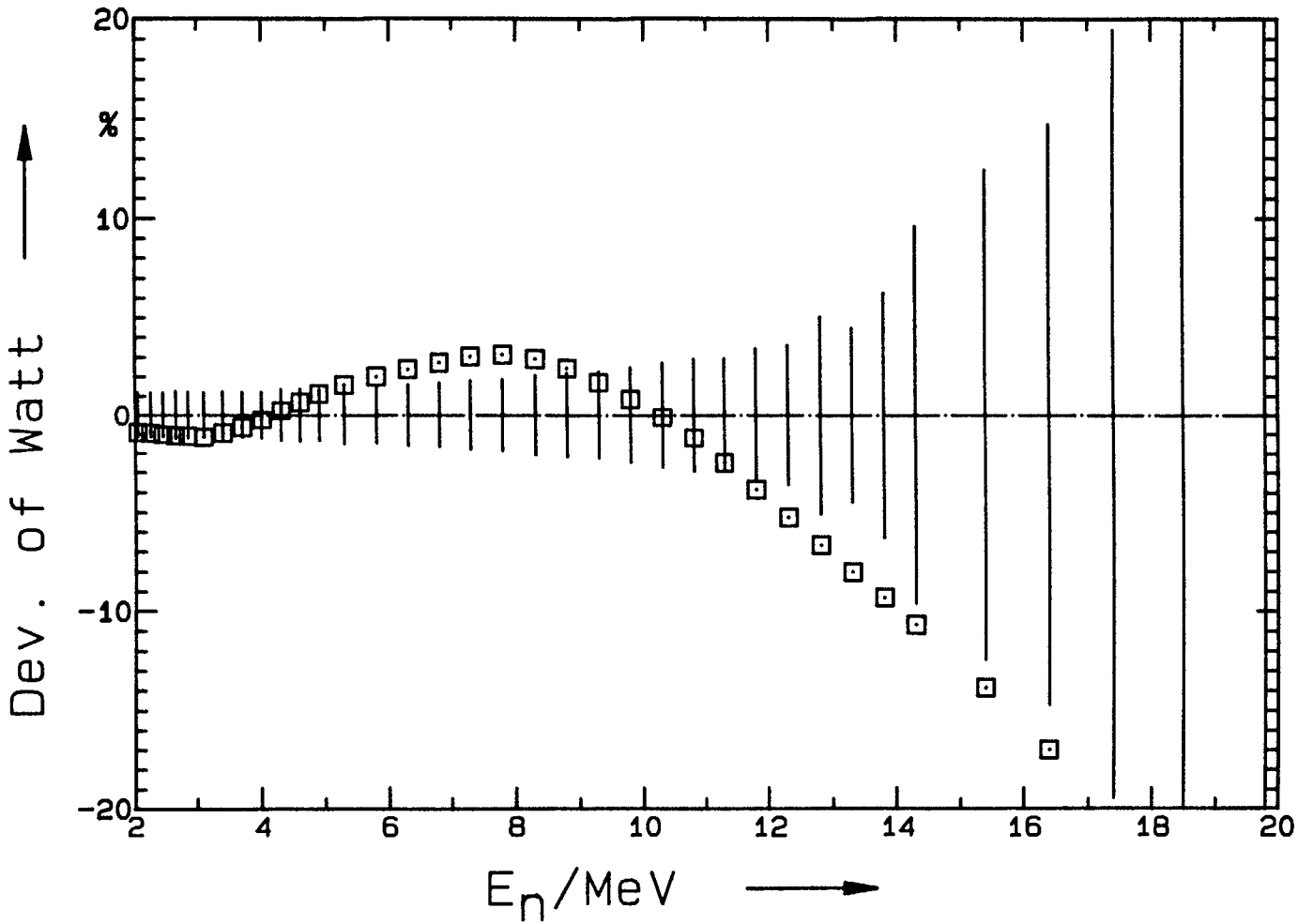

Fig. 13: As in Fig. 12, but for the high-energy portion of the Cf-252 neutron spectrum.

$$\rho\ (T_W,\ E_W) = -\ 0.984$$

The value of chi-square per degree of freedom was $x^2/f = 1.04$ and indicated a satisfactory description of the spectrum data.

Shortly after this, Fröhner also applied the fit to the present evaluated point data (see Fig. 1) and obtained

$$T_W = 1.174 \pm 0.008 \text{ MeV and } E_W = 0.361 \pm 0.014 \text{ MeV} \qquad (2)$$

without quoting further details.

This second fit has been repeated here. The parametrization of the Watt distribution was done in ENDF/B notation and was:

$$N_W\ (E) = \frac{2}{\sqrt{\pi\ b\ a^3}}\ \exp\left(-\frac{ab}{4}\right)\ \exp\left(-\frac{E}{a}\right)\ \sinh\left(\sqrt{bE}\right) \qquad (3)$$

This notation is slightly different from Fröhner's formula. Both are interconnected via the simple relationships:

$$T_W = a \text{ and } E_W = \frac{a^2 b}{4} \qquad (4)$$

It was found that Fröhner's result (Eq. (2)) could only be reproduced when the correlations between the evaluated point data are neglected. The result obtained was:

$$a = 1.174 \pm 0.008 \text{ MeV}$$
$$b = 1.043 \pm 0.056\ (\text{MeV})^{-1} \qquad (5)$$

with $\rho\ (a,b) = -\ 0.99$ and $x^2/f = 1.44$ and is consistent with Fröhner's result of eq. (2).

The high anti-correlation between the parameters and a and b or T_W and E_W is not unusual for such a two-parameter fit. The Watt distribution obtained with the parameters of eq. (5) is shown in Figs. 12 and 13. The deviations of the Watt distribution from the "continuous" evaluation are shown. The error bars given correspond to the evaluation. In general, there is good agreement between the

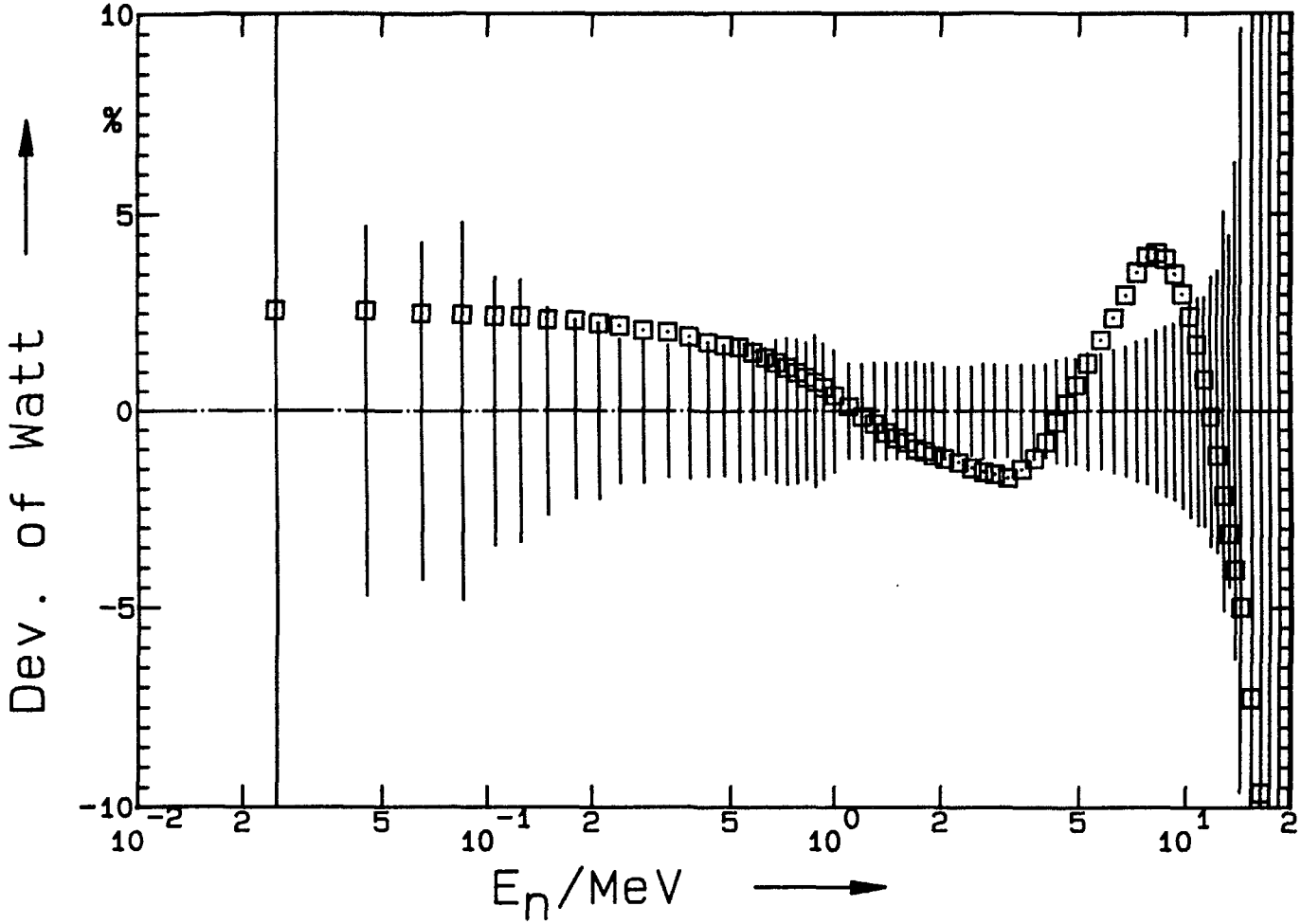

Fig. 14: Result obtained from the fit of a Watt distribution to the evaluated point data taking into account the data correlations. The deviations of this Watt distribution from the data of the "continuous" evaluation shown with error bars are plotted.

Watt distribution and the evaluation. In the high-energy part of the spectrum (see Fig. 13), the Watt distribution shows a tendency to overestimate the spectrum between 6 and 9 MeV and to underestimate it above 12 MeV. The error propagation with the parameters of eq. (5) given for a few neutron energies resulted in the following figures for the relative uncertainty:

$$E_n = 25 \text{ keV} : 0.40\ \% \quad (10.35\ \%)$$
$$E_n = 1.6 \text{ MeV} : 0.04\ \% \quad (1.23\ \%)$$
$$E_n = 19.8 \text{ MeV} : 3.01\ \% \quad (76.95\ \%)$$

with a value of less than 1 % between 25 keV and 11.8 MeV. For comparison, the corresponding uncertainty values obtained from the evaluation are given in brackets. These uncertainties are based on the experimental data available and are chiefly dominated by remaining systematical components. And now a very fundamental question arises: Does a parameter fit justify reducing such uncertainties by more than a factor of ten? In the case of purely statistical uncertainties and on the assumption that the Watt distribution is a valid representation of the neutron spectrum, the answer is obvious from a statistical point of view. But here the situation is somewhat more complex. On the one hand we know that the neutron detector calibration of each experiment is at least based on the hydrogen cross section (presently known with an accuracy of about 1 %), and on the other hand we have no information that the Watt distribution is the only valid description of the spectrum. It is therefore believed that an uncertainty reduction below the 1 % level is arbitrary and cannot be justified with regard to the original experimental data. Finally, a fit of a Watt distribution to the evaluated point data with full regard to the correlations between the data has been performed. The resulting parameters were quite different from those obtained before and shown in eq. (5). These parameters were:

$$a = 1.209 \pm 0.015 \text{ MeV}$$
$$b = 0.836 \pm 0.107 \text{ (MeV)}^{-1} \qquad (6)$$

with $\rho(a,b) = -0.98$ and $\chi^2/f = 0.90$.

The value of the reduced chi-square of eq. (6) promised a better approximation compared with the result of eq. (5). This can be

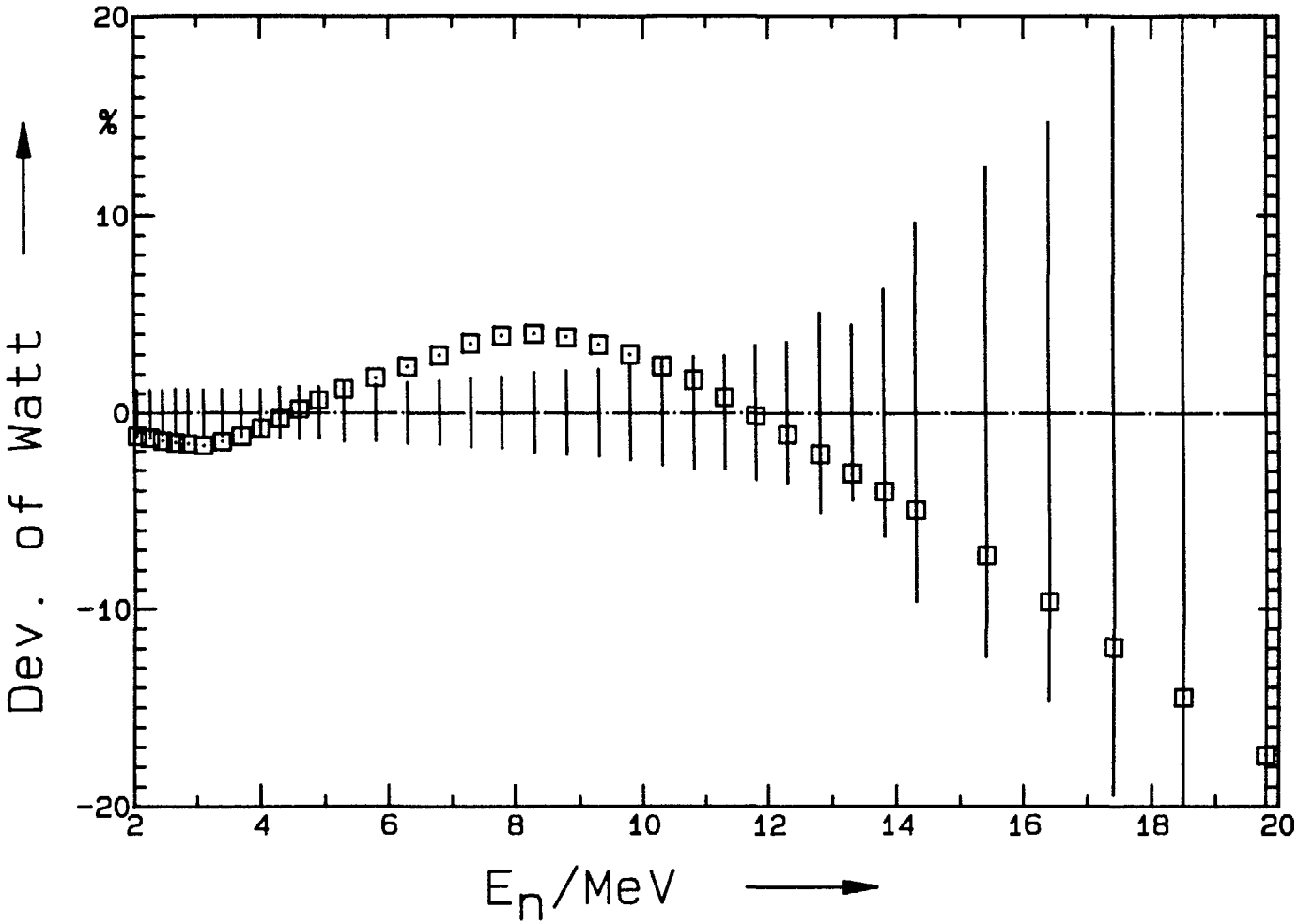

Fig. 15: As in Fig. 14, but for the high-energy portion of the spectrum.

clearly seen in Figs. 14 and 15. At low neutron energies the deviation of this second Watt distribution is somewhat larger than before, but at high neutron energies the agreement between the fitted Watt distribution and the evaluation is considerably improved. The propagated uncertainties derived from eq. (6) resulted in somewhat more realistic values of:

E_n = 25 keV : 1.08 % (10.35 %)
E_n = 1.8 MeV : 0.06 % (1.20 %)
E_n = 19.6 MeV : 3.81 % (76.95 %)

But here too, with a derived uncertainty value of < 1 % valid between 150 keV and 4.6 MeV, it is obvious that the same arguments as mentioned before remain valid.

Summarizing the results quoted above, it can be said that parametrization with a Watt distribution is useful for a fast and simple representation of the Cf-252 neutron spectrum. The Watt distribution obtained from a fit to the evaluated point data with regard to their uncertainties and their correlations is superior in the description of the neutron spectrum. The accuracy of such an approximation should not be overestimated, and it seems unrealistic to propagate the uncertainties of the fit parameters.

References:

[1] W. Mannhart: in "Properties of Neutron Sources", IAEA-TECDOC-410, IAEA, Vienna (1987) 158

[2] W. P. Poenitz, T. Tamura: in "Nuclear Data for Science and Technology" (K. H. Böckhoff, Ed.); D. Reidel Publ. Comp., Dordrecht (1983) 465
W. P. Poenitz, T. Tamura: Report INDC(NDS)-146/L (1983) 175

[3] M.V. Blinov, G. S. Boykov, V. A. Vitenko: in "Nuclear Data for Science and Technology", (K. H. Böckhoff, Ed.); D. Reidel Publ. Comp., Dordrecht (1983) 479
M. V. Blinov, G. S. Boykov, V. A. Vitenko: Report INDC(CCP)-238/L (1985)

[4] J. W. Boldeman, B. E. Clancy, D. Culley: Nucl. Sci. Eng. 93 (1986) 181

[5] A. Lajtai, P. P. Dyachenko, L. S. Kutzaeva, V. N. Konov, P. A. Androsenko, A. A. Androsenko: Report INDC(NDS)-146/L (1983) 177

[6] R. Böttger, H. Klein, A. Chalupka, B. Strohmaier: in "Nuclear Data for Science and Technology", (K. H. Böckhoff, Ed.); D. Reidel Publ. Comp., Dordrecht (1983) 484
R. Böttger, H. Klein, A. Chalupka, B. Strohmaier: in "Properties of Neutron Sources", IAEA-TECDOC-410, IAEA, Vienna (1987) 186

[7] H. Märten, D. Seeliger, B. Stobinski: in "Nuclear Data for Science and Technology", (K. H. Böckhoff, Ed.); D. Reidel Publ. Comp., Dordrecht (1983) 488
H. Märten, D. Richter, D. Seeliger: Report INDC(GDR)-28/L (1984)

[8] W. Mannhart: in "Nuclear Standard Reference Data", IAEA-TECDOC-335, IAEA, Vienna (1985) 294

[9] B. Strohmaier, S. Tagesen, H. Vonach: Physics Data 13-2 (1980)

[10] S. Tagesen, H. Vonach, B. Strohmaier: Physics Data 13-1 (1979)

[11] S. Tagesen, H. Vonach: Physics Data 13-3 (1981)

[12] W. Mannhart, D. L. Smith, J. W. Meadows: in "Nuclear Data for Basic and Applied Science", (P. G. Young, Ed.), Gordon and Breach, New York (1986) 577

[13] D. L. Smith, J. W. Meadows, I. Kanno: Report ANL/NDM-85 (1984)

[14] I. Kanno, J. W. Meadows, D. L. Smith: Report ANL/NDM-86 (1984)

[15] A. Pavlik, G. Winkler: Report INDC(AUS)-9/L (1983)

[16] D. L. Smith, J. W. Meadows: Nucl. Sci. Eng. 60 (1976) 187

[17) G. Winkler, D. L. Smith, J. W. Meadows: Nucl. Sci. Eng. 76 (1980) 30

[18] W. Mannhart: in "Reactor Dosimetry" (J. P. Genthon, H. Röttger, Eds.), D. Reidel Publ. Comp., Dordrecht (1985) 801
W. Mannhart: in "Handbook on Nuclear Activation Data", Techn. Rep. Series No. 273, IAEA, Vienna (1987) 413

[19] A. Lajtai, P. P. Dyachenko, E. A. Seregina, V. N. Kononov:

in "Nuclear Data for Science and Technology", (S. Igarasi, Ed.), Saikon Publ. Comp., Tokyo (1988) 737

[20] H. Klein: priv. communication (1989)

[21] H. Märten, D. Richter, D. Seeliger, W. D. Fromm, R. Böttger, H. Klein: Report INDC(NDS)-194/L (1987)

[22] A. Chalupka, L. Malek, S. Tagesen, R. Böttger: in "Properties of Neutron Sources", IAEA-TECDOC-410, IAEA, Vienna (1987) 190

[23] W. Mannhart: in "Nuclear Data for Science and Technology", (K. H. Böckhoff, Ed.), D. Reidel Publ. Comp., Dordrecht (1983) 429

[24] W. Mannhart: in "Properties of Neutron Sources", IAEA-TECDOC-410, IAEA, Vienna (1987) 194

[25] G. Tang, S. Bao, J. Wang, W. Zhoug, Y. Li, Z. Shi, F. Huang, J. Chen, J. Meng, A. Li, Z. Bao, S. Huang: in "Nuclear Data for Science and Technology", (S. Igarasi, Ed.), Saikon Publ. Comp., Tokyo (1988) 755

[26] C. Butz-Jørgenson, H. H. Knitter: contribution to the present meeting

[27] H. Märten: Proc. IAEA Advisory Group Meeting on Nuclear Theory for Fast Neutron Nuclear Data Evaluation, Beijing (China), 12 - 16 October 1987

[28] D. G. Madland, J. R. Nix: Nucl. Sci. Eng. 81 (1982) 213
D. G. Madland, J. R. Nix: in "Nuclear Data for Science and Technology", (K. H. Böckhoff, Ed.), D. Reidel Publ. Comp., Dordrecht (1983) 473
D. G. Madland, R. J. LaBauve, J. R. Nix: in "Nuclear Standard Reference Data", IAEA-TECDOC-335, IAEA, Vienna (1985) 267

[29] H. Märten, D. Neumann, D. Seeliger: Report INDC(NDS)-146/L (1983) 199
H. Märten, D. Seeliger: in "Nuclear Standard Reference Data", IAEA-TECDOC-335, IAEA, Vienna (1985) 255

[30] J. A. Grundl, C. Eisenhauer: in "Nuclear Cross Sections and Technology", NBS Spec. Publ. 425, Washington (1975) 250
J. Grundl. C. Eisenhauer: in "Neutron Cross Sections for Reactor Dosimetry", IAEA-TECDOC-208, IAEA, Vienna (1978) 53

[31] D. Madland: in "Nuclear Data for Science and Technology", (S. Igarasi, Ed.), Saikon Publ. Comp., Tokyo (1988) 759

D. G. Madland, R. J. LaBauve, J. R. Nix: contribution to the present meeting

[32] R. L. Walsh, G. Chircu: contribution to the present meeting

[33] B. F. Gerasimenko, V. A. Rubchenya: in "Properties of Neutron Sources", IAEA-TECDOC-410, IAEA, Vienna (1987) 208
B. F. Gerasimenko, V. A. Rubchenya: contribution to the present meeting

[34] I. O. Batenkov, A. B. Blinov, M. V. Blinov, S. N. Smirnov: in "Nuclear Data for Science and Technology", (S. Igarasi, Ed.), Saikon Publ. Comp., Tokyo (1988) 771

[35] H. Märten, D. Richter, A. Ruben, D. Seeliger, W. Neubert, A. Lajtai: in "Nuclear Data for Science and Technology", (S. Igarasi, Ed.), Saikon Publ. Comp., Tokyo (1988) 683

[36] F. H. Fröhner: Proc. IAEA Advisory Group Meeting on Nuclear Theory for Fast Neutron Nuclear Data Evaluation, Beijing (China), 12 - 16 October 1987

LIST OF PARTICIPANTS

AUSTRALIA:

J.W. Boldeman (Chairman)
Lucas Heights Research Laboratory
Private Mail Bag 1
Menai, N.S.W. 2234

CHINA:

Huang Shengnian
Institute of Atomic Energy
P.O. Box 275 (41)
Beijing

FRANCE:

J.E. Fréhaut
Service de Physique Neutronique
et Nucléaire
Commisariat a l'Energie Atomique
B.P. No. 12
F-91680 Bruyères-le-Châtel

GERMAN DEM. REP:

D. Seeliger
Technische Universität Dresden
Sektion Physik
Mommsenstr. 13
DDR-8027 Dresden

H. Märten
Technische Universität Dresden
Sektion Physik
Mommsenstr. 13
DDR-8027 Dresden

GERMANY, FED. REP.:

W. Mannhart
Physikalisch-Technische
Bundesanstalt
Abteilung 6
Bundesallee 100
D-3300 Braunschweig

INDIA:

S.S. Kapoor
Nuclear Physics Division
Bhabha Atomic Research Centre
Trombay, Bombay 400 085

JAPAN:

M. Baba
Dept. of Nuclear Engineering
Tohoku University
Aoba, Aramaki
Sendai-shi, 980

N. Hirakawa
Dept. of Nuclear Engineering
Tohoku University
Aoba, Aramaki
Sendai-shi, 980

JAPAN (cont.):

S. Igarasi (Meeting Organization)
Nuclear Data Center
Physics Department
Japan Atomic Energy Research
Institute (JAERI)
Tokai-Mura, Naka-Gun
Ibaraki-ken 319-11

I. Kanno (Meeting Organization)
Dept. of Nuclear Engineering
Japan Atomic Energy Research
Institute (JAERI)
Tokai-mura, Naka-gun
Ibaraki-ken 319-11

I. Kimura
Research Reactor Institute
Kyoto University
Kumatori-Cho, Sennan-Gun
Osaka-fu 590-04

K. Kobayashi
Research Reactor Institute
Kyoto University
Kumatori-cho, Sennan-gun
Osaka 590-04

Y. Nakagome
Research Reactor Institute
Kyoto University
Kumatori-cho, Sennan-gun
Osaka 590-04

T. Ohsawa
Faculty of Engineering
Kyushu University - 36
6-10-1 Hakozaki
Higashi-ku
Fukuoka 812

U.S.A.:

D.G. Madland
Theoretical Division
Los Alamos National Laboratory
Los Alamos, New Mexico 87545

F.G. Perey
Engineering Physics Division
Oak Ridge National Laboratory
P.O. Box X
Oak Ridge, TN 37830

U.S.S.R.:

M.V. Blinov
Radievyj Institut V.G. Khlopina
Ul. Rentgena 1
Leningrad 197022

B.D. Kuzminov
Fiziko-Energeticheskij Institut
Ploshchad Bondarenko
249 020 Obninsk, Kaluga Region

INTERNATIONAL ORGANIZATIONS

European Communities:

H.H. Knitter
Bureau Central de Mesures
Nucléaires
Steenweg Naar Retie
B-2440 Geel, Belgium

I.A.E.A.:

H.D. Lemmel (Scientific Secretary)
Nuclear Data Section
International Atomic Energy Agency
Wagramerstr. 5, P.O. Box 100
A-1400 Vienna, Austria